Lecture Notes in Civil Engineering

T. G. Sitharam
Sreevalsa Kolathayar
Ravi Jakka *Editors*

Earthquakes and Structures

Select Proceedings of 7th ICRAGEE 2021

Springer

Lecture Notes in Civil Engineering

Volume 188

Lecture Notes in Civil Engineering (LNCE) publishes the latest developments in Civil Engineering - quickly, informally and in top quality. Though original research reported in proceedings and post-proceedings represents the core of LNCE, edited volumes of exceptionally high quality and interest may also be considered for publication. Volumes published in LNCE embrace all aspects and subfields of, as well as new challenges in, Civil Engineering. Topics in the series include:

- Construction and Structural Mechanics
- Building Materials
- Concrete, Steel and Timber Structures
- Geotechnical Engineering
- Earthquake Engineering
- Coastal Engineering
- Ocean and Offshore Engineering; Ships and Floating Structures
- Hydraulics, Hydrology and Water Resources Engineering
- Environmental Engineering and Sustainability
- Structural Health and Monitoring
- Surveying and Geographical Information Systems
- Indoor Environments
- Transportation and Traffic
- Risk Analysis
- Safety and Security

To submit a proposal or request further information, please contact the appropriate Springer Editor:

– Pierpaolo Riva at pierpaolo.riva@springer.com (Europe and Americas);
– Swati Meherishi at swati.meherishi@springer.com (Asia - except China, and Australia, New Zealand);
– Wayne Hu at wayne.hu@springer.com (China).

All books in the series now indexed by Scopus and EI Compendex database!

More information about this series at https://link.springer.com/bookseries/15087

T. G. Sitharam · Sreevalsa Kolathayar · Ravi Jakka
Editors

Earthquakes and Structures

Select Proceedings of 7th ICRAGEE 2021

Springer

Editors
T. G. Sitharam
Indian Institute of Technology Guwahati
Guwahati, Assam, India

Ravi Jakka
Department of Earthquake Engineering
Indian Institute of Technology Roorkee
Roorkee, Uttarakhand, India

Sreevalsa Kolathayar
Department of Civil Engineering
National Institute of Technology
Surathkal, Karnataka, India

ISSN 2366-2557 ISSN 2366-2565 (electronic)
Lecture Notes in Civil Engineering
ISBN 978-981-16-5672-9 ISBN 978-981-16-5673-6 (eBook)
https://doi.org/10.1007/978-981-16-5673-6

This Springer imprint is published by the registered company Springer Nature Singapore Pte Ltd.
The registered company address is: 152 Beach Road, #21-01/04 Gateway East, Singapore 189721, Singapore

Preface

The behaviour of structures subjected to dynamic loads during earthquakes needs special attention in making the infrastructure resilient. The advancements in the research on the response of structures under earthquake loading can go a long way in reducing the risk through best practices.

This volume presents select papers presented at the 7th International Conference on Recent Advances in Geotechnical Earthquake Engineering and Soil Dynamics. The papers discuss advances in the fields of earthquake engineering connected with structures. Some of the themes include soil structure interaction, dynamic analysis, underground structures, vibration isolation, seismic response of buildings, etc. A strong emphasis is placed on connecting academic research and field practice, with many examples, case studies, and best practices.

We thank all the staff of Springer for their full support and cooperation at all the stages of the publication of this book. We thank and acknowledge the service of authors and reviewers for their valuable time and efforts. We do hope that this book will be beneficial to students, researchers, and professionals working in the field of geotechnical earthquake engineering. The comments and suggestions from the readers and users of this book are most welcome.

Guwahati, India — T. G. Sitharam
Karnataka, India — Sreevalsa Kolathayar
Roorkee, India — Ravi Jakka

Contents

About the Editors

Prof. Dr. T. G. Sitharam is the Chairman of 7th ICRAGEE, and President of Indian Society for Earthquake Technology. Presently, he is the Director of Indian Institute of Technology, Guwahati, Assam since July 2019. He is a Senior Professor at Department of Civil Engineering, Indian Institute of Science, Bangalore. He is also the Director of Central Institute of Technology, Kokrajhar, Assam (additional charge) since May 2021. He holds Masters in Civil engineering from Indian Institute of Science and Ph.D. from University of Waterloo, Canada and worked for his postdoctoral at University of Texas, USA. He has served as a visiting or honorary/visiting professor at several overseas universities. He has guided 40 Ph.D., more than 35 Masters Students, 20 postdoctoral students and several thousand industry professionals and teachers through continuing education workshops. Over the last 35 years, he has carried out research and development in the area of geotechnical and infrastructure engineering, seismic microzonation & soil dynamics and Geotechnical earthquake engineering leading to about 500 technical papers, 20 books and 5 patents. He has 2 start-up companies and many technological innovations to his credit. Prof Sitharam has recently delivered the IGS annual lecture in IGC 2020 and recipient of several National and International awards. In 2020, He was listed in the world's top 2% of scientists for the most-cited scientists (with more than 6700 citations with an H-index of 46) in various disciplines by Stanford University in 2020. He is the Fellow of American Society of Civil Engineering, Fellow of the Institution of Civil Engineers (UK), Diplomate of Geotechnical Engineering from Academy of Geoprofessionals, ASCE, USA, and holds many other fellowships to his credit.

Dr. Sreevalsa Kolathayar pursued his M.Tech. from Indian Institute of Technology (IIT) Kanpur, Ph.D. from Indian Institute of Science (IISc) and served as International Research Staff at UPC BarcelonaTech Spain. He is presently Assistant Professor in the Department of Civil Engineering, National Institute of Technology (NIT), Karnataka. Dr. Kolathayar has authored six books and over 75 research articles. He is Associate Editor of two International Journals. His broad research areas are geotechnical earthquake engineering, geosynthetics & geonaturals, and water geotechnics. He is currently the Secretary of the Indian chapter of International Association for

Coastal Reservoir Research (IACRR), and Executive Committee Member of Indian Society of Earthquake Technology. In 2017, The New Indian Express honored Dr. Kolathayar with 40 under 40 - South India's Most Inspiring Young Teachers Award. He is the recipient of ISET DK Paul Research Award from Indian Society of Earthquake Technology, IIT Roorkee. He received "IEI Young Engineers Award" by The Institution of Engineers (India), in recognition of his contributions in the field of Civil Engineering. He was recently featured in Geostrata Magazine by American Society of Civil Engineers (ASCE). Dr. Sreevalsa is the Organizing Secretary of 7th International Conference on Recent Advances in Geotechnical Earthquake Engineering.

Prof. Ravi Jakka is working as Associate Professor in the Department of Earthquake Engineering, Indian Institute of Technology, Roorkee. He is also currently serving as Secretary, Indian Society of Earthquake Technology(ISET). He has graduated in Civil Engineering from Andhra University Engineering College in the year 2001. He has obtained masters and doctorate degrees from IIT Delhi in the years 2003 and 2007 respectively. His areas of interest are Dynamic Site Characterization, Soil Liquefaction, Seismic Slope Stability of Dams, Landslides, Foundations & Seismic Hazard Assessment. He has published over 100 articles in reputed international journals and conferences. He has supervised over 35 Masters Dissertations and 6 Ph.D. thesis, while he is currently guiding 10 Ph.D. Thesis. He has received prestigious DAAD and National Doctoral fellowships. He has obtained University Gold Medal from Andhra University. He also received 'Young Geotechnical Engineer Best Paper Award' from Indian Geotechnical Society. He was instrumental in the development of Earthquake Early Warning System for northern India, a prestigious national project. He is also the Organizing Secretary to 7th International Conference on Recent Advances in Geotechnical Earthquake Engineering. Recently, he took the responsibilities of the International Journal of Geotechnical Earthquake Engineering as an Editor.

Dynamic Analysis of SSI Effects on Underground Structures

Vijay Kumar, Mithilesh Kumar, Madan Kumar, and Akash Priyadarshee

Abstract This paper describes the Dynamic Soil-Structure Interaction (SSI) effects on the underground structures. The finite element model for Nuclear Power Plant (NPP) and a tunnel was considered to analyze the effects of SSI. Dynamic analysis was carried out considering three transmitting boundary conditions. The effect of embedment for NPP founded on soft soil and seismic responses of a reinforced concrete building in proximity with an underground circular tunnel were studied. The lateral spacing of the circular tunnel from the center line of the building was varied while maintaining a constant depth below the ground level. The effect of embedment has been investigated and the result shows acceleration and displacement responses of the system are smaller with the infinite boundary as compared to viscous and kelvin boundary conditions. In tunnel analysis, the results shows maximum building response occurs when the tunnel is positioned directly below the centre line of the building.

Keywords SSI · Transmitting boundaries · Underground structures · Embedment

1 Introduction

The process in which the motion of the soil influences the response of the structure and the motion of the structure influences the response of the soil is termed as soil-structure interaction (*SSI*). The soil-structure interaction effect plays an important role in the seismic analysis of infrastructure and industrial facilities, especially for underground structures. It is more observed when massive or elevated structures are situated at soft soil thus it is one of the most widely studied phenomena in earthquake engineering. Over the past four decades, broad research has been performed to study

V. Kumar (✉) · A. Priyadarshee
Muzaffarpur Institute of Technology, Muzaffarpur 842003, India

M. Kumar
Saharsa College of Engineering, Saharsa 852201, India

M. Kumar
Government Polytechnic, Muzaffarpur 842001, Bihar, India

T. G. Sitharam et al. (eds.), *Earthquakes and Structures*, Lecture Notes in Civil Engineering 188, https://doi.org/10.1007/978-981-16-5673-6_1

the phenomenon of SSI, and its impact on the seismic response of structures. One of the major challenges in the analysis of dynamic soil-structure interaction problems is to achieve stable and economical modeling. In the numerical simulation of wave propagation problems by finite element, it is necessary to eliminate the boundary events which are generated by the boundary of the numerical grids. Artificial boundaries in numerical analysis generally introduce spurious reflected waves. The numerical modeling of waves in underground structures is a challenging task for several reasons. One of the primary obstacles is formulating an accurate yet inexpensive procedure for dynamic interaction analysis is the modeling of unbounded medium beneath the structures. Many approaches of modeling have been developed in both time and frequency domains. A critical review of the existing literature suggests that various available techniques could be grouped into the following two major categories:

(a) Rigorous Approach,
(b) Approximate Approach.

A rigorous approach which is global in space and time: first solving in the frequency domain and then in the time domain. To obtain a solution in the time domain, the procedures involve the convolution process, which uses Fourier transform. Therefore, these have no errors other than discretization and truncation errors. In this modeling approach, radiation condition is exactly satisfied at infinity. On the basis of the review of literature, the following rigorous boundaries can be reckoned:

(i) Consistent Boundary [1],
(ii) Boundary Element Method [2],
(iii) Consistent Infinitesimal Finite Element Cell Method [3],
(iv) Scaled Boundary Finite Element Method [4],
(v) Perfectly Matched Layer [5].

Approximate approach boundaries are used in the direct method of analysis in the time domain. As we know that most of the transmitting boundaries are simple in their formulation in the time domain and can be easily implemented in finite element code. On the basis of the review of literature, the following approximate boundaries could be cited:

(i) Viscous Boundary [6],
(ii) Paraxial Boundary [7],
(iii) Superposition Boundary [8],
(iv) Infinite Element [9],
(v) Extrapolation Algorithm [10],
(vi) Transient Transmitting Boundary [11].

The behavior of soil-structure interaction effects in the analysis of structures founded on the surface or embedded in the soil is still one of the most discussed issues in the field of seismic design. The importance of underground structures such as nuclear power plants, underground tunnels is required that the design should be such that it can withstand safely in severe conditions. For a safe design, several artificial boundaries have been studied in the literature and can be mostly classified into

Local (Viscous), Consistent boundaries. Local boundary conditions are commonly used in engineering practice because the radiation condition is satisfied approximately at the artificial boundary, as the solution is local in space and time. On the other hand, consistent boundaries such as Lysmer and Wass [1] and [12] have mathematically complex formulations and satisfy exactly the radiation condition at the artificial boundary. Lysmer and Kuhlemeyer [6] recommended a system of dashpots (independent of wave frequency) known as the viscous boundary, positioned at an artificial boundary, which can absorb both harmonic and non-harmonic scattering waves effectively. Lysmer and Wass [1] proposed a transmitting boundary (dependent on the frequency), which is intended to absorb body waves and surface waves on the lateral infinite boundary. Kosloff and Kosloff [13] proposed the technique which absorbs radiating wave from the interior region to outward on the absorbing region around about an interior region. The first model has been analyzed with three boundaries conditions, viz. viscous, consistent, and infinite boundaries. In developing cities, the underground tunnels for transport facilities (subways, underpasses, sewers, etc.) are being constructed on a large scale. A lot of buildings have been constructed directly above or near the underground tunnels. The complex behavior of the reinforced concrete structures in the presence of underground tunnels and their vulnerability to earthquakes have been the major topic of interest for the past few years among structural engineering researchers. Nonlinear time history analysis is the most rigorous technique to compute seismic responses. However extensive studies have been done by various researchers [14–17], on the effects of tunneling, stability of tunnels, and on interactions between tunnels and overground constructions. Major research studies have aimed to predict the movement of the earth around the tunnels through experimental, analytical, and numerical methods. The seismic response of a soil-structure system during an earthquake is affected by many factors including the soil type and its parameters (shear modulus, mass density, and damping), structure height, and its materials properties in addition to the frequency content of the earthquake and soil-structure interaction [16, 23]. Analytically described the impact of the tunnel excavation on the adjacent structures using PLAXIS-2D software under seismic loading conditions. Mangushev et al. [18] investigated the role of deep excavation and its effects on nearby existing buildings for shallow foundations. Korff [19] described the axial pile deformation due to the vertical soil displacement and observed that deep excavations may cause settlement and damage to adjacent buildings even if the building is situated on deep piles.

The present study aims at understanding the seismic behavior of multi-storeyed buildings standing in proximity to an underground tunnel excavation and also to determine the influence of an underground tunnel excavation on the response of the nearby building subjected to earthquake excitation. The analytical study has been carried out using finite element by modeling the building-tunnel-soil system.

2 Statements of Problem

In numerical modeling, boundary conditions plays an important role. To study the dynamic SSI on underground structures, two models have been considered using ABAQUS 6.14. The models are validated with the [6] boundary condition. Further results have been compared with two more boundary conditions, viz. Novak and Mitwally [20] boundary and Bettess [21] Infinite element boundary. The three boundary conditions will be called further as BC-1, BC-2, and BC-3 corresponding to Lysmer and Kuhlemeyer [6], Novak and Mitwally [20], and Bettess [21], respectively. The problems which have been considered are as follows:

I. Outer containment shell of a typical nuclear reactor building with an embedment in surrounding soils Fig. 1.
II. Seismic performance of multistoried buildings constructed in proximity to an underground tunnel excavation and influence of underground tunnel excavation on the response of the nearby building subjected to earthquake excitation.

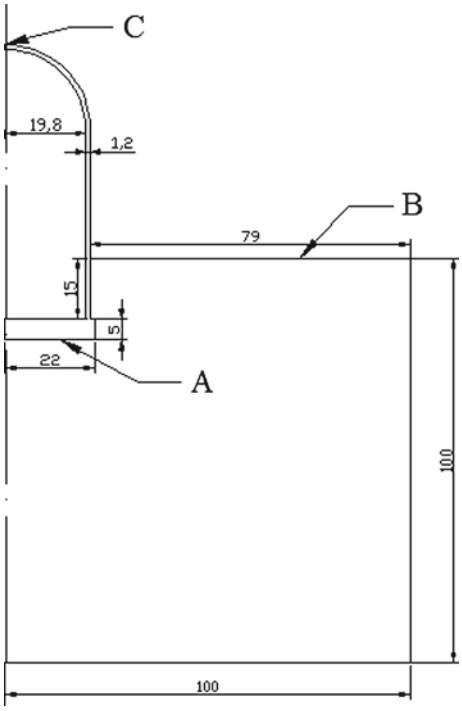

Fig. 1 Model with embedment

2.1 Example I: Nuclear Reactor Building

It consists of a reinforced concrete cylindrical shell capped with a spherical dome and resting on a raft. The geometrical properties of the model are the height of the structure from the base of the foundation to the top of the superstructure is 72.9 m, the base of the foundation is 22 m in width, and thickness of the foundation is 5 m, the thickness of the superstructure is 1.2 m, the distance from the axis of symmetry to the inner part of the shell of the structure is 19.8 m. Material properties of containment shell and soil are shown in Table 1 [22]. For non-linearity, Mohr–Coulomb material model is used. For soil modeling, an 8-noded quadrilateral element in plane strain condition is used. For containment shell 'shell element' is used.

Nuclear power plant founded on soft soil is modeled using finite elements and dynamic analysis is carried out. To rationally consider SSI, the unbounded soil needs to be modeled properly for this, Lysmer and Kuhlemeyer [6], Novak and Mitwally [20], and Bettess [21] boundary conditions are used and referred to as BC-1, BC-2, and BC-3, respectively. Further dynamic analysis is carried out considering no embedment and embedment effect. A time history of maximum acceleration of 0.13 g is applied at the base of the system. The frequency of the system is observed and also the effect of embedment with (SSI) is compared with no embedment with SSI.

Table 1 Properties of Material Parameters

Properties of Soil	
Modulus of elasticity	25×10^3 kN/m^2
Poisson's ratio	0.35
Unit weight of Soil	1700 kg/m^3
Damping in soil	15%
Rayleigh damping Co-efficient α and β	0.2805 & 0.1212
Dilation angle	0.1
Shear Modulus	250×10^6 N/m^2
Cohesion	7×10^6 N/m^2
Friction angle	37^0
Slope angle	45^0
Properties of containment shell	
Modulus of elasticity	25×10^6 kN/m^2
Poisson's ratio	0.25
Unit weight of Soil	2400 kg/m^3
Damping in soil	5%

2.1.1 Numerical Analysis and Modeling

For the analysis, the model was assumed without embedded in its surrounding soil, and its response was compared with that of the same model embedded in the surrounding soil. A site-specific data of the Northridge earthquake (1994) having the maximum acceleration of 0.29 g has been taken as the input motion. But this, acceleration time history can't be directly put on the surface of the ground as an input motion.

This observed input motion is applied at the base of the foundation soil/rock, i.e., 100 m depth so the ground motion must be de-convoluted to get the input response at the base of the soil/rock. The basic stipulation of the de-convolution is shown in Fig. 2.

The procedure of de-convolution can be easily understood through the following steps:

Motion at rock outcrop (time domain)

↓ (Fast Fourier Transformation)

Motion at rock outcrop (Frequency domain)

↓ (Compute transfer function in frequency domain)

Motion at base of the foundation soil/rock (Frequency domain)

↓ (Inverse Fast Fourier Transformation)

Desired motion at base of the foundation soil/rock (Time domain)

After de-convolution of the motion, the peak value of the acceleration is reduced to 0.13 g (Pro-Shake's User Manual) which is shown in Fig. 3.

There are two cases for the analysis part: one is without embedment and part two is with embedment. The width of soil is considered 100 m from the axis of symmetry

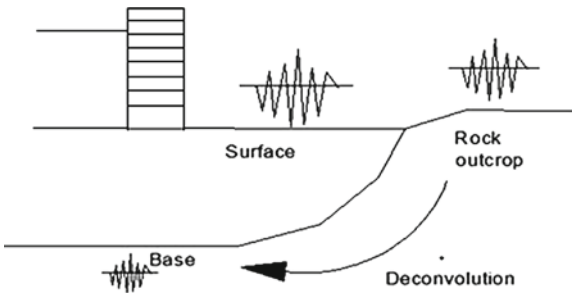

Fig. 2 De-convolution of Motion

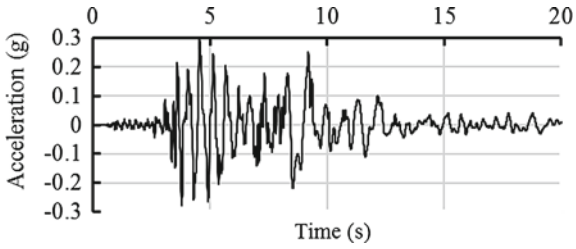

Fig. 3 Northridge (1994) earthquake acceleration-time history

and depth has also been considered 100 m from the base of the foundation. In case of no embedment, only the base foundation will come under the contact of soil. But in case of the embedment, it is assumed that 15 m of structural part from the top of the base of the foundation is embedded in the soil. All this information regarding geometrical data and without embedment and with embedment conditions of the model are shown in Fig. 4a, b, respectively.

For the analysis, the model was assumed without embedded in its surrounding soil, and its response was compared with that of the same model embedded in the surrounding soil. Therefore, two cases were assumed.

(1) Without embedment of structure in the surrounding soil and
(2) With embedment of structure in the surrounding soil.

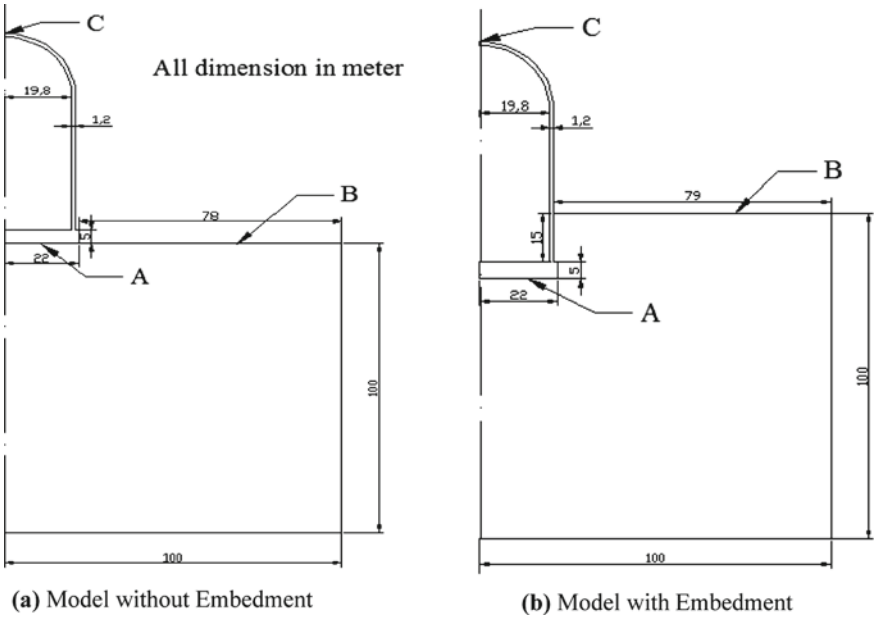

Fig. 4 Model for Analysis

Various points are indicated in Fig. 4 as A, B, and C. All these notations are used for getting the response of the system. In Fig. 4, point A represents a node between the foundation and soil media interface. Point B is representing a node in the soil media and it is named as free-field (FF). Point C represents a node that is the topmost nodal point of the structure. Point A can be treated as an interface, Point B can be treated as FF, and Point C can be treated as the crest. Two cases, i.e., without embedment and with embedment were considered for the response of the structure, with the above discussed boundaries.

The response was obtained with the FEM meshing of the model using ABAQUS. The shell element is used for the analysis of the system, because the shell element gives better results for the axisymmetric system. The response was obtained in terms of acceleration and displacement corresponding to applied time history.

2.1.2 Response of the System

In this section, first the effect of soft soil is considered then the effect of different boundary conditions is examined. The effect of different boundary conditions is carried out without embedment and with embedment. The effect of these boundary conditions is expressed in terms of acceleration and displacement response. The response has also been plotted for top node C of the structure and tabulated for three nodes A, B, C.

2.1.3 Effect of Soft Soil on the Response

The response of the structure is compared for two cases, when situated on soft soil and assumed to be situated on a rock. Table 2 shows the response obtained without embedment effect when the structure is on rock and soil. It can be observed from Table 2 that due to the presence of soft soil, the response at each node increases significantly. The acceleration at node C is observed 0.55 g and displacement as 65 mm for node C when situated on the soil.

Table 2 Responses of Structure situated on Rock and Soil

Without Embedment Structure is Situated on				
Nodes	Rock		Soil	
	Acceleration (g)	Displacement (mm)	Acceleration (g)	Displacement (mm)
A	0.14	15	0.18	20
B	0.16	20	0.26	35
C	0.30	50	0.55	65

Table 3 Response of the system

Response Points	BC-1 [6]		BC-2 [20]		BC-3 [21]	
	Without Embedment	With Embedment	Without Embedment	With Embedment	Without Embedment	With Embedment
Acceleration response						
A	0.29	0.19	0.20	0.18	0.175	0.15
B	0.38	0.28	0.36	0.26	0.22	0.20
C	0.53	0.48	0.51	0.45	0.49	0.42
Displacement response						
A	26	19	19	16	18	12
B	36	31	33.4	29	31	22
C	72	64	69	58	64	50

Table 4 Time period of system (sec)

Without embedment			With embedment
Modes	Structure on rock	Structure on soil	Structure on soil
1	0.153	0.428	0.408
2	0.108	0.343	0.310
3	0.089	0.192	0.187

2.1.4 Effect of Embedment

In this section, various boundaries were used at the boundary of the soil media to get the response without embedment and with embedment, respectively. Our main focus is to show the variation of acceleration response of point C of the NPP system. Without embedment and with embedment, acceleration time history is plotted for node C which is as follows (see Table 3).

2.1.5 Time Period of the System

The time period of the system is calculated for the first three modes. Initially, it is assumed that the structure is situated on the rock though its stiffness is high, so its natural frequency will be high. When the structure is situated on the rock without embedment, the time period for the first mode is 0.153 s and decreased for further modes. When the structure is situated on the soft soil, the system gets less stiff than the previous case, so its frequency decreased by some amount hence time period of the system increased more. Further, when the structure is embedded in the soil medium its stiffness would be more than the without embedment. Since frequency is more in the case of embedment hence the time period of the system decreased by some amount. Table 5 shows the time period of all three modes of the system. It can

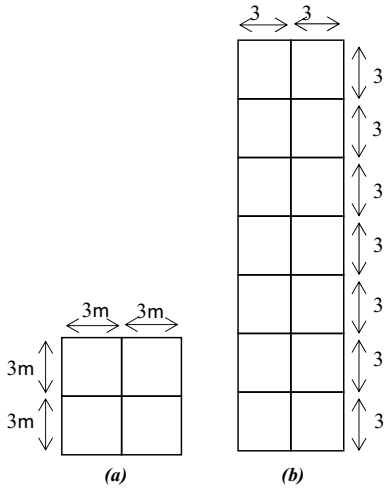

Fig. 5 **a** Plan and **b** elevation of the building

be observed from the Table 5 that as structure gets stiffer its time period decreased. Due to the embedment of the structure in the surrounding soil, the time period is observed for the first mode is 0.408 s (Table 4)

2.2 Example II: Multistoryed Building in Proximity to an Underground Tunnel Excavation

The building consists of 7-storey two-bay moment-resistant frame building whose two storeys are situated under the ground (like basement). The plan and elevation of the building are shown in Fig. 5. Each storey height is taken as 3 m. The cross sections of columns and beams are taken as 0.3 m × 0.3 m. Three different types of foundation systems, viz. isolated footing, mat footing, and pile foundation are taken for the study. The dimensions of each isolated and mat footings are considered as 2 m × 2 m × 1 m and 8 m × 8 m × 1 m, respectively. The depth and diameter of the pile foundation considered are 10.0 m and 1.0 m, respectively. The foundation can be visualized as a beam resting on the soil mainly responsible for distributing the structural load uniformly to the soil. The diameter of the tunnel in all cases is taken as 8 m. It is located 11 m below the ground level. Four different horizontal tunnel locations with respect to the center line of the building are considered below the ground surface. These four horizontal distances are 0, 5, 10, 15 m from the centre line of the building.

The mass of this building has been considered to be concentrated at each floor level and the floor systems were assumed to be rigid rectangular floors supported by relatively massless, axially inextensible columns. The building has been analyzed as a 2D frame. Beams and columns have been modeled as two-noded beam elements.

The performance of deep excavations is strongly influenced by the soil behavior. In finite element analysis, it is absolutely important to use realistic soil models [22, 24] to obtain more consistent results. ABAQUS includes several basic models for soils (e.g., Mohr–Coulomb, Drucker-Prager, and Modified Cam clay). In this study, the Mohr–Coulomb plasticity is used to model slipping and gapping of the soil elements because it is a criterion used to model the inelastic behavior of soils.

The bottom of the soil is assumed as bedrock where ground motions were applied for the analysis and assumed fixed. The properties of the bedrock were considered the same as for concrete. The two-dimensional soil was simulated as a rectangle with 160 m width and 32 m depth. The soil under the building has been modeled and meshed as the 8-noded quadrilateral plane strain elements.

For numerical analysis of wave propagation, the size of an element (Δl) should satisfy the condition as per Eq. (1) so that numerical distortion of transmitted waves is avoided [6]

$$\Delta l \leq \frac{\lambda}{10} \sim \frac{\lambda}{8} \tag{1}$$

where λ is the wavelength of the transmitted wave in the soil model and it is related to the shear wave velocity of the soil and the highest frequency of the input motion ($f_{\max}$) by the following relation:

$$\lambda = \frac{v_s}{f_{\max}} \tag{2}$$

In order to achieve convergence in computations, size of the element (Δl) has been taken as 1.1 m. The finite element meshing for different positions of the tunnel is shown in Fig. 6. Considering Eqs. (1–2), shear wave velocity of the soil is 850 m/s and the highest frequency of the input motions adopted is 25 Hz. The properties of soil and concrete used for the analysis are presented in Table 5.

2.2.1 Soil-Foundation Interface Modeling

In ABAQUS, mechanical contact between the soil and foundation system can be modeled either as node-based interaction or surface-based interaction. In surface-based interaction, mechanical contact of soil and foundation has been modeled using surface elements. Surface-based interaction is suitable because of its capability to model both normal and tangential interaction behavior. Generally, interface modeling has three steps: (a) definition of the contact surfaces which could potentially be in contact, (b) identification of master and slave surfaces that interact with one another, (c) definition of the mechanical (tangent and normal) and thermal properties of the surface. In the surface-based contact approach, two surfaces are required to be defined based on their rigidity; the more deformable surface is defined as a slave surface and the more rigid surface is defined as a master surface. Master surfaces should be

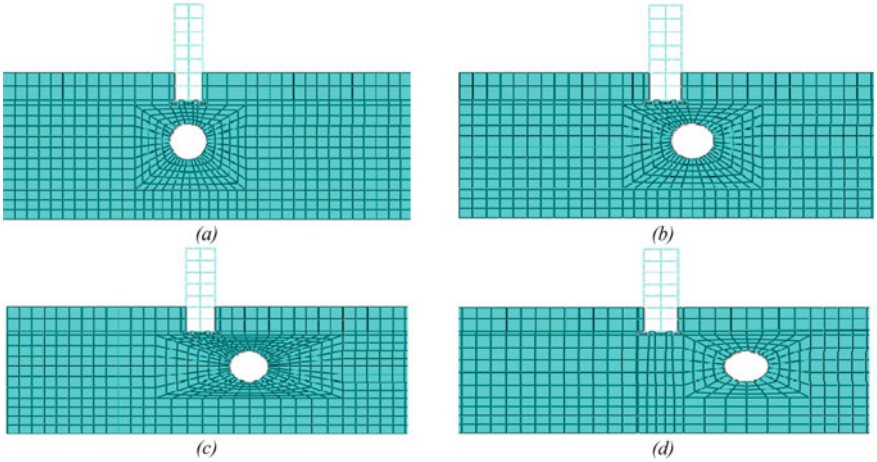

Fig. 6 Meshing of soil and building models with tunnel positions at **a** 0 m **b** 5 m **c** 10 m **d** 15 m

Table 5 Properties of soil and concrete

Parameters	Density (kg/m^3)	Modulus of elasticity (GPa)	Poisson's ratio (ν)	Cohesion (MPa)	Friction angle	Dilation angle	Grade
Soil	2050	4.0	0.30	7.0	0	0	–
Concrete	2400	48.3	0.15	–	–	–	M25

defined as element-based surface. However, slave surfaces can be defined as either element based or node-based surfaces. In this study, the foundation and soil were considered as master and slave surfaces, respectively.

2.2.2 Input Excitations

In this study, the acceleration time histories of the El-Centro, 1979 (PEER 2013) and Moravian Disaster Response (MDR), 2014 earthquakes were used for numerical analyses, as shown in Fig. 7. In order to consider the influence of different seismic wave inputs on the structural system, seismic wave excitations are considered acting horizontally from the bedrock.

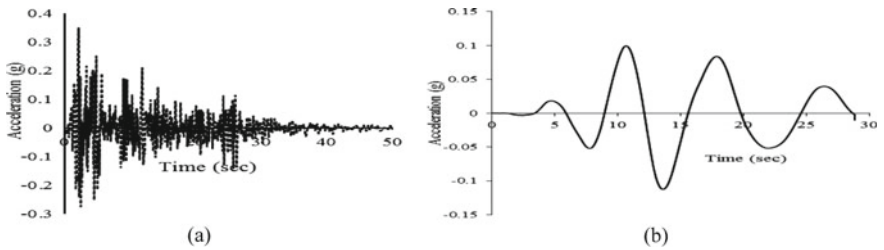

Fig. 7 **a** El-Centro N-S **b** MDR earthquake motion

2.2.3 Analysis and Results

The analysis has been carried out for the whole soil structure-foundation system using ABAQUS 6.14 considering the three foundation types. Rayleigh damping coefficients have been considered in which damping parameters of the soil and concrete have been taken through frequency analysis. For calculating Rayleigh damping coefficients, the damping of soil and concrete was taken to be 20% and 5%, respectively. The Rayleigh viscous damping coefficient for a given frequency ω_i can be expressed in terms of critical damping, ξ_i, as

$$\xi_i = \frac{\alpha}{2\omega_i} + \frac{\beta\omega_i}{2} \tag{3}$$

where α and β are the Rayleigh damping coefficients. For calculation of the value of α and β, first two modes of natural frequencies of the building standing on the soil-tunnel system $\omega_1$and $\omega_2$were considered. In this study, the value of α and β was calculated using Eq. (3) for each case by considering the frequency analysis of the structure soil-tunnel system. The above procedure has been considered for the buildings with the three types of foundations (mat foundation, isolated foundation, and pile foundation) for the study of the response of the structures. The response computations were carried out for two cases. Both El-Centro and MDR earthquake ground motions as mentioned earlier were used to calculate the displacements of the buildings. The whole analysis of soil, tunnel, and structure interaction was carried out in two steps. In the first step, only gravity load was used whereas in the second step dynamic implicit step for earthquake analysis was used. The peak displacements experienced by the building with and without tunnel excavations were determined to study the impact of the position of the underground tunnel on the seismic displacement of the building. In the first case, the seismic analysis of the building before excavating the underground tunnel was done. In the second case, the dynamic analysis of the building system was carried out, in the presence of the underground tunnel.

The peak displacement experienced on the top-left corner node c of the structure under different tunnel positions is shown in Fig. 8 under MDR earthquake loading

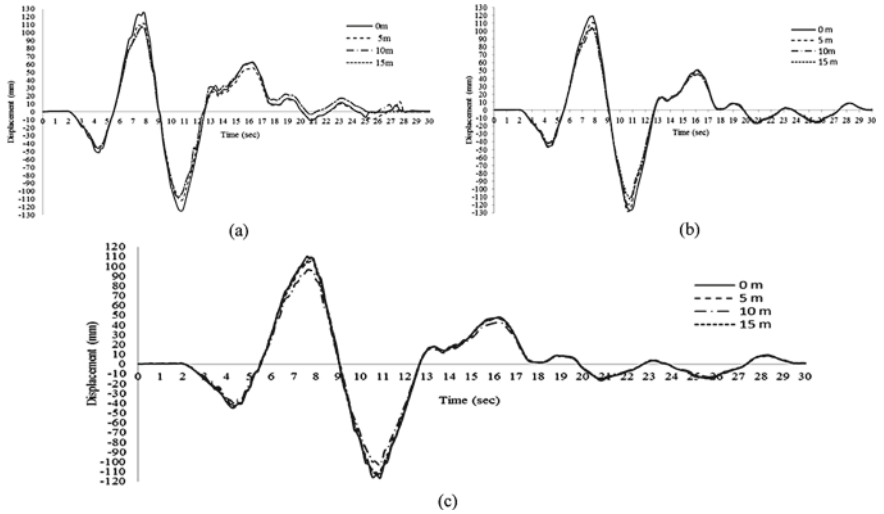

Fig. 8 Displacement Time history for **a** Isolated and **b** Mat and **c** Pile Foundation

for isolated and mat foundation in presence of varying horizontal tunnel locations of 0, 5, 10, 15 m from the center line of the building frame.

The maximum peak displacement for various tunnel positions and also for different types of foundation systems experienced by the building due to MDR earthquake excitation are presented in Table 6. The peak displacement of the building with an isolated foundation is 6.048% more than that of the building with the mat foundation in absence of tunnel condition.

It is seen that the peak displacement of the building system is decreasing when the tunnel is shifted away from the center line of the building. The comparative values of peak displacements under MDR earthquake are shown in Fig. 9.

The comparative study of maximum displacement of building top-left corner for different foundation systems due to El-Centro earthquake is shown in Fig. 10.

Further, Table 7 presents the maximum displacement experienced by the building due to the El-Centro earthquake for different types of foundation systems and the tunnel positions. It is seen that the maximum displacement experienced by the building system is in the case of an isolated foundation when the tunnel is located at the center line of the building.

Finally, the impact of the underground tunnel on the adjacent buildings during different earthquake loadings can be evaluated. Table 8 represents the comparative changes of maximum seismic displacement before tunnel and after tunnel.

Table 6 Maximum peak displacement (mm) at a constant vertical depth of 11 m below ground level

Position of tunnel	Isolated foundation	Increase relative to no tunnel	Decrease relative to 0 m	Mat foundation	Increase relative to no tunnel	Decrease relative to 0 m	Pile foundation	Increase relative to no tunnel	Decrease relative to 0 m
No tunnel (m)	105.45	0.00	–	102.96	0.00	–	99.24	0.00	–
0	119.19	13.74	0.00	118.85	15.89	0.00	109.08	9.84	0.00
5	112.15	6.70	7.04	111.07	8.11	7.78	104.86	5.62	4.22
10	107.40	1.95	11.79	105.25	2.29	13.60	101.65	2.41	7.43
15	106.81	1.36	12.38	104.42	1.46	14.43	100.58	1.34	9.27

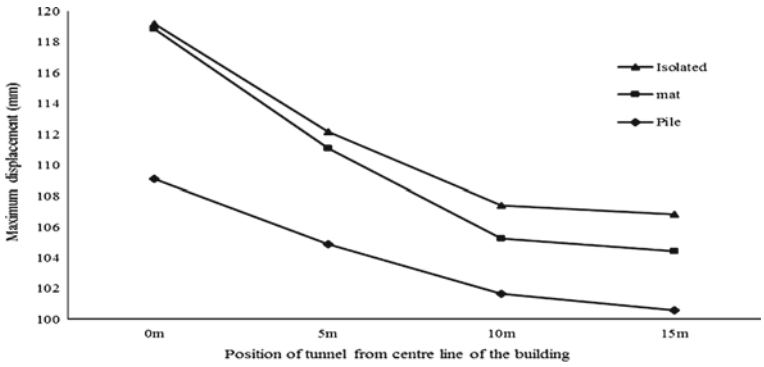

Fig. 9 Maximum displacement versus position of the tunnel under MDR earthquake

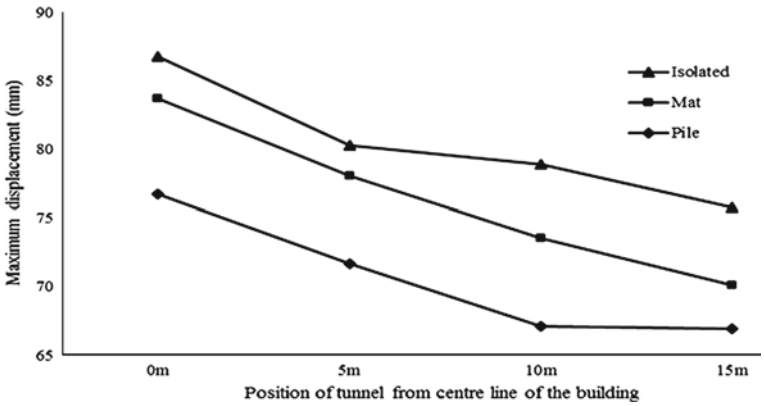

Fig. 10 Maximum displacement of building top for different lateral positions of the tunnel

2.2.4 Discussion of the Result

When the tunnel is shifted away from the center line of the building, it is observed that the peak displacement of the building system is decreasing. From the study, it is observed that maximum displacement was experienced when frame models are situated on an isolated foundation system. From Table 8, it was clearly observed that the maximum displacement occurs in the case of MDR earthquake irrespective of the El-Centro earthquake for all cases of structures.

Table 7 Maximum displacement (mm) at top of building for various horizontal tunnel positions due to El-Centro earthquake

Position of tunnel	Isolated foundation	Increase relative to no tunnel condition	Decrease relative to 0 m	Mat foundation	Increase relative to no tunnel condition	Decrease relative to 0 m	Pile foundation	Increase relative to no tunnel condition	Decrease relative to 0 m
No tunnel (m)	70.17	0.00	–	69.88	0.00	–	66.70	0.00	–
0	86.74	16.57	0.00	83.72	13.84	0.00	76.71	10.01	0.00
5	80.25	10.08	6.49	78.05	8.17	5.67	71.66	4.96	5.05
10	78.90	8.73	7.84	73.56	3.68	10.16	67.09	0.39	9.62
15	75.74	5.57	11.00	70.12	0.24	13.60	66.92	0.22	9.79

Table 8 Comparison of changes in maximum seismic displacement of building before and after tunnel placement due to El-Centro and MDR earthquakes excitation

Earthquakes	No. of storeys	Max. seismic displacements before the tunnel (mm)	Max. seismic displacements after tunnel (mm)	Changes in max. displacement (mm)	Percentages of changes in max displacements (%)
El-Centro	7 storey	70.17	86.74	16.57	23.61
MDR	7 storey	105.45	119.19	13.74	13.03

3 Summary

An analytical study has been presented to demonstrate the displacement response of a reinforced concrete building frame founded on isolated, mat, and pile foundations and standing over the soil through which an underground tunnel runs at a constant depth. The response was also studied when the off-center tunnel positions change. A seven-storey building along with a soil-tunnel system was modeled with viscous boundary conditions and the system was analyzed using ABAQUS software under El-Centro and MDR earthquake excitations. The results show that when the tunnel is located directly below the center line of the building, the maximum influence on the building response is obtained. For this position of the tunnel, the interaction between soil, tunnel, and building structure is the most significant and produces maximum displacement. The displacement response of the building decreases with the increasing horizontal position of the tunnel from the center line of the building. Also, considering the mat, isolated, and pile foundations system, the isolated foundation system produces maximum response irrespective of the spacing of the tunnel positions. The response of the building in each case is maximum when the building is situated on the isolated footing. The study confirms that the building responses in presence of the underground tunnel depend on the tunnel position.

4 Conclusions

1. The response of an NPP structure situated on soil is considerably higher than that situated on the rock. For the case considered here, the response increased by a margin of about 67%.
2. The time period of the system decreases due to the embedment effect of structure which indicates that the system is stiffer.
3. The acceleration and displacement responses of the system, are smaller with the infinite boundary as compared to kelvin and viscous boundary.
4. The maximum influence on the building is observed when the tunnel is located directly below the center line of the building.

5. The displacement response of the building decreases with the increasing horizontal position of the tunnel from the center line of the building.
6. The isolated foundation system produces maximum response irrespective of the spacing of the tunnel positions.

Future Recommendations Future studies can be extended considering different soil conditions, structure types, and structure heights.

References

1. Lysmer J, Waas G (1972) Shear waves in plane infinite structures. ASCE. https://doi.org/10.1016/S0895-7177(98)00155-1
2. Beskos DE (1987) Boundary element methods in dynamic analysis. Appl Mechan Rev ASME 40:1–23
3. Wolf JP, Song C (1995) Doubly asymptotic multi-directional transmitting boundary for dynamic unbounded medium-structure-interaction analysis. Earthq Eng Struct Dyn. https://doi.org/10.1002/eqe.4290240204
4. Song C, Wolf JP (2002) Semi-analytical representation of stress singularities as occurring in cracks in anisotropic multi-materials with the scaled boundary finite-element method. Comput Struct 80(2):183–197
5. Basu U, Chopra AK (2003) Perfectly matched layer for time-harmonic elastodynamics of unbounded domains: theory and finite-elemet implimentation. Comput Methods Appl Mech Eng. org/https://doi.org/10.1016/S0045-7825(02)00642-4
6. Lysmer J, Kuhlemeyer L (1969) Finite-dynamic model for infinite media. J Eng Mech Div
7. Clayton W, Engquist B (1980) Geophsyics. Absorbing Bound Condition Wave Equ Migr. https://doi.org/10.1190/1.1441094
8. Zienkiewicz OC, Emson C, Bettess P (1983) A novel boundary infinite element. Int J Numer Meth Eng 19(3):393–404
9. Bettess P (1977) Infinite elements. Int J Numer Methods Eng
10. Lio ZP, Wong HL (1984) A transmitting boundary for the numerical simulation of elastic wave propagation. Int J Soil Dyn Earthq Eng. https://doi.org/10.1016/0261-7277(84)90033-0
11. Al Assady AKMS (2005) Modeling of nonlinear dynamic soil-structure interaction problems. PhD dissertation, Indian Institute of technology Roorkee, Roorkee, India
12. Kausel E (1994) Thin-layer method: formulation in time domain. Int J Numer Meth Eng 37:927–941
13. Kosloff R, Kosloff D (1986) Absorbing boundaries for wave propagation problems. J Comput Phys 10.1016/0021-9991(86)90199-3
14. Besharat V, Davoodi M, Jafari MK (2012) Effect of underground structures on free-field ground motion during earthquakes. In: Proceedings of 15th world conferences on earthquake Engineering, pp 1–10
15. Abdullah MH, Taha MR (2013) A review of the effects of tunneling on adjacent piles. Electron J Geotech Eng 18N:2739–2762
16. Azadi M, Hosseini M (2014) The influence of tunnels on the nearby buildings under seismic loadings conditions, case study: Shiraz underground-Iran. Proc 14th World Conf Earthq Eng 1–8
17. Bhatkar T, Barman D, Mandal A, Usmani A (2016) Prediction of behaviour of a deep excavation in soft soil: a case study. Int J Geotech Eng 6362:1–10. https://doi.org/10.1080/19386362.2016.1177309

18. Mangushev R, Rybnov E, Lashkova E, Osokin A (2016) Examples of the construction of deep excavation ditches in weak soils. Procedia Eng 165:673–681. https://doi.org/10.1016/j.proeng.2016.11.765
19. Korff M (2009) Deformations and damage to buildings adjacent to deep excavations in soft soils 143
20. Novak M, Mitwally H (1988) Transmitting boundary for axisymmetric dilation problems. J Eng Mech Div ASCE 104(4):953–956
21. Bettess P (1977) Infinite elements. Int J Numer Meth Eng 11:53–64
22. Farghlay AA (2014) Evaluation of seismic performance of buildings constructed on hillside slope of Dronka village—Egypt. Int J Geotech Eng 9(2)
23. Cong S, Tang L, Ling X et al (2018) Boundary effect on the seismic response of a three-dimensional soil slope with a shallow foundation on top. KSCE J Civ Eng 22:1130–1140. https://doi.org/10.1007/s12205-017-1535-4
24. Kumar A, Choudhury D (2016) DSSI analysis of pile foundations for an oil tank in Iraq. ICE Proceed Geotech Eng 169(2):129–138. https://doi.org/10.1680/jgeen.15.00025

Joint Time Frequency Analysis Based Synthesis of Acceleration-Time History and Response Spectra for Japanese Earthquakes

R. Ramkrishnan, Deepa Devaraj, Sreevalsa Kolathayar, and T. G. Sitharam

Abstract Time–Frequency Analysis (TFA) techniques help to obtain the ideal time and frequency occurrence characteristics of earthquake motion confined in a seismic recorded signal. Time-histories from recording stations in Japan has been adopted in the present analysis, considering a large number of available data. The seismograms were transformed using Gabor transform, a Linear Joint TFA method, to assess their frequency content by generating their Gabor coefficients. Average Gabor coefficients were estimated for recorded seismograms within a magnitude range of 5.5–6.0 and hypocentral distances ranging from 0 to 50 km. The estimated average Gabor coefficients were used to synthesize a generalized acceleration-time history for the specific distance and magnitude ranges using Gabor Expansion, without compromising the frequency content of the waves. Additionally, it is demonstrated that the response spectra of the synthesized signal and the original signal match very well. These response spectra will be valuable for the nonlinear investigation of structures in this region.

Keywords Joint time–frequency analysis · Gabor transform · Linear TFA · Time-history · Response spectra

R. Ramkrishnan (✉) · D. Devaraj
Department of Civil Engineering, Amrita School of Engineering, Coimbatore, Amrita Vishwa Vidyapeetham, Coimbatore, India
e-mail: r_ramkrishnan@cb.amrita.edu

S. Kolathayar
Department of Civil Engineering, National Institute of Technology Karnataka, Surathkal, Mangalore, India
e-mail: sreevalsa@nitk.edu.in

T. G. Sitharam
Department of Civil Engineering, Indian Institute of Science, Bangalore, Bangalore 560012, India
e-mail: sitharam@iisc.ac.in

T. G. Sitharam et al. (eds.), *Earthquakes and Structures*, Lecture Notes in Civil Engineering 188, https://doi.org/10.1007/978-981-16-5673-6_2

1 Introduction

Japan is positioned along the world's most active earthquake zone, the Pacific Ring of Fire. This 'ring' is an imaginary horseshoe-shaped zone that accompanies the Pacific Ocean rim, where earthquakes and eruptions are a frequent phenomenon. The 2011 Tohoku earthquake and tsunami was the largest earthquake ever to strike Japan (magnitude 9.0) and this earthquake triggered a tsunami up to 40.5 m (133 ft) high that moved up to 10 km (6 mi) inland [1, 2].

Synthetic seismograms are advantageous in the analysis of patterns based on different types of structures and in the prediction of certain drawbacks in the study of structural complexity [3]. In most scenarios, it is not possible to record strong motion at a defined site. There is no reason to expect a potential earthquake to cause the same or comparable ground movement even if these records are available. For seismic time-history evaluation of a structure, synthetic time-histories need to be generated for specific locations [4]. In earthquake seismology, synthetic time history is either used to fit the anticipated impacts of a particular earthquake with measured seismogram data, to evaluate the breakdown mechanism during major earthquakes or to help determine the frequency distribution [5]. Synthetic seismograms may also be used in specific geophysical software.

Earthquake waves are non-stationary. In past decades, seismic investigations have been carried out considering the waves to be stationary. Such studies lack accurate assessment of the behavior and characteristics of these motions, which calls for a non-stationary analysis of the same. Analyzing the time–frequency domain instead of independent time domain and frequency domain is important. Traditional strategies like Fourier examination is inadmissible for analyzing seismic records because of its inadequacy in providing the details of individual frequency contents. Seismic motions have different time factors such as amplitude and frequency due to the non-stationary behavior of earthquake waves [6]. The critical aspect is to study changes in frequency content over time. Fourier analysis has been used in seismic signals for decades to represent the frequency plane. The Fourier spectrum incorporates the frequency content in time series; however, the time position of the peak frequency and the time–frequency shift are not defined in the above spectrum, which essentially means it has a different time and frequency domain [7]. To study the time–frequency domain, time-variable spectral analysis is implemented [8]. Time–Frequency Analysis (TFA) explains the shift in the ground motion spectral content as a seismogram time history by subsequently mapping one-dimensional time domain signal to the two-dimensional time and frequency function and describing how well the spectral data of the signal fluctuates. The joint time–frequency analysis allows the signal information to be evaluated in time and frequency domains at the same time [9, 10]. Time–frequency distribution also reveals how much signal energy is distributed over time and frequency domain concurrently [11]. TFA techniques are composed of two methods: linear TFA and quadratic TFA. Linear transformation focuses on signal and noise processing. Different linear methods are Short Time Fourier Transform (STFT),

Gabor Transformation (GT), and Wavelet Transformation (WT). Quadratic transformation describes the energy distribution in signals. Various methods associated with quadratic transformation are Wigner-Ville Distribution (WVD), Choi-William (CWD), Cone shaped distribution (CSD) and Spectrogram (SP). Gabor Transformation (GT) is better than STFT because the Gaussian functions are more concentrated than the rectangular function in the frequency domain, and the frequency resolution of Gabor Transform is higher than that obtained using STFT [4].

One of the important parameters of any structure in a dynamic loading point of view is its natural frequency. Every structure has its natural frequency for a series of distinct modes, which influences its dynamic behavior. When the natural frequency of the vibration mode of a body coincides with the frequency of external force, resonance occurs leading to excessive deflections and possible catastrophic failures [12]. Therefore, analyzing the frequency content of the signal is a key step in any dynamic analysis and resistance measures that follow.

In this study, acceleration-time histories from Kik-NET was Gabor transformed and Gabor expanded to synthesize a new seismogram representative of different magnitude and distance ranges for the area under scrutiny. The magnitude of 5.5–6.0 and hypocentral distance from 0-50 km is considered. A generic response spectrum is also created for specific magnitude and distance ranges from the synthesized time history.

2 Review on STFT and Gabor Transform

2.1 STFT

The Fourier Transform doesn't precisely indicate where the time and frequency elements are located. Such time localization can be obtained by STFT. Short Time Fourier Transform (STFT) is the easiest time–frequency illustration technique [8, 13]. The width of the selected window must be equal to the segment of the signal where the analyzed signal is being assumed stationary and STFT of the signal is obtained based on FFT algorithms. The Short-Time Fourier Transforms the amplitude spectrum by integrating linearly as.

$$STFT(\tau, F) = \int_{-\infty}^{+\infty} s(t)\gamma(\tau - t)e^{-2j\pi ft}dt \tag{1}$$

Where, *s(t)* → time-domain seismogram, $\gamma\ (\tau - t)$ → windowing function and $e^{-2j\pi ft}$ → Fourier kernel. STFT is the signal spectrum *x(t)* chosen by the location window *h(t)* around time *t*.

Because of the restriction provided by the principle of uncertainty, the result of STFT suffers from windowing impacts [6, 12, 13] and another issue connected with

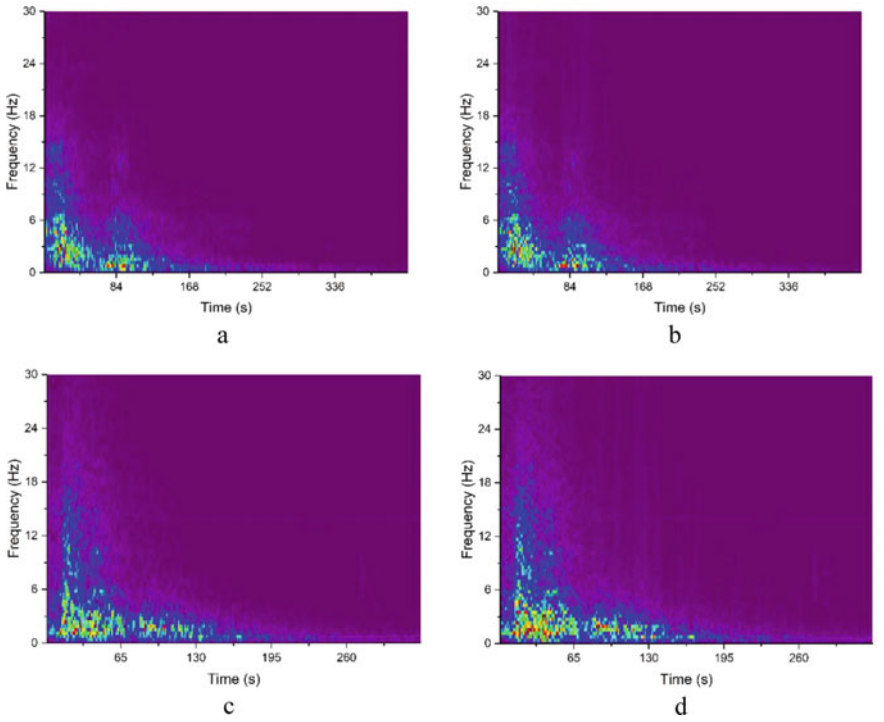

Fig. 1 Spectrogram showing the difference of STFT and Gabor transform **a** STFT for distance 0-25 km **b** Gabor for distance 0-25 km **c** STFT for distance 25-50 km **d** Gabor for distance 25-50 km

STFT is the quantity of spectral leakage [13, 14]. STFT spectrogram images of sample acceleration time-history are shown in Fig. 1a, c.

2.2 Gabor Transform (GT) and Gabor Expansion (GE)

The Gabor transformation is a unique case of short-term transformation of Fourier, where the window function used is a Gaussian function. Because the Gaussian function signals are more focused than the rectangular function in the frequency domain, the Gabor Transform frequency resolution is much better than the Short-Time Fourier Transforms. Gabor Expansion is a very useful tool in signal processing. Gabor Transform maps the time domain into the time–frequency domain whereas Gabor Expansion reconstructs the time domain signal after some modification being made in the time–frequency domain. For signal x(t) Gabor Expansion is defined as

$$s(i) = \sum_{m=D}^{M-1} * \sum_{n=D}^{N-1} C_{m,n} h_{m,n}(i) \tag{2}$$

$$h_{m,n}(i) = h(i - mdm)\exp(\frac{2j\pi ni}{N}) \tag{3}$$

The coefficients $c_{m,n}$ are the Gabor coefficients, which are computed by the Gabor Transform or the sampled STFT.

$$c_{m,n} = \sum_{i} s[i]\gamma[i - mdm]\exp(-\frac{2j\pi ni}{N}) \tag{4}$$

where the function *[i-mdm]* is called the analysis window and is a dual function of the synthesis window *h(t)*. Gabor transformation of sample acceleration-time histories are shown in Fig. 1b, d.

3 Methodology

To evaluate earthquake-resistant structures, realistically strong ground movement is required. Earthquake waves used for the present study were obtained from KiK-net (http://www.kyoshin.bosai.go.jp/). The seismic signal's time–frequency feature reveals impressive characteristics from a seismographic perspective. Earthquake waves in E-W direction taken for synthesis was obtained at stations lying between latitudes 31–44° N and longitude 130–145° E. Higher magnitudes from Mw 5.5 to 6.0 were sorted for a hypocentral distance of 0–50 km. 15 earthquake data for each distance ranges under consideration were obtained and processed for the study. Offset correction was carried out and the corrected acceleration data is divided by its absolute maximum acceleration to obtain a normalized time-history. Seismogram acceleration values are completely different in range. Because of their variance, these values cannot be merged or assessed in a similar window and range. Hence, the values are normalized and a seismogram with values ranging from ?1 to 1 is therefore created and used for further evaluation.

Gabor transformation is adopted here among the methods of time–frequency analysis owing to its superiority in spectrogram, like less spectral leakage and better resolution [15]. Inversion can also be achieved by Gabor Expansion so we can recreate a new acceleration-time history taking into account the temporal components of frequency [16]. All signals were transformed using the Eq. (4) and Gabor coefficients shown in Fig. 2a, c were created and obtained from the transform. The mean of these Gabor coefficients, representative of the transforms of all signals in that selected magnitude and distance range is then obtained to be used in Gabor Expansion as shown in Eqs. (2) and (3). The reason for considering the mean transformation of Gabor is to smooth the undesirable signal characteristics as well [3, 13]. The flow chart given below demonstrates the TFA approach in synthesis of time-histories and response spectra.

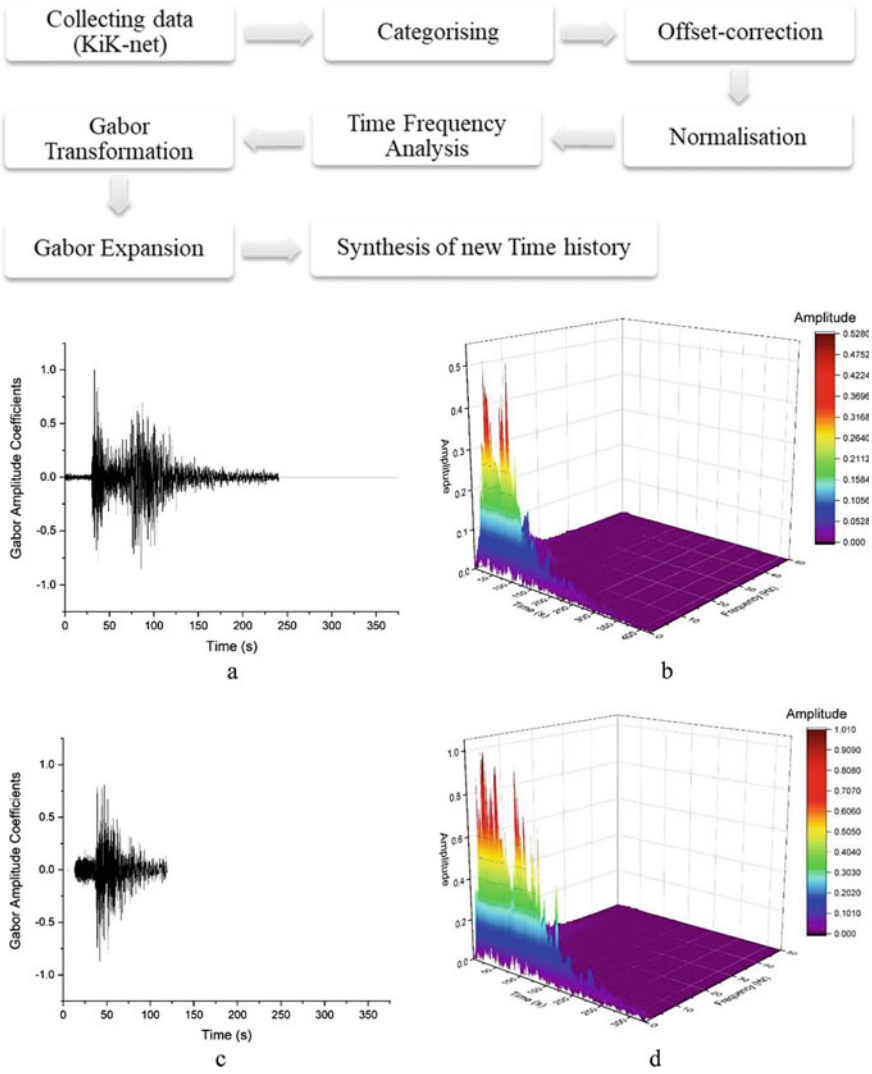

Fig. 2 Gabor coefficient and physiograms of sample recorded signals of Magnitude (Mw)5.9 within different hypocentral distance ranges **a** Gabor coefficients $M_{5.9}D_{0\text{-}25}$ **b** Physiogram $M_{5.9}D_{0\text{-}25}$, **c** Gabor coefficients $M_{5.9}D_{25\text{-}50}$ **d** Physiogram $M_{5.9}D_{25\text{-}50}$

The response spectra developed by the TFA method can be introduced to the structure. Response spectra analysis (RSA) is a linear-dynamic statistical analysis method that analyzes the presence of each natural vibration mode to imply an elastic structure's peak seismic response. It provides information on dynamic behavior by assessing pseudo-spectral acceleration, velocity, or displacement as a function of the

Table 1 Coefficient of determination factor of seismograms for a specific distance range of magnitude

Magnitude (Mi)	Distance (Dj)	Coefficient of determination (R^2)
$M_{5.5–6.0}$	D_{0-25}	0.90
	D_{25-50}	0.88

structural period for specified time history and damping level [17]. Response spectrum analysis is useful for decisions during development as it relates to structural dynamic efficiency [18]. Table 1 provides the R^2 value of the actual and synthetic response spectra. The R^2 value must lie between 0–1. As the value approaches towards 1, it indicates best fitting.

4 Results and Discussions

To establish synthetic seismic signals, available recorded seismograms from the selected magnitude range were transformed to obtain a mean representative Gabor Coefficient. Gabor expansion was carried out on the mean Gabor coefficient for different magnitude and distance ranges to obtain a representative synthetic seismic signal. A comparison is made between the TFA based synthetic seismogram and the actual recorded seismogram. Response spectra for these signals were developed and were compared as well. The synthesized acceleration vs time graph and response spectra was observed to make a good fit, respectively, with the actual recorded seismogram and response spectra.

The R^2 value for response spectra developed from synthetic signals and actual signal is presented in Table 1. The comparison of actual and synthetic seismogram and response spectra for magnitude 5.5–6.0 and hypocentral distance 0–25 and 25–50 are given in Figs. 3 and 4 respectively.

The response spectra computed from synthetic time-history generated by the time–frequency approach is compared with the actual response spectra. It can be seen that the response spectrum of recorded histories matches quite well with the response spectrum of synthetic time-history. These response spectra produced by considering the frequency element of the signals can provide better results in structural analyses.

5 Conclusion

Synthesis of earthquake motions are vital in areas with limited recorded data for seismic studies. The current study presents a new technique and addresses few shortcomings of the past techniques to synthesize earthquake motions. Due to variable window functioning and less spectral leakage, the signals synthesized with Gabor

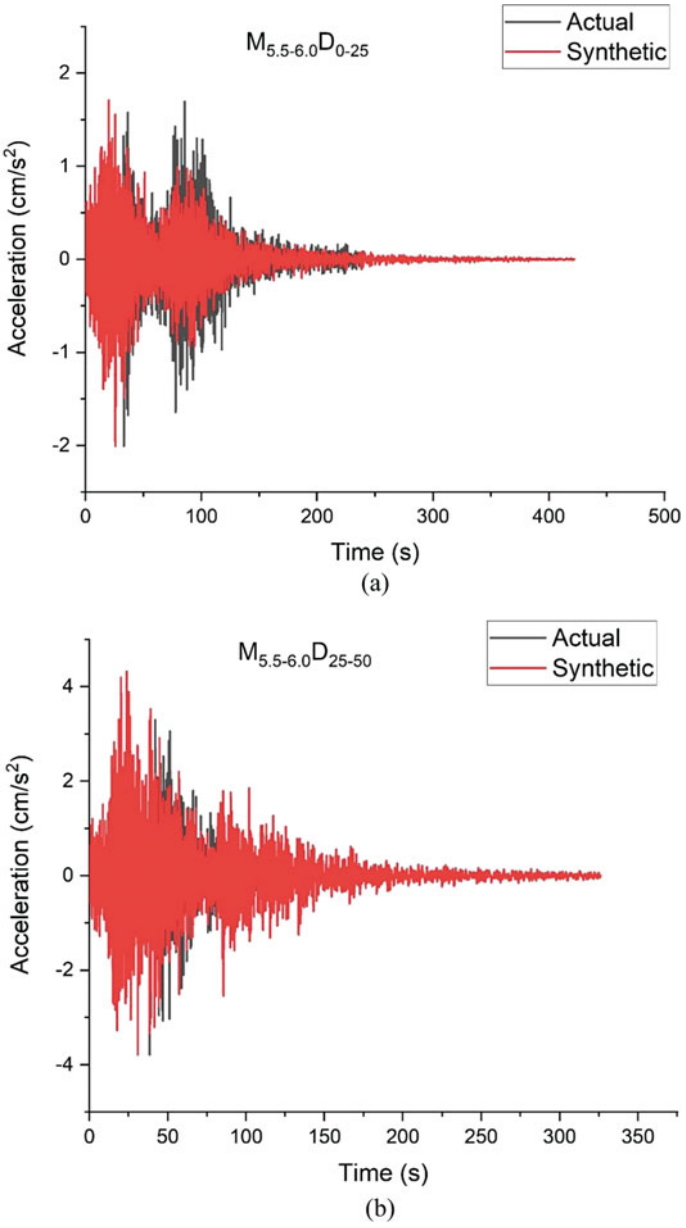

Fig. 3 Comparison of the actual and synthetic seismogram **a** magnitude 5.5–6.0 and distance 0-25 km, **b** magnitude 5.5–6.0 and distance 25-50 km

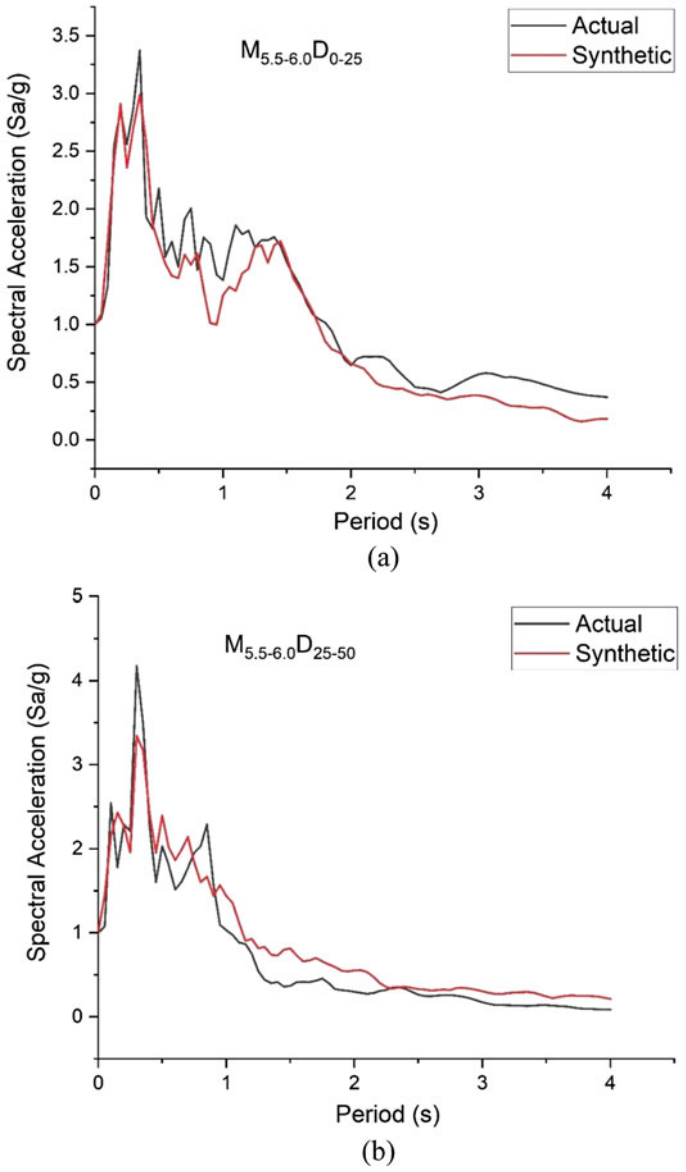

Fig. 4 Comparison of response spectra of the actual and synthetic seismogram **a** magnitude 5.5–6.0 and distance 0-25 km, **b** magnitude 5.5–6.0 and distance 25-50 km

Transformation and Gabor Expansion produce better outcomes. The synthesized seismogram closely represents the actual recorded seismogram, but with the removal of unwanted frequencies and noise. By removing unwanted noise and smoothing the frequency content, better representation of the signal features is obtained from the response spectrum produced from the synthetic seismogram. Additionally, synthetic time-history produced using Gabor techniques, when compared with the time history developed from standard techniques like Fourier Transform and STFT showed that the distribution of frequency elements over the time–frequency plane matches well with the realistic signal pattern in the event of the synthetic signal produced by standard techniques. The coefficient of determination factor R^2 was estimated for the original vs synthetic response spectra and was found to have a good fit with R^2 values of 0.90 and 0.88. The new method suggested here can be used effectively for seismically active areas with limited recording stations and data for developing synthetic signals and response spectra to be used in various applications like structural analysis and hazard studies.

References

1. Norio O, Ye T, Kajitani Y, Shi P, Tatano H (2011) The 2011 Eastern Japan great earthquake disaster: overview and comments, vol 2, no 1, pp 34–42
2. Matsu RS (2017) A short history of Japanese historical seismology: past and the present. Geosci Lett
3. Dak Hazirbaba Y, Tezcan J (2016) Image based modeling and prediction of nonstationary ground motions. Comput Struct 174:85–91
4. Kumar Roshan Kumar A, Sumitha P (2013) Denoising of seismic signal based on gabor transform, pp 1997–2001
5. Michael Campillo Fabrice Cotton (1994) Application of seismogram synthesis to the study of earthquake source from strong motion records
6. Pugliese A, Sabetta F (1996) Estimation of response spectra and simulation of nonstationary earthquake ground motions. Bull Seismol Soc Am 86(April):1996
7. Upegui-Botero F, Huerta-López C (2012) Joint time-frequency analysis of seismic records. Wcee
8. Huerta-Lopez C, Shin Y (2000) Time-frequency analysis of earthquake records. Earthquake 1–8
9. Devi V, Sharma ML (2018) Advances in extraction of signal from ground motion time histories using time-frequency analysis, 1–30
10. Devi V, Sharma ML (2016) Spectral estimation of noisy seismogram using time-frequency analyses. Int J Geotech Earthq Eng 7(1):19–32
11. Black CJ, Ventura CE (1998) Building during two earthquakes, 896–902
12. Qamaruddin S (2017) Seismic response study of multi- storied reinforced concrete building seismic response study of multi-storied reinforced concrete building with fluid viscous dampers. A dissertation work submitted in partial fulfilment of the requirements for the master of
13. Chen D, Qian S (1999) Joint TFA analysis
14. Kumar R, Sumathi P, Kumar A (2016) A time–frequency approach for generation of synthetic time-histories of earthquake signals. Acta Geod Geophys 51(1):57–67
15. Søndergaard P (2009) An efficient algorithm for the discrete Gabor transform using full length windows. Computer 6:1–5

16. Zielinski TP (2001) Joint time-frequency resolution of signal analysis using Gabor transform. IEEE Trans Instrum Meas 50(5):1436–1444
17. Freeman SA (2007) Response spectra as a useful design and analysis tool for practicing structural engineers. ISET J Earthq Technol 44(1):25–37
18. Nigam NC, Jennings PC (1969) Calculation of response spectra from strong-motion earthquake records. Bull Seismol Soc Am 59(2):909–922

Parametric Studies on Overturning Moment Ratio of Buildings with Shallow Foundation for Tsunami Loading

P. Kamatchi, P. Hema Malini, and K. Sathish Kumar

Abstract As reported in literature number of buildings including five reinforced concrete and one steel framed buildings in the town of Onagawa and two buildings in the city of Miyako have failed by overturning during past 2011 Gear East Japan Tsunami. During Tsunami, exceedance of the instantaneous overturning moment due to buoyancy force and hydrodynamic force above the resisting moment due to self-weight of the building has been found to cause the overturning failure of building. In the present study, residual air space ratio (C_b), inundation depth (R) and height of the building (h) are identified as important parameters which influence the action of overturning. Residual air space ratio is defined in such a way that C_b equal to 1 means no water enters into building and C_b equal to 0 represents entire building is filled with water. The variation of overturning ratio of building *w.r.t.* the identified parameters are studied for four inundation depths, five heights of building and five air void ratios for the chosen 8mx8m plan of building. From the limited studies made, it is observed that when C_b is equal to 1 i.e. when no water enters the building, there is a maximum possibility for overturning. O_R is found to increase linearly with C_b. Similarly, when the inundation depth is more, there is a maximum possibility of overturning of building, however the variation of O_R with R is not linear. Based on the parametric study a model has been proposed for calculation of overturning ratio.

Keywords Tsunami loading · Overturning ratio · Building damage · Buoyancy force · Foundation

1 Introduction

It is well documented that, past tsunamis have caused huge losses in terms of causality, economic loss and destruction of coastal environment. In addition to tsunami, ground

P. Kamatchi (✉) · P. H. Malini · K. S. Kumar
CSIR-Structural Engineering Research Centre, CSIR Campus, Taramani, Chennai, India
e-mail: kamat@serc.res.in

K. S. Kumar
e-mail: ksk@serc.res.in

T. G. Sitharam et al. (eds.), *Earthquakes and Structures*, Lecture Notes in Civil Engineering 188, https://doi.org/10.1007/978-981-16-5673-6_3

shaking, soil liquefaction, impact due to debris have contributed for the failures of buildings. During December 26th, 2004 Indian Ocean Tsunami, destruction of many fishing facilities, compound walls, concrete posts, roofs and walls of brick masonry residential buildings were observed in Indian Coast [1]. Structural and nonstructural damages to infrastructure in Thailand and Indonesia during 2004 Sumatra earthquake and Indian Ocean Tsunami were reported by Murat et al. [2]. March 2011, Great East Japan Tsunami which affected 650 km long Pacific coast has resulted in failures of many Reinforced Concrete (RC) and steel buildings [3]. Further, failures of nonstructural elements viz., infill walls, finishes, claddings and foundation failures viz., overturning and slicing of foundation from super structure were also reported during 2011 Great East Japan Tsunami. During this event, number of buildings including five reinforced concrete and one steel framed buildings in the town of Onagawa and two buildings in the city of Miyako have failed by overturning [4, 5]. The large inundation depths of successive tsunami waves have caused the hydrodynamic force and huge buoyancy force instantaneously and the buildings of lesser height than that of the inundation depth have suffered failure due to overturning. Studies on response of reinforced concrete buildings for tsunami loading are reported in literature [6–8]. Michitaka et al. [9] have carried out two dimensional and three dimensional simulation of tsunami and studied the reason for overturning of two adjacent buildings during 2011 Great Tohoku Earthquake and Tsunami. In this paper, residual air space ratio (C_b), inundation depth (R) and height of the building (h) are identified as important parameters which influence the action of overturning and the results of the parametric studies are presented and a model has been fitted for evaluation of overturning ratio.

2 Forces Considered in Tsunami

Federal Emergency Management Agency [10] has specified the following forces to be considered for design of structures for vertical evacuation due to Tsunami: (1) hydrostatic forces; (2) buoyant forces; (3) hydrodynamic forces; (4) impulsive forces; (5) debris impact forces; (6) debris damming forces; (7) uplift forces; and (8) additional gravity loads from retained water on elevated floors. As it is also reported in literature, hydrostatic forces are mainly due to standing water and not contributing much for the overturning effect, hence not included in the present study. Panon et al. [4] have studied the effect of hydrodynamic force and buoyancy force causing overturning against the self weight and pile resistance of the building. In the present study only shallow foundations are studied and hence the hydrodynamic force, buoyancy forces and the building self weight are only considered. Hydrodynamic and buoyancy forces for the chosen building are estimated as per FEMA P 646 [10] for different cases.

2.1 Hydrodynamic Force

Hydrodynamic force also known as drag force is the lateral force caused by the water travelling at a varying velocity and hits the building. Hydrodynamic force (F_d) is a function of fluid velocity, fluid density and structural geometry estimated using Eq. 1 [10] and applied as uniform load on the structure.

$$F_d = \frac{1}{2}\rho_s C_d B(hu^2)_{\max} \tag{1}$$

$$(hu^2)_{\max} = gR^2[0.125 - 0.235(\frac{z}{R}) + 0.11(\frac{z}{R})^2] \tag{2}$$

where ρ_s is the density of sea water which is equal to1100 kg/m^3, C_d is the drag coefficient (a value of 2.0 has been adopted) [10], B is the width of building in the plane normal to the direction of flow, h is flow depth, and u is flow velocity at the location of the building, z is the height of elevation of the building from the sea, R is the inundation depth of tsunami and g is the acceleration due to gravity.

2.2 Buoyancy Force

Buoyancy force or the vertical uplift force is acting vertically through the center of gravity of the building and below the building. Panon et al. [4] have specified the buoyant force as a function of residual air space ratio C_b as given in Eq. 3. Where C_b equal to 1 means no water enters into building and C_b equal to 0 represents entire building is filled with water, B_r and D_r are the width and depth of the raft foundation of the building and H is inundation Depth or Height of building.

$$F_b = \rho_s C_b B_r D_r H \tag{3}$$

2.3 Overturning and Resisting Moment

Overturning moment (O_M) and resisting moment (R_M) are estimated using Eqs. 4 and 5 respectively for the different cases using the total weight of building (W_s) which includes weight of raft foundation.

$$O_M = F_d H/2 + F_b B_r/2 \tag{4}$$

$$R_M = W_s B_r/2 \tag{5}$$

3 Parametric Study

In the present study, residual air space ratio, inundation depth and height of the building are identified as important parameters which can contribute for the action of overturning.

For carrying out the parametric study, a square building of plan dimension 8mx8m as shown in Fig. 1a is considered. Five buildings consisting of one storey to five stories as shown in Fig. 1b–f with column and beam dimensions as shown in Table 1 are included in the study. Slab thickness of buildings is assumed as 125 mm and a live load of 3kN/m^2 has been considered for all the cases. Seismic loads consistent with Indian seismic code IS 1893 (Part 1) 2016 [11], for Zone III, importance factor 1 and response reduction factor 3 are adopted in the present study. Structural design of beams and columns are carried out for load combinations prescribed in Indian Standard for reinforced concrete design IS 456 2000 [12].

3.1 Residual Air Space Ratio (C_b)

Residual air space ratio is defined in such a way that C_b equal to 1 refers to the case of no water entering into building and C_b equal to 0 represents entire building is filled with water [4]. In the present study C_b values of 0.2, 0.4, 0.6, 0.8, and 1.0 have been considered and the variations of overturning ratio for different heights of building and inundation depths are shown in Fig. 2. From Fig. 2a, it is seen that when C_b is equal to 0.2 i.e. while the building is filled with 80% of water, O_R values are less than 1 which indicates that there is no chance of overturning for all the five buildings considered and for all the inundation depths studied. Similarly, when the values of C_b is equal to 0.4, wherein, 60% of the building is filled with water, there are less chances of overturning for all the cases considered, except for one case of two storey building with 12.5 m inundation depth. Chances of overturning exist for about nine cases out of eighteen (50%) when the C_b is equal to 0.6. Further, twelve cases out of eighteen (67%) have chances of overturning when the value of C_b is equal to 0.8. On the other hand, when the value of C_b is equal to 1, i.e. when the building is fully closed and no water enters the building, O_R values are more than 1 for fourteen cases out of eighteen (78%) with the maximum value of O_R being 2.18 for two storey building for 12.5 m inundation depth. An observation demonstrates the importance of air void ratio in causing the overturning of building.

*3.2 Inundation Depth (*R*)*

Typical inundation depths of 5, 7.5, 10 and 12.5 m are considered for the parametric study and the variation of O_R with C_b for different inundation depths are shown in

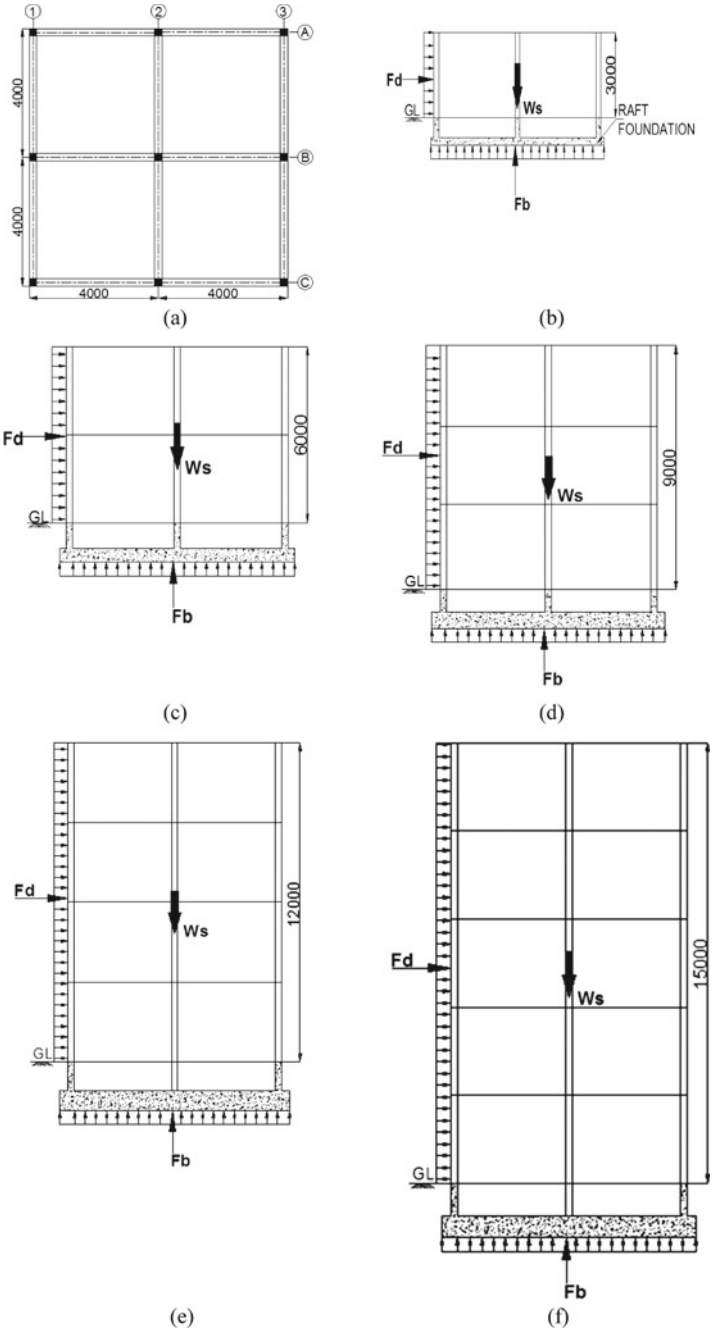

Fig. 1 Plan and elevation of building indicating the direction of hydrodynamic and buoyancy forces **a** plan **b** one storey **c** two stories **d** three stories **e** four stories **f** five stories

Table 1 Structural details of buildings

Sl. No	No. of stories	Dimensions of beams (m)	Dimensions of colum (m)	Thickness of slab (m)	Thickness of raft foundation (m)
1	One	0.23 × 0.23	0.3 × 0.3	0.125	0.15
2	Two	0.23 × 0.23	0.3 × 0.3	0.125	0.2
3	Three	0.23 × 0.325	0.325 × 0.325 (From Bottom Storey No.1)	0.125	0.3
		0.23 × 0.3	0.3 × 0.3 (Storey Nos. 2, 3)	0.125	0.3
4	Four	0.23 × 0.325	0.35 × 0.35 (Storey No.1)	0.125	0.4
		0.23 × 0.3	0.35 × 0.35 (Storey No. 2)	0.125	0.4
		0.23 × 0.3	0.3 × 0.3 (Storey Nos. 3, 4)	0.125	0.4
5	Five	0.23 × 0.325	0.4 × 0.4 (Storey Nos 1, 2)	0.125	0.5
		0.23 × 0.3	0.35 × 0.35 (Storey No. 3)	0.125	0.5
		0.23 × 0.3	0.3 × 0.3 (Storey Nos 4, 5)	0.125	0.5

Fig. 3. Linear variation of O_R with C_b for different inundation depths are observed from Fig. 3. Single and two storey buildings only have the potential hazard of overturning for the inundation depth of 5 m. Similarly, for the inundation depth of 7.5 m, four and five storey buildings do not possess the chance of overturning. Single storey building has maximum potential for overturning for 10 m and 12.5 m inundation depths and these cases have not been included in the present study. About nine cases out of eighteen (50%) and 13 cases out of eighteen (72%) have chances of overturning for 10 m and 12.5 m inundation depths respectively.

*3.3 Heights of the Building (***h***)*

Five buildings of heights 3, 6, 9, 12 and 15 m representing one to five stories are considered in the present study and the variations of O_R with R for different heights of building are shown in Fig. 4. From Fig. 4 it can be seen that, while the inundation depth is more than the height of the building and the C_b values are more than 0.8 there are maximum chances of overturning. Further, even while the inundation depths are

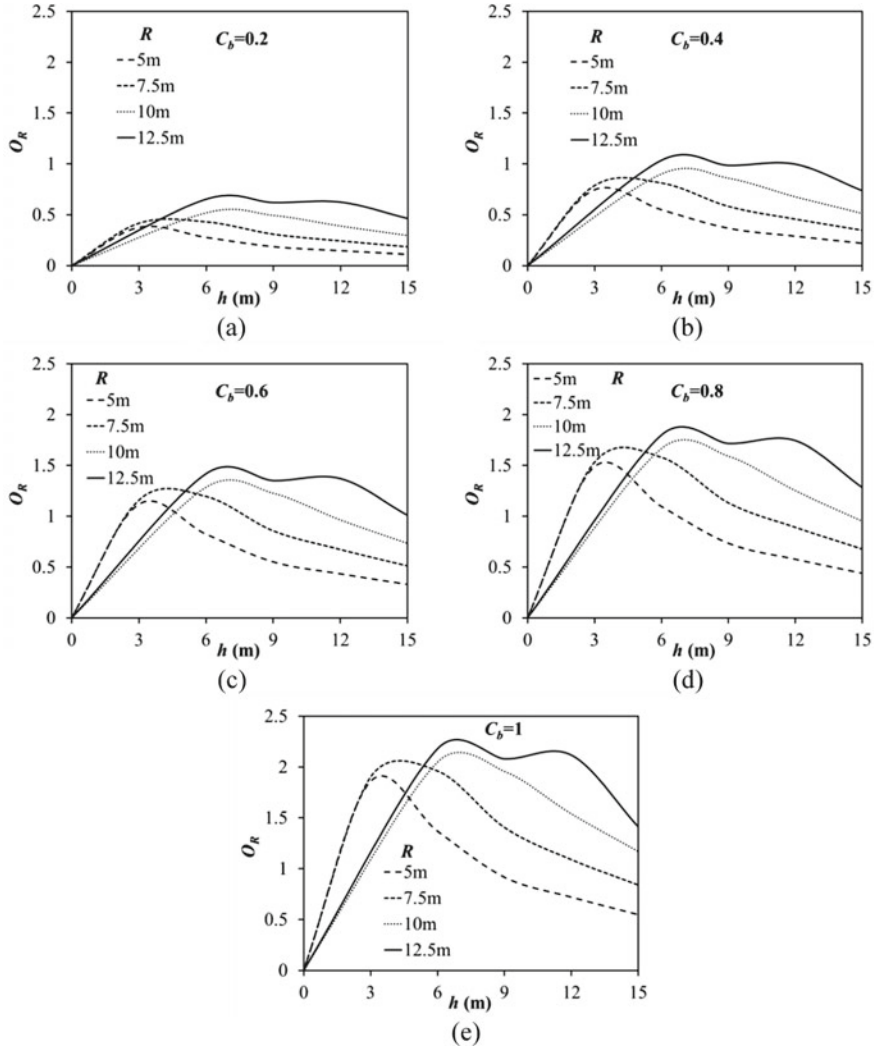

Fig. 2 Variation of Overturning ratio with height of building for different inundation depths and air void ratios **a** $C_b = 0.2$ **b** $C_b = 0.4$ m **c** $C_b = 0.6$ m **d** $C_b = 0.8$ m **e** $C_b = 1.0$

lesser than the height of building, there are chances of overturning for C_b values of more than 0.8% of buildings overturned among the cases considered in the present study are 60%, 60%, 40%, 30% and 20% respectively for the heights of 3 m, 6 m, 9 m, 12 m and 15 m.

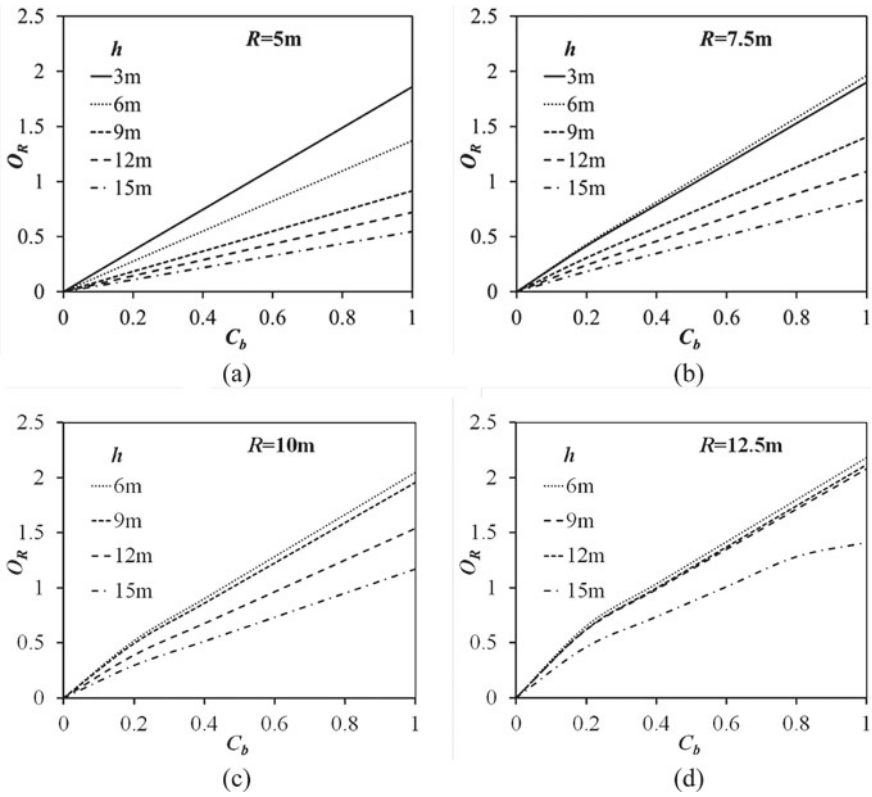

Fig. 3 Variation of Overturning ratio with air void ratio for different Inundation depths **a** $R = 5$ m **b** $R = 7.5$ m **c** $R = 10$ m **d** $R = 12.5$ m

4 Model for Prediction of O_R

Based on the parametric study, a model has been fitted for estimation of O_R as given in Eq. 6. Coefficient of correlation for the fit is 0.985, coefficient of determination is 0.97 and root mean square error of fit is 0.0972. Plot of comparison of actual and predicted O_R for the data set of the parametric study is shown in Fig. 5.

$$O_R = 0.089459 + 1.5151C_d + 0.00032127R - 0.028721h + 0.10242C_dR - 0.098968C_dh + 0.0033186Rh \quad (6)$$

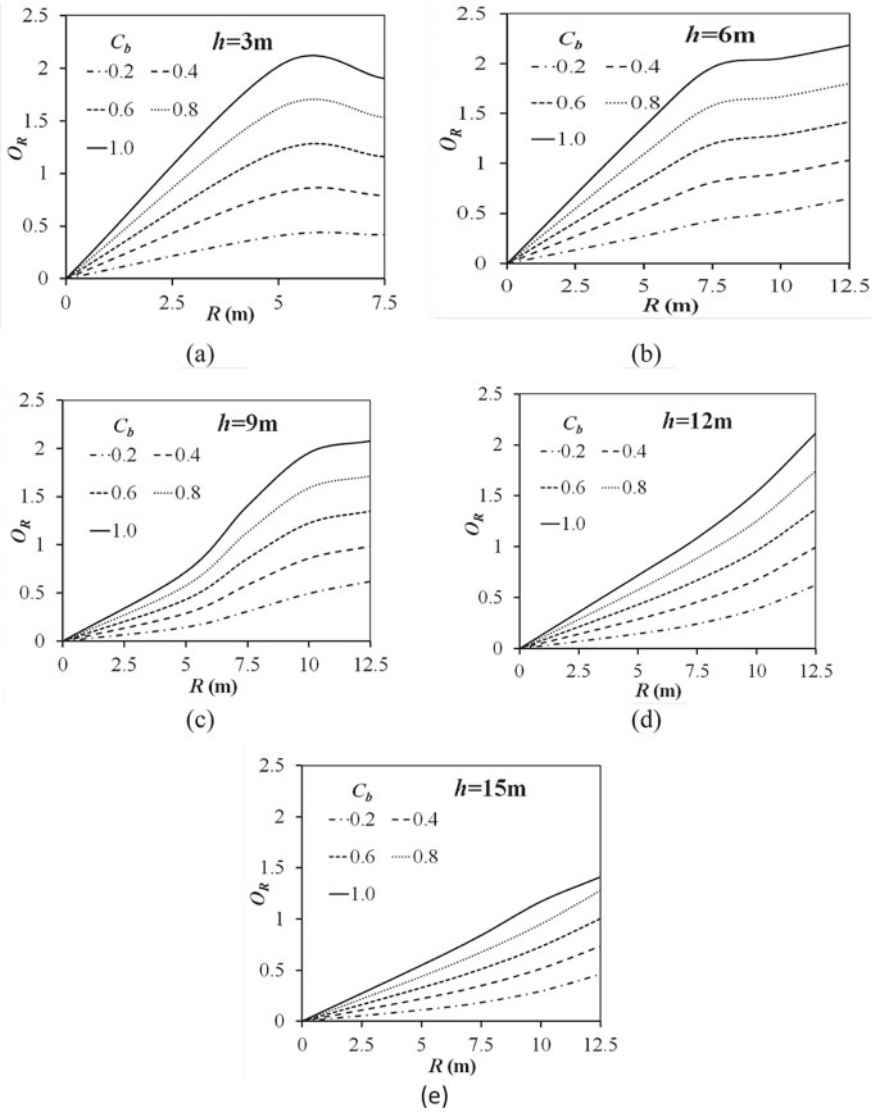

Fig. 4 Variation of Overturning ratio with Inundation depthfor different heights of building **a** $h =$ 3 m **b** $h = 6$ m **c** $h = 9$ m **d** $h = 12$ m **e** $h = 15$ m

5 Conclusions

In this paper, variation of overturning ratio of building with residual air space ratio, inundation depth and height of the building are studied. From the limited studies made, it is observed that when C_b is equal to 1 or 0.8 while the building is enclosed

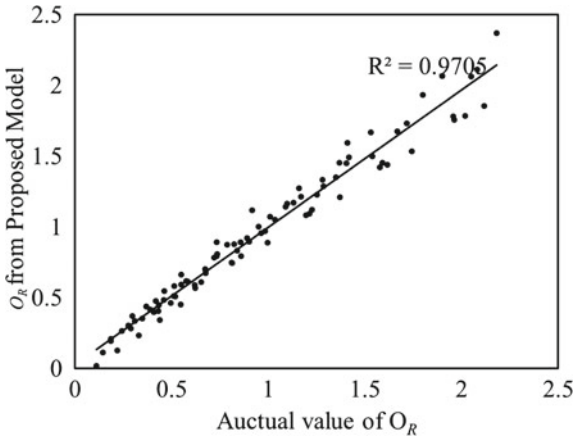

Fig. 5 Validation of the model proposed for O_R

by walls when no water or minimum water enters the building, there are maximum possibilities for overturning. O_R is found to increase linearly with C_b. Similarly, when the inundation depth is more, there is a maximum possibility of overturning of building, however the variation of O_R with R is not linear. Further, different heights of buildings are observed to be vulnerable for different inundation depths which can cause maximum O_R. Based on the results of the parametric study a model for overturning ratio has been proposed, which can be used for preliminary evaluation of overturning ratio of building.

Acknowledgements This paper is published with the kind permission of the Director CSIR-Structural Engineering Research Centre, Chennai.

References

1. Maheshwari BK, Sharma ML, Narayan JP (2005) Structural damages on the coast of Tamil Nadu due to tsunami caused by December 26, 2004 Sumatra earthquake. ISET J Earthq Technol 42(2–3):63–78
2. Murat S, Ahmed G, Ioan N (2005) Effects of the December 26, 2004 Sumatra earthquake and Tsunami on physical infrastructure. ISET J Earthq Technol 42(4):79–94
3. Joshua M, Ioan N, Alison R, Sean W, Antonios P, Tiziana R (2018) Tsunami design procedures for engineered buildings: a critical review. Ice Publishing, pp 1–13 (2018) https://doi.org/10.1680/jcien.17.00043
4. Panon L, Anawat S, Akane Y, Bruno A, Shunichi K, Yoshiro K, Fumihiko I (2017) Possible failure mechanism of buildings overturned during the 2011 great east Japan Tsunami in the town of Onagawa. Front Built Environ 3(16):1–18
5. Kohji T, Shuji T, Hiroko S, Kota K (2012) Building damage associated with geotechnical problems in the 2011 Tohoku Pacific Earthquake. Soils Found 52(5):956–974
6. Piyawat F, Anat R, Panitan L, Nuttawut T (2015) Behaviours of reinforced concrete building under tsunami loading. The IES J Part A, Civ Struct Eng 8(2):101–110. https://doi.org/10.1080/19373260.2015.1013998

7. Fauzan FAI, Annisa El H, Zev Al J (2018) Effect of tsunami loads on Ulak Karang shelter building in Padang City. Int J Trend Sci Res Dev (IJTSRD). Int Conf Adv Eng Inf Technol (ICAEIT-2017), ISSN No: 2456, 165–172
8. Kabeyasawa T, Okuda Y, Fukai A, Fukuyama H, Kato H, Ishihara T, Tajiri S, Tani M (2012) Evaluation of lateral and buoyant forces on reinforced concrete buildings by the tsunami of the 2011 east japan earthquake. In: 15th world conference on earthquake engineering Lisboa
9. Michitaka I, Kohji T, Shusaku I (2016) Factors affecting tsunami-induced overturning of building in the 2011 great Tohoku earthquake. In: Civil engineering conference in the Asian region (CECAR7), pp. 1–10
10. FEMA P-646 (2012) Guidelines for design of structures for vertical evacuation from tsunamis (2nd ed.). Federal Emergency Management Agency, Washington, D.C., p 174
11. IS 1893 (Part-1) (2016) Indian standard criteria for earthquake resistant design of structures (Sixth Revision). Bureau of Indian Standards, New Delhi
12. IS 456 (2000) Indian standard plain and reinforced concrete—code of practice (Fourth Revision). Bureau of Indian Standards, New Delhi

Semi-active Seismic Vibration Control Offshore Jacket Platforms

Minaruddin Khan and Diptesh Das

Abstract A semi-active control scheme for the vibration control of offshore steel jacket platforms is developed. Decentralized sliding mode control (SMC) algorithm is adopted for applying the control force to the structure with the help of Magneto-rheological (MR) damper for alleviating the earthquake-induced vibrations. SMC method is used due to its robustness against the parametric variations of the structures. The command voltage to the MR dampers is regulated through the clipped-optimal algorithm. A steel jacket platform, available in the literature, is modelled in MATLAB as an example to investigate the dynamic responses under the environmental loads. The earthquakes ground motions, scaled to 0.3 g PGA, considered in the present study are the El Centro (1940), Northridge (1994), San Fernando (1971) and Chichi (1999). Results indicate that sliding mode controller is able to reduce the responses of the offshore jacket platform significantly, subjected to different earthquake loads. It is observed that the positions and the number of MR dampers affect the performance of the controller to a great extend in the offshore jacket platforms. The control algorithm is stable against the variations and uncertainties in structural parameters.

Keywords Offshore jacket platform · Semi-active control · Decentralized sliding mode control · MR damper · Earthquake loads

1 Introduction

Recently offshore platforms play a key factor for the growth of industry, as the platforms are mainly used to extract, drill and store oil and natural gases. The fixed steel jacket platform is generally slender, flexible in nature, and installed in the water at different required depths. The environment surrounding the structures is harsh and hostile and make complexity for the erection and difficulties for employment of control device. There are some major environmental loads act to the structures during

M. Khan (✉) · D. Das
Department of Civil Engineering, National Institute Technology, Durgapur 713209, India

D. Das
e-mail: diptesh.das@ce.nitdgp.ac.in

T. G. Sitharam et al. (eds.), *Earthquakes and Structures*, Lecture Notes in Civil Engineering 188, https://doi.org/10.1007/978-981-16-5673-6_4

their lifetime, which are nonlinear and dynamic in nature. The vibrations due to the major dynamic forces induced by wave [1–3] and earthquake [4–6] and to some lesser extent current [7] and ice [8] have the substantial affect to the structure and cause large deformation and fatigue damage. Therefore, for the structural productivity, safety and for the smooth and continuous operation, the amplitude of deformation due to the vibrations should be a certain limit. During the last few decades, researchers have been given afford to mitigate the vibrations using different isolator. State-of-the-arts [9] reflect that the general trend for the vibration control system go along from passive to active and towards semi-active and hybrid as because these controller utilized the advantages of both passive active control system.

Literature survey [4, 5, 10–12] show that the passive isolators, mainly, Tuned Liquid Dampers (TLD), Viscous Dampers, Friction Damper Devices (FDD), Tuned Liquid Column-Gas Dampers (TLCGD) and Hydrodynamic Buoyant Mass Dampers are used to attenuate the vibrations of the platforms. Passive controllers have the drawback of their inadaptability to the changes in structural properties and loading conditions. There are many active control schemes [6, 13, 14] has been performed to overcome the shortcomings the passive dampers for the mitigation of the structural vibrations. However, complexity arise for the implementation of active control scheme in the platform due to their sensibility and disruption during power failure. Moreover, modelling error, time-delay and limited frequency bandwidth are the disadvantages for the execution of the active controller.

Semi-active control scheme [15, 16] is an excellent approach for the vibration control as these controllers utilized the benefits of both passive and active control system. The major control algorithms, clipped optimal control algorithm [14], Bang-Bang control algorithm [17], LQG algorithm [30], linear quadratic control algorithm [18] and non-resonance control algorithm [19], are used for implementation of semi-active control schemes. There are lot of assumptions and parameter variations taken under consideration to develop a mathematical model for the water-structure controller and even it is more challenging for random earthquake excitations. Sliding mode control algorithm [20] works more effectively under the complex environment for its implicit robustness and efficiency to cope up with parameter variations and imprecisions. MR damper has considered as a semi-active control device for its excellence fluid properties. In presence of magnetic field, the MR fluid changes its state from fluid to semi solid within millisecond and provides sufficient yield strength to the platform to alleviate the vibrations against external excitations [21]. For controlling large-scale civil structures, decentralized control strategy have better efficiency and robustness as compared to the conventional centralized control approach [22].

The objective of the present work to develop a robust control scheme to work effectively under the adverse environmental condition and capable to reduce structural responses to be a satisfactory level. A semi-active control scheme with MR damper device is proposed to mitigate the vibrations subjected to seismic ground motions, namely, El Centro (1940), Northridge (1994), San Fernando (1971) and Chichi (1999). Decentralized SMC algorithm is developed to supply the control force to the MR dampers due to its inherent robustness with parameter variations and uncertainties. For the supply of the required command voltage to MR dampers,

Clipped Optimal algorithm is used. The proposed control scheme fulfill the objective and motivation of the present study in terms response reduction in the deck of the platform. A parametric study on the optimum number and place of installation of MR dampers is carried out to get best results in terms of response reduction of the platform. Results show that control scheme is effective and bear significant contributions toward structural stability and integrity.

2 Theoretical Formulation

Presence of water around the offshore structures make it differences with the conventional civil structures. Therefore, water-structural interaction is also an important factor has to be taken under consideration for the control of the vibrations. The drag force due to the motion of the structures in the water act as dampers and enhance structural stability. The equation of motion of the structures subjected to seismic ground motion, written as [11]

$$\mathrm{M}\ddot{\mathrm{x}}(\mathrm{t}) + \mathrm{C}\dot{\mathrm{x}}(\mathrm{t}) + \mathbf{K}\mathrm{x}(\mathrm{t}) = \mathbf{H}\mathrm{U}(\mathrm{t}) + \eta\ddot{\mathrm{x}}_g(t) + \mathrm{f} \tag{1}$$

$$\text{where,}\quad \mathbf{f} = -\mathbf{K}_\mathrm{d}\left(\{\dot{\mathrm{x}}\} + [1]\dot{\mathrm{x}}_\mathrm{g}\right)\left|\{\dot{\mathrm{x}}\} + [1]\dot{\mathrm{x}}_\mathrm{g}\right| \tag{2}$$

$$\mathbf{M} = \mathbf{M}_\mathrm{s} + \mathbf{M}_\mathrm{a},\ \mathbf{M}_\mathrm{a} = \rho(\mathrm{C}_\mathrm{l} - 1)\mathbf{B},\ \mathbf{K}_\mathrm{d} = \rho\mathrm{C}_\mathrm{D}\mathrm{A} \tag{3}$$

In Eq. 1 the term f reflects the effect water-structure interaction, which is considered as the absolute velocity dependent nonlinear dashpots, explain in Eq. 2. $\mathbf{M}_\mathrm{a}$ $\mathbf{M}_\mathrm{s}$, **C** and **K** are the added mass, the jacket platform mass, damping, and stiffness matrices, respectively; ρ, C_l, C_D, **A** and **B** are the sea water density, inertia coefficient, drag coefficient, area and volume matrices; $\ddot{\mathrm{x}}_\mathrm{g}$ is earthquake ground motion; **U**(t) is vector to apply control forces; and η is an n-vector denoting the influence of the earthquake excitation. The placement of the dampers are incorporate with the denoting matrix (**H**). The formulation of damping matrix is based on Rayleigh damping concept, which is proportional to mass and stiffness matrix [23].

2.1 Modelling of MR Damper

MR damper has excellence property that in presence of electrical field, the MR fluid change it's state from semi-liquid to solid within millisecond. To describe the dynamic properties of MR Dampers, a numerical Bouc-Wen model is considered. It is highly versatile and simple mechanical model consisting of Bouc-Wen element in parallel with a viscous damper, used for denominating hysteretic behavior of the MR damper. The numerical equations incorporating with Bouc-Wen model to produce

force in the MR dampers [21] are given as follows

$$f = c_o\dot{x} + \alpha z \tag{7}$$

$$\dot{z} = -\gamma|\dot{x}|z|\dot{z}|^{n-1} + \beta\dot{x}|\dot{z}| + A_m\dot{x} \tag{8}$$

z is the evolutionary variable important for the hysteretic loop which depends on the response; γ β, n, and A_m are carry their usual meanings. Two parameters α and c_o depends on the control input voltage u as follows:

$$\alpha = \alpha(u) = \alpha_a + \alpha_b u \tag{9}$$

$$c_o = c_o(u) = c_{oa} + c_{ob}u \tag{10}$$

The expression of control voltage is given as first-order filter dynamics equation induced in the system as follows:

$$\dot{u} = -\eta(u - v) \tag{11}$$

where, u is required voltage applied to the current driver, and η is the time constant of the first-order filter.

3 Methodology

A four legged, 70 m high steel jacket offshore platform available in literature Mousavi et al. [11] is taken to investigate the efficiency and usefulness of the proposed control scheme in terms of response reductions against seismic induced excitations. The platforms have same properties in the both directions and all the elements are under elastic limit. The density of water is 1000 kg/m^3, the density of steel is 7800 kg/m3, the drag and inertia coefficients are 0.7 and 2, respectively, and the deck mass of the platform is 1000 tons. Lumped mass model of the platform as five degree-of-freedom system mentioned in literature [11], and its mass M and stiffness K matrix are given below

$$K = 10^9 \times \begin{bmatrix} 1 & -0.444 & 0 & 0 & 0 \\ -0.444 & 0.819 & -0.375 & 0 & 0 \\ 0 & -0.375 & 0.661 & -0.286 & 0 \\ 0 & 0 & -0.286 & 0.353 & -0.067 \\ 0 & 0 & 0 & -0.067 & 0.067 \end{bmatrix} (\text{N/m}),\ M = \begin{bmatrix} 157 & 0 & 0 & 0 & 0 \\ 0 & 154 & 0 & 0 & 0 \\ 0 & 0 & 151 & 0 & 0 \\ 0 & 0 & 0 & 137 & 0 \\ 0 & 0 & 0 & 0 & 1087 \end{bmatrix} \times 10^3 \text{ kg}$$

The diagonal elements of the area (A_P) and volume (V_P) matrices of the structural [294, 289, 282, 202, 0] m^2 and [258, 253, 248, 177, 0] m^3, respectively. To formulate the Rayleigh damping matrix, a value of 2% is taken as the damping ratio of all modes in air [23]. MR damper is considered as an isolator in semi-active control system for its excellence properties of fluid. The value of the parameters for 100-ton capacity MR damper is adopted from [21]. The main motive of the sliding mode controller is to enter the structural responses into the sliding surface. The formulation of the sliding mode control algorithm is carried out according to the formulae given in literature [20]. The Clipped-Optimal algorithm proposed by Dyke [21] is used to govern the input voltage delivered to the MR damper. The study is carried out on the base of state space formulation in MATLAB Simulink. The time history responses, mainly, top deck displacement, top deck acceleration, and base shear are the major interest to reduce its amplitudes. The comparative study of controlled and uncontrolled of these responses are carried for the earthquake ground motions (0.3 g peak ground acceleration), namely, El Centro (1940), Northridge (1994), San Fernando (1971) and Chichi (1999) [11]. A parametric study on the optimum number and place of installation of MR dampers is carried out to get best results in terms of response reduction of the platform.

4 Importance Outcomes

To investigate the effectiveness of semi-active control scheme, a steel jacket platform is taken based on assumption that all elements of the structure remain elastic during the external excitation. Control of top deck displacement and acceleration is investigated for different arrangement of 100-ton capacity MR dampers placed in the offshore platform. Following arrangement have been considered to analysis the efficiency of the scheme for structural integrity.

1. Single MR damper placed in the fifth storey.
2. Two MR dampers placed in the four and fifth storeys.
3. Three MR dampers placed in the alternate storeys.
4. Four MR dampers placed in the top four storeys.
5. Five MR dampers placed all storey level.

Time histories responses of top deck displacement, acceleration and RMS value of displacement for both controlled and uncontrolled with different arrangement of MR dampers are shown in Figs. 1, 2 and 3 subjected to El ecntro (1940) ground motion.

Results indicate that positioning five MR dampers towards the storey is the best arrangement to get optimum response reduction. The top deck responses are effectively reduced with the increase of MR dampers. It may be noted that MR dampers are placed on five floors have slight greater reduction of responses other than four dampers are placed towards top four floors but, the position of MR damper near the base of the structure is not a feasible option to install due to requirement of high cost,

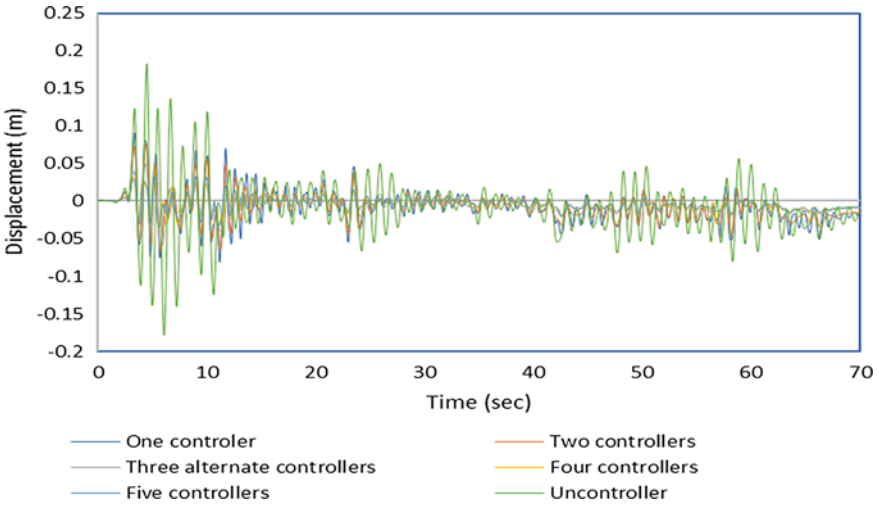

Fig. 1 Variation of top deck displacement with different arrangement of MR dampers subjected to El ecntro (1940)

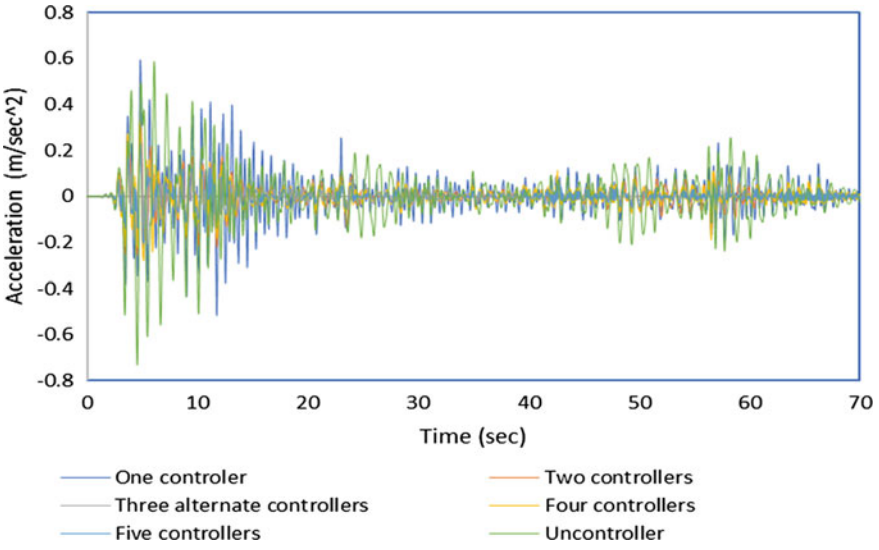

Fig. 2 Variation of top deck acceleration with different arrangement of MR dampers subjected to El ecntro (1940)

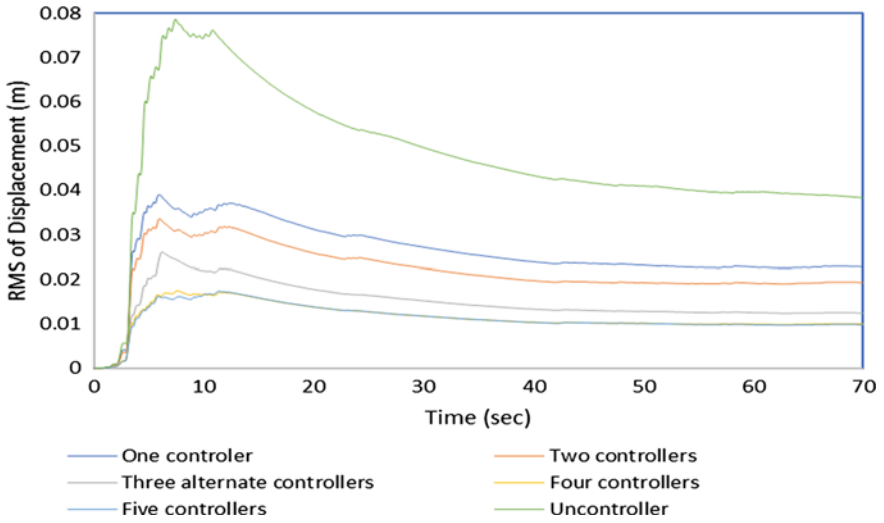

Fig. 3 Variation of top deck RMS value of displacement with different arrangement of MR dampers subjected to El ecntro (1940)

maintenance and operation. Controlled and Uncontrolled responses of displacement, acceleration, velocity and RMS values of displacement, and their corresponding percentage of reduction (%R) for various arrangement of MR dampers against El ecntro (1940) ground motion are shown in Table 1. Therefore, based on the results, four dampers placed on top four floors is taken as an optimum option to study the performance of the scheme against earthquake excitations. Table 2, also reflects similar trend in terms of top deck amplitude reduction for displacement, acceleration, 4th interstory drift and base shear against various earthquake motions. Reduction of base shear bears important for cost optimization; the proposed scheme reduces the base shear (Fig. 4) effectively, which implies less cost involvement for construction. The proposed scheme reduces the inter-storey drift (Fig. 5) and provide stability to some extent.

The effectiveness of the controller does not vary with the sling margin (Fig. 6), therefore, the controller is robust against the parameter uncertainties. As per theory, Sliding surface (S) should be zero but, Fig. 7 shows that response trajectory does not coincide with the sliding surface; this is due to presence of external distribution but the average values of the sliding function tend to be zero. The clipped control algorithm operates as an "on–off" mode, maximum 10 V supplied to the MR damper. The voltage operation, switch between 0 to 10 V to the 100 ton MR Dampers is shown in Fig. 8.

Table 1 Controlled (C) and Uncontrolled (UC) responses (RMS values of displacement) and corresponding percentage of reduction (%R) for El ecntro (1940)

			Displacement (cm)			Acceleration (cm)			Velocity (cm)			RMS displacement (cm)		
	EQ	DOF	UC	C	%R	UC	C	%R	UC	C	%R	UC	C	%R
El Centro31	Alternate	1	2.81	0.95	66.26	26.43	8.46	68.01	2.12	0.43	79.70	1.11	0.33	70.60
		2	5.77	1.78	69.21	50.25	15.48	69.19	4.37	0.87	80.15	2.26	0.62	72.58
		3	8.42	2.30	72.68	64.38	19.66	69.46	6.20	1.16	81.30	3.31	0.82	75.29
		4	10.58	1.97	81.33	82.55	15.60	81.10	7.28	0.95	86.92	3.31	0.73	77.85
		5	18.24	4.88	73.25	58.67	30.58	47.88	8.85	2.66	70.00	7.86	2.61	66.83
	One controller	1	2.81	1.06	62.28	26.43	11.39	56.92	2.12	0.84	60.52	1.11	0.40	64.20
		2	5.77	2.10	63.68	50.25	21.97	56.29	4.37	1.68	61.44	2.26	0.77	65.77
		3	8.42	2.87	65.85	64.38	29.04	54.90	6.20	2.26	63.59	3.31	1.04	68.68
		4	10.58	2.61	75.35	82.55	23.62	71.38	7.28	1.85	74.51	3.31	0.92	72.27
		5	18.24	9.05	50.41	58.67	59.38	-1.21	8.85	4.42	50.12	7.86	3.90	50.41
	Two controllers	1	2.81	0.91	67.53	26.43	9.85	62.74	2.12	0.55	73.94	1.11	0.30	73.39
		2	5.77	1.72	70.17	50.25	12.75	74.63	4.37	0.80	81.77	2.26	0.54	76.26
		3	8.42	2.24	73.33	64.38	14.59	77.33	6.20	0.90	85.52	3.31	0.71	78.55
		4	10.58	1.89	82.18	82.55	21.43	74.04	7.28	0.83	88.65	3.31	0.59	82.14
		5	18.24	7.56	58.55	58.67	30.14	48.63	8.85	3.40	61.61	7.86	1.04	86.72
	Four controllers	1	2.81	0.87	69.13	26.43	15.10	42.86	2.12	0.58	72.66	1.11	0.28	74.77
		2	5.77	1.62	71.99	50.25	18.69	62.82	4.37	1.07	75.55	2.26	0.52	77.10
		3	8.42	2.08	75.25	64.38	24.43	62.06	6.20	1.37	77.83	3.31	0.66	79.94
		4	10.58	1.70	83.93	82.55	25.00	69.71	7.28	1.07	85.26	3.31	0.55	83.51
		5	18.24	3.44	81.14	58.67	32.64	44.38	8.85	3.76	57.57	7.86	1.75	77.80

(continued)

Table 1 (continued)

			Displacement (cm)			Acceleration (cm)			Velocity (cm)			RMS displacement (cm)		
	EQ	DOF	UC	C	%R	UC	C	%R	UC	C	%R	UC	C	%R
	Five controllers	1	2.81	0.80	71.65	26.43	6.50	75.42	2.12	0.39	81.75	1.11	0.26	76.40
		2	5.77	1.48	74.40	50.25	12.55	75.03	4.37	0.64	85.29	2.26	0.49	78.51
		3	8.42	1.95	76.83	64.38	15.75	75.54	6.20	0.82	86.76	3.31	0.65	80.53
		4	10.58	1.62	84.65	82.55	17.88	78.34	7.28	0.61	91.58	3.31	0.54	83.77
		5	18.24	3.30	81.92	58.67	23.16	60.53	8.852	2.71	69.36	7.86	1.74	77.92

Table 2 Controlled (C) and Uncontrolled (UC) amplitude of top deck displacement, acceleration, 4th inter-storey drift and base shear for optimum condition

Forces	Top deck displacement (cm)		Top deck acceleration (cm/s^2)		Base-shear (ton)		Inter storey drift (cm)	
	UC	Semi-active	UC	Semi-active	UC	Semi-active	UC	Semi-active
El ecntro (1940)	18.244	3.440	58.673	32.64	494.88	433.02	2.694	0.474
Chi-Chi (1999)	22.902	6.352	32.187	16.03	305.33	275.35	4.423	1.093
San Fernando (1971)	20.628	4.960	49.813	26.75	495.10	439.02	3.854	0.891
Northridge (1994)	15.643	3.896	57.123	47.18	446.41	439.80	3.155	0.624

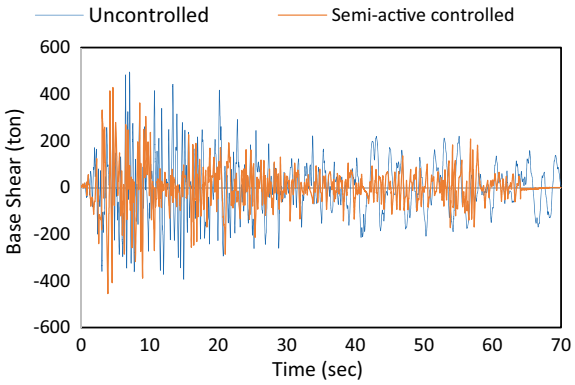

Fig. 4 Time–history variation of base shear subjected to El Centro earthquake

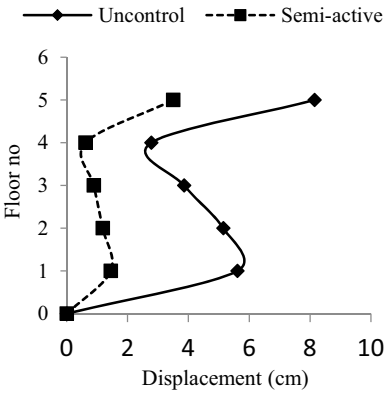

Fig. 5 Variation of maximum amplitude of 4th inter-storey drift subjected to El Centro earthquake (extreme) wave load, and (**c**) irregular (JONSWAP)

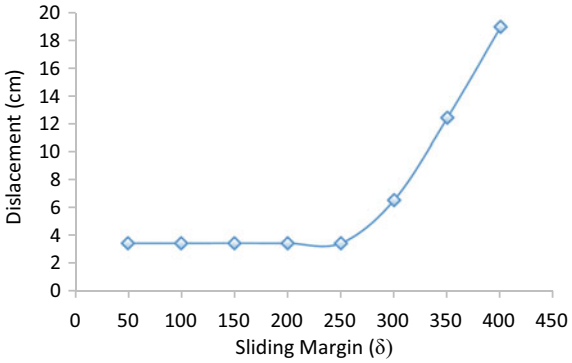

Fig. 6 Variation of top deck displacement with the variation of sliding margin corresponding to El Centro earthquake

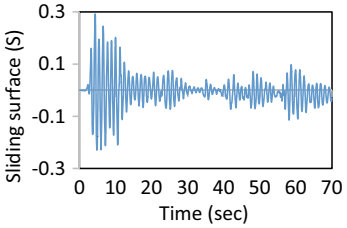

Fig. 7 Variation of sliding surfaces of the controller against El Centro earthquake

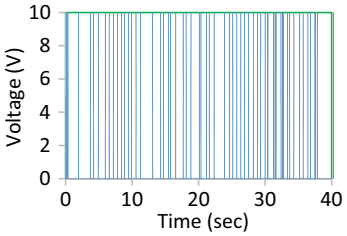

Fig. 8 Variation of command voltage applied to the MR damper subjected to El Centro earthquake

5 Outcomes

There are some certain major conclusions brought out from the present numerical study are enlightened below. The decentralized sliding mode controller using MR damper isolator is capable to reduce the vibrations of the fixed jacket platform against multiple earthquake loads and the number of the MR dampers and its position of installation affect the performance of the controller largely to improve the safety, stability and integrity of the platform. To control structural damage like, cracks and

fatigue, displacement reduction is inevitable and for human easement acceleration, reduction is essential. The control scheme is effective to fulfill the bi-objective, acceleration and displacement reduction. The control system is robust against parametric uncertainties and work function is smooth under the harsh and hostile environment and to some extent reduce base shear effectively.

References

1. Wu Q, Zhao X, He S, Tang W, Zheng R (2016) A bufferable tuned-mass damper of an offshore platform against stroke and response delay problems under earthquake loads. J Shock Vib 2016:1–18
2. Lin CS, Liu F, Zhang J, Lin CC (2017) Multiple tuned mass dampers for vibration control of offshore platform against natural loadings. The world congress on advance in structural engineering and mechanics, Ilsan(Seoul), Korea, pp 1–18
3. Wu Q, Zhao X, Zheng R, Minagawa K (2016) High response performance of a tuned mass damper for vibration suppression of offshore platform under earthquake loads. J Shock Vib 2016:1–11
4. Ha M, Cheong C (2016) Pitch motion mitigation of spar-type floating substructure for offshore wind turbine using multilayer tuned liquid damper. Ocean Eng 116:157–164
5. Tabeshpour MR, Rokni HJ (2018) Spectral fatigue analysis of jacket platform under wave load equipped with viscous damper. J Mar Sci Technol
6. Zhang BL, Jiang X, Wu Q, Tang GY (2019) Vibration reduction for offshore platforms via delayed sliding mode H∞ control. Int J Control Autom Syst 17(1):107–116
7. Haritos N (2007) Introduction to the analysis and design of offshore structures-an overview. Electron J Struct Eng 7:55–65
8. Mostafa YE, El Naggar MH (2004) Response of fixed offshore platforms to wave and current loading including soil-structure interaction. Soil Dyn Earthq Eng 24(4):357–368
9. Wang S, Yue Q, Zhang D (2013) Ice-induced non-structure vibration reduction of jacket platforms with isolation cone system. Ocean Eng 70:118–123
10. Komachi Y, Tabeshpour MR, Golafshani AA, Mualla I (2011) Retrofit of Ressalat Jacket platform (Persian Gulf) using friction damper device. J Zhejiang Univ 12(9):680–691
11. Mousavi SA, Zahrai SM, Bargi K (2012) Optimum geometry of tuned liquid column-gas damper for control of offshore jacket platform vibrations under seismic excitation. J Earthq Eng Eng Vib 11(4):579–592
12. Moharrami M, Tootkaboni M (2014) Reducing response of offshore platforms to wave loads using hydrodynamic buoyant mass dampers. Struct Eng 81:162–174
13. Zhang BL, Han QL, Zhang XM, Yu X (2014) Sliding mode control with mixed current and delayed states for offshore steel jacket platforms. IEEE Trans Control Syst Technol 22(5):1769–1783
14. Huang S, Cai M, Xiang Z (2017) Robust sampled-data H∞ control for offshore platforms subject to irregular wave forces and actuator saturation. J Nonlinear Dyn 88(4):2705–2721
15. Sarrafan A, Zareh SH, Khayyat AA, Zabihollah A (2011) Performance of an offshore platform with MR dampers subjected to wave. In: Proceedings of the 2011 IEEE international conference on mechatronics, Istanbul, Turkey, pp 242–247. https://doi.org/10.1109/icmech.2011.5971289
16. Babaei S, Amirabadi R, Taghikhany T (2016) Assessment of semi-active tunes mass damper application in suppressing seismic-induced vibration of an existing jacket platform. Int J Marit Technol 6:1–10
17. Paul S, Datta TK, Kapuria S (2009) Control of fixed offshore jacket platform using semi-active hydraulic damper. ASME J Offshore Mech Arct Eng 131(4):041–106

18. aul, S., and Datta, T. K. (2012) Semiactive control of a fixed offshore jacket platform using LQR algorithm. J Eng Marit Environ 227(4):367–380
19. Leng D, Xiao H, Sun L, Liu G, Wang X, Sun L (2018) Study on a magnetorheological elastomer-base device for offshore platform vibration control. J Intell Mater Syst Struct 30(2):243–255
20. Yang JN, Wu JC, Agrawal AK, Li Z (1994) Sliding mode control for seismic-excited linear and nonlinear civil engineering structures. Nat Ctr Earthq Eng Res State Univ New York, Buffalo. Tech Rep NCEER-94–00/7
21. Dyke SJ, Spencer BF Jr, Sain MK, Carlson JD (1996) Modeling and control of magnetorheological dampers for seismic response reduction. J Smart Mater Struct 5(5):565–575
22. Lei Y, Wu DT, Lin Y (2012) A decentralized control algorithm for large-scale building structures. Comput Aided Civ Infrastruct Eng 27(1):1–13
23. Chopra AK (1995) Dynamic of structures, theory and applications to earthquake engineering. Prentice Hall, Englewood Cliffs, N.J

Lateral Capacity of Skirted Footing Resting on Level Ground

Khalid Bashir, Rajesh Shukla, and Ravi S. Jakka

Abstract The paper presents the performance of a square footing with structural skirts resting on sand and subjected to a lateral load through a numerical study. Strip footings are subjected to lateral forces induced by earthquake movements, wind loads. The lateral forces acting on the footings may be predominant in certain structures such as waterfront structure, earth retaining structure and transmitting power towers. There has been a lack of information about the performance of skirted footings subjected to lateral loads. The results of this study revealed that skirted foundations exhibit lateral capacity values that are near, but not exact, to those of block foundations of the same width and depth. The enhancement in the lateral capacity of skirted foundation increases with increasing skirt depth and shearing resistance of sand.

Keywords Skirts · Lateral load · Enhancement

1 Introduction

The term skirted foundations are used to identify strip foundations with driven sheet piles fixed at their circumference. The skirts form a plug in which soil is strictly confined and works as a unit with the overlain foundation to transfer the load of superstructure to soil essentially at the level of skirt tip. Vertical skirts can be used with new and existing shallow foundations of square, rectangular, and circular shapes. Skirted foundations have been used extensively for offshore structures based on their ease and short time of installation compared with deep foundations such as piers and piles. Behavior of skirted foundations for such structures has been studied by several researchers using both numerical and physical modeling [e.g., 1, 2, 3, 4]. Because the offshore structures usually involve cohesive marine deposits, these studies have

K. Bashir (✉) · R. S. Jakka
Department of Earthquake Engineering, Indian Institute of Technology, Roorkee, India
e-mail: kbashir@eq.iitr.ac.in

R. Shukla
Department of Civil Engineering, National Institute of Technology, Srinagar, India

T. G. Sitharam et al. (eds.), *Earthquakes and Structures*, Lecture Notes in Civil Engineering 188, https://doi.org/10.1007/978-981-16-5673-6_5

been focused on predicting the undrained shear strength behavior of the deposits enclosed and overlain by skirted foundations.

Tani and Craig [5] studied Bearing Capacity of Circular Foundations on Soft Clay of strength increasing with depth, and they mentioned that the lower-bound solutions underestimate the bearing capacity at deeper embedments, although their results are limited to embedments of only 30% of the foundation diameter. Bransby and Randolph [1] mentioned that little work has been done to study the effect of the shape of skirted foundations under the combined loads. Bransby and Randolph [6] studied the effect of embedment depth on the undrained response of skirted foundation. Hu et al. [7] Studied a circular bucket offshore foundation on non-homogeneous soil and commented on the effect of side friction in enhancing bearing capacity. Aghbari and Mohamedzein [8] studied Bearing Capacity of Skirted Foundation and suggested Inclusion of Skirts can enhance the bearing capacity 1.5–3.9 times. Yun and Bransby [9] studied this case using centrifuge modeling and compared the test results with the existing raft foundation without skirts to see how much skirts increase the bearing capacity. They proved that the skirts increase the horizontal bearing capacity up to 3–4 times. Watson and Randolph [10] mentioned that in soils with low strength at the surface, skirted foundations are being used as an alternative solution to deep foundations. Tani and Craig [5] suggested that the soil above the level of the skirt tips has a little effect on the foundation response especially for the case of strip footings. Hu et al. [] studied the bearing capacity response of skirted foundation on nonhomogeneous soils; they concluded that the effect of the topsoil layer disappears once the embedment of the footing is greater than two times the diameter, as the failure mode changes to confined plasticity rather than a plastic mechanism reaching the soil surface.

2 Problem Definition

The main objective of this study is to determine the lateral capacity for a skirted footing of width B, which is placed horizontally on the ground surface having, as shown in Fig. 1. The soil is assumed to be entirely plastic and, it follows the Mohr–Coulomb failure criterion and an associated flow rule; the latter assumption ensures that the theorems of the limit analysis remain applicable.

2.1 Numerical Simulation

In order to estimate a solution, a domain as illustrated in Fig. 1, is being chosen. The domain and the associated different stress boundary conditions which are applicable along the footing-soil interface, ground surface, and the chosen boundaries, are illustrated in Fig. 1. The extent of the domain is kept sufficiently large so that in

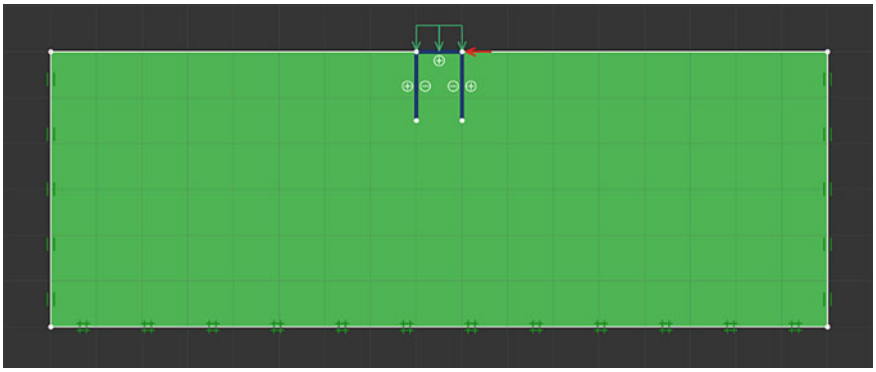

Fig. 1 Chosen domain and boundary conditions

the event of collapse, the region of the soil mass around the selected boundaries does not yield.

An extensive 3D finite-element analysis was carried out using the OptumG2 software package (Krabbenhoft 2017) 1] to study the effects of skirts on the behavior of axially loaded surface foundations resting on sand. An limit analysis based on the Mohr–Coulomb failure criterion and following associated flow rule was used for soil modeling in FELA, as this constitutive model has been widely accepted both in static and pseudo-static analysis of slope stability [1]. The foundation shapes and dimensions used in the analysis are shown in Fig. 1. Rigid plates having a thickness of 50 mm were considered in the analysis to represent the skirts. This thickness was selected to yield skirt stiffness (moment of inertia) similar to those of the commercially available typical steel sheet-pile sections used for foundation skirts. To study the effect of meshing and element type and size, FE models of the foundation on level ground (H = 40 m with properties as shown in Table 11) were developed using conventional and adaptive meshing options with lower bound (LB), upper bound (UB), 6-node Gauss, and 15-node Gauss, triangular plane strain elements available in OptumG2. Fifteen-node gauss plate elements composed footing and skirts. No particular elements were utilized at the concrete-sand or the steel-sand interfaces. Instead, a sand interface strength factor of 1.0 that is suitable for representing rough

Table 1 Parameters considered for numerical analysis

Parameters	Value
Cohesion (c)	0
Angle of internal friction (°)	25–45
Dry unit weight (kN/m^3)	18
Drainage condition	Drained
Failure criteria	Mohr–Coulomb
Skirt soil interface	Rough

Table 2 Percentage increase in bearing capacity for various soils with an increase in the length of skirts

L/B	$\varphi = 30$	$\varphi = 35$	$\varphi = 40$	$\varphi = 45$
0.5	237.4	186.9	144.7	114.6
1	67.09	59.3	52.97	47.4
1.5	42.2	38.3	34.6	31.1
2	30.9	29.8	28.2	25.9

surface-soil interaction was used in the analysis of surface, pier, and skirted foundations. To minimize the boundary effect, the distance of the finite-element mesh boundary from the foundation edges was set to 7B. A similar distance was taken for the vertical extension of sand below the base of surface foundations and the tip of skirts for skirted foundations. The properties used to describe the materials employed in the numerical analysis are shown in Table 12–14.

3 Results and Discussion

The effects of the skirt length on lateral capacity were analysed for various internal friction angles of the soil. The effects of these parameters are discussed separately in the following two sections, i.e., the effect of skirt length, the effect of angle of internal friction. Some of the typical results are presented for soil of internal friction 30º only.

3.1 Effect of Skirt Length (L/B)

Figure 2 shows the effect of the length of the skirts on the lateral capacity for various internal friction angles of the soil. The lateral capacity increases with an increase in the length of skirts, but the percentage increase is high during the initial embedment of skirt length. For the internal friction angle of 30, the effect of the skirt depth is significant when the length of the skirt is 0.5B. The percentage increase of 238% is seen for length of skirt 0.5B, while as for length of skirt 2B percentage increase of 31% is seen. Similar trends are seen for soils with increased internal friction angles as shown in Table 1. This is because an increase in the length of skirts leads to an increase in the depth of foundation. Further, with an increase in depth of skirts, the percentage increase is lower for higher depths is due to moments caused by the application of lateral loads. Figure 3 presents the failure pattern of skirted footing with varying skirt depth when subjected to lateral loads. Results indicate sliding failure predominates during small length of skirts and with an increase in length of skirts moment also comes into play (Table 2).

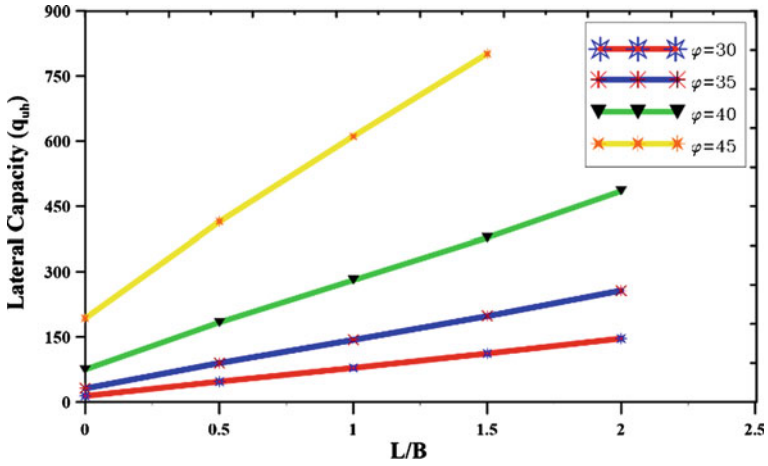

Fig. 2 Variation of lateral load capacity with length of skirts

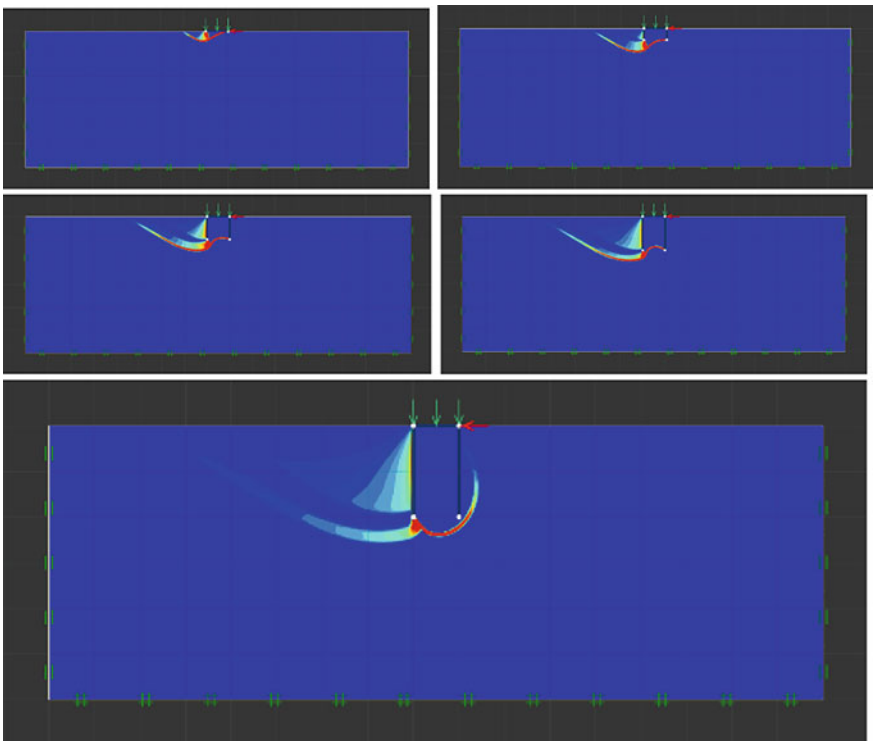

Fig. 3 Failure patterns for $\varphi = 30^{o}$ with varying skirt lengths

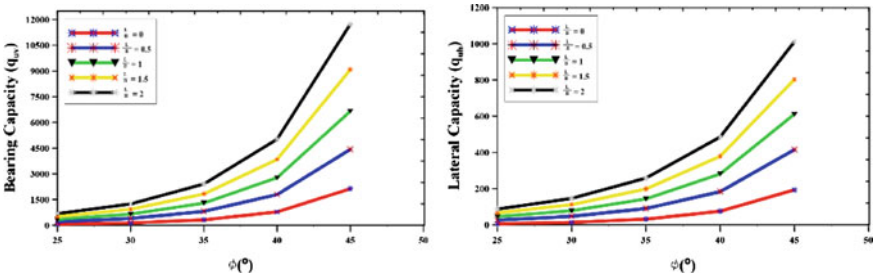

Fig. 4 Variation of bearing capacity and lateral capacity with angle of shearing resistance

3.2 Effect of Angle of Internal Friction

The effect of the angle of internal friction of soil on the bearing capacity is presented in Fig. 4. In addition to the surface footing, the results are presented for the skirted footing with varying skirt depth. For a particular skirt length, the bearing capacity increases with an increase in the friction of the soil. Furthermore, the increase in the bearing capacity is varying with the length of skirts, and this variation is depending significantly on the angle of friction. The increase in the bearing capacity with an increase in the friction angle of soil is higher for angle of friction greater than 35. In comparison to the soil with a low internal friction angle, the pressure is distributed over a relatively large area in the case of soils with higher friction angle. To mobilize the strength of the soil thoroughly, the footing resting on the dense sand requires a relatively large area. In the loose sands, the failure is either a local shear failure or a punching shear failure, and in both cases, the footing sinks without affecting the surrounding area. Similar to the present study, almost all previous studies also found that the bearing capacity increases with the increase in the angle of shearing resistance or the relative density of the soil. Figure 5 presents the failure pattern of skirted footing with varying skirt depth when subjected to vertical loads.

3.3 Effect of Embedment Depth of Footing

Table 3 represents the comparison between the bearing and lateral load capacities of strip and skirted footing with the same embedment. The results are presented for strip footing at same embedment as the length of skirts.

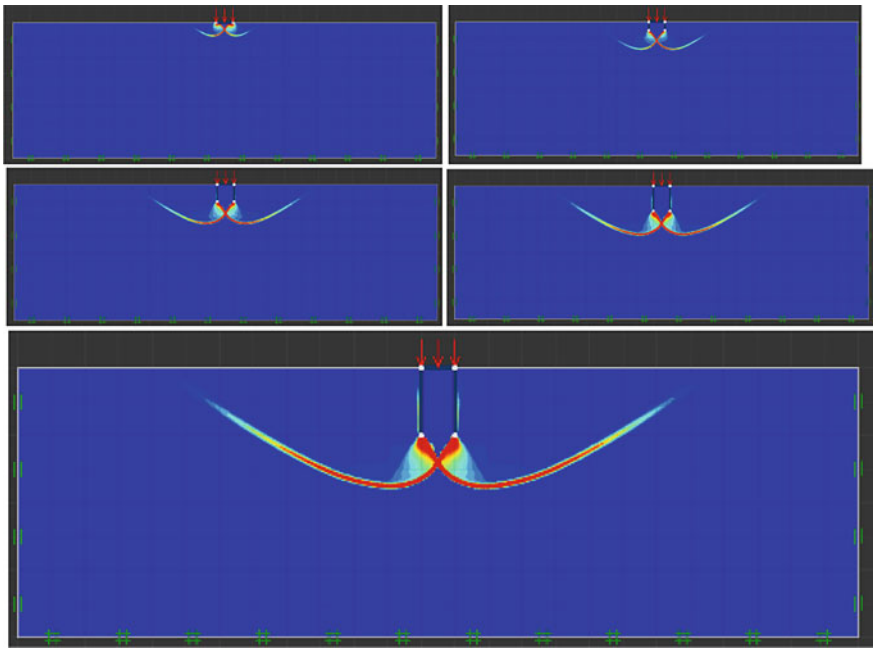

Fig. 5 Bearing capacity failure patterns for $\varphi = 30°$ with varying skirt length

Table 3 Comparison between the bearing and lateral load capacities of the strip and skirted footing with the same embedment

Embedment (D/B)	Bearing capacity		Lateral capacity	
	Strip footing (kN)	Skirted (kN)	Strip footing (kN)	Skirted (kN)
0.5	396.76	393.84	48.86	46.98
1	576.72	579.94	87.43	76.12
1.5	747.7	754.7	129.04	102.21
2	944.69	936.75	178.42	127.51
0.5	396.76	393.84	48.86	46.98

4 Conclusions

The study was carried out to understand the effect of skirts on the lateral capacity of skirted footing resting on cohesionless soils. The lateral-capacity for a skirted foundation was determined using an limit analysis for various soil-friction angles and skirt lengths. The lateral carrying capacity of skirted footing increases with increase in the length of skirts. The percentage increase is highest for small skirt lengths and for all internal friction angles of the soil. Further the lateral capacity increases with the increase in the angle of shearing resistance due to more area

taking part in mobilizing the shear strength. The deformation of sand underneath the skirted foundation is also investigated up to the failure. The mode of failure changes from sliding to rotational with the increase in length of skirts. The failure surface of footing without skirts is just below the foundation base and fails by sliding failure.

Acknowledgements The authors are grateful to Optum Computational Engineering (OptumCE) for providing a free academic license to perform the present study.

References

1. Bransby MF, Randolph MF (1998) Combined loading of skirted foundations. Geotechnique 48(5):637–655
2. Byrne BW, Houlsby GT (2002) Experimental investigations of the response of suction caissons to transient vertical loading. J Geotech Geoenviron Eng 128(11):926–939
3. Dewoolkar MM, Hwang J, Ko HY (2008) Physical and finite element modeling of lateral stability of offshore skirted gravity structures subjected to iceberg impact load. Ocean Eng 35(16):1615–1626
4. Gourvenec S, Randolph MF (2010) Consolidation beneath skirted foundations. Int J Geomech 10(1):22–29
5. Tani K, Craig WH (1995) Bearing capacity of circular foundations on soft clay of strength increasing with depth. Soils Found 35(4):21–35
6. Bransby MF, Randolph MF (1999) The effects of embedment on the undrained response of caisson foundations to combined loadings. Soils Found 39(4):19–34
7. Hu Y, Randolph MF, Watson PG (1999) Bearing response of skirted foundation on nonhomogeneous soil. J Geotech Geoenviron Eng, ASCE 125(11):924–935
8. Al-Aghbari MY, Mohamedzein YE-A (2004) Bearing capacity of strip foundations with structural skirts. J Geotech Geol Eng 22(1):43–57
9. Yun GI, Bransby MF (2003) Centrifuge modelling of the horizontal capacity of skirted foundations on drained loose sand. In: Proceedings, British geotechnical association international conference on foundations (ICOF), Dundee, UK. Thomas Telford
10. Watson PG, Randolph MF (1998) Skirted Foundations in Calcareous Soil. Geotech Eng J Proc Inst Civ Eng 131:171–179
11. Krabbenhoft K (2017) OptumG2:materials. Optum Comput Eng. www.optumce.com
12. Abramson LW, Lee TS, Sharma S, Boyce GM (2001) Slope stability and stabilization methods, 2nd edn. John Wiley & Sons, Hoboken, NJ
13. Bromhead E (2005) The stability of slopes. Taylor and Francis, London
14. Changwei Y, Jingyu Z, Jing L, Wenying Y, Jianjing Z (2017) Slope earthquake stability. Springer, Singapore

A Case Study of Las Palmas Tailings Dam Failure

T. S. Aswathi, Ravi S. Jakka, and David Frost

Abstract The increasing demand for minerals and their subsequent mining causes tailings to be produced in large amounts. Hence, tailings dams have increased in number as well as height to accommodate more storage capacity. Failure of these structures is dangerous with respect to toxic exposure, landslides, liquefaction, etc. In this study, the possible failure mechanisms of the Las Palmas tailings dam, which failed following the 2010 Maule, Chile earthquake, have been examined. Numerical simulation of the dam is carried out using the GeoStudio package to assess the condition of the dam during this seismic event and a pseudo-static analysis is carried out. The strong ground motion of the 2010 Maule, Chile earthquake recorded at three of the stations near the dam site was used as input since there is no record available at the tailings dam site. Slope stability analysis is performed to understand the possible failure mechanism. The Mohr–Coulomb failure criterion is used to define the material properties. Furthermore, the simulation results are compared with the final dam failure scenario.

Keywords Tailings dam · Earthquake · Slope stability · Pseudo-static analysis

1 Introduction

Tailings are the by-product of the mining industry from the mineral extraction process. Normally, the particle size distribution of tailings varies from medium sand to silt and clay size. These by-products in the form of slurry are transported to

T. S. Aswathi (✉) · R. S. Jakka
Department of Earthquake Engineering, IIT Roorkee, Roorkee 247667, India
e-mail: as@eq.iitr.ac.in

R. S. Jakka
e-mail: ravi.jakka@eq.iitr.ac.in

D. Frost
School of Civil & Environmental Engineering, Georgia Institute of Technology, 790 Atlantic Drive, Atlanta, GA 30332, USA
e-mail: david.frost@ce.gatech.edu

T. G. Sitharam et al. (eds.), *Earthquakes and Structures*, Lecture Notes in Civil Engineering 188, https://doi.org/10.1007/978-981-16-5673-6_6

a disposal area through pipelines. There are different disposal techniques such as sub-aerial discharge, subaqueous discharge and thickened discharge which can be used for distributing the slurry. In the process of distribution, the coarser particles settle close to the point of discharge, and the fine particles run down the beach into the pond and settle there. Tailings are generally stored in surface impoundments, which commonly consist of raised embankments. The raised embankment is generally constructed with either of the following raising methods: upstream, downstream or centerline [1]. Of the raised embankment construction, the downstream method is the most stable construction [2, 3, 1].

With an increase in mineral extraction annually, the tailings containing toxic chemicals that are harmful to the environment are produced hugely in large quantities. Therefore, it is necessary to store the tailings in an environmentally safe and economical way. In order to contain the increased amounts of tailings, the height of the tailings has to be increased. With increasing tailings height, there is a risk of tailings dam failure [4–7, 3, 8, 9]. The main concern with a tailings dam is the stability during the mining operation and after its closure. From the studies, it is seen that a total of 198 tailings dam failure has occurred before the year 2000, about 20 failure cases between the years 2000 and 2010 [4] and 11 other cases from 2010 to 2015 [10]. According to these statistical results, the rate of failure of tailings dams is estimated to be 1.2%, which is more than the failure rate of conventional water retention dams which is about 0.01% [4, 11]. The high failure rate of tailings dams has led to increasing awareness of the need for enhanced safety in the design and operation of tailings dams.

In this paper, the stability of the Las Palmas tailings dam under the February 27, 2010, Maule, Chile earthquake is studied. This earthquake is the sixth-largest recorded earthquake since 1900 and occurred at 3:34 am local time with a moment magnitude of 8.8 with its epicenter of the coast of Bio Bio, Chile. The hypocenter is located at an approximate depth of 35 km (21.7 miles) at about 95 km (60 miles) off the coast and 335 km (210 miles) southwest of the capital of Santiago. The Las Palmas tailings dam contains the tailings from a gold mine operated between 1981 and 1997. The tailings dam was constructed in four stages during the operation span of the mine. During the earthquake the tailings dam became unstable and the flow slide happened. The failed tailings traveled approximately 500 m. The collapse of the dam caused the death of 4 people living nearby. The sand boils in the tailings indicated liquefaction failure (Villavicencio 2014).

2 Methodology

The analysis was carried out using the GeoStudio package (SLOPE/W) with the model being made with respect to the longitudinal cross-section of Las Palmas tailings dam (Fig. 1). In this paper to distinguish the slopes in the dyke of tailings with ease, three terms were introduced, namely upstream dyke, downstream dyke and middle dyke. The two dykes constructed using the upstream method of construction

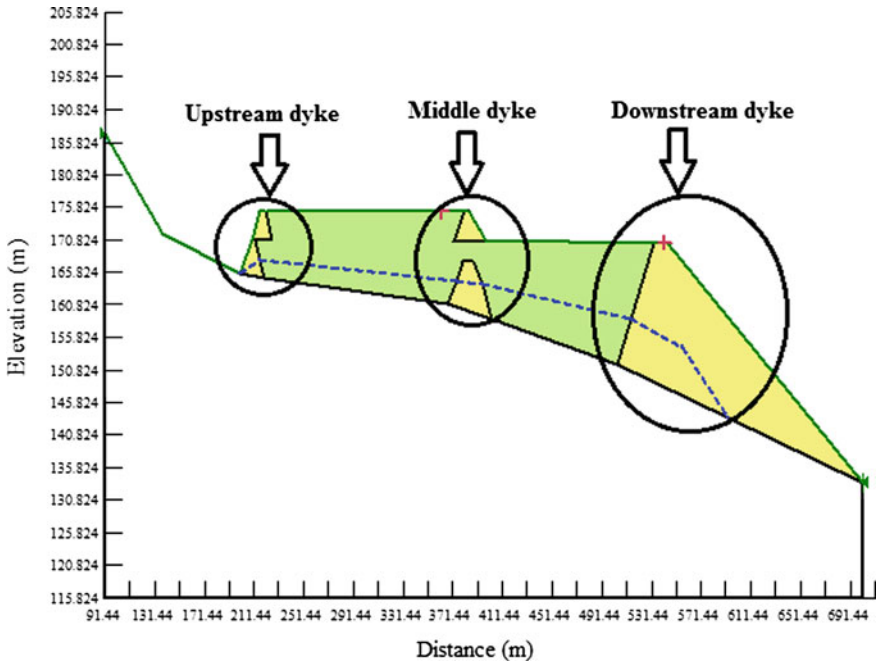

Fig. 1 Cross-sectional view of Las Palmas tailings dam (Note: The horizontal and vertical scales are different)

in the left-hand side of the cross-section are referred to as upstream dykes. Likewise, on the right-hand side, the dykes constructed using the downstream method of construction are referred to as downstream dykes. Similarly, in the middle of the cross-section, the dykes constructed similar to the centerline method of construction (but there were tailings between the two dykes) are referred to as middle dykes (Fig. 1).

In order to study the dynamic response of the tailings dam, a pseudo-static method is used. The pseudo-static method is an extension of the static slope stability method. The inertial forces created during earthquake shaking are represented using seismic coefficients in this process. These inertial forces are disintegrated into vertical (F_v) and horizontal (F_h) components. Hence, the two seismic coefficients are horizontal seismic coefficient (k_h) and vertical seismic coefficient (k_v). The selection of an appropriate seismic coefficient is the most important, and difficult, aspect of a pseudo-static stability analysis.

In theory, the seismic coefficient k_h is taken as PGA recorded at different stations though typically it is taken as 1/3 to 1/2 of crestal acceleration. Due to the unavailability of studies on crestal amplification, this assumption of seismic coefficient equal to recorded PGA is taken in order to take into account the crestal amplification. Here, the seismic coefficients are considered by dividing the peak ground acceleration by gravity. As with any other slope stability analysis, slope/w considers a possible slip

surface and divides the failure mass into slices. The seismic coefficients are used to calculate the forces created by the earthquake (Fig. 2). Then the overall equilibrium computation for the individual slices composing the failure surface is done.

For doing this, initially the model is prepared by drawing the cross-section of the dam. Then defining the material properties using the Mohr–Coulomb failure criteria (Table 2),the water table is defined approximately from SPT bore logs given in [12]. The stability analysis is carried out using Morgenstern–Price method and for the pseudo-static analysis additionally seismic coefficients (Table 1) are inputted. As there were no earthquake records for the tailings site, three nearby stations Curico, Talca and Hualane stations (Fig. 3) were taken for the study. Then the analysis is run, the minimum factor of safety obtained from possible slip surfaces are considered as a critical factor of safety and it is stated in the result section (Fig. 4).

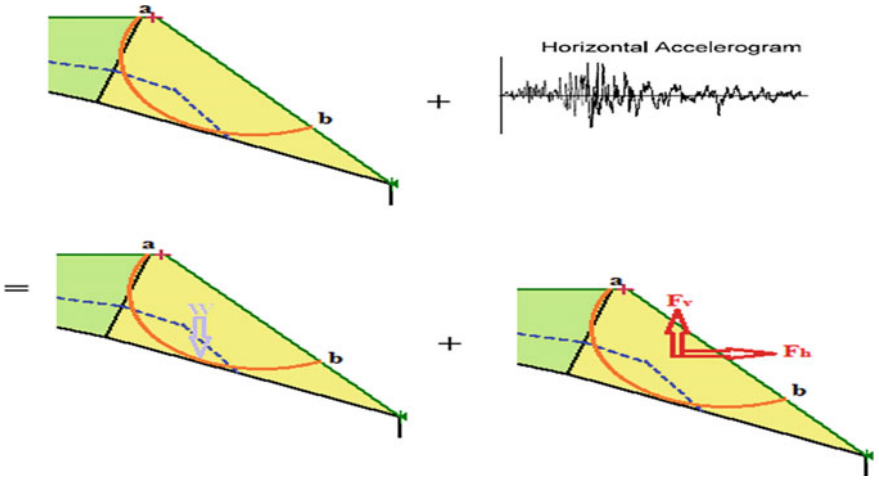

Fig. 2 Pseudo-static procedure illustration considering downstream dyke

Table 1 Stations and their corresponding PGA and k_h values

Station	PGA (cm/s^2)	k_h
Curico	461.07	0.47
Hualane	382.59	0.39
Talca	470.88	0.48

Table 2 Material properties considered in the study

Material type	Phi, ∅°	Cohesion (in kN/m^2)	Unit weight (in kN/m^3)
Containment wall	26	23.9	15.7
Tailings	10.5	11.97	14.9

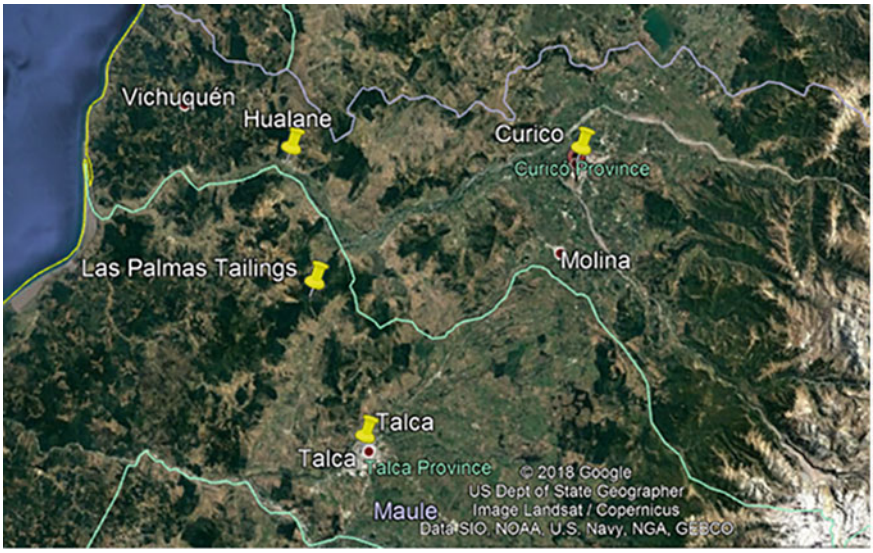

Fig. 3 Location of Las Palmas tailings dam along with Curico, Talca and Hualane stations

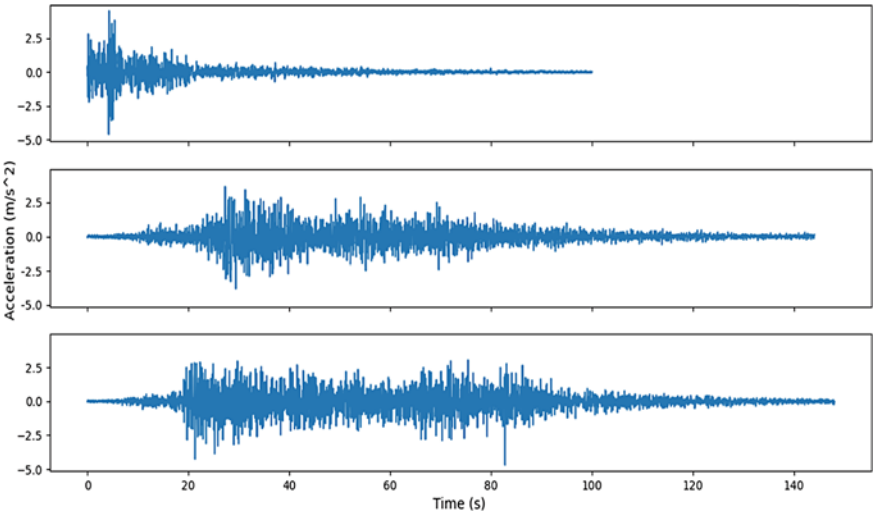

Fig. 4 Time history records at Curico, Hualane and Talca stations

3 Results and Discussion

The analysis was carried out in the following way: first, the static slope stability and then the seismic slope stability using the pseudo-static method. The pseudo-static analysis has been carried out for the motions which are recorded at three nearby

stations to the tailings dam. This was done as there was no strong motion record recorded on the site. As the effect of the vertical seismic coefficient is negligible, only horizontal seismic coefficients are considered for this study. Table 1 gives the PGA and horizontal seismic coefficients of the three stations. Figure 5 shows that the factor of safety in the middle and downstream dyke are 2.325 and 1.472, respectively, indicating the tailings dam is stable under static conditions. Figure 6 shows that the factor of safety corresponding to the seismic coefficients 0.47, 0.39 and 0.48 in the downstream dyke are 0.806, 0.846 and 0.796, respectively. And Fig. 7 shows that the factor of safety corresponding to the seismic coefficients 0.47, 0.39 and 0.48 in the middle dyke are 0.935, 1.061 and 0.922, respectively.

From Table 3, it is seen that there is a decrease in stability under earthquake loading. Further, the pseudo-static factor of safety is less than one in all the cases for the downstream dyke, i.e., it is unstable during earthquakes, whereas the middle

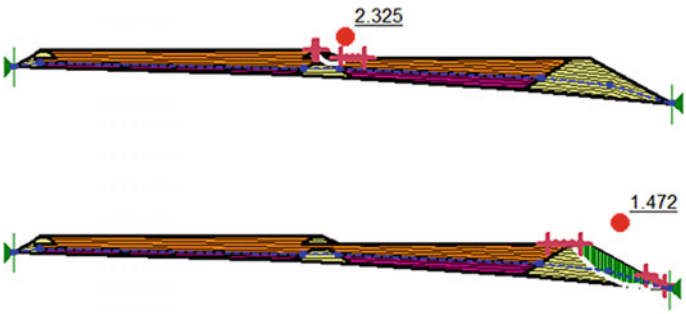

Fig. 5 The static slope analysis of Las Palmas tailings dam before an earthquake

Fig. 6 The Pseudo-static factor of safety of downstream dyke corresponding to horizontal seismic coefficients of 0.47, 0.39 and 0.48

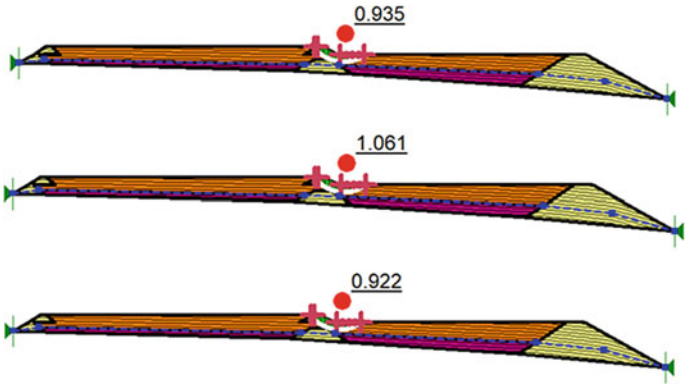

Fig. 7 The Pseudo-static factor of safety of middle dyke corresponding to horizontal seismic coefficients of 0.47, 0.39 and 0.48

Table 3 Factor of safety of dykes at different conditions

Condition	Middle dyke	Downstream dyke
Static	2.325	1.472
Pseudo-static for k_h 0.47	0.935	0.806
Pseudo-static for k_h 0.39	1.061	0.846
Pseudo-static for k_h 0.48	0.922	0.796

dyke is more stable in the static as well as pseudo-static cases when compared to that of downstream dyke. However, the factor of safety is around one (slightly more or less than one) indicating that a slight increase in seismic force is enough to make the middle dyke unstable.

4 Summary and Conclusions

Las Palmas tailings dam was built from a gold mine operated between 1981 and 1997. It was constructed in four stages. All three types of raised construction have been used in the construction of this tailings dam. In the middle dyke, there is a layer of tailings because of stage 3 and stage 4. This layer happens to be the weak layer. Many literature points this to cause the failure of the middle dyke. In this paper, the Las Palmas tailings dam stability during the Maule, Chile earthquake is studied using pseudo-static analysis.

The following conclusions are drawn from the study. The tailings dam is stable under static conditions. However, the pseudo-static analysis representative of stability under earthquake indicates that the dam is unstable under the Chile earthquake. The slope stability of the middle dyke is more in the case of both the static as well as pseudo-static cases when compared to the downstream slope. This proposes the

mechanism that the downstream dyke failed first and then the middle dyke during the earthquake. Upon the failure of the downstream dyke, the contained tailings flowed down which further triggered the failure of the middle dyke, that is, the flow failure occurred.

References

1. Vick SG (1983) Planning, design, and analysis of tailings dams. Wiley, New York
2. Jakka RS, Ramana GV, Datta M (2011) Seismic slope stability of embankments constructed with pond ash. Geotech Geol Eng 29(5):821–835
3. Psarropoulos PN, Tsompanakis Y (2008) Stability of tailings dams under static and seismic loading. Can Geotech J 45(5):663–675
4. Azam S, Li QR (2010) Tailings dam failures: a review of the last one hundred years. Geotech News 28(4):50–53
5. Davis MP (2002) Tailings impoundment failures: are geotechnical engineers listening? Geotechnical News, BiTech Publishers, Richmond, BC, Canada, pp 31–36
6. Ferdosi B, James M, Aubertin M (2015) Investigation of the effect of waste rock inclusions configuration on the seismic performance of a tailings impoundment. Geotech Geol Eng 33(6):1519–1537
7. Ferdosi B, James M, Aubertin M (2015) Numerical simulations of seismic and post-seismic behavior of tailings. Can Geotech J 53(1):85–92
8. Klohn EJ (1997) Tailings dams in Canada. Geotechnical news. BiTech Publishers, Richmond, BC, Canada, pp 117–123
9. Rico M, Benito G, Salgueiro AR, Díez-Herrero A, Pereira HG (2008) Reported tailings dam failures: a review of the European incidents in the worldwide context. J Hazard Mater 152(2):846–852
10. WISE (World Information Service on Energy) (2015) Chronology of major tailings dam failures. www.wise-uranium.org/mdaf.html
11. ICOLD (International Commission on Large Dams) (2001) Tailings dams—risk of dangerous occurrences—lessons learnt from past experiences. Commission Internationale des Grands Barrages, Paris
12. Moss RES, Gebhart TR, Frost DJ, Ledezma C (2019) Flow-failure case history of the Las Palmas, Chile, Tailings Dam. PEER Report No. 2019/01

Soil-Structure-Interaction Study and Safety Assessment of Ventilation Stack for Extreme Wind Events

Soumalya Das, Shrikant D. Mishra, R. N. Sarangi, Raghupati Roy, and Arvind Shrivastava

Abstract Ventilation Stack structure of a typical Nuclear Power Plant (NPP) is analysed and designed for a design basis wind velocity corresponding to 1000 years return period. Subsequent to the Fukushima Event, as a part of safety assessment of NPP structures, assessment of structural integrity of stack structures has been taken up against extreme natural events i.e., beyond design basis wind loading in both along and across wind direction using non-linear. In the present work, detailed Soil-Structure-Interaction (SSI) analysis of typical stack structure of NPP modeled as 3D finite element along with soil has been carried out in Abaqus software under sustained plus along and across wind load corresponding to extreme wind condition. Mohr–coulomb plasticity model is used for continuum soil medium. Elasto-plastic behaviour of the raft-soil interface is simulated using Coulomb friction model available in Abaqus. Steel reinforcements have been introduced at relevant layers/sections of the stack. Transverse shear deformation in element formulation and geometric non-linearity due to large deformation has been considered during the analysis. Non-linear analysis with detailed material characterization and failure models for both concrete and reinforcement has been carried out for a realistic estimation of post-cracking margins and to understand the non-linear behaviour of the stack at various load steps. This paper presents the analysis methodology for safety assessment of wind sensitive stack structures against beyond design basis wind with due consideration to SSI effects. The analysis procedures, material models adopted for the analysis, etc. and the analysis results under extreme wind have been discussed in this paper. Based on the results of the nonlinear analysis safety margin with respect to beyond design basis wind speed has been established.

Keywords Soil-Structure-Interaction · Along and across Wind · Elasto-plastic · Mohr–Coulomb Plasticity · Non-linear Analysis

S. Das (✉) · S. D. Mishra · R. N. Sarangi · R. Roy · A. Shrivastava
NPCIL, Mumbai, India
e-mail: soumalyadas@npcil.co.in

T. G. Sitharam et al. (eds.), *Earthquakes and Structures*, Lecture Notes in Civil Engineering 188, https://doi.org/10.1007/978-981-16-5673-6_7

1 Introduction

Safety is the ultimate objective in the process of design, construction and operation of Nuclear Power Plants (NPPs). It is given the prime importance as it has to sustain all environmental, accidental and human-induced loads under all operating conditions. Defence-in-depth approach is embedded as safety philosophy in the entire plant engineering so that multiple barriers protect the release of radioactivity in an event of nuclear accident inside the containment. Consequent to the Beyond Design Basis Events (BDBE), i.e., Extreme Earthquake Event (EEE) and subsequent Tsunami, that affected Fukushima Nuclear Power Plants (NPP); it was required to evaluate the safety of NPPs under similar conditions. For evaluation of safety of NPPs against extreme natural events beyond design basis; consideration of site specific postulated scenarios for each of the extreme natural events viz., Earthquake, Tsunami, and Wind has been emphasized. Ventilation stack being the wind-sensitive structure is required to remain functional during BDBE and the collapse of the same may endanger the functionality of the surrounding buildings supporting essential systems required under beyond design basis condition. In this paper assessment of structural integrity of ventilation stack structures has been taken up against extreme natural events beyond design basis wind using non-linear analysis in Abaqus software. As a first order estimate, the beyond design basis wind speed have been estimated to the one corresponding to 1000 years return period wind increased by 50% and rounded off to nearest 10 m/s speed. In the present analysis, site specific beyond design basis wind speed value considered is 100 m/s.

Detailed Soil-Structure-Interaction (SSI) analysis of typical ventilation stack structure of NPP has been carried out under sustained plus along and across wind load corresponding to extreme wind condition. The ventilation stack is modeled as 3D reinforced concrete shell element along with the 3D solid element of soil. Mohr–coulomb plasticity model is used for simulating the behaviour of soil medium. The initial state of stress in the soil is modeled by activating the geo-static step. The interface behaviour of raft and soil (frictional force vs. relative displacement) is simulated using Coulomb friction model available in Abaqus [1]. The unbounded or infinite soil medium is approximated by extending the finite element mesh to a far distance, where the influence of the surrounding medium on the region of interest is considered small enough to be neglected. Steel reinforcements have been introduced at relevant layers/sections of the stack. Transverse shear deformation in element formulation and geometric non-linearity due to large deformation has been considered to account for changes in geometry during the analysis. Non-linear analysis with detailed material characterization and failure models for both concrete and reinforcement has been carried out for a realistic estimation of post-cracking margins and to understand the non-linear behaviour of the stack at various load steps under beyond design basis wind speed. This paper presents the analysis methodology for safety assessment of wind sensitive stack structures against beyond design basis wind with due consideration to SSI effects. The analysis procedures, material models adopted for the analysis, etc. and the analysis results of a typical ventilation stack under extreme wind have

been discussed in this paper. Based on the results of the nonlinear analysis safety margin with respect to beyond design basis wind speed has been established.

2 Development of Integrated Finite Element Modeling of Stack and Soil Medium

Developing the integrated finite element model involves geometric and finite element modeling of stack and soil medium.

2.1 Finite Element Modeling of Stack and Soil Medium

The ventilation stack structure consists of a reinforced concrete (RC) shell and RC raft foundation. Stack is modelled as 3D finite element (FE) along with raft and opening for underground ventilation tunnel on north face. The ventilation stack is 140 m above ground level. The cylindrical shell is rigidly connected at base with the annular raft foundation. The outer and inner diameters of annular raft foundation are 24 m and 8 m respectively. Opening of size 2.2 m wide and 1.8 m deep is made in the shell for taking the underground ventilation tunnel provided to carry the exhaust duct into the stack. Stack is divided into different sections to account for variation of thickness of RC shell structure of stack varying linearly from bottom to top. Steel reinforcements have been introduced at relevant layers/sections of the element. Reinforcement in stack has been modelled as a smeared layer with a constant thickness equal to the area of each reinforcing bar divided by the reinforcing bar spacing. Quadrilateral four noded shell elements are used for modeling the ventilation stack. Nine integration points are used in thickness direction of the shell help in tracing the progress of cracks through the depth of the shell. Transverse shear deformation is considered in the element formulation by assuming that the normal to the mid-surface of the element remains straight but not necessarily normal during deformation. Geometric non-linearity due to large deformation has been considered to account for changes in geometry during the analysis. 3D geometric and FE model of stack is shown in Fig. 1. The founding media of site considered in the present analysis is soft alluvium. The annular raft of stack is founded on alluvium soil which has been modelled using combination of 3D solid tetrahedral and wedge element. 3D geometric and FE model of soil medium is shown in Fig. 2. The geometric and FE model of the ventilation stack along with the soil medium is shown in Fig. 3.

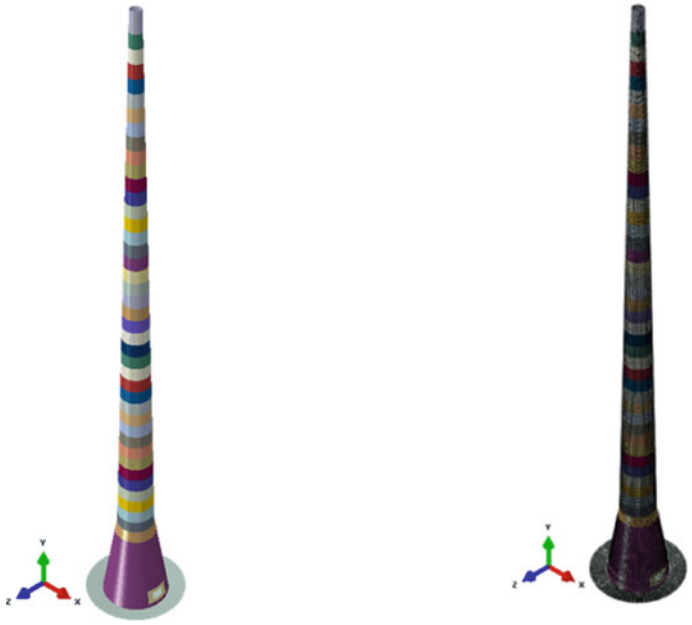

Fig. 1 Geometric and Finite Element Model of Stack

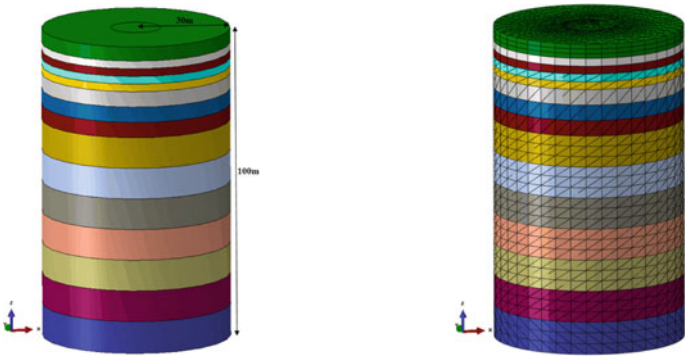

Fig. 2 Geometric and Finite Element Model of Soil Medium

2.2 Elasto-Plastic Constitutive Relationship for the Soil Medium

In the present work, Mohr–coulomb plasticity model is used for simulating the behavior of soil medium. The Mohr–Coulomb criterion considers that failure is controlled by the maximum shear stress and that this failure shear stress depends on the normal stress. The Mohr–Coulomb failure line is the best fit straight line that

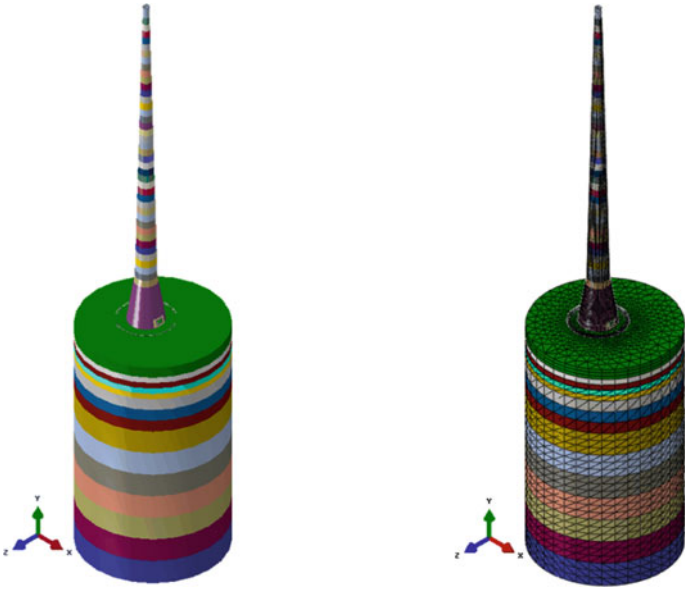

Fig. 3 Geometric and Finite Element Model of Stack Along with Soil Medium

touches the Mohr's circles.

$$\tau = \mathrm{c} + \sigma \tan\phi \tag{1}$$

where, τ is the shear strength, σ is the normal stress, c is the cohesion and ϕ is the angle of internal friction.

2.3 Simulation of In-Situ Stress State

The initial state of stress in the soil is considered to be geo-static in nature. The geostatic stress condition means that at any point of time, soil is subjected by vertical stress, $\sigma_z = \gamma \times h$, and lateral stress, $\sigma_L = k_0 \times \gamma \times h$, where γ is the density of soil, h is depth and k_0 is the lateral coefficient of earth pressure at rest. It is required to consider this initial state of stress in the soil before application of the load to structure. The value of k_0 is specified as follows:

$$k_0 = 1 - \sin\phi \tag{2}$$

2.4 Modeling of Semi-Infinite Soil Medium

The unbounded or infinite soil medium can be approximated by extending the finite element mesh to a far distance, where the influence of the surrounding medium on the region of interest is considered small enough to be neglected. This approach calls for iteration with mesh sizes and assumed boundary conditions at the truncated edges of the mesh and the same approach is used for finalizing the extent of boundary of soil medium. This process of finalization of boundary is problem specific. In the present work, finite element model of soil medium of 60 m diameter and 100 m depth has been considered based on the iterative analysis wherein effect of the boundary condition is not observed.

In all the cases, *x* (North–South), *y* (East–West) and *z* (vertical) translations at the bottom of the soil are not allowed. Similarly, *x*-translation is not allowed in *yz* plane of soil, and *y*-translation is not allowed on *xz* plane of soil.

2.5 Modeling of Contact Zones (Raft-Soil Interface)

The soil-structure interaction analysis requires considerations of the interaction or coupling between the structure and the founding media. When stack is subjected to wind loading, raft interacts with the soil. Hence, for simulating normal and tangential behavior of the interface between raft and soil, Coulomb friction model available in Abaqus has been utilized for raft-soil interaction.

Tangential Behaviour: The interface behavior of the raft and soil (Frictional force vs. relative displacement) is pictorially shown in Fig. 4. The interaction behavior is divided into two parts (a) Sticking phase and (b) Slipping phase. Initially, during the sticking phase, raft-soil interface allows some relative motion (elastic slip) between the raft and the soil surface. Once the induced shear stress between the raft and soil reaches the critical shear stress, the interface enters in the slipping phase. The above sticking and slipping phase of the raft-soil interface is simulated using elastic coulomb friction model. In this model, the critical shear stress (τ_{crit}) is defined as:

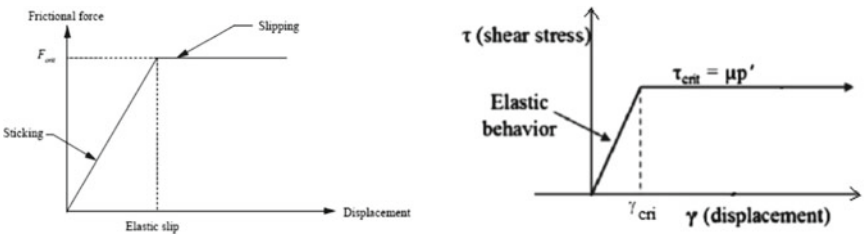

Fig. 4 Raft soil interface behavior (Tangential Direction)

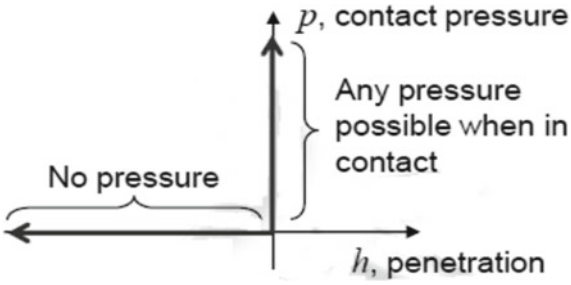

Fig. 5 Behavior of raft-soil interface in normal direction

$$\tau_{\text{crit}} = \min\left(\mu p', \tau_{\max}\right) \tag{3}$$

Normal Behaviour: Normal contact pressure develops, when raft moves vertically towards the soil. Under such situation, area of the raft, which is in contact with soil, will develop normal stress. This phenomenon is simulated in the analysis using relationship as shown in Fig. 5.

To model the contact property between the raft and soil surface material, it is essential to obtain the friction factor (μ), maximum shear stress (interface shear strength, $\tau_{\max}$) and elastic slip (γ_{crit}) values. The design value of the friction or adhesion below the raft and walls to be mobilized at an interface with the structure is usually considered as 75% of the design shear strength to be mobilized in the soil itself [2]. Values of friction factor considered as:

$$\mu = 0.75 * \tan\phi \tag{4}$$

The design value of strength to be mobilized below the raft and walls to be an interface with the structure is usually considered as 75% of the design shear strength of the soil itself [2]. The design interface shear strength is:

$$\tau_{\max} = 0.75 * \left(c + \sigma' \tan\phi\right) \tag{5}$$

An elasto-plastic model is used to define the behavior of the interface for the modeling of soil-structure interaction. The above-mentioned criterion is used to distinguish between elastic and plastic interface behavior. For the interface to remain elastic the shear stress τ is given by:

$$\tau < \tau_{\max} \tag{6}$$

The minimum slip required for the full mobilization of frictional resistance is known as critical slip (γ_{crit}). The default value given in Abaqus is used in the present study.

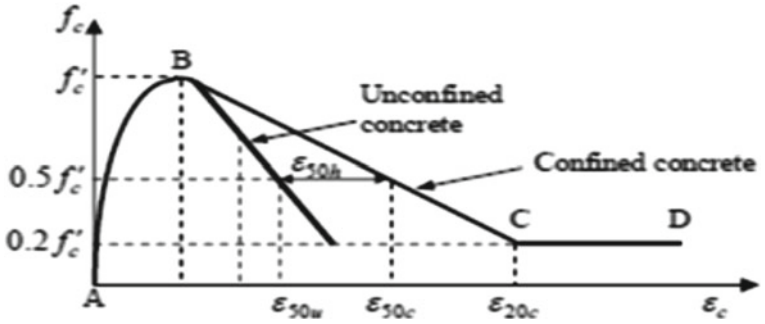

Fig. 6 Stress–strain behaviour of concrete under compression

3 Material Model

The concrete damage plasticity model is used for concrete reinforcement in the present nonlinear analysis. The material model is a continuum, plasticity-based, damage model for concrete. It assumes that the main two failure mechanisms are tensile cracking and compressive crushing of the concrete material. Kent and Park Model have been used to consider the stress strain behaviour of concrete under compression. The material model in tension as suggested in Japanese codes JSCE JGC-15 has been considered for concrete. The grade of concrete considered in the analysis is M20 and for steel is FE415.

3.1 Stress–Strain Behaviour of Concrete Under Compression (Kent & Park Model)

Kent and Park proposed a stress–strain curve for concrete confined by rectangular hoops as shown in Fig. 6. A second-degree parabola represents the ascending part of curve and assumes that the confining steel has no effect on the shape of this part of curve or the strain at maximum stress. This essentially means that the ascending curve is exactly the same for both confined and unconfined concrete. It is also assumed that the maximum stress reached by confined concrete is equal to the cylinder strength f_c, that is reached at a strain of 0.002.

3.2 Stress–Strain Behaviour of Concrete Under Tension (JSCE JGC15)

The material model in tension as suggested in Japanese codes JSCE JGC15 [3] has been considered for concrete. Fracture Energy (G_f) based approach is adopted

for simulating tension in concrete. The crack width is treated as displacement perpendicular to the direction of crack and the same is correlated with the tensile stress.

3.3 Material Model for Reinforcement Steel

A linear elastic and plastic hardening behaviour is assumed for the reinforcing steel. The grade of steel considered is FE415.

3.4 Soil Properties

The founding media of site considered in the present analysis is soft alluvium. Linear variation of static modulus of elasticity of different soil layers has been considered in the present analysis. Since, Mohr–Coulomb model has been used for defining the failure criteria of soil, values of cohesion 'c' and internal friction 'ϕ' used in the analysis are obtained from soil testing at the alluvium soil site. The soil layering system below the foundation raft of stack is shown in Fig. 2. As suggested in literature for sandy soil [4], dilation angle, $\Psi = \phi - 30$ has been considered for all soil layers.

4 Loading

Two types of loads are applied on stack to get the structural capacity against beyond design basis wind; i.e., constant load and variable load. Constant load consists of static earth pressure applied all along the periphery of stack towards inward direction and self-weight applied as gravity force; whereas, the variable load consists of combination of along wind load corresponding to beyond design basis wind speed and across wind load generated due to vortex shedding phenomenon.

4.1 Varying Load

Stack is designed to resist the wind forces in both the along-wind and across wind directions. The along wind load (mean plus fluctuating component of wind) per unit height of the stack at any level is calculated as per clause 4.2.2 of ACI 307–98 and is based on mean hourly wind (MHW). Fluctuating component of wind is based on gust factor and base bending moment due to mean wind. In the present analysis, site specific basic beyond design basis wind speed value considered is 100 m/s.

Across wind load on the stack is generated due to vortex shedding phenomenon. As per clause no. 4.3.2.2 of ACI 307–98 any method using the modal characteristics of the stack shall be used to estimate the across-wind response in the critical mode. Thus the equations given in clause A-5.3 of IS: 4998–1992 is used for calculating across-wind response in the critical mode of stack vibration. Calculation of across-wind load is made by first calculating the peak response amplitude at the specified mode of vibration (critical mode).

Combination of Along and Across Wind Load: As per clause no. 4.2.3.5 of ACI 307–98, across wind load is combined with the coexisting component of along wind load (mean component due to hourly mean wind).

$$M_w(z) = \left\{[M_a(z)]^2 + [M_1(z)]^2\right\}^{0.5}$$

where, $M_a(z)$ = moment induced by across-wind loads and $M_l(z)$ = moment induced by the mean component of along-wind load.

5 Analysis Methodology

Ventilation stack is analyzed to resist the wind forces in the along-wind directions. The along wind load consist of mean and fluctuating component of wind is computed at different elevations as per clause 4.2.2 of ACI 307–98 and are applied as equivalent nodal load uniformly at the respective location of nodes in the full perimeter. Further, stack is also analysed for a combination of along wind loads (mean or static component of wind load due to Hourly Mean Wind (HMW)) with across wind loads as per clause no. 4.2.3.5 of ACI 307–98.

The detailed SSI analysis of stack for BDB wind loading in ABAQUS is performed according to the sequence of applied loads, which has been defined in different steps. In the initial step boundary conditions are applied followed by geostatic step to simulate the in-situ stress in the soil medium. In the next step, sustained loading (i.e., self weight of stack and earth pressure) is applied along with BDB wind loading. Following two cases have been considered in the present analysis as given in Table 1 and shown in Fig. 7.

Table 1 Different cases considered in the analysis

S. no	Cases	Description
1	Case I	Along wind load (mean component) is applied in N–S direction and across wind load in E–W direction
2	Case II	Along wind load (consist of mean component due to HMW and fluctuating component due to gust) is applied in N–S direction

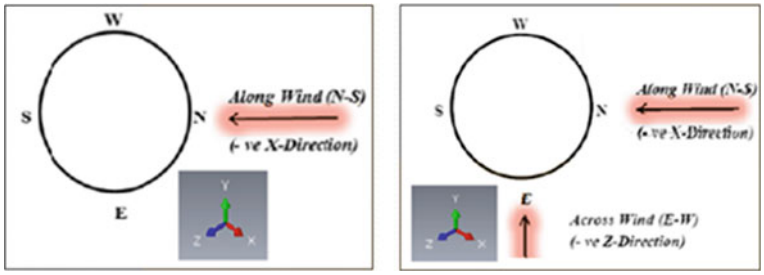

Fig. 7 Different cases considered in the analysis

Table 2 Failure criteria of stack under BDB wind loading

Failure criteria	Limits
Crushing of concrete	Strain of 0.02
Tearing of reinforcements	Strain of 0.05
Yielding of all layer of reinforcements	
Non-convergence due to high deformation and cracking	

6 Failure Criteria

Failure of reinforced concrete structure may be due to different mechanisms, such as crushing of concrete under compression, cracking of concrete, reinforcement tearing, etc. The limits of the different modes of failure of ventilation stack are considered to evaluate the structural capacity are presented in Table 2.

7 Results

7.1 Maximum Top Deflection of Stack

The maximum top deflections of stack for Case I is 1.07 m along N–S direction and 0.36 m along E–W direction. Similarly, the maximum top deflections of stack for Case II is 2.89 m along N–S direction and negligible along E-W direction.

7.2 Variation of Principal Strain in Inner and Outer Face of Concrete

The variation of principal strain at inner and outer face of concrete is shown in Fig. 8

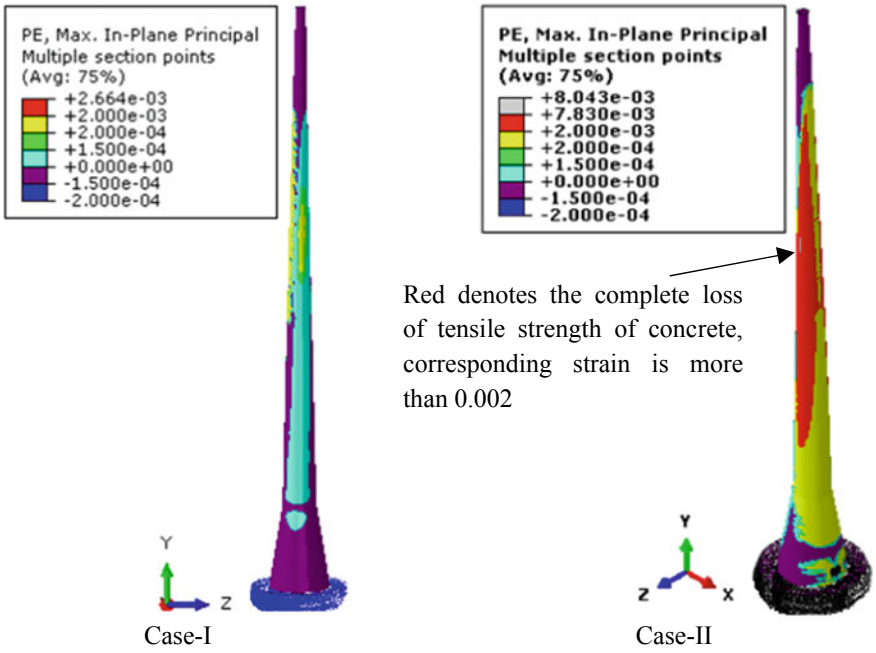

Fig. 8 Variation of principal strain in concrete at outer surface for Case I and Case II

for Case I and Case II. Here six colours are used to differentiate the type of strain. Red denotes the complete loss of tensile strength of concrete; the corresponding strain value is 0.002. Yellow is for tensile strain more than 0.0002 and green is for tensile strain more than 0.00015 (cracking strain). Cyan and blue denote compressive strain of concrete less and more than 0.00015, respectively. As per CEB-FIP model code the crack propagation of concrete starts at a strain of 0.00015. When each integration point along the thickness of concrete at any section reaches that strain, concrete is said to be through and through cracked in that section. Loss of complete tensile stress of concrete is considered in case of through and through cracking of concrete at strain 0.002 at each integration point along the thickness. The through and through cracking has been observed in a large portion at different elevation of stack.

7.3 Variation of Principal Stresses in Rebar Layer

The variation of maximum in-plane principal stress in outer vertical and horizontal rebar layer is shown in Fig. 9 for Cases I and II. The maximum in-plane principal stress observed in outer vertical rebar layer is 203 MPa for Case I and 356 MPa for Case II. Similarly, the maximum in-plane principal stress observed in inner rebar layer is 83 MPa for Case I and 200 MPa around opening for Case II.

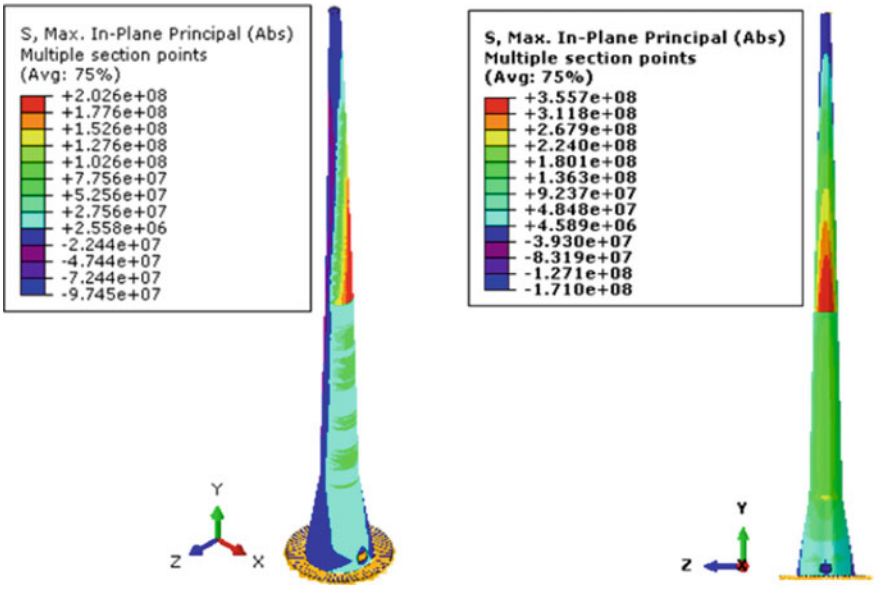

Case-I Case-II

Fig. 9 Variation of principal stress in outer rebar layer for Case I and Case II

7.4 Load-Deformation (P-Δ) Curve of Stack

The load-deformation (i.e., base shear vs. top deflection) curve of stack under BDB wind for two different cases is shown in Fig. 10.

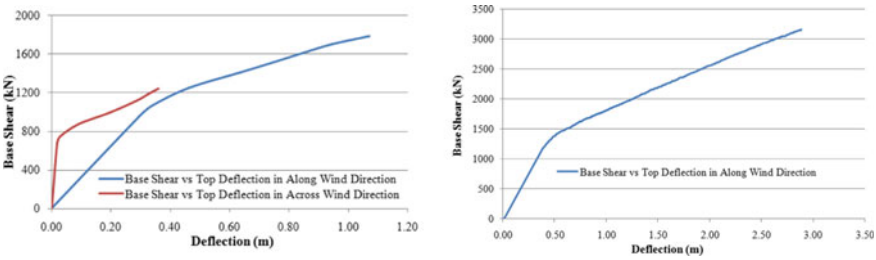

Case-I Case-II

Fig. 10 Load deformation curve of stack under BDB wind loading for Case I and Case II

8 Discussion and Conclusion

The analysis results are studied in terms of stresses and displacements. It is observed from the non-linear load–deflection curve that the response of stack is linear at initial steps, further, as cracking of concrete starts, then it behaves non-linearly. It has been observed that the distribution of stiffness degradation in stack becomes un-symmetrical at higher wind loading due to presence of the across wind load. This un-symmetrical distribution of stiffness degradation causes torsional deformation of the stack, due to which the component of the deformation in the along-wind direction reduces. This, in return, shows the pseudo-stiffening of the stack at higher wind load as observed in Fig. 10 of Case I. This effect is not observed if the stack is subjected to only along or only across wind load. The rebar stresses obtained is higher around 70 m height due to discontinuity in the rebar area. However, the maximum principal stresses in the rebar at outer and inner layer are within limit.

The structural strength and stiffness of the 140 m high ventilation stack is adequate to withstand the beyond design basis wind speed of 100 m/s without collapse and there exists sufficient margin even when subjected to wind loads higher than the beyond design basis wind.

Acknowledgements The authors are grateful to Executive Director (Engineering) and Director (Technical), NPCIL for their constant support and encouragement throughout the present work.

References

1. Abaqus 6.14, Analysis User's Manual
2. BS 8002–94: British standards institution, Code of practice for Earth retaining structures
3. JSCE JGC15 (2008) Japan Society of Civil Engineers Standards, Japan
4. Kowalska M (2014) Numerical study of the influence of dilatancy angle on bearing capacity and rotation of a gravity retaining wall. Paper No. 186, European Conference on Geotechnical Engineering (DECGE 2014), Vienna, Austria

Soil-Structure-Interaction Study of a Nuclear Structure Supported on Alluvium Soil and Estimation of Stiffness of Its Foundation System

Soumalya Das, Shrikant D. Mishra, R. N. Sarangi, Raghupati Roy, and Arvind Shrivastava

Abstract One of the proposed site in Northern part of India for twin unit 700MWe Nuclear Power Plant (NPP) (based on Indian PHWR) is founded on alluvial soil. Considering the founding medium of alluvial soil, the effect of the deformation of foundation, both total and differential, is required to be accounted for in the analysis/design of the structural system. Since the deformation of such founding media has direct bearing on the structural response, detailed analysis and design considering soil structure interaction effects for safety related structures supported on raft foundation system shall be carried out. In the analysis of raft foundation, the most important parameter is determination of exact contact pressure distribution underneath the raft, which is a complex function of rigidity of the superstructure, raft itself and the supporting soil. In this paper, detailed soil structure interaction analysis of typical safety related structure of NPP, modeled as 3D finite elements along with soil has been carried out using Abaqus software [1] for both vertical sustained and lateral loads (seismic loads with pseudo-static approach) using site-specific geotechnical parameters. Elasto-plastic behavior of the raft-soil interface is simulated using three parameter model i.e. elastic slip, maximum shear strength and frictional coefficient. Mohr–coulomb plasticity model is used for modeling continuum soil medium. This paper presents the methodology for estimation of stiffness's of raft foundation system under static condition and compares the same with conventional formulations for static springs as per Vesic's approach using modulus of subgrade reaction.

Keywords Soil-structure-interaction · Contact pressure · Elasto-plastic · Raft-soil interface · Mohr–Coulomb plasticity

1 Introduction

The structures, system and components (SCC) of a Nuclear Power Plant (NPP) are designed ensuring adequate safety of public, occupational workers and protection of

S. Das (✉) · S. D. Mishra · R. N. Sarangi · R. Roy · A. Shrivastava
NPCIL, Mumbai, India
e-mail: soumalyadas@npcil.co.in

T. G. Sitharam et al. (eds.), *Earthquakes and Structures*, Lecture Notes in Civil Engineering 188, https://doi.org/10.1007/978-981-16-5673-6_8

environment. Any safety related structure in a NPP is to be designed to have a very low probability of failure. Safety related structures in the Nuclear Island of a NPP are generally heavily loaded with a high stiffness of its structural members. In a NPP a number of system and components acts in tandem which requires various services (e.g. piping, cable trays) to move through different buildings. Determination of total and differential settlement at raft with due considerations to soil-structure-interaction effects becomes an important part of structural design to ensure safety of structure as well as other system and components. When the structure is founded on alluvium soil medium, this aspects becomes further more critical as these have a direct bearing on the development of stresses in the structural elements.

For analyzing the behaviour of raft foundation, correct evaluation of three basic parameters, i.e., rigidity of the raft, pressure distribution of the raft and value of sub-grade modulus become important in addition to other geotechnical parameters received from soil investigation report. Contact pressure distribution under the raft depends on many parameters viz., upon the nature of the soil below the raft, i.e., single homogenous mass or a layered formation, thickness of various layers and their locations, properties of the soil, the nature of the foundation, i.e., whether rigid, flexible or soft, rigidity of the superstructure, the quantum of loads and their relative magnitude, presence of adjoining foundation, size of raft etc. In general foundation rafts are analysed as a plate on elastic foundation (conventional method) with the representation of the foundation media using the Winkler idealisation i.e. series of linear uncoupled springs. The elastic constant of the Winkler springs is derived using the modulus of sub-grade reaction. Modulus of sub-grade reaction also called a coefficient of sub-grade reaction is generally determined by performing a simple plate load test. Major problems associated with the determination of modulus of subgrade reactions are; soil is not perfectly elastic and results are affected by the magnitude of the soil pressure and deflection, foundation size and shape, depth of foundation and soil stratification. Thus, the modulus of subgrade reaction estimated from simple plate load test differ much from the actual value in the field. Further, various authors have suggested different methods and factors to compute the modulus of subgrade reaction. It would thus be seen that even for the same soil data value of modulus of subgrade reaction determined by methods suggested by different authors and codes will be different. Which value to be adopted for the correct design, is an important question. Further, the Winkler approach has limitations due to incompatibility of the deflections at raft-soil interface. The deflection of the raft at the point of contact and the deformation of the foundation media at this point of contact are incompatible in this approach. This particularly influences flexible rafts and further if the founding media is soil. It would thus be seen that the conventional method as per Winkler idealisation does not correctly predict the behaviour of the raft both qualitatively and quantitatively and could lead to underestimation of contact pressures leading to unconservative design.

The approach involving detailed soil structure interaction analysis like the one presented here is hence recommended for important structures like those nuclear

facilities which are founded on soft alluvium soil. In the present study, methodology for estimation of stiffness's of raft foundation system under static and pseudo-dynamic (equivalent static) condition has been suggested by performing detailed SSI analysis with appropriate simulation of raft-soil interaction. The analysis results obtained as per detailed SSI analysis have been compared with the same using conventional formulations for static springs as per Vesic's approach using modulus of subgrade reaction and dynamic springs as per ASCE 4–16.

2 Proposed Methodology for the Analysis of Structure Supported on Raft Foundation System for Alluvium Soil

The proposed methodology in this paper for the analysis of raft foundation system of safety related structures of NPP involves basically three steps as shown in Fig. 1. In step-1, detailed SSI analysis of structure supported on raft foundation system along with soil medium is carried out. In step-2, stiffness of founding medium/raft foundation system under static and dynamic (pseudo dynamic/equivalent static) condition is estimated by dividing the contact pressure or forces with the contact displacement obtained from step-1. Finally, in step-3, detailed analysis of structure supported on parallel springs computed in step-2 representing the founding medium is carried out.

In the present study, detailed soil structure interaction analysis of typical structure of NPP, modeled as 3D finite elements along with soil has been carried out using Abaqus software for both vertical sustained and lateral loads (seismic loads with pseudo-static approach) using site-specific geotechnical parameters. Detailed SSI

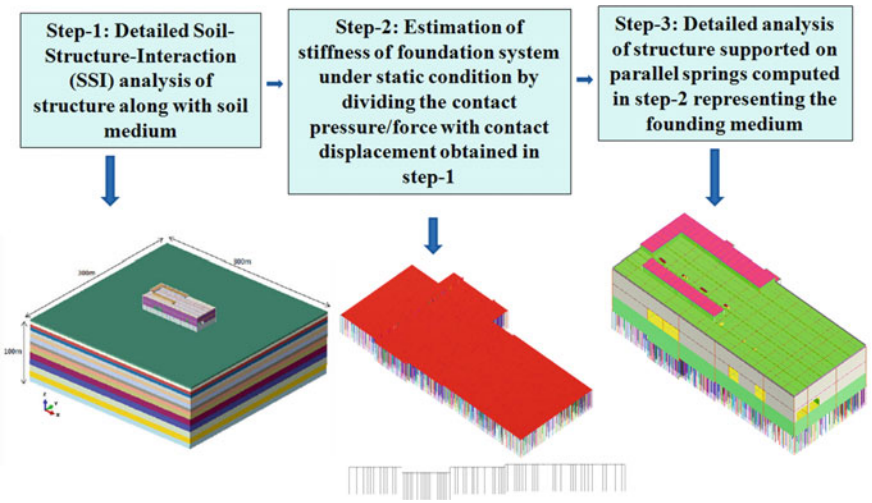

Fig. 1 Steps involved in the proposed methodology

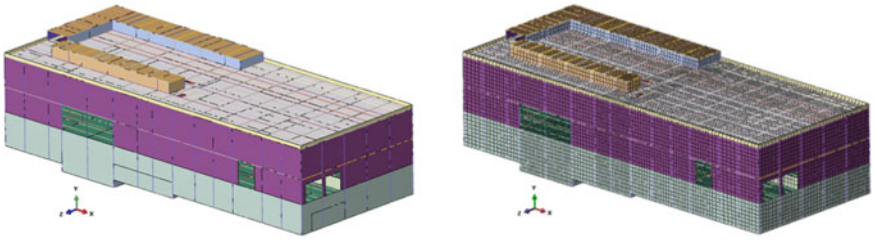

Fig. 2 Geometric and finite element model of a typical NPP structure

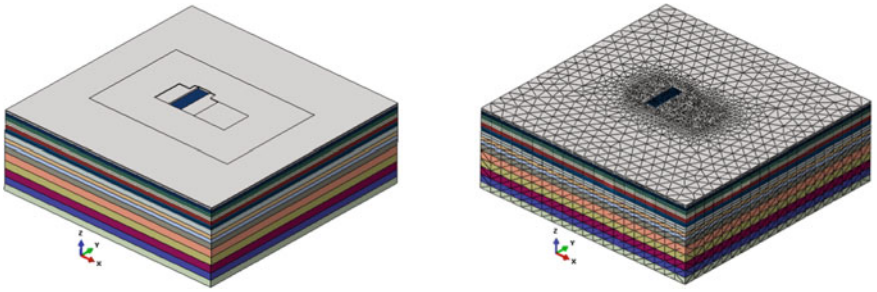

Fig. 3 Geometric and finite element model of a typical NPP structure

analysis includes modeling of the superstructure and soil medium, simulation of the behaviour of the soil media using Mohr–Coulomb plasticity model, simulation of in-situ stress of soil, modeling of contact zones, application of loads and simulation of raft-soil interaction.

2.1 Geometric and Numerical Modeling

The typical structure considered is a RCC framed structure with shear walls, supported on raft foundation system on alluvial soil site. Developing the integrated FE model involves (i) geometric and FE modelling of the structure, (ii) geometric and FE modelling of founding medium (soil medium). The geometric and FE model is shown in Figs. 1 and 2 have been carried out in Abaqus software.

2.2 Elasto-Plastic Constitutive Model for Soil

In the present work, Mohr–coulomb plasticity model is used for simulating the behavior of soil medium. The Mohr–Coulomb failure line is the best fit straight line that touches the Mohr's circles.

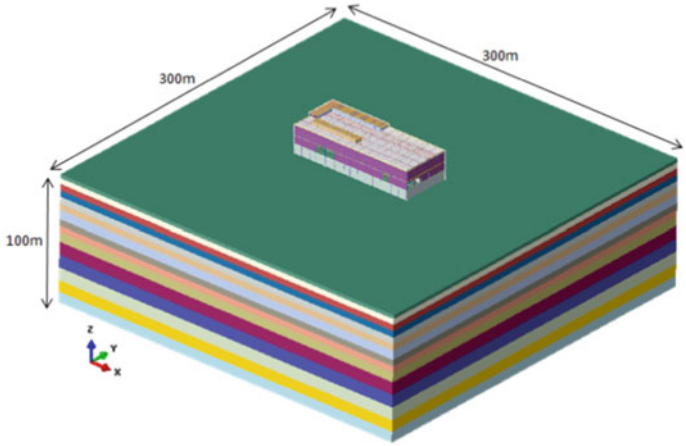

Fig. 4 Combined model of structure and soil medium

$$\tau = c + \sigma \tan \phi \tag{1}$$

where, τ is the shear strength, σ is the normal stress, c is the cohesion and ϕ is the angle of internal friction.

Simulation of In-situ Stress State: The initial state of stress in the soil is considered to be geo-static in nature. The geostatic stress condition means that at any point of time, soil is subjected by vertical stress, $\sigma_z = \gamma \times h$, and lateral stress, $\sigma_L = k_0 \times \gamma \times h$, where γ is the density of soil, h is depth and k_0 is the lateral coefficient of earth pressure at rest. It is required to consider this initial state of stress in the soil before application of the load to structure. The value of k_0 is specified as follows:

$$k_0 = 1 - \sin \phi \tag{2}$$

Modeling of Semi-Infinite Soil Medium: The unbounded or infinite soil medium is approximated by extending the finite element mesh to a far distance, where the influence of the surrounding medium on the region of interest is considered small enough to be neglected. In the present work, finite element model of soil medium of 300 m × 300 m and 100 m depth has been considered based on the iterative analysis wherein effect of the boundary condition is not observed.

2.3 Modeling of Contact Zones (Raft-Soil Interface)

The soil-structure interaction analysis requires considerations of the interaction or coupling between the structure and the founding media. When stack is subjected to loading, raft interacts with the soil. Hence, for simulating normal and tangential

behavior of the interface between raft and soil, Coulomb friction model available in Abaqus has been utilized for raft-soil interaction.

Tangential Behaviour: The interface behavior of the raft and soil (Frictional force vs. relative displacement) is pictorially shown in Fig. 5. The interaction behavior is divided into two parts (a) Sticking phase and (b) Slipping phase. Initially, during the sticking phase, raft-soil interface allows some relative motion (elastic slip) between the raft and the soil surface. Once the induced shear stress between the raft and soil reaches the critical shear stress, the interface enters in the slipping phase. The above sticking and slipping phase of the raft-soil interface is simulated using elastic coulomb friction model. In this model, the critical shear stress (τ_{crit}) is defined as:

$$\tau_{crit} = \min\left(\mu p',\ \tau_{\max}\right) \tag{3}$$

Normal Behaviour: Normal contact pressure develops, when raft moves vertically towards the soil. Under such situation, area of the raft, which is in contact with soil, will develop normal stress. This phenomenon is simulated in the analysis using relationship as shown in Fig. 6.

To model the contact property between the raft and soil surface material, it is essential to obtain the friction factor (μ), maximum shear stress (interface shear strength, $\tau_{\max}$) and elastic slip (γ_{crit}) values. The design value of the friction or adhesion below the raft and walls to be mobilized at an interface with the structure is usually considered as 75% of the design shear strength to be mobilized in the soil itself [2]. Values of friction factor considered as:

$$\mu = 0.75 * \tan\phi \tag{4}$$

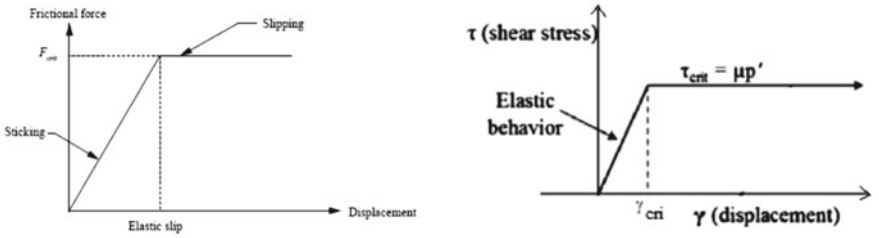

Fig. 5 Raft soil interface behavior (tangential direction)

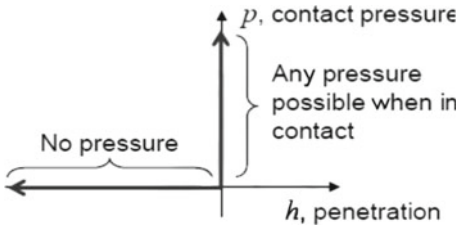

Fig. 6 Behavior of raft-soil interface in normal direction

The design value of strength to be mobilized below the raft and walls to be an interface with the structure is usually considered as 75% of the design shear strength of the soil itself [2]. The design interface shear strength is:

$$\tau_{\max} = 0.75 * \left(c + \sigma' \tan \phi\right) \tag{5}$$

An elasto-plastic model is used to define the behavior of the interface for the modeling of soil-structure interaction. The above-mentioned criterion is used to distinguish between elastic and plastic interface behavior. For the interface to remain elastic the shear stress τ is given by:

$$\tau < \tau_{\max} \tag{6}$$

The minimum slip required for the full mobilization of frictional resistance is known as critical slip (γ_{crit}). The default value given in Abaqus is used in the present study.

2.4 Material Properties of Soil

The founding media of site considered in the present analysis is soft alluvium. Linear variation of static modulus of elasticity of different soil layers has been considered in the present analysis. Since, Mohr–Coulomb model has been used for defining the failure criteria of soil, values of cohesion 'c' and internal friction 'ϕ' used in the analysis are obtained from soil testing at the alluvium soil site. As suggested in literature for sandy soil [3], dilation angle, $\Psi = \phi - 30$ has been considered for all soil layers.

3 Analysis as Per the Proposed Methodology

3.1 Analysis Steps

SSI analysis under static condition in Abaqus is performed according to the sequence of applied loads, which has been defined in different steps. The steps followed are: (a) Geostatic step and (b) Loading step (Gravity, other dead loads, equipment loads and live loads).

Geostatic Step: Geostatic step simulates the in-situ soil stress developed in the soil medium before the placement of the structure. The in-situ stresses developed in the soil medium is shown in Fig. 7.

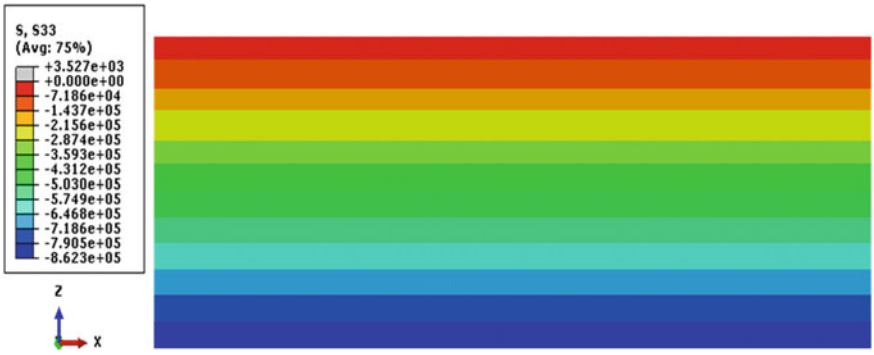

Fig. 7 Geostatic stress contour (vertical stress, S33 unit: N/m^2) for soil

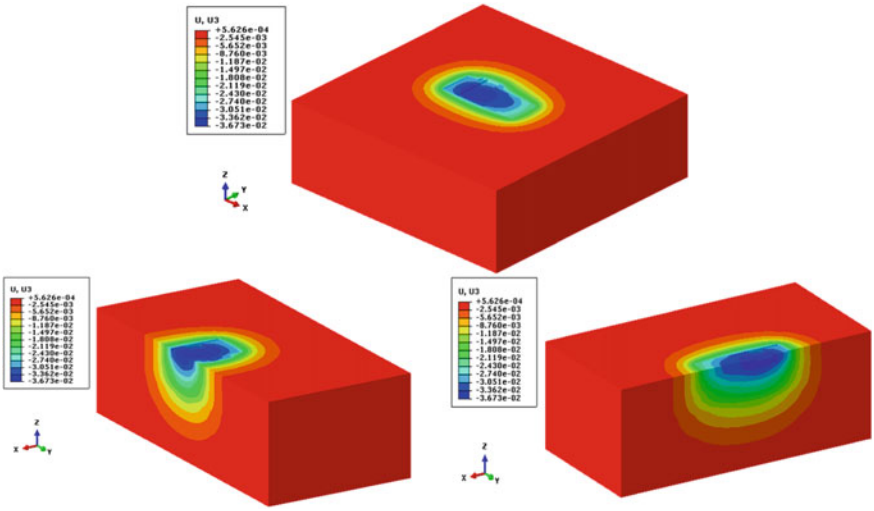

Fig. 8 Vertical displacement (U3: unit in m) contour of soil medium

Loading Step: After the completion of geostatic step, vertical loading is applied on the structure. Settlement observed in the soil medium and raft foundation is shown in Fig. 7, 8, 9 and 10 respectively.

3.2 Estimation of Stiffness of Soil Spring Under Sustained Loading by SSI Analysis

The vertical stiffness of soil spring to be modeled below foundation raft has been estimated based on the modulus of subgrade reaction computed at each nodes of the

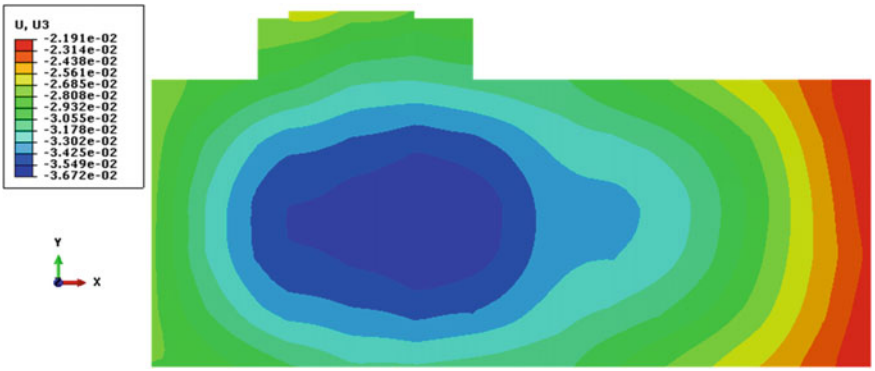

Fig. 9 Vertical settlement contour (U3: unit in m) at raft under sustained loadings

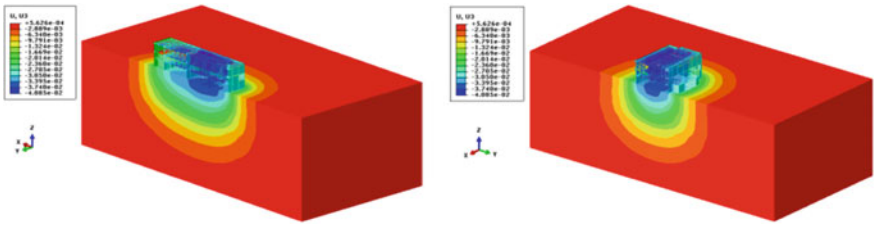

Fig. 10 N-S/E-W cross section of vertical settlement contour (U3: unit in m) under sustained loadings

raft from detailed SSI analysis. Modulus of subgrade reaction values is estimated by dividing the induced contact pressure at each nodes of the raft with displacement of that node. The modulus of subgrade reaction thus obtained is multiplied by the induced contact nodal area of that node to obtain the vertical stiffness of soil spring.

3.3 Estimation of Stiffness of Soil Spring by Vesic's Formulation (Conventional Approach)

Spring stiffness's under this approach have been estimated by Vesic's equation as given below.

$$K_s = \frac{0.65 \times E_r}{1 - \mu_s^2 \times B} \times \sqrt[12]{\frac{E_r \times B^4}{E_c \times I}} \tag{7}$$

where, E_r = modulus of elasticity of soil (kN/m^2), B = least dimension of the mat foundation (m), E_c = weighted static elastic modulus of concrete foundation (kN/m^2), f_{ck} = characteristic compressive strength of concrete (MPa), I = cross sectional moment of inertia of foundation (m^4) and μ_s = Poison's ratio of the founding medium.

3.4 *Comparison of Soil Spring Stiffness's Obtained from Proposed SSI Analysis Methodology and as Per Vesic's Formulation*

Comparative plots of vertical soil spring stiffness obtained from proposed SSI analysis methodology and as per conventional approach using Vesic's formulation is shown in Figs. 11 and 12 for lines along-*x* and *y*.

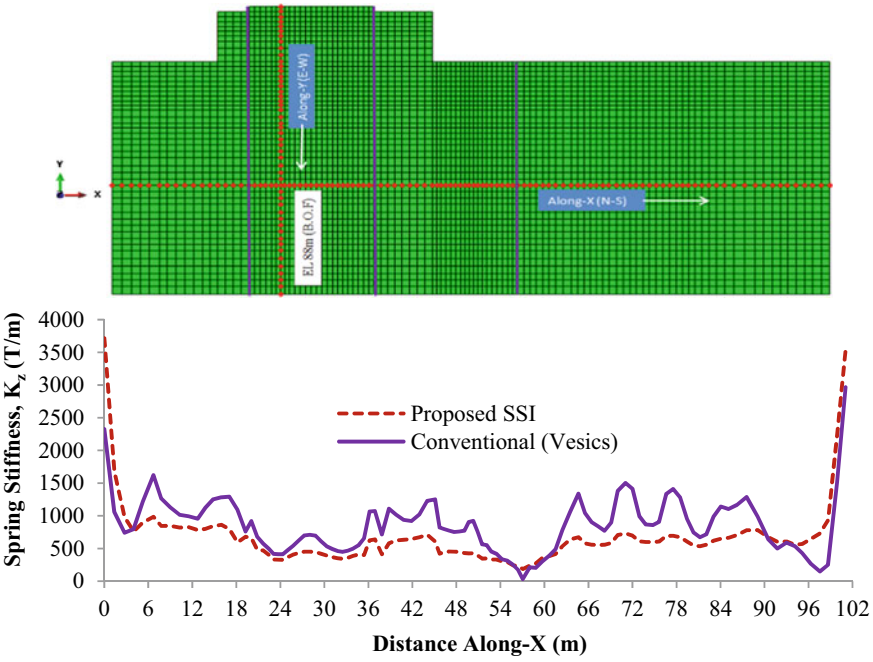

Fig. 11 Comparison of variation of vertical spring stiffness along line X at raft under sustained loading as per proposed SSI analysis methodology and as per Vesic's equation

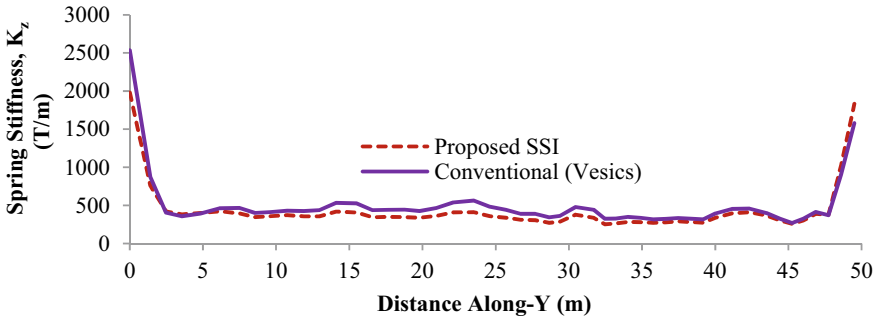

Fig. 12 Comparison of variation of vertical spring stiffness along line Y at raft under sustained loading as per proposed SSI analysis methodology and as per Vesic's equation

3.5 Comparison of Displacement

Comparison of vertical displacement contour under sustained loadings (vertical) with that obtained from proposed SSI analysis methodology and as per Vesic's equation (conventional method) is shown in Fig. 13. Similarly, the comparison of variation of vertical displacement along line-x and along line-y is shown in Figs. 14 and 15.

4 Discussion and Conclusion

Static soil-structure-interaction analysis of typical building of NPP founded on soft alluvium soil has been carried out to study the behaviour of raft foundation system under vertical sustained loading. Further, static analysis with soil spring stiffness estimated using subgrade modulus as per conventional Vesic's formulation has been also performed. The outcome of the analysis in terms of vertical spring stiffness and displacement has been compared with the two approaches. From the comparison of analysis results it is observed that the trend of variation of vertical spring stiffness obtained from proposed SSI analysis approach and as per conventional Vesic's formulation is more or less same. However, the settlement observed using subgrade modulus as per Vesic's formulation is on the lower side.

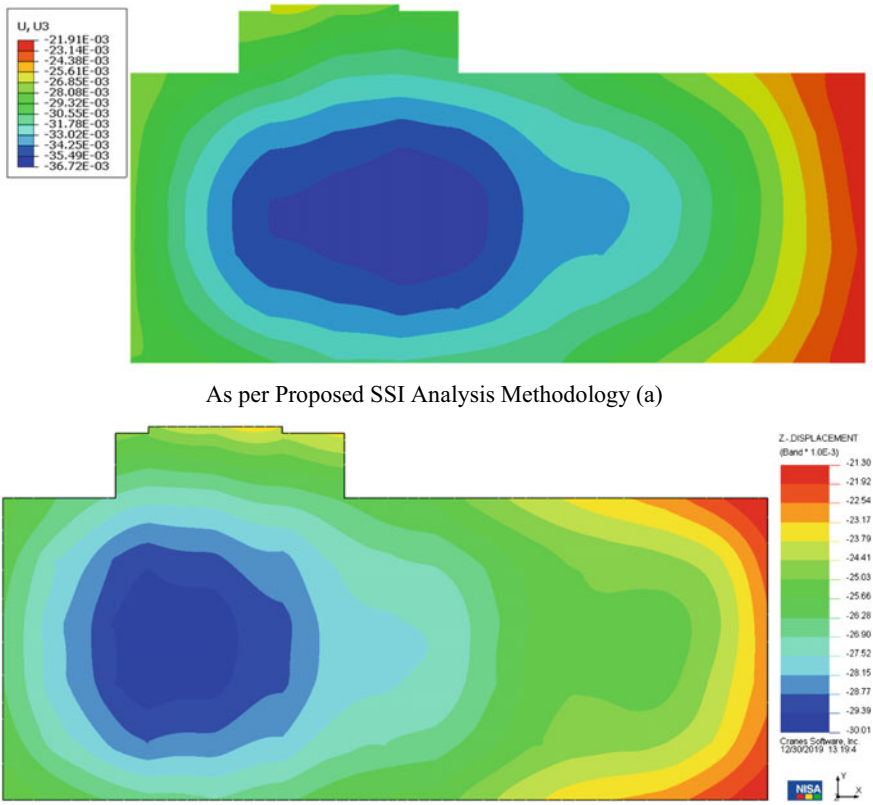

Fig. 13 Comparison of vertical displacement (U3: unit in m) contour at raft under sustained loading as per proposed SSI analysis methodology (**a**) and as per Vesic's equation (**b**)

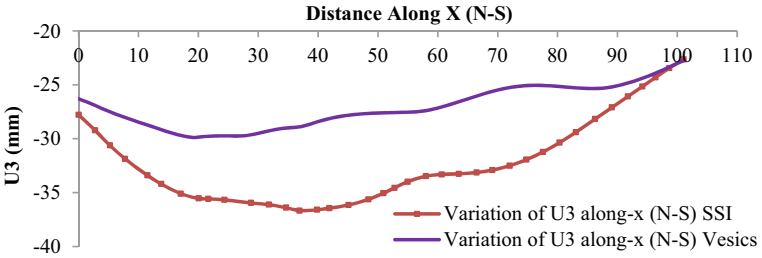

Fig. 14 Comparison of variation of vertical displacements along-X (N-S) at raft under sustained loading as per proposed SSI analysis methodology and as per Vesic's equation

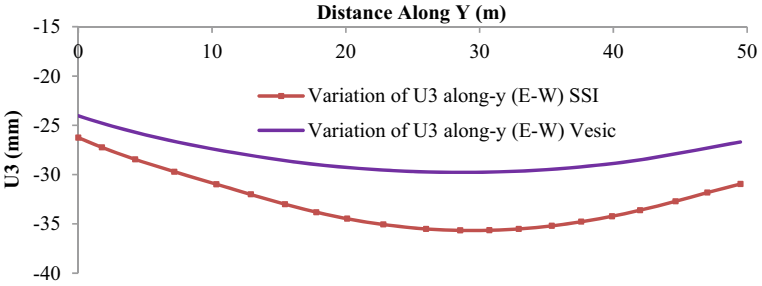

Fig. 15 Comparison of Variation of Vertical Displacements Along-Y (E-W) at Raft Under Sustained Loading as per Proposed SSI Analysis Methodology and as per Vesic's Equation

Acknowledgements The authors are grateful to Executive Director (Engineering) and Director (Technical), NPCIL for their constant support and encouragement throughout the present work.

References

1. Abaqus 6.14, Analysis User's Manual
2. BS 8002–94: British Standards Institution, Code of practice for Earth retaining structures
3. Kowalska M (2014) Numerical study of the influence of dilatancy angle on bearing capacity and rotation of a gravity retaining wall. Paper No. 186, European Conference on Geotechnical Engineering (DECGE 2014), Vienna, Austria

Seismic Vulnerability Assessment of Lifeline Buildings at Gangtok

Pretam Dahal, Guru Prasad Sharma, and Shantharam Patil

Abstract The M6.9 Sikkim earthquake of September 18, 2011, caused widespread damage in the state of Sikkim and adjoining areas and it exposed the seismic vulnerability of the multi-storied construction. Damage that occurred in and around Gangtok was disproportionately high to the observed intensity of shaking, primarily due to poor compliance with seismic codes, inferior quality of raw materials and shoddy workmanship. The main objective of the survey was to observe the effects of the 18th September earthquake and aftershocks on the build environment in terms of seismological, geotechnical and structural damages. From this Earthquake, it can be clearly seen that there is a need for seismic vulnerability assessment of buildings in and around Gangtok town. This paper presents the study of seismic vulnerability of buildings by rapid visual screening method and detailed vulnerability assessment method.

Keywords Seismic risk · Vulnerability · Assessment · Gangtok

1 Introduction

Earthquakes are one of the most dangerous, destructive and unpredictable natural hazards, which can leave everything up to a few hundred kilometres in complete destruction in seconds. India has enough experience with earthquakes and the kind of damage that they can leave behind within seconds and it is not rare or unusual anymore. About 59% of India's land is prone to moderate to severe earthquakes which makes it one of the highest seismic risk-prone areas in the world [1]. More than 25,000 people died in eight major earthquakes during the last 20 years and the last major earthquake in India was a decade earlier in Bhuj, Gujarat, which occurred on 26th

P. Dahal · G. P. Sharma
Sikkim Manipal Institute of Technology, Sikkim Manipal University, Gangtok, Sikkim 737136, India

S. Patil (✉)
Manipal School of Architecture and Planning, Manipal Academy of Higher Education, Manipal 576104, India
e-mail: patil.s@manipal.edu

T. G. Sitharam et al. (eds.), *Earthquakes and Structures*, Lecture Notes in Civil Engineering 188, https://doi.org/10.1007/978-981-16-5673-6_9

January 2001 and claimed over 14,000 lives and caused severe damage to buildings and infrastructure resulting in high economic losses [2–4]. Due to the collision of the Indian Plate with the Eurasian Plate, the Himalayan region has emerged as one of the seismically active regions of the world, resulting in many disastrous earthquakes in the past and recent times, and North East India alone has emerged as one of the most seismically active regions in the country. The northeastern region of the country as well as the entire Himalayan belt is susceptible to great earthquakes of magnitude more than 8.0.

An earthquake of 6.9 magnitude with its epicentre near the India-Nepal border located at (27.7° N, 88.2° E) shook the northeast and large parts of northern and eastern India on September 18, 2011, at 6:11 p.m. IST. Gangtok, the capital city of Sikkim, which is around 68.74 km southwest from the epicentre, experienced an earthquake intensity of VI on the MMI scale. It caused extensive damage and widespread panic, and those who experienced the earthquake realised that the event was large enough and the majority of their buildings were not strong enough to sustain another earthquake of the same or higher magnitude.

The major lifeline buildings in and around the capital city of Gangtok have been constructed at least 40 to 50 years ago whose earthquake resistance capabilities cannot be ascertained due to the absence of detailed drawings and test reports. The purpose of an earthquake-resistant design is to provide a structure with features, which will enable it to respond satisfactorily to seismic effects [5–7]. These features are related to five major objectives, which are listed in order of importance:

1. The likelihood of collapse after a very severe earthquake should be as low as possible.
2. Damage to non-structural elements caused by moderate earthquakes should be kept within reasonable limits. Although substantial damage due to severe earthquakes which have a low probability of occurrence is acceptable, such damage is unacceptable in the case of moderate tremors which are more likely to occur.
3. Buildings in which many people are usually present should have deformability features that will enable occupants to remain calm even in the event of strong shocks.
4. Personal injury should be avoided.
5. Damage to neighbouring buildings should be avoided.

2 Methodology

Gangtok town is highly vulnerable to future earthquakes, there is an urgent need to assess the seismic vulnerability of school buildings at Sikkim town as an essential component of a comprehensive earthquake disaster risk management policy. India's national vulnerability assessment methodology, as a component of the earthquake disaster risk management framework is included in the following procedures.

1. Rapid visual screening (RVS) procedure requiring only visual evaluation and limited additional information (level 1 procedure). This procedure is recommended for all buildings.
2. Simplified vulnerability assessment (SVA) procedure requiring limited engineering analysis based on information from visual observations and structural drawings or on-site measurements (level 2 procedure). This procedure is recommended for all buildings with a high concentration of people.
3. Detailed vulnerability assessment (DVA) procedure requiring detailed computer analysis, similar to or more complex than that required for the design of a new building (level 3 procedure). This procedure is recommended for all important and lifeline buildings.

The main objective of this paper is to compare the results of vulnerability assessment by Rapid Visual Screening method and by detailed vulnerability assessment using software SAP v8i 2000.

2.1 Rapid Visual Screening Method

The building profile for different construction types that is developed on the basis of application of the first procedure (rapid visual screening) will be useful to shortlist the buildings to which a simplified vulnerability assessment procedure should be applied. The simplified vulnerability assessment procedure will provide a more reliable assessment of the seismic vulnerability of the building and will form the basis for determining the need for a more complex vulnerability assessment. The rapid visual screening will be useful for all buildings except critical structures where detailed vulnerability assessment is always required. Rapid Visual Screening is a form of survey to identify the buildings which are expected to be more vulnerable under an earthquake. It is used to prioritise the buildings in a jurisdiction for further evaluation and retrofit for seismic forces [8]. RVS is designed to evaluate the primary lateral load resisting system and to identify the building attributes that modify the seismic performance of the lateral load resisting system along with the non-structural components. A building may require 15–30 min for RVS depending upon the size of the building. Data collection and decision-making process will occur at the building site.

The objective of the study is to:

1. To carry out RVS of selected lifeline buildings in Gangtok town.
2. To access the necessary data and drawings from this RVS study which will be useful to carry out a detailed vulnerability study of buildings which are vulnerable to seismic activities.
3. To comment on the seismic vulnerability of selected lifeline buildings in Gangtok town.

The RVS score evaluation is based on a few parameters of buildings. The parameters of the buildings are building height, frame action, pounding effect, structural

irregularity, short columns, heavy overhang, soil conditions, falling hazard, apparent building quality, diaphragm action, etc. On the basis of above-mentioned parameters, the performance score of the buildings has been calculated. The formula of the performance score is given as

$$PS = (BS) + \sum [(VSM) \times (VS)] \tag{1}$$

where VSM represents the Vulnerability Score Modifiers and VS represents the vulnerability Score that is multiplied with VSM to obtain the actual modifier to be applied to the BS or Basic Score. For RC Frame buildings and masonry buildings, the base score, vulnerability score and vulnerability modified score are given in references [9–12]. A building with a higher seismic zone and more number of the storey will get a low score, i.e. building will be more vulnerable. In this study, an attempt has been made to survey 11 buildings in Sikkim (Gangtok Town). The buildings include only that constructed of reinforced concrete. As a part of this study, RVS forms are generated for reinforced concrete buildings. RVS scores have been calculated for the buildings. A performance score for all eleven buildings is shown in Table 1.

The building with a higher performance score performs better compared to a lower performance score. However, the buildings which are in the middle range of performance is large in number, and drawing a meaningful conclusion is a difficult task because of the non-availability of standard results for the Indian code provisions.

Table 1 Performance score of buildings by RVS method

Sl. No	Name of the building	Score
1	Govt. Senior Secondary School, Enchey, Old Hostel Building	90
2	Tashi Namgyal Academy School Hostel Building	100
3	Tashi Namgyal Academy School Old Staff Quarter	55
4	Tashi Namgyal Academy School Building	100
5	Tashi Namgyal Academy School New Staff Quarter	100
6	Tashi Namgyal Academy School Golden Temple	100
7	Sir Tashi Namgyal Senior Secondary School Primary School	115
8	Sir Tashi Namgyal Senior Secondary School Auditorium	30
9	Sir Thutob Namgyal Memorial Hospital Main Hospital Building	90
10	Sir Thutob Namgyal Memorial Hospital Orthopedic Block	65
11	Govt. Senior Secondary School, Enchey, Main Building	90

2.2 Detailed Vulnerability Assessment

In the present study, the various model of RC frame buildings of different stories has been designed as per IS 1893 (part I): 2000 using SAP 2000.v.14. The capacity design has been done as per the Euro code to achieve a strong column weak beam concept. The performance of the RC frame building has been evaluated by Nonlinear static and dynamic analysis. Nonlinear static analysis involves Pushover analysis and nonlinear dynamic analysis involves Time History analysis. In this study, five different buildings (Model-1, Model-2, Model-3, Model-4 and Model-5) have been taken whose Rapid Visual Screening test has already been done. These buildings are evaluated by nonlinear static and dynamic analysis using SAP 2000.v.14. The basic concept of capacity-based design of structures is the spreading of inelastic deformation demands in a structure in such a way so that the formation of plastic hinges takes place at predetermined positions and sequences. In multistory multi-bay reinforced concrete frames, plastic hinges are allowed to form only at the ends of the beams. To achieve this flexural capacity of the column, sections at each joint are made more than the joining beam sections. This will eliminate the possible sway mechanism of the frame.

The capacity design is also the art of avoiding failure of structure in brittle mode. This can be achieved by designing the brittle modes of failure to have higher strength than ductile modes. Shear failure is a brittle mode of failure hence the shear capacity of all components is made higher than their flexural capacities.

A plot of total base shear versus top displacement in structure is obtained by this analysis that would indicate any premature failure or weakness, and the analysis is carried out up to failure, thus it enables determination of collapse load and ductility capacity. On the building frame, the load is applied incrementally, the formation of plastic hinges, stiffness degradation, plastic rotation, and lateral inelastic force versus displacement response for the complete structure is monitored. Figure 1 shows the plot of total base shear versus top displacement of one of the models and Fig. 2. the hinge pattern in beams and columns due to nonlinear static pushover load case.

A plot of base shear and displacement was obtained from pushover analysis. Table 2 gives the maximum displacement of each model obtained from the pushover curve and maximum allowable deflection according to IS 1893:2002.

From the table it is seen that for Model-1, the maximum displacement is greater than the maximum allowable displacement and for other Models, the maximum displacement is less than the maximum allowable displacement; therefore, it can be concluded that Model-1 is vulnerable for static pushover load case. The frame members in pushover analysis with hinge patterns indicate the performance levels. The absence of colour indicates the elastic condition. Plastic hinges having pink colour indicate IO level, blue colour indicate LS level and cyan colour indicate CP level; other colours indicate performance beyond CP level. The performance levels of all the buildings were found to be the same. The maximum displacement of roof one of the building obtained from nonlinear time history analysis is represented below.

Figure 3 represents the maximum roof displacement of different models, and it

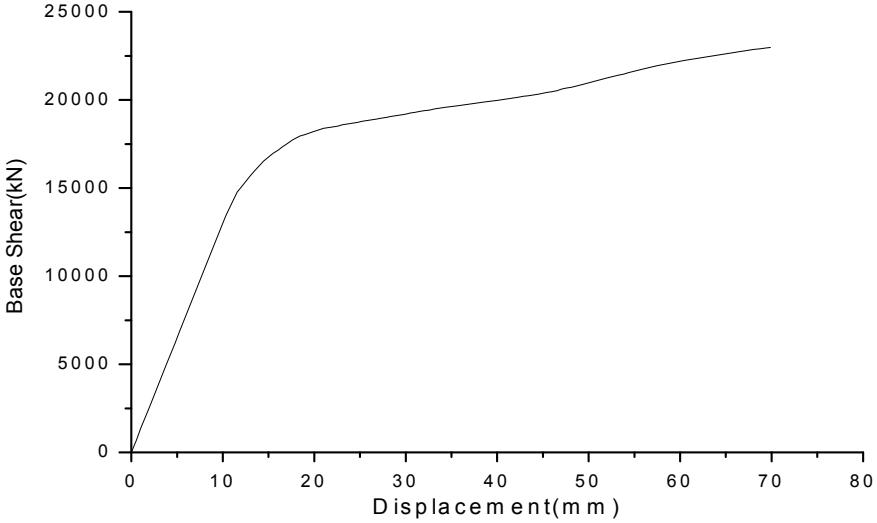

Fig. 1 Pushover curve in long direction for Model-1

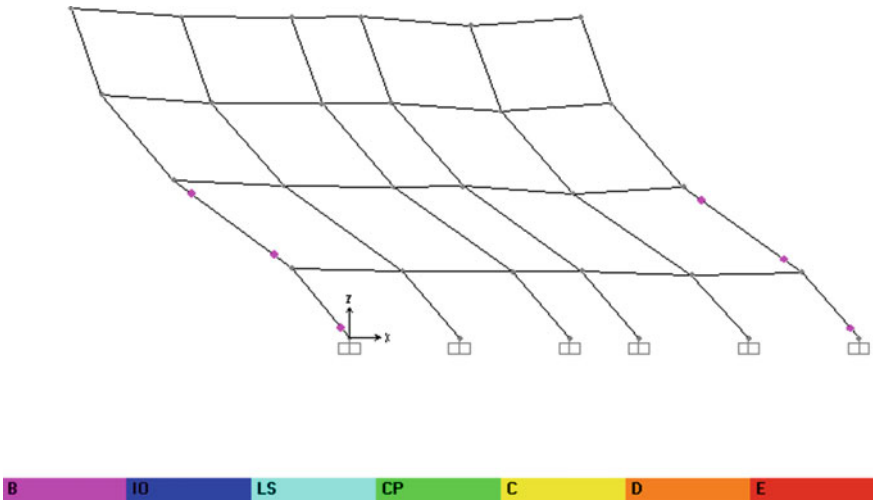

Fig. 2 Pushover analysis hinge pattern in long direction for Model-1

was observed that the buildings are failing within 5 s of strong motion, hence the buildings are vulnerable to earthquake. The hinge pattern obtained from nonlinear time history analysis of different models is shown Fig. 4. Different colours on frames indicate the performance levels of the buildings. It was found that the performance levels of all the buildings fall under the same level.

Table 2 Maximum displacement of models

Model	Base shear (kN)	Maximum displacement (mm)	Maximum allowable displacement (mm)
Model-1	23,151	69.9	37.6
Model-2	49,340	4.4	20.3
Model-3	324.31	15.2	33.83
Model-4	1286.37	22.997	68.2
Model-5	3099.84	58.995	85.9

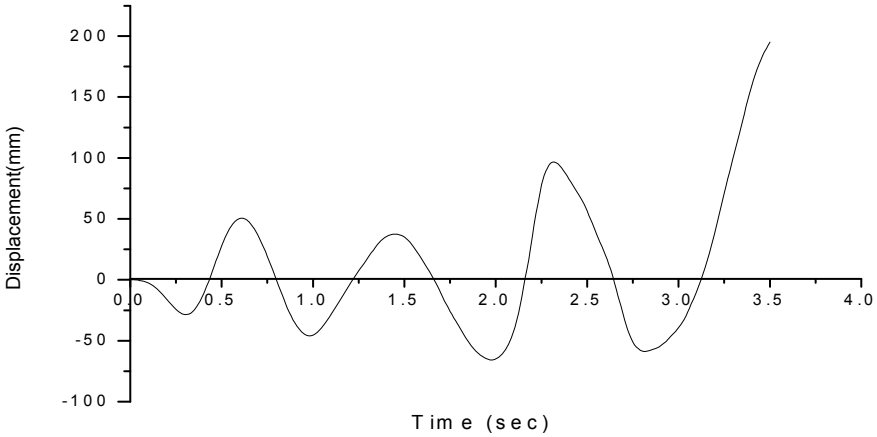

Fig. 3 Nonlinear roof displacement in long direction for Model-1

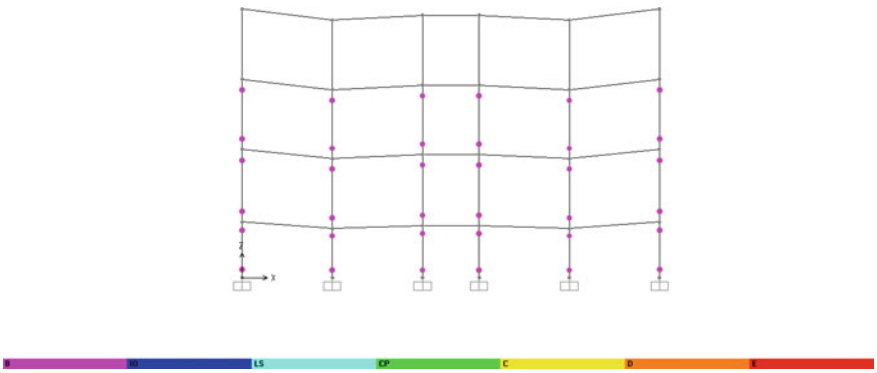

Fig. 4 NLTH hinge pattern in long direction for Model-1

Table 3 Comparison of results of RVS and DVA

Model	Performance score by RVS method	Maximum displacement by DVA (mm)
Model-1	55	195.08
Model-2	100	62.50
Model-3	100	71.30
Model-4	100	85.56
Model-5	115	57.90

2.3 Comparison Between RVS Method and Detailed Analysis

From RVS method, it was found that the Model-1 was most vulnerable and Model-5 was the least vulnerable among all buildings. Table 3, Figs. 5 and 6 show the comparison of results of RVS and DVA.

The building having the least performance score and having a high value of displacement is the most vulnerable. From Table 3, it is clear that the vulnerability level is found to be the same by both methods. However, it is seen that the performance score of Model-5 is 115 which should perform well during the earthquake but it is failing within 5 s of strong motion.

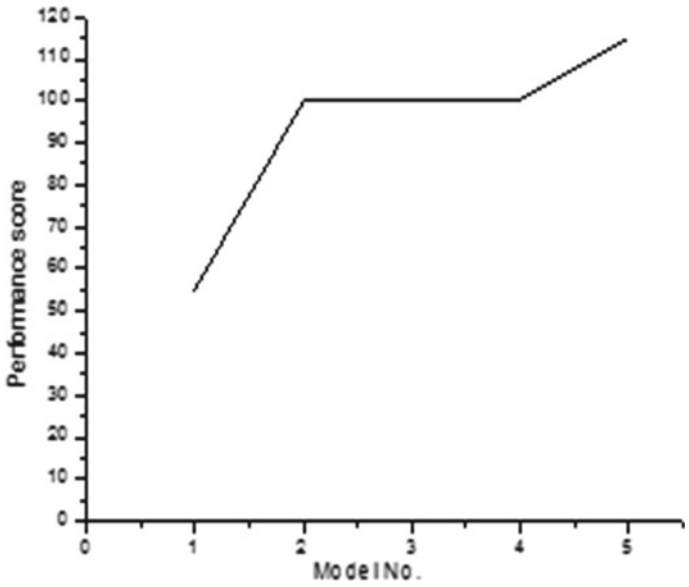

Fig. 5 Graph showing performance score of buildings

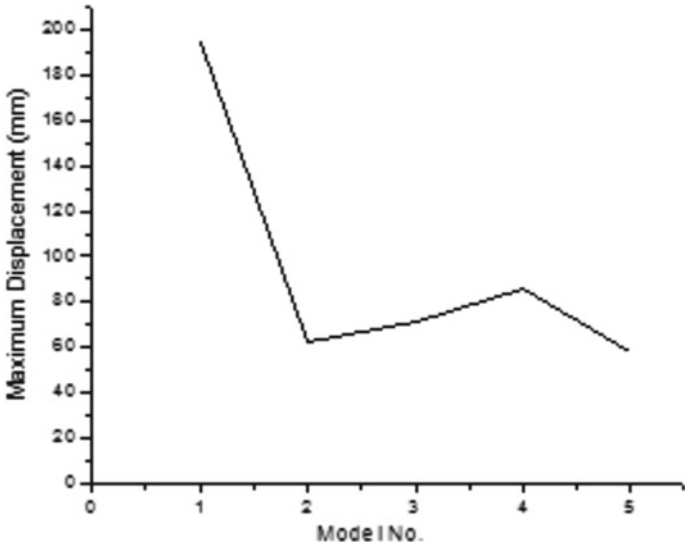

Fig. 6 Graph showing maximum displacement of building

3 Conclusion

The performance of buildings whose performance score was known to have been evaluated under nonlinear pushover and nonlinear time history analysis. It was seen that the buildings were failing due to the formation of plastic hinges at beam-column joint and the buildings failed against the strong ground motion. All the buildings considered for this study are vulnerable to strong ground motion. In this study, it was found that the level of vulnerability of buildings was the same using RVS methodology and DVA. But the buildings having high performance score also failed within 5 s of strong ground motion. Therefore, it can be concluded that RVS can be used only for the early stage of vulnerability assessments but detailed vulnerability assessment must be done for a more reliable result.

References

1. BMTPC (2006) Vulnerability atlas of india: building materials and technology promotion council, New Delhi
2. Arya AS (2000) Recent developments toward earthquake risk reduction in India. Curr Sci 79(9):1270–1277
3. Ghosh C (2008) Earthquake risk mitigation strategies in India. In: The 12th international conference of international association for computer methods and advances in geomechanics. Goa, India, pp 2985–2991
4. NDMA (2011) Development of probabilistic seismic hazard map of India technical report. National Disaster Management Authority, New Delhi
5. IS 1893–2002: Indian standard criteria for earthquake resistant design of structures
6. IS 4326–1993: Earthquake resistant design and construction of buildings-code of practice
7. IS 13935–2009: Seismic evaluation, repair and strengthening of masonry buildings: guidelines.
8. CPWD (2007) Handbook on seismic retrofit of buildings
9. Jain SK, Mitra K, Kumar M, Shah M (2010) A proposed rapid visual screening procedure for seismic evaluation of RC-frame buildings in India. Earthquake Spectra 709–729
10. Jain SK, Mitra K, Kumar M, Shah M (2010) A rapid visual seismic assessment procedure for RC-frame buildings in India. In: Proceedings of the 9th U.S. National and 10th Canadian conference on earthquake engineering, 2010, Toronto, Ontario, Canada
11. Singh Y, Gade P, Lang DH, Erduran E (2012) Seismic behaviour of buildings located on slopes-an analytical study and some observations from Sikkim earthquake of September 18, 2011. In: World conference in earthquake engineering
12. FEMA 154 (2002) Rapid visual screening of buildings for potential seismic hazards, a handbook, 2nd edn. Redwood City, CA

Analysis of Knee-Braced, x-braced Moment Frame for Ductility Based Seismic Design

Eshanya Tongper Nongsiej, Karthiga N. Shenbagam, A. Mohanraj, and Kartik Kapoor

Abstract Multistory structures are the type of structures which are often subjected to seismic and wind effects simultaneously. The actual strength in the plan of multistory building is the regularity in planning, the type of materials, construction techniques used during constructions. The structure is mostly constructed to have adequate horizontal solidness to oppose the lateral loads caused by the seismic action and to control the parallel float of the structures. The steel supporting framework in strengthened solid edges is suitable for preventing horizontal powers. In this paper we are preparing and analysing a G + 20 with 3 m spacing of each floors. In this structure we will distinguish exposed casing and edges having X-type bracings or knee bracings at the corners. A three dimensional structure is taken, and 20 stories is taken with story tallness of 3 m. The bars and segments are intended to withstand dead and live load only. Seismic tremor loads are taken by bracings. The bracings are given just on the fringe sections. Analysis and design has been carried out using ETABS software, and the results are discussed.

Keywords Steel frame · X bracings · Knee · Moment resisting · Seismic

1 Introduction

Braced frame is type of a structural system commonly used in structures subjected to lateral loads such as wind and seismic loadings. The members in a braced frame are generally made of structural steel, which can work effectively both in tension and compression.

E. T. Nongsiej (✉) · K. N. Shenbagam · A. Mohanraj · K. Kapoor
Tamil Nadu, Sathyamangalam, India
e-mail: eshanyatongpernongsiej.ce18@bitsathy.ac.in

A. Mohanraj
e-mail: mohanraja@bitsathy.ac.in

K. Kapoor
e-mail: kartikkapoor.ce18@bitsathy.ac.in

T. G. Sitharam et al. (eds.), *Earthquakes and Structures*, Lecture Notes in Civil Engineering 188, https://doi.org/10.1007/978-981-16-5673-6_10

Beams and columns are the structural members that are constructed to carry vertical loads, and the bracing system are the structural members which carries lateral loads. The positioning of braces is found to problematic or very difficult due to the positioning of braces and its connections in a proper way with or without openings. Buildings adopting high-tech or post-modernist styles have responded to this by expressing bracing as an internal or external design feature.

To oppose lateral earthquake loads, braces or shear dividers are usually constructed in RC and Steel structures. RC structures with steel supporting elements were generally used as a retrofitting measure to strengthen earthquake-harmed structures.

2 Literature Survey

Vishwanatha et al. [1] proposed that the seismic performance of concrete and composite buildings for different parameters of vertical irregularities in buildings and composite columns are installed in the structure to increase the strength and fire resistance of the column and also to resist lateral forces. Finally, they concluded that the maximum storey drift and displacement will increase as the vertical irregularities increases.

Jingbo et al. [2] proposed the behaviour of steel concrete composite frame structure system under seismic loads. In this study four types of columns such as composite beam concrete filled square tubular column, Equivalent stiffness RC column and other two types are analysed under response spectrum analysis. And from the analysis of those columns and frame they come to a conclusion that in composite frames, the maximum storey drift angle is reduced by 18% and in composite we can achieve greater span and height, but in RC the columns must be enlarged to meet the desired bearing capacity.

Dhruvil [3] proposed the seismic analysis of tall building having different structural systems by using response spectrum method. The tall building comprises of shear wall system and shear wall combined bracing system. Their study is mainly based on the behaviour of the shear wall system under response spectrum analysis under varying storey height. From the study they suggested that for 15 storey building shear wall was recommended and for 25 stories shear wall and bracing combined and for 35 stories shear wall is recommended.

Rahul Pandey [4] proposed the response of the RCC, steel and steel concrete composite frame under earthquake loading. Comparative analysis of all the three is done based on the material, cost benefit and behaviour. The analysis is done in SAP 2000 software, and the behaviours are studied. They found that base shear is maximum in RCC frame. Base shear is reduced by 40% for composite frame and 45% for steel frame. Reduction in cost of composite is 33% and steel is 27%. RC frame has the least value of storey drift because of its high stiffness.

Prabhu Booshan [5] proposed that the behaviour of RCC and composite structures with different and various vertical irregularities were considered, and the structures

were modelled and analysed using ETABS software. On comparing the results steel concrete composite structures' performance was better than that of RC structures.

Patil et al. [6] proposed that the behaviour of RCC and composite structure which has a soft storey was analysed using response spectrum method and equivalent static method in ETABS software. Those obtained results are compared, and they came to a conclusion that the storey drift reduces what parameter in composite structures, self-weight of the composite structure reduces, bending moment and shear force in composite columns are less when compared to RC columns. And they found that composite structures are exhibiting high ductility and lateral load resisting capacity greater than RC structures.

Chandak [7] proposed that the reinforced concrete buildings in structural walls and moment resisting frames were analysed using response spectrum method with the help of SAP 2000 software. The analysis is based on Indian standard code and two other codes such as Uniform Building Code and Euro Code. The main observation of his study is to find the difference in the response of the building based on the three codes. On successful analysis he found that IS Code method gives higher values of base shear. And IS method gives maximum displacement values when compared to other two methods.

Youcef et al. [8] proposed that the Seismic Performance of RC Building Using Spectrum Response and Pushover Analysis was carried out. This investigation is based on the Euro Code. They compared the storey drift, displacement, base shear using response spectrum and push over analysis. The modelling of the eight storey structure is done using ETABS software. The analysis of absolute displacements of a building using linear response spectrum was taken into account indirectly, and the nonlinear behaviour of structural elements by introducing the behaviour factor was considered; the nonlinear static analysis using pushover procedure was also done. The results showed a large difference between the two methods explain the results in detail.

Shirule et al. [9] proposed the response spectrum analysis of asymmetrical building. This study is based on the Indian Standard code on an asymmetrical building modelled in SAP 2000. After the performance of analysis was done, it is concluded that the provision of shear wall is necessary for asymmetrical building as it helps in the prevention of collapse and damage to the structure. It also decreases the storey drift (if it increases what happens) of the structure. And they also found that the IS code gives higher value of base shear when compared with Uniform building code.

Md. Akberuddin et al. [10] analysed the structure using Pushover Analysis. This method had been utilized to obtain the deformation capability of frame by inelasticity, and it is found that irregularity in height of the structure decreases the structure's performance level. This induces a decrease in the deformation or displacement of the structure, and the bare frame without irregularity has more lateral load carrying capacity compared to bare frames with vertical irregularity (i.e., the vertical irregularity decreases the flexure and shear demand). The lateral displacement of the structure is reduced with an increase in the percentage of irregularity.

Saisaran et al. [11] proposed a study on static nonlinear method i.e. push over analysis which utilizes to evaluate the deformations of the structure to evaluate the

displacement force relationship or the capacity curve for a building or structural element. The analysis includes application of horizontal loads, in a recommended pattern, to the structure incrementally. There would be a progressive change in the slant of weakling bend with increment in the horizontal relocation of the building in which part of the structures. This is because of the progressive formation of plastic hinges in beams and columns throughout the structure.

Mindaye et al. [12] proposed that the seismic response of a residential G + 10 RC frame building structure has been investigated by equivalent static analysis and response spectrum analysis, and finally it was concluded that the results obtained from response spectrum analysis resulted in a more accurate for storey drift, displacements etc. The model created was analysed for different seismic zones in accordance with the Indian standard codes of practice as per I 1893:2002. The results predicted were further studied in a detailed manner for nonlinear seismic analysis.

Srikanth et al. [13] proposed that the responses of earthquake loadings for symmetric multi-storied structure were carried out by using equivalent static and response spectrum methods. It was finally concluded that the response of the structures obtained by static method was found to be much higher than that of response spectrum analysis. Hence response spectrum analysis gives a more accurate value, and it is reliable.

Ahirwar et al. [14] evaluated seismic loads on multistory RC framed structures, they considered three, five, seven and nine storey buildings, and each were analysed using seismic coefficient method, response spectrum method and modal analysis method. Seismic responses viz. storey shear and base shear were computed for all the four buildings, and the results were compared. The following conclusions were brought up from the above study: In both versions of codes IS: 1893–1984 and IS: 1893–2002, the seismic plan approach is to plan solid and flexible structure to deal with latency powers produced by quakes. The new version of IS: 1893–2002 plainly reflects that the seismic force configuration is much lesser than what can be normal from strong ground shaking. Seismic forces obtained from IS: 1893–2002 are relatively higher than that forces acquired by IS: 1893–1984. As per, IS: 1893–1984, when compared to response spectrum method and modal analysis method, the base shear value of seismic coefficient method would be higher. Modal analysis method gives higher values of lateral forces for upper storey.

Gottala et al. [15] proposed a similar investigation of static and dynamic seismic examination of a multi-story building that was done on a multi-storied encircled structure of nine storey. Direct seismic examination was completed for the working by seismic coefficient method and response spectrum method using STAAD-Pro as per 1893–2002-Part-1. A detailed examination was completed between the static and dynamic investigation, and the outcomes of the analysis, bending moment, nodal displacements and mode shapes were observed for beams and columns.

3 Methodology

The methodology includes the following:

1. Structure with a steel building of 20 storey's with its various structural and construction techniques. Its analysis methods and deign aspects.
2. Structure with a steel building of 20 storey's having knee bracings with its various structural and construction techniques. Its analysis methods and deign aspects.
3. Structure with a steel building of 20 storey's having X bracings with its various structural and construction techniques. Its analysis methods and deign aspects.

The analysis and the design of 20 storey's steel building and various types of bracings was done according to IS codal provisions for steel and concrete sections.

4 Modelling

For the analysis and design of the structure, ETABS software is used and the deign results and the various outputs are explained in detail.

The details of the structure are listed in Table 1.

Table 1 Structural details

Description	Values
Number of storey	20
Number of bays in X direction	9
Number of bays in Z direction	7
Storey height	3.5
X Direction width of bay	4
Z Direction width of bay	4.5
Grade of concrete	M25
Grade of steel	FE415
Live load	2 kN/m^2
Zone	V
Response reduction	5
Importance factor	1.5
Thickness of slab	110 mm
Steel bracing	As per IS 800 codal provisions-ISMB
Knee bracings	As per IS 800 codal provisions-ISMB

Earthquake loads are determined as per IS 1893:2016. Design of steel and concrete sections was done according to the limit state design, and the load combinations are considered which are determined with consideration to IS 800:2007 from Table 2.

5 Results

See Table 2, Figs. 1, 2, 3, 4, 5, 6, 7, 8, 9, 10.

Table 2 Results of the structure with its performance level

Sl. no	Model type	V	D	Sa	Sd
1	Plane frame	521.54	0.128	0.165	0.997
2	X Bracings	2034.5	0.018	0.790	0.014
3	Knee Bracings	2027.4	0.024	0.796	0.019

Fig. 1 Frame with loadings

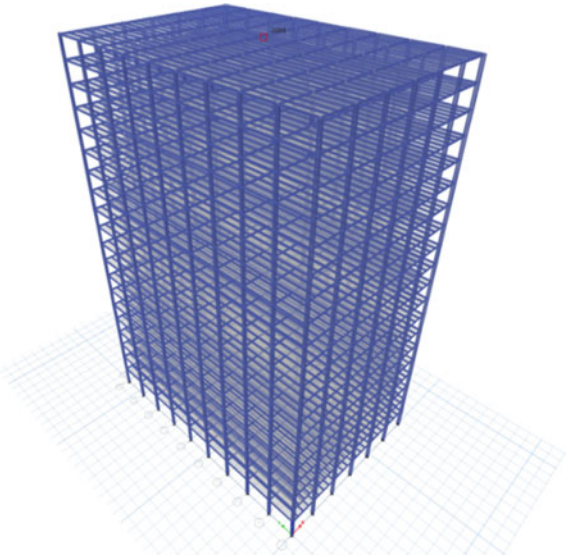

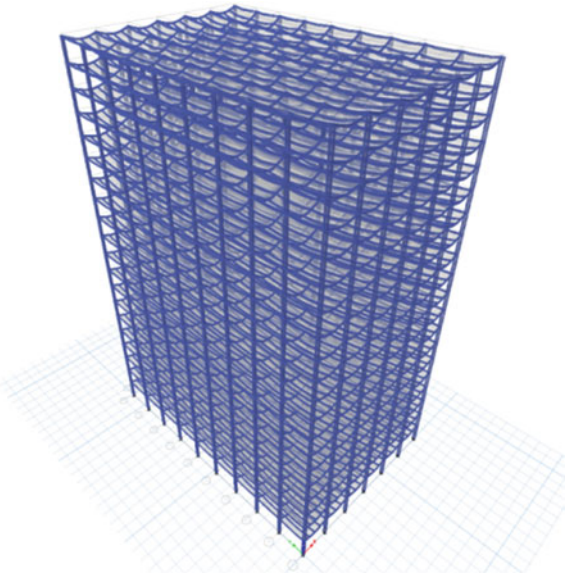

Fig. 2 Deflected shape of the building after analysis

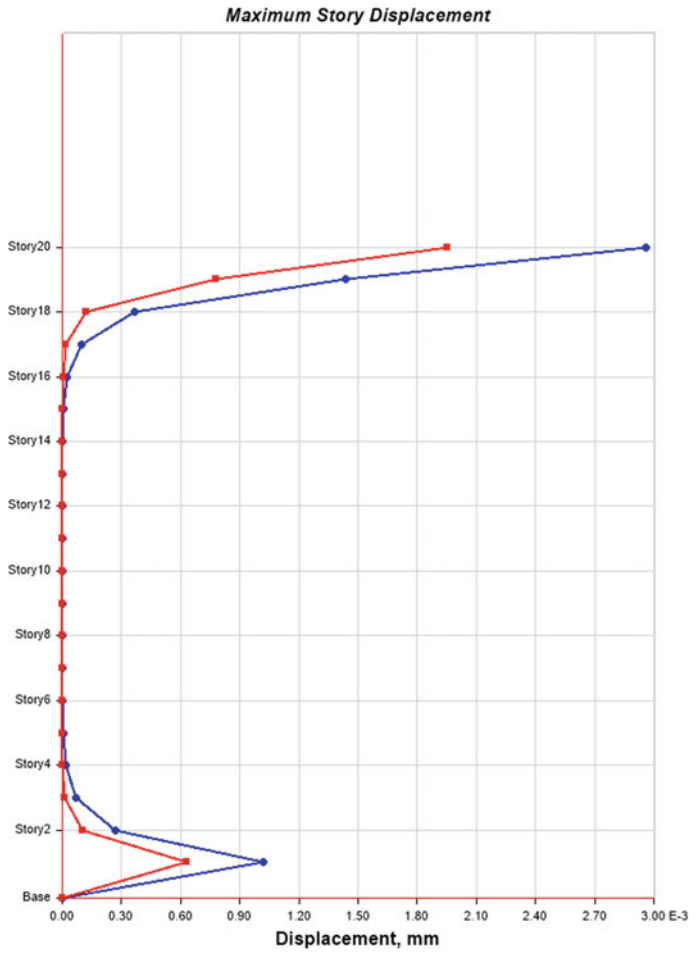

Fig. 3 Maximum storey displacement without bracings

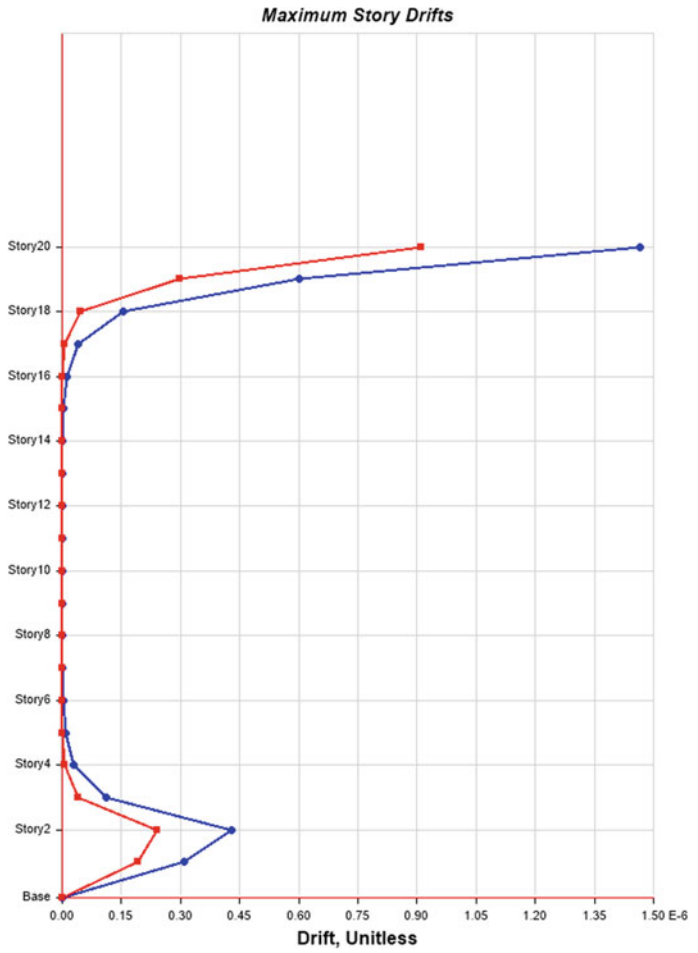

Fig. 4 Maximum storey drift without bracings

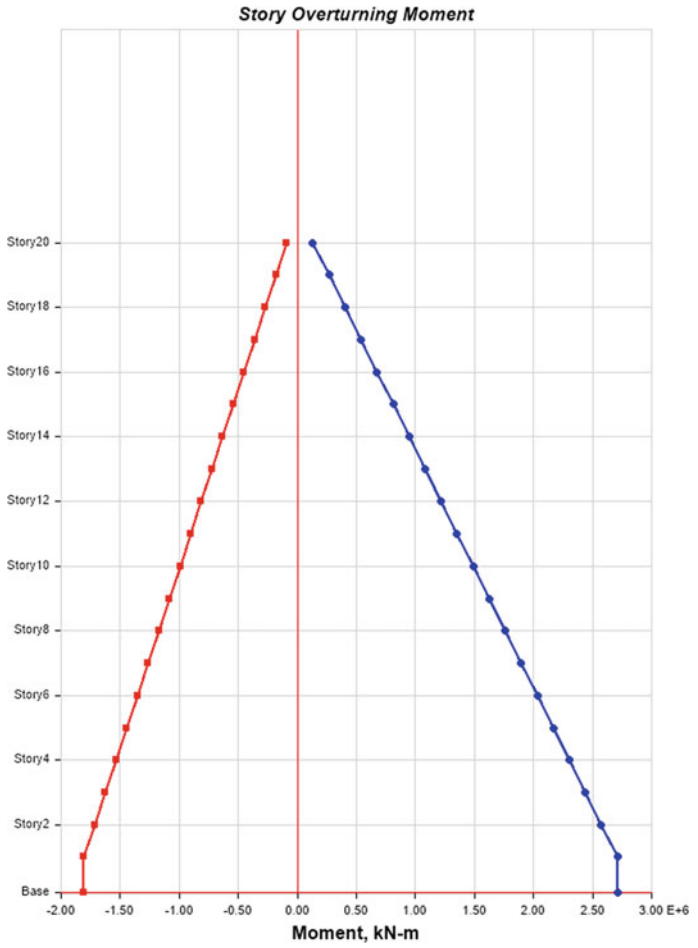

Fig. 5 Storey overturning momnet

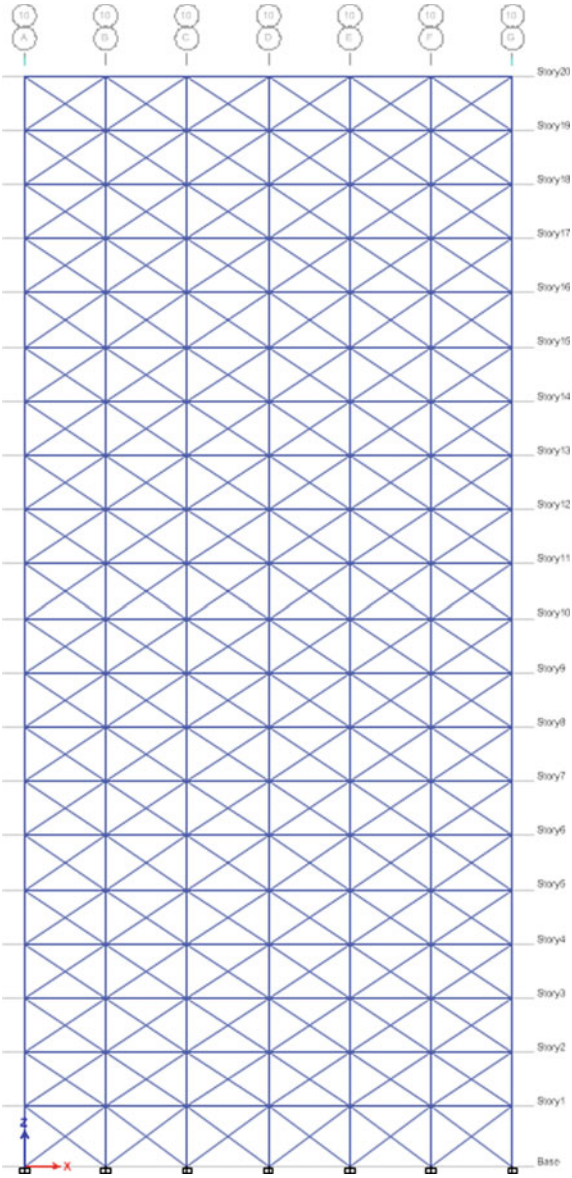

Fig. 6 Storey overturning momnet

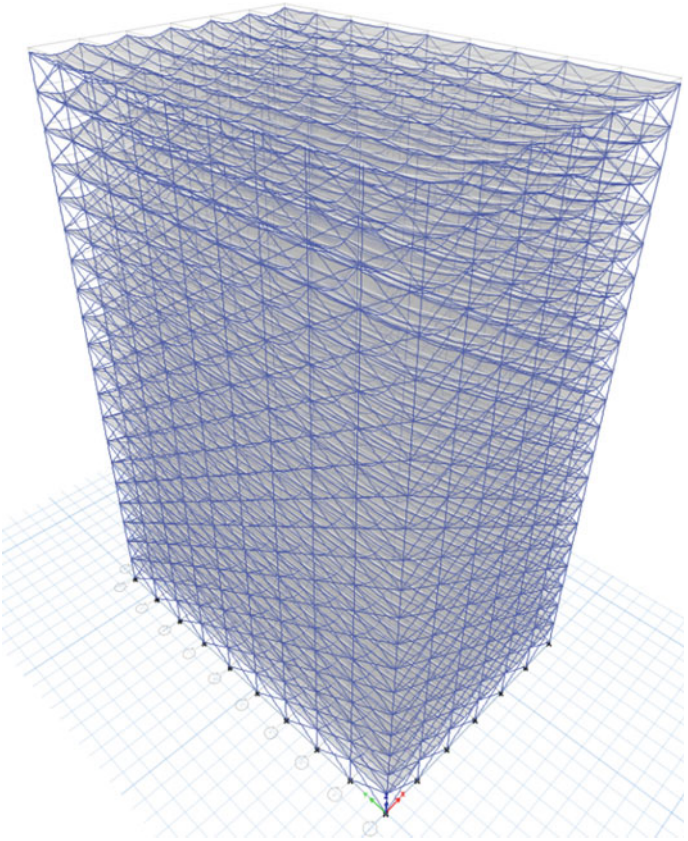

Fig. 7 Frame with loadings with X bracings

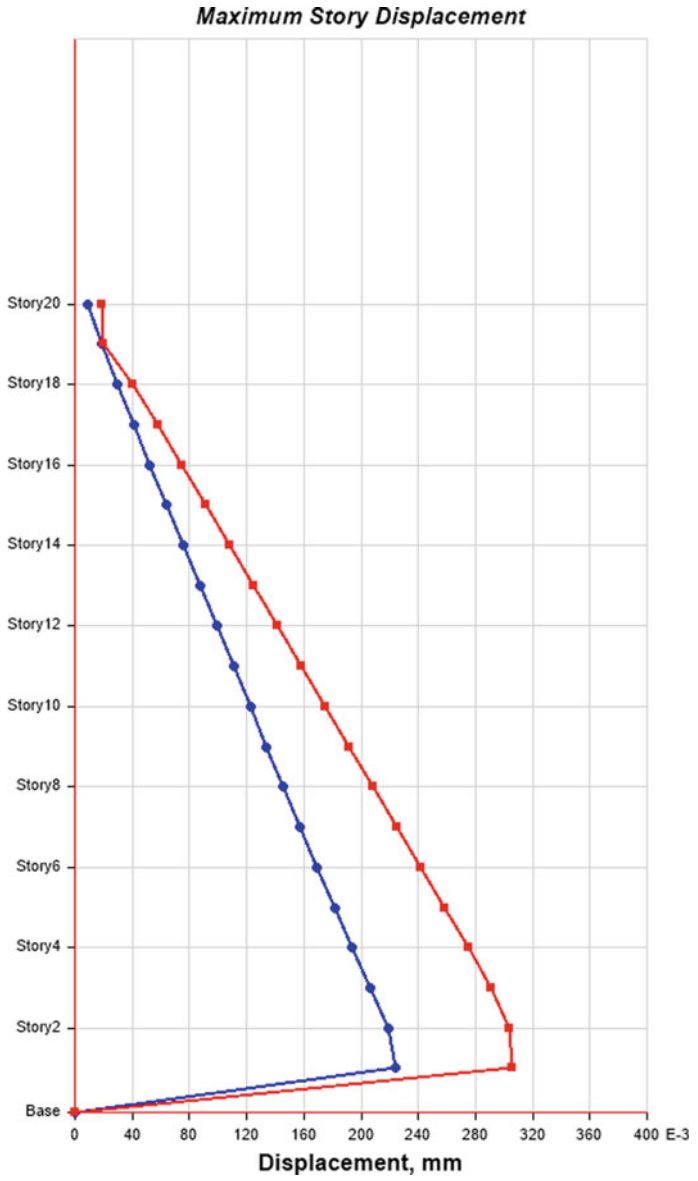

Fig. 8 Deflected shape of the building after analysis with X bracings

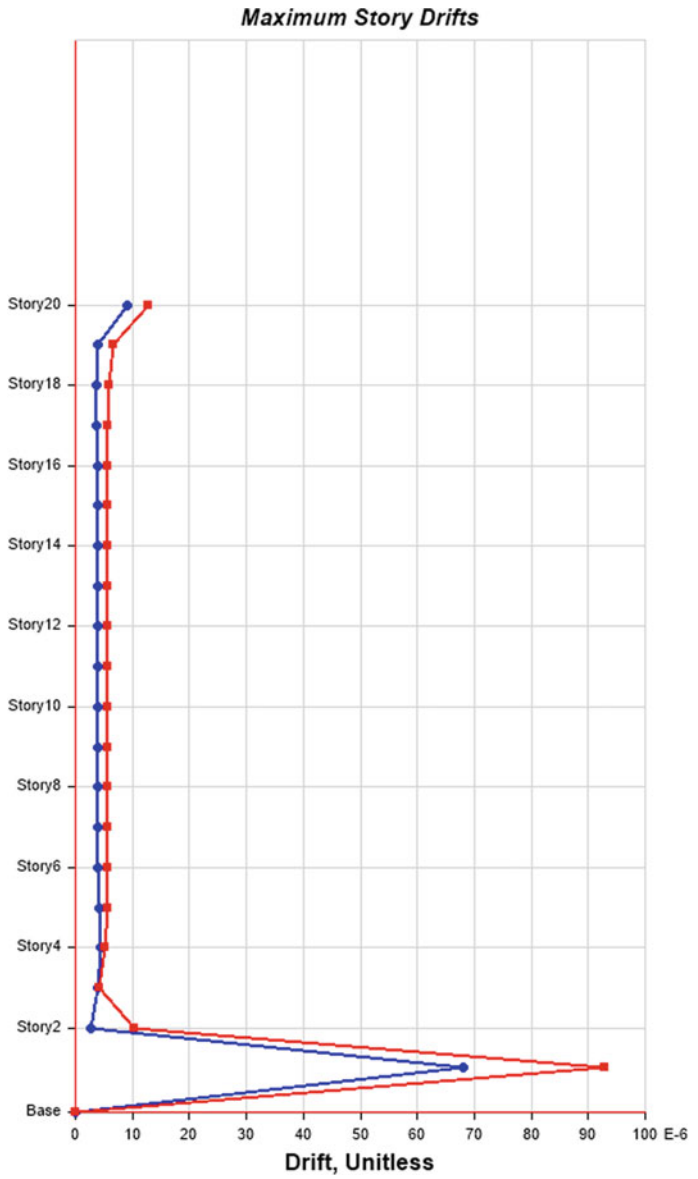

Fig. 9 Maximum storey displacement with X bracings

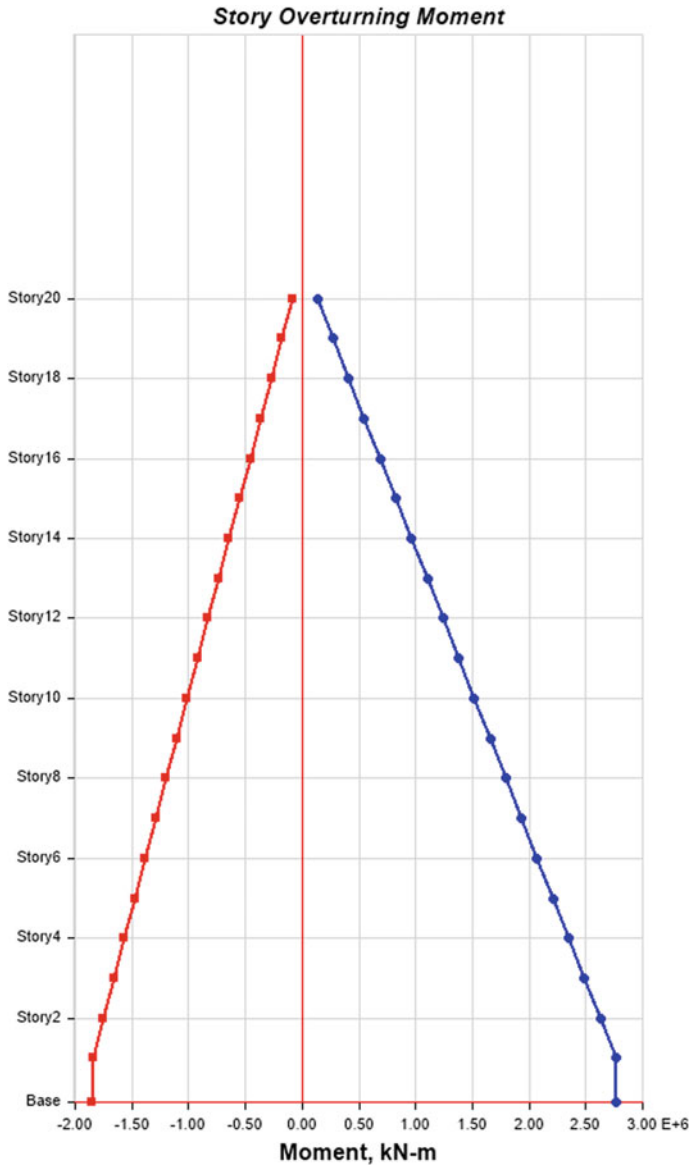

Fig. 10 Maximum storey drift with X bracings

6 Conclusions

The structural system with two types of bracing system for a twenty storey building has been analysed and designed.

And the conclusions of the research have been given below.

1. The drift in the storey without any bracing is nearly the same as specified in the IS 1893 codal provisions. With the use fob arcing systems out of X and knee bracing, X bracing is found to be more effective than knee bracing as there is significant reduction in the global lateral displacement in both X and Y directions.
2. After determining the performance of the structure with X and knee bracing, it was found that knee bracing is found economical as the overall capacity gets increased when compared to X bracing.

References

1. Gottala A, Kishore KSK, Yajdhani S (2015) Comparative study of static and dynamic seismic analysis of a multistoried building. Int J Sci Technol Eng 2(1)
2. Srikanth B, Ramesh V (2013) Comparative study of seismic response for seismic coefficient and response spectrum methods. Int J Eng Res Appl 3(5):1919–1924
3. ETABS DesignManuals
4. Saisaran GS, Yogendra Durga Prasad V, Venkat Das T (2016) Push over analysis for concrete structures at seismic zone-3 using ETABS Software. Int J Eng Res Technol (IJERT) 5(3)
5. Gardner L (2005) The use of stainless steel in structures. Prog Struct Mat Eng 7(2):45–55
6. Mindaye G, Yajdani S (2016) Seismic analysis of a multistorey RC frame building in different seismic zones. Int J Innov Res Sci Eng Technol 5(9)
7. Govindan SK, Madhavan M (2017) The flexural strength behavior of profiled steel sheet–with hot rolled plate panel system with bolted connection. CE/papers 1(2–3):1786–1795
8. IS 1893(Part 1) (2002) Criteria for earthquake resistant design of structures, part 1, general provisions and buildings (Fifth Revision), New Delhi–110002: Bureau Indian Standards
9. IS 456 (2000) Plan and reinforced concrete code for practice (fourth revision), New Delhi-110002. Bureau Indian Standards
10. IS 875 (Part 1, Part 2, Part 3) (1987) Code of practice for design loads (other than earthquake) for buildings and structures. New Delhi-110002. Bureau Indian Standards
11. Jingbol L, Yangbing L (2008) Seismic behaviour analysis of steel-concrete composite frame structure systems. World Conference on Earthquake Engineering
12. Madhavan M, Davidson JS (2009) Theoretical evaluation of flange local buckling for horizontally curved I-girders. J Bridge Eng 14(6):424–435
13. Youcef M, Abderrahmane K, Benazouz C (2018) Seismic performance analysis of an irregular existing building using the future seismic code RPA 2018 and non linear dynamic analysis. Int Civil Eng Conf
14. Anwaruddin M, Akberuddin M, Saleemuddin ZM (2013) Pushover analysis of medium rise multi-story RCC frame with and without vertical irregularity. Int J Eng Res Appl 3(5):540–546. www.ijera.com
15. Patel DY, Jain P, Patel VR (2017) Response spectrum analysis of tall building having different structural systems. Int J Adv Eng Res Develop. ISSN number: 2348–4470

16. Chandak NR (2012) Response spectrum analysis of reinforced concrete buildings. J Inst Eng India. https://doi.org/10.1007/s40030-012-0012-9
17. Natesan V, Madhavan M (2017) Rotational behavior of cold formed steel beams connected through clip angles. CE/papers 1(2–3):1580–1589
18. Agarwal P, Shrikhande M (2006) Earthquake resistant design of structures. Prentice Hall of India Private Limited
19. Pardeshisameer, Gore NG (2016) Study of seismic analysis and design of multi storey symmetrical and asymmetrical building. Int Res J Eng Technol (IRJET) 3(1)
20. Shirule PA, Mahajan BV (2013) Response spectrum analysis of asymmetrical building. Int J Sci Spiritual Business Technol 1. ISSN number: 2277–7261
21. Pandey R (2014) Comparative seismic analysis of RCC, steel & steel-concrete composite frame. National Institute of Technology, Rourkela
22. Prabhu Booshan S, Sindhu Nachiar S, Anandh S (2017) Comparative analysis of R.C.C. and composite structures with different vertical irregularities. Department of Civil Engineering, SRM University, ISSN number: 2312–7791
23. Ahirwar SK, Jainand SK, Pande MM (2008) Earthquake loads on multistorey buildings as per IS:1893–1984 and IS:1893–2002: a comparative study. In: 14th world conference on earthquake engineering (WCEE). Beijing, China
24. Selvaraj S, Madhavan M (2018) Improvements in AISI design methods for gypsum-sheathed cold-formed steel wall panels subjected to bending. J Struct Eng 145(2):04018243
25. Shanmugam NE, Mahendrakumar M, Thevendran V (2003) Ultimate load behaviour of horizontally curved plate girders. J Constr Steel Res 59(4):509–529
26. Patil UP, Suryanarayana (2015) Analysis of G+15 RC and composite structure having a soft storey at ground level by response spectrum and equivalent static methods using Etabs 2013. Int J Adv Eng Res Develop 2. ISSN number: 2395–0056
27. Vishwanatha SN, Sandeep Kumar DS (2018) Seismic analysis of Multi-storeyed RC and composite building Subjected to vertical irregularity. Int Res J Eng Technol 5. ISSN number: 2395–0056
28. Wang L, Young B (2015) Behavior of cold-formed steel built-up sections with intermediate stiffeners under bending. II: parametric study and design. J Struct Eng 142(3):04015151

Effect of Non-homogeneity of Seabed Soil on Natural Frequency of Offshore Free Spanning Pipeline

Goutam Sarkar and Pronab Roy

Abstract Determination of natural frequency of free spanning pipeline is essential as it governs the allowable length and also fatigue life of the pipeline. From the literature survey, it is seen that a considerable amount of works have been studied to determine the effect of seabed soil on natural frequency of free span by the previous researchers. However, researchers have assumed that soil of the supports of free span is homogeneous. Well-used code DNVGL-RP-F105 (for free span analysis of offshore pipeline) also considers soil as homogeneous. But, recently, researchers state that non-homogeneity of soil has significant effects on dynamic soil stiffness. The objective of this paper is to determine the effect of non-homogeneity of soil on the natural frequency of free spanning pipeline. In this paper, a frequency analysis of the free spanning pipeline on homogeneous soil is carried out by Det Norske Veritas (DNV) guidelines and finite element modelling. A free spanning pipeline is analysed considering it on a non-homogeneous soil using soil mesh finite element modelling. The non-homogeneous soil model is designed with different layered soil combinations. Finally, it has been observed that finite element analysis software can be incorporated for pipe-soil interaction effectively. For layered soil profile, if the topmost soil stratum is thin, it has been found out that there is a significant variation in both inline and cross-flow natural frequencies compared to those of homogeneous soil having same topmost soil. Whereas if the topmost soil stratum is thick, it will not significantly affect in-line natural frequency, but cross-flow natural frequency tends to be same as that of homogeneous soil.

Keywords Free span · Natural frequency · Dynamic soil stiffness · Layered soil · Finite element analysis

G. Sarkar · P. Roy (✉)
Department of Civil Engineering, NIT Durgapur, Durgapur 713209, India
e-mail: pronab.roy@ce.nitdgp.ac.in

T. G. Sitharam et al. (eds.), *Earthquakes and Structures*, Lecture Notes in Civil Engineering 188, https://doi.org/10.1007/978-981-16-5673-6_11

1 Introduction

One of the important issues in submarine pipeline design is free span calculation. The free span of submarine pipelines is a common and inevitable phenomenon in offshore oil and gas engineering, due to seabed unevenness, change of topology, scouring, or sand waves [1]. When the subsea wave or current flows across a free span, vorticities are formed behind the pipeline on the top and bottom. The frequency induced due to these vorticities is called vortex-induced vibration (VIV). Apart from this, the pipeline has also its natural frequency. Now, if VIV-induced frequency synchronizes with one of its natural frequencies, resonances will be more likely to happen. If resonance happens, the pipeline integrity will be threatened by fatigue damage on the pipeline welds, and ultimately pipeline will fail. Due to this, the computation of natural frequencies of the free span pipeline is a very important aspect of the offshore pipeline industry. Figure 1 shows a typical free span scenario. The middle unsupported portion of the free span pipeline will not remain straight due to the submerged weight of the pipeline.

Researchers have already recognized the importance of pipe soil interaction on the shoulders of the free span pipeline since the late 1980s and early 1990s. Hobbs [2], developed a non-dimensional graph of effective length to incorporate the effects of seabed elasticity on the dynamic behaviour of the free span pipeline. Choi [3], studied the effect of axial force on free span analysis. Fyrileiv and Mørk [4], used improved beam theory and developed a semi-empirical approximate expression. The DNV recommended practice DNV-RP-F105 [5] updates new expression for an effective length of free span pipeline based on the work of Fyrileiv and Mørk. Bakhtiary [6] investigated the effect of real seabed conditions and axial force on natural frequencies by using modal analysis with the Euler–Bernoulli beam equation. Ruby and Hartving [7] used transmitting boundary elements and included various environmental conditions, structural data, soil parameters, damping parameters, and safety factors. Xiao and Zhao [8] studied single and multi-span pipelines by using dynamic finite-element analysis. Mehdi et al. [9] examined the influence of different types of soil natural frequency of free spanning pipeline by both mathematical modelling and

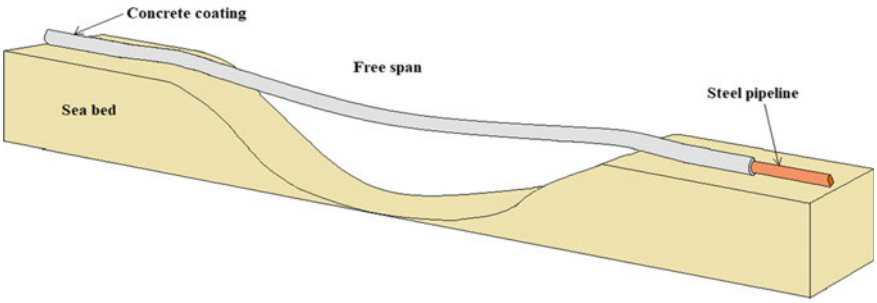

Fig. 1 A Sketch of a typical free spanning offshore pipeline

finite element analysis. Vedled and Sollund [1] developed a semi-analytical method to carry out a modal analysis of free span pipelines by applying the Rayleigh–Ritz method. Sollund et al. [10] performed dimension analysis by using the Buckingham Pi theorem for the modal response of the free span pipeline. Guha and Randolph et al. [11], proposed a new form of axial soil stiffness calculation, which depends on the embedment of pipe and degree of soil non-homogeneity. DNVGL-RP-F105 [12] gives guidelines for distinguishing between interacting multi-span and isolated single spans. A separate expression has been given for determining the lowest frequency and maximum amplitude for very short spans in this new guideline. Li et al. [13] investigated the modal response of the free span pipeline by using a general integral transform technique (GITT).

Thus, to study the dynamic response of the free span pipeline, great effort has been made by carrying out both mathematical and finite element analysis by a large number of researchers. All of them concluded that the soil in the supports of the free span pipeline played a significant role on the dynamic response. However, in the free spanning pipeline analyses, the previous researchers considered only homogeneous soil, but in reality, it is not homogeneous. The seabed profile is normally mixed or layered in nature. The layered profile of seabed soil is a composite of very soft clay to hard clay and silt or sand. Thus, the effects of layered profile or mixed profile of seabed soil on the dynamic response of the free span pipeline should be analysed.

In this present paper, the dynamic behaviour of a free span offshore pipeline and the effect of the layered profile of seabed soil on its dynamic behaviour have been studied. The dynamic behaviour of the single-span pipeline has been analysed in terms of extracting the fundamental natural frequencies of the free spanning pipeline by using DNV guidelines and finite element analysis (FEA) modelling. The main aim of this study is to understand the effects of layered seabed soil characteristics on the natural frequencies. Here, a 60 m free span pipeline has been considered with L/D ratio 60. In this paper, two different cases have been investigated, at first, the soil has been assumed to be homogeneous (stiff clay or hard clay) at the shoulder of the free span pipeline. Then, the results of FEA modelling have been validated by DNV guidelines. Next, the soil has been assumed to be a two-layer system, a hard clay stratum is considered to be underneath the stiff clay. Finally, a parametric study has been carried out to analyse the influence of layered soil profile on the natural frequencies of free spanning offshore pipeline by varying stiff clay depth while keeping the total depth of soil constant.

2 Methodology

2.1 Structural and Functional Data of Pipeline

The geometry of the free spanning pipeline has been modelled as a free span in the middle and two equally sized shoulders, which are supported on soil. Here in this free

Table 1 Geometric properties of pipeline

Variable	Symbol	Unit	Value
Free span length	L	m	60
Shoulder-length	L_{sh}	m	180
Outer diameters	D	mm	1000
Wall thickness	T	mm	30
Concrete coating thickness	t_c	mm	68

Table 2 Material properties of pipeline

Variable	Symbol	Unit	Value
Modulus of elasticity for steel	E_{st}	GPa	207
Poisson's ratio for steel	ν	–	0.3
Density of steel	ρ_s	kg/m^3	7850
Density of concrete	ρ_c	kg/m^3	3040
Density of hydrocarbon	ρ_h	kg/m^3	200
Density of water	ρ_w	kg/m^3	1025

span model, the shoulder-length on each side of free span has been considered as three times of free span length [1] and the geometric properties of pipeline are tabulated in Table 1. To increase the submerged weight, pipe has been coated with a concrete coating. It should be noted that in these analyses, only the mass contribution due to concrete coating has been taken into consideration, while the structural stiffness due to concrete coating has been neglected for simplicity in FEA modelling. The total effective mass has been determined as 2355.069 kg/m. The effect of axial force on the free span pipeline has also been neglected here. The submerged weight of the pipe is determined as 7308.48 N/m.

For modelling the pipeline, API 5L X65 grade of stainless steel is used, which is taken from API 5L [14] specification. The pipe material is assumed to be isotropic. The material properties of the pipeline are given in Table 2. The seabed soil properties are tabulated in Table 3. C_L and C_V are the simplified lateral and vertical dynamic stiffness factors for the soil, respectively, which are required for determining horizontal and vertical dynamic soil stiffnesses, respectively. The dynamic shear modulus

Table 3 Soil properties of the seabed

Soil type	Undrained shear strength (kN/m^2)	Coefficient of friction w.r.t. concrete	Submerge unit weight (kN/m^3)	Poisson's ratio	Modulus of elasticity (N/m^2)	C_V (kN/m$^{5/2}$)	C_L (kN/m$^{5/2}$)
Stiff clay	50-100	0.35	7–12	0.45	21.75×10^6	4500	3900
Hard clay	200	0.50	10–13	0.45	58×10^6	12,000	10,500

of soil is determined according to DNVGL-RP-F114 [15] clause 4.5.3.2 and clause 4.5.3.3 by using dynamic soil stiffness. Finally, the modulus of elasticity of soil is determined from shear modulus. The coefficient of friction for different types of soil with respect to concrete has been provided according to Potyondy [16].

2.2 Determination of Natural Frequency by DNVGL-RP-F105 (2017) Guidelines

The DNVGL-RP-F105 [12] is a guideline for free span subsea pipeline. In this code at clause 6.8.2, a simple formula (Eq. 1) is provided to calculate the lowest natural frequency of free spanning subsea pipeline considering pipeline specifications, seabed soil conditions, concrete coating, effective axial force, and vertical out-of-straightness. There is a limitation of this semi-empirical expression; the span length should be less than 140 D_s (outer steel pipe diameter) and compressive effective axial force up to 0.5 P_{cr} and ratio of static deflection (δ) to the outer diameter of the pipe (D) should be less than 2.5. The expression is as follows:

$$f_1 = C_1 \sqrt{\frac{E_{st} I_{st}}{m_e L_{eff}^4} \left(1 + \frac{S_{eff}}{P_{cr}} + C_3 \left(\frac{\delta}{D}\right)^2\right)} \tag{1}$$

C_1 and C_3 are boundary condition coefficients. The E_{st} and I_{st} are Young's modulus and moment of inertia of the steel pipe, respectively. L_{eff} is the effective length of pipeline corresponding to seabed soil in free span. Equation 2 shows the expression of the effective length according to DNVGL-RP-F105 [12], clause 6.8.8.

$$\frac{L_{eff}}{L_s} = \begin{cases} \frac{4.73}{0.066\beta^2 + 1.02\beta + 0.63} for \beta \geq 2.7 \\ \frac{4.73}{0.036\beta^2 + 0.61\beta + 1.0} for \beta < 2.7 \end{cases} \tag{2}$$

The β is a non-dimension parameter and calculated by using Eq. 3,

$$\beta = \log_{10}\left(\frac{K {L_s}^4}{E_{st} I_{st}}\right) \tag{3}$$

where L_s is free span length of pipeline. K is dynamic seabed soil stiffness (vertical or horizontal). For inline frequency determination, lateral dynamic stiffness (K_L) is used. According to DNVGL-RP-F114 [15] clause 7.2.4, the K_L can be determined by the following Eq. 4,

$$K_L = C_L \times (1 + \nu) \times \left(\frac{2}{3} \times \frac{\rho_s}{\rho} + \frac{1}{3}\right)\sqrt{D} \tag{4}$$

For cross-flow frequency, the vertical dynamic stiffness (K_V) is used, and it is given by Eq. 5 according to DNVGL-RP-F114 [15] clause 7.2.4.

$$K_V = \frac{C_v}{(1-\nu)} \times \left(\frac{2}{3} \times \frac{\rho_s}{\rho} + \frac{1}{3}\right)\sqrt{D} \tag{5}$$

C_L and C_V are the coefficients with respect to soil and taken from Tables 7.3 to 7.4 of DNVGL-RP-F114 [15], respectively, and are tabulated in Table 3. ν is the Poisson's ratio of corresponding seabed soil, $\frac{\rho_s}{\rho}$ is the ratio of density pipe mass (not including added mass) and displaced water, and D is outer diameter of pipe including coating thickness.

2.3 *Determination of Natural Frequency by Numerical Method*

Commercial finite element software Abaqus 6.12 [17] has been used to determine natural frequency of free spanning offshore pipeline. A finite element analysis in Abaqus includes various modules such as creating a model, defining material property, assembling various parts, creating step module, specifying boundary conditions and external loads, specifying the interaction property between different parts, discretization of parts, and finally post-processing. Here, the geometric and material properties used in FEA analysis are same as in analytical method.

The geometry of the model

In Abaqus CAE software, free span pipeline has been modelled as pipeline supported by two equal sizes of soil shoulders. To model a free span pipeline, reasonable and practical 3D-FE models have been established here. The pipeline model has been created as a 3D deformable shell model due to thin thickness of pipeline and soil in shoulder modelled as a 3D deformable solid body as shown in Figs. 2 and 3. Pipe has been assumed to be half diameter embedded into soil [11].

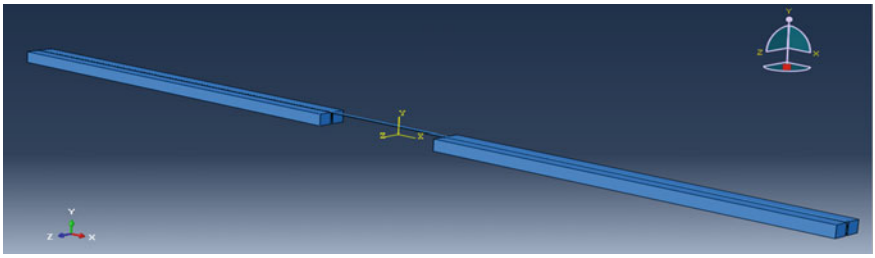

Fig. 2 Free span offshore pipeline model with homogeneous soil in FEA

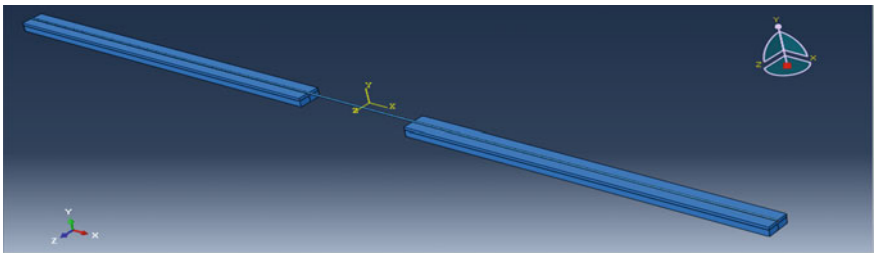

Fig. 3 Free span offshore pipeline model with layered soil in FEA

Pipeline model

A 3D reduced shell continuum element with four nodes as a first-order (or linear) interpolation (S4R) has been chosen for the pipe. Length, outer diameter, and wall thickness of pipe are given in Table 1. The total length of pipeline is 420 m. Shoulder-length on each side of free span is taken as three times of free span length [1]. The material property of pipeline has been shown in Table 2. Steel pipeline has been chosen, considered as an elastic and isotropic in this study.

Soil model

The soil is modelled as a rectangular block, and both vertical and horizontal boundaries are placed at 6.25 m (6.25D) away from the centreline of the embedded portion of pipe [11]. The 3D reduced integration continuum element with eight nodes as a first-order (or linear) interpolation (C3D8R) is used to model soil in the shoulder. The "R" denotes reduced integration formulations. In this study, two different soil models have been taken. The first one is homogeneous soil (Fig. 2) model (stiff clay or hard clay), and the second one is layered soil with topsoil as stiff clay and followed by hard clay (Fig. 3). Soil is assumed to be an elastic–perfectly plastic material, thus here Mohr–Coulomb failure criteria has been adopted.

Meshing and Seed

It is an important module since the accuracy of the result depends on meshing of the assemblies. A biased discretization is provided near the contact surface of pipe and soil, as finer elements are required near the contact region to incorporate the pipe-soil interaction more efficiently.

The mess sensitivity analysis has been performed to find out the optimum size of element. To do this, first soil shoulders are modelled with 540 numbers of C3D8R elements, and pipe is modelled with 2100 numbers S4R elements. With this messing, total time required to complete the analysis of the model was 36 s, and obtained inline and cross-flow fundamental natural frequencies of the model were 0.66296 Hz and 0.73149 Hz, respectively. Secondly, while doing the meshing of pipe, the numbers of element have been kept same, whereas the soil shoulders have been messed with 3584 numbers of C3D8R element. With this messing, the total time required to complete the analysis of the model was 66 s, and the obtained inline and cross-flow

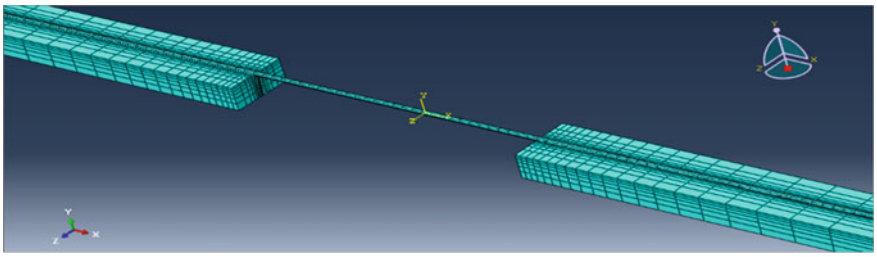

Fig. 4 Applied meshes in a free span model with elements in 100 m models

fundamental natural frequencies were 0.66201 Hz and 0.74438 Hz, respectively. Again, while doing the meshing of pipe, the numbers of element have been kept same, whereas the soil shoulders have been messed with 22,176 numbers of C3D8R element. Now, the model has taken a total time of 549 s, and the obtained inline and cross-flow fundamental natural frequencies are 0.66212 Hz and 0.74469 Hz, respectively. So, it was concluded that the optimum number of C3D8R elements at shoulders is 3584. Lastly, the optimum number of pipe elements were studied and it was considered that the number of pipe elements at the bottom of pipe and the contact region of soil is same. The optimum number of S4R element is 2100 in this study. Figure 4 shows enlarged picture of applied meshes on free span model.

Load

The self-weight of the model is applied by providing gravity loading. The mass of concrete cover and added mass are considered as the non-structural mass because the stiffness contribution to structural stiffness matrix is assumed as negligible. The submerged weight of pipe is also added to the non-structural mass.

Model boundary conditions

Two types of boundary conditions (hinge and fix) are considered in this analysis. To restrain the translation movement along the sides of soil shoulder (i.e. "Z" axis) and shoulder ends (i.e. "X" axis), hinge supports are provided. The bottom surface of the soil shoulder is to be restrained from translation and rotational movements. To achieve this, fix support has been assigned to the bottom surface. So, an infinitely long pipeline which is resting on a seabed soil, has been represented by this assumption of boundary condition [18]. The boundary conditions provided in this model are shown in Fig. 5.

Interactions

To execute the study for interaction between soil and subsea pipeline under a dynamic excitation, the portion of pipe surface embedded in soil was treated as fully rough and also assumed that a frictional property exists between soil surface and pipe surface, thus "surface to surface contact" has been used with penalty friction. In the case of

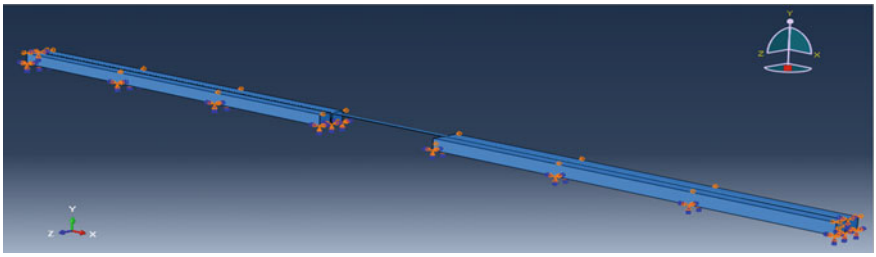

Fig. 5 The boundary conditions of the free span offshore pipeline model in FEA

layered soil model, the interaction between two types of clay "tie constraint" has been used, as it is assumed that both clay surfaces are fully bonded to each other.

3 Results and Discussion

3.1 Homogeneous Soil

Here, a free span having homogeneous seabed has been studied by both numerical models and DNV guidelines. Two different types of clay in the shoulder are selected for this analysis, homogeneous stiff clay and hard clay. The *L/D* ratio of the model is 60. The mode shapes of free span offshore pipeline for first inline and cross-flow frequencies with stiff clay soil are shown in Figs. 6 and 7, respectively.

Table 4 shows the comparison of results from FEA with DNV for the two selected verification cases. It is observed that both models show around 5% variation in inline flow frequency and cross-flow frequency. Thus, the inline and cross-flow frequencies vary for both DNV and FEA within the permissible limit (i.e. 5% according to clause

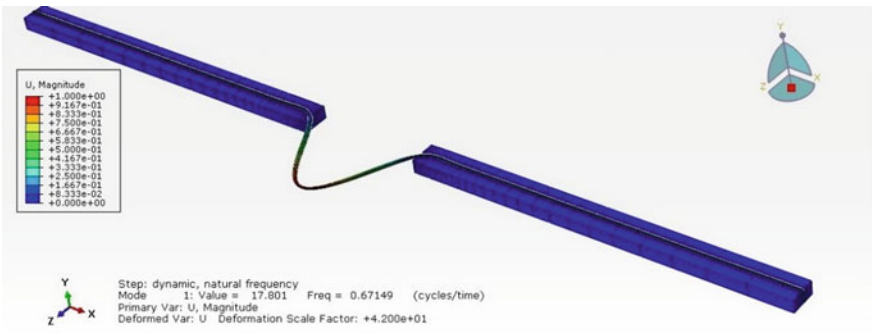

Fig. 6 1st inline mode shape in the FE model with homogeneous stiff clay

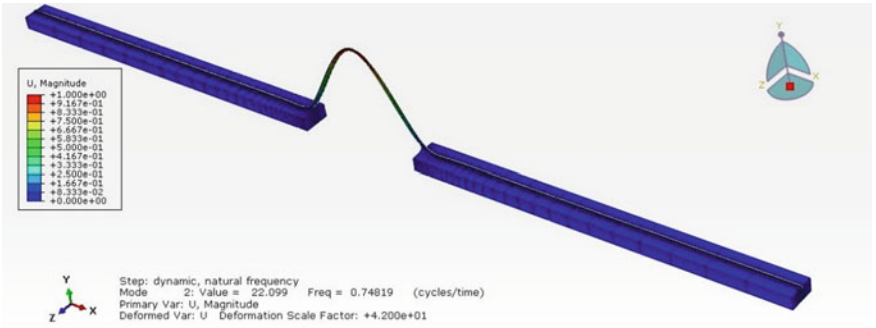

Fig. 7 1st cross-flow mode shape in the FE model with homogeneous stiff clay

Table 4 Comparison of fundamental natural frequencies from FEA with those of DNV for the two selected verification cases

Soil type	Direction of flow	DNV (Hz)	FEA (Hz)	Percentage variation
Stiff clay	Inline	0.6738	0.6715	0.34
Stiff clay	Cross-flow	0.7072	0.7482	5.48
Hard clay	Inline	0.7297	0.7187	1.51
Hard clay	Cross-flow	0.7565	0.8039	6.72

6.7.4 of DNVGL-RP-F105) [12]. This observation validates the FE model prepared in Abaqus.

3.2 Non-Homogeneous Soil

The non-homogeneity of seabed soil in free span soil shoulder has been incorporated by introducing a layered profile. The seabed soil is assumed to be a two-layer system. A stiff clay stratum is considered to be overlaid above the hard clay stratum, and the pipeline is laid on the top of the stiff clay. In this section, a parametric study of varying stiff clay depth while keeping the total depth of soil constant has been carried out, to analyse the influence of this layered soil profile on the natural frequencies of free spanning pipelines. For this, total five different free span models have been generated with 1 m, 2 m, 3 m, 4 m, and 5 m depth of stiff clay. The total depth (6.25 m) of soil shoulder is considered to be the same for all free span models by providing hard clay underneath the stiff clay stratum. Figures 8 and 9 show the first inline and cross-flow mode shapes of the free spanning pipeline with 1 m stiff clay layer over 5.25 m hard clay, respectively. Table 5 gives a summary of the frequencies computed by Abaqus CAE for this parametric study of layered soil.

Here, in these analyses, it is shown that the effect of increasing stiff clay depth (1 m, 2 m, 3 m, 4 m, and 5 m) on inline natural frequency is very negligible (no change

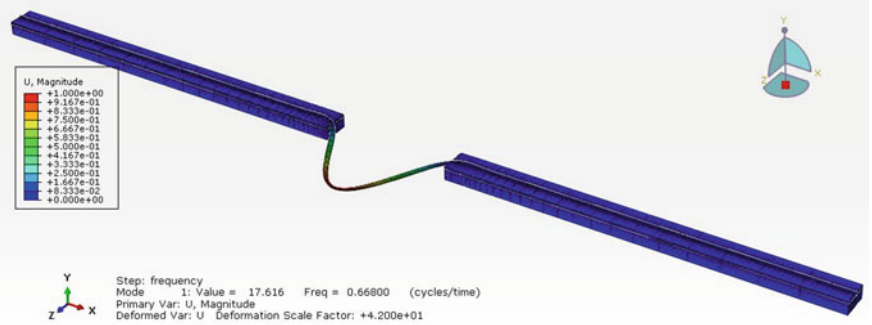

Fig. 8 1st inline mode shape in the FE model with 1 m stiff clay and 5.25 m hard clay

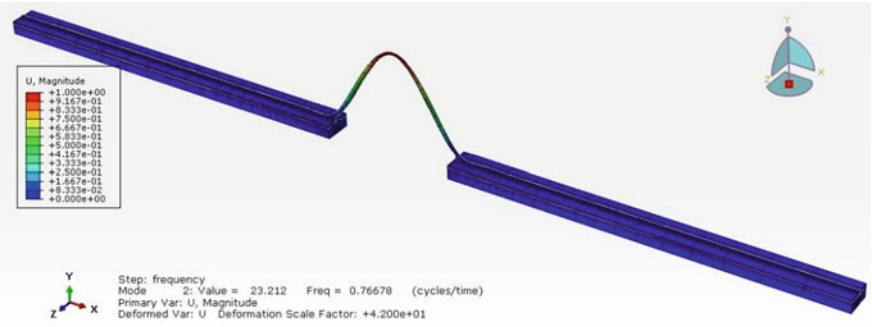

Fig. 9 1st cross-flow mode shape in the FE model with 1 m stiff clay and 5.25 m hard clay

Table 5 Results of the parametric study of layered soil computed on Abaqus CAE

Depth of stiff clay (m)	Depth of hard clay (m)	Direction of flow	Frequency (Hz)
1.00	5.25	Inline	0.6680
		Cross-flow	0.7668
2.00	4.25	Inline	0.6613
		Cross-flow	0.7570
3.00	3.25	Inline	0.6586
		Cross-flow	0.7493
4.00	2.25	Inline	0.6569
		Cross-flow	0.7427
5.00	1.25	Inline	0.6562
		Cross-flow	0.7399

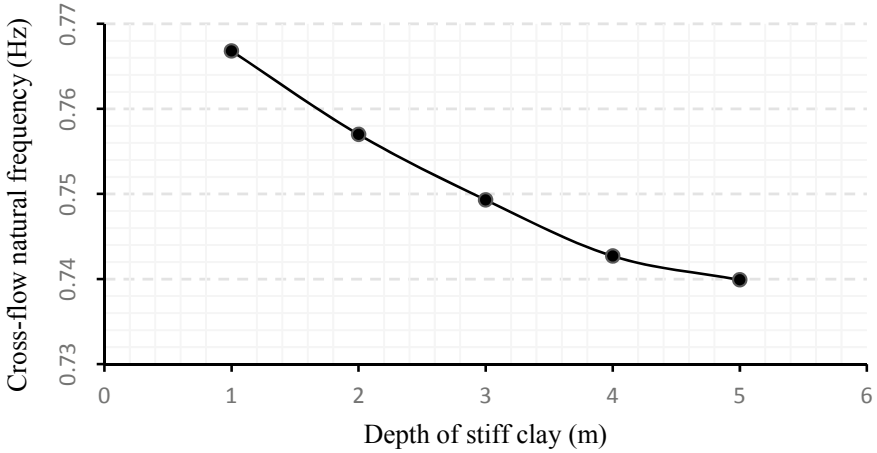

Fig. 10 The variation of cross-flow frequency with increasing depth of stiff clay soil

up to two decimal places) except stiff clay with 1 m and 2 m depth model. The cross-flow natural frequency for stiff clay with 1 m thickness comes as 0.7668 Hz, which is close to the cross-flow frequency of homogeneous hard clay model (0.8039 Hz). But, it is observed that when the depth of stiff clay is increased (2 m, 3 m, 4 m, and 5 m), the natural frequency approaches to the cross-flow natural frequency of homogeneous stiff clay (0.74814 Hz). To visualize this phenomenon, a graph has been plotted between depth of stiff clay and cross-flow natural frequency (Fig. 10).

4 Conclusions

The lowest inline and cross-flow natural frequencies have been calculated by both numerical and DNVGL-RP-F105 [12] guidelines for a free span having homogeneous soil shoulders. The FE analysis shows a variation of around 1% for inline natural frequency and 6% for cross-flow natural frequency when compared with DNV guideline. So, there is a good agreement between the FEA model and the DNV guidelines, which validates the FEA model.

A non-homogeneous free span soil shoulder has been modelled by assuming stiff clay laid over hard clay stratum.

From this study, the following conclusions can be drawn:

For non-homogeneous soil having a layered profile, if the topmost soil is a thin stratum (1 m or less), then there are significant variations in both inline and cross-flow natural frequencies compared to those of homogeneous soil having the same soil throughout. So, in a layered soil, if the topmost soil stratum is thin, then it cannot be assumed as homogeneous soil.

If the topmost soil stratum is more than 1 m, the increasing depth of topsoil will not significantly affect the inline natural frequency as compared to that in case of homogeneous soil having the same topmost soil. Whereas as the depth of the top layer is increasing, the cross-flow frequency will approach that of homogeneous soil.

References

1. Vedeld K, Sollund H, Hellesland J (2013) Free vibrations of free spanning offshore pipelines. J Eng Struct 56:68–82
2. Hobbs RE (1986) Influence of structural boundary conditions on pipeline free span dynamics. In: Proceedings of 5th international conference on offshore mechanics and arctic engineering, Tokyo, pp 685–690
3. Choi HS (2001) Free spanning analysis of offshore pipelines. Ocean Eng 28:1325–1338
4. Fyrileiv O, MØrk K (2002) Structural response of pipeline free spans based on beam theory. In: Proceedings of 21st international conference on offshore mechanics and arctic engineering. Oslo, Norway, pp 1–9
5. Det Norske Veritas, DNV-RP-F105 (2006) Free spanning pipelines, Norway
6. Bakhtiary YA, Ghaheri A, Valipour R (2007) Technical note on: analysis of offshore pipeline allowable free span length. Int J Civil Eng 5(1):84–91
7. Ruby K, Hartving PA (2008) Free span analyses of an offshore pipeline. Master thesis, Aalborg University, Denmark
8. Xiao ZG, Zhao XL (2010) Prediction of natural frequency of free spanning subsea pipelines. Int J Steel Struct 1(1):81–89
9. Mehdi Y, Said M, Ebrahim J (2012) Determining natural frequency of free spanning offshore pipelines. J Persian Gulf (Marine Sci) 3(8):25–34
10. Sollund H, Vedled K, Fyrileiv O (2015) Modal response of free spanning pipelines based on dimensional analysis. J Appl Ocean Res 50:13–29
11. Guha I, Randolph MF, White DJ (2016) Evaluation of elastic stiffness parameters for pipeline–soil interaction. ASCE J Geotech Geoenviron Eng 142(6)
12. Det Norske Veritas (2017) DNVGL-RP-F105: Free spanning pipelines, Norway
13. Li T, An C, Liang W, Duan M, Estefen SF (2018) Semi-analytical solution for soil constrained vibration of subsea free-spanning pipelines. J Ships Offshore Struct 13(6):666–676
14. API 5L (2004) Specification for line pipe. American Petroleum Institute, USA
15. DNVGL-RP-F114 (2017) Pipe-soil interaction for submarine pipelines. Det Norske Veritas, Norway
16. Potyondy JG (1961) Skin friction between various soils and construction material. Géotechnique 11(4):339–353
17. Simulia (2008) Abaqus FEA user's manual, version 6.12: Dassault systems. Velizy-Villacoublay, France
18. Lee H (2010) Finite element analysis of a buried pipeline. Master thesis, University of Manchester, United Kingdom

Seismic Performance of Buildings in Hilly Regions with and Without Base Isolation and Cable Support System

V. S. Athira, S. Nair Minnu, and S. C. Mohan

Abstract The construction of buildings in hilly areas faces several challenges, such as slope stability, suitable building configuration, etc. The capacity of buildings on the sloping ground reduces as it has to accommodate different length columns in a single storey. These buildings possess both vertical and horizontal irregularities. The current study is an effort to comprehend the effect of seismic forces on the buildings in hilly regions and suitable protection systems. A comparative study of a fixed base, base-isolated, cabled-supported, and base-isolated building with cable support is carried out. The base isolator is designed according to the UBC-97 guidelines. Seismic analysis results show that the base isolator building outperformed other protection systems. Moreover, the base-isolated building with cable support also performed equally sound as base-isolated building. The reaction forces in the cables reduced the stiffness requirement of the isolator. On the other hand, the cabled building did not show any effect on the building.

Keywords Building in hilly regions · Base isolation · Cable support · Irregularity · Seismic analysis

1 Introduction

An earthquake is considered to be a major threat in the unrecorded and recorded human history [1]. An earthquake can be described as a result of a sudden movement of tectonic plates, which results in the release of energy. Its impact affects larger areas and is usually unpredictable, causing loss of life and property and poses problems to the communication systems, transport systems, etc., and results in social and financial weakening of the country. From previous earthquakes, it is confirmed that hilly areas are most vulnerable to earthquakes. Hilly regions are the toughest, and most exciting features to carry any developmental activities. Construction of buildings in hilly terrain is inhibited by their difficult terrain, steep inclines, complicated geological structure, climatic settings, and rich flora. In retort to these settings, various built

V. S. Athira (✉) · S. N. Minnu · S. C. Mohan
Birla Institute of Technology and Science Pilani, Hyderabad Campus, Hyderabad, India

T. G. Sitharam et al. (eds.), *Earthquakes and Structures*, Lecture Notes in Civil Engineering 188, https://doi.org/10.1007/978-981-16-5673-6_12

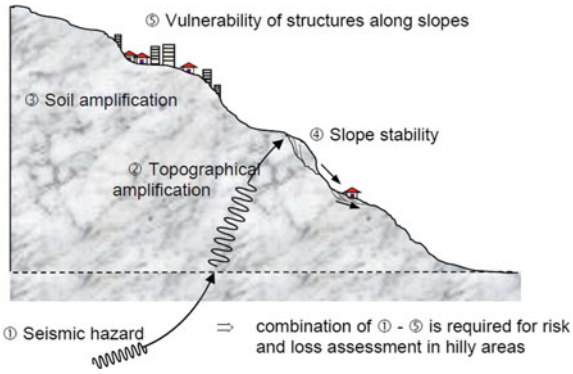

Fig. 1 Seismic safety issues associated with buildings on slopes [2]

form construction techniques and patterns of development have arisen in different hill regions of the country. Fast urbanisation has led to an increase in the population size of the hill towns and, at the same time, the development of hilly areas. Thus, there is an increased demand for the development of multi-story buildings on sloping ground. Lesser availability of plain ground also makes these construction activities on the sloping ground necessary. Buildings in hilly areas are different from those in plains. They possess vertical and horizontal irregularities and are torsionally coupled. As a result, those buildings built on slanted grounds are highly susceptible to earthquakes. These irregularities result in complex seismic behaviour, not anticipated by any of our current seismic codes. The buildings in hilly areas possess columns of different length in the ground storey due to the sloping nature of the ground. Wind load may also be considered critical when the upward slope exceeds 3°. Construction in hilly areas poses several challenges, as depicted in Fig. 1 such as topographic amplification of seismic ground motion due to the geometric features, slope failure hazard, and irregular configurations of buildings due to foundations at different levels, etc.

1.1 Current Scenario in Hilly Regions of India

The most serious concern for the engineering community during the planning and design of buildings in hill regions is their safety against natural hazards. Many vernacular practices like the Dajji wall, Kath-Kuni, Koti-banal, taaq, and wooden buildings have good responses during previous earthquakes (Fig. 2). However, current construction practices in hilly areas lack good seismic resistance and cause serious loss of human life and other precious resources. Therefore, conventional methods can be adopted with suitable modifications for the construction of better earthquake-resistant buildings in hilly areas. Materials like timber and thatch used in old-style buildings that are susceptible to fire and termite attacks can be replaced with more robust and fire-resistant materials like steel or aluminium.

Thathara Style

Kath-Kuni style

Dajji Diwari and Kath-Kuni Sytle

Mud Houses

Fig. 2 Vernacular practices in hilly areas [5]

1.2 Configurations of Buildings in Hilly Areas

Buildings in hilly areas possess exceptional structural configurations compared to normal buildings. Normally adopted configurations of buildings in hilly zones are shown in Fig. 3 [3]. In step-back buildings, successive floors step back towards

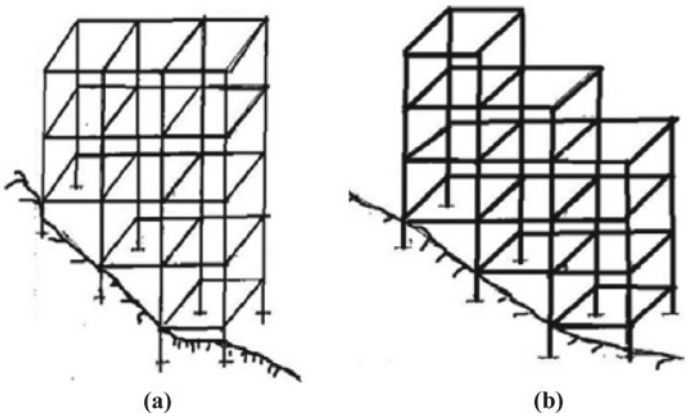

Fig. 3 **a** Step back building. **b** Set back and step back building [3]

the hill slope. Step back buildings have unequal column heights that cause stiffness variations in along-slope and cross-slope directions. Thus, even buildings with symmetric horizontal configurations are torsionally coupled and have high vulnerability to earthquakes. Considering the inefficiency of current construction practices adopted in hilly areas and the loss of life and resources, methods like base isolation, additional stiffness provision, etc. should be adopted to improve the performance of buildings in hilly areas during an earthquake. In this study, the effects of the provision of base isolation and the provision of cables for additional stiffness in buildings of hilly areas are studied.

1.3 Base Isolation

Base isolation is the most safest method that can be adopted in earthquake-prone areas [1]. The objective of a seismic isolation system is to separate a building from its foundation soil so that the building is least affected during an earthquake. Base isolations devices are usually provided to reduce stiffness in the horizontal direction. The basic idea behind base isolation is to shift the time-period of the building and avoids the resonance condition [4]. In an isolated base building, the base isolation device is placed between the superstructure and the foundation of the building. This enables to detach building from the ground; by doing so, the energy induced by an earthquake is not transmitted up through the building. The use of base isolation in a building reduces base shear and acceleration. It avoids seismic damage to the building. However, the use of base isolation is a challenge in hilly regions as isolators have to be designed for various levels according to the reaction force. Designing all the isolators with the highest force is not economical; hence a separate design is required for forces at different levels of foundation.

The following are three major requirements of a good seismic isolation system:

1. Sufficient horizontal flexibility to increase the time-period of the building.
2. Sufficient capacity to dissipate energy or damping to reduce the displacement.
3. Sufficient rigidity to the structure under service loading.

1.3.1 Lead-Rubber Bearing

Lead-rubber bearing (LRB), applied to buildings and bridge constructions, is a cost-effective way for seismic isolation. An LRB is composed of a ***laminated elastomeric bearing*** pad, top, and bottom sealing & connecting plates, and a lead plug which is inserted in the middle of the bearing. The lead core provides rigidity to the building under service loads, and this facilitates energy dissipation during major earthquakes. When subjected to minor earthquakes, the lead-rubber bearing provides lateral and vertical stiffness. The lateral stiffness is a result of the high elastic stiffness of the lead plug and the vertical rigidity.

The main advantage of lead-rubber bearing is that in a single compact unit, it provides rigidity at service load levels, flexibility at earthquake load levels and provide damping. The LRB possesses energy absorbing capacity through additional hysteretic damping through the yielding of the lead core, which helps in reducing lateral displacements of the isolator.

1.4 Cable Supports

Cables are tensile members which can be provided as beams and membranes or to assist beams, columns, other member types as stay wires or suspended members. The application of cables can be seen cranes, ships, towers, bridges, roofs, etc. In cable structures, ropes, strands, chains, etc., are provided as tensile members as main load-bearing elements and give support to other members, resist lateral forces. In this study, cables are provided along one side of the building with the longest columns. The cables are attached to the joints and assigned fixed supports at the other end (at 6 m away from the building). The idea behind the provision of cables was to study the effect of increasing the stiffness of superstructure.

2 Objectives and Methodology

The present study emphasises on the comparison of the seismic performance of a building in a hilly region with and without suitable earthquake protection systems. In addition to base isolation, cable support is assigned to the building and analysed with the following objectives:

- Study the behaviour of a building in the hilly region during an earthquake.
- Study the seismic response of the building when the base isolator is provided.
- Study the effect of providing cable support to the building under seismic activity.
- Study the effect of providing a combination of cable support and base isolation on the seismic performance of the building.

The software used for the study is ETABS. Dynamic analysis was carried out for the building. The building is modelled, and analysis was carried according to IS 1893: 2016 and IS 456: 2000. The building was subjected to Koyna ground motion. Lead core rubber bearing was designed according to UBC 97 code. The building is modelled as a five-storeyed set back building in seismic zone V. The building details are given in Table 1.

Table 1 Building details

Plan dimension	30 × 15 m
Beam	450 × 550 mm
Column	600 × 600 mm
Slab	125 mm thick
Storey height	3 m

3 Models Considered for Analysis

The study involves the analysis of four models: building with fixed base, base-isolated building, cable-supported building, and the one with cable support and base isolation. The plan view of the top floor of the models is shown in Fig. 4. The four models are shown in Figs. 5, 6, 7 and 8. The four models are titled as:

1. Model A—Building with a fixed base (Fig. 5).
2. Model B—Building with base isolation (Fig. 6)
3. Model C—Building with cable support. (Fig. 7).
4. Model D—Building with cable support and base isolation. (Fig. 8).

The fixed base building is analysed for static and seismic loads. From the reactions obtained base isolators for different levels are designed. For Model C, the building was given cable support. Steel cables of diameter 100 mm were provided. The reactions were determined, and the base isolator was designed for the same.

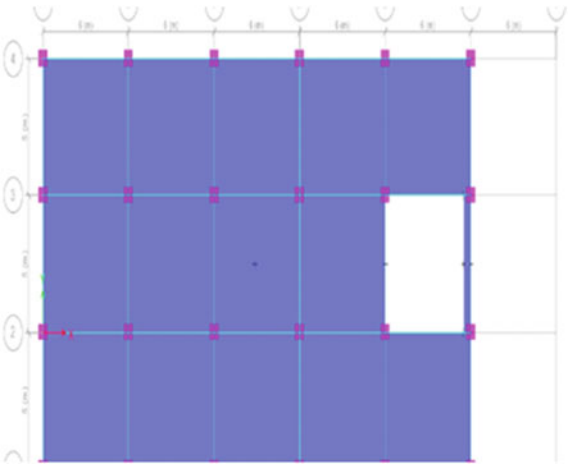

Fig. 4 Top floor plan view of the building

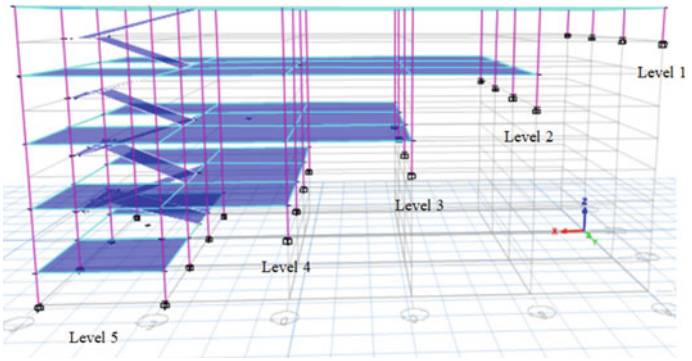

Fig. 5 3D view of Model A

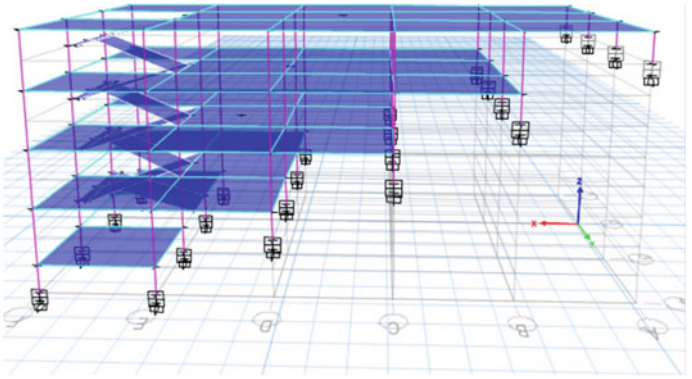

Fig. 6 3D view of Model B

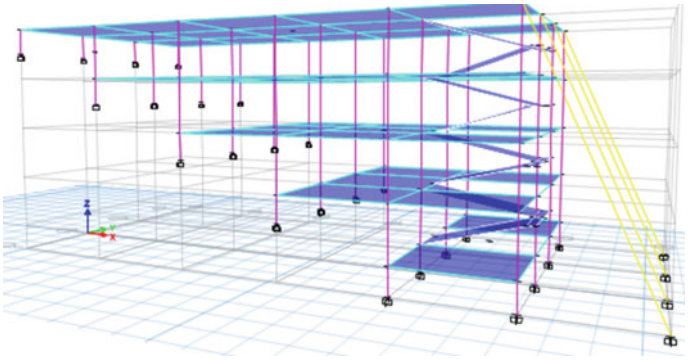

Fig. 7 3D view of Model C

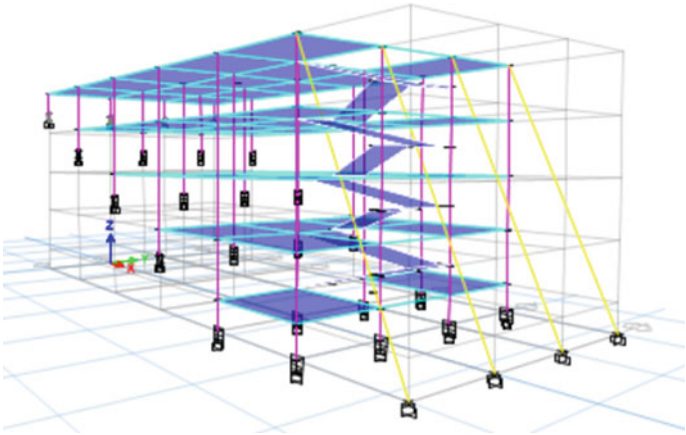

Fig. 8 3D view of Model D

3.1 Properties of Isolator

For building Model B and Model D, different isolators were designed according to the reactions in each storey level. Both base isolators are designed according to the UBC-97 guidelines. The properties of the two isolators are given in Table 2.

Table 2 Base isolator properties

Models	Levels	Maximum reaction (kN)	Horizontal stiffness (kN/m)	Vertical stiffness (kN/m)	Height of isolator (mm)
B	1	131.17	72.399	25750.05	540
	2	386.11	212.81	75691.8	475
	3	624.85	344.47	122516.8	450.4
	4	872.69	480.92	171048.65	442
	5	1126.96	621.13	220916.2	442.4
D	1	76.85	42.354	15064.15	577.6
	2	230.16	126.85	45118.25	500.8
	3	378.78	208.85	74281.86	475
	4	533.51	293.9	104558.5	458
	5	1124.59	619.88	2204709.5	442.4

4 Results and Discussions

4.1 Modal Analysis

The modal analysis was done first to get an idea of possible mode shapes of the buildings. The models were then studied under the response spectrum analysis technique to observe the response of both conventional and base-isolated buildings concerning time. Mode shapes are the deformation pattern of the building when vibrating at a particular natural frequency. The mode shapes of all the four models were analysed to study the behaviour of all the storeys in the fundamental mode. The fundamental mode in X-direction is opted for the study.

From Fig. 9a–d it can be seen that Model A and C behaved similarly. This can be due to the futility of the cable under seismic action. Models B and D behaved similarly, and the displacement was found to be higher for these models. The parameters considered for evaluating the building are time-period, storey acceleration, base shear, storey shear, overturning moment, storey displacement, and storey drift.

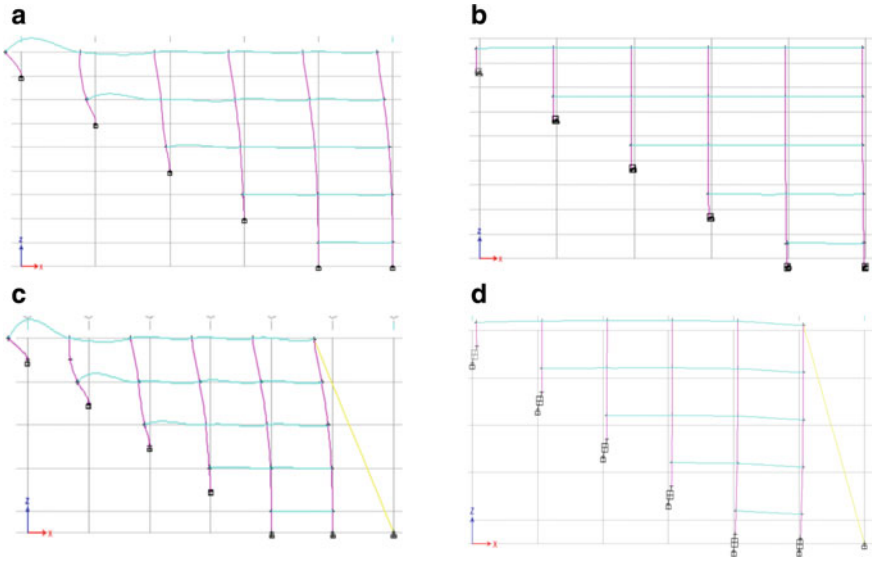

Fig. 9 **a** Fundamental mode shape of Model A**. b** Fundamental mode shape of Model B. **c** Fundamental mode shape of Model C. **d** Fundamental mode shape of Model D

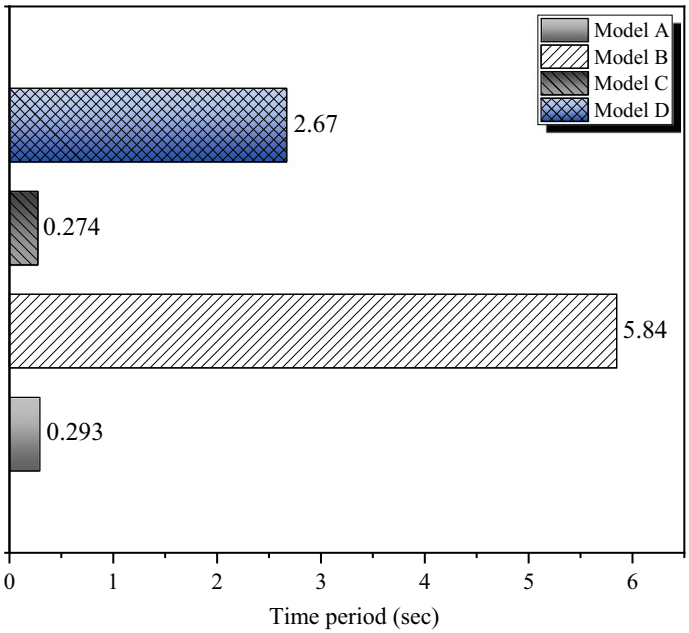

Fig. 10 Variation in time-period

4.2 Variation in Time-Period

This study demonstrated that the overall response was mainly affected by the incorporation of rubber bearings used as base isolators. The predominant time-period has been lengthened for the seismically isolated building as logically expected. Figure 10 shows the variation of the time-period in the fundamental mode. The base isolation (Model B) has increased the fundamental time-period of building to 5.8 s compared to that of 0.2 s for the fixed base building (Model A). The cabled building does not show much change in time-period, whereas Model D shows an increased fundamental time-period to 2.67 s; hence it is comparable with Model B. Base isolators make the building more flexible at the base and helps in less transfer of lateral forces at the time of an earthquake. Thus the time-period is found to be higher for base-isolated buildings.

4.3 Variation in Storey Acceleration

Figure 11 shows the variation of storey accelerations in different storey levels. They are indicators of inertia forces acting at different storey levels. As a general rule, the force acting on a building is directly proportional to its acceleration. Hence, the main

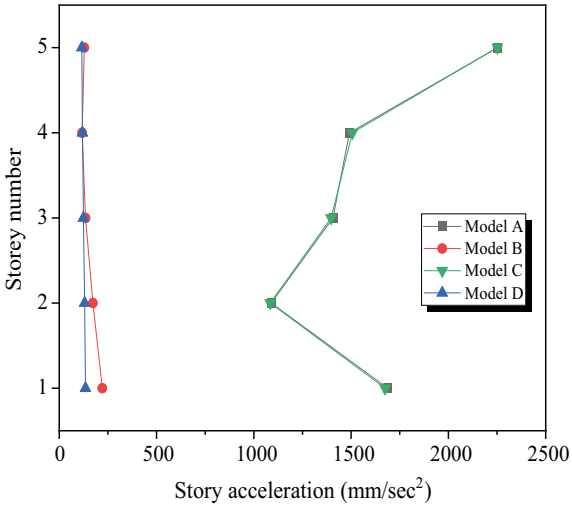

Fig. 11 Variation in storey acceleration

aim should be to reduce the acceleration to decrease the seismic forces on the building. According to the results obtained, a reduction in acceleration at storey levels by the use of isolators is observed. The accelerations are found to decrease significantly for Model D also. The cabled building is found to face the same accelerations as that of fixed building.

4.4 Variation in Base Shear

Base shear is the maximum lateral force acting at the base of the building during seismic activity. When a building is base-isolated, the maximum elastic forces are reduced due to the shift in time-period and energy dissipation by the isolator. Thus, a considerable reduction in base shear is witnessed in the base-isolated building. It is obvious from Fig. 12 that base shear is high for fixed and cabled buildings, whereas for Model B and D base shear has considerably reduced and are almost similar which shows the effectiveness of the isolator. The less stiff isolated building gave the same results as that of high stiff isolated buildings.

4.5 Variation in Storey Shear

Storey shear is the seismic force acting at different storeys. For the top storeys, Model, D performed better than all other models, as observed in Fig. 13. However, at the second and first storey, the results were reversed as storey shear was found to be more for Models B and D. The storey shear was found not to follow a uniform

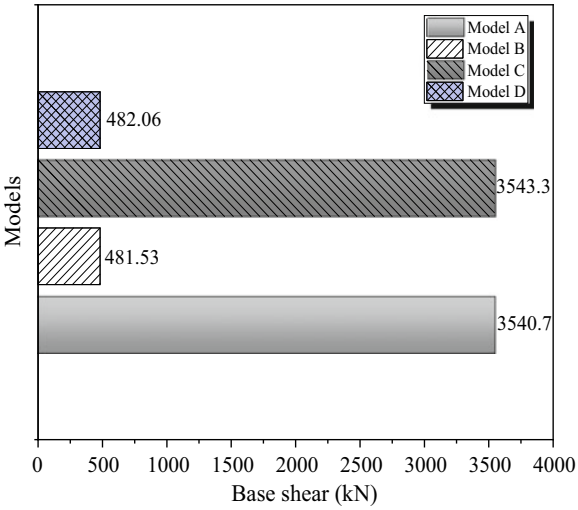

Fig. 12 Variation in base shear

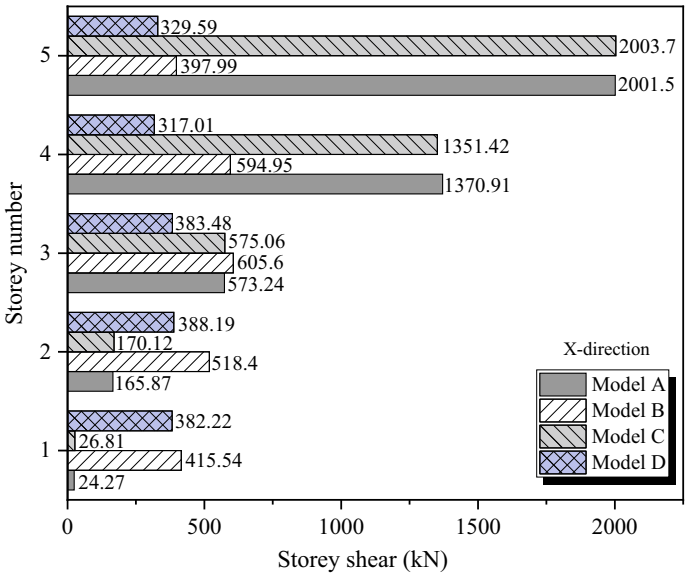

Fig. 13 Variation in storey shear

pattern of change with the storeys for the models studied. This might be due to the difference in the floor area for each storey.

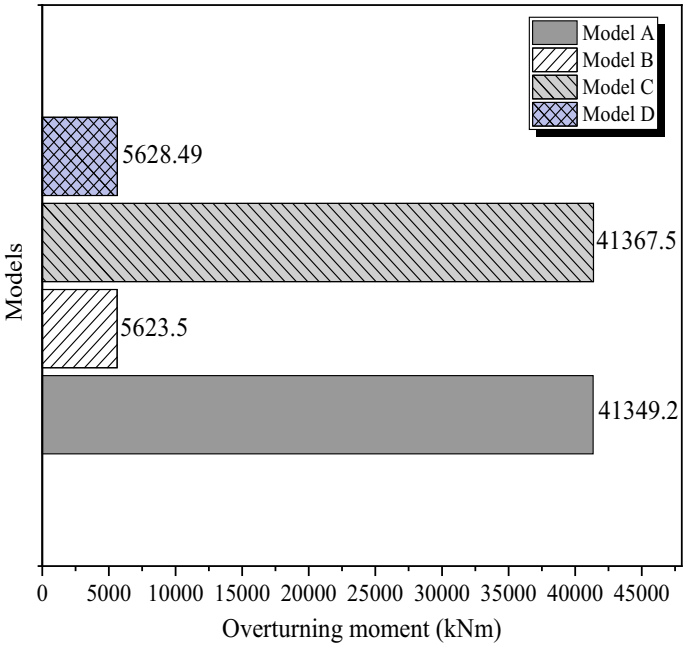

Fig. 14 Variation in overturning moments

4.6 Overturning Moments

The overturning moment is experienced by the structure when it is subjected to lateral forces such as wind force, seismic force, etc. The force causes lateral deflection of the structure in the direction of the force and hence leads to the formation of overturning moments. Stability of the structure considerably increases if the overturning moment is considered for analysis. From Fig. 14, it is evident that moments are considerably reduced for Models B and D. This is because less force is acting on the super building for isolated buildings; hence less moment is observed.

4.7 Variation in Storey Displacement

Storey displacement refers to the maximum total displacement experienced by the storey. Higher displacement of storeys creates uneasiness to the occupants (Fig. 15).

It was observed that Model A and C had similar displacements in all the storeys. The highest displacement was found for Model B in all the storeys, which reduced to 60% in Model D in all the storeys. This was because cables provided extra stiffness to the building, which reduced displacement. Model B had 90% more displacement than

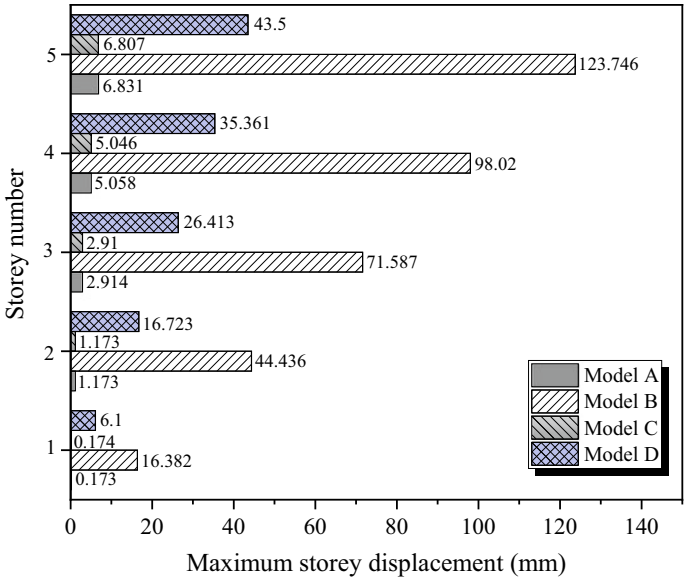

Fig. 15 Variation in storey displacement

Models A and C. Base-isolated buildings were found to have higher displacements as it is more flexible than fixed base building.

4.8 Variation in Storey Drift

It is observed that in the top storey drift is very less for Models C and D. It is evident that storey drift is high for base-isolated building (Model B) however, the presence of cable has reduced the storey drift to a very great extent (Model D). The effect of cables in reducing storey drift is found to decrease in the lower storeys; however, it was found to perform better than base-isolated building (Model B) (Fig. 16).

5 Conclusions

The study focused on a comprehensive analysis of seismic responses of a building in the hilly area. Earthquake protection systems used in the study were base isolation and cable supports. The primary focus of the study is to make base isolators economical by combining with cable support technique. The challenge was high as this had to be implemented in hilly terrain. By introducing cables to the base-isolated building, the stiffness of the building increases, thus reducing the demand of highly

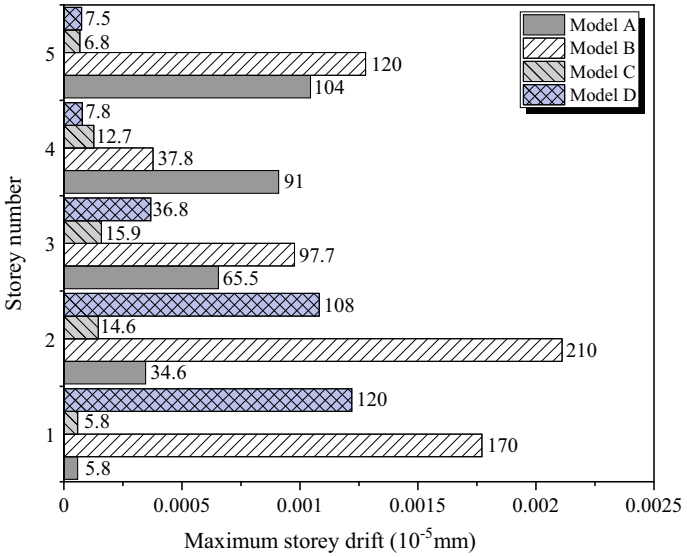

Fig. 16 Variation in storey drift

stiff base isolator. Therefore the cost of the base isolator can also be reduced considerably, making it available for the common people. Parameters such as time-period, storey accelerations, base shear, storey shear, overturning moments, storey displacements and storey drift in different models were considered for the comparative study. From the results obtained, it was found that the base-isolated building showed better seismic performance. In contrast, cable with base-isolated building gave comparable results as that of base-isolated building. It can be inferred that cables act as extra stiffness providers which reduce the reactions hence reducing the material and stiffness required for the isolator. It can be seen that the low stiffness isolator performs as good as the high stiffness isolator. On the other hand, only providing cables is not effective to reduce seismic demand on the building.

References

1. Tamang P, Kumar B (2016) Study on earthquake resistant building—(Base Isolation) Y LIMIT, vol 33, pp 417–420
2. Singh Y, Lang DH, Narasimha DS (2015) Seismic risk assessment in hilly areas : case study of two cities in Indian Himalayas, pp 1–10
3. Singh Y, Gade P (2011) Seismic behavior of buildings located on slopes—an analytical study and some observations from Sikkim earthquake of September 18, 2011
4. Jain M, Sanghai SS (2017) A review : on base isolation system
5. Kumar A, Pushplata (2013) Vernacular practices: as a basis for formulating building regulations for hilly areas. Int J Sustain Built Environ 2:183–192. https://doi.org/10.1016/j.ijsbe.2014.01.001

Damage Assessment of Tunnels in Seismic Prone Zone During Earthquakes: A Part of Hazard Evaluation

Abdullah Ansari, K. Seshagiri Rao, and A. K. Jain

Abstract Tunnels are generally constructed in urban areas and metro cities to fulfill the rising need of space and passage due to urbanization. These infrastructure may get damaged because of earthquakes occurring in that particular area where tunnels are constructed. While designing tunnels in seismic prone zones, it is ensured that tunnels must withstand under both seismic and static loading. Recently occurred large magnitude earthquakes caused significant damages of the tunnels including the 1995 Kobe earthquake in Japan, the 1999 Chi-Chi earthquake in Taiwan and the 2008 Wenchuan earthquake in China. During damage evaluation, tunnel damages are broadly categorized into five classes based on damage index including no damage, minor damage, moderate damage, major damage and collapse. This paper gathers the materials of tunnels affected by the 1995 Kobe earthquake in Japan and the 1999 Chi-Chi earthquake in Taiwan, and the grades of damage are calculated based on seismic performance. Earthquake intensity, distance from fault, rock classification, tunnel length and overburden depth are considered as the tunnel damage factors while doing analysis. Considering these parameters, the formula for seismic damage evaluation for tunnel is deducted using the least square method. Further, this formula is modified after taking into account additional factors like construction time, seismic fortification strength and portal stability.

Keywords Tunnel damage · Damage assessment · Earthquake · Regression analysis

A. Ansari (✉) · K. S. Rao · A. K. Jain
Department of Civil Engineering, Indian Institute of Technology Delhi, New Delhi 110016, India
e-mail: cez188391@iitd.ac.in

K. S. Rao
e-mail: raoks@iitd.ac.in

A. K. Jain
e-mail: akjain@iitd.ac.in

T. G. Sitharam et al. (eds.), *Earthquakes and Structures*, Lecture Notes in Civil Engineering 188, https://doi.org/10.1007/978-981-16-5673-6_13

1 Introduction

The large magnitude earthquakes may cause the damage of surface as well as underground structures [1, 3]. Tunnels are generally constructed in urban areas and metro cities to fulfill the rising need of space and passage due to urbanization. They may be subjected to different types of dynamic loading conditions like impact load, blast load and seismic load. Construction of tunnels in seismically active region involves a unique challenge for geotechnical as well as structural engineers to make earthquake-proof underground structures. These structures are subjected to strong damage in case of earthquakes if designed without considering seismic effects [2]. Seismically induced tunnel damage with surface peak ground acceleration correlated using data from 70 case histories and employing relevant attenuation relationships [7]. The rock tunnels are subjected to damage for Peak Ground Acceleration (PGA) below 0.4 g [13]. Tunnels constructed at greater depth are safer while damage will be more extensive with increasing magnitude of an earthquake and decreasing epicentral distance [16].

Minor damage on tunnels for Peak Ground Acceleration (PGA) values lower than 0.2 g and slight to heavy damage for Peak Ground Acceleration (PGA) greater than 0.2 g observed during the 1995 Hyogoken-Nambu earthquake in Kobe, Japan [14]. It is worth noticing that the 1995 Hyogoken-Nambu earthquake was a rather destructive event for tunnels, as more than 12% of the tunnels in the epicentral area were heavily damaged [4, 19]. The damage mechanisms were extensively studied by several researchers. They all highlighted that most of the damaged tunnels were designed and built neglecting an appropriate seismic assessment [8]. The collapse of the twin Bolu tunnel (Turkey) during the 1999 Kocaeli earthquake caused by the combined effects of ground shaking and ground permanent deformation [8, 10]. The collapse took place during construction in the unfinished section of the tunnel, which was deformed in an oval shape, causing crushing of the shotcrete and buckling of the steel ribs at the shoulder and at the knees. A large number of mountain tunnels suffered significant damage during the 1999 Chi-Chi earthquake in Taiwan [11, 12]. In this event, 26% of the 50 tunnels located within 25 km of the earthquake fault were severely damaged, while over 20% of the tunnels were moderately damaged. Various types of damage were observed like lining cracks, portal failures, displaced lining, spalling of the concrete lining, groundwater inrush, rockfalls in unlined sections ad lining collapses.

Similar to Chi-Chi earthquake, devastating damages were observed in mountain tunnels during the 2004 Mid Niigata Prefecture earthquake in Japan, the 2007 Niigata Prefecture Chuetsu Offshore Earthquake and the 2008 Wenchuan earthquake in China [9, 15, 18, 20]. Earthquake magnitude, depth and epicentral distance of the seismic source, geometrical properties of the lining, burial depth and sudden changes of tunnel dimensions are the most critical parameters affecting mountain tunnel damages during the seismic activity. A damage classification for tunnels was proposed based on 254 damage reports from the 1999 Chi-Chi earthquake, the 2004 Mid Niigata Prefecture earthquake and the 2008 Wenchuan earthquake [18]. The ring

Table 1 Major tunnel damages due to historical earthquakes

Tunnel name	Usage	Location	Earthquake magnitude (M_w)	Date
Wrights	Railway	San Francisco, USA	7.9	18 Apr 1906
Tanna	Railway	North Izu, Japan	7.2	26 Nov 1930
Kern County	Railway	Kern Co., CA, USA	7.5	21 Jul 1952
Inatori	Railway	Izu Oshima, Japan	7.0	14 Jan 1978
Pavoncelli	Water supply	Irpinia, Italy	6.8	23 Nov 1980
Rokko	Railway	Kobe, Japan	7.2	17 Jan 1995
Shioya-Danigawa	Railway	Kobe, Japan	7.2	17 Jan 1995
outlet tunnel of Kakkonda 2 hydropower station	Diversion tunnel of dam	Iwate, Japan	6.1	3 Sep 1998
Bolu	Istanbul-Ankara highway	Izmit, Turkey	7.4	17 Aug 1999
Intake tunnel of Shih-Kang dam	Intake	Chi-Chi, Taiwan	7.6	23 Sep 1999
Intake tunnel of Omiya dam	Intake	Tottori, Japan	7.3	6 Oct 2000
Tottori	Hydropower plant	Tottori, Japan	7.3	6 Oct 2000
Uonuma	Railway	Chuetsu, Japan	6.8	23 Oct 2004
Longxi	Road	Wenchuan, China	8.0	12 May 2008

cracks were found on the Tawarayama tunnel with a spacing of 10 m in around 20% of the spans of the tunnel during 2016 Kumamoto Earthquake [21]. A back analysis of damages suffered by Benedetto tunnel during the 2016 Norcia earthquake (Italy) carried out to evaluate the ability of available methods for analysis to predict seismic performance of tunnels [5]. Damage of tunnels due to earthquakes will lead to failure of transportation network and economical loss. Hence, it is very important to understand the damage pattern of tunnel in seismically prone zones so as to mitigate the damages of these infrastructure postured by such catastrophism (Table 1).

2 Damage Assessment of Tunnels

The relationship of tunnel damage level with the magnitude and intensity of earthquake as well as epicenter developed considering 71 rock tunnel response to earthquake motions [7]. Ground moment acceleration $\leq$0.19 g and ground moment

velocity ≤20 cm/s will lead to no tunnel damage. Ground moment acceleration ranging between 0.19 g and 0.5 g and ground moment velocity ranging between 20 cm/s and 80 cm/s will cause minor tunnel damage. In case, if ground moment acceleration and ground moment velocity become greater than 0.5 g and 80 cm/s respectively, then tunnel will be subjected to severe damage. Increasing in tunnel lining thickness will result into more damage. The 40 cm and 30 cm thickness of tunnel lining contribute around 85% and 35% damage, respectively. The percentage of damages are 16%, 40% and 60% for hard rock, soft rock and earth, respectively.

The correlation between Peak Ground Acceleration (PGA) at surface, overburden depth and damage was developed to study the stability of underground structures by considering the 85 historical earthquakes that occurred across the world [16]. Tunnels constructed in soft soil can be damaged easily. Safety index for tunnel damages due to fault and liquefaction analyzed which proved that damage level can be decided based on fault displacement and tunnel lining materials [6]. Tunnels passing through the fault zone will be subjected to serious damage in case if portals located nearby fault line. In case of severe damage, there is strong probability of portal landslide.

2.1 Earthquake Induced Tunnel Damages

Earthquake induced tunnel damages can be broadly categorized as follows:

(a) Damages due to rock failure including landslides and liquefaction
(b) Damages due to fault displacement
(c) Damages due to vibration and ground shaking.

The damages of tunnels due to ground failure can be controlled by means of doing proper geological investigation as well as geotechnical analysis. Damage due to fault displacement may cause serious destruction of tunnel lining and tunnel portals. There would be chances of minor damage in cases of any ground shaking compared to fault displacement. For the case of firm type of surrounding geology, tunnel structures would not be able to resist the deformation due to propagation of seismic waves during any earthquake activity.

2.2 Types of Damage Grade and Damage Index

The tunnel damages are broadly categorized into five grades. There are (a) no damage, (b) minor damage, (c) moderate damage, (d) severe damage and (e) collapse.

(a) No Damage: In case of no damage case, small cracks are developed with no rock fall.
(b) Minor Damage: Tunnel linings start showing cracks in case of minor damage with rock fall.

(c) Moderate Damage: Lots of destructive cracks are developed while having moderate case of damage.
(d) Severe Damage: In this case, big cracks developed in tunnel lining, falls of big rocks and sinking of road surfaces. Tunnels get heavy damages and remain useless without repair.
(e) Collapse: This is the extreme destructive case of tunnel damage during earthquakes, where serious cracks and clear deformation can be observed in the tunnel lining. Tunnel structure gets collapsed and there occurs need of reconstruction as traffic gets blocked completely and traffic network is interrupted.

For above mention five types of damage classes, there corresponding damage index ranges are (0, 0.2), (0.2, 0.4), (0.4, 0.6), (0.6, 0.8) and (0.8, 1), and the characteristic values are 0.1, 0.3, 0.5, 0.7 and 0.9.

3 Development of Damage Assessment Model

Recently occurred 1995 Kobe earthquake in Japan and 1999 Chi-Chi earthquake in Taiwan caused significant damages of the tunnels. In this study, the materials of tunnels affected by the 1995 Kobe earthquake in Japan and the 1999 Chi-Chi earthquake in Taiwan, and the grades of damage are calculated based on seismic performance [4, 11, 12, 17].

A large number of mountain tunnels suffered significant damage during the 1995 Kobe earthquake in Japan and the 1999 Chi-Chi earthquake in Taiwan whose damage grade as well as damage index are decided based on their damage level as described in the previous Sect. 2.1. Earthquake intensity, distance from fault, rock classification, tunnel length and overburden depth are considered as the earthquake damage factors while developing damage assessment model as mentioned in Table 2.

For analysis, least square method was used assuming damage index as a linear function. Total five governing parameters and "n" number of tunnels considered where number j factor has r_j categories when ith tunnel response is $\delta_{i(j.k)}$ ($j = 1 \ldots 5$). The damage function is represented as follows:

$$y_i = \sum_{j=1}^{5} \sum_{k=1}^{r_j} \delta_{i(j,k)} b_{jk} + e_i i = 1 \ldots n \tag{1}$$

In the above mentioned mathematical equation, $b_{jk}(k = 1, 2, \ldots, r_j)$ is a coefficient; $e_i (i = 1, 2, \ldots, n)$ is a residual number for ith tunnel; $\delta_{i(j,k)}$ is the response of the factor j. The value of $\delta_{i(j,k)}$ will be equal to 0 if ith tunnel does not have category k for the factor j. The y_i mentioned in the above equation can be represented as $y = xb + e$ where coefficient "b" can be calculated using regression analysis based on the least square method which is represented in the following Table 3. Here, the correlation coefficient and stand deviation are 0.834 and 0.094, respectively.

Table 2 Tunnels damaged during 1995 Kobe and 199 Chi-Chi earthquake

Tunnel name	Earthquake intensity	Rock classification	Tunnel length (km)	Overburden depth (m)	Through the fault	Damage grade
Rokko	10	Hard rock	16.25	460	Yes	Severe
Kitakshi	10	Hard rock	6.91	350	Yes	Severe
Keihaku	10	Hard rock	1.8	20.25	Yes	Severe
Shinkobe	10	Hard rock	6.85	330	Yes	Moderate
Kobe	10	Hard rock	7.95	272	Yes	Moderate
Nishitakura	10	Hard rock	0.25	42	No	Minor
Nagasaka	9	Soft rock	0.63	20	No	Minor
Seikotsudaini	9	Hard rock	0.20	40	No	Minor
Getsnmi	9	Soft rock	0.31	45	Yes	Severe
Rokoyama	9	Hard rock	2.85	280	No	Minor
Takakura	9	Hard rock	0.58	87	No	Minor
Yekana	8	Soft rock	1.25	145	No	Minor
Gosha	8	Hard rock	0.12	40	No	Minor
Arima	8	Hard rock	0.45	6.5	No	Minor
Tonglu	7	Soft rock	0.33	6.3	No	No damage
Sanyi - 1	7	Soft rock	7.5	24.1	Yes	Severe
Sanyi - 2	7	Soft rock	0.52	3.5	No	No damage
Miaoli	7	Soft rock	0.98	4.5	No	No damage
Doufu	7	Soft rock	0.65	6.5	No	No damage

Modification of Damage Assessment Model

The damage assessment model was developed based on five important factors including earthquake intensity, distance from fault, rock classification, tunnel length and overburden depth. But from the historical earthquakes, it is clear that construction time also plays a role for tunnel damage as tunnels constructed after 1990 showed better performance when subjected to earthquakes in 1995 and 1999.

Tunnels construed before 1990 had small cracks in tunnel lining and not designed properly considering seismic loading conditions. In case of any major earthquake having intensity 9 or 10, the tunnel portals are affected a lot resulting into portal landslides. Hence, few more factors, construction time and seismic fortification strength as well as portal stability considered to modify the already developed damage assessment model. Following formula evaluated after doing regression using least square method.

Table 3 Factors considered and resulting coefficient for damage assessment model

Factor	Category	Coefficient	
		Calculated	Suggested
Earthquake intensity	7	−0.0911	0
	8	0.1840	0.03
	9	0.3144	0.3
	10	0.3712	0.4
Rock classification	Soft rock	0.0565	0.06
	Hard rock	0	0
Tunnel length (km)	<1 km	0	0
	>1 km	0.0696	0.07
Overburden depth (m)	<30	0.1565	0.15
	30–100	0.346	0.03
	>100	0	0.01
Through the fault	Yes	0.2891	0.22
	No	0	0
Construction time and seismic fortification strength	No fortification		0
	7 fortification		−0.03
	8 fortification		−0.12
	9 fortification		−0.18
	10 fortification		−0.22
Portal stability	Very bad		025
	Bad		0.17
	Good		0.1
	Very good		0

$$y_{i(modified)} = \sum_{j=1}^{7} \sum_{k=1}^{r_j} \delta_{i(j,k)} b_{jk} i = 1 \ldots n \tag{2}$$

In the above equation, the suggested coefficient "b" can be calculated using least square method represented in the following Table 3.

4 Conclusion

In a way to fulfill the needs of space and passage due to rapid growth in population and industrialization, sometime it becomes impossible to construct the tunnels in a seismically prone zones. From the historical earthquakes, we get a lesson that tunnels are subjected to damages ranging from no damage to collapse depending on earthquake intensity and other geological parameters. In this study, types of earthquake-induced

tunnel damage as well as their damage mechanics discussed. Using the technique of regression analysis based on least square method, damage assessment model was developed considering tunnel materials affected during the 1995 Kobe earthquake and 1999 Chi-Chi earthquake. For this purpose, earthquake intensity, distance from fault, rock classification, tunnel length and overburden depth, construction time and seismic fortification strength as well as portal stability like factors considered which influence the tunnel damage. This technique is effective and feasible and helps to design the future tunnels considering seismic loading conditions. There are some other damage factors which are not considered in this study, but can be used for further research in a way to modify the existing damage formula. This study will be helpful to formulate and design the mitigation measures with the early warning systems as a part of hazard evaluation, which may eventually lead to less damage of the tunnel structures.

References

1. Ameen AAMM (2018) Modeling the 2004 Andaman-Sumatra tsunami and historical tsunamis from Andaman and Nicobar Island: towards estimation of tsunami hazard along the adjoining areas of Indian Ocean. M.Tech., thesis, Indian Institute of Technology Kanpur, India
2. Ansari A, Rao KS, Jain AK (2021) Seismic hazard and risk assessment in Maharashtra: a critical review. In: Sitharam TG, Kolathayar S, Sharma ML (eds) Seismic hazards and risk. Lecture notes in civil engineering, Springer, Singapore 116:35-45 https://doi.org/10.1007/978-981-15-9976-7_4
3. Ansari A, Satake K, Malik JN (2017) Modelling the 2004 Indian Ocean Tsunami to estimate tsunami heights and its amplitude and to study its effects on coastal areas. ERI Earthquake Conference, University of Tokyo, Japan
4. Asakura T, Sato Y (1998) Mountain tunnels damage in the 1995 Hyogoken-nanbu earthquake. Q Rep RTRI 39:9–16
5. Callisto L, Ricci C (2019) Interpretation and back-analysis of the damage observed in a deep tunnel after the 2016 Norcia earthquake in Italy. Tunn Undergr Space Technol 89:238–248
6. Changshi PAN (1996) Study and summarization on the aseismic problem of tunnel and underground structure. World Tunnel 5:7–16
7. Dowding CH, Rozan A (1978) Damage to rock tunnels from earthquake shaking. ASCE J Geotech Eng Div 104(2):175–191
8. Hashash YMA, Hook JJ, Schmidt B, Yao JIC (2001) Seismic design and analysis of underground structures. Tunn Undergr Space Technol 16(2):247–293
9. Jiang Y, Wang C, Zhao X (2010) Damage assessment of tunnels caused by the 2004 Mid Niigata prefecture earthquake using Hayashi's quantification theory type II. Nat Hazards 53(3):425–441
10. Kontoe S, Zdravkovic L, Potts DM, Menkiti CO (2008) Case study on seismic tunnel response. Can Geotech J 45(12):1743–1764
11. Lu CC, Hwang JH (2018) Damage analysis of the new Sanyi railway tunnel in the 1999 Chi-Chi earthquake: necessity of second lining reinforcement. Tunn Undergr Space Technol 73:48–59
12. Lu CC, Hwang JH (2019) Nonlinear collapse simulation of Daikai Subway in the 1995 Kobe earthquake: Necessity of dynamic analysis for a shallow tunnel. Tunn Undergr Space Technol 87:78–90
13. Owen GN, Scholl RE (1981) Earthquake engineering of large underground structures. Report No. FHWA/RD-80/195, Federal Highway Administration and National Science Foundation, 279

14. Power M, Rosidi D, Kaneshiro J, Gilstrap S, Chiou SJ (1998) Summary and evaluation of procedures for the seismic design of tunnels. Final report for task 112-d-5.3 (c). National Center for Earthquake Engineering Research, Buffalo, New York
15. Saito T, Mukouyama M, Taguchi Y (2007) Damages to railroad tunnels in the Niigataken Chuetsu-oki Earthquake Shinetsu line Yoneyama to kashiwazaki. Tunn Undergr 38(12):891–900
16. Sharma S, Judd WR (1991) Underground opening damage from earthquakes. Eng Geol 30(3–4):263–276
17. Wang WL, Wang TT, Su JJ, Lin CH, Seng CR, Huang TH (2001) Assessment of damage in mountain tunnels due to the Taiwan Chi-Chi earthquake. Tunn Undergr Space Technol 16(3):133–150
18. Wang ZZ, Zhang Z (2013) Seismic damage classification and risk assessment of mountain tunnels with a validation for the 2008 Wenchuan earthquake. Soil Dyn Earthq Eng 45:45–55
19. Yashiro K, Kojima Y, Shimizu M (2007) Historical earthquake damage to tunnels in Japan and case studies of railway tunnels in the 2004 Niigataken-Chuetsu earthquake. Q Rep RTRI 48(3):136–141
20. Yu H, Chen J, Bobet A, Yuan Y (2016) Damage observation and assessment of the Longxi tunnel during the Wenchuan earthquake. Tunn Undergr Space Technol 54:102–116
21. Zhang X, Jiang Y, Sugimoto S (2018) Seismic damage assessment of mountain tunnel: a case study on the Tawarayama tunnel due to the 2016 Kumamoto earthquake. Tunn Undergr Space Technol 71:138–148

Pushover Analysis of Existing Asymmetrical Building Using Modal Load Pattern, Soil Flexibility and Infill Walls—A Case Study

Karismita Pathak and Atanu Kumar Dutta

Abstract This work studies seismic vulnerability of an irregular block of Jorhat Engineering College old building, constructed in 1960 with predated code situated in Seismic Zone-V. Non-linear Static Pushover Analysis performed in SAP 2000® using modal load pattern with infill walls modelled as strut as per IS IS1893 (Part-I):2016. Sub-soil exploration is conducted and stiffness of the spring for the spring base structure is calculated as per ATC-40 guidelines. Detail plan of the structure showing different beams and column dimension is made using Autodesk AutoCAD®. The structure is simulated in SAP2000. Infill walls are designed as per IS1893 (Part-I):2016. Modeling of infill is done as Equivalent Strut, pin-jointed to the RC frame. Plastic hinges are assigned to the members as per FEMA-356, to identify the critical members which have exceeded their capacities. Non-linear analyses are performed for both the fixed and flexible base conditions. Inter-storey drift ratios and plastic hinge locations were selected as response parameters. From the analysis, it is observed that the pushover curves at the calculated target displacements are linear for both the cases, which indicate that the deformation of the structure is in elastic range.

Keywords Modal pushover analysis · Displacement controlled method · Target displacement

1 Introduction

Structure suffers significant inelastic deformation during major earthquakes and the dynamic characteristics of the structure changes with time. The non-linear static procedure (NSP) or pushover analysis, as described in FEMA-273 [1] and its successor FEMA-356 [2] is presently used extensively by structural engineers as a standard tool for estimating seismic demands for buildings. However, these procedures are often restricted to a fundamental mode response of a structure. Therefore, these are inappropriate for high-rise buildings with an asymmetric plan where torsion

K. Pathak (✉) · A. K. Dutta
Jorhat Engineering College, Jorhat, Assam 785007, India

T. G. Sitharam et al. (eds.), *Earthquakes and Structures*, Lecture Notes in Civil Engineering 188, https://doi.org/10.1007/978-981-16-5673-6_14

and higher modes have a significant impact. A modal pushover procedure is one of the pushover methods that have been developed to consider these effects [3]. In this present work, this procedure would be adopted to evaluate the seismic vulnerability of An irregular block of Jorhat Engineering College Old Building (year of construction 1960). The place where it is lies falls in Zone-V, the most vulnerable seismic zone as the Indian Seismic Zoning Map of 2002 [4].

2 Description of the Frame

2.1 Geometry

The building under consideration is a Plan-Irregular block of Jorhat Engineering College as shown in Fig. 1. The dimensions are actually measured in the field.

Indian Seismic Code [5] defines plan irregularities for such L-type-buildings as in Fig. 2.

With reference to Figs. 1 and 2, the ratio of outstands along Y-direction A/L_1 is 9.2/29.96 i.e. 0.30 > 0.15. Thus, the classification of the structure as plan-irregular is

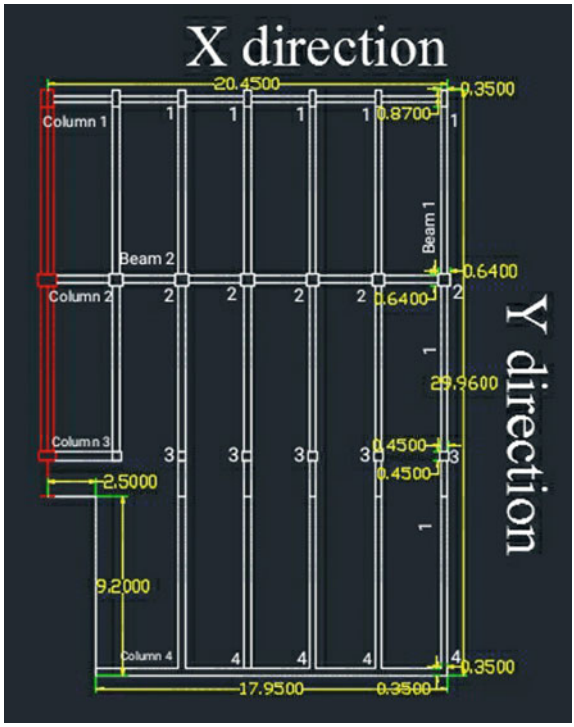

Fig. 1 Plan view of the model showing different sizes of beams and columns

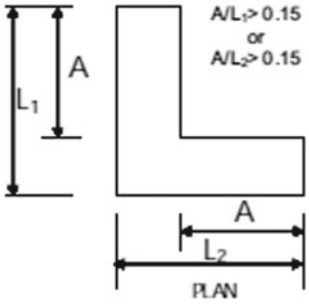

Fig. 2 Criterion for Plan Irregularity of L-type building [4]

valid. The structure is modelled as a 3-D frame using SAP2000®. The element sizes are as follows:

Beam 1 (along Y-axis): 350 mm × 870 mm.
Beam 2 (along X-axis): 380 mm × 970 mm.
Column 1: 350 × 870 mm.
Column 2: 640 × 640 mm.
Column 3: 450 × 450 mm.
Column 4: 350 × 350 mm.
Slab thickness = 150 mm.
Plan area (sq m.) = 20.45 m × 29.96 m.
Floor to floor height = 4.48 m (ground storey) and 4.14 m (other floors).

2.2 Material Properties

Concrete strength of the building is measured by Non-Destructive testing using Rebound Hammer. The reinforcement details of the members could not be ascertained from field observation due to lack of proper instrumentation. The design documents could not be traced either. It is however, gathered from authoritative source, that seismic analysis of precode era for Assam's building such as Assam Engineering College building of 1950, was done based on assumed seismic coefficient (8% of the storey weight). Accordingly, seismic analysis was done using the prevalent Indian Seismic Code with specified load combinations. Reinforcement details against the measured dimension of the structural members are arrived at using working stress method of the IS 456: 2000. These reinforcements are used in the numerical model.

Modulus of Elasticity (E_c) of concrete considering M20 concrete = $5000\sqrt{f_{ck}}$ = $5000\sqrt{20}$ = 22,360.68 N/mm^2 [7].

3 Numerical Modelling

3.1 Modelling of Strut

Infill walls are modelled as equivalent concentric diagonal strut modelled as per the provisions of Clause 7.9.2.2 of IS 1893: 2016 [4]. The struts are connected at the beam-column joints by pin joint as suggested in the same clause. It may be noted here that the same clause makes no distinction between walls, with and without opening. As such, when there is an opening in infill wall, no reduction of strut width is made.

To calculate the initial stiffness of the equivalent strut, effective width, length, thickness and elastic modulus are important. The infill properties of the equivalent strut are listed in Table 1. The infill panel is represented by an equivalent diagonal strut of width a, and net thickness t_w as shown in Fig. 1.

The width of equivalent struts without openings are calculated as per the following relations (Figs. 3, 4, 5, 6, 7 and 8)

$$\text{Width}\left(W_{eff}\right) = 0.175(\lambda_1 \times H)^{-0.4} \times w' \tag{1}$$

Table 1 Properties of infill wall [5]

Infill material properties	Values
Modulus of elasticity	5500 Mpa
Shear modulus	1018 Mpa
Thermal coefficient	0.0000081/°C
Poisson's ratio	0.15

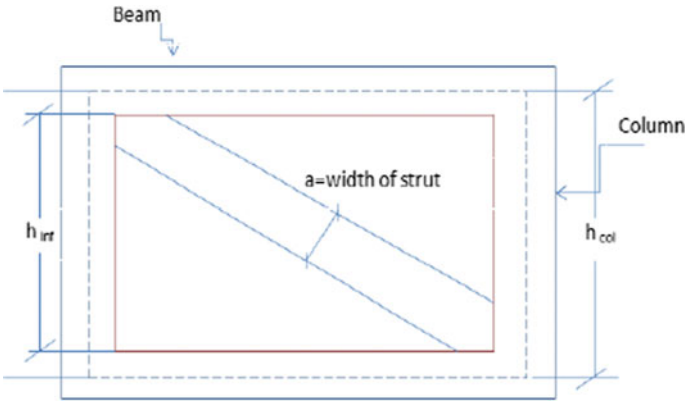

Fig. 3 Equivalent strut idealization of infill walls [4]

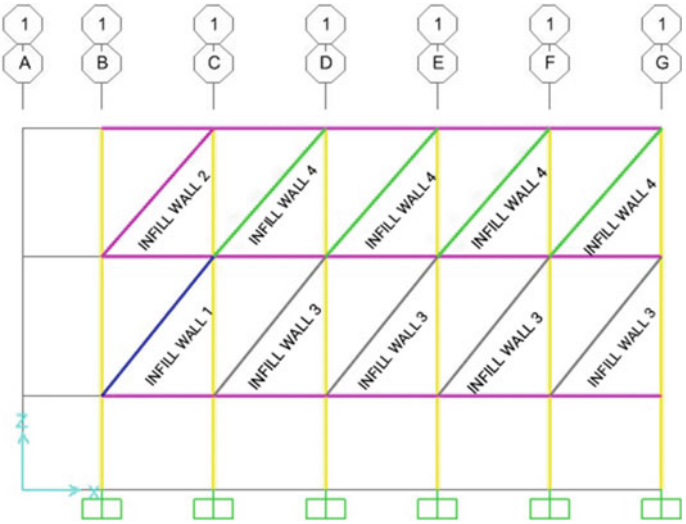

Fig. 4 Infill wall positions for equivalent strut calculation

Fig. 5 Pushover curve along X-direction as per Indian code

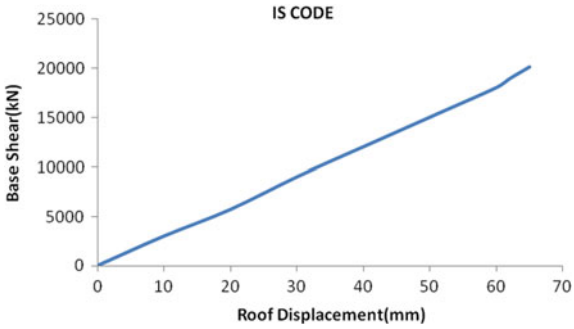

Fig. 6 Pushover curve along X-direction as per FEMA-273

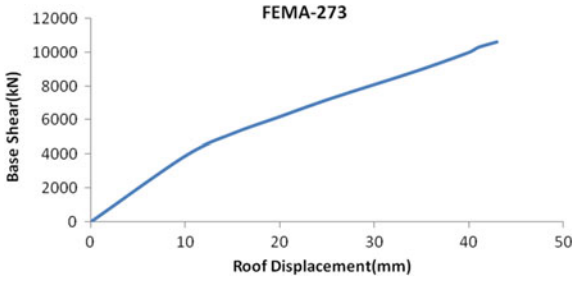

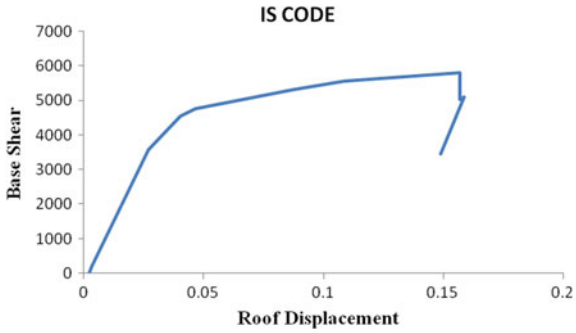

Fig. 7 Pushover curve along Y-direction as per Indian code

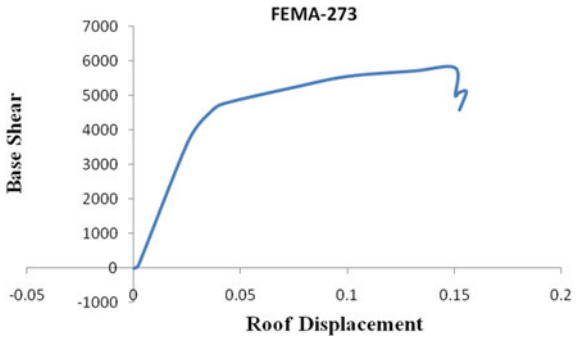

Fig. 8 Pushover curve along Y-direction as per FEMA-273 [1]

$$\lambda_1 = \left[\frac{E_m t \sin(2\theta)}{4E_{fe} I_{col} H_{\inf}}\right]^{1/4} \tag{2}$$

where,

H column height between centre lines of beams.
H_{inf} height of infill panel.
E_{fe} expected modulus of elasticity of frame material.
E_m Expected modulus of elasticity of infill material.
I_{col} moment of inertia of column.
w' diagonal length of infill panel.
t thickness of infill panel and equivalent strut.
θ diagonal angle $= \tan^{-1}\frac{H}{L}$

Unit weight of Masonry = 19 kN/m^3.
Unit weight of Concrete = 25 kN/m^3.
L = bay length of the frame.
External wall thickness = 230 mm.
Internal wall thickness = 230 mm.
Calculations

Infill Wall 1 (without openings)
$w' = 5.74$ m.
$h = 4.48$ m.
$t_w = 0.230$ m.
$\theta = \tan^{-1} \frac{4.48}{3.59}$
$= 51.29°$
$\lambda_h = [\frac{5500 \times 230 \times \sin(2 \times 51.29)}{4 \times 22360.68 \times 0.875 \times 10^9 \times 4.48 \times 10^3}]^{1/4}$.
$= 1.369 \times 10^{-3}$/mm.
$W_{eff} = 0.175(\lambda_h \times H)^{-0.4} \times w'$
$= 0.175(1.369 \times 10^{-3} \times 4.48 \times 10^3)^{-0.4} \times 5.74 \times 10^3$.
$= 486.27$ mm.
$= 0.48627$ m.
Infill Wall 3 (with openings).
$w' = 5.74$ m.
$h = 4.48$ m.
$t_w = 0.230$ m.
opening % = 4.32/16.083 = 0.268.
$\lambda = 1–2 \times (0.268)^{0.54} + (0.268)^{1.14}$.
$= 0.241$/mm.
$W_{eff} = 0.175(0.241 \times 4.48 \times 10^3)^{-0.4} \times 5.74 \times 10^3$.
$= 61.465$ mm.
The above procedure is repeated for 20 other infill walls.

As per Clause 7.9.9.2(b) [4], the relation to calculate the width of equivalent strut without openings is same as FEMA-273, where ends of diagonal struts shall be considered to be pin-jointed to RC frame.

But if there is a presence of openings in the infill wall, no reduction of strut width is required as per Clause 7.9.2.2(c) [4].

The calculated width of strut as per Indian Seismic Code [4] code is given in Table 2.

Table 2 Width of strut as per Indian code

Infill wall no (without openings)	Width (mm)	Infill wall no (with openings)	Width (mm)	Infill wall no (with openings)	Width (mm)
2	473.72	4	473.72	15	110.52
7	487.17	5	473.72	16	72.86
8	468.77	6	486.27	17	110.52
9	487.17	11	486.27	18	110.52
10	468.77	12	486.27	21	144.17
19	622.60	13	473.27	22	144.78
20	638.88	14	110.52		

3.2 Comparative Pushover Analysis

Analysis result as per as per SAP2000® is presented in this section.

From the above curve, it has been observed that the displacement is more along X and Y direction in the model as per IS code [4] in comparison to that as per FEMA-273 [1].

3.3 Types of Models Based on Foundation Modelling

Two types of models are considered for the study considering the bases as Fixed base and bases with soil springs, considering soil flexibility.

Fixed base model: The columns are assumed to be fixed at footing level. For want of exact depth of foundation, the embedment depth is assumed to be 3.0 mts. The variation of embedment depth will however, affect the modal properties and thereby, response of the structure against seismic load. Widths of strut are assumed as per Table 2. The 3-D model is presented in Fig. 9.

Spring base model: Springs are provided at the base of the structure with calculated stiffness in order to accommodate mechanisms related to soil failure. The stiffnesses of the spring along three directions, i.e. vertical, horizontal and rotation are calculated as per ATC-40 [9] guidelines, as shown in Table 3.

The basic steps followed for determining the stiffness properties of shallow bearing geotechnical components are as follows [9].

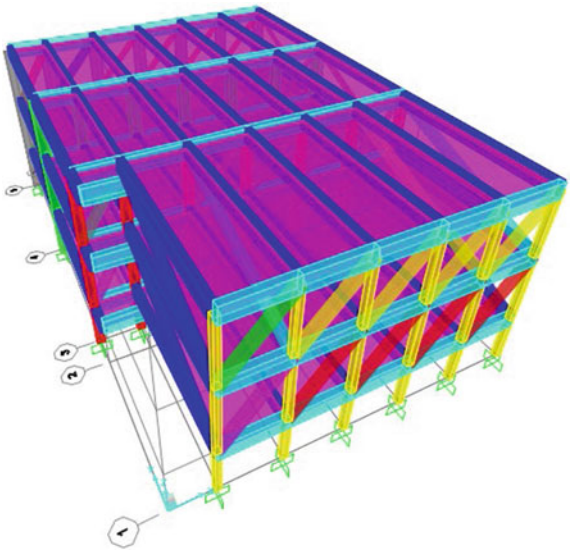

Fig. 9 3D view of fixed-base model with infill wall modelled as strut

Table 3 Surface stiffnesses for a rigid plate on a semi-infinite homogenous elastic half-space, adapted from Gazetas 1991 (ATC-40, Table: 10-2) [9]

Stiffness parameters	Rigid plate stiffness at surface, K_i
Horizontal translation along X-axis, k_x	$k_x = \frac{GL}{2-v}\left[2 + 2.5\left(\frac{B}{L}\right)^{0.85}\right] - \frac{GL}{0.75-v}\left[0.1\left(1 - \frac{B}{L}\right)\right]$
Horizontal translation along Y-axis, k_y	$k_y = \frac{GL}{2-vv}\left[2 + 2.5\left(\frac{B}{L}\right)^{0.85}\right]$ $ky = \frac{GL}{2-v}\left[2 + 2.5\left(\frac{B}{L}\right)^{0.85}\right] ky = \frac{GL}{2-v}\left[2 + 2.5\left(\frac{B}{L}\right)^{0.85}\right]$
Vertical translation along Z-axis, k_z	$k_z = \frac{GL}{1-v}\left[0.73 + 1.54\left(\frac{B}{L}\right)^{0.75}\right]$
Rotation about X-axis $k_{\theta x}$	$k_{\theta x} = \left(\frac{G}{1-v}\right)(I_{xx})^{0.75}\left(\frac{L}{B}\right)^{0.25}\left(2.4 + 0.5\left(\frac{B}{L}\right)\right)$
Rotation about Y-axis $k_{\theta y}$	$k_{\theta y} = \left(\frac{G}{1-v}\right)(I_{yy})^{0.75}\left[3\left(\frac{L}{B}\right)^{0.15}\right]$

(1) Determine the uncoupled total surface stiffness Ki, of the foundation element by assuming it to be a rigid plate bearing at the surface of semi-infinite elastic half-space.
(2) Adjust the uncoupled total surface stiffness Ki for the effects of the depth of bearing by multiplying by the embedment factors, i.e., to generate uncoupled total stiffness.

The embedment factors are calculated as in Table 4.

Table 4 Stiffness embedment factors for a rigid plate on a semi-infinite homogenous elastic half-space [9]

Stiffness parameters	Embedment factors, e_i
Horizontal translation along X-axis, e_x	$e_x = \left[1 + 0.15\left(\frac{2D}{L}\right)^{0.5}\right]\left\{1 + 0.52\left[\frac{\left(D - \frac{d}{2}\right)16(L+B)d}{LB^2}\right]^{0.4}\right\}$
Horizontal translation along Y-axis, e_y	$e_y =$ $\left[1 + 0.15\left(\frac{2D}{B}\right)^{0.5}\right]\left\{1 + 0.52\left[\frac{\left(D - \frac{d}{2}\right)16(L+B)d}{BL^2}\right]^{0.4}\right\} ky =$ $\frac{GL}{2-v}\left[2 + 2.5\left(\frac{B}{L}\right)^{0.85}\right] ky = \frac{GL}{2-v}\left[2 + 2.5\left(\frac{B}{L}\right)^{0.85}\right]$
Vertical translation along Z-axis, e_z	$e_{xz} = \left[1 + 0.095\frac{D}{B}\left(1 + 1.3\left(\frac{B}{L}\right)\right)\right]\left[1 + 0.2\left(\frac{(2L+2B)d}{LB}\right)^{0.67}\right]$
Rotation about X-axis,$e_{\theta x}$	$e_{\theta x} = 1 + 2.52\frac{d}{B}\left(1 + \frac{2d}{B}\left(\frac{d}{D}\right)^{-0.20}\left(\frac{B}{L}\right)^{0.50}\right)$
Rotation about Y-axis,$e_{\theta x}$	$e_{\theta y} = 1 + 0.92\left(\frac{2d}{L}\right)^{0.60}\left(1.5 + \left(\frac{2d}{L}\right)^{1.9}\left(\frac{d}{D}\right)^{-0.60}\right)$

In absence of exact design data the bearing stiffnesses are calculated assuming the footing details as follows:

Thickness of the foundation (d) = 0.2 m.

Total depth of foundation (embedment depth) from ground level(D) = 3 m.

Width of footing (B) = 3 m.

Length of footing (L) = 3 m $\cdot \frac{E}{2(1+\vartheta)} \frac{E}{2(1+\vartheta)}$

Geotechnical site investigation is carried out for this study, by conducting the Standard Penetration Test (SPT) in a borehole to determine the SPT N values. Since the corrected N value is less than 10 so the soil is considered as soft soil (N < 10).

Based on the classification of foundation soil as soft soil, other required values for calculation of Ki values are taken from standard literature [10] as follows:

Poisson's ratio = 0.33.

Modulus of Elasticity, E = 61,200 kN/m^2.

Bulk unit weight of soil = 17 kN/m^3[as per field test].

It must be mentioned here that in absence of exact geometrical data of the foundation and material properties of the foundation soil, values are assumed close to the soil type of the site. As much variation of these data is not anticipated, the results should not vary much from the field reality.

Calculated Shear modulus,

$$\begin{aligned} G &= E/2(1+\upsilon) \\ &= 6120/2(1+0.33) \\ &= 23007.51 \text{ kN/m}^2 \end{aligned}$$

Calculated values of Rigid Plate Stiffness at Surface, K_i.

Horizontal Translation along X-axis, k_x = 185,454.57 kN/m.

Horizontal Translation along Y-axis, k_y = 185,454.57 kN/m.

Vertical Translation along Z-axis, k_z = 237,476.95 kN/m.

Rotation about X-axis, $k_{\theta x} = 310.604 \times 10^6$ kNm/rad.

Rotation about Y-axis, $k_{\theta y} = 183.58 \times 10^6$ kNm/rad.

Calculated values of embedment factors, e_i.

Horizontal Translation along X-axis, e_x = 2.902 kN/m.

Horizontal Translation along Y-axis, e_y = 2.902 kN/m.

Vertical Translation along Z-axis, e_z = 2.726 kN/m.

Rotation about X-axis, $e_{\theta x}$ = 1.435 kNm/rad.

Rotation about Y-axis, $e_{\theta y}$ = 2.052 kNm/rad.

Calculation of total Embedded stiffness, K_{emb}.

Translation along X-axis, $K_{emb(x)} = 185{,}454.57 \times 2.902 = 538{,}189.16$ kN/m.

Translation along Y-axis, $K_{emb(y)} = 185{,}454.57 \times 2.902 = 538{,}189.16$ kN/m.

Translation along Z-axis, $K_{emb(z)} = 237{,}476.95 \times 2.726 = 647{,}362.16$ kN/m.

Rotation along X-axis, $K_{emb(\theta x)} = 310.604 \times 10^6 \times 1.435 = 445{,}716{,}740$ kNm/rad.

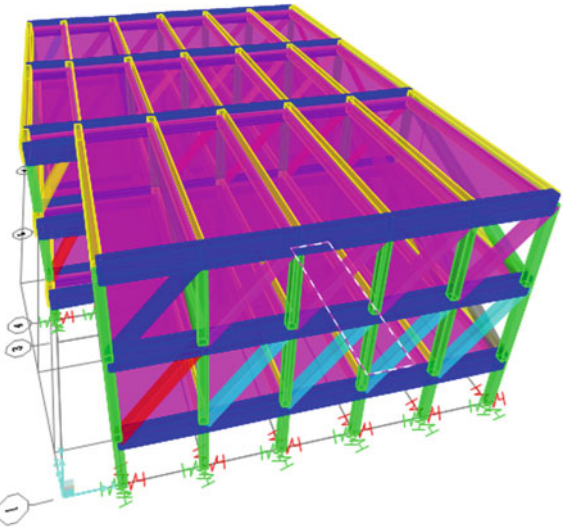

Fig. 10 3D view of spring base model

Rotation along Y-axis, $K_{emb(\theta y)} = 183.58 \times 10^6 \times 2.052 = 376{,}706{,}160$ kNm/rad.

The springs of above-calculated stiffnesses are inserted into the model at foundation level to represent soil flexibility. The strut properties are given as per Table 2. The 3-D model is shown in Fig. 10.

4 Modal Pushover Analysis

4.1 Pushover Analysis (PA)

Pushover analysis is a term used for the non-linear static analysis of a structure wherein the structure is subjected to monotonically increasing predefined lateral load pattern distributed along with the building height until some target displacement is reached. Using Pushover Analysis, a characteristic non-linear force-displacement relationship can be determined. The target displacement can be found out by various methods like Capacity spectrum method of ATC 40 [9] or the Displacement Coefficient method of ASCE 41-13 [10] and FEMA-356 [2]. The target displacement is intended to represent the maximum displacement the structure is likely to undergo under the design earthquake. Target displacements are found out for units with fixed and flexible base foundations for both X-axis and Y-axis loadings.

4.2 The Modal Pushover Analysis (MPA)

It has been developed to include the contributions of all modes of vibration that contribute significantly to seismic demands. This procedure fits well to the structure under the present study as seismic response of this plan-asymmetric structure will have significant contribution from higher modes. This procedure has been improved upon the common Pushover analysis procedure, especially in its treatment of P − Δ effects due to gravity loads and calculation of plastic hinge rotations. The P − Δ effect can be best summarized by the Fig. 11. Additional moment is inflicted upon the structure by gravity load P and change in geometry Δ due to lateral load F.

In MPA, the seismic demand due to individual terms in the modal expansion of the effective earthquake forces is determined by a pushover analysis using the inertia force distribution for each mode. Combining these 'modal' demands due to the first two or three terms of the expansion provides an estimate of the total seismic demand on inelastic systems.

A step-by-step summary of the MPA procedure to estimate the seismic demands is presented as a sequence of steps:

1. Compute the natural frequencies ω and modes $\emptyset_n$ for linearly elastic vibration of the building.
2. Run pushover analyses with the loading patterns ($S_n = m \times \emptyset_n$) based on each mode independently.
3. Idealize each pushover curve as bilinear curves considering negative post-yield stiffness if necessary.
4. Convert the idealized pushover curves into a set of capacity spectrum curves of the corresponding SDOF system using the ADRS (acceleration deformation response spectrum) conversion from MDOF to SDOF (guidelines are provided in ATC-40, capacity spectrum procedure can be used for this purpose).
5. Compute the peak response corresponding to each SDOF system via a non-linear response history analysis (NRHA) based on an input ground motion for each SDOF system or via inelastic design spectrum.
6. Convert the peak response of SDOF system to the target displacement of MDOF system for each mode separately.

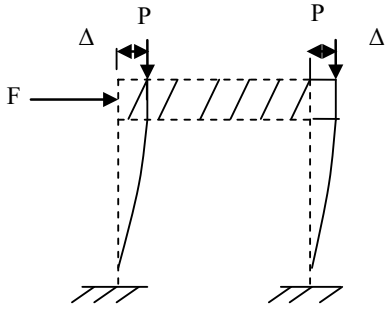

Fig. 11 Explanation of P − Δ effect on shear building

7. From the pushover database (Step 2), extract the peak inelastic response quantities of interest, such as interstory drift and plastic hinge rotations independently for each mode.
8. By using SRSS, determine the combined peak response.

5 Detailed Calculation for Model Input in SAP 2000®

This is shown in Appendix 1.

6 Results and Discussion

6.1 Pushover Curves

The target displacements are calculated as per Displacement Coefficient Method [2, 10] and it is found to be 72.16 mm for X-axis loading and 28.89 mm for Y-axis loading. The structure analysed to the target displacement limit has shown no failure. The pushover curves (Figs. 1, 2, 3, 4, 5, 6, 7, 8, 9, 10, 11, 12, 13, 14 and 15) at the target displacement 72.16 mm are linear which indicate that the deformation of the building is in the elastic range. Non-linearity in the building response can be observed clearly for roof displacement 100 mm. The results are, nevertheless, affected by the assumption of foundation data, soil parameters and reinforcement in RCC.

The capacity curves for the fixed base and flexible base foundations show that in case of flexible bases, the structure can undergo greater displacements for the

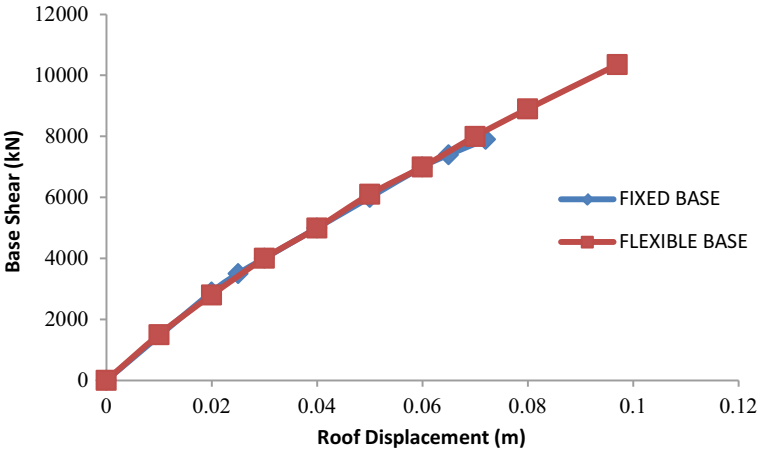

Fig. 12 Pushover curve for target displacement 72.16 mm along X-axis

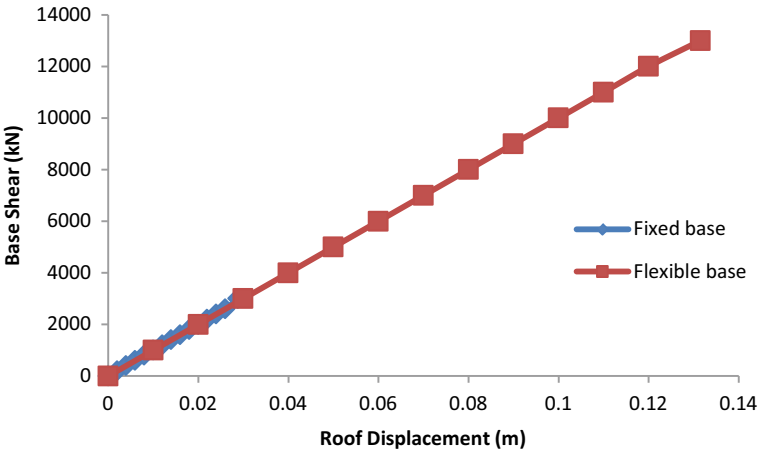

Fig. 13 Pushover curve for target displacement 28.89 mm along Y-axis

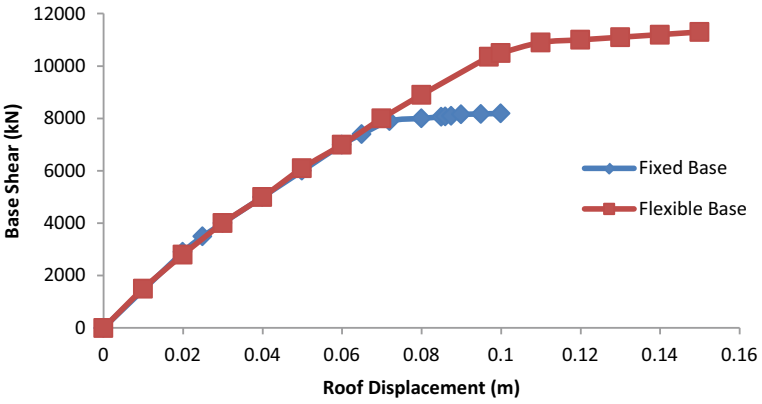

Fig. 14 Pushover curve for monitored displacement 100 mm along X-axis

same yielding point. The ultimate collapse point for structures with flexible bases is more than that of the structures with fixed base foundations. This clearly shows that serviceability aspect of the structure is underestimated in terms of deflection while taking the models as fixed base.

6.2 Inter-Storey Drift Ratios

The accurate estimate of inter-storey drift ratio and its distribution along the height of the structure is very critical for seismic performance evaluation purposes since the

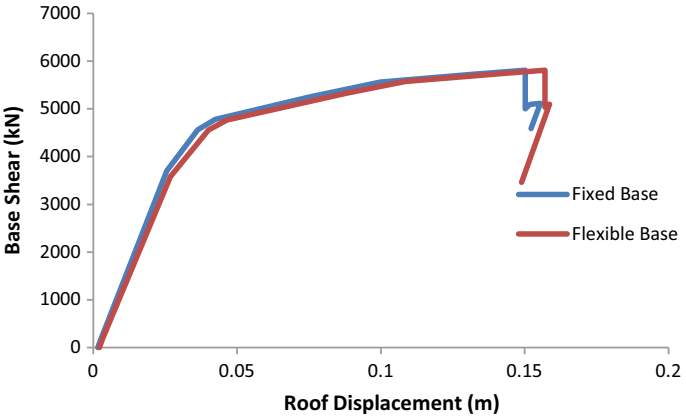

Fig. 15 Pushover curve for monitored displacement 150 mm along Y-axis

Fig. 16 Storey number versus storey drift curve along X-direction

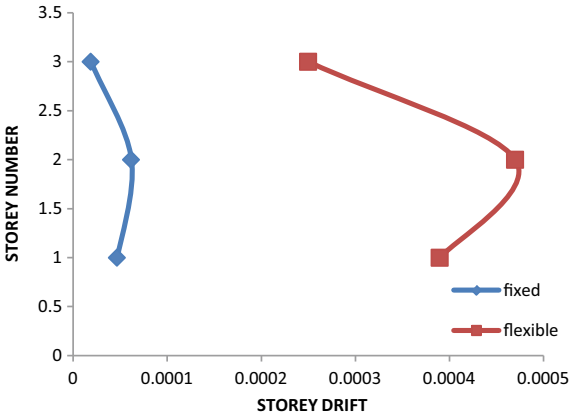

structural damage is directly related to the inter-storey drift ratio. Interstory drifts have been shown in Figs. 16 and 17. It has been observed as inter-storey drift is much more pronounced in the case of flexible base which again reinforces that the neglecting soil flexibility results in stiffer structure.

6.3 Plastic Hinge Location

Plastic hinge locations give us some idea of the locations where inelastic behaviour is expected. As the structure moves from elastic range to the inelastic range under the applied earthquake, these plastic hinges make it possible to trace the yielding and

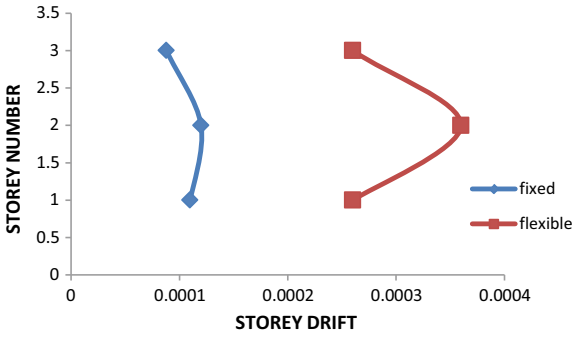

Fig. 17 Storey number versus storey drift curve along Y-direction

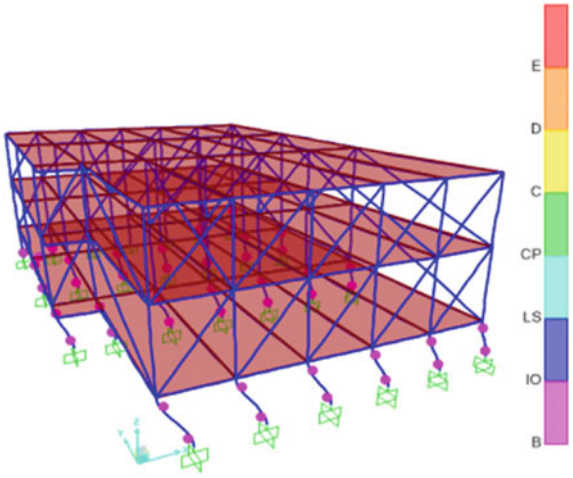

Fig. 18 Formation of plastic hinges in X-direction for fixed base condition for target displacement 72.16 mm

failure on a member and structural level. Plastic hinge locations for various cases of loadings are shown in Figs. 18, 19, 20 and 21.

The plastic hinge formation starts with beam ends and base of the columns of lower stories, then propagates to upper stories and continues with the yielding of interior intermediate columns in the upper stories. It is observed that fixed base model overestimates the occurrence of plastic hinges.

7 Conclusion

The Non-linear Static Pushover Analysis is carried out using Modal load Pattern in SAP2000® on structural models of old plan-irregular college building utilizing the effect of infill walls as per recent Indian Code. Comparison in made with models with Fixed base and Flexible base condition representing soil with springs. Comparison

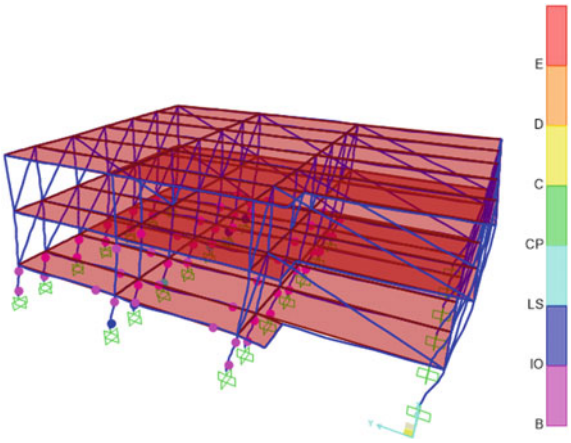

Fig. 19 Formation of plastic hinges in Y-direction for fixed base condition for target displacement 28.89 mm

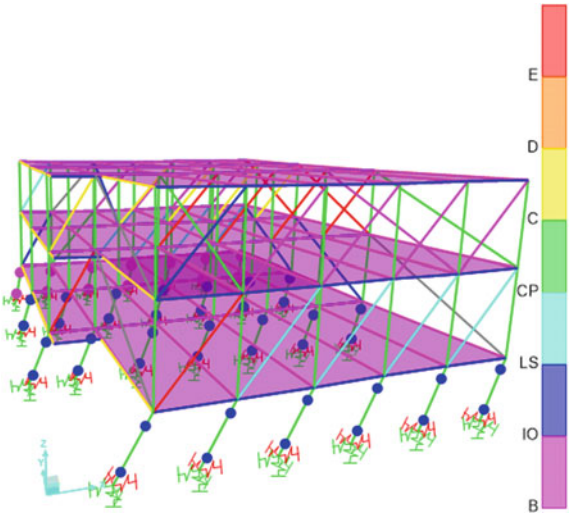

Fig. 20 Formation of plastic hinges in X-direction for flexible base condition for target displacement 97.83 mm

is also made between models of infills as strut with and without voids. The present study emphasizes the necessity of accurate representation of the support condition for evaluation of seismic vulnerability of a structure. It is realized that the serviceability aspects of the structure are underestimated in terms of deflection while taking the models as fixed base. The analysis concludes that building, though constructed in 1960, has adequate capacity to resist the seismic demands imposed on it as per the earthquake excitation applied in the analysis. The pushover curves at the calculated target displacements are linear which indicate that the deformation of the building is in the elastic range. The building analysed to the target displacement limit has shown no failure.

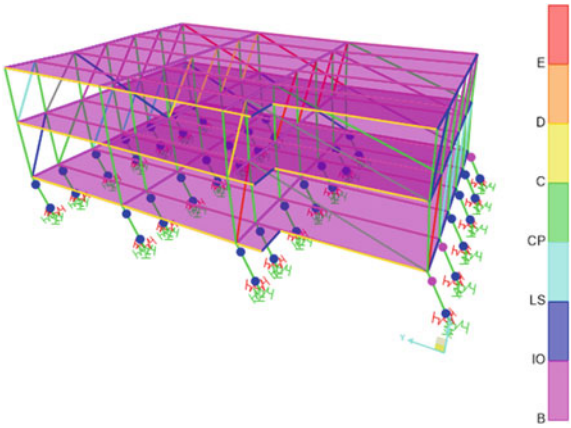

Fig. 21 Formation of plastic hinges in Y-direction for flexible base condition for target displacement 131.53 mm

Appendix 1

Calculations for Modal Pushover Analysis

Computation of Seismic Weights

Dead loads are calculated considering the unit weight of concrete as 25 kN/m^3 and
Unit weight of masonry as 22.5 kN/m^3[5]
Imposed load = 1.5 kN/m^2 (for roof) and 3 kN/m^2 (for floors) [6].
Seismic Weights for each floor of the buildings are calculated using procedure enumerated in IS 1893: 2016 [4]
$W_1 = W_2 = 6787.22$kN
$W_3 = 5222.31$kN (Roof)
Corresponding seismic masses-
M1 = M2 = 691.86×10^3 kg
M3 = 532.34×10^3 kg

Floor stiffness

Storey stiffness of a particular storey is calculated in the weaker direction based on shear building concept. Lateral stiffness of each column is calculated on the gross cross-section of the column of M20 grade concrete.
MI of different column nomenclature as per Fig. 1:

$$I_{C1} = 1.344 \times 10^{10}\text{mm}^4$$
$$I_{C2} = 0.973 \times 10^{10}\text{mm}^4$$
$$I_{C3} = 2.394 \times 10^{9}\text{mm}^4$$
$$I_{C4} = 0.875 \times 10^{19}\text{mm}^4$$

Young's modulus of M20 grade concrete as per IS 456 2000:

$E_C = 5000(f_{CK})^{0.5} = 5000(20)^{0.5} = 22{,}360.68$ MPa $= 22.36 \times 10^9$ N/m^2.

As all the columns are of equal cross-section throughout the height of the building, storey stiffnesses are equal. K1 = K2 = K3 = 0.6965×10^9 N/m.

Natural frequencies and mode shape

$$\text{Mass matrix, M} = \begin{bmatrix} M1 & 0 & 0 \\ 0 & M2 & 0 \\ 0 & 0 & M3 \end{bmatrix} = \begin{bmatrix} 691.68 & 0 & 0 \\ 0 & 691.86 & 0 \\ 0 & 0 & 532.34 \end{bmatrix} \times 10^3 \text{kg}$$

$$\text{Stiffness matrix, K} = \begin{bmatrix} K1 + \text{K2} & -K2 & 0 \\ -K2 & K2 + K3 & K3 \\ 0 & -K3 & K3 \end{bmatrix}$$

$$= \begin{bmatrix} 1.393 & -0.6965 & 0 \\ -0.6965 & 1.393 & -0.6965 \\ 0 & -0.6965 & 0.6965 \end{bmatrix} \times 10^9 \text{N/m}$$

Solving the Eigen equation, $[\text{K} - \text{M}\omega^2] = 0$, we get Eigen value and corresponding Eigen vectors as,

$$\text{Natural frequencies, } \omega = \begin{Bmatrix} 14.96 \\ 41.93 \\ 57.73 \end{Bmatrix} \text{ rad/sec.}$$

Mode shapes are $\{[\text{k}] - \omega^2\ [\text{M}]\}\varphi_\text{n} = 0$.

For $\omega^2 = 223.67$.

$\emptyset_{11} = 1, \emptyset_{21} = 1.76, \emptyset_{31} = 2.15$.

For $\omega^2 = 1758.81$.

$\emptyset_{12} = 1, \emptyset_{22} = 0.24, \emptyset_{32} = -0.726$.

For $\omega^2 = 3332.47$.

$\emptyset_{13} = 1, \emptyset_{23} = -1.30, \emptyset_{33} = 0.846$.

$S_n^* = \emptyset_n \times \text{M}$.

where $= \emptyset_n$ is a shape factor and M is the mass.

MODE-1

$$\Rightarrow \begin{bmatrix} 691.86 & 0 & 0 \\ 0 & 691.86 & 0 \\ 0 & 0 & 532.34 \end{bmatrix} \times 10^3 \times \begin{Bmatrix} 1 \\ 1.76 \\ 2.15 \end{Bmatrix} = \begin{Bmatrix} 691.86 \times 10^3 \\ 1217.67 \times 10^3 \\ 1144.53 \times 10^3 \end{Bmatrix}$$

MODE-2

$$\Rightarrow \begin{bmatrix} 691.86 & 0 & 0 \\ 0 & 691.86 & 0 \\ 0 & 0 & 532.34 \end{bmatrix} \times 10^3 \times \begin{Bmatrix} 1 \\ 0.24 \\ -0.726 \end{Bmatrix} = \begin{Bmatrix} 691.86 \times 10^3 \\ 166.04 \times 10^3 \\ -386.47 \times 10^3 \end{Bmatrix}$$

MODE-3

$$\Rightarrow \begin{bmatrix} 691.86 & 0 & 0 \\ 0 & 691.86 & 0 \\ 0 & 0 & 532.34 \end{bmatrix} \times 10^3 \times \begin{Bmatrix} 1 \\ -1.3 \\ 0.846 \end{Bmatrix} = \begin{Bmatrix} 691.86 \times 10^3 \\ -899.42 \times 10^3 \\ 450.36 \times 10^3 \end{Bmatrix}$$

Combined lateral forces.
Storey 1 = 780.51 kN.
Storey 2 = 1304.03 kN.
Storey 3 = 1312.02 kN.

References

1. ATC (1993) NEHRP guidelines for the seismic rehabilitation of buildings. 2–31
2. ASCE (2000) Prestandard and commentary for the seismic rehabilitation of buildings. 2-11
3. Chopra AK, Goel RK (2002) A modal pushover analysis procedure for estimating seismic demands for building. Earthq Eng Struct Dyn 31:561–582
4. Bureau of Indian Standards (2016) IS 1893-part I: criteria for earthquake resistant design of structure, general provisions and buildings, New Delhi
5. Agrawal, Kulkarni PB, Pooja R (2013) Analysis of masonary infilled R.C. frame with & without opening including soft storey by using equivalent diagonal strut method. Int J Sci Res Pub 3(9) (2013)
6. Bureau of Indian Standards (1897) IS:875 (Part1): code of practice for design loads for buildings and structures, New Delhi
7. Bureau of Indian Standards (1897) IS:875 (Part 2): code of practice for design loads for buildings and structures, New Delhi
8. Bureau of Indian Standards (2000) IS 456: code of design reinforcement. Bureau of Indian Standards, New Delhi
9. Applied Technology Council, Seismic Safety Commission, State of California, ATC 40 (1996) Seismic evaluation and retrofit of concrete buildings, vol 1
10. ASCE 41-13. Seismic evaluation and Retrofit of existing buildings. American Society of Civil Engineers
11. Raheem SEA, Mohamed MA, Tarek MAA (2014) Soil-structure interaction effects on seismic response of multi-story buildings on raft foundation. J Eng Sci Assiut Univ Fac Eng Res Gate 17
12. Surendran S, Kaushik HB (2012) Masonry infill RC frames with openings: review of in-plane lateral load behaviour and modeling approaches. Open Constr Build Technol J

Non-linear Analysis of Base-Isolated Building Having Optimized Number of Base Isolators

Ahmed Bilal and Zaid Mohammad

Abstract In the present study, a base isolation system has been designed for an eight-story framed building. Non-linear time history analysis has been performed to compare the non-linear response of the base-isolated building and conventionally designed building. The computer program SAP 2000 has been used for modelling and analysis. The comparative response of the fixed base building and the base-isolated building has been studied in terms of base shear, roof displacement, and roof acceleration. In addition to this, a cost-effective approach for designing a base-isolated building has been proposed. In this approach, the total number of base isolators to be used in the building have been gradually decreased to optimize the cost. The base isolators have been redesigned for each case, and linear and non-linear performances have been checked to ensure that the performance of the building has not been compromised.

Keywords Base isolation · Seismic performance evaluation · Pushover analysis · Non-linear time history analysis · Laminated lead rubber bearing

1 Introduction

Base isolation is one of the most efficient and economical structural control measures and can dissipate most of the seismic energy without damage to the superstructure [1–4]. Most of the practical aspects regarding the concepts and design procedures of base isolation have been addressed by International Building Code 2000 [5] and Eurocode 8 [6]. Although the behavior of the isolation devices is non-linear, linear analysis is commonly used to design most base-isolated structures [7, 8]. Krawinkler [9] states that non-linear analysis is increasingly used as a tool for evaluating the performance of structures under seismic loads. Inelastic time history analysis is a well-known method for performance evaluation of structures as the forces and deformation in

A. Bilal (✉)
University Polytechnic, Aligarh Muslim University, Aligarh, India

Z. Mohammad
Department of Civil Engineering, ZHCET, Aligarh Muslim University, Aligarh, India

T. G. Sitharam et al. (eds.), *Earthquakes and Structures*, Lecture Notes in Civil Engineering 188, https://doi.org/10.1007/978-981-16-5673-6_15

every element of the structural system can be defined with sufficient reliability using time history analysis [10, 11]. However, the computational time required for inelastic time history is much more as compared to pushover analysis.

If a building would be designed for the equivalent level of seismic performance, then a base-isolated structure would always be more cost-efficient as compared to a conventionally designed building. However, since the base-isolated structures are designed for higher performance levels, the cost of a base-isolated building comes out to be around 5% more than its counterpart [12]. The cost of a Laminated Lead Rubber Bearing (LLRB) isolator may range from ₹ 1.5 lacs to 4 lacs based on their capacities. In addition to this, there is a die cost, which may range from ₹ five lacs to ten lacs. There are various other charges as well. Therefore, if the number of isolators to be used in a structure is reduced without compromising with the performance of the structure, then this alternative can be very promising from the economic considerations of the project.

In the present study, lead laminated rubber bearings (LLRB) have been designed according to the procedure given by Datta [1] for a multi-storey building, and the response has been studied using non-linear time history analysis. The performance of the structure has been checked for different number of isolators using linear analysis and non-linear pushover analysis. The optimum number of base isolators to be used for the building was found based on the least cost of base isolators.

2 Numerical Modelling and Analysis

The dimensions of the considered building have been shown in Fig. 1. M25 grade concrete and Fe415 grade steel were used, and the building was assumed to lie in seismic zone IV. Computer Program SAP 2000 [13] was used for modelling and analysis. Beams and columns were modelled using frame elements, while the base isolators were modelled using non-linear link elements. Non-linear time history analysis was performed to compare the response of the fixed base and base-isolated building. Elcentro time history was considered, and linear scaling was done for PGA $= 0.24$ g.

The building under consideration has 20 columns. Each column was resting on an isolator. In this approach, isolators have been gradually removed (2 at a time) from below the columns and the load transferred to the remaining supports through rigid beams. This process was continued until any further decrease in the number of isolators made the structure unstable, and the beams above started to fail under gravity or earthquake loads. The isolators have been redesigned for the new loads coming on them, such that the total effective stiffness at the isolation level remains nearly the same. A base slab 200 mm thick has also been provided above the isolation level. The base slab has been modelled as a thick shell.

The linear as well as non-linear analysis, has been performed for each case to ensure that the performance of the structure has not been compromised by reducing

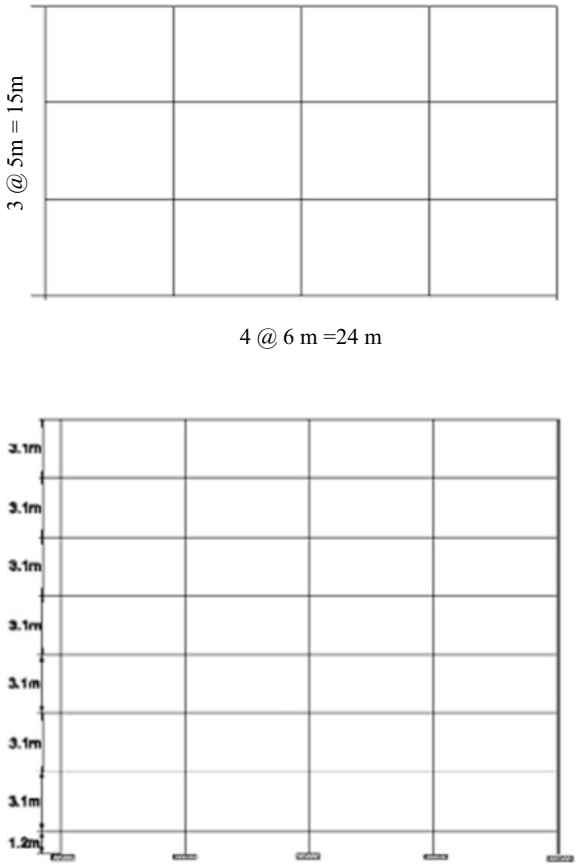

Fig. 1 Dimensions of the building

the number of isolators. A comparison of the total cost of isolators used in each case has been made based on the costs obtained from a registered merchant.

3 Results and Discussion

Elcentro ground motion time history, which was considered for Non-Linear Time History Analysis, has been shown in Fig. 2. The results of the time history analysis have been shown in Figs. 3, 4, 5, 6, 7 and 8. From the time history analysis, it can be seen that there is a 54.4% reduction in base shear, 60.8% reduction in top storey acceleration, and 40.4% reduction in plinth level acceleration when the base isolators have been used in the building.

When the isolators were removed from the two locations shown in Fig. 9, only two sizes of isolators were found to be sufficient for the combination. The details of the cost are given in Tables 1 and 2. The total approximate cost of the isolators came

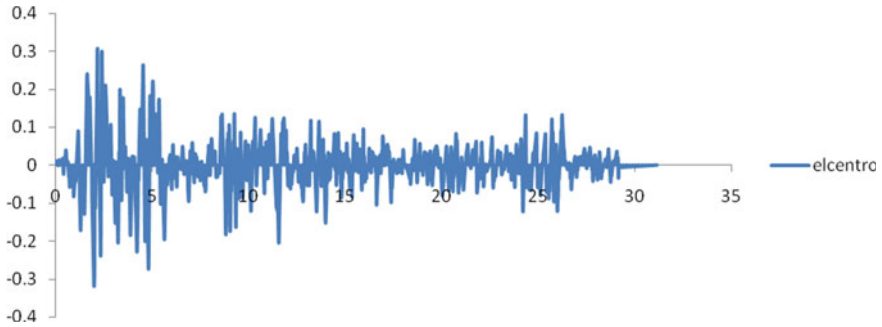

Fig. 2 Elcentro ground motion time history

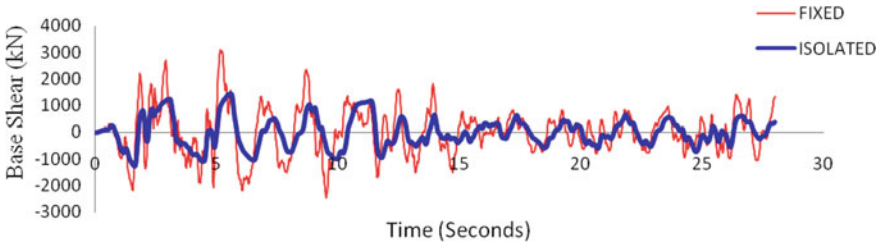

Fig. 3 Comparison of base shear in base building and base-isolated building

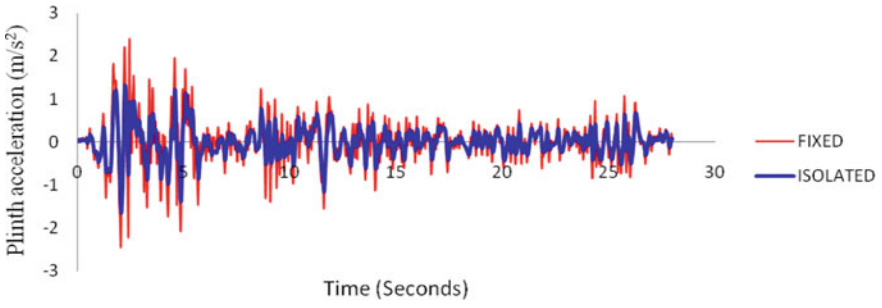

Fig. 4 Comparison of plinth level acceleration for the fixed base and base-isolated building

out to be 4,520,000 Indian Rupees (71,000 USD), which is about 21% less than the previous case where 20 isolators were used. This difference may vary depending upon the variation in the market rates of the base isolators. The cost has been calculated for other positions also, but the given position has been found out to be most economical.

From Figs. 10, 11 and 12, it has been seen that if the number of isolators is reduced and the remaining isolator are appropriately designed for the new loads, then there is no significant change in the linear and non-linear response of the structure. It has been shown that, for the given structure, the optimum number of isolators considering

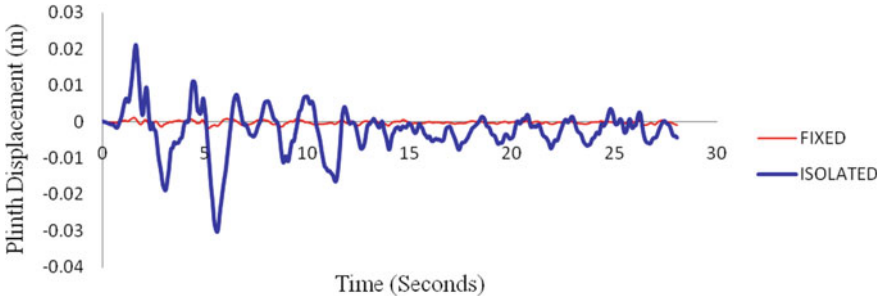

Fig. 5 Comparison of plinth level displacement for the fixed base and base-isolated building

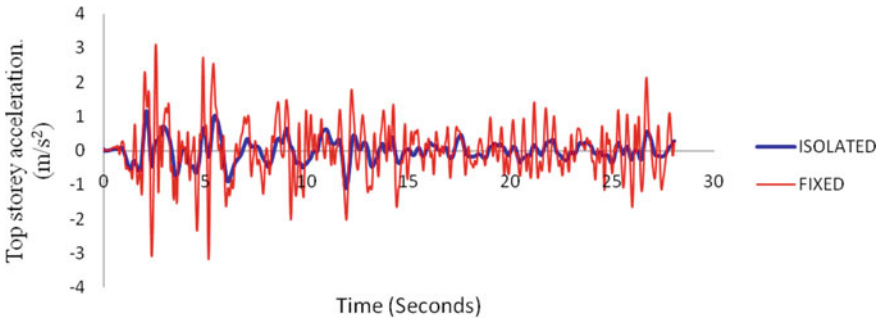

Fig. 6 Comparison of top storey acceleration for the fixed base and base-isolated building

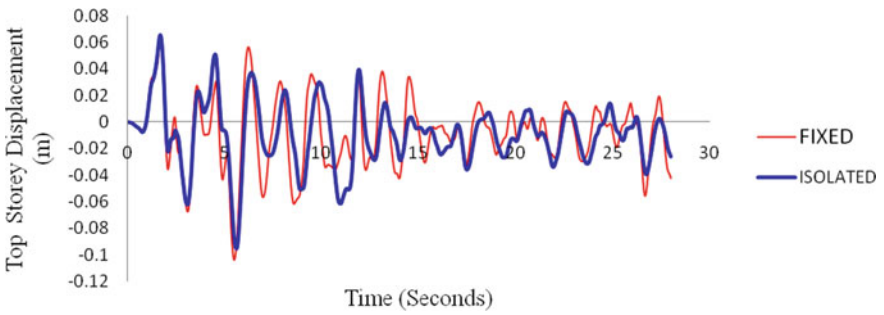

Fig. 7 Comparison of top storey displacement for the fixed base and base-isolated building

the isolator cost is 18. There is a saving of nearly 21% on the isolator cost. A much more rigorous cost analysis, including the reinforcement cost, installation cost, and other service charges, may be required to have the exact estimate of saving.

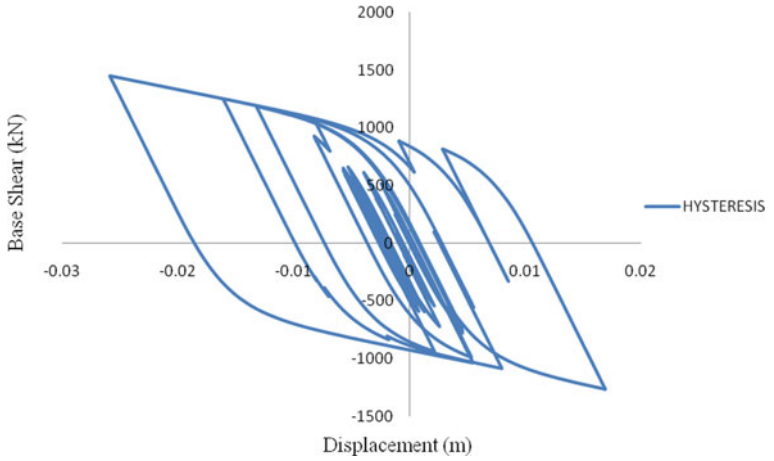

Fig. 8 Hysteresis curve for base isolator

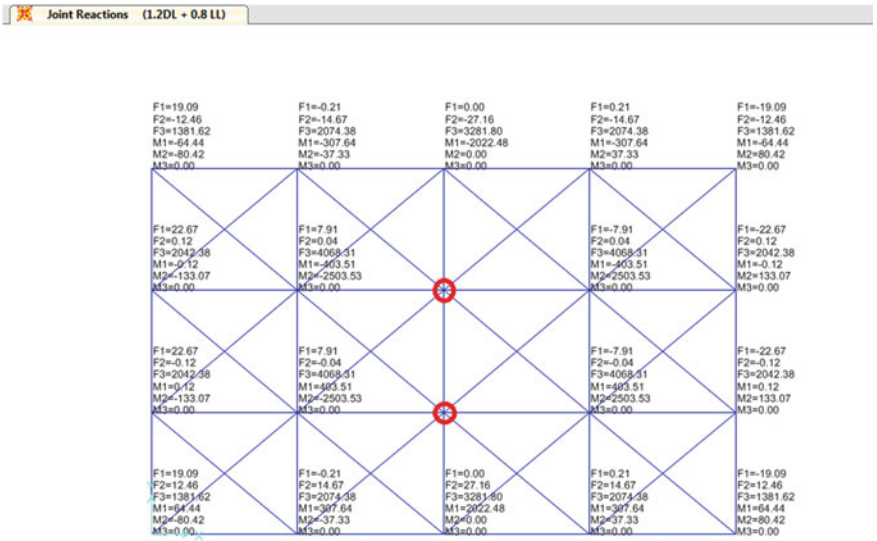

Fig. 9 Base reactions after removing 2 isolators from beneath the central columns

Table 1 Total cost of 18 base isolators

Reaction (kN)	Size (mm)	Quantity	Approximate cost		
			Isolator cost	Die cost	Total (in Indian Rupees)
4068	900	6	200,000	800,000	2,000,000
2000	600	12	165,000	540,000	2,520,000
	Total	18		Total	4,520,000

Table 2 Summary of the cost of base isolators

S. No	No. of isolators used	Sizes of isolators (mm)	Cost (in Indian Rupees)
1	20	800, 650, 500	5,740,000
2	18	900, 600	4,520,000
3	16	1000, 750, 600	5,530,000
4	14	1000, 800, 450	5,250,000
5	12	1000, 900, 750	5,400,000

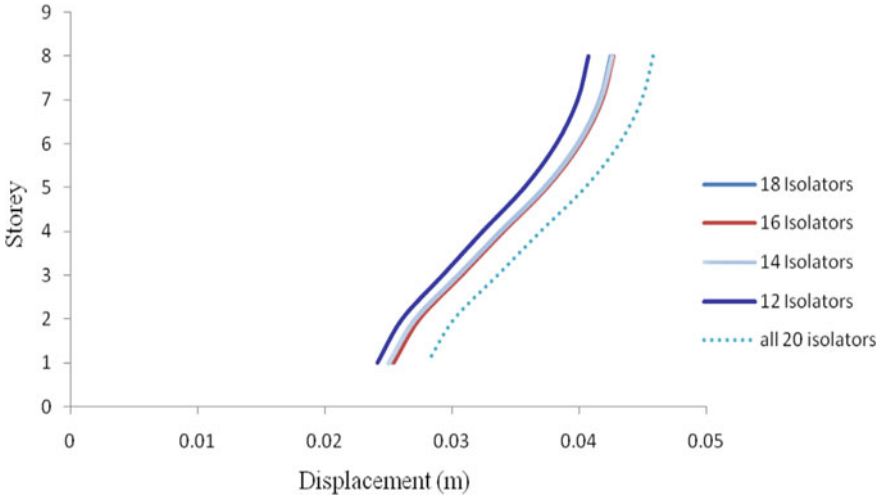

Fig. 10 Displacement in longitudinal direction when different number of isolators are used

4 Conclusion

The results of non-linear time history analysis show that the base shear of the building has reduced by 54.4% on using base isolators, and consequently, the forces in the members of the building also reduced. Thus, it can be said that base isolation should be used in the buildings instead of the conventional earthquake-resistant design for higher performance levels like life safety and immediate occupancy and to reduce damage during earthquakes.

A cost-effective approach of designing the base isolation system has been presented here in which the number of base isolators has been optimized to get the most economical combination of base isolators. It is a general practice to use base isolators beneath every column of a building, but it has been shown in the present paper that the same level of performance can be achieved using lesser number of base isolators if they are appropriately designed. The results of linear and non-linear analyses presented in the paper support this inference. Thus, it can be concluded that

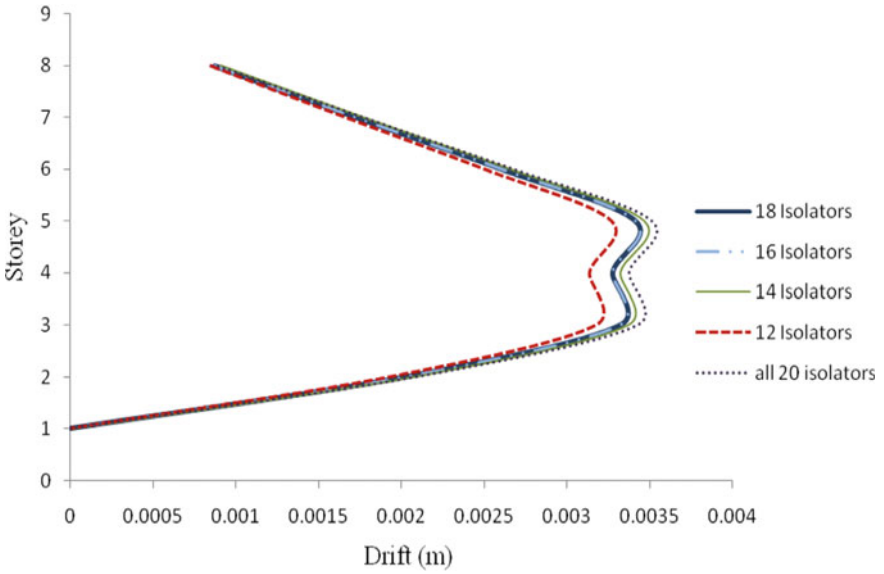

Fig. 11 Storey drift in longitudinal direction when different number of isolators are used

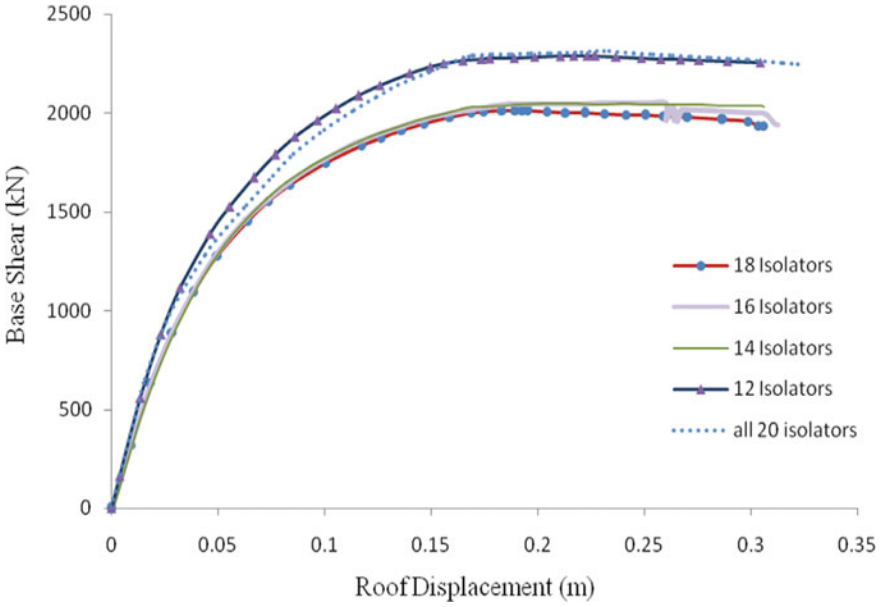

Fig. 12 Pushover curves in the longitudinal direction when different numbers of isolators are used

for designing a base isolation system for any building, an optimization study should be conducted to know the combination which gives the least cost.

References

1. Datta TK (ed) (2010) Seismic control of structures. In: Seismic analysis of structures. Wiley (Asia), pp 369–429
2. Martelli A, Forni M (2000) The most recent applications of seismic isolation and passive energy dissipation. In: Proceedings of the 3rd international workshop on structural control. Structural control for civil and infrastructure engineering, pp 351–364
3. Skinner RI, Robinson WH, McKerry GH (1993) An introduction to seismic isolation. Wiley, Chichester
4. Baratta A, Corbi I (2004) Optimal design of base-isolators in multi-storey buildings. Comput Struct 82:2199–2209
5. International Code Council (ICC), International Building Code (IBC), Falls Church, VA (2000)
6. Eurocode8 (2004) Design of structures for earthquake resistance. In: European committee for standardization (CEN), Brussels
7. Bilal A, Agarwal P, Sadique MR (2021) Performance evaluation of base isolated building. In: Advances in geotechnics and structural engineering. Select proceedings of TRACE 2020. Lecture Notes in Civil Engineering, vol 143. Springer, Singapore. https://doi.org/10.1007/978-981-33-6969-6_23
8. Chopra AK (2001) Dynamics of structures: theory and applications to earthquake engineering, 2nd edn. Prentice-Hall, New Jersey
9. Krawinkler H (2006) Importance of good non-linear analysis. Struct Des Tall Spec Build 15:515–531. Wiley Online Library. https://doi.org/10.1002/tal.379
10. Providakis CP (2008) Pushover analysis of base-isolated steel–concrete composite structures under near-fault excitations. Soil Dyn Earthq Eng 28:293–304
11. Mwafy AM, Elnashai AS (2001) Static pushover versus dynamic analysis of RC buildings. Eng Struct 23(5):407–424
12. Naeim F, Kelly JM (1999) Design of seismic isolated structures-from theory to practice. Wiley, New York
13. SAP 2000 (2014) Linear and non linear static and dynamic analysis and design of three dimensional structures. Computers and Structures Inc, 1995, Berkley, CA 94704, USA

Metro Train-Induced Vibration Measurement on Buildings

M. Bharathi, Dhiraj Raj, and Yogendra Singh

Abstract Vibrations in four buildings located at different positions along the Delhi Metro Rail Corporation (DMRC) network have been measured and reported. Vibrations developed due to the passage of metro trains through tunnels located at a depth up to 30 m from the ground level were measured on the considered buildings at different floor levels. To interpret the effect of vibrations on buildings, different vibration parameters, viz. Peak Ground Acceleration (PGA), Peak Ground Velocity (PGV) and frequency content are obtained from the recorded vibrations. These parameters change with the location, depending on the dynamic characteristics of the soil profile at the site of measurement and the building. It is observed that the maximum amplitude of vibrations measured during this study is more than the threshold provided by standards of different countries and can cause vibration of rigid building components, annoying physical sensations in the human body, interference with activities such as sleep and conversation, rattling of window panes and loose objects and fear of damage to the building and its contents.

Keywords Vibrations · Buildings · Field measurements

1 Introduction

In modern cities, transportation systems are coming closer and being integrated like never before, with the residential, commercial and office buildings. As a result, the buildings and their occupants are subjected to a wide spectrum of vibrations produced from various sources including industrial, construction and transportation activities.

M. Bharathi
Swami Keshvanand Institute of Technology, Management and Gramothan (SKIT), Jaipur, Rajasthan 302017, India

D. Raj (✉)
Malaviya National Institute of Technology Jaipur, Jaipur, Rajasthan 302017, India
e-mail: dhiraj.ce@mnit.ac.in

Y. Singh
Indian Institute of Technology Roorkee, Roorkee, Uttarakhand 247667, India

T. G. Sitharam et al. (eds.), *Earthquakes and Structures*, Lecture Notes in Civil Engineering 188, https://doi.org/10.1007/978-981-16-5673-6_16

Among the various sources, the traffic-induced vibrations are mostly complained about, by the common public. These vibrations may be attributed to the variety of traffic lines, underground, on the ground and overhead, extending and intruding into crowded residential areas, commercial centers and even cultural and high-tech research zones. The vibrations thus generated propagate through the soil medium and excite the supporting structures. These vibrations need to be quantified and checked with the permissible limits. On the other hand, traffic flows are increasing, traffic loads are becoming heavier and vehicles are moving at much faster speeds. All these factors contribute to the seriousness of traffic-induced vibrations on the surrounding environment. Especially in urban areas, a rail transit system is of necessity and it is placed near population centers and often causes significant noise and vibration.

When these vibrations propagate through the structures, the parameters, including structural material, building configuration, potential degradation due to structural age, soil supporting the structure, soil–structure interaction, etc., influence the vibration response. According to Zou et al. [1] the vibration energy directly gets transmitted through vertical support structures on both sides of tracks, such as columns and walls, to the platform and then to the upper floors. In addition, excessive vibrations transmitted into the buildings, hinder the performance of vibration-sensitive equipment, causing adverse effects on the living quality of the occupants and lead to microcracks, minor/architectural damage or major/ structural damage to the structures Xia et al. [2]. In the past, several researchers have reported the vibration measurements in the buildings, imparted from the underground/ overhead railway tracks [1, 3–6]. For greater insights, numerical models were developed by various researchers to understand the train-induced ground vibrations dealing with different aspects [7–19].

This paper presents the field measurements of the vibrations in four buildings located at different positions along the Delhi Metro Rail Corporation (DMRC) network. Vibrations were measured at the basement, ground level and at the top (at an intermediate floor level also in case of some multi-storey buildings). The vibration parameters viz. Peak Ground Acceleration (PGA), Pseudospectral acceleration (PSA), Peak Ground Velocity (PGV) and predominant frequency (f) are obtained from the recorded vibrations and checked with the threshold values provided in different codes and standards.

2 Effects of Vibration

BIS [20] and ISO [21] classifies the source of vibration broadly as continuous or semi-continuous, e.g. industry, permanent intermittent, e.g. traffic and limited (or non-permanent) duration activities, e.g. construction. NSW [22] developed on the basis of [23] classifies vibrations as continuous (vibrations that continue uninterrupted for a defined period with magnitudes varying or remaining constant with time), impulsive (a rapid build up to a peak followed by a damped decay that may or may not involve several cycles of vibration such as in shocks) and intermittent (interrupted periods of continuous or repeated periods of impulsive vibration or continuous

vibration that varies significantly in magnitude). Most of the available guidelines in design codes and standards deal either with the vibration caused due to traffic, transportation and construction activities. Based on the available guidelines the effects of these vibrations on buildings and on human beings are summarized in the following sections.

2.1 On Buildings

Occupants of buildings subjected to vibration complain about cracks in walls and ceilings, separation of masonry blocks and cracks in the foundation. However, vibration levels are rarely high enough to be the direct cause of this damage, though they could contribute to the process of deterioration from other causes. Building components usually have residual strains as a result of uneven soil movement, moisture and temperature cycles, corrosion, poor maintenance or past renovations and repairs. Therefore, small vibration levels induced by road/rail traffic could trigger damage by "topping up" residual strains. Consequently, it is difficult to establish a vibration level that may cause building damage and, therefore, controversy continues.

The response of structures subjected to road, rail and ground-borne traffic vibration is in the frequency range of 1–100 Hz with a particle velocity range of 0.2–50 mm/s and particle acceleration range of 0.02–1 m/s^2 [24, 25]. In addition, the frequency and amplitude of vibrations measured at different locations for various sources of vibration have also been summarized based on French experiences [24, 25]. When the buildings are exposed to continuous vibrations, dynamic magnification occurs due to resonance especially at lower frequencies. In addition, vibration levels measured during impact pile driving, driven cast-in place piling, dynamic consolidation, vibro-flotation or vibro-replacement, use of casing vibrators, rotary bored piling, tripod bored piling, driven sheet steel piling, driving of bearing piles and vibratory pile drivers are also summarized in detail in BSI [26] based on historic case history data. Base curves and multiplying factors for satisfactory magnitudes of building vibration with respect to human response are also proposed in [23].

Swedish standard [27] sets the maximum allowable PPV value for transient vibration, V as a product of vertical component of uncorrected vibration velocity at the base of the building, V_0; building factor, F_b; material factor, F_m and foundation factor, F_g. German standard [28] provides guidelines to evaluate the effect on short and long term vibrations on structures. The vibration limits exceeding these values does not necessarily lead to damage, but when they are exceeded by significant amount further investigations are necessary. However, the maximum velocity at the centre of floor should not be greater than 20 mm/s for short-term vibrations. The guidance manual by U.S. Department of Transportation, Federal Railroad Administration [29] sets guidelines for noise and vibration assessment due to high-speed ground transportation. The details regarding the screening distance for vibration assessment applicable to steel-wheel/steel-rail high-speed rail systems are summarized for three-speed ranges and two different land use purpose. In addition, threshold of PPV at a

distance of 25 ft for some commonly used construction equipments are also provided in FRA [29]. Vibration assessment guideline [22] by Department of Environment and Conservation (NSW), Australia provides both preferred and maximum of root mean square (rms) acceleration and peak velocity values for continuous, impulsive and intermittent vibrations. To evaluate the architectural damage, PPV in the range of 0.10–0.75 mm/s is recommended by Chinese Standard, GB/T [30]. Italian Standard, UNI [31] also follows the same limit as BSI [32] and German standard [28].

2.2 On Human Beings

Building vibrations caused by road traffic are not a health and safety concern; they are more a problem of annoyance. The vibration impact on humans is within the frequency range 1–80 Hz when the posture of the occupant need not be defined (BIS [20] and ISO [21]). ISO [33] and BIS [34] states "Experience in many countries has shown that occupants of residential buildings are likely to complain if the vibration magnitudes are only slightly above the perception threshold". BIS [20] and ISO [21] also mentions "In some cases complaints arise due to secondary effects associated with vibration, e.g. reradiated noise". Approximate indications on likely reaction of passengers experiencing overall vibration in public transport are summarized in [33] and [34]. However, these reactions also depend on the expectation of the passenger regarding the duration of the trip and the type of activity (e.g. reading, writing, eating, etc.) they wish to accomplish during the travel. BSI [26] presents the guidelines on the effect of vibration levels on human response.

3 Field Mesurements

Vibrations developed due to the passage of metro trains through tunnels located at a depth up to 30 m from the ground level (Fig. 1) were measured on four buildings located at different positions along the Delhi Metro Rail Corporation (DMRC) network. Four buildings namely A, B, C and D which belong to multi-storey residential apartment, official building, residential bunglow and residential building type, respectively, has been considered in this field study. For measurement of vibrations at ground level and roof level of the buildings, triaxial accelerometers (Kinemetrics EpiSensor FBA ES-T with sensitivity of 10 v/g) and uniaxial seismometers (Kinemetrics SS-1 Ranger Seismometer with sensitivity of 337.08 v/m/s) were used (Fig. 2a, b). These sensors were connected to a multichannel data acquisition system (Kinemetrics Granite 12) shown in Fig. 2c. In case of multi-storey buildings, vibrations were also measured at some intermediate levels. The recording location in each building is depicted in Fig. 3.

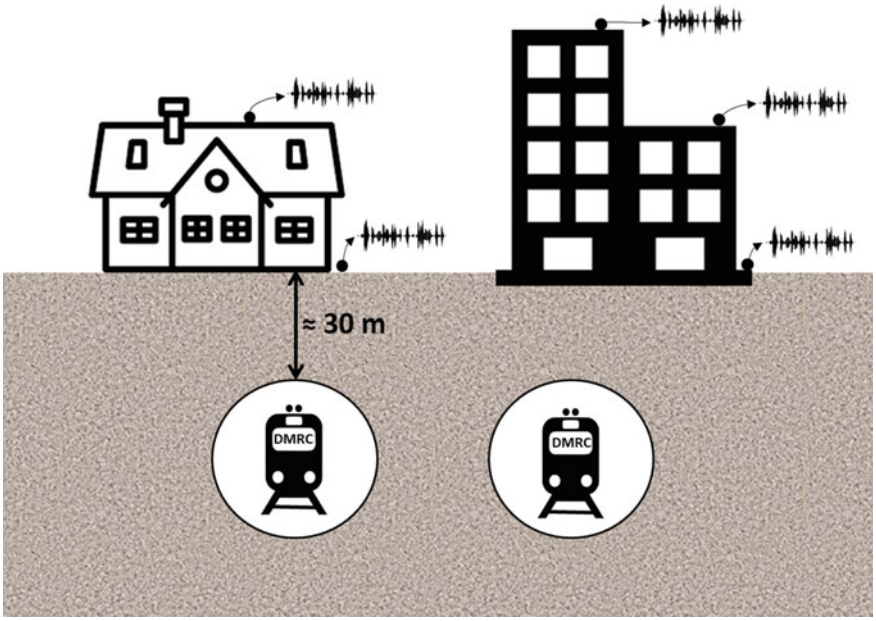

Fig. 1 Schematic representation of field vibration measurements

4 Processing of the Acquired Data

For each vibration record, both acceleration (using accelerometers) and velocity (using seismometers) were recorded in terms of voltage for five-minute duration at a sampling rate of 200 samples per second. Then the acceleration and velocity were converted into 'g' and 'm/s' units, respectively, using the sensitivity of the corresponding sensors. The 5 min recording duration usually contained more than one event (passage of one train). From the recorded data, the relevant signal corresponding to passage of each event (train) was manually extracted for further processing. Linear baseline correction was applied to the extracted signal and then Butterworth band-pass filter of fourth order was applied for frequency range 0.07–80 Hz. Fourier Spectra of each event was obtained. Fourier spectrum of a motion shows its frequency content, in different frequency ranges. In the present case, the Fourier spectrum indicates that most of the energy of vibration is in the high frequency range (60–80 Hz) and the energy content in the frequency range of 0–10 Hz is very small. Elastic response spectrum of each event was obtained for a damping value of 5%. The response spectrum shows the effect of the recorded motions on the building structure and content. All the stages indicating the processing of recorded vibrations is presented in Fig. 4a–f.

(a) (b)

(c)

Fig. 2 Instruments used for vibration measurement. **a** Uniaxial seismometers, **b** triaxial accelerometer and **c** data acquisition system

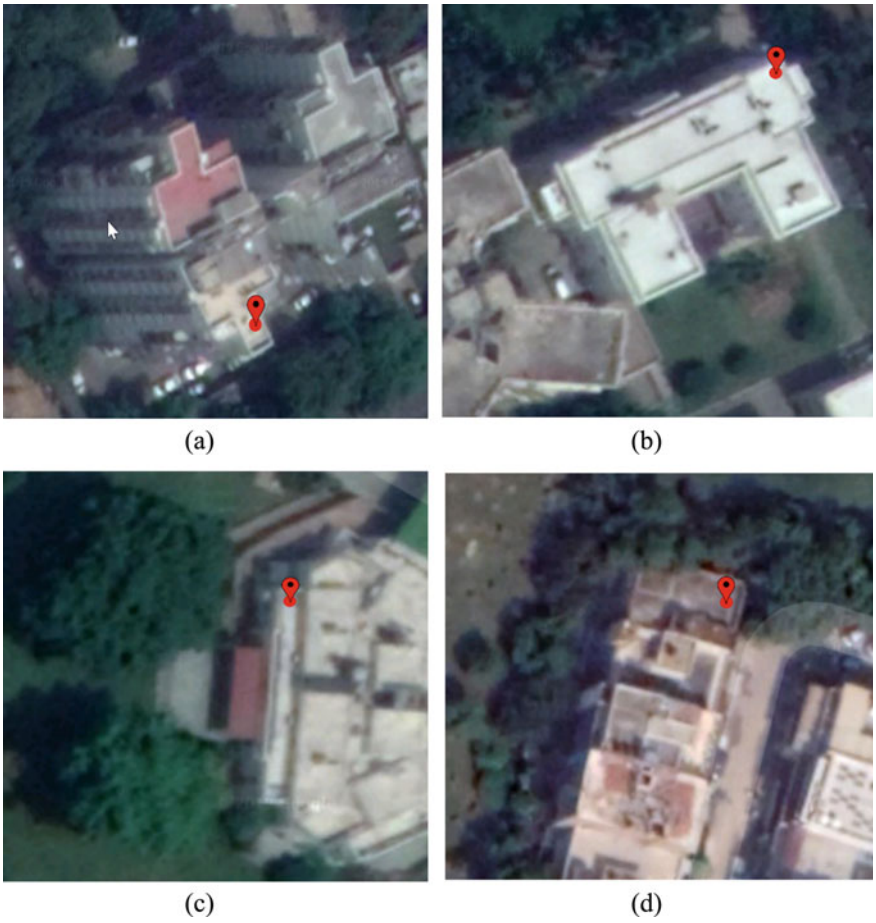

Fig. 3 Recording locations at buildings. **a** A, **b** B, **c** C and **d** D

5 Results and Discussion

While interpreting the effect of vibrations on buildings and occupants, two parameters, namely amplitude (PGA, PSA and PGV) and frequency content (represented by the range of predominant frequency) are important. As expected, both amplitude and frequency content change with location, depending on the dynamic characteristics of the soil column at the site of measurement and the building. X and Y direction represents the vibration component along the longest and shortest dimension of the building in plan whereas Z direction represents vertical component. Tables 1 and 2 summarize the amplitude and frequency content of the measured vibrations in terms of acceleration and velocity, respectively.

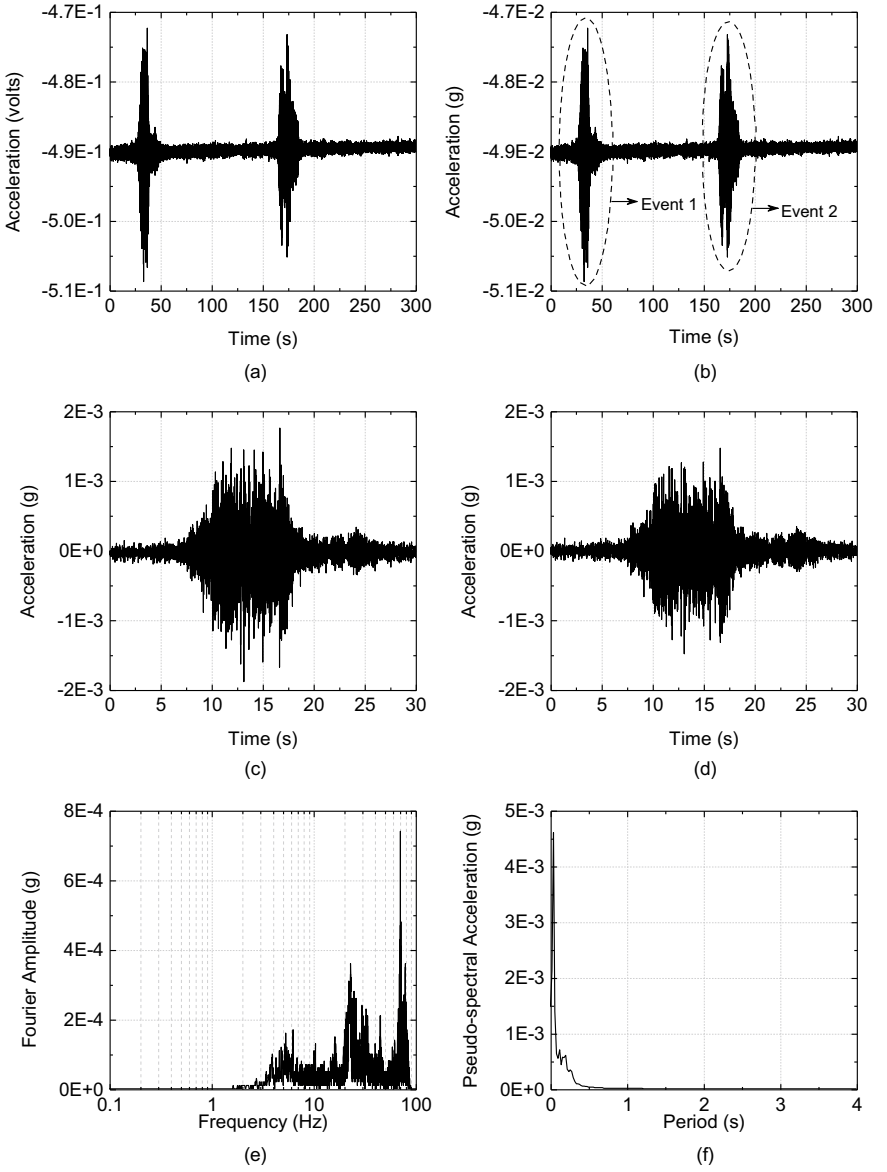

Fig. 4 Processing of raw data: **a** typical acceleration record (in volts), **b** typical acceleration record (in g), **c** extracted acceleration record for an event, **d** acceleration record for an event, after filtering the noise, **e** typical Fourier Spectrum for an event and **f** typical 5% damped elastic response spectrum for an event

Table 1 Summary of acceleration measurements

Building	Direction	PGA_{min} (cm/s^2)	PGA_{max} (cm/s^2)	PGA_{avg} (cm/s^2)	PGA_{SD}	Predominant frequency (Hz)
Building A (Top)	X	0.25	0.99	0.51	0.23	2–24
	Y	0.21	0.72	0.48	0.16	2–48
	Z	1.03	5.02	2.24	1.09	48–49
Building A (9th floor)	X	0.36	1.29	0.86	0.30	2–24
	Y	0.11	0.40	0.28	0.09	2–24
	Z	0.58	3.47	1.74	0.99	18–27
Building B (Top)	X	0.69	1.54	1.18	0.34	25–80
	Y	0.46	1.09	0.87	0.25	15–71
	Z	1.37	4.17	3.03	1.13	25–77
Building C (Roof)	X	0.89	3.49	2.04	0.80	42–56
	Z	1.63	5.54	3.16	0.99	15–57
Building D (Top)	X	0.61	2.24	1.19	0.38	34–46
	Y	0.68	1.79	1.17	0.33	10–38
	Z	1.78	7.46	4.65	1.56	28–42
Building D (Ground)	X	0.41	1.88	0.79	0.33	37–46
	Z	0.99	4.45	1.95	1.01	35–70

Table 2 Summary of velocity measurements

Building	Direction	PGV_{min} (cm/s)	PGV_{max} (cm/s)	PGV_{avg} (cm/s)	PGV_{SD}	Predominant frequency (Hz)
Building A (Top)	X	0.0061	0.0101	0.0078	0.0013	1.6–1.9
	Y	0.0039	0.0057	0.0048	0.0006	1.6–1.7
Building A (9th floor)	X	0.0057	0.0106	0.0080	0.0015	1.6–1.9
Building B (Top)	X	0.0023	0.0074	0.0048	0.0020	5–81
	Y	0.0026	0.0043	0.0034	0.0008	4.6–5.3
Building C (Roof)	X	0.0019	0.0051	0.0032	0.0009	10–56
	Y	0.0032	0.0082	0.0051	0.0017	10–67
Building D (Basement)	X	0.0016	0.0061	0.0035	0.0013	36–50
	Y	0.0014	0.0090	0.0041	0.0021	36–50

The maximum horizontal (X or Y) peak ground acceleration of 3.49 cm/s^2 (0.003 g) has been recorded at the roof of Building C. This is much higher than the limit (1.4 cm/s^2) specified by NSW [22] for residences during day time. But it is in frequency range of 42–57 Hz which is much beyond the frequency range of

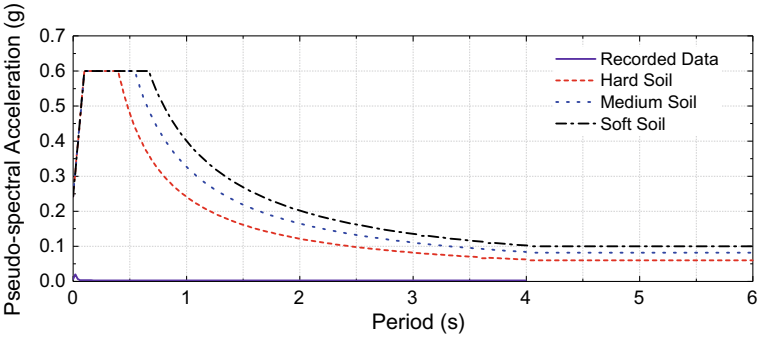

Fig. 5 Response spectrum corresponding to the maximum recorded horizontal peak ground acceleration, 3.49 cm/s^2 (0.003 g) and maximum horizontal peak ground acceleration, compared with the design response spectra for Zone IV (5% damping) as per BIS [35]

buildings (less than 10 Hz). Further, it is about 1/70 of the usual design acceleration values (0.24 g) for buildings located in seismic Zone IV (0.24 g). The maximum peak velocity at building roof has been observed to be 0.0106 cm/s which is well within the limits specified by almost all the standards of the world. The maximum horizontal peak ground acceleration of 3.49 cm/s^2 (0.0349 m/s^2) is much less than the threshold of 0.315 m/s^2 specified by ISO [33] and BIS [34] for not comfortable effect of vibration on human beings. Still, the occupants of the building were annoyed by the vibration sensations developed due to the passage of trains in the metro tunnel network.

Figure 5 compares the response spectrum of most severe record at Building C (recorded data) with the design response spectrum of BIS [35] for hard, medium and soft soil. It shows that the forces to be experienced by buildings of different heights are insignificant to cause any structural effect.

6 Conclusions

Vibrations developed due to the passage of metro trains through tunnels located at a depth up to 30 m from the ground level were measured on four buildings located at different positions along the Delhi Metro Rail Corporation network. The observations indicate that the maximum amplitude of vibrations measured during this study is more than the threshold provided by standards of some of the countries and can cause vibration of rigid building components, annoying physical sensations in the human body, interference with activities such as sleep and conversation, rattling of window panes and loose objects and fear of damage to the building and its contents. However, the amplitude and frequency range of these vibrations is not such that it can cause damage to the building structures. In some cases, as observed in case of the multi-storey apartment buildings, the pre-existing damage in the buildings, due to

ageing of material, corrosion of steel and reinforced concrete, uneven soil movement, moisture and temperature cycles, poor maintenance or past renovations and repairs, can be exposed by these vibrations.

References

1. Zou C, Wang Y, Moore JA, Sanayei M (2017) Train-induced field vibration measurements of ground and over-track buildings. Sci Total Environ 575:1339–1351. https://doi.org/10.1016/j.scitotenv.2016.09.216
2. Xia H, Chen J, Wei P, Xia C, De Roeck G, Degrande G (2009) Experimental investigation of railway train-induced vibrations of surrounding ground and a nearby multi-story building. Earthq Eng Eng Vib 8(1):137–148. https://doi.org/10.1007/s11803-009-8101-0
3. Degrande G, Schevenels M, Chatterjee P, Van de Velde W, Hölscher P, Hopman V, Wang A, Dadkah N (2006) Vibrations due to a test train at variable speeds in a deep bored tunnel embedded in London clay. J Sound Vib 293(3):626–644. https://doi.org/10.1016/j.jsv.2005.08.039
4. Xia H, Zhang N, Cao YM (2005) Experimental study of train-induced vibrations of environments and buildings. J Sound Vib 280(3):1017–1029. https://doi.org/10.1016/j.jsv.2004.01.006
5. Sanayei M, Kayiparambil PA, Moore JA, Brett CR (2014) Measurement and prediction of train-induced vibrations in a full-scale building. Eng Struct 77:119–128. https://doi.org/10.1016/j.engstruct.2014.07.033
6. EQ:2017-16 (2017) Delhi metro induced vibration measurement on various buildings. Department of Earthquake Engineering, Indian Institute of Technology Roorkee, Roorkee, India
7. Hung HH, Chen GH, Yang YB (2013) Effect of railway roughness on soil vibrations due to moving trains by 2.5D finite/infinite element approach. Eng Struct 57:254–266. https://doi.org/10.1016/j.engstruct.2013.09.031
8. Yang YB, Liang X, Hung H-H, Wu Y (2017) Comparative study of 2D and 2.5D responses of long underground tunnels to moving train loads. Soil Dyn Earthq Eng 97:86–100. https://doi.org/10.1016/j.soildyn.2017.02.005
9. Lopes P, Costa PA, Ferraz M, Calçada R, Cardoso AS (2014) Numerical modeling of vibrations induced by railway traffic in tunnels: from the source to the nearby buildings. Soil Dyn Earthq Eng 61–62:269–285. https://doi.org/10.1016/j.soildyn.2014.02.013
10. Bian X, Jiang H, Chang C, Hu J, Chen Y (2015) Track and ground vibrations generated by high-speed train running on ballastless railway with excitation of vertical track irregularities. Soil Dyn Earthq Eng 76:29–43. https://doi.org/10.1016/j.soildyn.2015.02.009
11. El Kacimi A, Woodward PK, Laghrouche O, Medero G (2013) Time domain 3D finite element modelling of train-induced vibration at high speed. Comput Struct 118(Supplement C):66–73. https://doi.org/10.1016/j.compstruc.2012.07.011
12. Mhanna M, Sadek M, Shahrour I (2012) Numerical modeling of traffic-induced ground vibration. Comput Geotech 39:116–123. https://doi.org/10.1016/j.compgeo.2011.07.005
13. Ju S-H (2009) Finite element investigation of traffic induced vibrations. J Sound Vib 321(3):837–853. https://doi.org/10.1016/j.jsv.2008.10.031
14. Shih JY, Thompson DJ, Zervos A (2016) The effect of boundary conditions, model size and damping models in the finite element modelling of a moving load on a track/ground system. Soil Dyn Earthq Eng 89:12–27. https://doi.org/10.1016/j.soildyn.2016.07.004
15. Galvín P, Romero A, Domínguez J (2010) Fully three-dimensional analysis of high-speed train–track–soil-structure dynamic interaction. J Sound Vib 329(24):5147–5163. https://doi.org/10.1016/j.jsv.2010.06.016

16. Kouroussis G, Van Parys L, Conti C, Verlinden O (2014) Using three-dimensional finite element analysis in time domain to model railway-induced ground vibrations. Adv Eng Softw 70:63–76. https://doi.org/10.1016/j.advengsoft.2014.01.005
17. Real T, Zamorano C, Ribes F, Real JI (2015) Train-induced vibration prediction in tunnels using 2D and 3D FEM models in time domain. Tunn Undergr Sp Tech 49:376–383. https://doi.org/10.1016/j.tust.2015.05.004
18. Hall L (2003) Simulations and analyses of train-induced ground vibrations in finite element models. Soil Dyn Earthq Eng 23(5):403–413. https://doi.org/10.1016/S0267-7261(02)00209-9
19. Hesami S, Ahmadi S, Ghalesari AT (2016) Numerical modeling of train-induced vibration of nearby multi-story building: a case study. KSCE J Civ Eng 20(5):1701–1713. https://doi.org/10.1007/s12205-015-0264-9
20. BIS (1992) Mechanical vibration and shock—evaluation of human exposure to whole body vibration—part 2: vibration in buildings (1 Hz to 80 Hz). IS 13276 (Part 2). Bureau of Indian Standards, Govt. of India, New Delhi, India
21. ISO (2003) Mechanical vibration and shock—evaluation of human exposure to whole-body vibration part 2: continuous and shock-induced vibration in buildings (1–80 Hz). ISO 2631-2. International Organization for Standardization, Geneva, Switzerland
22. NSW (2006) Assessing vibration: a technical guideline. Department of Environment and Conservation, New South Wales, Australia
23. BSI (1992) Evaluation of human exposure to vibration in buildings (1 Hz to 80 Hz). BS 6472. British Standards Institution, London, United Kingdom
24. ISO (2010) Mechanical vibration and shock—vibration of fixed structures—guidelines for the measurement of vibrations and evaluation of their effects on structures. ISO 4866. International Organization for Standardization, Geneva, Switzerland
25. BIS (2000) Mechanical vibration and shock—vibration of buildings—guidelines for the measurement of vibrations and evaluation of their effects on buildings. IS 14884. Bureau of Indian Standards, Govt. of India, New Delhi, India
26. BSI (2014) Code of practice for noise and vibration control on construction and open sites—part 2: vibration. BS 5228-2. British Standards Institution, London, United Kingdom
27. SIS (1999) Vibration and shock—guidance levels and measuring of vibrations in buildings originating from piling, sheet piling, excavating and packing to estimate permitted vibration levels (in Swedish). SS 02 52 11. Stockholm, Sweden
28. DIN (1999) Vibrations in buildings—part 3: effects on structure. DIN 4150-3. German Institute for Standardisation (Deutsches Institut für Normung), Berlin
29. FRA (2012) High-speed ground transportation noise and vibration impact assessment. DOT/FRA/ORD-12/15. Federal Railroad Administration, U.S. Department of Transportation, Washington, DC
30. GB/T (2008) Technical specifications for protection of historic buildings against man-made vibration. GB/T 50452. China Building Industry Press (in Chinese), Beijing
31. UNI (1991) Criteri di misura e valutazione degli effetti delle vibrazioni sugli edifice (Criteria for the measurement of vibrations and the assessment of their effects on buildings). UNI 9916. Ente Nazionale Italiano di Unificazione (UNI), Milano, Italia
32. BSI (1993) Evaluation and measurement for vibration in buildings. Part 2: guide to damage levels from ground borne vibration. BS 7385-2. British Standards Institution, London, United Kingdom
33. ISO (1997) Mechanical vibration and shock—evaluation of human exposure to whole-body vibration part 1: general requirements. ISO 2631-1. International Organization for Standardization, Geneva, Switzerland
34. BIS (2000) Mechanical vibration and shock—evaluation of human exposure to whole body vibration—part 1: general requirements. IS 13276 (Part 1). Bureau of Indian Standards, Govt. of India, New Delhi, India
35. BIS (2016) Criteria for earthquake resistant design of structures—part 1: general provisions and buildings IS 1893 (Part 1). Bureau of Indian Standards, Govt. of India, New Delhi, India

Seismic Performance of the Amritesvara Temple: Shake Table Test of a Dry Stone Masonry Structure

Vasantha Lakshmi Gudasali, Vijayalakshmi Akella, and B. K. Raghuprasad

Abstract Ancient structures were constructed by considering only vertical static loads. The seismic response of ancient masonry structures depends on their material properties, the geometry of the structure, the types of connections between various structural components, the stiffness of the floors and the strength of the non-structural elements. The rich and diverse architectural traditions across India provide evidence of the structural efficiency and technological skill of Indian craftsmen and builders. Studying the structural behaviour of Indian heritage buildings has national importance. In this study, the seismic vulnerability of the Amritesvara temple was evaluated. Built in 1196 and is located 260.8 km from Bengaluru, India. This study involved a shake table test of the temple. Experiments were conducted at the Earthquake and Vibration Research Centre, Bengaluru. According to the size and payload capacity of the shaking table, a 1:3 scale model was adopted. The model was subjected to various peak ground accelerations from 0.05 to 0.1 g. The dynamic properties of the model were evaluated through the experiments. The experimental results were used for validating the numerical model, which was used to conduct further investigations on the prototype.

Keywords Shake table test · Dry stone masonry structure · Seismic analysis · Heritage building

V. L. Gudasali (✉) · V. Akella
Department of Civil Engineering, K. S. School of Engineering and Management, Visvesvaraya Technological University, Belgaum, India

V. Akella
e-mail: hod.civil@kssem.edu.in

B. K. Raghuprasad
IISC, Bangalore, India

T. G. Sitharam et al. (eds.), *Earthquakes and Structures*, Lecture Notes in Civil Engineering 188, https://doi.org/10.1007/978-981-16-5673-6_17

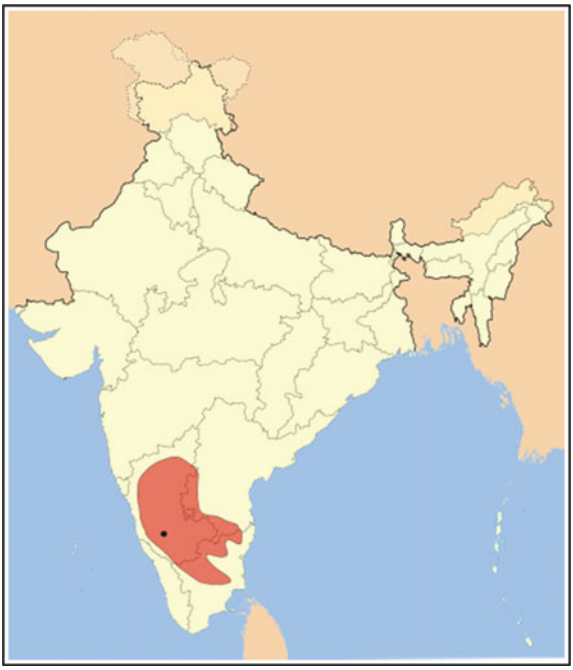

Fig. 1 Map of the hoysala empire

1 Introduction

1.1 Hoysala Architecture

The Hoysala Empire ruled southern India between 1026 and 1343 (Fig. 1) and constructed many large and small temples, including the Chennakesava temple at Belur (1117), the Hoysaleswara temple at Halebidu (1160) and the Kesava temple at Somanathapura (1268). These temple complexes have been proposed to be listed as UNESCO world heritage sites.

1.2 History of Earthquakes in Karnataka

In the present seismic zonation map of India (Fig. 2), Karnataka lies in zones 2 and 3 (i.e., seismically less active to moderately active). A literature survey indicates that 33 earthquakes have occurred in Karnataka from 1828 to 2001 [1]. Karnataka experienced high seismic activity during the 1970s, with five earthquakes occurring in 1971, four earthquakes occurring in 1972 and three earthquakes each occurring in 1970 and 1974. The aforementioned earthquakes had a magnitude ranging from 3.8 to 5 on the Richter scale.

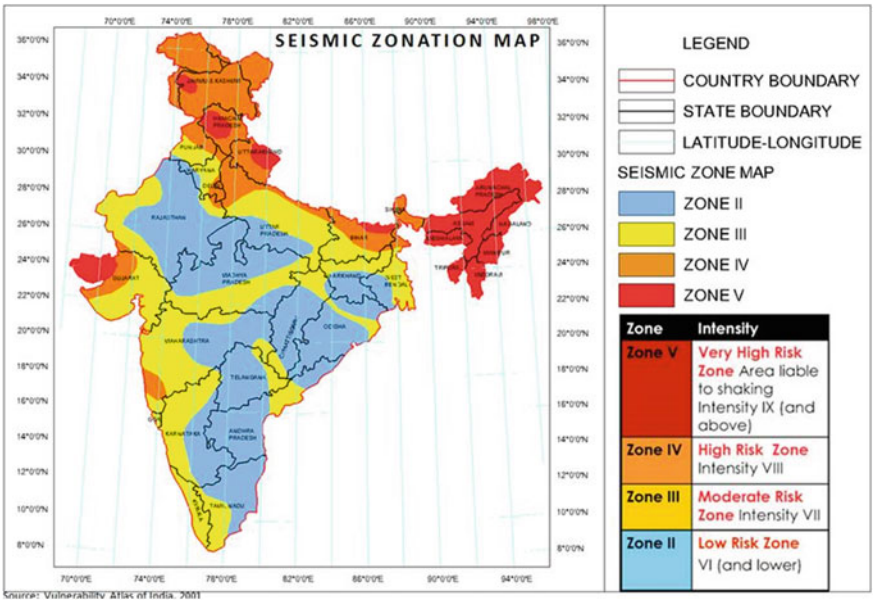

Fig. 2 Seismic zonation map of India

1.3 Literature Review

Analysis of historic masonary monuments by numerical modeling has been carried out by other investigators, few with dynamic characteristics analysis. Benjapon Wethyavivon et al. [2] carried out analysis on Thai historic masonary monuments at the Ayuthaya world heritage site to understand structural behaviour and provide critical information for planning and prioritizing restoration as well as assess their safety. Measured in-situ frequency was found to be 3.9 Hz and 2.3 Hz for 62.1 m high bell-shaped and 31.6 m high corn-shaped structure, respectively. From numerical modeling, the frequency with fixed base is 2.98 Hz and 3.10 Hz whereas with subsoil inclusion it was found to be 1.23 Hz and 2.41 Hz, respectively. The properties considered for modeling are elastic modulus are 3.020 Mpa, poison's ratio is 0.21 and compressive strength is 3.92 Mpa. Jaishi et al. [3] carried out analysis on dynamic and seismic performance of old multi-tiered temples in Nepal. The in-situ measured frequency by ambient vibration test and analytical natural periods were compared. An empirical formula is established to estimate the natural period of vibration for nepalese temples. It was found that the largest period was 0.6 s for the highest tower (21.93 m).

The problem of testing the scaled model and subject them to ground motion tests was addressed by Daniel Ruiz et al. [4] for sixteenth and seventeenth century rammed earth-built churches in the Andean highlands. The purpose of testing the model was to conduct a comparative evaluation of the seismic performance of scaled model of

rammed earth-built doctrinal churches, with and without confining reinforcements by wood elements. The displacements were reinforcement by wood elements. The displacements were found to be between 4 and 7.1 mm for unreinforced model and 1.2–1.4 mm with LVDT located at different positions.

A Meher Prasad, Arun Menon et al. [5] worked on seismic vulnerability of south Indian temples, in their effort to protect the monuments from earthquakes as the studies focussing on south Indian temples are not reported in the literature. The temple considered for the study is Ekambaranathar temple in Kanchipuram. Fundamental frequency of the site is estimated to be 3.63 Hz which is closely matching with the fundamental frequency of the mandapam. From FEM analysis using commercially available package ABAQUS 6.6.4 the frequency for 4 pillared mandapam is 3.53 Hz and for 16 pillared mandapam is 3.46 Hz in Y-direction being the first mode. Through ambient vibration the frequency was found to be 3.56 Hz for 4 pillared mandapam and 3.10 Hz for 16 pillared mandapam.

2 Description of the Amritesvara Temple

The Amritesvara temple is a heritage stone masonry structure that was constructed in the ekakuta style (single Vimana). The temple comprises the sanctum sanctorum, which is also known as the garbhagriha and is where the deity resides; the mandapa, which is a pillared hall provided in front of the garbhagriha for devotees to gather for activities such as chanting and meditation; and the antara, which is a chamber that joins the main sanctuary and the mandapa of the temple. The various components of the temple are illustrated in Fig. 3.

Fig. 3 Various components of the Amritesvara temple

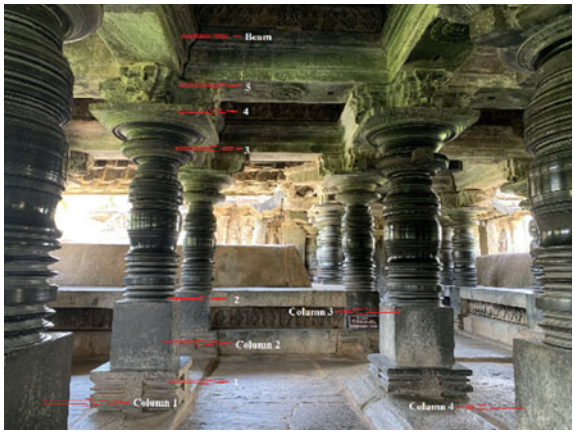

Fig. 4 View of the mandapa at the Amritesvara temple

To study the behaviour of the Amritesvara temple (a heritage structure) under seismic loads, a part of the temple, namely the mandapa (a space frame), was considered. The mandapa consists of four columns, four beams and a dome.

2.1 Structural System Modelling

The geometric scaling factor of the model was decided on the basis of shake table dimensions of 1.5 m × 1.5 m. The actual space frame measures 2.92 m × 2.92 m. Therefore, a 1:3 scale model was adopted. The temple columns comprise five table joints. The beams are placed on the capital and are tied using clamps, as observed in the prototype. The dome is placed on the beam without any joints. The joints of the temple column were replicated in the model (Figs. 4, 5, 6 and 7). The column base (pedestal) was fixed to a steel base plate, and this arrangement was assumed to be the fixed condition. The base plate was connected to the shake table by using 20 mm bolts (Fig. 5).

2.2 Scaling Factors

Simulation laws were followed when performing geometric scaling. Material used in the prototype and model is the same. Scale factors obtained using modelling principles are specified in Table 1 ($S_i = S_p/S_m$).

Fig. 5 Model of the mandapa of the Amritesvara temple

Fig. 6 Table joints provided in the prototype for different components of the column

2.3 Experimental Setup

The designed components with shear keys (model elements) were assembled on the shake table at the Earthquake and Vibration Research Centre, Central Power Research Institute, Bengaluru (Fig. 8). The provisional assemblage is displayed in Fig. 9. A

Fig. 7 Table joints provided in the model for various elements of the column

Table 1 Scaling factors [6]

Sr. no	Parameters	Scale factor
1	Acceleration (a)	S_i^{-1}
2	Gravitational acceleration (g)	Neglected
3	Time (t)	S_i
4	Linear dimension (l)	S_i
5	Displacement (δ)	S_i
6	Frequency (ω)	S_i^{-1}
7	Modulus (E)	1
8	Stress (σ)	1
9	Strain (ε)	1
10	Poison's ratio (υ)	1
11	Mass density (ρ)	1

fully assembled model of the space frame and the instrumentation are depicted in Fig. 5.

2.4 Seismic Loading Characteristics

Sine sweep tests were conducted on the assembled structure with peak ground accelerations (PGAs) of 0.05 g, 0.075 g and 0.1 g in the X-direction from 1 to 50 Hz at the rate of 1 octave per minute. Figures 10 and 11 display a typical input time history for the sine sweep tests corresponding to PGAs of 0.05 and 0.075 g, respectively.

Fig. 8 Assembling the model on the shake table

3 Experimental Testing on the Shaking Table

Four accelerometers were mounted on different components of the model (shake table, column, beam and dome), and an infrared linear variable displacement transducer was projected on the part of the dome where the maximum displacement was expected. After assembling the model, the accelerometers were placed on it and seismic testing was initiated. Three shake table tests were performed with PGAs of 0.05 g, 0.075 g and 0.1 g. The PGA was not increased further because the maximum displacement was observed at 0.1 g. The maximum displacement for a PGA of 0.1 g was 20.67 mm. At a PGA of 0.1 g, the column rotated due to torsion (Fig. 12) and the gap between the beams visibly widened at the joints. Therefore, the test was discontinued (Fig. 13).

4 Damping

The logarithmic decrement method was used to determine the damping value of the constructed scaled temple model from the free vibration records collected during the

Fig. 9 Provisional assemblage

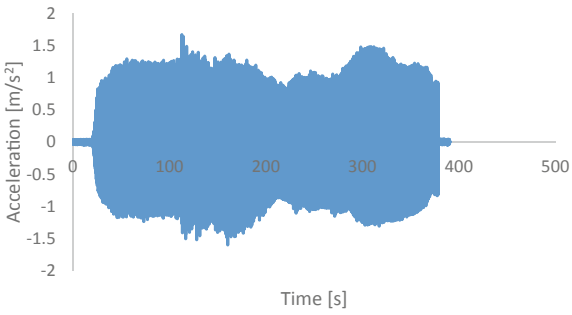

Fig. 10 Time history in the sine sweep test when the PGA is 0.05 g

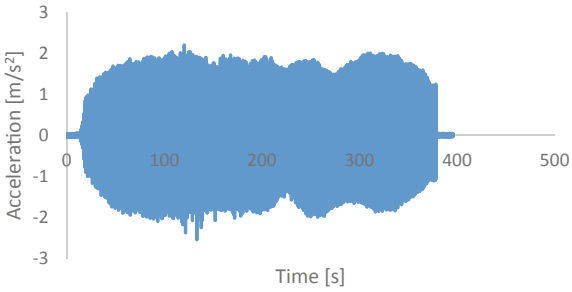

Fig. 11 Time history in the sine sweep test when the PGA is 0.075 g

Fig. 12 Rotation of the columns

Fig. 13 Displacement of the beams

shake table test. The damping value was found to be 6%. The structural damping ratio obtained through the experimental process was used for numerically modelling of the scaled temple model. The graph of the free vibration records is displayed in Figs. 14 and 15.

5 Numerical Modelling of the Scaled Temple Model

Considering the details of the scaled temple model, which is a replica of a part of the Amritesvara temple, a finite element (FE) model with joints was designed in ANSYS Workbench 16.0 by using 45 solid elements (Fig. 16). The numerical model consisted of four columns, four beams, one slab, and one dome. The material properties used in the design were obtained by conducting various experiments, such as the uniaxial

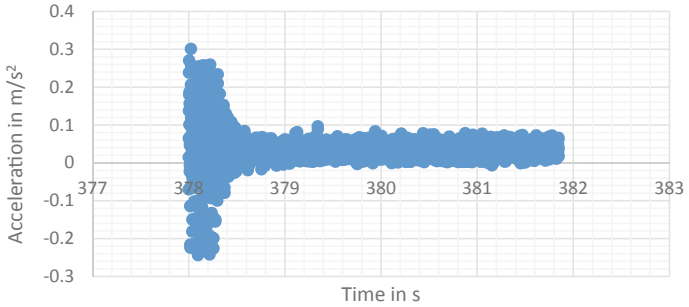

Fig. 14 Free vibration graph

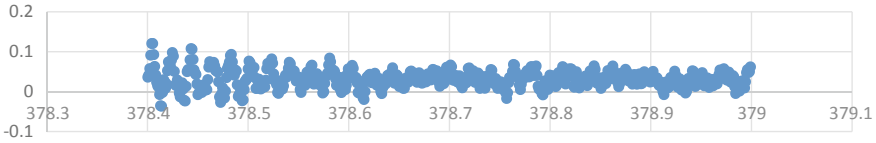

Fig. 15 Enlarged section of the free vibration graph

Fig. 16 FE model of the mandapa

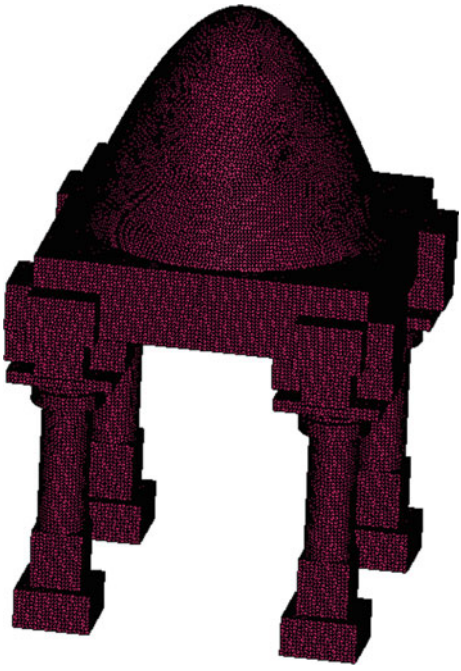

Table 2 Experimental results for the tested samples

Material	Density (kg/m^3)	Compressive strength (MPa)	Young's modulus (MPa)	Poisson's ratio	Tensile strength (MPa)
Soapstone	2798.6	48.88	3354	0.263	7.55

Table 3 Natural frequency obtained from the resonance test

Components	Natural frequency (in Hz)
Dome	3.375
Beam	3.375
Column	2.688

compression test for determining the Young's modulus and Poisson's ratio as well as the compressive strength and Brazilian tests for determining the tensile strength. The obtained results are summarised in Table 2. In the designed model, the building materials were assumed to be homogenous, isotropic and linearly elastic. Constraints were applied to the joints; the base was considered to be rigid; and the domes were designed to rest on the beams.

6 Results

6.1 Natural Frequency

The natural frequencies obtained from the resonance test of the shake table are presented in Table 3. Because the space frame did not act as a single unit, different frequencies were observed for different components of the space frame (Figs. 17, 18 and 19). Table 4 summarises the results obtained from the numerical model for the natural frequency. Table 5 provides a comparison of the natural frequency obtained through experiments and numerical analysis.

7 Conclusion

In the present study, a scaled model of the Amritesvara temple with the Hoysala architecture style was designed, constructed and commissioned. Shake table tests were conducted on the scaled model, and the natural frequency and damping were determined. Furthermore, a numerical model of the constructed scaled model was designed, and numerical analysis was performed. The results from numerical analysis and the laboratory measurements are in good agreement. Thus, the scaled structural model can replicate the behaviour of the real temple model with reasonable accuracy.

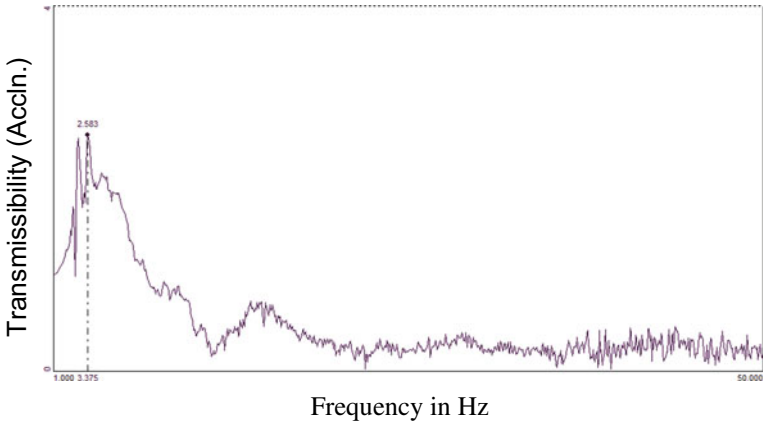

Fig. 17 Transmissibility graph for the beams

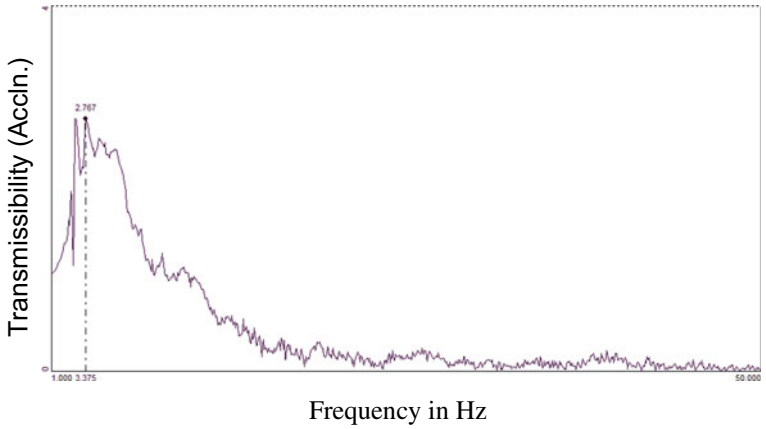

Fig. 18 Transmissibility graph for the dome

In conclusion, the scaled temple model is a valid and qualified model that can be used for further experimental investigations. The numerical results indicated that the vulnerability of the mandapa is mainly due to a lack of suitable interconnection between structural members.

In the experimental tests, the columns were rotated and hairline cracks were observed. Moreover, the gap between the beams at the joints visibly widened. This behaviour suggests that the beam and column behaved independently during the testing, as indicated by the obtained results. Thus, the experimental results also indicate that the vulnerability of the mandapa is primarily due to a lack of proper interconnection between structural members.

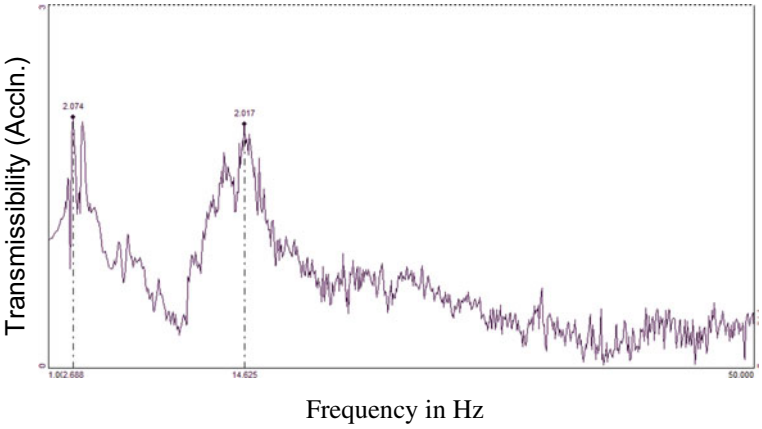

Fig. 19 Transmissibility graph for the column

Table 4 Results obtained from the numerical model of the scaled temple

Modes	Mode of vibration	Natural frequency (in Hz)
1	Transition in X	2.561
2	Transition in Y	2.568
3	Torsion	3.505
4	Transition in X	12.134
5	Transition in Y	12.954

Table 5 Comparison of the fundamental frequencies obtained through experimental and numerical analysis

Modes	Frequency obtained through shake table testing in Hz	Frequency obtained through numerical modelling in Hz
1	2.688	2.561

This study conclusively proves that torsion is the primary mode of vibration of the temple structure, and the temple structure may collapse during future earthquakes, even those of relatively low magnitude.

Acknowledgements This research was supported by the Vision Group of Science and Technology (VGST). The authors acknowledge the Archaeology Department of Karnataka for providing the structural details of the temple; the National Institute of Rock Mechanics, Kolar, for testing the stone samples; the Central Power Research Institute for their assistance; and K. S. School of Engineering and Management for their encouragement. The authors also thank the reviewers for their helpful comments and suggestions.

References

1. Sitharam TG, Anbazhagan P, Mahesh GU, Bharathi K, Nischala Reddy P (2005) Seismic hazard studies using geotechnical borehole data and GIS. In: Symposium on seismic hazard analysis and microzonation, 23–24 Sept 2005, Roorkee
2. Wethy Avivorn B et al (2014) Model verification of Thai historic masonary monuments. J Perform ASCE. https://doi.org/10.1061/(ASCE)CF.1943-5509.0000697
3. Jaishi B, Ren et al (2003) Dynamic and seismic performance of old multi-tiered temples in Nepal. Eng Struct 25(14):1827–1839
4. Ruiz D et al (2014) Seismic rehabilitation of sixteenth and seventeenth century rammed earth-built Churches in the Andean highlands: field and laboratory study. J Perform ASCE. https://doi.org/10.1061/(ASCE)CF.1943-5509.0000605
5. Ronald JA, Menon A et al (2018) Modelling and analysis of South Indian temple structures under earthquake loading. Indian Academy of Science
6. Harris HG, Sabnis GM (1999) Structural modelling and experimental techniques. CRC Press, USA
7. Lakshmana Murthy K (1997) Structural conservation of monuments in South India. Bharatiya Kala Prakashan, Delhi
8. Sharma A, Reddy GR, Vaze KK (2012) Shake table tests on a non-seismically detailed RC frame structure. Struct Eng Mech 41:1–24. https://doi.org/10.12989/sem.2012.41.1.001
9. Mikolic Z, Krstenska L, Maronic P, Smoljanovic H (2017) Shaking table test of scaled model of protiron dry-stone masonry structure. In: X international conference on structural dynamics, EVRODYN (2017)

Effect of Base Isolation on the Seismic Performance of Hill Buildings

Zaid Mohammad, Ahmed Bilal, and Abdul Baqi

Abstract RC buildings constructed on hill slopes pose complex structural behaviour as compared to conventional buildings resting on a plain ground. The hill buildings come under the category of irregular buildings, which are asymmetric in elevation as well as plan at different floor levels, due to which the centre of gravity and stiffness at subsequent floor levels always vary and cause additional torsional moments in the buildings. Further, the length of the columns in hill buildings also varies pertaining to steep slopes, resulting in variation of lateral stiffness in all columns. Moreover, the base isolation systems have shown a profound effect to reduce the seismic vibrations in the buildings. Thus, in this study, the influence of a commonly used base isolation system, i.e. Laminated Lead Rubber Bearing (LLRB) on the seismic performance of two hill building configurations, viz. stepback and setback-stepback, was investigated. All the configurations have been modelled using a finite element software, and examined by Response Spectrum analysis and Non-linear Static Pushover analysis. The dynamic parameters obtained from the numerical study were discussed as variations in storey shear, base shear, time period, drift, maximum top storey displacement values and plastic hinge development pattern in the building structure. finally, the vulnerability and suitability of the different configurations against seismic excitations were compared.

Keywords Hill buildings · Push-over analysis · Base isolation · Laminated lead rubber bearing

1 Introduction

The population growth has led to an increase in infrastructural development in hilly areas. Due to the scarcity of plain ground in hills, the construction of RC buildings

Z. Mohammad · A. Baqi
Department of Civil Engineering, Z.H.C.E.T., Aligarh Muslim University, Aligarh, India

A. Bilal (✉)
Faculty of Engineering & Technology, Civil Engineering Section, University Polytechnic, Aligarh Muslim University, Aligarh, India

T. G. Sitharam et al. (eds.), *Earthquakes and Structures*, Lecture Notes in Civil Engineering 188, https://doi.org/10.1007/978-981-16-5673-6_18

has to be carried out on steep sloping grounds. Thus, the buildings constructed on hill slopes show different dynamic behaviour as compared to those resting on the levelled ground under seismic forces [1]. The stepback configuration is generally preferred for the buildings on the steep slopes, however, a setback-stepback configuration is also common. Buildings resting on hill slopes have unsymmetrical structural configuration due to which the centre of mass and centre of stiffness varies along various floors and impart twisting moment in structural members, in addition to the lateral loads, when subjected to earthquake loads. Further, due to the short column effect in hill buildings, the shorter column on the uphill side has higher stiffness and attracts much more forces as compared to that of the column on the downhill side. Hence, it is found to be more vulnerable to damage under earthquake loads [2].

Previous studies have shown that a base isolation system is the most effective control measure for reducing the earthquake vibrations induced in the structural systems [3–5]. In conventional earthquake-resistant design of RC structures, the capacity of the structure is increased to provide the seismic demand through adequate reinforcement and ductility. Whereas, in a base isolation system, the dynamic properties of the building are modified in such a way that the shear demand for which the building has to be designed is reduced. In this technique, some flexible system is introduced between the foundation system and the column base of the structure, which increases the damping as well as the horizontal flexibility of the building. The fundamental time period of the RC structures is generally found in the range of the predominant period of the earthquake ground motions which causes a high dynamic amplification effect [6, 7]. Thus, the time period of the building can be increased beyond 2.0 s using base isolation, which significantly brings down the seismic demand [3]. The most common type of base isolator is the laminated lead rubber bearing isolator, as it is found to be very effective in reducing the high accelerations or the high-frequency motions. These are characterized by low horizontal stiffness to isolate the horizontal vibrations and high vertical stiffness [8, 9].

The state-of-the-art studies carried out so far, emphasized the structural behaviour of hill buildings and frame-infill interaction in normal buildings constructed on the plain ground [1, 2, 10–16]. But none of the studies were conducted on the behaviour of hill buildings with base isolation systems under earthquake loads. Moreover, IS 1893 (Part 1) has recommended to carry out three-dimensional dynamic analysis for the buildings with geometrical, mass and stiffness irregularity to ascertain the true response of buildings subjected to lateral loads [17]. Also, the inelastic behaviour of hill buildings should be analysed in order to get the true response of the structure. Thus, the present study explores the influence of a commonly used base isolation system, i.e. Laminated Lead Rubber Bearing (LLRB) on the seismic performance of two hill building configurations, viz. stepback and setback-stepback. All the configurations were modelled using a finite element software, and examined by employing Response Spectrum analysis and Non-linear Static Pushover analysis. The seismic parameters obtained from the numerical study were discussed as variations in storey shear, base shear, time period, drift, maximum top storey displacement values and

plastic hinge development pattern in the building structure. Finally, the vulnerability and suitability of the different configurations against seismic excitations were compared.

2 Materials and Methods

The present study investigates the structural behaviour of two different types of buildings resting on an inclined terrain, viz. stepback and setback-stepback, under seismic loads. The influence of laminated lead rubber bearing (LLRB) base isolation system on the seismic performance of the considered configurations was analysed. The Response Spectrum and Non-linear Static Pushover methods were employed to ascertain the seismic response of building configurations. The obtained seismic parameters from the analyses were compared as variation in the values of the fundamental time period, lateral drift, lateral shear at foundation level and plastic hinge development pattern in along as well as across hill slope direction. The elasticity modulus and Poisson's ratio of concrete material are taken as 25,000 N/mm^2 and 0.2, respectively. The concrete mix and reinforcement steel grade were assumed as M25 and Fe500, respectively. For seismic analysis, rigid frame diaphragm is considered in the floor systems and support conditions are assumed to be fixed at foundation level. Due to accidental eccentricity, the torsional effects have been considered in the analysis in accordance with IS 1893 (Part 1): 2016. For non-linear analysis, plastic hinges were allocated at the ends of all the frame elements in all the models. The load application was considered to be displacement control in pushover analysis. When the load was incrementally increased, structure members may start to yield and lead to failure. The members experience changes in stiffness sequentially and demonstrate various stages as shown in Fig. 1, viz. immediate occupancy, life safety and collapse prevention levels [18].

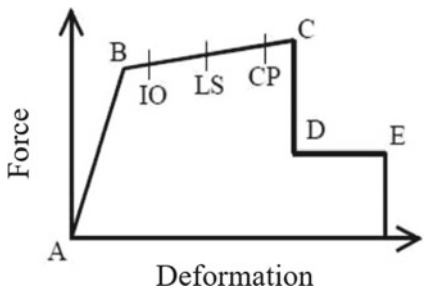

Fig. 1 Force versus deformation curve for plastic hinge at different stages

Table 1 Parameters considered in different building configurations [11]

Geometric parameters	Seismic parameters
Thickness of slab = 0.150 m	Zone = V
Height of each storey = 3.5 m	I = 1.5
Depth of foundation = 1.75 m	R = 5
Column size = 0.23 m × 0.50 m	Soil condition = II (i.e. medium)
Beam size = 0.23 m × 0.50 m	Live load = 3 kN/m^2

2.1 Building Configuration

Four different models of stepback and setback-stepback building configurations with and without base isolator systems were analysed. The buildings were modelled with 4 bays in along as well as across slope directions. The length of each bay in along and across the slope in all the models was taken as 7 and 5 m, respectively. The inclination of the ground was assumed to be 27° with the horizontal [11].

The load due to the masonry infills has been considered at the periphery of the building frames. The various parameters considered in the analysis of different building configurations are mentioned in Table 1.

2.2 Design of Base Isolation System

For the design of an effective base isolation system, the main requirements are: (a) capability to carry vertical loads, (b) sufficiently low stiffness in the horizontal direction which can increase the time period of the building to the required value, (c) large vertical stiffness so that the amplification in the vertical direction can be minimized, (d) sufficient damping to prevent excessive isolation level displacements, and (e) initial stiffness to prevent movement due to small vibrations [19]. While designing a base-isolated building, the following steps are followed [3]:

(i) Base isolators were designed based on the vertical load coming on them for the specified zone and soil type.
(ii) Base isolated building was designed to achieve the desired criteria.
(iii) Finally, the design was checked using non-linear dynamic analysis.

The base isolators were designed using the relationships given by Datta [3]

$$K_{eff} = \frac{W}{g}\frac{4\pi^2}{T_b^2} \tag{1}$$

where K_{eff} is the effective stiffness of the base isolator, W is the maximum vertical load under any column for the load case '$1.2DL + 1.6LL_o$' (where LL_o reduced live

load) [19], T_b is the isolated time period, '$T_b = nT$', (where n may be taken as 3 to 4), T represents the time period for building having a fixed base.

$$A_r = W/p \tag{2}$$

$$T_r = GA_r/K_d \tag{3}$$

$$A_{pb} = F/\sigma_{pb} \tag{4}$$

where T_r is the thickness of one rubber layer, G is the modulus of rigidity of rubber, G varies from 0.69 to 0.86 MPa for the range of strain specified for rubber bearing, i.e. $\gamma = 100 - 150\%$ [6], A_r represents the area of rubber layer, F is the characteristic strength calculated while determining the bilinear curve properties of the base isolator, σ_{pb} is the yield shear strength of the lead. σ_{pb} has a value of 8–10 MPa [4].

In order to account for sufficient over strength, peak design earthquake forces are used directly to design isolation system and substructure, that is, the R factor is taken as unity for designing the isolation system and the substructure. For the design of superstructure, the response reduction factor, R_I is kept lesser than that of fixed base building. As per FEMA P751 (2009) [20], R_I is taken as three-eighth of the R factor considered for the fixed base structure. For superstructure, R_I is considered as 2. For substructure, R_I is considered as 1. In IBC 2006, 1605.2.1 [21], three load cases, are available for the design of isolators.

In this paper, hill buildings with two configurations, viz. stepback and setback-stepback have been analysed. Base isolators were designed for both the buildings and the responses were compared with the buildings having fixed supports (see Fig. 2). In order to keep the design economical, base isolators were not provided beneath all the columns. Base isolators were provided at supports that were at higher levels from the base supports as shown in Fig. 3 and were subjected to higher shear forces under earthquake.

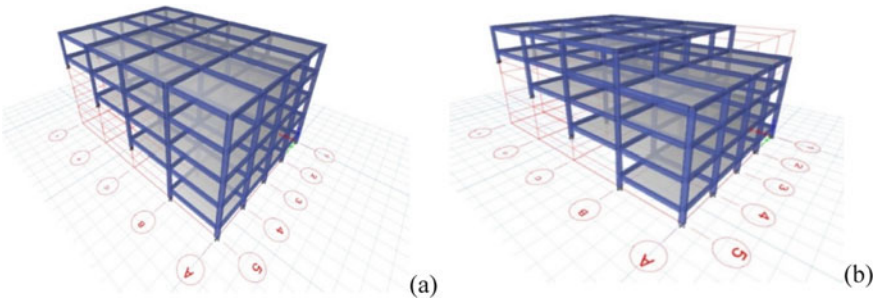

Fig. 2 Different hill building configurations: **a** Stepback building and **b** Setback-stepback building

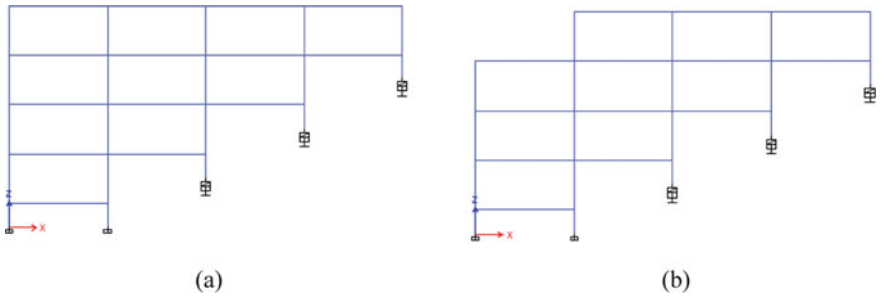

Fig. 3 Hill building configurations with a base isolator in **a** Stepback building and **b** Setback-stepback building

Initially, the buildings were analysed using the response spectrum method where input spectrum was taken from IS 1893:2016 [17]. The vertical load at each column was evaluated and the base isolator was designed individually. For example, while designing the base isolator under an interior column for setback-stepback configuration, the values of effective stiffness, design displacement and energy dissipation per cycle have been calculated as $K_{eff} = 2112$ kN/m, $\Delta_d = 0.213$ m, *and* $W_d = 82.56$ kNm, respectively, from Eq. 1, for zone V and damping coefficient $\xi_{eff} = 0.15$. Final values of parameters of the backbone curve of the base isolator have been obtained after iterations (Tables 2 and 3). Furthermore, the geometric properties have been calculated from Eqs. 2–4 as shown in Tables 4 and 5 [19]. Four sets of base isolators were designed for each building. Lumped plasticity approach was adopted for modelling non-linearity in the beams and columns. Hinges were defined as per FEMA 356 [18]. M3 hinges were provided for beams and P-M2-M3 hinges were provided for columns.

Table 2 Bilinear properties of the isolators used in stepback building

Isolator id	R (kN)	K_{eff} (kN/m)	F_y (kN)	K_u (kN/m)	K_d (kN/m)
RUB2000	2000	1222	70	9236	924
RUB1500	1500	964	55	7292	729
RUB1000	1000	643	37	4861	486
RUB650	650	418	24	3159	315

Table 3 Bilinear properties of the isolators used in setback-stepback building

Isolator id	R (kN)	K_{eff} (kN/m)	F_y (kN)	K_u (kN/m)	K_d (kN/m)
RUB2800	2800	1801	104	13,611	1361
RUB2000	2000	1222	70	9236	924
RUB1300	1300	836	48	6319	632
RUB850	850	546	31	4139	414

Table 4 Geometric properties of the base isolators used in stepback building

Geometric properties (in mm)	RUB2000	RUB1500	RUB1000	RUB650
Bearing diameter	600	550	450	35
Diameter of lead core	95	85	70	60
Thickness of each rubber layer	13	13	13	12
Layers of rubber	18	20	20	15
Thickness of the plates	3	3	3	3
Thickness of end plates	25	25	25	25
Bearing height	338	370	370	275

Table 5 Geometric properties of the base isolators used in setback-stepback building

Geometric properties (in mm)	RUB2800	RUB2000	RUB1300	RUB850
Bearing diameter	720	600	500	400
Diameter of lead core	100	95	75	65
Thickness of each rubber layer	13	13	13	13
Layers of rubber	18	18	18	18
Thickness of the plates	3	3	3	3
Thickness of end plates	25	25	25	25
Bearing height	338	338	338	338

3 Results and Discussion

The hill building configurations with fixed support and base isolator systems were analysed for the seismic loads in along as well as across slope directions including the effect of accidental eccentricity as per code provisions [17]. The three-dimensional models were analysed using the Response spectrum method and Push-over method of analysis. The results obtained from the analysis were discussed in terms of the fundamental time period, total base shear, lateral shear force at foundation and plastic hinge patterns in structural members, and compared within the considered configurations.

The dynamic properties obtained from the numerical analyses have been described in Table 6. It can be clearly observed that the base isolator system has significantly

Table 6 Seismic response of different building configurations

Building type	Support type	FTP by RSA (sec)		Base shear (kN)	
		Along	Across	Along	Across
Stepback	Fixed	0.718	0.417	2986	2258
	Base isolated	1.675	1.217	1521	884
Setback-stepback	Fixed	0.894	0.580	2502	1603
	Base isolated	2.165	1.613	989	638

influenced the seismic performance of both stepback and setback-stepback configurations. In the case of stepback buildings, the fundamental time period (FTP) in along slope direction was found to be increased by 133.3% with the introduction of a base isolator system in place of fixed isolated supports. The variation in FTP was found to be 191.8% in across slope direction. Similarly, base-isolated setback-stepback buildings exhibited a 142.1 and 178.1% increase in the FTP in along and across slope direction, respectively, as compared with that of fixed supported building.

There was a prominent decrease in the total base shear was observed in building configurations with base isolation in along as well as across slope directions, which indicates the less shear demand attracted by the structural members of base-isolated buildings as compared with those of fixed support systems. The base shear values were found to be reduced to 50.9 and 38.6% in along and across slope directions, respectively, after the base isolation system was introduced in the stepback building. Also, the base shear values in the base-isolated setback-stepback configuration were found to be decreased to 39.5 and 39.8% in along and across slope directions, respectively. Moreover, it can be ascertained that the setback-stepback buildings attract less base shear than the setback configuration of the hill buildings, thus proved to be less prone to earthquake forces.

Figures 4 and 5 describe the lateral shear force distribution in an interior frame of hill building configurations. It was observed that the building with fixed support

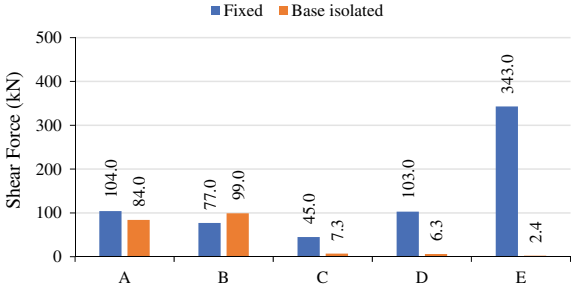

Fig. 4 Shear force distribution in columns at foundation level in stepback building in along slope direction

Fig. 5 Shear force distribution in columns at foundation level in setback-stepback in along slope direction

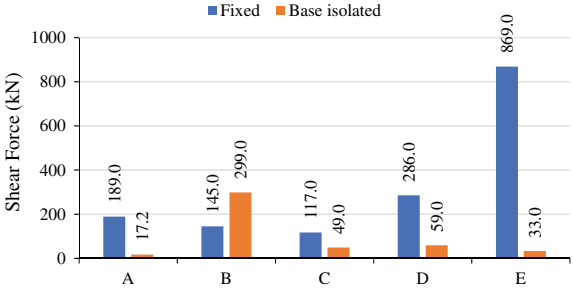

systems tends to attract higher shear forces in columns at upper storey level pertaining to higher lateral stiffness and short overall length. However, after the introduction of base isolators at columns C, D, and E, a significant reduction in the base shear values could be observed, especially at uppermost storey level at location E. Thus, it can be concluded that the introduction of base isolation systems in hill building configurations reduces the lateral shear demand in the structural members with higher lateral stiffness. A subsequent decrease in the values of base shear at C and D levels was also observed. However, the columns at frame A and B were remained fixed to reduce the lateral drift in the building structure.

The building configurations were also analysed using non-linear static pushover analysis after designing the reinforced concrete frames for assessing the seismic response of the structure. The plastic hinge pattern in structural members of different hill building configurations with and without base isolators was ascertained and compared in along as well as across hill slope directions at intermediate, upper and lower storey levels (see Figs. 6 and 7). The colour coding of the hinge represents the deformation and performance behaviour at various load levels. In the case of stepback configurations with fixed support systems, the plastic hinge was first formed in columns of the topmost storey due to high storey shear, also, complete yielding of foundation at upper hill frame was observed. However, after the introduction of base isolators, the formation of hinges could be observed in beams followed by the columns in lower storeys. Thus, a significant decrease in the shear demand in columns with high lateral stiffness was observed. Further, the performance of the building in across hill slope was observed to be significantly increased with the use of base isolators. It can be observed that the columns at uphill and downhill side have yielded prior to beams, while the base-isolated model displayed hinge formations in safe levels in only beam members. Moreover, due to less seismic weight, the setback-stepback configuration performed better and exhibited minimal yielding in fixed support condition, whereas, none of the frame members in base-isolated configuration displayed yielding at any location, showing the effectiveness of base isolation systems in the performance of hill building configurations.

4 Conclusion

In this study, the seismic behaviour of two different hill building configurations with fixed and base-isolated support systems was investigated. The three-dimensional models were analysed using the Response spectrum method and Push-over method. The dynamic properties of the hill buildings were evaluated and compared. It was observed that the fundamental time period of both stepback and setback-stepback buildings was increased significantly with the introduction of base isolators at the foundations. A prominent reduction in base shear value in along as well across hill slope direction was observed in both configurations. Further, in the case of step-back building with fixed support systems, the plastic hinges were first formed in the columns of topmost storey due to high storey shear, also, complete yielding

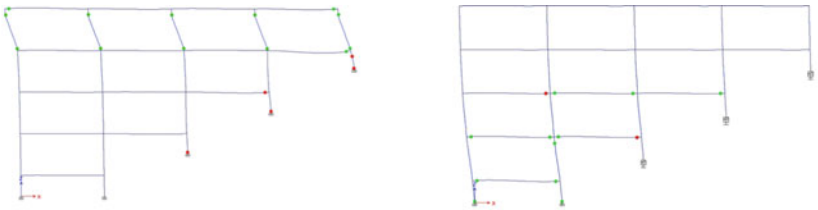

Fixed supports Base isolated supports

(a) Along slope direction (Intermediate frame)

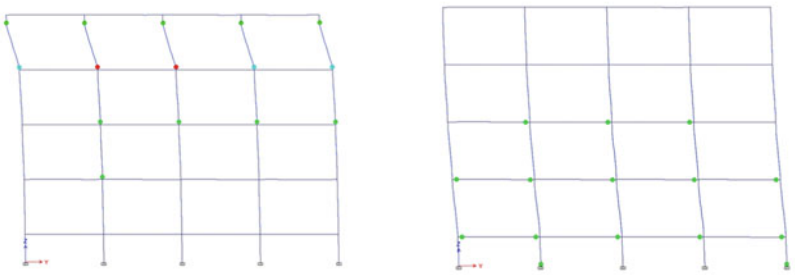

Fixed supports Base isolated supports

(b) Across slope direction (Downhill side)

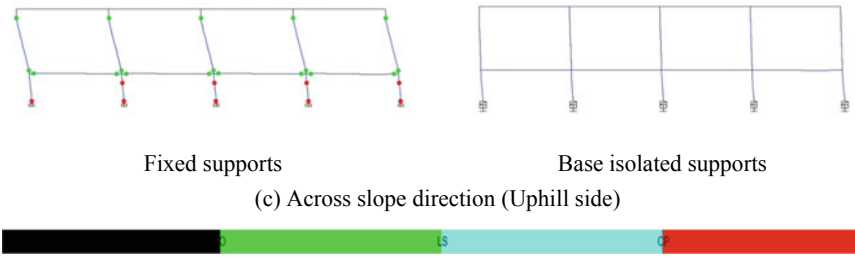

Fixed supports Base isolated supports

(c) Across slope direction (Uphill side)

Fig. 6 Plastic hinge formation pattern in stepback building

of the foundations at upper hill frame was observed. However, after the introduction of base isolators, the formation of hinges could be observed in beams followed by the columns in lower storeys only. Moreover, due to less seismic weight, the setback-stepback configuration performed better and exhibited minimal yielding in fixed support condition, whereas, none of the members in base-isolated configuration displayed yielding at any location, showing the effectiveness of base isolation systems. Thus, it can be concluded that the introduction of base isolation systems in hill building configurations reduces the lateral shear demand in the structural members with high lateral stiffness. Additionally, it could be ascertained that the

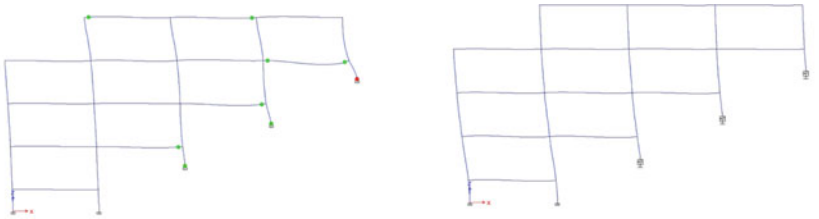

Fixed supports Base isolated supports

(a) Along slope direction (Intermediate frame)

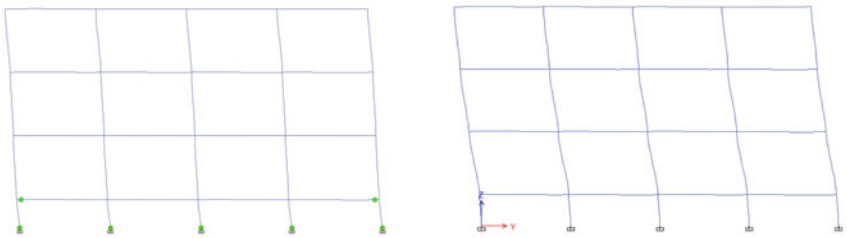

Fixed supports Base isolated supports

(b) Across slope direction (Downhill side)

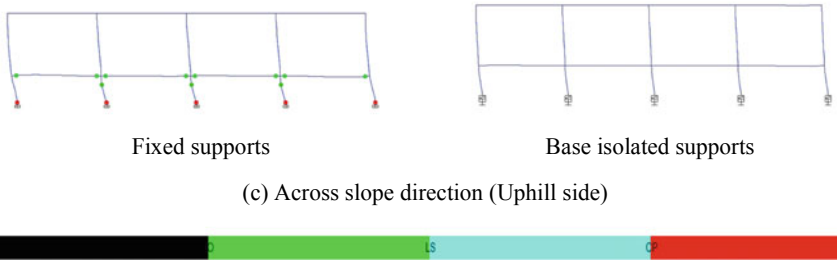

Fixed supports Base isolated supports

(c) Across slope direction (Uphill side)

Fig. 7 Plastic hinge formation pattern in setback-stepback building

setback-stepback buildings attract less base shear than the setback configuration of the hill buildings, thus proved to be less prone to earthquake forces.

References

1. Mohammad Z, Baqi A, Arif M (2017) Seismic response of RC framed buildings resting on hill slopes. In: 11th international symposium on plasticity and impact mechanics (IMPLAST 2016). Procedia Engineering, vol 173. Elsevier, New Delhi, pp 1792–1799. https://doi.org/10.1016/j.proeng.2016.12.221
2. Mohammad Z, Razi MA, Baqi A, Influence of masonry infill panels on the seismic performance of irregular buildings. In: Advances in geotechnics and structural engineering. Lecture notes in civil engineering, vol 143. Springer, Singapore, pp 1–11. https://doi.org/10.1007/978-981-33-6969-6_1
3. Datta TK (2010) Seismic control of structures. In: Seismic analysis of structures. Wiley (Asia) Pvt Ltd., pp 369–429
4. Skinner RI, Robinson WH, McKerry GH (1993) An introduction to seismic isolation. Wiley, Chichester
5. Alessandro B, Ileana C (2004) Optimal design of base-isolators in multi-storey buildings. Comput Struct 82:2199–2209
6. Kelly JM (1997) Earthquake-resistant design with rubber. Springer, London
7. Providakis CP (2008) Pushover analysis of base-isolated steel–concrete composite structures under near-fault excitations. Soil Dyn Earthq Eng 28:293–304
8. Wu YM, Samali B (2002) Shake table testing of a base isolated model. Eng Struct 24:1203–1215
9. Kelly JM, Leitman G, Soldatos AG (1987) Robust control of base isolated structures under earthquake excitation. J Optim Theory Appl 53:159–180
10. Kumar S, Paul DK (1998) A simplified method for elastic seismic analysis. J Earthquake Eng 2(2):241–266. https://doi.org/10.1080/13632469809350321
11. Birajdar BG, Nalawade SS (2004) Seismic analysis of buildings resting on sloping ground. In: 13th world conference on earthquake engineering (13WCEE). Paper no. 1472, Vancouver, BC, Canada. https://www.iitk.ac.in/nicee/wcee/article/13_1472.pdf
12. Kadid A, Boumrkik A (2008) Pushover analysis of reinforced concrete frame structures. Asian J Civil Eng (Building & Housing) 75–83. https://doi.org/10.1007/s11803-013-0179-8
13. Kaushik HB, Rai DC, Jain SK (2008) A rational approach to analytical modelling of masonry infills in reinforced concrete frame buildings. In: 14th world conference on earthquake engineering (14WCEE). Corpus ID: 165155308, Beijing, China. https://www.iitk.ac.in/nicee/wcee/article/14_05-01-0317.PDF
14. Davis R, Krishnan P, Menon D, Prasad AM (2004) Effect of infill stiffness on seismic performance of multi-storey RC framed buildings in India. In: 13th world conference on earthquake engineering (13WCEE). Paper no. 1198, Vancouver, BC, Canada. https://www.iitk.ac.in/nicee/wcee/article/13_1198.pdf
15. Murty CVR, Jain SK (2000) Beneficial influence of masonry infill walls on seismic performance of RC frame buildings. In: 12th world conference on earthquake engineering (12WCEE). Paper no. 1790, Auckland, New Zealand. https://www.iitk.ac.in/nicee/wcee/article/1790.pdf
16. Mohammad Z (2019) Effect of unreinforced masonry infills on seismic performance of hill buildings. VW Appl Sci 1(1):37–47. https://doi.org/10.36297/vw.applsci.v1i1.29
17. IS 1893 (Part 1): 2016 (2016) Criteria for earthquake resistant design of structures. BIS, New Delhi
18. FEMA 356, Federal Emergency Management Agency (FEMA) (2000) Prestandard and commentary for the seismic rehabilitation of buildings, Washington, DC
19. Bilal A, Agarwal P, Sadique MR, Performance evaluation of base isolated building. In: Advances in geotechnics and structural engineering. Lecture notes in civil engineering, vol 143. Springer, Singapore, pp 247–256. https://doi.org/10.1007/978-981-33-6969-6_23
20. FEMA P-751 (2012) NEHRP recommended seismic provisions: design examples. Federal Emergency Management Agency, Washington, DC
21. International Code Council (ICC) (2000) International Building Code (IBC), Falls Church, VA

Seismic Response Perspective for the Proposed Subway Tunnel Near Kamalapur Railway Station

Tahmeed M. Al-Hussaini, Sagar Barua, and Mahbubah Ahmed

Abstract To mitigate ever-growing traffic congestion in Dhaka city, the Government of Bangladesh is implementing the Mass Rapid Transit (MRT) project. The MRT Project consists of several metro rail routes in the city, some of these routes are elevated rail, while some are planned to be partly elevated and partly underground. Construction of MRT Line 6 consisting of elevated rail is in progress, while the second route (MRT Line 1) being planned for construction consists of some underground portions. Bangladesh, located near the plate boundaries of the Indian Plate colliding with the Eurasian Plate, possesses significant seismic hazard. According to the latest updated version of the Bangladesh National Building Code (BNBC-2020), Dhaka city has a seismic zone coefficient of 0.20 (maximum considered earthquake) for rock sites. For local soil conditions, ground motions may exceed 0.25 g. This paper considers a site near Kamalapur Railway station, the Railway Hub in Dhaka city, where MRT Line 1 will end. The seismic response of a typical cross-section of subway tunnel is analyzed using the finite element software PLAXIS 2D. Time history analysis under 2D plane strain conditions is conducted for various intensity levels of earthquake motion incorporating site effects.

Keywords Subway tunnel · Seismic response · Site amplification · Dhaka MRT · FEM

1 Introduction

During an earthquake, underground structures move with the soil, while structures above ground are free to sway back and forth. For this, underground structures are less prone to damage in comparison to surface engineering works. From this belief for a long-time, underground structures were designed without seismic considerations. However, some significant damages of underground tunnels during recent strong earthquakes have drawn attention. Researchers have conducted different case studies on the damages of the tunnel due to different earthquakes. Damages in tunnel lining

T. M. Al-Hussaini (✉) · S. Barua · M. Ahmed
Bangladesh University of Engineering and Technology, Dhaka 1000, Bangladesh

T. G. Sitharam et al. (eds.), *Earthquakes and Structures*, Lecture Notes in Civil Engineering 188, https://doi.org/10.1007/978-981-16-5673-6_19

like cracking, spalling, collapsing have been identified after earthquakes [1]. Later, to minimize the damage suffered by tunnels during the earthquakes, many studies have been carried out. These studies recommend special treatment in designing tunnels for earthquake hazards. To obtain an optimum tunnel seismic design, a correct evaluation of stresses in tunnel lining and its relative displacement under seismic waves is necessary. The variation of internal forces induced in the tunnel lining during earthquakes can be calculated following several approaches that model in different ways the soil-structure interaction [2]. Although existing guidelines suggest pseudo-static or uncoupled dynamic analyses, usually adopted for a preliminary stage of design, it has been shown that full dynamic analyses must be performed of the soil-structure interaction taking into account the influence of the pre-existing stress state around the tunnel [3, 4].

The government of Bangladesh has undertaken massive infrastructure projects in the transportation sector across the country, including a Mass Rapid Transit (MRT) System in Dhaka city to ease traffic congestions in this densely populated megacity. An elevated metro rail (MRT Line 6) under construction is expected to be completed next year. This will be the first metro rail of the capital city. The second metro rail under planning is MRT Line 1, which has portions of it underground. This paper deals with the underground portion of MRT Line 1. A recent publication [5] addresses geotechnical considerations and prospects for underground construction, including the underground metro in Dhaka City. This study attempts to have an assessment of the seismic response of the proposed tunnel-soil system in Dhaka soil. Full dynamic analysis of the soil-structure system has been conducted using the finite element software PLAXIS 2D.

2 Site Information

2.1 Route Location

The MRT Line-1 will have both elevated rail and underground rail [6] as shown in Fig. 1. Line 1 will have two branches: (i) 16.5 km Airport line running from Dhaka airport southward to Kamalapur Rail Station and (ii) 10 km Purbachal line running from Bhatara (Natun Bazar) eastward to Purbachal. The major portions of Line 1 will be above ground. However, there will also be significant underground portions (shown in blue in Fig. 1): (i) Khilkhet to Bhatara (ii) Malibag to Kamalapur (iii) Bhatara to Bashundhara. A typical underground cross-section of MRT line-1 tunnel near Kamalapur railway station has been considered for analysis in our study.

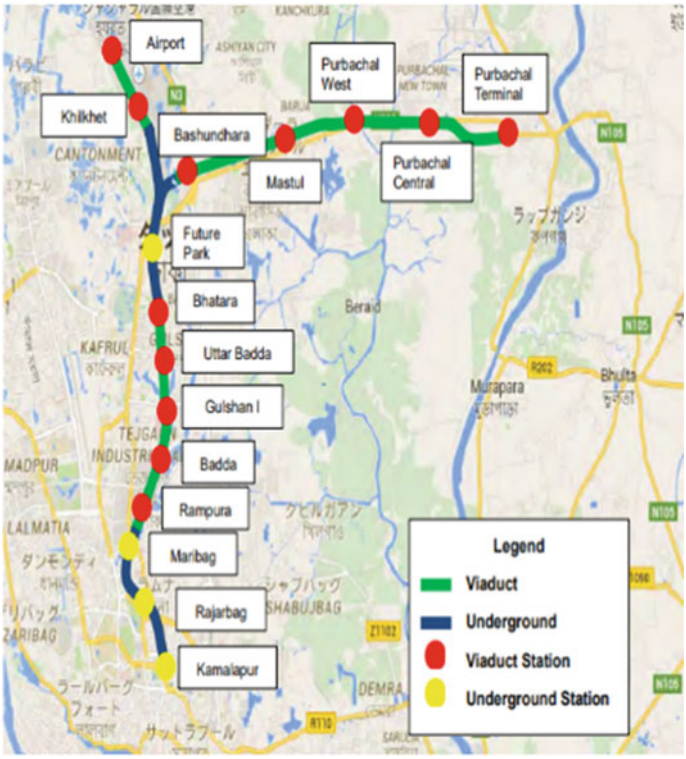

Fig. 1 Layout plan of MRT Line 1 [6]

2.2 Soil Profile

Soil investigations through 41 borings conducted under project feasibility study [6] provide information about the soil condition along the proposed route of MRT Line 1. A site (Borehole BH-1) near Kamalapur railway station is considered for this study (Fig. 2).

The subsoil information shows that there is 7.5 m of grayish brown medium stiff to very stiff clay on top of 3 m sandy silt layer. Below the sandy silt layer, 13.5 m of silty sand overlies firm support ($N > 50$) consisting of very dense sand or hard clay. Corresponding Standard Penetration Test (SPT) values are also shown in the figure.

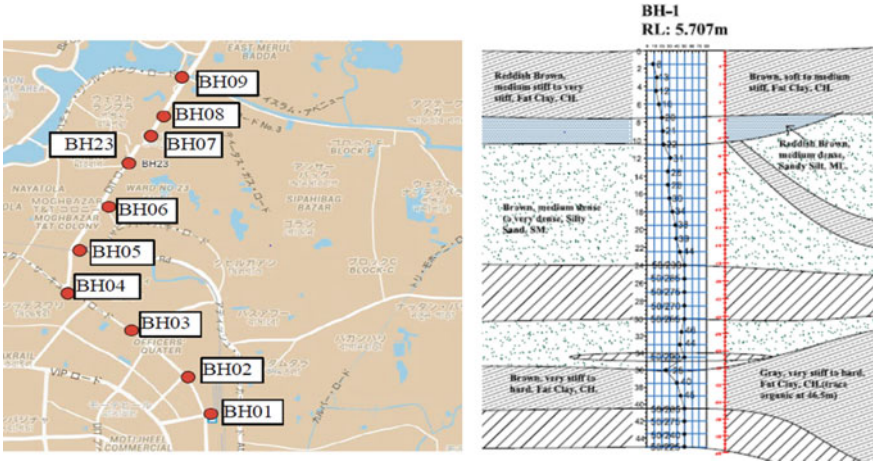

Fig. 2 Location of Borehole BH-1 and corresponding Bore Log [6]

3 Seismic Site Response Analysis

The software 'DEEPSOIL' has been used to conduct one-dimensional seismic site response analysis adopting the equivalent linear method. Shear wave velocities are estimated from SPT values of BH-1 using empirical relations given by the Japan Road Association [7].

Three earthquake records with different characteristics (listed in Table 1) but scaled to values consistent with Bangladesh's seismic zoning map have been used

Table 1 PGA (g) values obtained at 44 m depth from seismic site response analysis for different intensity levels of earthquakes

Earthquake Record	PGA (g) at 44 m depth		
	Case 1 $PGA_{rock} = 0.25$ g	Case 2 $PGA_{rock} = 0.2$ g	Case 3 $PGA_{rock} = 0.15$ g
January 17, 1995 $M_w = 6.9$ Kobe, Japan (PGA = 0.82 g)	0.15	0.12	0.08
October 15, 1979 $M_w = 6.4$ Imperial Valley, USA (PGA = 0.17 g)	0.18	0.14	0.1
January 17, 1994 $M_w = 6.9$ Northridge, USA (PGA = 0.22 g)	0.18	0.15	0.12

as input for site response analysis. The motions are hereafter termed as Kobe, Imperial Valley, and Northridge earthquake. The magnitude of the earthquakes and the peak ground acceleration (PGA) values of the three earthquake records are given in Table 1.

According to the updated version of the Bangladesh National Building Code (BNBC-2020), Dhaka city has a seismic zone coefficient of 0.20, implying PGA = 0.2 g at rock site [8] for maximum considered earthquake (MCE). For local site conditions consisting of alluvium, site amplification is expected, which is assessed by conducting seismic site response analysis. For this analysis, three different intensity levels are considered with PGA_{rock} equal to 0.25, 0.2, and 0.15 g. Each of the records of Imperial Valley, Northridge, and Kobe earthquakes scaled down to 0.25, 0.2, and 0.15 g are chosen as input (outcrop) motion in DEEPSOIL. As a result, nine sets of earthquake motion are considered. Through one-dimensional wave propagation analysis adopting an equivalent linear method, ground motion at a depth of 44 m is obtained. Table 1 also presents PGA values obtained at 44 m depth for nine sets of input earthquake motion. It is observed that the Imperial Valley and Northridge earthquake result in significantly greater PGA compared to that for the Kobe earthquake. The ground motion records obtained for 44 m depth are finally used as input to the base of the soil-tunnel system's numerical model for further numerical analysis in PLAXIS 2D.

4 Seismic Tunnel Response Analysis

4.1 Numerical Model

Figure 3 presents a schematic view of the tunnel-soil system considered for numerical analysis. A 7 m diameter tunnel with a reinforced concrete lining thickness of 0.3 m is assumed to have 8 m of overburden soil. High-strength concrete (fc' = 7000 psi) is considered for the tunnel lining. The soil profile up to firm soil is considered here, i.e., up to 44 m depth. The ground motion obtained through site response analysis (Sect. 3) is applied here at a depth of 44 m. As shown in Fig. 3, the soil profile is divided into eleven layers. The corresponding shear wave velocity and density are also shown.

A 2D plain strain model adopting 15-noded triangular elements is used to generate the finite element mesh for the problem shown in Fig. 3. The mesh, as developed in PLAXIS-2D, is shown in Fig. 4. The model is provided with viscous boundary conditions on the vertical boundaries described as absorbing boundary conditions in [9], while input motion (acceleration time history) obtained from site response analysis (Sect. 3) is applied to the base of the model as shown in Fig. 4.

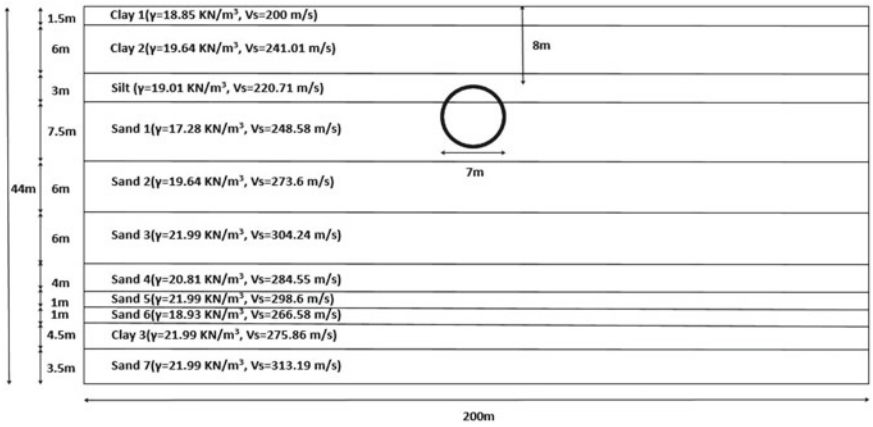

Fig. 3 Schematic view of the soil-tunnel system

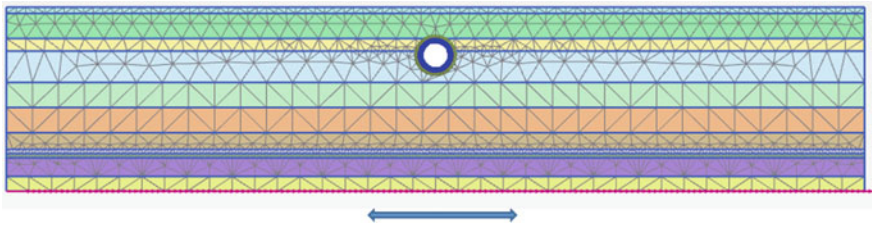

Fig. 4 PLAXIS 2D plain strain model with generated mesh

4.2 Numerical Results

Time history analysis is performed in PLAXIS-2D to evaluate the seismic response of the tunnel-soil system. Two parameters are considered in this paper, which affects the tunnel lining design:

(i) Induced horizontal distortions.
(ii) Induced moments.

Figure 5 presents horizontal distortion in the tunnel lining, which is defined as the relative lateral displacement between the tunnel left and tunnel right. For different intensity levels of earthquake, the relative displacement is found to be of the order of mm. The maximum distortion is found to be around 4.5 mm, which corresponds to the Imperial Valley earthquake. It may also be noted that the distortion is not proportional to the different intensity levels for the same earthquake. It is also worth mentioning that the Northridge earthquake has the maximum PGA value (Table 1) but still results in minimum distortion.

As shown in Fig. 6, the Kobe earthquake which has the lowest PGA (Table 1) results in the maximum bending moment (88.06 kN-m/m) in the tunnel lining. The

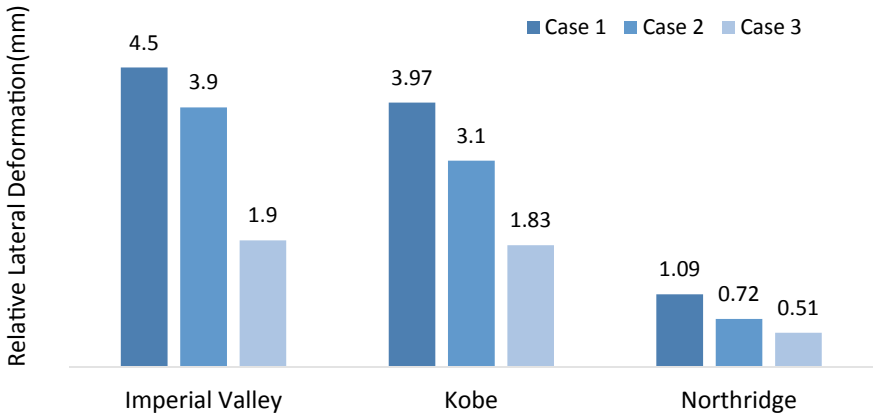

Fig. 5 Maximum relative horizontal deformation for various earthquake intensity levels

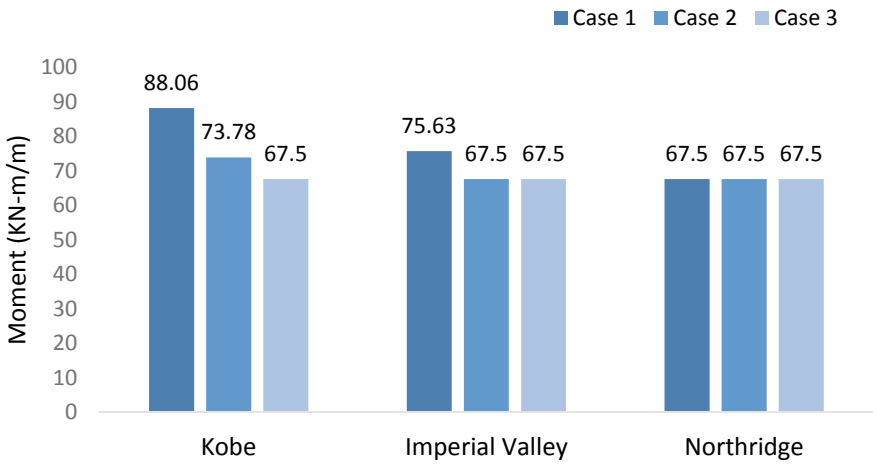

Fig. 6 Maximum bending moment in tunnel lining for different earthquake intensity levels

value of the bending moment without any earthquake is around 62.5 kN-m/m. Hence, the increase in bending moment is 5 to 25.56 kN-m/m, whereas corresponding input PGA at 44 m depth increases from 0.08 to 0.15 g. Hence, the bending moment increases by a much larger factor.

5 Conclusions

This paper presents preliminary results on ongoing research work for seismic response analysis for a typical tunnel-soil section for the proposed underground metro Line 1 near the Kamalapur Railway Station in Dhaka city. The study includes a two-step procedure with a seismic site response analysis to obtain ground motion at a certain depth, which is then used to perform finite element analysis on the tunnel-soil system using PLAXIS-2D. A variety of earthquake records with varying intensity levels have been considered. The seismic motion may generate appreciable bending moment in the tunnel lining, whereas the induced horizontal distortion is not that significant. The bending moment can increase at a much higher rate than the increase in the rate of intensity level. It is also observed that the earthquake with the lowest PGA at the bottom yields the largest bending moment. This highlights the importance of characteristics of earthquakes other than PGA. The results presented here are expected to be useful for conducting further studies on assessing the effect of an earthquake on tunnel design in the context of Dhaka City.

Acknowledgements This work was carried out as part of undergraduate thesis work by the second and third authors at the civil engineering department, BUET. PLAXIS-2D computations were performed at the computational laboratory of BUET-Japan Institute of Disaster Prevention and Urban Safety. PLAXIS-2D was procured under a research development fund (HEQEP CP-3140) from the University Grants Commission of Bangladesh.

References

1. Wang W, Wang T, Su J, Lin C, Seng C, Huang T (2001) Assessment of damage in mountain tunnels due to the Taiwan Chi-Chi Earthquake. Tunn Undergr Space Technol 16(3):133–150
2. Hashash Y, Hook J, Schmidt B, I-Chiang Yao J (2001) Seismic design and analysis of underground structures. Tunn Undergr Space Technol 16(4):247–293
3. Bilotta E, Lanzano G, Madabhushi S, Silvestri F (2014) A numerical Round Robin on tunnels under seismic actions. Acta Geotech 9(4):563–579
4. Fabozzi S, Bilotta E (2016) Behaviour of a segmental tunnel lining under seismic actions. Procedia Eng 158:230–235
5. Al-Hussaini TM, Ameen SF, Ahmed KS (2018) Geotechnical considerations and prospects for underground construction in Dhaka City. In: Proceedings of international conference on geotechnical engineering and architecture, St. Petersburg
6. ALMEC-Oriental-Nippon-Katahira (2018) The Preparatory Study on The Dhaka Mass Rapid Transit Development Project (Line 1) In Bangladesh. Report prepared by ALMEC CORPORATION, Oriental Consultants Global Co., Ltd., Nippon Koei Co., Ltd. and Katahira & Engineers International for Japan International Cooperation Agency
7. Japan Road Association (JRA) (1980) Specification and interpretation of bridge design for highway—Part V: Resilient Design
8. Al-Hussaini TM, Hossain TR, Al Noman MN (2012) Proposed changes to the geotechnical earthquake engineering provisions of the Bangladesh National Building Code. *Geotechnical Engineering Journal of the SEAGS & AGSSEA, 43*(2), 1–7

9. Kontoe S, Zdravkovic L, Potts D, Salandy N (2007) The use of absorbing boundaries in dynamic analysis of soil-structure interaction problems. In: Proceedings of 4th international conference on earthquake geotechnical engineering, Greece

Assessment of the Global Ductility of Mid-rise RC Buildings and Comparison with Varying Plan Aspect Ratio in High Seismic Zone

C. K. Sushma and Vijayalakshmi Akella

Abstract A structure in high seismic regions must perform under large forces without failing; hence, in this scenario, inelastic energy dissipation plays an important role in resisting large forces mainly caused by an earthquake. A ductile structure can deform and dissipate energy during an earthquake because it keeps deforming without reaching ultimate failure or collapse. In this study, the ductility of mid-rise RC buildings was compared under high seismic zones for different aspect ratios. Investigations were performed by following the Indian standard code with respect to plan aspect ratios. Reinforced concrete buildings with 10, 20 and 30 stories were modelled using five different plan aspect ratios of 1:1, 1:2, 1:3, 1:4, 1:5 and 1:6 under two categories, viz., category 1 with different plan aspect ratio and category 2 with the same plan area. The buildings were analysed by employing response spectrum and non-linear static analysis to obtain the results using Etabs software.

Keywords Pushover analysis · Mid-rise building · Ductility ratio · Performance point · Hinge

1 Introduction

1.1 Aspect Ratio

When the earthquake occurs, inertia force is distributed in a building, at floor levels where the mass is large and then this force is disseminated to lateral load resisting systems that this is, columns and/or structural walls. When floor slabs do not deform in large quantities in their own plane, due to rigid diaphragm action, a considerably good possibility of the distribution of inertia forces to lateral load resisting systems

C. K. Sushma (✉)
Department of Civil Engineering, DSCE, Bengaluru, India
e-mail: cvl@dayanandasagar.edu

V. Akella (✉)
Department of Civil Engineering, KSSEM, Bengaluru, India
e-mail: hod.civil@kssem.edu.in

T. G. Sitharam et al. (eds.), *Earthquakes and Structures*, Lecture Notes in Civil Engineering 188, https://doi.org/10.1007/978-981-16-5673-6_20

in proportion to their capacities emerges. However, when considerable deformation occurs in slabs in their own planes the inertia force is distributed based on the tributary area which causes members overloading with a low capacity and thus leads to buildings damage. Hence, floor slabs in buildings with a large plan aspect ratio may not provide rigid diaphragm action. Thus, constructing buildings with a large plan aspect ratio is not favorable [1].

1.2 Pushover Analysis

The non-linear static analysis, or pushover analysis, is a reliable procedure for seismic performance evaluation. It is a static analysis that includes nonlinear material characteristics. The non-linear static analysis can be performed to predict redistribution of forces during progressive yielding and thus to predict failure mechanisms or to accurately detect the possibility and location of any premature failure because it considers the inelastic behavior of structures. This analysis can help identify critical members likely to reach critical states during an earthquake to which attention should be paid during design and detailing. The pushover analysis includes several successive elastic analyses, superimposed to estimate the force–displacement curve of the complete structure [2].

1.3 Ductility

"The idea of designing earthquake resistant structures is based on the concept of energy absorption in inelastic deformations. The inelastic deformation capacity of structures is defined by a factor called ductility factor, which is the ultimate deformation to yield deformation. This factor indicates the rate of delay caused by the structure between yield and damage states. Thus, the structure behavior factor depends directly on the ductility factor" [3].

Mahmoodi (2000) studied the behavior of concrete moment resisting frames with different stories by inelastic analysis with a nonlinear static method and considered global and local (members) ductility capacity of the frames. They used displacement and rotational ductility to determine global and local ductility, respectively, and proposed a formula in two states to obtain the global ductility capacity of the structure based on the ductility capacity of beams and on that of columns [3].

1.4 IS Code

"IS 16700: 2017 code provides guidelines to prevent the progressive collapse of tall buildings. Progressive collapse can be defined as the failure that initiates at the local

element level and then propagates from element to element, finally leading to the collapse of entire building. As per the code, progressive collapse can be precluded by, selecting a suitable structural system, selecting critical member and providing adequate redundancy to the building. The Code also suggests the use of key elements to safeguard the building from progressive collapse. In addition to the methods indicated in the code to minimize the possibility of progressive collapse, other methods are suggested in various literature; these methods include improvement of member ductility, identification and strengthening of critical locations of buildings and provision of alternate load paths. Section 8.2 of the code emphasizes to ensure various aspects of ductility in tall buildings" [4, 5].

2 Present Work

Objective

1. To understand the effects of lateral force distribution on the lateral force-resisting system for different plan aspect ratios.
2. To understand the global ductility of buildings under investigation.

Three RC buildings of 30, 20, and 10 stories were considered in this study. Six models were prepared under each story for different plan aspect ratios of 1:1, 1:2, 1:3, 1:4, 1:5, and 1:6 for each story. The models have been discussed in detail in the below sections.

2.1 Modeling

Category 1

Six 30-, 20-, and 10-storied building were modeled using Etabs software, Table 1 presents the description of the input considered for modeling (Fig. 1).

Category 2

Six 30-storied buildings with the same area and the following input description were modeled (Table 2).

2.2 Analysis

The nonlinear analysis of the structures under static and dynamic loading was performed "ETABS" software. The response spectrum and pushover analyses were performed to determine maximum displacement and yield displacement of the whole

Table 1 Description of the model

Sl. no	Particulars		Remarks
1	Model 1	1:1	Area = 182.25 SQM
2	Model 2	1:2	Area = 364.5 SQM
3	Model 3	1:3	Area = 546.75 SQM
4	Model 4	1:4	Area = 723.6 SQM
5	Model 5	1:5	Area = 904.5 SQM
6	Model 6	1:6	Area = 1085.4 SQM
7	Zone	4	
8	Soil type	2	
9	Grade of concrete	M35	
10	Grade of steel	FE500	

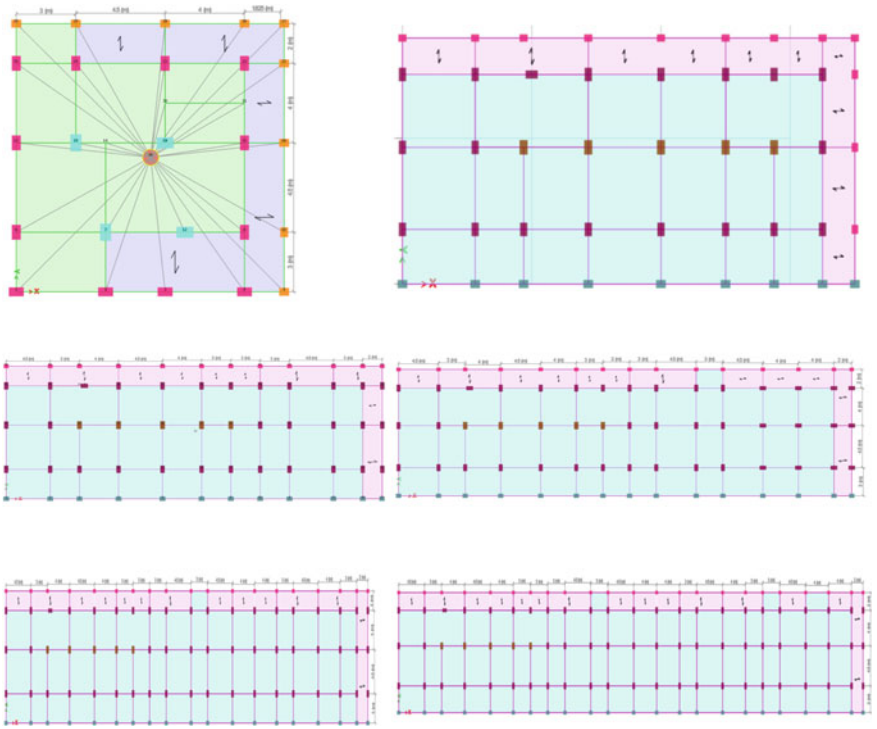

Fig. 1 Plan of the building with varying aspect ratio 1:1, 1:2, 1:3, 1:4, 1:5, and 1:6

Table 2 Description of the model

Sl. no	Particulars		Remarks
1	Model 1	1:1	Area = 1100 SQM
2	Model 2	1:2	Area = 1100 SQM
3	Model 3	1:3	Area = 1100 SQM
4	Model 4	1:4	Area = 1100 SQM
5	Model 5	1:5	Area = 1100 SQM
6	Model 6	1:6	Area = 1100 SQM
7	Zone	4	
8	Soil type	2	
9	Grade of concrete	M35, M30	
10	Grade of steel	FE500	

structure, respectively. According to IS 1893:2016, Zone 4 and Soil type 2 were considered for the analysis. The building models were analyzed and the designing process was conducted according to the IS codes 456 and 13920. Subsequently, global ductility was calculated using the formula

$$\mu(\text{global}) = \Delta\text{max} / \Delta\text{y},$$

where Δmax is = the maximum displacement at the roof level and Δy is the yield displacement of the whole building.

3 Results and Discussion

3.1 Maximum Displacement

According to the results of maximum displacement at each story, a trend of increase in displacement value from lower stories to the roof was observed and this trend occurred for all the aspect ratios (Figs. 2, 3, 4, 5, 6, and 7).

The maximum displacement at the roof level for aspect ratio 1:4 decreased by 76.5% in comparison with the aspect ratio 1:5 which decreased by 69.12%.

The percentage increase from 4th story to 30th story is approximately 78%, however for the building with an aspect ratio of 1:4, the percentage increase from 4th to roof level is 73%.

After the 24th floor in all the buildings, the increase in displacement is decreased by 4%.

In the building with the plan aspect ratio of 1:4 at the roof level the displacement is decreased by 0.23 mm in comparison with that on the 28th story.

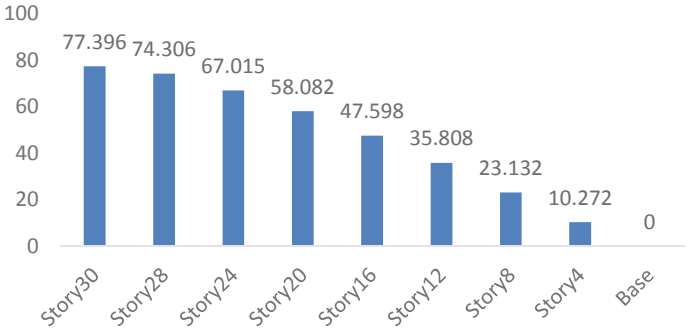

Fig. 2 Maximum displacement for the building with aspect ratio 1:1 story versus displacement

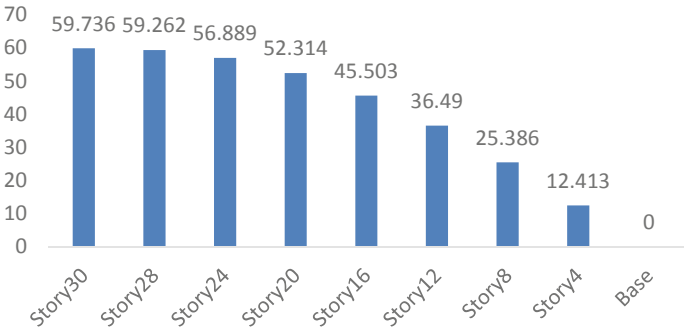

Fig. 3 Maximum displacement for the building with aspect ratio 1:2 story versus displacement

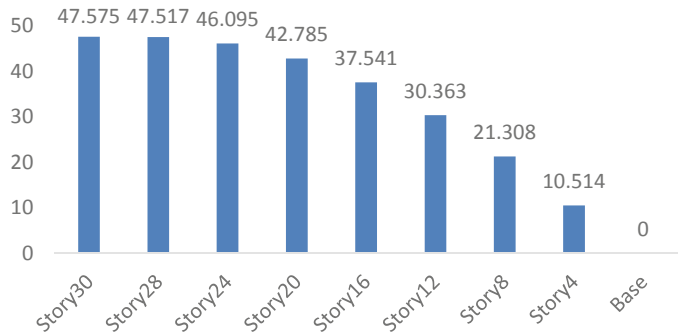

Fig. 4 Maximum displacement for the building with aspect ratio 1:3 story versus displacement

3.2 Story Drift

The story drift values obtained from the different plan aspect ratios are as follows (Figs. 8, 9, 10, 11, 12, and 13).

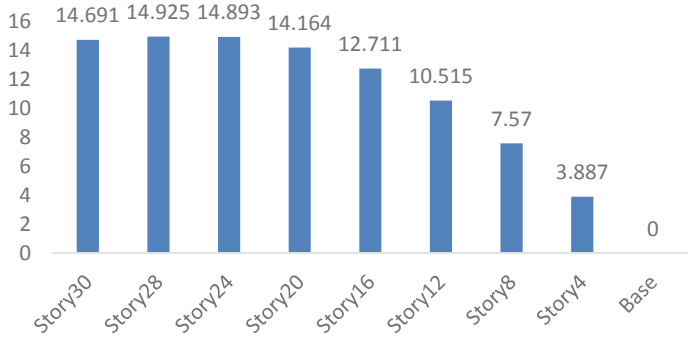

Fig. 5 Maximum displacement for the building with aspect ratio 1:4 story versus displacement

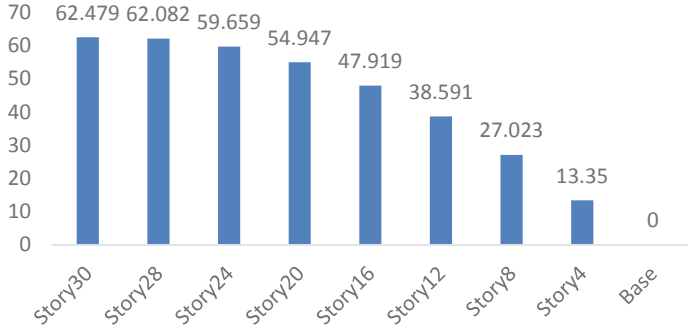

Fig. 6 Maximum displacement for the building with aspect ratio 1:5 story versus displacement

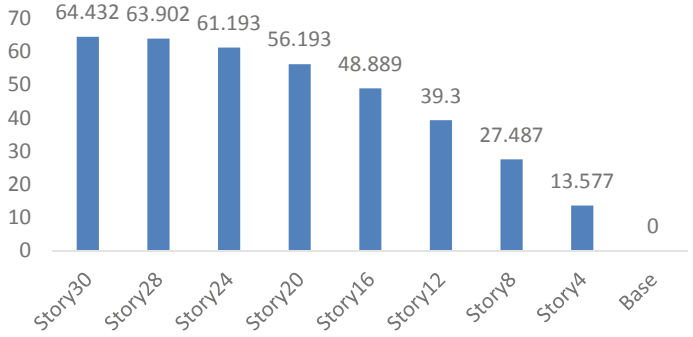

Fig. 7 Maximum displacement for the building with aspect ratio 1:6 story versus displacement

The story drift shows a decreasing trend from the ground floor to the roof level.

The building with the plan aspect ratio 1:4 exhibits behavior where the story drift at the 28th story decreases compared with that at the lower stories, but the story drift increases by 59% at the roof level.

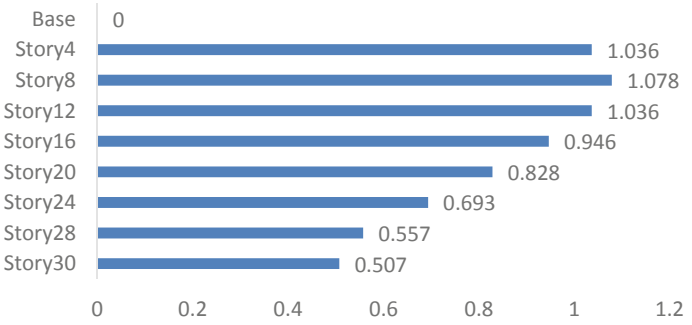

Fig. 8 Story drift for the building with aspect ratio 1:1

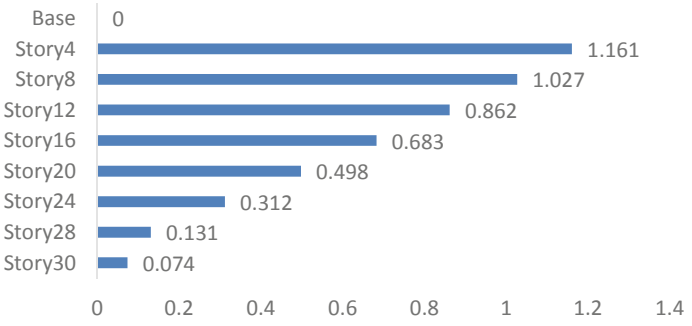

Fig. 9 Story drift for the building with aspect ratio 1:2

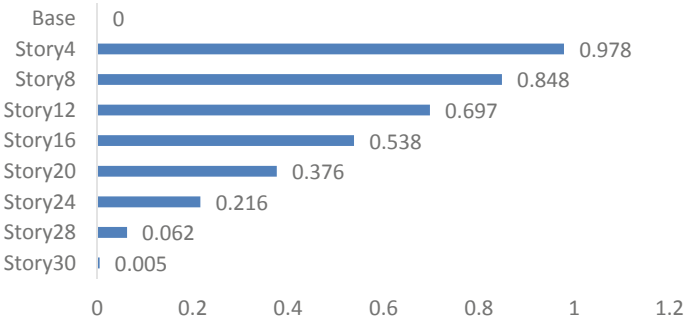

Fig. 10 Story drift for the building with aspect ratio 1:3

For the buildings with the aspect ratios of 1:2, 1:3, 1:4, 1:5, and 1:6 story drift decreased by approximately 93% However for those with an aspect ratio of 1:4 the story drift decreases by 86% and for those with the aspect ratio 1:1 the story drift decreases by 51%.

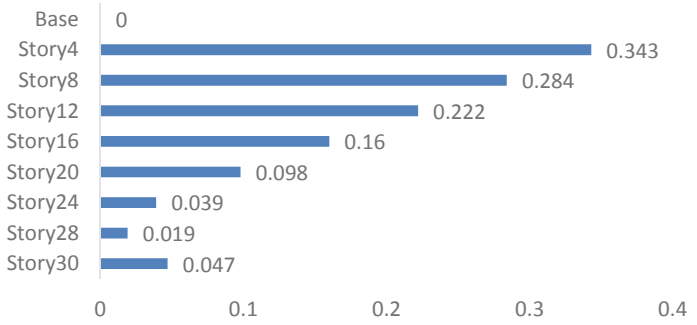

Fig. 11 Story drift for the building with aspect ratio 1:4

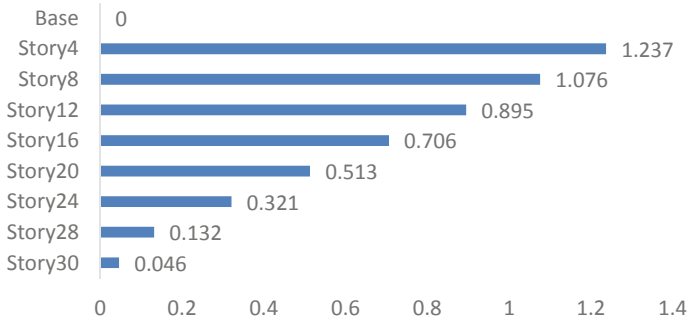

Fig. 12 Story drift for the building with aspect ratio 1:5

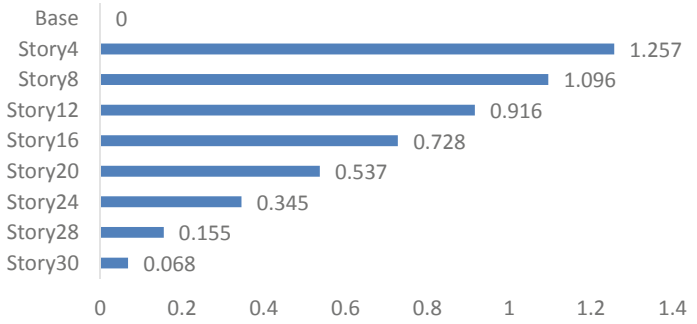

Fig. 13 Story drift for the building with aspect ratio 1:6

Story Stiffness

The presence of stiffness irregularity, together with strength irregularity, along the building height leads to undesirable performance throughout severe earthquake

shaking, including the localization of lateral deformations in select stories and initiation of story collapse mechanism. The existence of stiffness and strength irregularity, contributes to the undesirable output during an extreme earthquake, along the construction height, including the location of lateral deformations in the selected stories and to the mechanism of story collapse. The lateral stiffness Ks of a story is defined as the ratio of the story shear to story drift.

The following results show the variation in the stiffness for different stories and aspect ratios (Figs. 14, 15, and 16).

Global Ductility

The Global Ductility graph indicates that the ductility ratio decreases for the building with respect to the aspect ratio of 1:2 by 23% compared with the aspect ratio 1:1 and then increases for the aspect ratio 1:4 and again shows a trend of decrease by 36% for the aspect ratios 1:5 and 1:6.

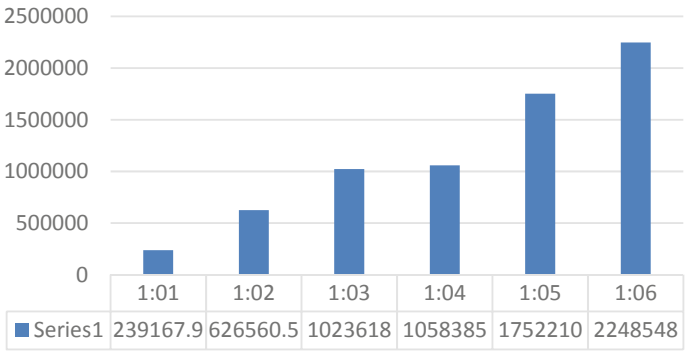

Fig. 14 Stiffness for 10 story along X-axis

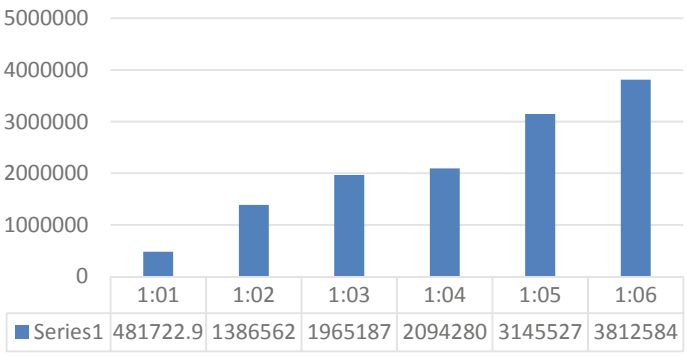

Fig. 15 Stiffness for 20 story along X-axis

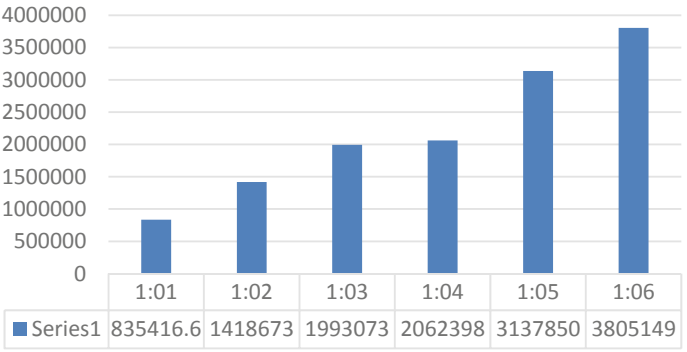

Fig. 16 Stiffness for 30 story along X-axis

4 Conclusion

This paper mainly focuses on the behavior of buildings with respect to the plan aspect ratios. In this paper, the calculation of global ductility for a high-rise building with a symmetrical plan and is mainly emphasized. Ductility is not directly proportional to the aspect ratio. Figures 17, 18, 19, and 20 indicate the variation pattern of the ductility ratio.

A detailed study was conducted by comparing the ductility ratio by varying the plan aspect ratio with the building height. When the number of stories increases from 10 to 30, the variation pattern becomes considerably similar. The ductility ratio decreases at 1:2 ratio and shows an increasing trend till the plan aspect ratio of 1:4 and then decreases at plan aspect ratio 1:5 and again increases for the aspect ratio of 1:6.

Ductility for the aspect ratio of 1:4 decreased by 29% and 36.2% compared with that for the aspect ratio of 1:3 and 1:5, respectively.

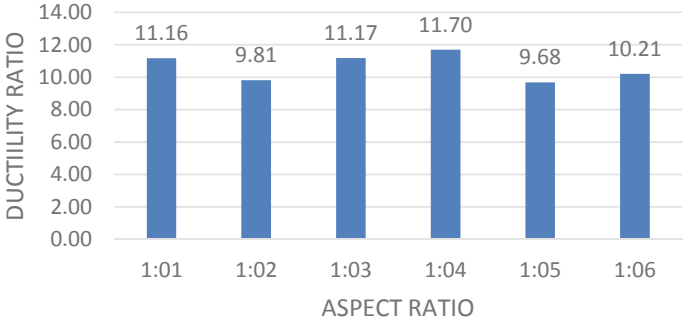

Fig. 17 Global ductility demand of the 10-story building

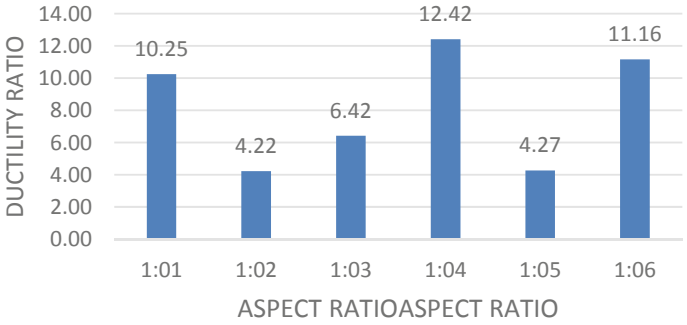

Fig. 18 Global ductility demand of the 20-story building

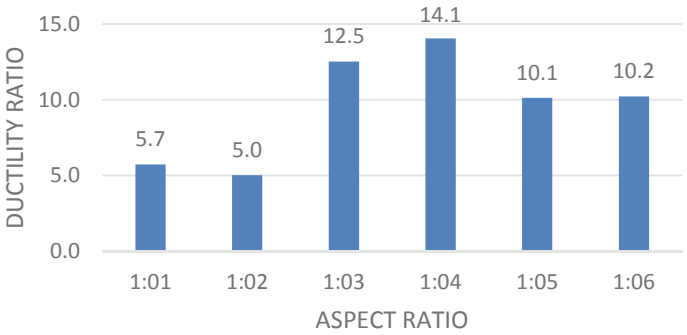

Fig. 19 Global ductility demand of the 30-story building

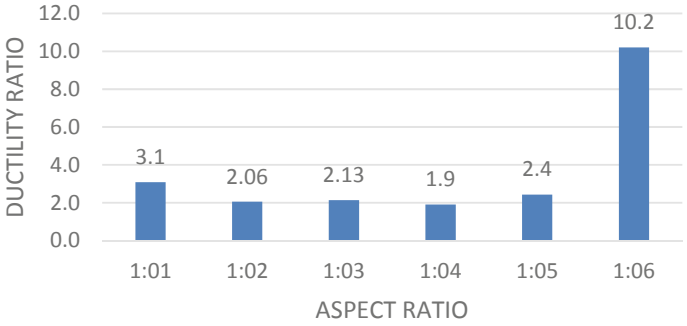

Fig. 20 Global ductility ratio for the 30-story building with the same area

In this study, the building dimension was kept constant along the Y-axis and the number of bays was increased along the X-axis. The maximum displacement at the roof level along X-axis shows a trend of decrease with an increase in the plan aspect ratio.

Figures 14, 15, and 16 show the variations in buildings stiffness. The ductility ratio is directly influenced by the stiffness variation.

References

1. Murty CVR, Goswami R, Vijayanarayanan AR, Mehta VV (2012) Some concepts in earthquake behavior of buildings
2. Aswin PT (2013) Thesis on seismic evaluation of 4-story reinforced concrete structure by non-linear static pushover analysis. NIT, Rourkela
3. Kia SM, Yahyai M (2004) Relationship between local and global ductility demand in steel moment resisting frames. In: 13th world conference on earthquake engineering, Paper no. 885
4. Krishna GV, Kumar R, International conference on issues in design of tall concrete buildings in India with reference to IS 16700: 2017 code
5. IS 13920 (2016) Ductile design and detailing of reinforced concrete structures subjected to seismic forces—code of practice

Sloshing Response of Water Tanks Under Seismic Excitation

Jogi Pranitha and B. R. Jayalekshmi

Abstract Liquid storage tanks are the predominant structures and they have to be designed to withstand major earthquake loads. In the present study, an elevated intze water tank of capacity 700 m^3 was considered and analyzed for seismic effects. Finite element modeling of the tank was made in ANSYS. A series of transient analyses was carried out for El Centro and Kobe earthquakes which are applied in the horizontal direction. The fluid inside the tank accelerates and causes additional hydrodynamic pressures on the tank. Past studies reveal that the convective hydrodynamic pressure is more than the impulsive hydrodynamic pressure. Time history plots were made to describe the sloshing phenomenon in the tank for various levels of the liquid. The sloshing displacements for the one-third level of the liquid were found to be maximum. The sloshing displacements in the horizontal direction are more than in the vertical direction.

Keywords Elevated intze water tank · Impulsive and convective hydrodynamic pressures · Sloshing displacement · ANSYS

1 Introduction

Elevated water tanks are constructed to store and supply the water at high pressure. There are lot of failures that has taken place due to earthquakes. The fluid behavior has to be analyzed. There are many approaches to evaluate the fluid-structure interaction effects. This study was made by formulating the fluid as the Lagrangian element. The behavior of liquid inside the tank during earth shaking is an important phenomenon as it exerts hydrodynamic pressures on the tank wall and base. They have to be analyzed for earthquake effects and designed accordingly. The study of fluid-structure interactions is necessary to find the hydrodynamic pressure distribution along the tank height and tank base. There are mainly three finite element approaches to represent fluid motion. Namely, Eulerian, Lagrangian, and mixed methods. In the Eulerian

J. Pranitha (✉) · B. R. Jayalekshmi
Department of Civil Engineering, National Institute of Technology Karnataka, Surathkal, India
e-mail: Jogipranitha.197cv019@nitk.ac.in

T. G. Sitharam et al. (eds.), *Earthquakes and Structures*, Lecture Notes in Civil Engineering 188, https://doi.org/10.1007/978-981-16-5673-6_21

approach, velocity potential or pressure is used to describe the behavior of the fluid. In the Lagrangian approach, the displacement field is used to express the fluid behavior. And in mixed-method, both pressure and displacement field are used in element formulation. In this study, fluid behavior is expressed by Lagrangian fluid element formulation.

Adem Dogangun et al. studied the hydrodynamic pressure distribution based on wall flexibility, the hydrodynamic pressure for flexible tanks is generally more than that of the rigid tanks [1]. Adem Dogangun et al. did a comparative study of hydrodynamic pressures for different codal provisions, they found that the impulsive time period is the difficult parameter to find, and the Eurocode 8 gives the practical formulations for the impulsive period. And the lateral displacement has to be determined to get this period [2]. Sivy martin et al. found that the hydrodynamic pressure by using a simplified mechanical model in which the fluid is replaced by impulsive and convective mass. The flexibility of the tank wall has an impact on impulsive liquid mass that experiences accelerations greater than peak ground accelerations and there is no effect on convective liquid mass and corresponding hydrodynamic pressure [3]. Kamila Kotrasova analyzed the rectangular endlessly long tank by using the finite element method. The fluid is formulated by using arbitrary Eulerian-Lagrangian formulation in which the two-way FSI is incorporated to account for the interaction effects. The hydrodynamic pressure was developed in the ground-supported rectangular endlessly long tank during the Loma Prieta earthquake was 16.03% [4]. Sloshing can be defined as the motion of the free surface inside its container. It is caused by any disturbances when the container is in partially filled condition. Based on the type of disturbance and the shape of the container, there are different types of motions as planar, non-planar, rotational, symmetric, and asymmetric. The main problem of liquid sloshing involves the estimation of hydrodynamic pressure distribution, forces, moments, and natural frequencies of the free liquid surface [5].

The present study describes the importance of convective hydrodynamic pressure, the critical condition in elevated intze water tank, and the variations of sloshing displacements and total hydrodynamic pressures in different directions for the tank full, two-third full, and one-third full conditions for two different seismic excitations.

2 Input Ground Motion

In this study, the structure is analyzed using time history data of two different ground accelerations, the El Centro earthquake and the Kobe earthquake. El Centro earthquake happened in 1940 in the Imperial Valley in southeastern Southern California near the international border of the United States and Mexico. It had a moment magnitude of 6.9. It was the first major earthquake that happened next to fault rupture. Kobe earthquake happened in Japan in 1995 with a magnitude of 7. To get the nonlinear behavior of the structure, it was analyzed for time-history data. The seismic forces were applied along the X-direction for all the models in ANSYS (Figs. 1 and 2).

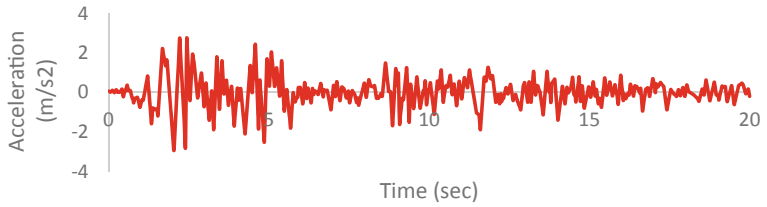

Fig. 1 Time history of El Centro earthquake (1940)

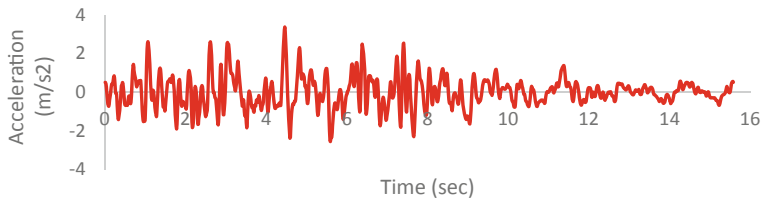

Fig. 2 Time history of Kobe earthquake (1995)

3 Estimation of Hydrodynamic Pressures as per IS 1893 Part 2

The interaction of fluid on the structure causes hydrodynamic pressures, these are impulsive and convective hydrodynamic pressures, respectively. The estimation of these pressures has been done according to IS 1893 part 2. The results show that the convective pressure is more than that of the impulsive pressure.

Elevated intze water tank is idealized as an equivalent cylindrical tank and analyzed for the hydrodynamic pressures. Figure 3 shows the vertical cross-section of the tank.

Impulsive hydrodynamic pressure on the wall

$$p_{iw}(y) = Q_{iw}(y)(A_h)_i \rho g h \cos\varphi$$

where

$$Q_{iw}(y) = 0.866[1 - \left(\frac{y}{h}\right)^2 \tanh(0.866D/h)$$

$$D = \text{diameter of the tank}$$

$$h = \text{depth of liquid}$$

Maximum pressure will occur at $\phi = 0$.

Impulsive hydrodynamic pressure on the base slab

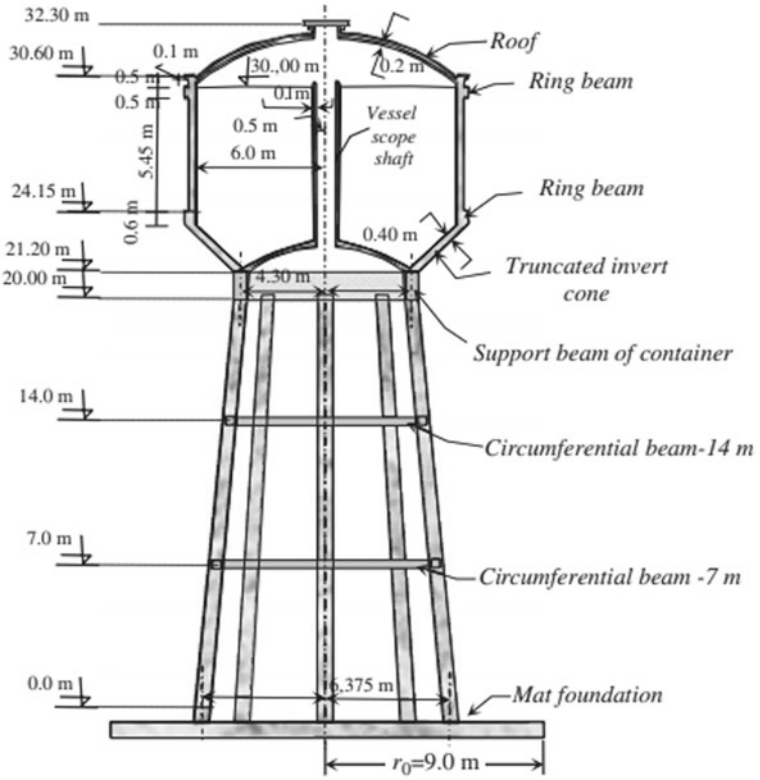

Fig. 3 Vertical cross-section of the tank (*Courtesy* Livaoglu et al. [6])

$$P_{ib} = 0.866(A_h)_i \rho g h \frac{\sinh \frac{0.866x}{L}}{\cosh \frac{0.866l'}{h}}$$

Convective hydrodynamic pressure on wall

$$P_{cw} = Q_{cw}(y)(A_h)_c \rho g D\left[1 - \frac{1}{3}\cos^2 \emptyset\right]\cos \emptyset$$

where

$$Q_{cw}(y) = 0.5625 \frac{\cosh\left(\frac{3.674y}{D}\right)}{\cosh\left(\frac{3.674h}{D}\right)}$$

Maximum pressure will occur at $\phi = 0$.
Convective hydrodynamic pressure on the base slab

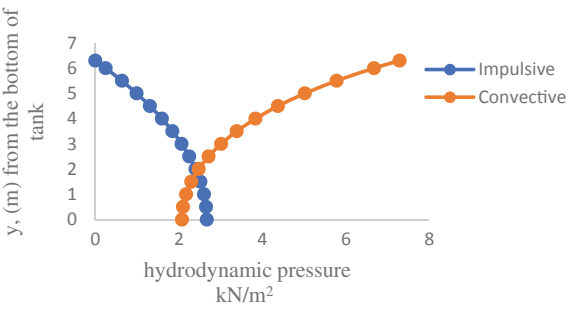

Fig. 4 Hydrodynamic pressure variation along the tank wall

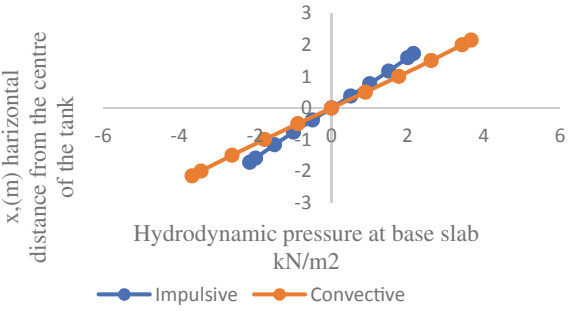

Fig. 5 Hydrodynamic pressure along the base slab

$$P_{cb} = Q_{cb}(x)(A_h)_c \rho g D$$

where

$$Q_{cb}(x) = 1.125\left[\frac{x}{D} - \frac{4}{3}\left(\frac{x^3}{D}\right)\right]\text{sech}\left(0.3674\frac{h}{D}\right)$$

The impulsive and convective hydrodynamic pressures along the tank wall and base are estimated and plotted (Figs. 4 and 5).

4 Methodology

The finite element software ANSYS [7] was used to evaluate the sloshing response of an elevated intze water tank of frame type staging. Figure 3 shows the vertical elevation of an elevated intze tank, which was analyzed and reported in [6]. The cross-sectional and the material properties of the water tank are shown in Tables 1 and 2.

ANSYS offers a wide variety of element libraries suitable for different applications. Each element has its own specific properties. The behavior of these elements is

Table 1 Cross-sectional details of various components

Component	Dimension (mm)
Top dome	200 thick
Top ring beam	300 × 500
Cylindrical wall	400 thick
Bottom ring beam	450 × 600
Circular ring beam	500 × 1200
Bottom dome	200 thick
Conical dome	400 thick
Braces	350 × 1200
Columns	300 (diameter)

Table 2 Material properties

Concrete	M30
	Poisson's ratio: 0.15
	Density: 2500 kg/m^3
	Modulus of elasticity: 3.2E10 N/m^2
Water	Density: 1000 kg/m^3
	Sonic velocity 1500 m/sec^2

defined through the use of element real constants. Generally, there are two methods to generate models in ANSYS, Direct generation method, and Solid modeling. Finite element analysis is performed in ANSYS in three major steps:

(1) Building the model (Pre-processing Phase);
(2) Applying the loads and obtaining the solutions (Solution Phase);
(3) Review the results (Post Processing Phase).

To evaluate the sloshing response of the tank the fluid-structure interaction is taken into account. During the seismic activity, the bottom portion of the liquid mass moves along with the tank wall which is rigidly connected to the tank called as impulsive mass. Whereas the top portion of the liquid mass is connected to the springs which are accountable for liquid sloshing. The FSI flag is assigned at the free surface of the liquid in order to get the fluid-structure interaction behavior.

5 Finite Element Model of Elevated Intze Tank

ANSYS mechanical APDL was used in the present study, beams and columns were modeled by structural 3D two-noded BEAM 188 element having 6 DOF at each node, the container walls, raft, top, and bottom domes were modeled by 3D four-noded structural SHELL 181 element having 6 DOF at each node, the soil medium was modeled by 3D eight-noded structural solid BRICK 185 element having 3 DOF

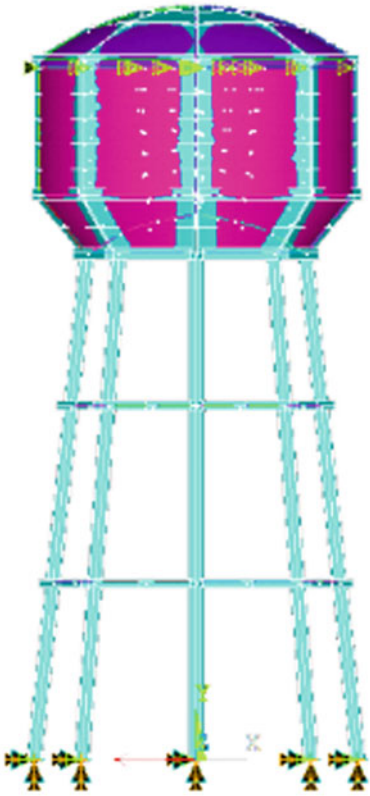

Fig. 6 Finite element model of the tank

at each node. Fluid is modeled by 3D eight-noded acoustic fluid element FLUID 30 having 5 DOF at each node (Fig. 6).

6 Results and Discussions

A series of transient analyses was carried out for tank full, two-third full, and one-third full conditions under El Centro and Kobe earthquake data. The following results are obtained and the corresponding time history plots were shown below.

6.1 Sloshing Displacement

Figures 7, 8, 9, and 10 show the variation of sloshing displacement in both horizontal and vertical directions for El Centro and Kobe earthquake excitation. The sloshing

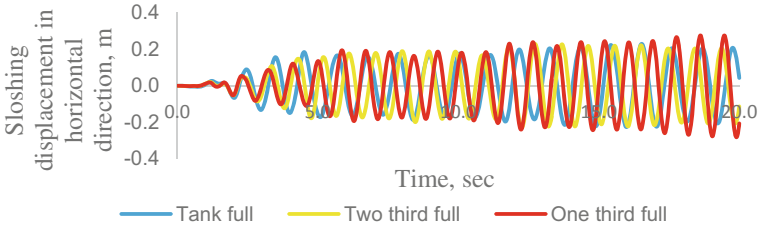

Fig. 7 Variation of sloshing displacement in the horizontal direction for El Centro earthquake

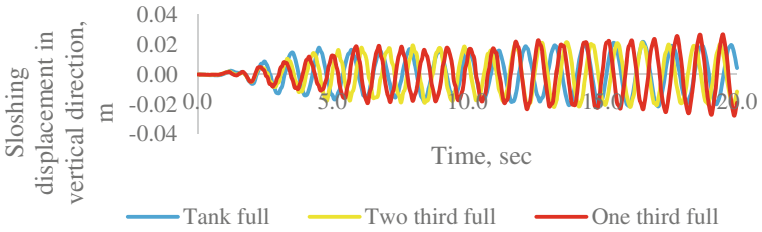

Fig. 8 Variation of sloshing displacement in the vertical direction for El Centro earthquake

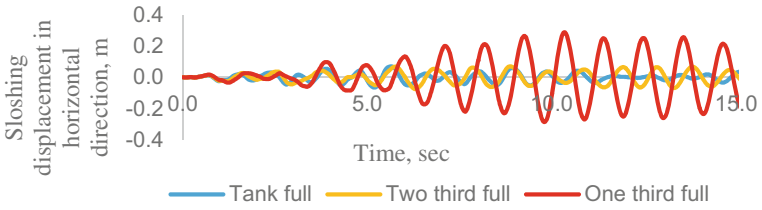

Fig. 9 Variation of sloshing displacement in the horizontal direction for Kobe earthquake

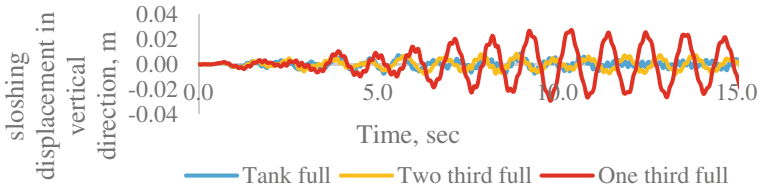

Fig. 10 Variation of sloshing displacement in the vertical direction for Kobe earthquake

displacement in horizontal direction is more than the vertical direction, i.e. the tank gives the maximum response in the applied earthquake force. The sloshing increases with the reduction in the water level in the container as it has more free space to accelerate (Figs. 11, 12, 13, 14, 15, and 16).

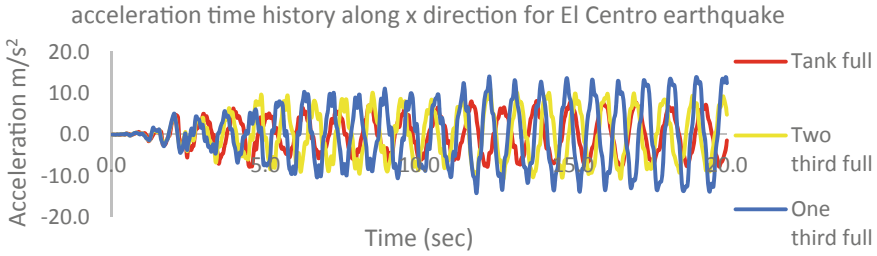

Fig. 11 Variation of acceleration in the X direction for El Centro earthquake

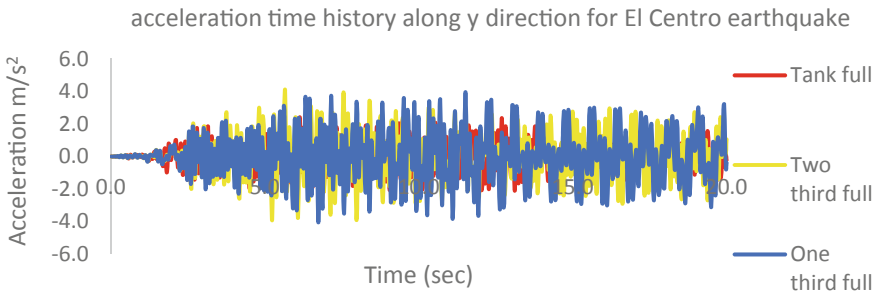

Fig. 12 Variation of acceleration in the Y direction for El Centro earthquake

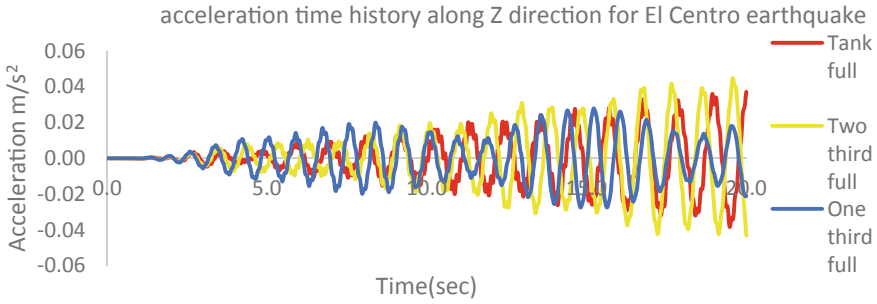

Fig. 13 Variation of acceleration in the Z direction for El Centro earthquake

6.2 Total Hydrodynamic Pressure

Figures 17 and 18 show the variation of total hydrodynamic pressure under El Centro, Kobe earthquakes for tank full, two-third full, and one-third full conditions. The maximum hydrodynamic pressure was reported in tank full condition. The variation of total hydrodynamic pressure for two-third full and one-third full was considerably low in the Kobe earthquake.

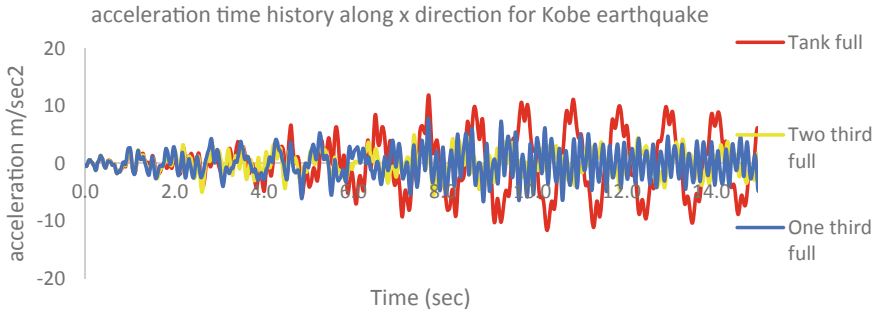

Fig. 14 Variation of acceleration in the X direction for Kobe earthquake

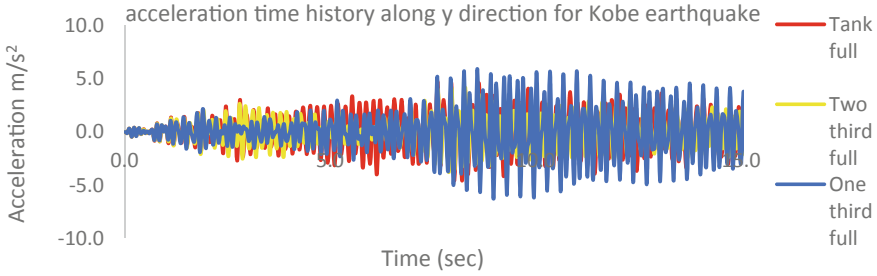

Fig. 15 Variation of acceleration in the Y direction for Kobe earthquake

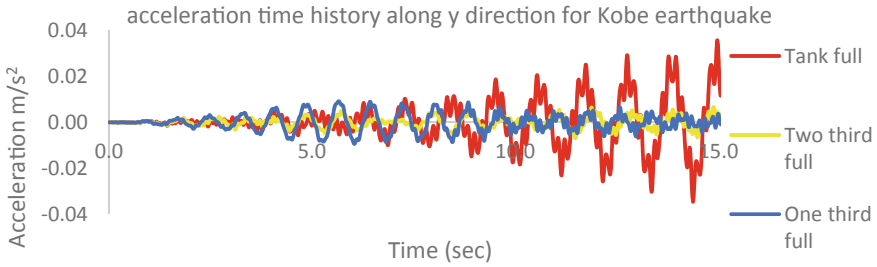

Fig. 16 Variation of acceleration in the Z direction for Kobe earthquake

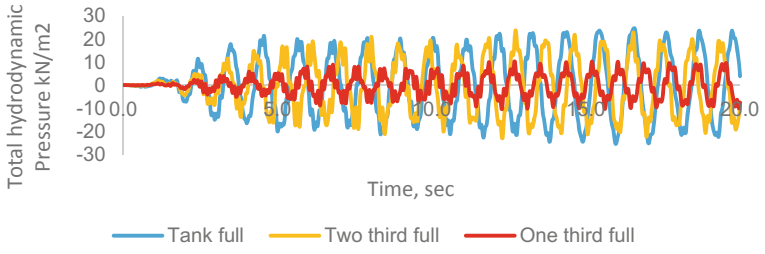

Fig. 17 Variation of total hydrodynamic pressure for El Centro earthquake

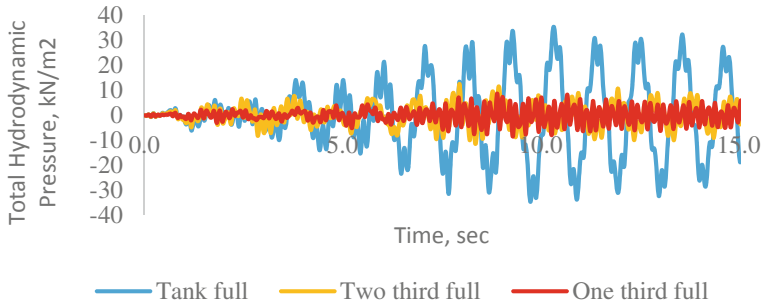

Fig. 18 Variation of total hydrodynamic pressure for Kobe earthquake

7 Conclusion

The dynamic response parameters such as the sloshing displacement, total hydrodynamic pressures, and the acceleration time history plots for El Centro and Kobe earthquakes were drawn and the following conclusions are made

1. The maximum impulsive and convective hydrodynamic pressure on the tank walls are 2.66, 7.28 kN/m^2, respectively. It clearly shows the importance of sloshing displacement in the design of the tank.
2. The sloshing displacements in applied earthquake direction (horizontal) is more in one-third full condition which is equal to 0.258 m for the El Centro earthquake and 0.268 m for the Kobe earthquake.
3. The maximum sloshing displacement in the vertical direction is more in one-third full condition which is equal to 0.0259 m for the El Centro earthquake and 0.0258 m for the Kobe earthquake.
4. The total hydrodynamic pressure is more in tank full condition as it contains huge liquid mass which will exert both impulsive and convective hydrodynamic pressures.
5. The maximum hydrodynamic pressures are equal to 24,650 N/m^2 for the El Centro earthquake and 35,450 N/m^2 for the Kobe earthquake.

References

1. Dogangun A, Livaoglu R (2013) Hydrodynamic pressures acting on the walls of rectangular fluid containers. Struct Eng Mech 17(2):203–214
2. Dogangun A, Livaoglu R (2008) A comparative study of the seismic analysis of rectangular tanks according to different codes. In: The 14th world conference on earthquake engineering, Beijing, China
3. Sivy M, Musil M (2016) Analysis of hydrodynamic pressures induced in liquid storage tanks during a seismic event. J Appl Math Eng 8. ISSN: 1337-6365

4. Kotrasova K (2017) Study of hydrodynamic pressure on wall of tank. Struct Phys Aspects Construct Eng Procedia Eng 190:2–6
5. Ibrahim RA (2005) Liquid sloshing dynamics, theory and applications. Cambridge University Press
6. Livaoglu R, Dogangun, Simplified seismic analysis procedures for elevated tanks considering fluid–structure–soil interaction. Elsevier J Fluids Struct 22:421–439 (2006)
7. Kohnke P, ANSYS theory reference release 5.6. ISO 9001:1994

Seismic Response of Hill Buildings with Base Isolation and URM Infills

Ahmed Bilal, Zaid Mohammad, and Abdul Baqi

Abstract RC frame structures resting on a hill slope exhibit diverse seismic responses in comparison with conventional buildings built on plain ground. Due to asymmetric structural configuration at different floor levels, the hill buildings attract additional lateral shear force and torsional moments in the structural members. Further, unreinforced masonry infills play a critical role in the energy dissipation during seismic excitements and are often neglected in the seismic analysis of buildings. Moreover, base isolation systems have also been shown to reduce the seismic vibrations in the buildings. Thus, in the present study, the effect of unreinforced masonry infill panels as well as a commonly used base isolation system, i.e. Laminated Lead Rubber Bearing (LLRB) on the seismic performance of two hill building configurations, viz. stepback and setback-stepback, was studied. All the configurations have been modelled using finite element software, and analysed by Response Spectrum and Non-linear Static Pushover method. The seismic parameters obtained from the numerical study were discussed in terms of base shear, fundamental time period, maximum top storey displacement and plastic hinge formation pattern in the building structure. Finally, the vulnerability and suitability of the different configurations against earthquake were compared in along and across slope directions.

Keywords Hill buildings · Base isolation · Laminated lead rubber bearing · Masonry infills

1 Introduction

Infrastructural development has considerably increased the population growth in hilly regions. The scarcity of plain ground in hills has lead to the construction of RC buildings on steeply sloping grounds. However, the buildings constructed on steep

A. Bilal
Civil Engineering Section, University Polytechnic, Aligarh Muslim University, Aligarh, India

Z. Mohammad (✉) · A. Baqi
Department of Civil Engineering, ZHCET, Aligarh Muslim University, Aligarh, India

T. G. Sitharam et al. (eds.), *Earthquakes and Structures*, Lecture Notes in Civil Engineering 188, https://doi.org/10.1007/978-981-16-5673-6_22

terrain show different dynamic behaviour as compared to that resting on the level ground when subjected to earthquakes [1]. RC-framed structures in hilly areas are commonly built in stepback and setback-stepback configuration. Buildings resting on hill slopes have unsymmetrical structural configuration due to which the centre of mass and centre of stiffness vary along various floors and impart twisting moment in structural members, in addition to the lateral shear forces, when subjected to earthquake loads. Further, due to the short column effect in hill buildings, the columns on the uphill side exhibit higher stiffness and attract larger forces as compared to that of the columns on the downhill side and hence, are found to be more vulnerable to damage under earthquake loads [2].

Previous investigations have shown that a base isolation system is the most effective control measure for reducing the earthquake vibrations induced in the structural systems [3–5]. In conventional earthquake-resistant designs of RC structures, the capacity of the structure is increased to provide the seismic demand through adequate reinforcement and ductility. Whereas, in a base isolation system, the dynamic properties of the building are modified in such a way that the shear demand for which the building has to be designed is reduced. In this technique, some flexible system is introduced between the foundation system and the column base of the structure, which increases the damping as well as the horizontal flexibility of the building. The fundamental time period of the RC structures is generally found in the range of the predominant period of the earthquake ground motions which causes a high dynamic amplification effect [6, 7]. Thus, the time period of the building can be increased beyond 2.0 s using base isolation, which significantly brings down the seismic demand [3]. The most common type of base isolator is the laminated lead rubber bearing isolator, as it is found to be very effective in reducing the high accelerations or the high-frequency motions. These are characterized by low horizontal stiffness to isolate the horizontal vibrations and high vertical stiffness [8, 9].

The state-of-the-art studies carried out so far, emphasized the structural behaviour of hill buildings and frame-infill interaction in normal buildings constructed on plain ground [1, 2]. Previous studies [10–16] show that infill panels significantly affect the seismic behaviour of hill buildings. The presence of masonry infills usually as partition walls and exterior coverings increases the lateral stiffness and strength considerably under seismic loading. On the contrary, it produces torsional effects due to irregular distribution at the same storey, soft storey effect due to differential stiffness, and short column effect due to partial infills. But none of the previous studies had explored the behaviour of hill buildings with base isolation systems under earthquake loads. Moreover, IS 1893 (Part 1) has recommended to carry out three-dimensional dynamic analysis for the buildings with geometrical, mass and stiffness irregularity to ascertain the true response of buildings subjected to lateral loads [17]. Also, the inelastic behaviour of hill buildings should be analyzed in order to get the true response of the structure. Thus, the present study explores the influence of a commonly used base isolation system, i.e. Laminated Lead Rubber Bearing (LLRB) on the seismic performance of two hill building configurations, viz. stepback and setback-stepback, with and without masonry infill panels. All the configurations were modelled using finite element software, and examined by employing Response

Spectrum analysis and Non-linear Static Pushover analysis. The seismic parameters obtained from the numerical study were discussed as variations in storey shear, base shear, fundamental time period and plastic hinge development pattern in the building structure. Finally, the vulnerability and suitability of the different configurations against seismic excitations were compared.

2 Materials and Methods

The present study investigates the structural behaviour of two different types of buildings resting on a hill slope, viz. stepback and setback-stepback, under seismic loads. The influence of unreinforced masonry infill panels with the introduction of laminated lead rubber bearing (LLRB) base isolation system, on the seismic performance of the considered building configurations was studied. The Response Spectrum and Non-linear Static Pushover methods were employed to ascertain the seismic response of building configurations. The obtained seismic parameters from the analyses were compared as variation in the values of the fundamental time period, total base shear, lateral shear force at foundation level, and plastic hinge formation in the structural members in along as well as across hill slope direction. The elastic modulus and Poisson's ratio of concrete material were taken as 25,000 N/mm^2 and 0.2, respectively. The concrete mix and reinforcement steel were assumed as M25 and Fe500, respectively. For seismic analysis, rigid frame diaphragm was considered in floor systems and support conditions are assumed to be fixed at foundation level. Due to accidental eccentricity, the torsional effects were considered in the analysis in accordance with IS 1893 (Part 1): 2016 [17]. For non-linear analysis, plastic hinges were allocated at the ends of all the frame elements in all the models. The load application was considered to be displacement control in pushover analysis. When the load was incrementally increased, structural members start to yield and lead to failure. The members experience changes in stiffness sequentially and demonstrate various stages as shown in Fig. 1, viz. immediate occupancy, life safety, and collapse prevention levels [18].

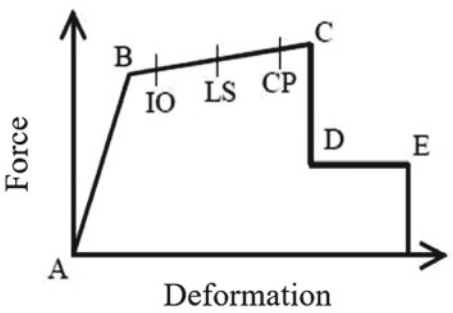

Fig. 1 Force versus deformation curve for plastic hinge at different stages

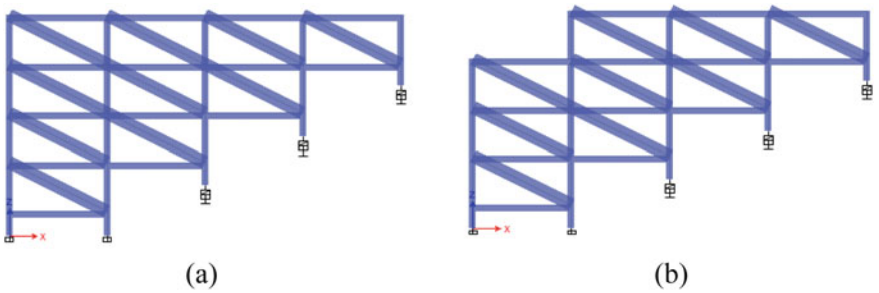

Fig. 2 Different building configurations with URM infills and base isolators **a** stepback and **b** setback-stepback

Table 1 Parameters considered in different building configurations [11]

Geometric parameters	Seismic parameters
Thickness of slab = 0.150 m	Zone = V
Height of each storey = 3.5 m	I = 1.5
Depth of foundation = 1.75 m	R = 5
Column size = 0.23 m × 0.50 m	Soil condition = II (i.e. medium)
Beam size = 0.23 m × 0.50 m	Live load = 3 kN/m^2

2.1 Building Configuration

Overall four finite element models of stepback and setback-stepback building configurations were modelled with 4 bays in along as well as across the slope directions. The un-reinforced masonry infills were introduced as an equivalent diagonal strut in place of the masonry wall. Further, the building configurations were also analysed with and without base isolator systems at the foundation level. The length of each bay in along and across the slope in all the models was taken as 7 and 5 m, respectively. The slope of the ground was assumed to be 27° with the horizontal (Fig. 2). The masonry infills have been considered at the periphery of the building frames and modelled as equivalent diagonal strut [2, 16]. The various parameters considered in the analysis of different building configurations are mentioned in Table 1.

2.2 Modelling of Un-reinforced Masonry Infills

In RC-framed buildings, the influence of infill panels on the lateral stiffness of the buildings under seismic loads can be represented by modelling the infills as a diagonal strut as shown in Fig. 2. In the present study, these diagonal struts are modelled as diagonal truss elements allowing only three degrees of freedom (translational) per

Table 2 Width of masonry strut

Direction	H (m)	L_{ds} (m)	E_f (GPa)	E_m (GPa)	Column size (mm)	T (m)	α_h	w_{ds} (m)
Across Slope	3.0	6.1	25	13.8	230 × 500	0.23	3.91	0.62
Along Slope	3.0	7.8	25	13.8	230 × 500	0.23	2.55	0.95

node at each end of the element so that only axial forces are able to transfer in the strut. The thickness and material properties of diagonal struts are kept similar to masonry infill panels. The width of struts is calculated as per IS 1893 (Part1): 2016. The values of different parameters taken for calculating width of the struts in along and across the slope directions are mentioned in Table 2, and the material properties for masonry were considered from Agarwal and Shrikhande [19] and approximated as per IS 1905. The value of Young's modulus of masonry is assumed as 13,800 N/mm^2 and Poisson's ratio is taken to be 0.16.

$$w_{ds} = 0.175 \propto_h^{-0.4} L_{ds} \tag{1}$$

where

$$\propto_h = h\left(\sqrt[4]{\frac{E_m t \sin 2\theta}{4E_f I_c h}}\right) \tag{2}$$

where w_{ds} = width of strut; L_{ds} = length of strut; E_m = Young's modulus of masonry panel; E_f = Young's modulus of RC beams and columns; t = thickness of masonry panel; θ = angle of strut with horizontal; I_c = moment of inertia of adjoining column; h = clear height of panel.

2.3 Design of Base Isolation System

For the design of an effective base isolation system, the main requirements are; (a) capability to carry vertical loads, (b) sufficiently low stiffness in the horizontal direction which can increase the time period of the building to the required value, (c) large vertical stiffness so that the amplification in the vertical direction can be minimized, (d) sufficient damping to prevent excessive isolation level displacements and (e) initial stiffness to prevent movement due to small vibrations [20]. While designing a base-isolated building, the following steps are followed [3, 23]:

(i) Base isolators were designed based on the vertical load coming on them for the specified zone and soil type.
(ii) Base isolated building was designed to achieve the desired criteria.
(iii) Finally, the design was checked using non-linear time history analysis.

The base isolators were designed using the relationships given by Datta [3]

$$K_{eff} = \frac{W}{g}\frac{4\pi^2}{T_b^2} \tag{3}$$

where K_{eff} is the effective stiffness of the base isolator, W is the maximum vertical load under any column for the load case '$1.2DL + 1.6LL_o$' (where LL_o reduced live load) [20], T_b is the isolated time period, '$T_b = nT$', (where n may be taken as 3 to 4), T represents the time period for the building having a fixed base.

$$A_r = W/p \tag{4}$$

$$T_r = GA_r/K_d \tag{5}$$

$$A_{pb} = F/\sigma_{pb} \tag{6}$$

where T_r is the thickness of one rubber layer, G is the modulus of rigidity of rubber, G varies from 0.69 to 0.86 MPa for the range of strain specified for rubber bearing, i.e. γ = 100–150% [6], A_r represents the area of rubber layer, F is the characteristic strength calculated while determining the bilinear curve properties of the base isolator, σ_{pb} is the yield shear strength of the lead. σ_{pb} has a value of 8–10 MPa [4].

In order to account for sufficient over strength, peak design earthquake forces are used directly to design isolation system and substructure, that is, the R factor is taken as unity for designing the isolation system and the substructure. For the design of superstructure, the response reduction factor, R_I is kept lesser than that of fixed base building. As per FEMA P751 (2009) [21], R_I is taken as three-eighth of the R factor considered for the fixed base structure. For superstructure, R_I is considered as 2. For substructure, R_I is considered as 1. In IBC 2006, 1605.2.1 [22], three load cases, are available for design of isolators.

In this paper, hill buildings with two configurations, viz. stepback and setback-stepback have been analysed. Base isolators were designed for both the buildings and the responses were compared within the configurations. In order to keep the design economical, base isolators were not provided beneath all the columns. Base isolators were provided at supports that were at higher levels from the base supports as shown in Fig. 2 and were subjected to higher shear forces under earthquake.

Initially, the buildings were analysed using the response spectrum method where input spectrum was taken from IS 1893:2016 [17]. The vertical load at each column was evaluated and the base isolator was designed individually. For example, while designing the base isolator under an interior column for stepback-setback configuration, the values of effective stiffness, design displacement and energy dissipation per cycle have been calculated as K_{eff} = 1800 kN/m, Δ_d = 0.213 m, and W_d = 49.53 kNm, respectively, from Eq. 3, for zone V and damping coefficient $\xi_{eff} = 0.15$. Final

Table 3 Bilinear properties of the isolators used

Isolator id	R (kN)	K_{eff} (kN/m)	F_y (kN)	K_u (kN/m)	K_d (kN/m)
LLRB2800	2800	1800	104	13,611	1361
LLRB2000	2000	1286	74	9722	972
LLRB1400	1400	900	52	6805	680
LLRB800	800	514	30	3888	388

Table 4 Geometric properties of the base isolators used

Geometric properties (in mm)	LLRB2800	LLRB2000	LLRB1400	LLRB800
Bearing diameter	720	600	520	400
Diameter of lead core	100	95	80	60
Thickness of each rubber layer	13	13	12	12
Layers of rubber	18	18	20	20
Thickness of the plates	3	3	3	3
Thickness of end plates	25	25	25	25
Bearing height	338	338	350	350

values of parameters of the backbone curve of the base isolator have been obtained after iterations (Table 3). Furthermore, the geometric properties have been calculated from Eqs. 4–6 as shown in Table 4. Four sets of base isolators were designed for each building [23]. Lumped plasticity approach was adopted for modelling non-linearity in the beams and columns. Hinges were defined as per FEMA 356 [18]. M3 hinges were provided for beams and P-M2-M3 hinges were provided for columns.

3 Results and Discussion

The hill building configurations with fixed and isolated foundation systems were analysed for the seismic loads in along as well as across slope directions including the effect of masonry infill struts [2, 16, 17]. All models were analysed using Response spectrum and Pushover method of analysis. The results obtained from the analysis were evaluated in terms of the fundamental time period, total base shear, lateral shear force values at foundation level and plastic hinge patterns in structural members, and compared within the considered configurations.

The seismic parameters ascertained from the finite element study have been tabulated in Table 5. It was observed that the earthquake performance of both hill building configurations significantly increased with the introduction of base isolators. The fundamental time period (FTP) of the buildings was found to be reduced. In the case of stepback buildings, FTP in along slope direction was found to be increased by 139.1% with the introduction of a base isolator system in place of fixed isolated

Table 5 Seismic response of different building configurations

Building type	Support type	FTP by RSA (sec)		Base shear (kN)	
		Along	Across	Along	Across
Stepback	Fixed	0.516	0.310	3822	3822
	With base isolator	1.234	1.464	3043	1685
Setback-stepback	Fixed	0.486	0.297	3530	3530
	With base isolator	1.222	1.536	2951	1572

supports. The variation in FTP was found to be 372.2% in across slope direction. Similarly, base-isolated setback-stepback buildings exhibited 151.4 and 417.2% increase in the time period in along and across slope direction, respectively, as compared with that of fixed supported building.

A significant amount of reduction in the total base shear values was observed in building configurations with isolated foundation systems in both along and across slope directions, which indicates the less shear demand attracted by the structural members of base-isolated buildings as compared with those of fixed support systems. After the introduction of the base isolation system in the stepback building, the base shear values were found to be reduced to 79.6 and 44.1% in along and across slope directions, respectively. Also, the base shear values in base-isolated setback-stepback configuration were found to be decreased to 83.6 and 44.5% in along and across slope directions, respectively (Table 5). Moreover, it can be ascertained that the setback-stepback buildings attract less base shear than the stepback configuration of the hill buildings, thus proved to be less prone to earthquake forces. Further, it was observed that due to the inclusion of masonry infill as a structural member in the analysis, the dynamic response of the building has been changed as compared to a bare frame building as studied in previous works by the same author [2].

The lateral shear force distribution in an exterior frame of the hill building configurations in along hill slope direction has been described in Figs. 3 and 4. It was

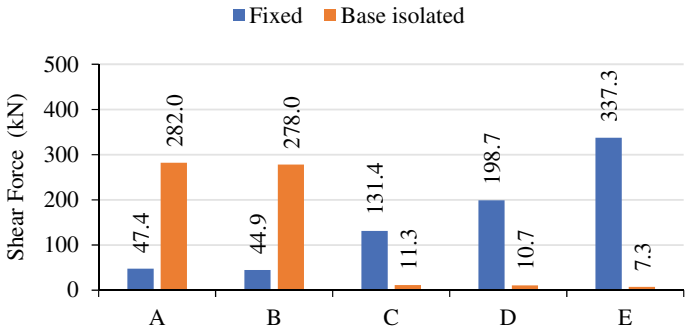

Fig. 3 Shear force distribution in columns at foundation level in stepback building in along slope direction

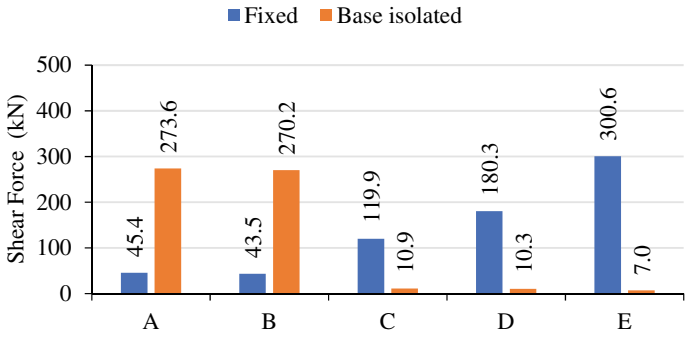

Fig. 4 Shear force distribution in columns at foundation level in setback-stepback in along slope direction

observed that the buildings with fixed support system attract lateral shear force in columns at upper storey level due to high lateral stiffness and short overall length of the column members. However, after the introduction of base isolators at columns C, D and E, a significant reduction in the base shear values could be observed. Thus, it can be concluded that the introduction of base isolation systems in hill building configurations reduces the lateral shear demand in the structural members with higher lateral stiffness. However, the columns at frames A and B were remained fixed to reduce the lateral drift in the building structure, pertaining to which, the lateral shear force at the foundations at downhill side was increased, thus increasing the shear demand in the adjoining structural members.

Further, the stepback and setback-stepback configurations were also analysed using nonlinear static pushover analysis. The plastic hinge pattern in structural members of different hill building configurations with and without base isolators was ascertained and compared in along as well as across hill slope directions at intermediate, upper and lower storey levels (see Figs. 5 and 6). The color coding of the hinge represents the deformation and performance behavior at various load levels. In case of stepback configurations with fixed support systems, the plastic hinge was first formed in columns at foundation levels due to high storey shear, also, complete yielding of columns and the adjoining joint at upper hill frame was observed. However, after the introduction of base isolators, the formation of hinges at immediate occupancy level, could be observed in beams and columns in lower storey at the downhill side. Thus, a significant decrease in the shear demand in columns with high lateral stiffness was observed. Further, the performance of the building in across hill slope was observed to be significantly increased with the use of base isolators. It could be observed that the columns at uphill and downhill side have yielded prior to beams, while base-isolated model displayed hinge formations in fixed foundations at downhill storey only. Moreover, due to less seismic weight, the setback-stepback configuration performed better and exhibited minimal yielding in fixed support condition, whereas, a few members in base isolated configuration displayed yielding only at downhill side storeys of the hill building.

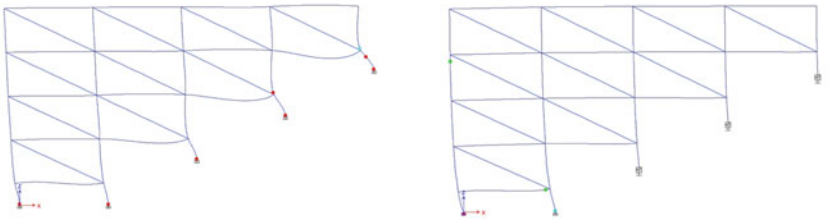

Fixed supports Base isolated supports

(a) Along slope direction

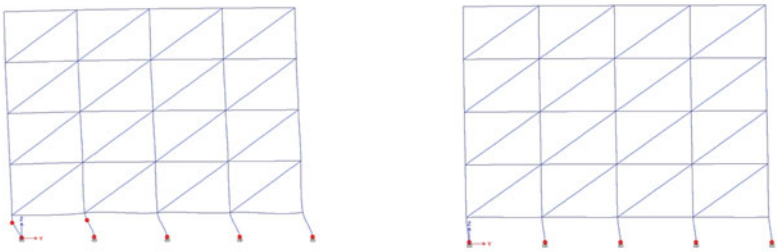

Fixed supports Base isolated supports

(b) Across slope direction (Downhill side)

Fixed supports Base isolated supports

(c) Across slope direction (Uphill side)

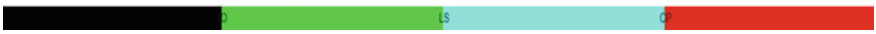

Fig. 5 Plastic hinge formation pattern in stepback building

4 Conclusion

The present study investigates the earthquake performance of two hill building configurations. The influence of unreinforced masonry infill panels and base isolators on the seismic behaviour of stepback and setback-stepback was evaluated and compared using the equivalent static and response spectrum method. It was observed that the fundamental time period of both stepback and setback-stepback buildings was increased significantly with the introduction of base isolators in the foundations. A

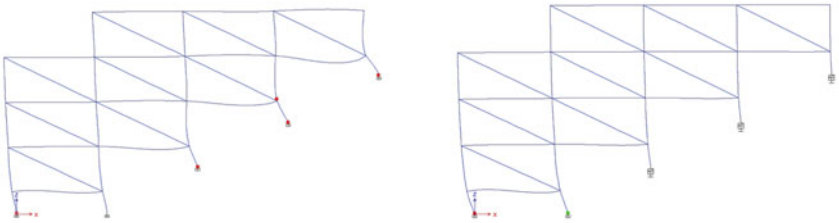

Fixed supports Base isolated supports

(a) Along slope direction (Intermediate frame)

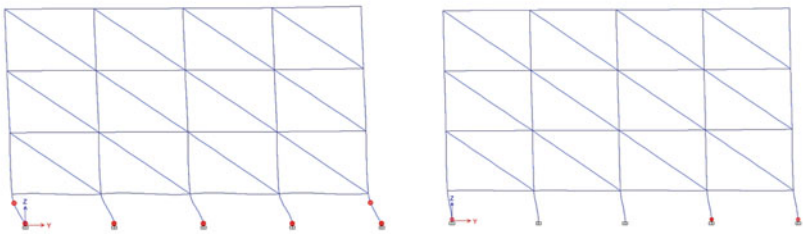

Fixed supports Base isolated supports

(b) Across slope direction (Downhill side)

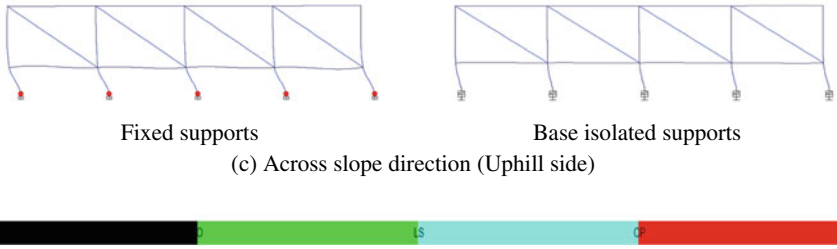

Fixed supports Base isolated supports

(c) Across slope direction (Uphill side)

Fig. 6 Plastic hinge formation pattern in setback-stepback building

prominent reduction in the base shear value in along as well across hill slope direction was observed in both configurations. Further, due to the introduction of masonry infills as equivalent strut members in the buildings, the overall shear demand was found to be increased. Moreover, the Pushover analysis of both hill building configurations revealed that the plastic hinges were formed in the fixed columns at the foundation levels. However, after the introduction of base isolators, the formation of hinges was observed only in the columns at the downhill side storey.

References

1. Mohammad Z, Baqi A, Arif M (2017) Seismic response of RC framed buildings resting on hill slopes. In: 11th international symposium on plasticity and impact mechanics (IMPLAST 2016). Procedia Engineering, vol 173. Elsevier, New Delhi, pp 1792–1799. https://doi.org/10.1016/j.proeng.2016.12.221
2. Mohammad Z, Razi MA, Baqi A, Influence of masonry infill panels on the seismic performance of irregular buildings. Advances in Geotechnics and Structural Engineering. Lecture Notes in Civil Engineering, vol 143. Springer, Singapore, pp 1–11. https://doi.org/10.1007/978-981-33-6969-6_1
3. Datta TK (2010) Seismic control of structures. In: Seismic analysis of structures. Wiley (Asia) Pvt Ltd., pp 369–429
4. Skinner RI, Robinson WH, McKerry GH (1993) An introduction to seismic isolation. Wiley, Chichester
5. Alessandro B, Ileana C (2004) Optimal design of base-isolators in multi-storey buildings. Comput Struct 82:2199–2209
6. Kelly JM (1997) Earthquake-resistant design with rubber. Springer, London
7. Providakis CP (2008) Pushover analysis of base-isolated steel–concrete composite structures under near-fault excitations. Soil Dyn Earthq Eng 28:293–304
8. Wu YM, Samali B (2002) Shake table testing of a base isolated model. Eng Struct 24:1203–1215
9. Kelly JM, Leitman G, Soldatos AG (1987) Robust control of base isolated structures under earthquake excitation. J Optim Theory Appl 53:159–180
10. Kumar S, Paul DK (1998) A simplified method for elastic seismic analysis. J Earthquake Eng 2(2):241–266. https://doi.org/10.1080/13632469809350321
11. Birajdar BG, Nalawade SS (2004) Seismic analysis of buildings resting on sloping ground. In: 13th world conference on earthquake engineering (13WCEE). Paper no. 1472, Vancouver, BC, Canada. https://www.iitk.ac.in/nicee/wcee/article/13_1472.pdf
12. Kadid A, Boumrkik A (2008) Pushover analysis of reinforced concrete frame structures. Asian J Civil Eng (Building & Housing), 75–83. https://doi.org/10.1007/s11803-013-0179-8
13. Kaushik HB, Rai DC, Jain SK (2008) A rational approach to analytical modelling of masonry infills in reinforced concrete frame buildings. In: 14th world conference on earthquake engineering (14WCEE). Corpus ID: 165155308, Beijing, China. https://www.iitk.ac.in/nicee/wcee/article/14_05-01-0317.PDF
14. Davis R, Krishnan P, Menon D, Prasad AM (2004) Effect of infill stiffness on seismic performance of multi-storey RC framed buildings in India. In: 13th world conference on earthquake engineering (13WCEE). Paper no. 1198, Vancouver, BC, Canada. https://www.iitk.ac.in/nicee/wcee/article/13_1198.pdf
15. Murty CVR, Jain SK (2000) Beneficial influence of masonry infill walls on seismic performance of RC frame buildings. In: 12th world conference on earthquake engineering (12WCEE). Paper no. 1790, Auckland, New Zealand. https://www.iitk.ac.in/nicee/wcee/article/1790.pdf
16. Mohammad Z (2019) Effect of unreinforced masonry infills on seismic performance of hill buildings. VW Appl Sci 1(1):37–47. https://doi.org/10.36297/vw.applsci.v1i1.29
17. IS 1893 (Part 1): 2016. Criteria for earthquake resistant design of structures. BIS, New Delhi (2016)
18. FEMA 356, Federal Emergency Management Agency (FEMA). Prestandard and commentary for the seismic rehabilitation of buildings, Washington, DC (2000)
19. Agarwal P, Shrikhande M (2006) Earthquake resistant design of structures (Ninth reprint, August, 2011) ed., Prentice Hall India (PHI)
20. Bilal A, Agarwal P, Sadique MR, Performance evaluation of base isolated building. Advances in Geotechnics and Structural Engineering. Lecture Notes in Civil Engineering, vol 143. Springer, Singapore, pp 247–256. https://doi.org/10.1007/978-981-33-6969-6_23
21. FEMA P-751 (2012) NEHRP recommended seismic provisions: design examples. Federal Emergency Management Agency, Washington, DC

22. International Code Council (ICC) (2000) International Building Code (IBC), Falls Church, VA
23. Mohammad Z, Bilal A, Baqi A, Effect of base isolation on the seismic performance of hill buildings. Earthquakes and Structures: Select Proceedings of 7th ICRAGEE 2021. Lecture Notes in Civil Engineering, vol 188. Springer, Singapore. https://doi.org/10.1007/978-981-16-5673-6_18

Ground Vibrations Due to Moving Load in the Proposed Subway Tunnel Near Kamalapur

Tahmeed M. Al-Hussaini, Mahbubah Ahmed, and Sagar Barua

Abstract Mass Rapid Transit (MRT) Line 1 is planned for the eastern part of Dhaka city connecting the capital's International Airport Terminal at Kurmitola with the Main Train Station Terminal at Kamalapur. This line also has a second branch from Future Park to Purbachal. While a significant portion of the proposed MRT Line 1 will be above ground, three significant portions will be underground: (i) Khilkhet to Bhatara (ii) Bhatara to Bashundhara (iii) Mailbag to Kamalapur. Subway tunnel construction for metro rail involves many unique geotechnical design considerations such as the effects of fast-moving trains in an underground tunnel on adjacent property. The resulting vibrations can be the subject of legal complaints by owners of buildings in the immediate vicinity. The primary objective of this paper is to perform a numerical study to have an impression of the ground vibrations generated in the surrounding soils due to moving loads in an underground tunnel near the Kamalapur Railway Station. A numerical model is created using the finite element software PLAXIS 3D for moving load on rails in an embedded tunnel in an idealized soil profile. Numerical analysis is performed for a two-wagon train running on an underground tunnel at various depths.

Keywords Subway tunnel · Ground vibrations · Dynamic moving loads · FEM

1 Introduction

Underground railway technology being introduced in mid of the nineteenth century has become an integral part of the transportation system worldwide with the rapid development of urban modernization. But, along with bringing comfort and ease in public transport, on another side, the metro subway tunnel has become a significant concern regarding environmental issues. A wide range of studies has concluded that significant vibrations are induced by the passage of underground trains sometimes exceeding the tolerance level of residents living in adjacent buildings [1]. This kind of vibration has been listed as one of the seven significant environmental hazards in the

T. M. Al-Hussaini (✉) · M. Ahmed · S. Barua
Bangladesh University of Engineering and Technology, Dhaka 1000, Bangladesh

T. G. Sitharam et al. (eds.), *Earthquakes and Structures*, Lecture Notes in Civil Engineering 188, https://doi.org/10.1007/978-981-16-5673-6_23

world [2]. With the advancement of computer-based software, numerical analysis is commonly used to predict ground-borne vibrations due to fast-moving trains. Different numerical techniques have been adopted by various researchers for studying this three-dimensional problem of wave propagation, finite element method (FEM) is one of them. Singh and Seth [3] have shown that this kind of modeling can be effectively simulated in 3D FEM.

The Government of Bangladesh is implementing the Mass Rapid Transit (MRT) project as part of its transportation solutions for the capital city of Dhaka, which is overburdened by high population density and severe traffic congestions. The project consists of several MRT railway lines [4] consisting of both elevated and underground portions. This paper is concerned with the underground portion of MRT line 1 near Kamalapur Railway Station. A numerical study is conducted to study the wave propagation problem caused by underground railways using the finite element method software PLAXIS 3D. To the best of the authors' knowledge, this study is a first attempt to have an impression on the ground vibrations generated by proposed subway traffic in Dhaka city.

2 Site Parameters

2.1 Site Location

The 26.5 km long MRT line-1 has been planned to be constructed with three underground portions, represented by orange lines in Fig. 1. This line will connect Kamalapur Railway Station with the International Airport at Kurmitola and will also have another branch Bhatara to Purbachal. The three underground branches are: (i) Khilkhet to Bhatara, (ii) Bhatara to Bashundhara, and (iii) Mailbag to Kamalapur. This study is dealing with an area near Kamalapur Railway Station.

2.2 Soil Stratigraphy

Borehole data are obtained from the preliminary study report [5]. As part of the geotechnical investigations, a total of 41 borings have been drilled along the route of MRT Line-1. Borehole BH-01, drilled to a depth of 45 m, is near the Kamalapur railway station, as such soil data from BH-01 is considered in this study. The subsoil information shows that there is 7.5 m of grayish brown medium stiff to very stiff clay on top of 3 m sandy silt layer. Below the sandy silt layer, 13.5 m of silty sand overlies firm support ($N > 50$) consisting of very dense sand or hard clay. Shear wave velocities are estimated from SPT values of BH-01 using empirical relations given by the Japan Road Association [6]. For this study, the soil profile has been divided into 11 layers, the corresponding soil properties are shown in Table 1.

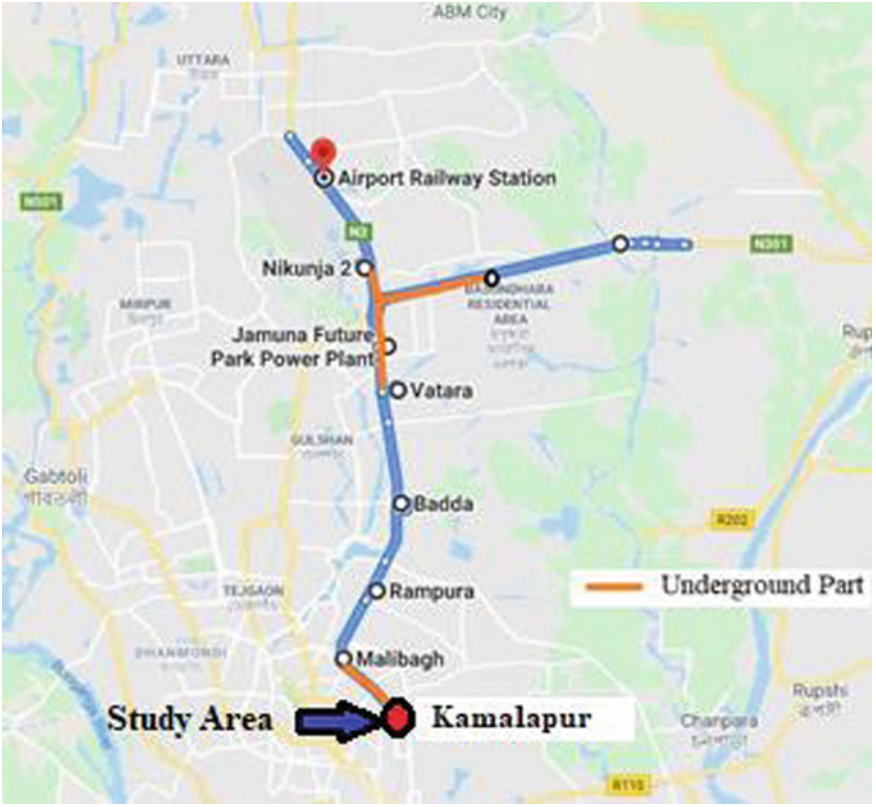

Fig. 1 Layout plan of MRT Line 1

Table 1 Soil parameters for different layers

Layer no	Depth (m)	Unit Weight (kN/m^3)	Poisson's ratio	Shear wave velocity (m/sec)
1	0–1.5	18.9	0.4	200
2	1.5–7.5	19.6	0.4	241
3	7.5–10.5	19.0	0.33	221
4	10.5–18	17.3	0.3	249
5	18–24	19.6	0.3	274
6	24–30	22.0	0.3	304
7	30–34	20.8	0.3	285
8	34–35	22.0	0.3	299
9	35–36	18.9	0.3	267
10	36–40.5	22.0	0.4	276
11	40.5–44	22.0	0.3	313

3 Numerical Analysis Under Moving Load

3.1 Numerical Model

A 30 m × 60 m × 44 m domain (Fig. 2) is considered in the numerical model for underground tunnel embedded in a layered soil medium with PLAXIS 3D. For the soil model, 1% hysteretic damping is considered. Dynamic load changing in time and location corresponding to two wagon train axle loads moving at speed 72 km/h is assigned on the rail track. The 7 m diameter tunnel is assumed to have a lining thickness of 0.3 m. High-strength concrete (fc' = 7000 psi) is considered for the tunnel lining. The rails used are UIC60A. Concrete sleepers are modeled with a base thickness of 250 mm and a height of 150 mm, with a length of 2.6 m. In this FEM model, the soil is modeled using 10-noded tetrahedral elements, the rails and sleepers are modeled using 3-noded beam elements, the tunnel is modeled with orthotropic 6-noded plate elements. The viscous boundary condition is applied at domain boundaries.

For introducing moving trainload, the X52 commuter train model [7] is considered, which consists of two wagons with a total length of 54 m and a load of 185 kN/axle. Figure 3 illustrates the configuration of axles and bogies of the train. Its speed is considered to be 72 km/hr. In terms of dynamics, a moving load changes its point of application with time compared to a static load, which is very different from a dynamic load that does not change its point of application. The dynamic load of

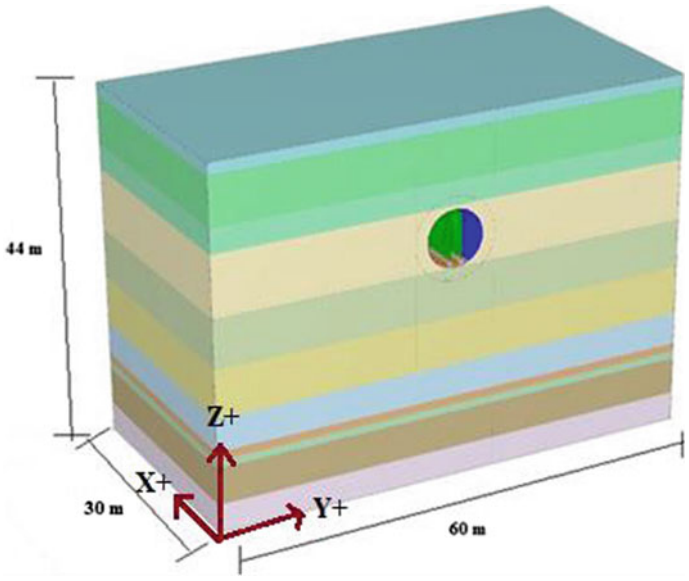

Fig. 2 PLAXIS 3D model of subway tunnel

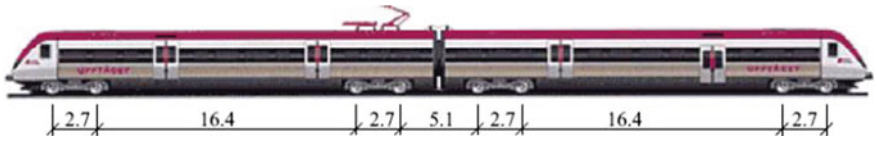

Fig. 3 X52 commuter train

this moving train is modelled using static point load and its corresponding dynamic multiplier. A pair of point loads, representing the wheels, together distribute the axle load. Rail spacing is 0.6 m. To simulate a train passage with 72 km/hr speed, the pairs of point loads are activated and deactivated in turn. Details of the numerical modeling are described by Ahmed [8].

3.2 Validation of PLAXIS 3D Model

To check the accuracy of the numerical model of moving train load developed with PLAXIS 3D, an example of a commuter train running at the ground surface is selected from the published literature. Comparison is done with field measurements [7] of track-bed acceleration over a buried culvert about 40 km north of Stockholm, Sweden. Figure 4 presents a comparison of numerical results computed by PLAXIS 3D with the field measurements. It is observed that there is a fair agreement between the field measurements and the FEM results of the time history of track-bed acceleration.

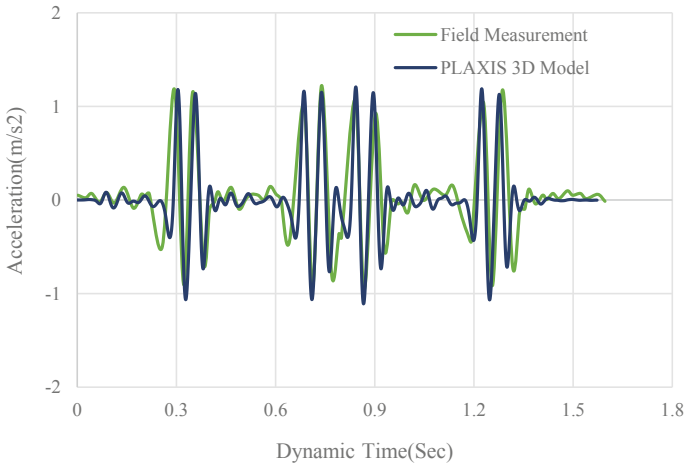

Fig. 4 Validation of PLAXIS 3D analysis for measured track-bed acceleration [7]

4 Numerical Results

Theoretically, ground vibration can be expressed either in terms of displacement, velocity, or acceleration. However, the response of humans, buildings, and equipment to vibrations can be more accurately described in terms of velocity or acceleration. As such, the ground-borne vibrations herein will be represented as acceleration on a logarithmic scale in decibels according to International Standard [9].

Figures 5, 6, and 7 present the free-field vibrations (at the ground surface) in X, Y, and Z directions (Fig. 2), respectively due to moving train (Sect. 3.1) in subway tunnel as a function of distance from the tunnel center line. Results are presented for three different depths of tunnel top (5, 8, and 11 m). The vibration level of the ground surface decreases with an increase in tunnel depth as expected. Wave Interference

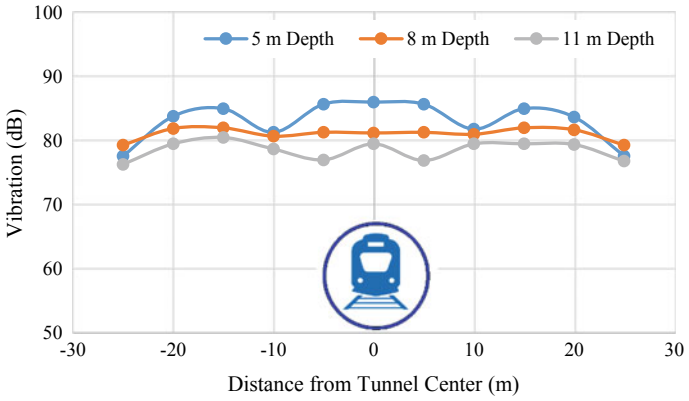

Fig. 5 Free-field horizontal vibration (in the direction of the tunnel) at various distances from tunnel centerline for subway train at three different depths

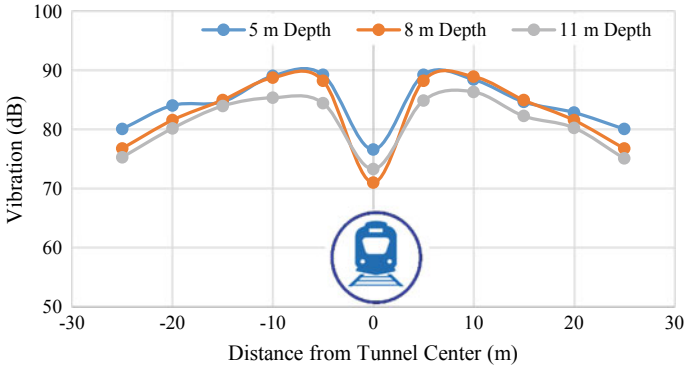

Fig. 6 Free-field horizontal vibration (perpendicular to the tunnel) at various distances from tunnel centerline for subway train at three different depths

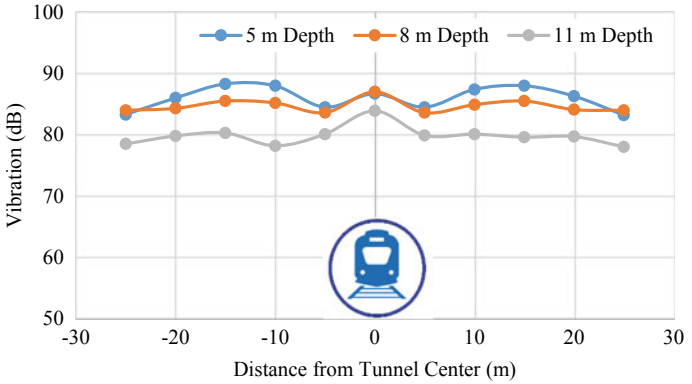

Fig. 7 Free field vertical vibration at various distances from tunnel centerline for subway train at three different depths

effects from waves generated from different points of the tunnel result in variation of vibration at ground level. Ground surface vibrations for different depths of tunnels can reach 70–90 dB. Even at distances of 25 m, vibrations may reach 75–85 dB, which is quite significant.

The maximum horizontal vibration (90 dB) is in a direction (Y dir) perpendicular to the tunnel length as shown in Fig. 6, which is in agreement with field measurements from published literature. This exceeds the safe vibration limit for human beings (85 dB) [10].

Figure 8 presents the vibration within the soil at points located at 2 and 4 m depth from the ground surface and 20 m distance from the tunnel center line. These are possible locations for shallow foundations or basement of nearby buildings. Vibrations at these locations range from 74 to 83 dB which can be significant enough to cause complaints.

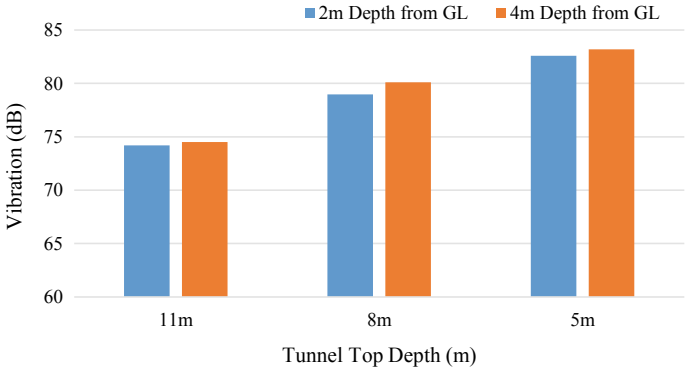

Fig. 8 Ground vibration at 2 and 4 m depths at a distance of 20 m from tunnel centerline due to subway train at three different depths

5 Conclusions

This paper presents preliminary results on ongoing research work for the prediction of ground vibrations caused by proposed underground metro Line 1 near the Kamalapur Railway Station in Dhaka city. Numerical analysis has been conducted using the three-dimensional FEM software PLAXIS 3D, simulating a two-wagon train moving at a speed of 72 kmph in a subway tunnel. Numerical results indicate that ground surface vibrations reduce with increased tunnel depth. Significant free field vibrations in the range of 70–90 dB can be caused by the train, exceeding the safe vibration limit for human beings (85 dB), and also exceeding tolerance limits for human discomfort. Significant vibrations are also induced at depths of 2 and 4 m which may affect adjacent structures at those depths.

Acknowledgements This work was carried out as part of undergraduate thesis work by the second and third authors at the department of civil engineering, BUET. PLAXIS-3D computations were performed at the computational laboratory of BUET-Japan Institute of Disaster Prevention and Urban Safety. PLAXIS-3D was procured under a research development fund (HEQEP CP-3140) from the University Grants Commission of Bangladesh.

References

1. Shyu RJ, Wang WH, Cheng CY, Hwang D (2002) The characteristics of structural and ground vibration caused by the TRTS trains. In: Metro's impact on urban living, proceedings of 2002 world metro symposium. Taipei City Government, Taipei, Taiwan, p 610
2. Xia H, Cao YM (2004) Problem of railway traffic-induced vibrations of environments. J Railway Sci Eng 1:44–51
3. Singh D, Seth Y (2017) 3D Modelling of ground surface vibration induced by underground train movement. Procedia Eng 173:1580–1586
4. Al-Hussaini TM, Ameen SF, Ahmed KS (2018) Geotechnical considerations and prospects for underground construction in Dhaka City. In: Proceedings of international conference on geotechnical engineering and architecture, St. Petersburg
5. ALMEC-Oriental-Nippon-Katahira (2018) The Preparatory Study on the Dhaka Mass Rapid Transit Development Project (Line 1) In Bangladesh. Report prepared by ALMEC CORPORATION, Oriental Consultants Global Co., Ltd., Nippon Koei Co., Ltd. and Katahira & Engineers International for Japan International Cooperation Agency (JICA)
6. Japan Road Association (JRA) (1980) Specification and interpretation of bridge design for highway—Part V: Resilient Design
7. Mellat P, Andersson A, Pettersson L, Karoumi R (2014) Dynamic behaviour of a short span soil–steel composite bridge for high-speed railways—field measurements and FE-analysis. Eng Struct 69:49–61
8. Ahmed M (2020) Ground vibrations due to proposed subway near Kamalapur Railway Station, B.Sc. Engg. Thesis, Department of Civil Engineering, BUET, under preparation
9. Griffin M (1996) Handbook of human vibration. Elsevier Academic, Amsterdam
10. Harmful noise levels. https://www.healthlinkbc.ca/health-topics/tf4173. Accessed 20 Sept 2020

SSI Effects on the Behavior of a Low-Rise RC Framed Building Including Foundation

Shivi Nigam, Meenu Sunil, Neha, and Navjeev Saxena

Abstract The process of soil response influencing the motion of the structure and vice versa is termed as soil-structure interaction. Conventionally, SSI has been considered to pose beneficial effects on the seismic response of a structure because of causing the structure to be more flexible resulting in an increased natural period and enhanced effective damping ratio. These modifications suggest a reduction in base shear demand for a structure as compared to its fixed-base counterpart. This study presents analyses of four-storeyed ordinary RC framed structures assuming the base of the column as fixed and supported on stiff, medium and soft soil springs. The study also includes isolated rectangular concrete footing fixed at the base and supported on the same springs as used in the structure. The results are somewhat different than the assumption of fixed-base analyses being always conservative. The study also suggests appropriate modeling to capture maximum response in structural members.

Keywords Soil-structure interaction · SSI · Dynamic · Earthquake · Seismic · Frame · Concrete · Foundation

1 Introduction

The process of soil response influencing the motion of the structure and vice versa is termed as soil-structure interaction (SSI). It is a phenomenon which comprises various mechanisms leading to the interdependence of soil and structural displacements. These mechanisms broadly fall under either the kinematic or inertial component of SSI. Roesset [1] and Kausel [2] presented reviews of the early-stage developments in the field of soil-structure interaction. In addition to the two components of SSI—kinematic and inertial, Roesset also discussed direct and substructure approaches to perform SSI analyses. Kausel presented chronological development in

S. Nigam (✉)
D.S.M.N.R.U, Lucknow, India

M. Sunil · Neha · N. Saxena
CSIR-CBRI, Roorkee, India
e-mail: navjeevsaxena@cbri.res.in

T. G. Sitharam et al. (eds.), *Earthquakes and Structures*, Lecture Notes in Civil Engineering 188, https://doi.org/10.1007/978-981-16-5673-6_24

SSI, starting from fundamental solutions (commonly termed as Green's functions) devised by mathematicians and scientists way back in the early nineteenth century. Kausel initiated the development of a substructure approach to solve SSI problems.

Conventionally SSI has been considered to pose beneficial effects on the seismic response of a structure. The usual reasoning provided in this regard is that considering SSI makes a structure more flexible, increases its natural period and enhances its effective damping ratio. These modifications suggest a reduction in base shear demand for a structure as compared to its fixed-base counterpart. With such assumptions, SSI has usually been disregarded by designers to reduce the complications involved in analyses. However, observations from many earthquake-damaged sites tell a different story. Noticeable instances include damage in a number of pile-supported bridge structures in the 1989 Loma Prieta earthquake as cited by Yashinsky [3] and the collapse of Hanshin Expressway Route 3 (Fukae section) in the 1995 Kobe earthquake as investigated by Mylonakis and Gazetas [4]. Further, Badry and Satyam [5] obtained SSI analysis for asymmetrical buildings supported on a piled raft which got damaged during the 2015 Nepal earthquake. They observed that detrimental effects of SSI can be greatly intensified by the asymmetry in the geometry of superstructures. These observations suggest that the traditional belief of SSI being ever-beneficial does not stand good for all structures on all soil conditions [6].

Ciampoli and Pinto [7] identified structure-to-soil stiffness ratio and aspect ratio of structures to be regulating the phenomenon. Nguyen et al. [8, 9] established the significance of foundation characteristics, viz., footing size in shallow foundations, pile size and load-bearing mechanism in pile foundations on seismic response of structure-soil systems. The possibility of differential settlement arising out of soil flexibility has been remarked by Raychowdhury [10] for low-rise steel moment-resisting framed buildings. She also concluded that SSI needs to be tackled more critically for heavily loaded footings owing to high inertial effects. This suggests a need to develop a rational basis for seismic design incorporating SSI.

Further, Jarernprasert et al. [11] studied the effects of SSI on the response of yielding single-storey structures embedded in an elastic half-space to a set of accelerograms representative of diverse geology. Unlike elastic structures, SSI may lead to an increase in ductility demands and total displacements in the case of inelastic structures. Aydemir [12] studied soil-structure interaction effects on structural parameters for stiffness degrading systems built on soft soil sites and found smaller strength reduction factors for interacting systems than those for corresponding fixed-base systems. This implies that neglecting SSI may result in an unconservative design.

Dutta and Roy [13] presented a critical review of idealization and modeling for interaction among various components of the soil-foundation-structure system. These modeling strategies are broadly classified as discrete and continuum depending on elements used at the structure-soil interface. In discrete modeling, springs and dashpots are usually used as interface elements. On the other hand, continuum modeling is achieved using either finite element or boundary element methods.

Vaseghiamiri et al. [14] proposed a novel probabilistic approach to account for SSI in the seismic design of building structures. In this approach, an SSI response modification factor is introduced to capture SSI effects on the seismic performance

of structures. The proposed procedure quantifies factors such that the probability distribution of the collapse capacity of the structure designed to account for SSI concurs with that of the structure designed using the default fixed-base provisions. It is employed for special steel moment frame buildings (3–15 storey) with surface foundation. To model the superstructure, a surrogate SDOF system with a multilinear backbone curve is used that represents the nonlinear response of the actual structure oscillating according to its fundamental mode of vibration. A lumped-parameter mass-spring-dashpot model representing a rigid disk foundation on a uniform half-space is used to represent the soil-foundation system. The results indicate that no reduction in the design base shear is advisable for structures located on moderately soft to firm soils with shear wave velocities above 150 m/s. This conclusion is at odds with the current prescription of SSI provisions of seismic design code, which allow some reduction in the design base shear for such buildings.

This study presents analyses of a four-storeyed ordinary framed structure assuming the base of the column as fixed as well as supported on stiff, medium and soft soil springs. The study also includes isolated rectangular concrete footing (with two sizes to transfer uniform load on supports) fixed at the base as well as supported on the same springs as used in the structure alone. The results are somewhat different than the assumption of the fixed-base analyses being always conservative. The study also suggests appropriate modeling to capture maximum response in structural members.

2 Modeling and Analyses

A typical four-storeyed ordinary moment-resistant framed building has been considered for the study. The details of the building are as follows:

- Grade of concrete used is M20 and grade of steel used is Fe415.
- Weight density of concrete is 25 kN/m^3 and that of masonry is 20 kN/m^3.
- Floor-to-floor height is 3.1 m.
- Plinth height above GL is 0.55 m.
- Depth of Foundation is 0.65 m below GL.
- Parapet height is 1.5 m.
- Slab thickness is 150 mm.
- External wall thickness is 230 mm and internal wall thickness is 150 mm.
- Size of columns is 300 mm $\times$ 450 mm and size of beams 300 mm $\times$ 450 mm.
- Live load on floor is 3 kN/m^2 and Live load on roof is 1.5 kN/m^2.
- Floor finish is 1 kN/m^2 and roof treatment is 1.5 kN/m^2.
- The building is located in Seismic Zone IV.
- Importance Factor is taken as 1.
- Building frame type is Moment Resting Frame (MRF).
- Damping for concrete and masonry is considered as 5%.

Table 1 Model parameters

Description	Modulus of elasticity (MPa)	Poisson's ratio
Concrete	22,360	0.15

The behavior of the materials has been assumed to be elastic. The foundation of columns is considered to be made of M20 concrete rectangular pedestal of thickness 0.6 m. The structure has been modeled in SAP2000.

The models have incorporated linear soil springs representing Type-I, Type-II and Type-III soils with their modulus of subgrade reaction as 90,000, 30,000 and 15,000 kN/m^3, respectively [15]. The beams and columns have been modeled as frame elements. For each soil type, 4 models were developed where for soil Type-I, A1 represents structure fixed at column base, A2 has soil spring below the columns, A3 has foundation below the column fixed at the base and A4 has foundation below the column supported on the same soil springs. Similarly, B1, B2, B3 and B4 models consider soil Type-II, and C1, C2, C3 and C4 models consider soil Type-III. The other model parameters considered are shown in Table 1.

The three-dimensional models of A1, A2, A3 and A4 are shown in Fig. 1. The Models B1–B4 and C1–C4 look alike in appearance. The minimum depth of foundation should be more than 1.0 m as per NBC Clause 7.4.1.5 of Part 6, Sect. 2 [15]. In this study, it has been considered as 1.8 m up to the base of the isolated footing. The foundation has been added as a frame element of length 0.6 m with section sizes of 1.8 × 4.8 m and 1.7 × 3.5 m to apply a uniform load below it. The 1.8 × 4.8 m foundation is placed below the middle eight columns and 1.7 × 3.5 m foundation below the outer columns all in the Y-direction.

The response spectrum analyses have been carried out on these models with the load combinations as per IS1893 [16] shown in Table 2. The last mode considered for the response belongs to have 34 Hzs frequency. The results have been obtained for the envelop case of these combinations.

3 Results and Discussion

The structures are generally designed assuming their base is fixed. In reality, all the structures have a foundation which is supported on soil. So, in this discussion, the emphasis has been given to know the models capturing the maximum response along with a comparison with the response obtained from fixed-base analyses.

3.1 Dynamic Characteristics and Base Shear of the Models

The dynamic characteristics and base shear induced in all models are shown in Table 3. The fundamental time period of fixed-base models is 0.789 s. The maximum

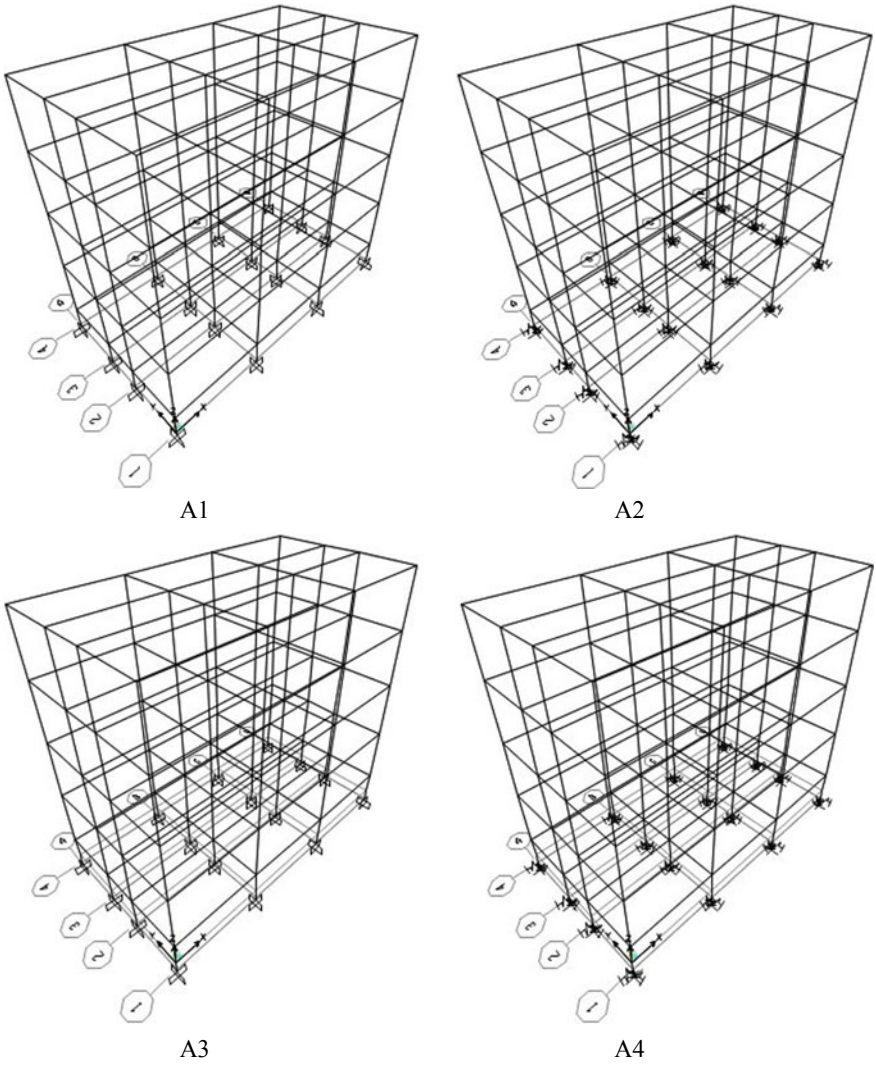

Fig. 1 Three-dimensional models of the framed building: A1—Column fixed at the base, A2—Column supported on springs, A3—Foundation fixed at the base, and A4—Foundation supported on springs

percent (%) increase of periods compared to fixed-base models are 8.9(A4), 35.3(B4) and 64.8(C4), respectively. The increases in peak values with soils Type-II and Type-III compared to Type-I are 24.3 and 51.2%, respectively.

The base shear of fixed-base models in the X-direction are 452.5(A1), 615.3(B1) and 755.6(C1) kN. The maximum values out of all models are 541.2(A3), 736.1(B3) and 903.9(C3) kN. It is found to be lesser with A2, B2, B4, C2 and C4 compared

Table 2 Load combinations considered in analyses

1. 1.5DL
2. 1.5(DL + LL)
3. 1.2(DL + LL + EQx)
4. 1.2(DL + LL + EQy)
5. 1.2(DL + LL-EQx)
6. 1.2(DL + LL-EQy)
7. 1.5(DL + EQx)
8. 1.5(DL-EQx)
9. 1.5(DL + EQy)
10. 1.5(DL-EQy)
11. 0.9DL + 1.5(EQx)
12. 0.9DL-1.5(EQx)
13. 0.9DL + 1.5(EQy)
14. 0.9DL-1.5(EQy)
15. 1.2(DL + LL + response spectrum-XY)
16. 1.5(DL + response spectrum-XY)
17. 0.9DL + 1.5 response spectrum-XY
18. Envelope load case

Table 3 Dynamic characteristics and base shear of the models

Models	First mode (s)	Second mode (s)	Third mode (s)	Base shear—X (kN)	Base shear—Y (kN)
A1	0.789	0.726	0.626	452.5	491.7
A2	0.858	0.842	0.695	424.0	415.7
A3	0.789	0.726	0.626	541.2	588.1
A4	0.859	0.842	0.695	506.8	496.7
B1	0.789	0.726	0.626	615.3	668.7
B2	1.064	0.939	0.780	516.8	456.2
B3	0.789	0.726	0.626	736.1	799.8
B4	1.068	0.942	0.783	616.0	543.6
C1	0.788	0.725	0.626	755.6	821.2
C2	1.290	1.070	0.865	556.8	461.8
C3	0.788	0.725	0.626	903.9	982.4
C4	1.299	1.079	0.874	660.5	548.9

to fixed-base models. The increases in peak values with soils Type-II and Type-III compared to Type-I are 36.0 and 67.0%, respectively. The base shear of fixed-base models in the Y-direction are 491.7(A1), 668.7(B1) and 821.2(C1) kN. The maximum values out of all models are 588.1(A3), 799.8(B3) and 982.4(C3) kN. It is found to be lesser with A2, B2, C2 and C4 compared to fixed-base models. The increases in peak values with soils Type-II and Type-III compared to Type-I are 36.0 and 67.1%, respectively.

It is found that in general there is an increase in the fundamental time period in all SSI systems. The models with foundation fixed at the base have maximum base shear in both the directions.

3.2 Peak Joint Displacements of the Models

The peak joint displacements in X-, Y- and Z-directions of the fixed-base model A1 are 23.1, 23.3 and 2.9 mm, respectively. The corresponding displacements of B1 are 31.5, 31.7 and 2.9 mm and those for C1 are 38.6, 38.9 and 3.0 mm. The percent (%) increase in peak joint displacements of A4 are 24.7, 37.8 and 489.7 compared to A1, B4 are 35.1, 65.2, and 1454.1 compared to B1 and those for C4 are 48.3, 94.3 and 2722.4 compared to C1. The percentage increases in peak values with soils Type-II and Type-III compared to Type-I are 47.8 and 98.7 in X, 63.1 and 135.5 in Y and 163.6 and 395.2 in Z directions, respectively (Table 4).

It is found that in general the displacements have increased in SSI systems but the increase is more pronounced in the Z-direction.

Table 4 Joint displacements of the models

Models	X (mm)	Y (mm)	Z (mm)
A1	23.1	23.3	2.9
A2	24.5	27.2	14.9
A3	27.3	27.4	2.9
A4	28.8	32.1	17.1
B1	31.5	31.7	2.9
B2	36.2	44.6	38.1
B3	37.1	37.3	2.9
B4	42.6	52.4	45.1
C1	38.6	38.9	3.0
C2	48.9	64.5	71.2
C3	45.5	45.8	3.1
C4	57.2	75.6	84.7

3.3 Peak Responses in Columns of the Models

The peak responses in columns are shown in Table 5. The peak axial forces of fixed-base models are 1172.2(A1), 1195.6(B1) and 1249.9(C1) kN. The maximum peak values out of all models are 1172.2(A3), 1238.0(B3) and 1301.9(C3) kN, which are 0, 3.5 and 4.2% higher compared to A1, B1 and C1, respectively. It is found to be lesser in A2, A4, B2, B4, C2 and C4 compared to fixed-base models. The increases in peak values with soils Type-II and Type-III compared to Type-I are 5.6 and 11.1%, respectively.

The peak shear force of fixed-base models is 88.7(A1), 119.0(B1) and 145.2(C1) kN. The maximum peak values out of all models are 104.9(A3), 141.1(B3) and 172.3(C3) kN, which are 18.3, 18.6 and 18.7% higher compared to A1, B1 and C1, respectively. It is found to be lesser in A2, A4, B2, B4, C2 and C4 compared to fixed-base models. The increases in peak values with soils Type-II and Type-III compared to Type-I are 34.5 and 64.3%, respectively.

The peak bending moments of fixed-base models are 129.5(A1), 174.8(B1) and 213.9(C1) kN m. The maximum peak values out of all models are 153.5(A3), 207.5(B3) and 254.1(C3) kN m, which are 18.5, 18.7 and 18.8% higher compared to A1, B1 and C1, respectively. It is found to be lesser in A2, A4, B2, B4, C2 and C4 compared to fixed-base models. The increases in peak values with soils Type-II and Type-III compared to Type-I are 35.2 and 65.5%, respectively.

The peak torsional moments of fixed-base models are 0.8(A1), 1.0(B1) and 1.3(C1) kN m. The maximum peak values out of all models are 1.2(A4), 2.5(B3) and 4.0(C3) kN m, which are 50.0, 149.4 and 208.1% higher compared to A1, B1 and C1, respectively. The increases in peak values with soils Type-II and Type-III compared to Type-I are 107.8 and 233.8%, respectively.

Table 5 Peak response of columns of the models

Models	Axial force (kN)	Shear force (kN)	Bending moment (kN m)	Torsional moment (kN m)
A1	1172.2	88.7	129.5	0.8
A2	1095.6	63.1	108.2	1.0
A3	1172.2	104.9	153.5	0.9
A4	1107.8	75.4	129.0	1.2
B1	1195.6	119.0	174.8	1.0
B2	1064.6	84.6	145.8	2.1
B3	1238.0	141.1	207.5	1.2
B4	1079.7	100.7	173.2	2.5
C1	1249.9	145.2	213.9	1.3
C2	1029.9	96.1	167.0	3.4
C3	1301.9	172.3	254.1	1.5
C4	1037.9	113.8	197.5	4.0

It is found that models with foundation fixed at the base have maximum axial force, shear force and bending moments. The models with foundations supported on springs have maximum torsional moments.

3.4 Peak Responses in Beams of the Models

The peak responses in beams are shown in Table 6. The peak axial forces of fixed-base models are 11.1(A1), 12.5(B1) and 14.6(C1) kN. The maximum peak values out of all models are 21.2(A4), 43.1(B4) and 60.7(C4) kN, which are 91.0, 244.7 and 315.5% higher compared to A1, B1 and C1, respectively. The increases in peak values with soils Type-II and Type-III compared to Type-I are 103.2 and 186.2%, respectively.

The peak shear forces of fixed-base models are 141.2(A1), 183.6(B1) and 220.1(C1) kN. The maximum peak values out of all models are 163.1(A3), 213.3(B3) and 256.7(C3) kN, which are 15.5, 16.2 and 16.6% higher compared to A1, B1 and C1, respectively. It is found to be lesser in A2, A4, B2, B4, C2 and C4 compared to fixed-base models. The increases in peak values with soils Type-II and Type-III compared to Type-I are 30.8 and 57.4%, respectively.

The peak bending moments of fixed-base models are 155.0(A1), 197.0(B1) and 237.3(C1) kN m. The maximum peak values out of all models are 174.3(A3), 229.9(B3) and 277.7(C3) kN m, which are 12.5, 16.7 and 17.0% higher compared to A1, B1 and C1, respectively. It is found to be lesser in A2, B2, C2 and C4 compared to fixed-base models. The increases in peak values with soils Type-II and Type-III compared to Type-I are 31.9 and 59.3%, respectively.

Table 6 Peak response of beams of the models

Models	Axial force (kN)	Shear force (kN)	Bending moment (kN m)	Torsional moment (kN m)
A1	11.1	141.2	155.0	2.5
A2	18.8	115.0	149.1	2.4
A3	11.5	163.1	174.3	2.9
A4	21.2	130.3	164.1	2.8
B1	12.5	183.6	197.0	3.3
B2	38.0	126.5	181.6	2.8
B3	14.2	213.3	229.9	3.9
B4	43.1	136.2	205.3	3.2
C1	14.6	220.1	237.3	4.0
C2	54.5	135.3	202.6	2.9
C3	16.8	256.7	277.7	4.7
C4	60.7	146.3	229.5	3.3

The peak torsional moments of fixed-base models are 2.5(A1), 3.3(B1) and 4.0(C1) kN m. The maximum peak values out of all models are 2.9(A3), 3.9(B3) and 4.7(C3) kN m, which are 16.0, 18.2 and 17.5% higher compared to A1, B1 and C1, respectively. It is found to be lesser in A2, B2, B4, C2 and C4 compared to fixed-base models. The increases in peak values with soils Type-II and Type-III compared to Type-I are 34.5 and 62.1%, respectively.

It is found that models with foundation fixed at the base have maximum shear force, bending moments and torsional moments. The models with foundations supported on springs have maximum axial force.

4 Conclusions

The study has been carried out on a four-storeyed ordinary framed structure. It has been analyzed with a base of the column as fixed and supported on stiff, medium and soft soil springs. The structure has also been analyzed considering isolated rectangular concrete footing (with sizes to transfer uniform load on supports) fixed at the base and supported on the same springs as used in the structure. Considering the structure to be in seismic zone IV, response spectrum analyses were carried out combining until the last mode with 34 Hzs frequency. The peak values of modal time periods, base shear, joint displacements, axial force, shear force, bending moment and torsional moment in both columns and beams were presented. The following conclusions have been drawn about SSI effects compared to fixed-base analyses:

- There is an increase in the fundamental time period in all SSI systems. The increase in peak values with soils Type-II and Type-III compared to Type-I have been computed to be 24.3 and 51.2%, respectively. This increase is due to SSI systems getting flexible from soils Type-I to Type-III.
- The models with foundation fixed at the base have maximum base shear in both the directions. The increase in peak values with soils Type-II and Type-III compared to Type-I have been computed to 36.0 and 67.1%, respectively due to higher spectral acceleration in the models.
- In general the displacements have increased in SSI systems. The percentage increases in peak values with soils Type-II and Type-III compared to Type-I are 47.8, 98.7 in X, 63.1 and 135.5 in Y and 163.6, 395.2 in Z directions. Thus, the increase is more pronounced in the Z (vertical) direction. This increase is due to SSI systems getting flexible from soils Type-I to Type-III.
- The models with foundation fixed at the base have maximum axial force, shear force and bending moment in columns. The increases in peak values, respectively, with soils Type-II and Type-III compared to Type-I are 5.6, 11.1% in case of axial force, 34.5, 64.3% in case of shear force and 35.2, 65.5% in case of bending moment due to the highest base shear in the models.

- The models with foundation restrained by springs have maximum torsional moments in columns with small magnitude. The increases in peak values, respectively, with soils Type-II and Type-III compared to Type-I are 107.8 and 233.8%. This may be due to the system being flexible about the vertical direction due to soil springs.
- The models with foundation fixed at the base have maximum shear force, bending moment and torsional moment in beams. The increases in peak values, respectively, with soils Type-II and Type-III compared to Type-I are 30.8 and 57.4% in case of shear force, 31.9 and 59.3% in case of bending moment and 34.5 and 62.1% in case of torsional moment due to the highest base shear in the models.
- The models with foundation restrained by springs have maximum axial force in beams. The increases in peak values, respectively, with soils Type-II and Type-III compared to Type-I are 103.2 and 186.2%. This may be due to the system being flexible in the horizontal plane due to soil springs.

Thus, the study infers that models with foundation fixed at the base cause maximum axial force, shear force and bending moment in columns and also maximum shear force, bending moment and torsional moment in beams. The SSI models with foundations restrained by soil springs cause maximum torsional moment in columns and maximum axial force in beams.

Acknowledgements The authors are highly grateful to Director CSIR-Central Building Research Institute, Roorkee, for providing all kinds of support to carry out the study and submit it to the conference for publication.

References

1. Roesset JM (2013) Soil structure interaction: the early stages. Appl Sci Eng 16(1):1–8
2. Kausel E (2010) Early history of soil-structure interaction. Soil Dyn Earthq Eng 30(9):822–832
3. Yashinsky M (1998) The Loma Prieta, California, earthquake of October 17, 1989—highway systems. Professional paper 1552-B. U.S. Geological Survey
4. Mylonakis G, Gazetas G (2000) Seismic soil-structure interaction: beneficial or detrimental? J Earthq Eng 4:377–401
5. Badry P, Satyam N (2017) Seismic soil structure interaction analysis for asymmetrical buildings supported on piled raft for the 2015 Nepal earthquake. J Asian Earth Sci 133:102–113
6. Anand V, Satish SR (2018) Seismic soil-structure interaction: a state-of-the-art. J Struct 16:317–326
7. Ciampoli M, Pinto PE (1995) Effects of soil-structure interaction on inelastic seismic response of bridge piers. J Struct Eng 121(5):806–814
8. Nguyen QV, Fatahi B, Hokmabadi AS (2016) The effects of foundation size on the seismic performance of buildings considering the soil-foundation-structure interaction. Struct Eng Mech 58(6):1045–1075
9. Nguyen QV, Fatahi B, Hokmabadi AS (2017) Influence of size and load-bearing mechanism of piles on seismic performance of buildings considering soil-pile-structure interaction. Int J Geomech 17(7):04017007
10. Raychowdhury P (2011) Seismic response of low-rise steel moment-resisting frame buildings incorporating nonlinear SSI. Eng Struct 33(3):958–967

11. Jarernprasert S, Bazan-Zurita E, Bielak J (2013) Seismic soil-structure interaction response of inelastic structures. Soil Dyn Earthq Eng 47:132–143
12. Aydemir ME (2013) Soil structure interaction effects on structural parameters for stiffness degrading systems built on soft soil sites. Struct Eng Mech 45(5):655–676
13. Dutta SC, Roy R (2002) A critical review on idealization and modelling for interaction among soil-foundation-structure system. Comput Struct 80:1579–1594
14. Vaseghiamiri S, Mahsuli M, Ghannad MA, Zareian F (2020) Probabilistic approach to account for soil-structure interaction in seismic design of building structures. J Struct Eng 146(9):04020184
15. National Building Code of India (2016) Bureau of Indian Standards, Part-6, Section-2, Annex B, p 38
16. IS 1893 (2016) Criteria for earthquake resistant design of structures. Bureau of Indian Standards

SSI Effects on the Behavior of a Low-Rise Load Bearing Masonry Building Including Foundation

Meenu Sunil, Neha, Shivi Nigam, and Navjeev Saxena

Abstract The process of soil response influencing the motion of the structure and vice versa is termed as soil-structure interaction. Conventionally, SSI has been considered to pose beneficial effects on the seismic response of a structure because of causing the structure to be more flexible resulting in the increased natural period and enhanced effective damping ratio. These modifications suggest a reduction in base shear demand for a structure as compared to its fixed-base counterpart. This study presents the analyses of a four-storeyed load-bearing brick masonry building. It has been analyzed with the base of the walls as fixed and supported on stiff, medium and soft soil springs. The structure has also been analyzed considering stepped brick masonry strip footing fixed at the base and supported on the same springs as used in the structure. The results are somewhat different than the assumption of fixed-base analyses being always conservative. The study also suggests appropriate modeling to capture maximum response in structural members.

Keywords Soil-structure interaction · SSI · Dynamic · Earthquake · Seismic · Masonry · Concrete · Foundation

1 Introduction

The process of soil response influencing the motion of the structure and vice versa is termed as soil-structure interaction (SSI). It is a phenomenon which comprises various mechanisms leading to the interdependence of soil and structural displacements. These mechanisms broadly fall under either the kinematic or inertial component of SSI. Roesset [1] and Kausel [2] presented reviews of the early-stage

M. Sunil (✉) · Neha · N. Saxena
CSIR-CBRI, Roorkee, India

N. Saxena
e-mail: navjeevsaxena@cbri.res.in

S. Nigam
D.S.M.N.R.U, Lucknow, India

T. G. Sitharam et al. (eds.), *Earthquakes and Structures*, Lecture Notes in Civil Engineering 188, https://doi.org/10.1007/978-981-16-5673-6_25

developments in the field of soil-structure interaction. In addition to the two components of SSI—kinematic and inertial, Roesset also discussed direct and substructure approaches to perform SSI analyses. Kausel presented chronological development in SSI, starting from fundamental solutions (commonly termed as Green's functions) devised by mathematicians and scientists way back in the early nineteenth century. Kausel initiated the development of a substructure approach to solve SSI problems.

Conventionally, SSI has been considered to pose beneficial effects on the seismic response of a structure. The usual reasoning provided in this regard is that considering SSI makes a structure more flexible, increases its natural period and enhances its effective damping ratio. These modifications suggest a reduction in base shear demand for a structure as compared to its fixed-base counterpart. With such assumptions, SSI has usually been disregarded by designers to reduce the complications involved in analyses. However, observations from many earthquake-damaged sites tell a different story. Noticeable instances include damage in a number of pile-supported bridge structures in the 1989 Loma Prieta earthquake as cited by Yashinsky [3] and the collapse of Hanshin Expressway Route 3 (Fukae section) in the 1995 Kobe earthquake as investigated by Mylonakis and Gazetas [4]. Further, Badry and Satyam [5] obtained SSI analysis for asymmetrical buildings supported on a piled raft which got damaged during the 2015 Nepal earthquake. They observed that detrimental effects of SSI can be greatly intensified by the asymmetry in the geometry of superstructures. These observations suggest that the traditional belief of SSI being ever-beneficial does not stand good for all structures on all soil conditions [6].

Ciampoli and Pinto [7] identified structure-to-soil stiffness ratio and aspect ratio of structures to be regulating the phenomenon. Nguyen et al. [8, 9] established the significance of foundation characteristics, viz., footing size in shallow foundations, pile size and load-bearing mechanism in pile foundations on seismic response of structure-soil systems. The possibility of differential settlement arising out of soil flexibility has been remarked by Raychowdhury [10] for low-rise steel moment-resisting framed buildings. She also concluded that SSI needs to be tackled more critically for heavily loaded footings owing to high inertial effects. This suggests a need to develop a rational basis for seismic design incorporating SSI.

Further, Jarernprasert et al. [11] studied the effects of SSI on the response of yielding single-storey structures embedded in an elastic half-space to a set of accelerograms representative of diverse geology. Unlike elastic structures, SSI may lead to an increase in ductility demands and total displacements in the case of inelastic structures. Aydemir [12] studied soil-structure interaction effects on structural parameters for stiffness degrading systems built on soft soil sites and found smaller strength reduction factors for interacting systems than those for corresponding fixed-base systems. This implies that neglecting SSI may result in an unconservative design.

Dutta and Roy [13] presented a critical review of idealization and modeling for interaction among various components of the a soil-foundation-structure system. These modeling strategies are broadly classified as discrete and continuum depending on elements used at the structure-soil interface. In discrete modeling, springs and dashpots are usually used as interface elements. On the other hand, continuum modeling is achieved using either finite element or boundary element methods.

Vaseghiamiri et al. [14] proposed a novel probabilistic approach to account for SSI in the seismic design of building structures. In this approach, an SSI response modification factor is introduced to capture SSI effects on the seismic performance of structures. The proposed procedure quantifies factors such that the probability distribution of the collapse capacity of the structure designed to account for SSI concurs with that of the structure designed using the default fixed-base provisions. It is employed for special steel moment frame buildings (3–15 storey) with surface foundation. To model the superstructure, a surrogate SDOF system with a multilinear backbone curve is used that represents the nonlinear response of the actual structure oscillating according to its fundamental mode of vibration. A lumped-parameter mass-spring-dashpot model representing a rigid disk foundation on a uniform half-space is used to represent the soil-foundation system. The results indicate that no reduction in the design base shear is advisable for structures located on moderately soft to firm soils with shear wave velocities above 150 m/s. This conclusion is at odds with the current prescription of SSI provisions of seismic design code, which allow some reduction in the design base shear for such buildings.

This study presents the analyses of a four-storeyed load-bearing brick masonry structure assuming the base of the walls as fixed as well as supported on stiff, medium and soft soil springs. The study also includes strip-stepped brick masonry footing with its width as 1.38 m at a depth of 1.0 m below the walls fixed at the base as well as supported on the same springs as used in the structure alone. The results are somewhat different than the assumption of the fixed-base analyses being always conservative. The study also suggests appropriate modeling to capture maximum response in structural members.

2 Modeling and Analyses

A typical four-storeyed load-bearing brick masonry building has been considered for the study. The details of the building are as follows:

- Grade of concrete used is M20 and grade of steel used is Fe415.
- Floor-to-floor height is 3.1 m.
- Plinth height above GL is 0.30 m.
- Depth of foundation is 1.15 m below GL.
- Parapet height is 1.2 m.
- Slab thickness is 150 mm.
- Masonry wall thickness is 230 mm.
- Live load on floor is 3 kN/m^2 and Live load on roof is 1.5 kN/m^2.
- Floor finish is 1 kN/m^2 and roof treatment is 1.5 kN/m^2.
- The building is located in Seismic Zone IV.
- Importance Factor is taken as 1.0.
- Damping for concrete and masonry is considered as 5%.

Table 1 Model parameters

Description	Modulus of elasticity (MPa)	Weight density (kN/m^3)	Poisson's ratio
Concrete	22,360	25.0	0.15
Masonry	4200	20.0	0.30

The behavior of the materials has been assumed to be elastic. The foundation below the walls is considered to be made of brick masonry with its width gradually increasing to 1.38 m at a depth of 1.15 m below the GL. The structure has been modeled in SAP2000.

The models have incorporated linear soil springs representing Type-I, Type-II and Type-III soils with their modulus of subgrade reaction as 90,000, 30,000 and 15,000 kN/m^3, respectively, as mentioned in NBC Clause 7.4.1.11 of Part 6, Sect. 2 [15]. The walls, slabs and foundation have been modeled as 4 noded shell elements. The material properties of the brick masonry have been taken from the literature [16]. For each soil type, 4 models were developed where for soil Type-I, A1 represents structure fixed at the base of the walls, A2 has soil springs below the walls, A3 has foundation below the walls fixed at the base and A4 has foundation below the walls supported on the same soil springs. Similarly, B1, B2, B3 and B4 models consider soil Type-II and C1, C2, C3 and C4 models consider soil Type-III. The other model parameters considered are shown in Table 1.

The three-dimensional models of A1, A2, A3 and A4 are shown in Fig. 1. The Models B1–B4 and C1–C4 look alike in appearance. The foundation has been added as a shell element with its width 0.46 m just below the walls and 1.38 m at a depth of 1.15 m below the GL.

The response spectrum analyses have been carried out on these models with the load combinations as per IS1893 [17] shown in Table 2. The last mode considered for the response belongs to have 34 Hzs frequency. The results have been obtained for the envelop case of these combinations.

3 Results and Discussion

The structures are generally designed assuming their base is fixed. In reality, all the structures have a foundation which is supported on soil. So, in this discussion, the emphasis has been given to know the models capturing the maximum response along with a comparison with the response obtained from fixed-base analyses.

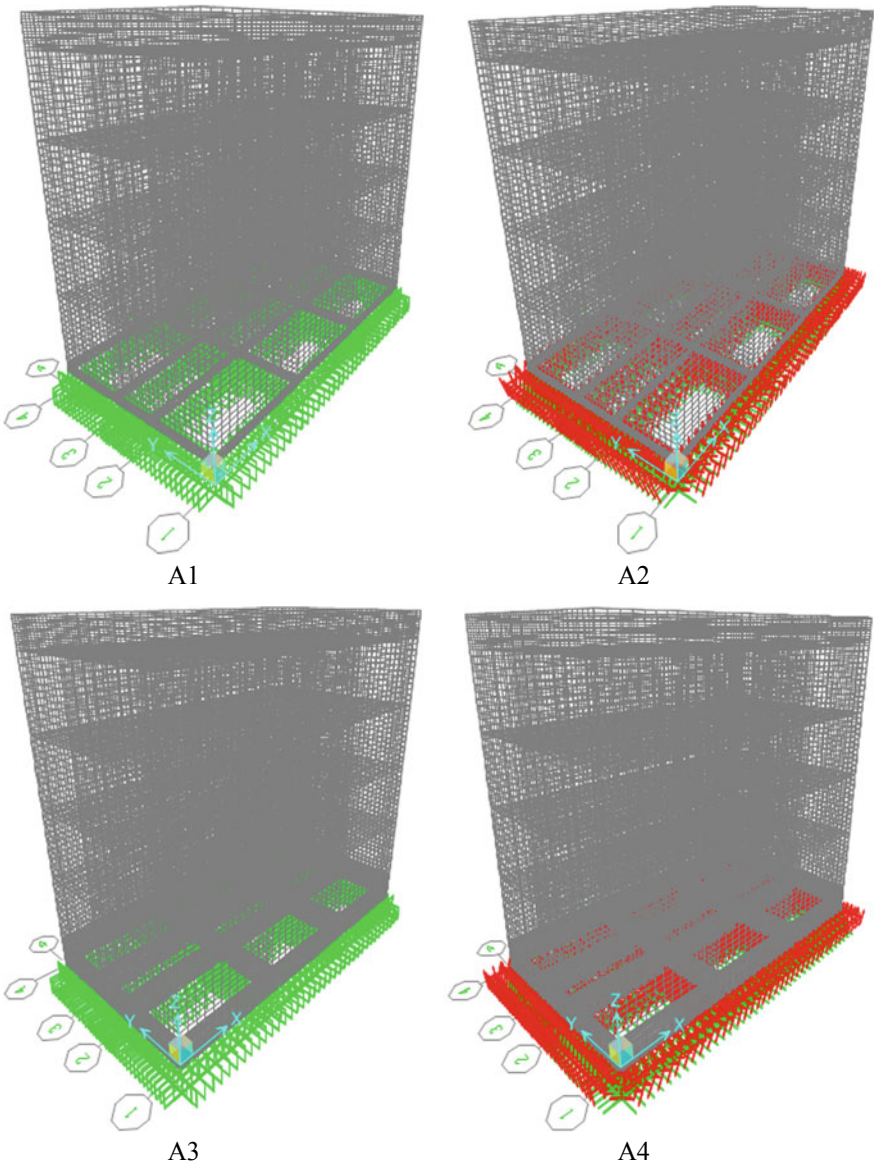

Fig. 1 Three-dimensional models of the masonry building: A1—Walls fixed at the base, A2—Walls restrained by springs, A3—Foundation fixed at the base, and A4—Foundation restrained by springs

Table 2 Load combinations considered in analyses

1. 1.5DL
2. 1.5(DL + LL)
3. 1.2(DL + LL + EQx)
4. 1.2(DL + LL + EQy)
5. 1.2(DL + LL-EQx)
6. 1.2(DL + LL-EQy)
7. 1.5(DL + EQx)
8. 1.5(DL-EQx)
9. 1.5(DL + EQy)
10. 1.5(DL-EQy)
11. 0.9DL + 1.5(EQx)
12. 0.9DL-1.5(EQx)
13. 0.9DL + 1.5(EQy)
14. 0.9DL-1.5(EQy)
15. 1.2(DL + LL + response spectrum-XY)
16. 1.5(DL + response spectrum-XY)
17. 0.9DL + 1.5response spectrum-XY
18. Envelope load case

3.1 Dynamic Characteristics and Base Shear of the Models

The dynamic characteristics and base shear induced in all models are shown in Table 3. The fundamental time period of fixed-base models is 0.165 s. The maximum percent (%) increase compared to fixed-base models are 12.8(A4), 28.7(B4) and 47.7(C4), respectively. The increases in peak values with soils Type-II and Type-III compared to Type-I are 14.1 and 31.0%, respectively.

The base shear of fixed-base models in the X-direction is 1660.4 kN which is the same in the Y-direction also. The maximum value is 1999.0 kN in both X- and Y-directions of models A3, A4, B3, B4, C3 and C4. It is found to be equal in A2, B2 and C2 models compared to fixed-base models. There is no change with soils Type-II and Type-III compared to Type-I in this problem.

It is found that in general there is an increase in the fundamental time period in all SSI systems. Models having foundation fixed at the base (A3, B3 & C3) and foundation restrained by soil springs (A4, B4 & C4) have maximum base shear in both the directions of same magnitude.

Table 3 Dynamic characteristics and base shear of the models

Models	First mode (s)	Second mode (s)	Third mode (s)	Base shear—X (kN)	Base shear—Y (kN)
A1	0.165	0.111	0.100	1660.4	1660.4
A2	0.181	0.121	0.104	1660.4	1660.4
A3	0.170	0.115	0.102	1999.0	1999.0
A4	0.186	0.125	0.106	1999.0	1999.0
B1	0.165	0.111	0.100	1660.4	1660.4
B2	0.207	0.137	0.107	1660.4	1660.4
B3	0.170	0.115	0.102	1999.0	1999.0
B4	0.213	0.142	0.109	1999.0	1999.0
C1	0.165	0.111	0.100	1660.4	1660.4
C2	0.240	0.158	0.110	1660.4	1660.4
C3	0.170	0.115	0.102	1999.0	1999.0
C4	0.244	0.164	0.112	1999.0	1999.0

3.2 Peak Joint Displacements of the Models

The peak joint displacements in X-, Y- and Z-directions of the fixed-base model A1 are −2.2, −4.9 and −1.9 mm, respectively. The corresponding displacements of B1 and C1 are the same as that of A1. The percent (%) increase in peak joint displacements of A4 are 34.2, 39.8 and 34.9 compared to A1, those for B4 are 64.8, 76.0 and 78.2 compared to B1 and those for C4 are 106.1, 123.7 and 138.4 compared to C1. The percentage increases in peak values with soils Type-II and Type-III compared to Type-I are 22.8 and 53.6 in X, 25.9 and 59.9 in Y and 32.1 and 76.7 in Z directions, respectively (Table 4).

It is found that in general the displacements have increased in SSI systems but the increase is more pronounced in the Z-direction.

3.3 Peak Responses in Walls of the Models

The peak responses in walls are shown in Table 5. The peak tensile stress of the fixed-base model A1 is 1.43 MPa which is the same in B1 and C1. The maximum peak values out of all models are 1.43(A1), 1.43(B4) and 1.80(C4) MPa which are 0, 0 and 25.8% higher compared to A1, B1 and C1, respectively. It is found to be lesser with A2, A3, A4, B2, B3, B4 and C3 compared to fixed-base models. The increases in peak values with soils Type-II and Type-III compared to Type-I are 0.0 and 25.8%, respectively. The tensile strength of the masonry can be considered as 0.07 and 0.14 MPa for induced tensile stresses normal and parallel to bed joint, respectively, as mentioned in NBC Clause 5.4.2, Part 6, Sect. 4 [15]. The results

Table 4 Joint displacements of the models

Models	X (mm)	Y (mm)	Z (mm)
A1	−2.2	−4.9	−1.9
A2	−2.5	−5.7	−2.3
A3	−2.7	−6.0	−2.2
A4	−3.0	−6.9	−2.6
B1	−2.2	−4.9	−1.9
B2	−3.0	−7.2	−3.0
B3	−2.7	−6.0	−2.2
B4	−3.7	−8.7	−3.4
C1	−2.2	−4.9	−1.9
C2	−3.8	−9.3	−4.0
C3	−2.7	−6.0	−2.2
C4	−4.6	−11.0	−4.6

Table 5 Peak response of walls of the models

Models	Tensile stress (MPa)	Compressive stress (MPa)	Shear stress (MPa)
A1	1.43	−2.67	0.54
A2	1.25	−2.68	0.67
A3	1.39	−2.92	0.65
A4	1.37	−2.99	0.67
B1	1.43	−2.67	0.54
B2	1.27	−2.83	1.02
B3	1.39	−2.92	0.65
B4	1.43	−3.09	0.94
C1	1.43	−2.67	0.54
C2	1.52	−3.13	1.41
C3	1.39	−2.92	0.65
C4	1.80	−3.30	1.28

indicate that the induced peak tensile stresses in the masonry are much higher than the tensile strength.

The peak compressive stress of the fixed-base model A1 is 2.67 MPa which is the same in B1 and C1. The maximum peak values out of all models are 2.99(A4), 3.09(B4) and 3.30(C4) Mpa, which are 11.9, 15.8 and 23.7% higher compared to A1, B1 and C1, respectively. The increases in peak values with soils Type-II and Type-III compared to Type-I are 3.5 and 10.5%, respectively. The compressive strength of the masonry would be 7.6 Mpa corresponding to the modulus of elasticity as 4200 Mpa [16]. It can be seen that the induced peak compressive stresses are significantly less than the compressive strength of the masonry.

The peak shear stress of the fixed-base model A1 is 0.54 MPa which is the same in B1 and C1. The maximum peak values out of all models are 0.67(A4), 1.02(B2) and 1.41(C2) MPa, which are 23.7, 88.8 and 160.1% higher compared to A1, B1 and C1, respectively. The increases in peak values with soils Type-II and Type-III compared to Type-I are 52.6 and 110.2%, respectively.

It is found that models with foundations restrained by soil springs have maximum tensile and compressive stresses. The shear stresses are maximum with walls restrained by soil springs in all soil types.

3.4 Peak Responses in Slabs of the Models

The peak responses in slabs are shown in Table 6. The peak tensile stress of the fixed-base model A1 is 2.15 MPa which is the same in B1 and C1. The maximum peak values out of all models are 2.16(A4), 2.16(B4) and 2.17(C4)MPa, which is close to the response of fixed-base models. The slabs are assumed to be made of concrete having characteristic compressive strength 20 MPa. The permissible direct tensile strength can be considered as 2.8 MPa as per NBC Clause B-2.1, Part 6, Sect. 5 [15]. The results indicate that the peak tensile stresses are less than the permissible strengths.

The peak compressive stress of the fixed-base model A1 is 2.03 MPa, which is the same in B1 and C1. The maximum peak values are close to the response of fixed-base models. The permissible direct compressive strength can be considered as 5.0 MPa as per NBC Clause B-2.1, Part 6, Sect. 5 [15]. The results indicate that the peak compressive stresses are significantly less than the permissible strengths.

Table 6 Peak responses of slab of the models

Models	Tensile stress (MPa)	Compressive stress (MPa)	Shear stress (MPa)
A1	2.15	−2.03	0.77
A2	2.16	−2.03	0.78
A3	2.15	−2.03	0.81
A4	2.16	−2.03	0.81
B1	2.15	−2.03	0.77
B2	2.16	−2.03	0.78
B3	2.15	−2.03	0.81
B4	2.16	−2.03	0.81
C1	2.15	−2.03	0.77
C2	2.17	−2.03	0.78
C3	2.15	−2.03	0.81
C4	2.17	−2.03	0.80

The peak shear stress of the fixed-base model A1 is 0.77 MPa, which is the same in B1 and C1. The maximum peak values out of all models is 0.81 MPa in A3, B3 and C3 models, which is 5.3% higher compared to respective fixed-base models. The increase in peak values of both soils Type-II and Type-III compared to Type-I is 0.4%.

Comparing the peak responses, it is found that SSI does not significantly affect the tensile and compressive responses. The shear stress is found to be maximum in models with foundation fixed at the base.

4 Conclusions

The study has been carried out on a four-storeyed load-bearing brick masonry building. It has been analyzed with the base of the walls as fixed and supported on stiff, medium and soft soil springs. The structure has also been analyzed considering stepped brick masonry strip footing fixed at the base and supported on the same springs as used in the structure. Considering the structure to be in seismic zone IV, response spectrum analyses were carried out considering the last mode with 34 Hzs frequency. The peak values of modal time periods, base shear, joint displacements, normal tensile stresses, normal compressive stresses and shear stresses in walls and slabs have been presented. The following conclusions have been drawn about SSI effects compared to fixed-base analyses:

- There is an increase in the fundamental time period in all SSI systems. The increase in peak values with soils Type-II and Type-III compared to Type-I have been computed to be 14.1 and 31.0%, respectively.
- The SSI models have a higher base shear in both the directions. There is no increase in peak values with soils Type-II and Type-III compared to Type-I.
- In general, the displacements have increased in SSI systems. The percent (%) increases in peak values with soils Type-II and Type-III compared to Type-I are 22.8 and 53.6 in X, 25.9 and 59.9 in Y and 32.1 and 76.7 in Z directions, respectively. Thus, the increase is more pronounced in the Z (vertical) direction.
- Comparing the peak responses in walls, it is found that maximum tensile and compressive stresses are found in the models with foundation restrained by soil springs except in the case of wall fixed at the base (soil Type-I). The increases in peak values of tensile stresses with soils Type-II and Type-III compared to Type-I are 0.0 and 25.8%, respectively. The increases in peak values of compressive stresses with soils Type-II and Type-III compared to Type-I are 3.5 and 10.5%. respectively. The shear stresses are maximum with walls restrained by soil springs in soils Types II and III. In the case of soil Type-I, it is maximum with foundation restrained by soil springs. The increases in peak values with soils Type-II and Type-III compared to Type-I are 52.6 and 110.2%, respectively.

- Comparing the peak responses in slabs, it is found that SSI does not significantly affect the tensile and compressive stress responses. However, the shear stress is found maximum in models with foundation fixed at the base.

Thus, the study infers that SSI models having foundations restrained by soil springs respond to maximum tensile and compressive stresses in walls except in the case of wall fixed at the base (soil Type-I). The maximum shear stress in walls is found in SSI models with walls restrained by soil springs. The maximum shear stress in slabs is found in the models with the foundation fixed at the base.

Acknowledgements The authors are highly grateful to Director CSIR-Central Building Research Institute, Roorkee, for providing all kinds of support to carry out the study and submit it to the conference for publication.

References

1. Roesset JM (2013) Soil structure interaction: the early stages. Appl Sci Eng 16(1):1–8
2. Kausel E (2010) Early history of soil-structure interaction. Soil Dyn Earthq Eng 30(9):822–832
3. Yashinsky M (1998) The Loma Prieta, California, earthquake of October 17, 1989—highway systems. Professional paper 1552-B. U.S. Geological Survey
4. Mylonakis G, Gazetas G (2000) Seismic soil-structure interaction: beneficial or detrimental? J Earthq Eng 4:377–401
5. Badry P, Satyam N (2017) Seismic soil structure interaction analysis for asymmetrical buildings supported on piled raft for the 2015 Nepal earthquake. J Asian Earth Sci 133:102–113
6. Anand V, Satish SR (2018) Seismic soil-structure interaction: a state-of-the-art. J Struc 16:317–326
7. Ciampoli M, Pinto PE (1995) Effects of soil-structure interaction on inelastic seismic response of bridge piers. J Struct Eng 121(5):806–814
8. Nguyen QV, Fatahi B, Hokmabadi AS (2016) The effects of foundation size on the seismic performance of buildings considering the soil-foundation-structure interaction. Struct Eng Mech 58(6):1045–1075
9. Nguyen QV, Fatahi B, Hokmabadi AS (2017) Influence of size and load-bearing mechanism of piles on seismic performance of buildings considering soil-pile-structure interaction. Int J Geomech 17(7):04017007
10. Raychowdhury P (2011) Seismic response of low-rise steel moment-resisting frame buildings incorporating nonlinear SSI. Eng Struct 33(3):958–967
11. Jarernprasert S, Bazan-Zurita E, Bielak J (2013) Seismic soil-structure interaction response of inelastic structures. Soil Dyn Earthq Eng 47:132–143
12. Aydemir ME (2013) Soil structure interaction effects on structural parameters for stiffness degrading systems built on soft soil sites. Struct Eng Mech 45(5):655–676
13. Dutta SC, Roy R (2002) A critical review on idealization and modelling for interaction among soil-foundation-structure system. Comput Struct 80:1579–1594
14. Vaseghiamiri S, Mahsuli M, Ghannad MA, Zareian F (2020) Probabilistic approach to account for soil-structure interaction in seismic design of building structures. J Struct Eng 146(9):04020184
15. National Building Code of India (2016) Bureau of Indian Standards
16. Kaushik HB, Rai DC, Jain SK (2007) Stress-strain characteristics of clay brick masonry under uniaxial compression. J Mater Civil Eng 19(9):728–739
17. IS 1893 (2016) Criteria for earthquake resistant design of structures. Bureau of Indian Standards

SSI Effects on Behavior of a Low-Rise Load-Bearing Structural Walled Building Including Foundation

Neha, Meenu Sunil, Shivi Nigam, and Navjeev Saxena

Abstract The process of soil response influencing the motion of the structure and vice-versa is termed as soil-structure interaction. Conventionally, SSI has been considered to pose beneficial effects on the seismic response of a structure because of causing the structure more flexible resulting in the increased natural period and enhanced effective damping ratio. These modifications suggest a reduction in base shear demand for a structure as compared to its fixed-base counterpart. This study presents analyses of a four-storeyed load-bearing structural walled building. It has been analyzed with the base of the walls as fixed and supported on stiff, medium and soft soil springs. The structure has also been analyzed considering stepped brick masonry strip footing fixed at base and supported on same springs as used in the structure. The results are somewhat different than the assumption of fixed-base analyses being always conservative. The study also suggests appropriate modeling to capture maximum response in structural members.

Keywords Soil-structure interaction · SSI · Dynamic · Earthquake · Seismic · Shear wall · Concrete · Foundation

1 Introduction

The process of soil response influencing the motion of the structure and vice-versa is termed as soil-structure interaction (SSI). It is a phenomenon that comprises various mechanisms leading to the interdependence of soil and structural displacements. These mechanisms broadly fall under either the kinematic or inertial component of SSI. Roesset [1] and Kausel [2] presented reviews of the early-stage developments

Neha (✉) · M. Sunil · N. Saxena
CSIR-CBRI, Roorkee, India

N. Saxena
e-mail: navjeevsaxena@cbri.res.in

S. Nigam
D.S.M.N.R.U, Lucknow, India

T. G. Sitharam et al. (eds.), *Earthquakes and Structures*, Lecture Notes in Civil Engineering 188, https://doi.org/10.1007/978-981-16-5673-6_26

in the field of soil-structure interaction. In addition to the two components of SSI—kinematic and inertial, Roesset also discussed direct and substructure approaches to perform SSI analyses. Kausel presented chronological development in SSI, starting from fundamental solutions (commonly termed as Green's functions) devised by mathematicians and scientists way back in the early nineteenth century. Kausel initiated the development of a substructure approach to solve SSI problems.

Conventionally, SSI has been considered to pose beneficial effects on the seismic response of a structure. The usual reasoning provided in this regard is that considering SSI makes a structure more flexible, increases its natural period and enhances its effective damping ratio. These modifications suggest a reduction in base shear demand for a structure as compared to its fixed-base counterpart. With such assumptions, SSI has usually been disregarded by designers to reduce the complications involved in analyses. However, observations from many earthquake-damaged sites tell a different story. Noticeable instances include damage in a number of pile-supported bridge structures in the 1989 Loma Prieta earthquake as cited by Yashinsky [3] and the collapse of Hanshin Expressway Route 3 (Fukae section) in the 1995 Kobe Earthquake as investigated by Mylonakis and Gazetas [4]. Further Badry and Satyam [5] obtained SSI analysis for asymmetrical buildings supported on the piled raft which got damaged during the 2015 Nepal Earthquake. They observed that detrimental effects of SSI can be greatly intensified by the asymmetry in the geometry of the superstructure. These observations suggest that the traditional belief of SSI being ever-beneficial does not stand good for all structures on all soil conditions [6].

Ciampoli and Pinto [7] identified structure-to-soil stiffness ratio and aspect ratio of structure to be regulating the phenomenon. Nguyen et al. [8, 9] established the significance of foundation characteristics, viz. footing size in shallow foundations and pile size and load-bearing mechanism in pile foundations on seismic response of structure-soil systems. The possibility of differential settlement arising out of soil flexibility has been remarked by Raychowdhury [10] for low-rise steel moment-resisting framed buildings. She also concluded that SSI needs to be tackled more critically for heavily loaded footings owing to high inertial effects. This suggests a need to develop a rational basis for seismic design incorporating SSI.

Further, Jarernprasert et al. [11] studied the effects of SSI on the response of yielding single-storey structures embedded in an elastic half-space to a set of accelerograms representative of diverse geology. Unlike elastic structures, SSI may lead to an increase in ductility demands and total displacements in the case of inelastic structures. Aydemir [12] studied soil-structure interaction effects on structural parameters for stiffness degrading systems built on soft soil sites and found smaller strength reduction factors for interacting systems than those for corresponding fixed-base systems. This implies that neglecting SSI may result in an unconservative design.

Dutta and Roy [13] presented a critical review of idealization and modeling for interaction among various components of the soil-foundation structure system. These modeling strategies are broadly classified as discrete and continuum depending on elements used at the structure-soil interface. In discrete modeling, springs and dashpots are usually used as interface elements. On the other hand, continuum modeling is achieved using either finite element or boundary element methods.

Vaseghiamiri et al. [14] proposed a novel probabilistic approach to account for SSI in the seismic design of building structures. In this approach, an SSI response modification factor is introduced to capture SSI effects on the seismic performance of structures. The proposed procedure quantifies factors such that the probability distribution of the collapse capacity of the structure designed to account for SSI concurs with that of the structure designed using the default fixed-base provisions. It is employed for special steel moment frame buildings (3–15 storey) with surface foundation. To model the superstructure, a surrogate SDOF system with a multilinear backbone curve is used that represents the nonlinear response of the actual structure oscillating according to its fundamental mode of vibration. A lumped-parameter mass-spring-dashpot model representing a rigid disk foundation on a uniform half-space is used to represent the soil-foundation system. The results indicate that no reduction in the design base shear is advisable for structures located on moderately soft to firm soils with shear wave velocities above 150 m/s. This conclusion is at odds with the current prescription of SSI provisions of seismic design code, which allow some reduction in the design base shear for such buildings.

This study presents analyses of a four-storeyed load-bearing structural walled building assuming the base of the walls as fixed as well as supported on stiff, medium and soft soil springs. The study also includes strip-stepped brick masonry footing with its width as 1.38 m at a depth of 1.0 m below the walls fixed at the base as well as supported on the same springs as used in the structure alone. The results are somewhat different than the assumption of fixed-base analyses being always conservative. The study also suggests appropriate modeling to capture maximum response in structural members.

2 Modeling and Analyses

A typical four-storeyed load-bearing structural walled building has been considered for the study. The details of the building are as below:

- Grade of concrete used is M20 and the grade of steel used is Fe415.
- Floor to floor height is 3.1 m.
- Plinth height above GL is 0.30 m.
- Depth of foundation is 1.15 m below GL.
- Parapet height is 1.2 m.
- Slab thickness is 150 mm.
- Structural wall thickness is 150 mm of concrete grade M20.
- Live load on the floor is 3 kN/m^2 and Live load on the roof is 1.5 kN/m^2.
- The load for floor finishes is 1 kN/m^2 and roof treatment is 1.5 kN/m^2
- The building is located in Seismic Zone IV.
- Importance Factor is taken as 1.0.
- Damping for concrete and masonry is considered as 5%.

Table 1 Model parameters

Description	Modulus of elasticity (MPa)	Weight density (kN/m^3)	Poisson's ratio
Concrete	22,360	25.0	0.15
Masonry	4200	20.0	0.30

The behavior of the materials has been assumed to be elastic. The foundation below the walls is considered made of brick masonry with its width gradually increasing to 1.38 m at a depth of 1.15 m below the GL. The structure has been modeled in SAP2000.

There are three classifications of soils namely Type-I (Rock or hard soils), Type-II (Medium of stiff soils) and Type-III (soft soils) for determining the response spectrum to be used to estimate design earthquake forces. In terms of penetration number (N), the soil Type-I, Type-II and Type-III have been categorized having $N > 30$, $10 < N > 30$ and $N < 10$, respectively [17]. The models have incorporated linear soil springs representing Type-I, Type-II and Type-III soils with their modulus of subgrade reaction as 90,000, 30,000 and 15,000 kN/m^3, respectively, as mentioned in NBC Clause 7.4.1.11 of Part 6, Sect. 2 [15]. The walls, slabs and foundation have been modeled as four noded shell elements. The material properties of the brick masonry have been taken from literature [16]. For each soil type, four models were developed where for soil Type-I, A1 represents structure fixed at the base of the walls, A2 has soil springs below the walls, A3 has foundation below the walls fixed at base and A4 has foundation below the walls supported on same soil springs. Similarly, B1, B2, B3 and B4 models consider soil Type-II and C1, C2, C3 and C4 models consider soil Type-III. The other model parameters considered are shown in Table 1.

The three-dimensional models of A1, A2, A3 and A4 are shown in Fig. 1. The Models B1 to B4 and C1 to C4 look alike in appearance. The foundation has been added as a shell element with its width as 0.46 m just below the walls and 1.38 m at a depth of 1.15 m below the GL.

The response spectrum analyses have been carried out on these models with the load combinations as per IS1893 [17] shown in Table 2. The last mode considered for the response belongs to have 34 Hzs frequency. The results have been obtained for the envelop case of these combinations.

3 Results and Discussion

The structures are generally designed assuming their base as fixed. In reality, all structures have a foundation that is supported on the soil. So, in this discussion, the emphasis has been given to know the models capturing the maximum response along with a comparison with the response obtained from fixed-base analyses.

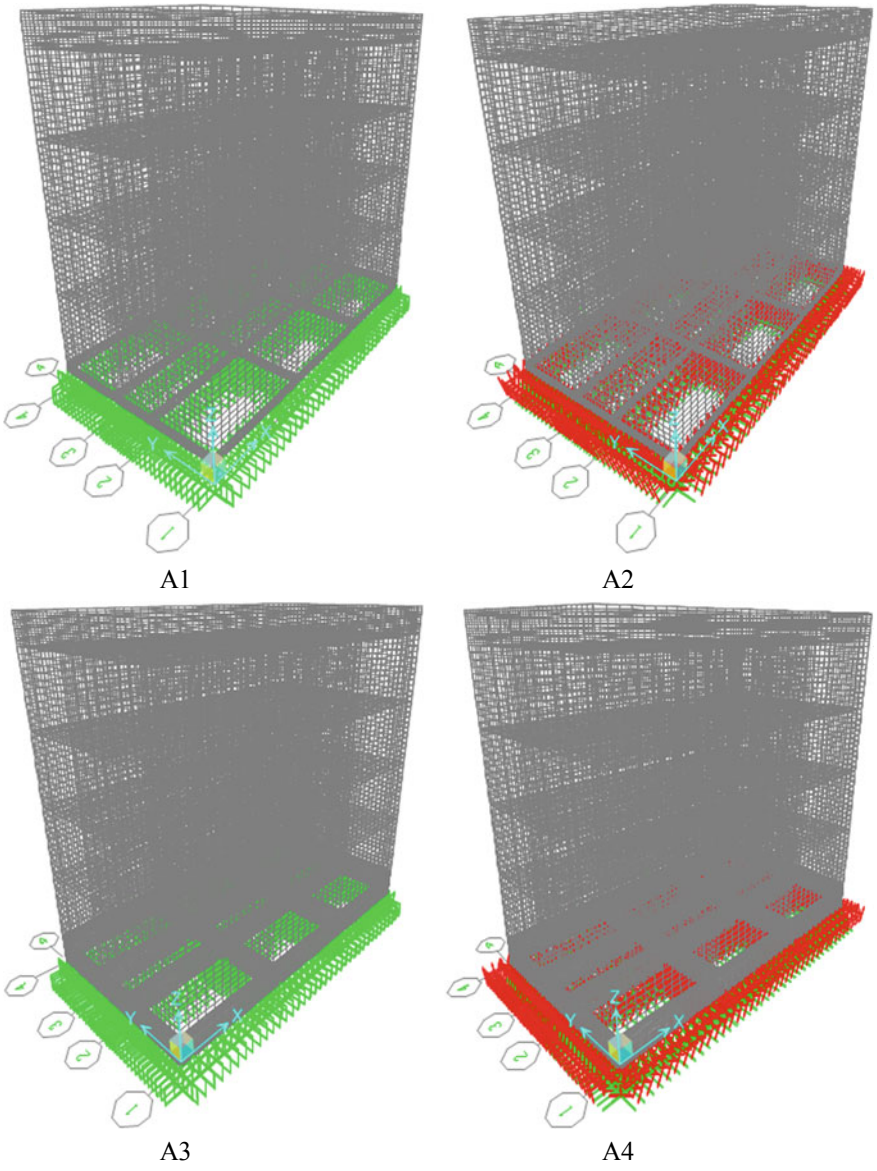

Fig. 1 Three-dimensional models of the structural walled building: A1—Walls fixed at the base, A2—Walls restrained by springs, A3—Foundation fixed at the base, A4—Foundation restrained by springs

Table 2 Load combinations considered in analyses

1. 1.5DL
2. 1.5(DL + LL)
3. 1.2(DL + LL + EQx)
4. 1.2(DL + LL + EQy)
5. 1.2(DL + LL-EQx)
6. 1.2(DL + LL-EQy)
7. 1.5(DL + EQx)
8. 1.5(DL-EQx)
9. 1.5(DL + EQy)
10. 1.5(DL-EQy)
11. 0.9DL + 1.5(EQx)
12. 0.9DL-1.5(EQx)
13. 0.9DL + 1.5(EQy)
14. 0.9DL-1.5(EQy)
15. 1.2(DL + LL + response spectrum-XY)
16. 1.5(DL + response spectrum-XY)
17. 0.9DL + 1.5response spectrum-XY
18. Envelope load case

3.1 Dynamic Characteristics and Base Shear of the Models

The dynamic characteristics and base shear induced in all models are shown in Table 3. The fundamental time period of fixed-base models is 0.084 s. The maximum percent (%) increase compared to fixed-base models is 37.6(A4), 78.6(B4) and 121.4(C4), respectively. The increases in peak values with soil Type-II and Type-III compared to Type-I are 29.8 and 61.0%, respectively.

The base shear of fixed-base models in X-direction is 1067.0 kN for all models. The maximum values out of all models are 1536.6 (A4), 1787.9(B4) and 1788.6(C4) kN. The increase in peak values with soil Type-II and Type-III compared to Type-I is the same as a value of 16.4%. The base shear of fixed-base models in Y-direction is 1308.6 kN for all models. The maximum value is 1788.6 kN which is the same for A4, B4 and C4. There is no increase in peak values with soil Type-II and Type-III compared to Type-I.

It is found that in general there is an increase in the fundamental time period in all SSI systems. The maximum base shear is found in the models with foundation restrained by soil springs.

Table 3 Dynamic characteristics and base shear of the models

Models	First mode (s)	Second mode (s)	Third mode (s)	Base shear—X (kN)	Base shear—Y (kN)
A1	0.084	0.056	0.051	1067.0	1308.6
A2	0.108	0.071	0.056	1196.3	1450.1
A3	0.091	0.061	0.054	1370.2	1692.3
A4	0.115	0.077	0.059	1536.6	1788.6
B1	0.084	0.056	0.051	1067.0	1308.6
B2	0.142	0.093	0.060	1388.3	1450.1
B3	0.091	0.061	0.054	1370.2	1692.3
B4	0.150	0.100	0.064	1787.9	1788.6
C1	0.084	0.056	0.051	1067.0	1308.6
C2	0.181	0.118	0.063	1450.0	1450.0
C3	0.091	0.061	0.054	1370.2	1692.3
C4	0.185	0.127	0.067	1788.6	1788.6

3.2 Peak Joint Displacements of the Models

The peak joint displacements in X, Y and Z-directions of fixed-base model A1 are −0.5, −1.4 and −0.7 mm, respectively. The corresponding displacements of B1 and C1 are the same as that of A1. The percent (%) increase in peak joint displacements of A4 are 98.1, 102.8 and 61.7 compared to A1, B4 are 236.9, 211.8 and 147.8 compared to B1 and C4 are 392.3, 353.6 and 278.7 compared to C1. The percentage increases in peak values with soil Type-II and Type-III compared to Type-I are 70.1 and 148.5 in X, 53.7 and 123.7 in Y and 53.2 and 134.2 in Z-directions, respectively (Table 4).

It is found that in general, the displacements have increased in SSI systems but the increase is more pronounced in X-direction.

3.3 Peak Responses in Walls of the Models

The peak responses in walls are shown in Table 5. The peak tensile stress of fixed-base model A1 is 1.66 MPa, which is the same in B1 and C1. The maximum peak values out of all models are 2.02(A4), 2.92(B4) and 4.10(C4) MPa, which are 22.0, 75.9 and 147.3% higher compared to A1, B1 and C1, respectively. It is found lesser with A3, B3 and C3 compared to fixed-base models. The increases in peak values with soil Type-II and Type-III compared to Type-I are 44.1 and 102.6%, respectively.

The peak compressive stress of fixed-base model A1 is 3.25 MPa, which is the same in B1 and C1. The maximum peak values out of all models are 4.20(A4), 5.19(B4) and 6.42(C4) MPa, which are 29.2, 59.6 and 97.3% higher compared to

Table 4 Joint displacements of the models

Models	X (mm)	Y (mm)	Z (mm)
A1	−0.5	−1.4	−0.7
A2	−0.8	−2.2	−1.0
A3	−0.7	−1.9	−0.8
A4	−1.0	−2.8	−1.2
B1	−0.5	−1.4	−0.7
B2	−1.3	−3.4	−1.5
B3	−0.7	−1.9	−0.8
B4	−1.8	−4.3	−1.8
C1	−0.5	−1.4	−0.7
C2	−2.0	−5.2	−2.3
C3	−0.7	−1.9	−0.8
C4	−2.6	−6.3	−2.7

Table 5 Peak response of walls of the models

Models	Tensile stress (MPa)	Compressive stress (MPa)	Shear stress (MPa)
A1	1.66	−3.25	0.71
A2	1.92	−3.62	1.53
A3	1.54	−3.49	0.93
A4	2.02	−4.20	1.63
B1	1.66	−3.25	0.71
B2	2.55	−4.60	2.69
B3	1.54	−3.49	0.93
B4	2.92	−5.19	2.90
C1	1.66	−3.25	0.71
C2	3.95	−6.01	4.20
C3	1.54	−3.49	0.93
C4	4.10	−6.42	4.49

A1, B1 and C1, respectively. The increases in peak values with soil Type-II and Type-III compared to Type-I are 23.5 and 52.7%, respectively.

The peak shear stress of fixed-base model A1 is 0.71 MPa, which is the same in B1 and C1. The maximum peak values out of all models are 1.63(A4), 2.90(B4) and 4.49(C4) MPa, which are 129.9, 310.4 and 533.9% higher compared to A1, B1 and C1, respectively. The increases in peak values with soil Type-II and Type-III compared to Type-I are 78.5 and 175.7%, respectively.

It is found that models with foundations restrained by soil springs have maximum tensile, compressive stresses and shear stresses.

Table 6 Peak responses of slab of the models

Models	Tensile stress (MPa)	Compressive stress (MPa)	Shear stress (MPa)
A1	2.14	−2.09	0.51
A2	2.15	−2.09	0.52
A3	2.14	−2.09	0.51
A4	2.15	−2.09	0.52
B1	2.14	−2.09	0.51
B2	2.15	−2.09	0.52
B3	2.14	−2.09	0.51
B4	2.15	−2.09	0.52
C1	2.14	−2.09	0.51
C2	2.15	−2.09	0.52
C3	2.14	−2.09	0.51
C4	2.15	−2.09	0.52

3.4 Peak Responses in Slabs of the Models

The peak responses in slabs are shown in Table 6. The peak tensile stress of fixed-base model A1 is 2.14 MPa, which is the same in B1 and C1. The maximum peak value out of all models is 2.15 MPa in A2, B2 and C2, which is close to the response of fixed-base models.

The peak compressive stress of fixed-base model A1 is 2.09 MPa, which is the same in all models.

The peak shear stress of fixed-base model A1 is 0.51 MPa, which is the same in B1 and C1. The maximum of peak values out of all models is 0.52 MPa in A2, B2 and C2 models, which is 1.7% higher compared to respective fixed-base models. The increase in peak values of both soil Type-II and Type-III compared to Type-I is 0.6%.

Comparing the peak responses, the maximum tensile, compressive and shear stresses are found in models with walls restrained by soil springs. However, the increase is not significant compared to fixed-base models.

4 Conclusions

The study has been carried out on a four-storeyed load-bearing structural walled building. It has been analyzed with the base of the walls as fixed and supported on stiff, medium and soft soil springs. The structure has also been analyzed considering stepped brick masonry strip footing fixed at base and supported on same springs as used in the structure. Considering the structure to be in seismic zone IV, response spectrum analyses were carried out considering the last mode with 34 Hzs frequency.

The peak values of modal time periods, base shear, joint displacements, normal tensile stresses, normal compressive stresses and shear stresses in walls and slabs have been presented. Following conclusions have been drawn about SSI effects compared to fixed-base analyses:

- There is an increase in the fundamental time period in all SSI systems. The increase in peak values with soil Type-II and Type-III compared to Type-I has computed to 29.8 and 61.0%, respectively. This increase is due to SSI systems getting flexible from soil Type-I to Type-III.
- The maximum base shear is found in the models with foundation restrained by soil springs. The increase in peak values with soil Type-II and Type-III compared to Type-I is the same as a value of 16.4% in X-direction due to higher spectral acceleration in the models. In Y-direction, there is no increase in peak values with soil Type-II and Type-III compared to Type-I due to unchanged spectral acceleration.
- In general, the displacements have increased in SSI systems. The percentage increases in peak values with soil Type-II and Type-III compared to Type-I are 70.1 and 148.5 in X, 53.7 and 123.7 in Y and 53.2 and 134.2 in Z-directions, respectively. The increase is more pronounced in X-direction. This increase is due to SSI systems getting flexible from soil Type-I to Type-III.
- It is found that models with foundations restrained by soil springs have maximum tensile, compressive stresses and shear stresses in walls. The increases in peak values of tensile stresses with soil Type-II and Type-III compared to Type-I are 44.1 and 102.6%, respectively. The increases in peak values of compressive stresses with soil Type-II and Type-III compared to Type-I are 23.5 and 52.7%, respectively. The increases in peak values of shear stresses with soil Type-II and Type-III compared to Type-I are 78.5 and 175.7%, respectively. This increase is due to higher base shear in the models.
- Comparing the peak responses in slabs, the maximum tensile, compressive and shear stresses are found in models with walls restrained by soil springs. However, the increase is not significant compared to fixed-base models.

Thus, the study infers that SSI models having foundation restrained by soil springs respond to maximum tensile, compressive and shear stresses in walls which is significant. In the case of slabs, the maximum tensile, compressive and shear stresses are found in SSI models with walls restrained by soil springs but it is not significant.

Acknowledgements The authors are highly grateful to Director CSIR-Central Building Research Institute, Roorkee, for providing all kinds of support to carry out the study and submit it to the conference for publication.

References

1. Roesset JM (2013) Soil structure interaction: the early stages. Appl Sci Eng 16(1):1–8
2. Kausel E (2010) Early history of soil-structure interaction. Soil Dyn Earthq Eng 30(9):822–832
3. Yashinsky M (1998) The Loma Prieta, California, earthquake of October 17, 1989—highway systems. Professional paper 1552-B. U.S. Geological Survey
4. Mylonakis G, Gazetas G (2000) Seismic soil-structure interaction: beneficial or detrimental? J Earthq Eng 4:377–401
5. Badry P, Satyam N (2017) Seismic soil structure interaction analysis for asymmetrical buildings supported on piled raft for the 2015 Nepal earthquake. J Asian Earth Sci 133:102–113
6. Anand V, Satish SR (2018) Seismic soil-structure interaction: a state-of-the-art. J Struct 16:317–326
7. Ciampoli M, Pinto PE (1995) Effects of soil-structure interaction on inelastic seismic response of bridge piers. J Struct Eng 121(5):806–814
8. Nguyen QV, Fatahi B, Hokmabadi AS (2016) The effects of foundation size on the seismic performance of buildings considering the soil-foundation-structure interaction. Struct Eng Mech 58(6):1045–1075
9. Nguyen QV, Fatahi B, Hokmabadi AS (2017) Influence of size and load-bearing mechanism of piles on seismic performance of buildings considering soil-pile-structure interaction. Int J Geomech 17(7):04017007
10. Raychowdhury P (2011) Seismic response of low-rise steel moment-resisting frame buildings incorporating nonlinear SSI. Eng Struct 33(3):958–967
11. Jarernprasert S, Bazan-Zurita E, Bielak J (2013) Seismic soil-structure interaction response of inelastic structures. Soil Dyn Earthq Eng 47:132–143
12. Aydemir ME (2013) Soil structure interaction effects on structural parameters for stiffness degrading systems built on soft soil sites. Struct Eng Mech 45(5):655–676
13. Dutta SC, Roy R (2002) A critical review on idealization and modelling for interaction among soil-foundation-structure system. Comput Struct 80:1579–1594
14. Vaseghiamiri S, Mahsuli M, Ghannad MA, Zareian F (2020) Probabilistic approach to account for soil-structure interaction in seismic design of building structures. J Struct Eng 146(9):04020184
15. National Building Code of India (2016) Bureau of Indian Standards
16. Kaushik HB, Rai DC, Jain SK (2007) Stress-strain characteristics of clay brick masonry under uniaxial compression. J Mater Civil Eng 19(9):728–739
17. IS 1893 (2016) Criteria for earthquake resistant design of structures. Bureau of Indian Standards

Seismic Effect on Underground Box Structure for Metro and Subways with Varying Soil Parameters

Chiranjib Sarkar, Sibapriya Mukherjee, and Narayan Roy

Abstract With the advancement in technology, urban transportation systems have been modernized with the construction of underground structures due to restricted movements and inadequate space. Many cities already have or plan to construct underground box structures for metros and subways. These structures may undergo severe damages caused by excessive deformation due to seismic shaking. Hence, it is necessary to have an accurate estimation of deformation and bending moment caused by the movement of the surrounding soil under seismic conditions. In the present investigation, an attempt has been made to carry out a parametric study for a typical box structure 9.6 m wide × 5.8 m high with varying soil parameters from loose to medium, medium to dense and very dense in different seismic zones. The results of the study reveal that about 16–26% of the variation in distortion and 8–12% of the variation in bending moment occur with different subsoil conditions (loose to medium, medium to dense and very dense) under the same seismic conditions. Once seismic conditions change from lower to higher seismic zone (zone-III to zone-IV), the deformation becomes almost double even for the same soil condition (loose to medium or medium to dense or very dense). The findings of the present study may be useful in the design of underground subways and metro box structures for practicing engineers.

Keywords Underground structure · Metro and subways · Seismic excitation

1 Introduction

With the rapid development in human societies and complexity of urban transportations, the construction of the underground structure is gaining popularity for transportation and other utilities due to the restrictions in transportation movement as

C. Sarkar (✉)
AECOM India Pvt Ltd, New Town, Kolkata 700156, India
e-mail: chiranjib.sarkar@aecom.com

S. Mukherjee · N. Roy
Civil Engineering Department, Jadavpur University, Kolkata 700032, India

T. G. Sitharam et al. (eds.), *Earthquakes and Structures*, Lecture Notes in Civil Engineering 188, https://doi.org/10.1007/978-981-16-5673-6_27

well as the limitation in the expansion of surface infrastructure. The underground tunneling and subway system are playing a vital role in improving the urban space congestion problem as well as sustainable development of the concerned locations. Almost every developing city already has or plans to construct underground structures for metros, subways, other utilities, etc. The increasing need in very recent years to expand the transportation networks is the main cause of studying the vulnerability of such underground structures due to seismic loading. It is imperative to fully examine the performance of these structures against natural hazards, like earthquakes, because of their importance for saving life and the economy.

The seismic design of underground structures has not received adequate attention in the past because they usually suffer lesser damage in comparison to the above-ground structures from earthquakes. However, Daikai underground subway station in Kobe, Japan, collapsed during the Hyogo-ken-Nambu earthquake in 1995. This event has been reported as the first modern underground structure failure due to seismic loading, rather than surrounding ground instability [1]. There are many more instances of severe damages due to earthquakes which have been reported in the recent literature. Significant among them are as follows: Loma Prieta earthquake in 1989; Kobe earthquake in 1995; the Duzce earthquake in 1999; the Chi-Chi earthquake in 1999; the Niigata earthquake in 2004; the Wenchuan earthquake in 2008; Tohoku earthquake in 2011. Therefore, it is very important to have an accurate estimation of deformation generated by the surrounding soil of underground structures under seismic loading conditions.

The seismic response of underground structures is considerably different from that of above-ground structures because the overall mass of the structure is generally less in comparison to the mass of the surrounding soil, and the overall confinement provides a high level of damping. Therefore, the seismic behavior of an underground structure is principally controlled by the response of the surrounding soil [1, 5] (Arango 2008) and by the imposed ground deformation, but not by the inertial characteristics of the hulk structure itself.

Underground structures are generally affected by earthquakes in two ways: (1) ground shaking and (2) ground failure through mechanisms such as liquefaction, slope instability and fault dislocation. Ground shaking basically refers to the deformation of the ground generated by seismic waves propagating through the earth's crust.

Owen and Scholl (1981) express that ground shaking mostly lead to three different types of deformation in underground structures: (1) axial compression and extension; (2) longitudinal bending and (3) ovaling/racking. The ovaling and racking deformations in the tunnel occur when shear waves propagate normal to nearly normal to the tunnel axis, resulting in the cross-section of a tunnel to deform. Transverse shear waves transmit the highest proportion of an earthquake's energy to underground box structures [1]. Therefore, racking deformations of an underground box structure produced by transverse shear waves are the type of deformation considered in this study.

This study highlights the behavior of underground box structures in different surrounding soil parameters under the same and different seismic conditions. A series

of parametric studies is carried out by developing the numerical model compared with available analytical solutions. A typical box structure 9.6 m wide × 5.8 m high having 5.8 m backfill is resting on varying soil parameters of (a) loose to medium, (b) medium to dense and (c) very dense at different seismic levels of seismic zone-III and zone-IV. Along with the analytical method, a detailed analysis has been performed by using STAAD.Pro [8] to investigate the complex behavior of underground box structures in similar and different soils under different seismic conditions. The outcome of the present analyses may help in the proper prediction of stresses and deformations of structure within the surrounding soil under seismic conditions.

2 Methodology

This paper estimates the seismic behavior of a box tunnel structure adopting Free-Field deformation/Racking analysis.

2.1 Mathematical Background

The term 'free-field deformations' defines ground strains produced by seismic waves in the absence of structures or excavations which generally ignores the interaction between the underground box structure and the surrounding ground but can deliver a first-order estimate of the expected deformation of the structure. Combined axial and curvature deformations can be estimated by treating the tunnel structure as an elastic beam. With beam theory, total free-field axial strains are found by adding the longitudinal strains generated by axial and bending deformation [1].

Racking deformation of rectangular tunnels is generated due to shear distortions during an earthquake. A rectangular box structure undergoes transverse racking deformations which can be computed from shear strains in the soil from Eq. (1).

2.2 Numerical Analysis and Computational Method

The expected free-field ground strains produced by the vertically propagating shear waves of the design earthquakes have been estimated using the following formula:

$$\gamma_{max} = V_s/C_{se} \tag{1}$$

where

γ_{max} = maximum free-field shear strain at the elevation of the tunnel,
V_s = S-wave peak particle velocity at the tunnel elevation and

C_{se} = effective shear wave velocity of ground surrounding the tunnel.

The seismic effect on the underground structure is determined from the racking force required to generate the deflection estimated with respect to the surrounding ground strain. A series of parametric studies for similar and different ground conditions under different seismic levels is carried out to assess the racking forces from numerical analysis followed by the comparison of the results found. The soil-structure interaction is considered by assigning linear springs with stiffnesses based on the modulus of subgrade reaction as per IS: 2950 (Part I) [9].

3 Model of the Study

A typical section of the Delhi Metro Rail Corporation (DMRC) Box tunnel in the Dwarka-Najafgarh corridor has been considered for analysis. This section is in the Najafgarh area which is constructed in Phase-III of the work of DMRC. This typical box structure as shown in Fig. 1 has the same geometrical parameters as considered in this study. Cut and cover method of construction with diaphragm wall has been considered as part of earth retaining structure as well as the main structure. Ground soil condition up to the depth of tunnel was varying mostly from loose silty fine sand to medium and dense sand at different stretches of tunnel alignment. Delhi lies in zone-IV of the earthquake zoning maps of India as per IS 1893 [10].

A similar type of section of Lucknow Metro Rail Corporation (LMRC) Box tunnel in North–South corridor from CCS Airport to Munshipulia has been further considered for analysis. Shape, size, depth and surrounding ground condition (mostly silty sand to tunnel depth) of underground box structures of above-mentioned two locations are mostly similar except Lucknow which lies in zone-III of the earthquake zoning maps of India.

The parametric study was initially conceptualized by comparing the bending moment and deformation of the same type of underground box section situated at the similar ground condition of Delhi (zone-IV) and Lucknow (zone-III). This study has been further elaborated with varying soil parameters mostly from loose silty fine sand to medium and dense sand at different stretches of tunnel alignment of the study area at Najafgarh, Delhi (zone-IV) and CCS Airport, Lucknow (zone-III). The following three types of ground conditions have been considered for the present analysis:

- Ground condition-I (GC-I): Loose to medium silty fine sand from ground level to the depth of 15.0 m below ground level.
- Ground condition-II (GC-II): Medium to dense silty sand from 3.0 m below ground level to the depth of 15.0 m below ground level. Top 3.0 m soil is with loose silty fine sand.
- Ground condition-III (GC-III): Very dense sand from 5.5 m below ground level to the depth of 15.0 m below ground level. Top 5.5 m soil is with loose to medium silty fine sand.

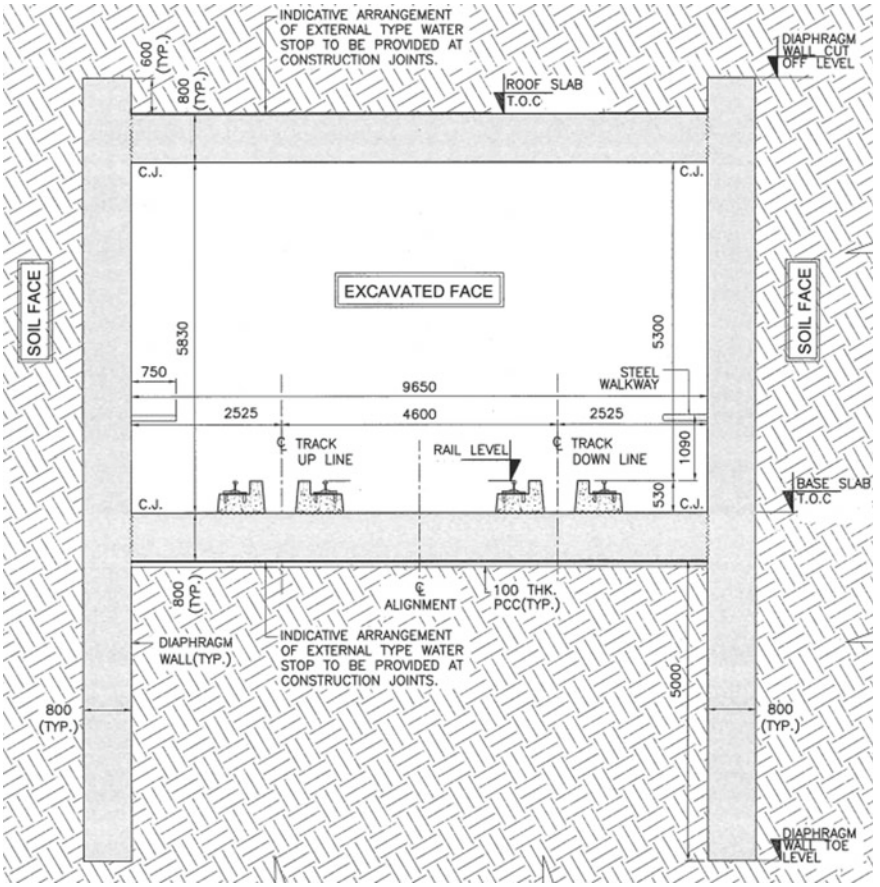

Fig. 1 A typical section of Delhi Metro Rail Corporation (DMRC) box tunnel in the Dwarka-Najafgarh corridor

Geotechnical parameters which are considered for present analysis are tabulated in Table 1 for the above three ground conditions.

During soil investigation, the actual water table was found 18 m below ground level. Also, the water level was not encountered during the excavation of the cut and cover box structure. Hence, the entire domain of soil has been considered as dry soil during analysis. The cohesion of Delhi and Lucknow silt has been taken as zero (cohesionless silt).

The entire analysis part of the parametric study has been conducted in six different situations for three different ground conditions (GC-I, GC-II and GC-III) within two different seismic zones (zone-III and zone-IV). The different soil parameters with different seismic levels cause the change in force application and deformation behavior of the concerned structure.

Table 1 Geotechnical parameters for three types of ground conditions

Ground condition	Soil type	Depth, m	SPT value (Avg.)	Φ′ (Avg.), deg	Bulk density (Avg.), kN/m^3	E′ (Avg.), MPa	ν′ (Avg.)
GC-I	Loose to medium silty fine sand	0–15	20	29	19.0	14.0	0.3
GC-II	Loose silty fine sand	0–3	10	28	18.0	12.0	0.3
	Medium to dense silty sand	3–15	35	32	19.5	15.0	0.3
GC-III	Loose to medium silty fine sand	0–5.5	20	29	19.0	14.0	0.3
	Very dense sand	5.5–15	50	35	20.0	17.5	0.3

The vertical surcharge and lateral earth pressure have been calculated based on adopted soil parameters of different ground conditions and the same have been applied on the numerical models with the appropriate load combinations.

4 Results and Discussions

The outcomes of the conducted study are as follows:

4.1 Racking Deformation Under Different Surrounding Soil and Seismic Conditions

Racking deformation of underground box structure for three different ground conditions (GC-I, GC-II and GC-III) having two different seismic zones (zone-III and zone-IV) is shown in Table 2.

From the above-mentioned free-field deflection values, it is observed that racking deformation gradually decreases with the improvement of surrounding ground conditions. For seismic zone-III, the racking deformation value reduces from 4.914 to 3.884 mm and from 3.884 to 3.344 mm with the improvement of ground conditions

Table 2 Racking deformation of underground box structure under different ground and seismic conditions

Ground condition	Soil type	Free-field deflection (MCE condition), mm	
		Seismic zone-III	Seismic zone-IV
GC-I	Loose to medium silty fine sand	4.914	10.481
GC-II	Medium to dense silty sand	3.884	8.286
GC-III	Very dense sand	3.344	7.133

from GC-I to GC-II and from GC-II to GC-III, respectively. Similarly, for seismic zone-IV, the racking deformation value reduces from 10.481 to 8.286 mm and from 8.286 to 7.133 mm with the improvement of ground conditions from GC-I to GC-II and from GC-II to GC-III, respectively. It is also further observed that racking deformation values increase noticeably once seismic condition changes from lower to higher seismic zone (zone-III to zone-IV) even for the same soil condition (GC-I, GC-II or GC-III).

4.2 Bending Moment Comparison of Underground Box Wall Under Different Surrounding Ground and Seismic Conditions

Bending moment comparison of underground box structure wall for three different ground conditions (GC-I, GC-II and GC-III) having different seismic conditions (non-seismic case and seismic zone-III and zone-IV) are shown in Tables 3, 4 and 5.

From the above-mentioned Bending Moment values at the Box Tunnel wall, it is noticed that the Bending Moment of the wall gradually decreases with the improvement of surrounding ground conditions within the same seismic level (non-seismic

Table 3 Bending moment comparison of underground box wall under different ground conditions with non-seismic condition

Ground condition	Soil type	Bending moment of underground box wall, kN m		
		At roof slab junction (hogging)	At midpoint of wall (sagging)	At base slab junction (hogging)
GC-I	Loose to medium silty fine sand	1552.5	−207.2	251
GC-II	Medium to dense silty sand	1547.5	−168.4	230
GC-III	Very dense sand	1543.2	−130.1	192

Table 4 Bending moment comparison of underground box wall under different ground conditions within seismic zone-III

Ground condition	Soil type	Bending moment of underground box wall, kN m		
		At roof slab junction (hogging)	At midpoint of wall (sagging)	At base slab junction (hogging)
GC-I	Loose to medium silty fine sand	1739.1	−222.5	350
GC-II	Medium to dense silty sand	1699.1	−178.8	298
GC-III	Very dense sand	1676.8	−136.5	255.4

Table 5 Bending moment comparison of underground box wall under different ground conditions within seismic zone-IV

Ground condition	Soil type	Bending moment of underground box wall, kN m		
		At roof slab junction (hogging)	At midpoint of wall (sagging)	At base slab junction (hogging)
GC-I	Loose to medium silty fine sand	1852.6	−232.7	512.9
GC-II	Medium to dense silty sand	1792.9	−198.4	421.2
GC-III	Very dense sand	1757.6	−156.3	359.5

case and seismic zone-III and zone-IV). With the improvement of surrounding ground conditions within the same seismic level, bending moment of wall reduces by 1–4% at Roof Slab Junction location, 17–31% at the midpoint of wall and 17–22% at Base Slab Junction. It is also further observed that Bending Moment values of the wall increase significantly once the seismic condition changes from lower to higher seismic zone (zone-III to zone-IV) even for the same soil condition (GC-I, GC-II or GC-III). With the changes of seismic level from non-seismic condition to Seismic zone-III and IV, bending moment of the wall is increased by 5–11% at Roof Slab Junction location, 5–13% at the Midpoint of wall and 23–32% at Base Slab Junction. Comparison of Bending moment is shown in Fig. 2 for different surrounding ground and Seismic Conditions.

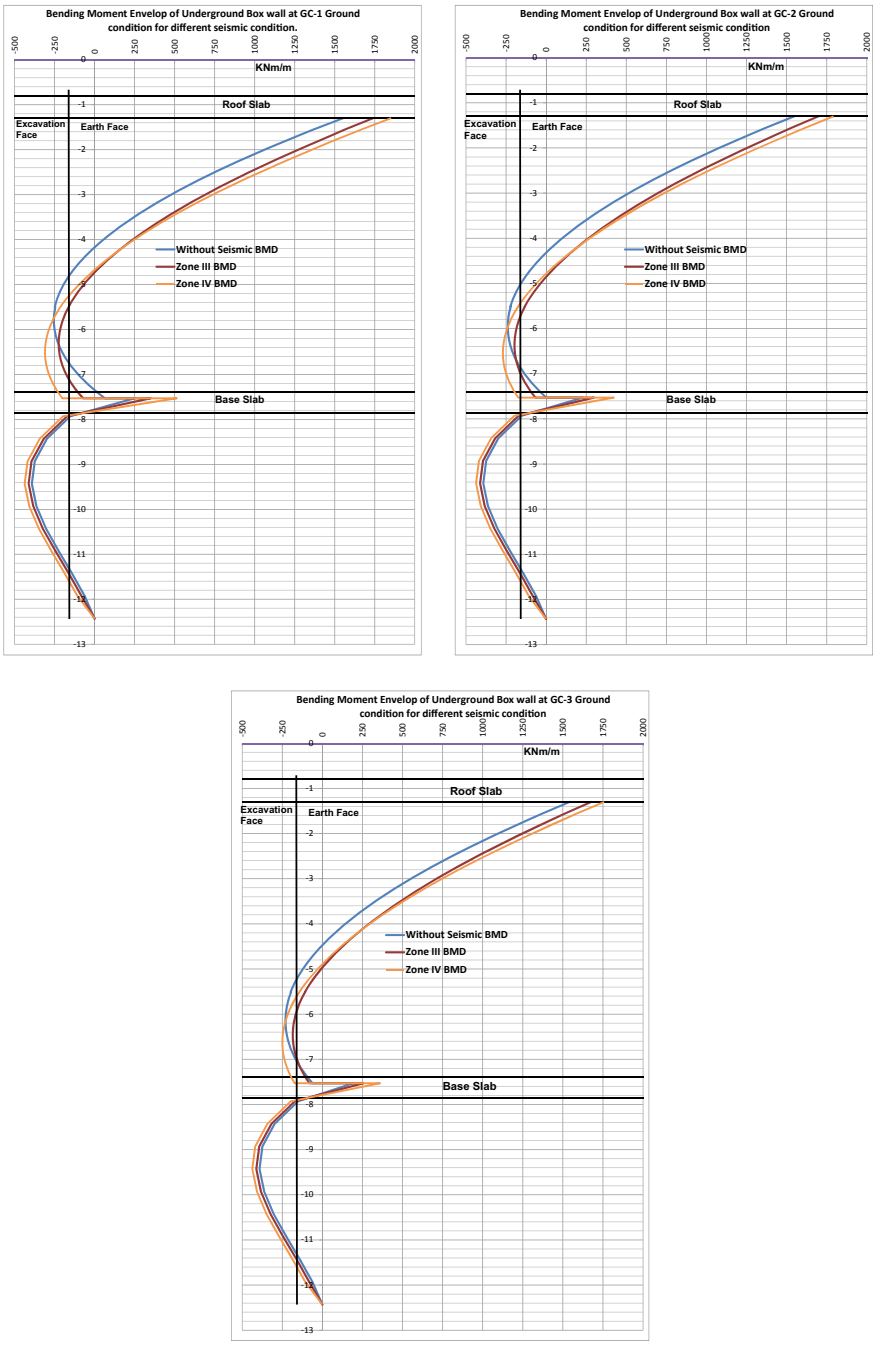

Fig. 2 Comparison of bending moment in underground box wall under different surrounding ground and seismic conditions

Table 6 Bending moment comparison of underground box structure roof slab under different ground and seismic conditions

Ground condition	Soil type	Bending moment of underground box roof slab at wall junction location, kN m		
		Non-seismic condition	Seismic zone-III	Seismic zone-IV
GC-I	Loose to medium silty fine sand	1320.2	1483.9	1603.2
GC-II	Medium to dense silty sand	1304.9	1435.9	1534.5
GC-III	Very dense sand	1290.8	1406.6	1491.3

4.3 Bending Moment Comparison of Underground Box Roof Slab Under Different Surrounding Ground and Seismic Conditions

Bending moment comparison of underground box structure roof slab for three different ground conditions (GC-I, GC-II and GC-III) within different seismic conditions (non-seismic case and seismic zone-III and zone-IV) are shown in Table 6.

From the Bending Moment values mentioned in Table 6, it is observed that the Bending Moment of the Roof Slab at the wall junction gradually decreases with the improvement of surrounding ground conditions within the same seismic level (non-seismic case and seismic zone-III and zone-IV). With the improvement of surrounding ground conditions within the same seismic zone, the bending moment of the Roof Slab is reduced by 1–5%. It is also further observed that Bending Moment values of the Roof Slab increase significantly once the seismic condition changes from lower to higher seismic zone (zone-III to zone-IV) even for the same soil condition (GC-I, GC-II or GC-III). With the changes of seismic level from non-seismic condition to seismic zone-III and IV, bending moment of Roof Slab at wall junction is increased by 6–12%.

4.4 Bending Moment Comparison of Underground Box Base Slab Under Different Surrounding Ground and Seismic Conditions

Bending moment comparison of underground box structure Base slab for three different ground conditions (GC-I, GC-II and GC-III) within different seismic conditions (non-seismic case and seismic zone-III and zone-IV) is shown in Table 7.

From the Bending Moment values mentioned in Table 7, it is noticed that the Bending Moment of Base Slab at the wall junction gradually decreases with

Table 7 Bending moment comparison of underground box structure base slab under different ground and seismic conditions

Ground condition	Soil type	Bending moment of underground box base slab at wall junction location, kN m		
		Non-seismic condition	Seismic zone-III	Seismic zone-IV
GC-I	Loose to medium silty fine sand	331.8	444.2	610.7
GC-II	Medium to dense silty sand	245	411.8	542.4
GC-III	Very dense sand	185	395.6	503.5

the improvement of surrounding ground conditions within the same seismic level (non-seismic case and seismic zone-III and zone-IV). With the improvement of surrounding ground conditions within the same seismic zone, the bending moment of the Base Slab is reduced by 4–13%. It is also further observed that Bending Moment values of the Base Slab increase significantly once the seismic condition changes from lower to higher seismic zone (zone-III to zone-IV) even for the same soil condition (GC-I, GC-II or GC-III). With the changes of seismic level from non-seismic condition to Seismic zone-III and IV, bending moment of Base Slab at wall junction is increased by 25–38%.

5 Conclusions

In the current study, the behavior of underground box structure placed on varying soil parameters under different seismic loading conditions has been studied. A series of parametric studies was carried out to examine the soil and tunnel interface under the same and different soil conditions with different seismic conditions. From the present study, the following conclusions may be drawn:

- Deformation caused by surrounding ground gradually decreases with the improvement of surrounding ground conditions. Racking deformation value reduced by 16–26% with the improvement of ground condition. With the improvement of ground condition from GC-I (Loose to medium silty fine sand) to GC-II (Medium to dense silty sand) and from GC-II (Medium to dense silty sand) to GC-III (Very dense sand), racking deformation value reduced by 26 and 16%, respectively. Racking deformation values increase noticeably once the seismic condition changes from lower to higher seismic zone even for the same soil condition (GC-I, GC-II or GC-III). With the increase in seismic level from zone-III to zone-IV, racking deformation is increased by 113% in the same soil condition.
- Bending Moment values of the Underground Box wall gradually decrease with the improvement of surrounding ground conditions within the same seismic level.

However, the decrease of Bending Moment of the Underground Box structure wall is not uniform throughout the wall. It is different at different points of the Underground Box structure wall. With the improvement of surrounding ground conditions within the same seismic level, bending moment of the wall is reduced by 1–4% at wall-roof slab Junction location, 17–31% at wall midpoint and 17–22% at wall-base slab Junction location.

- Once seismic condition changes from lower to higher seismic zone even for same soil condition (GC-I, GC-II or GC-III), Bending Moment values of wall increase significantly. However, this increase of Bending Moment of Underground Box structure wall is also not uniform throughout the wall. With the changes of seismic level from lower to higher, bending moment of the wall is increased by 5–11% at Roof Slab Junction location, 5–13% at Midpoint of wall and 23–32% at Base Slab Junction.
- With the improvement of surrounding ground conditions within the same seismic zone, the bending moment of Roof Slab at wall junction location is reduced by 1–5%.
- Bending Moment values of Underground Box structure Roof Slab increase significantly once seismic condition changes from lower to higher seismic zone even for same soil condition (GC-I, GC-II or GC-III). With the changes of seismic level from zone-III to zone-IV, the bending moment of Roof Slab at wall junction is increased by 6–12%.
- Bending Moment of Underground Box structure Base Slab gradually decreases with the improvement of surrounding ground conditions within the same seismic level (Seismic zone-III, zone-IV or non-seismic case). With the improvement of surrounding ground conditions within the same seismic zone, the bending moment of Base Slab at wall junction location is reduced by 4–13%.
- Once seismic condition changes from lower to higher seismic zone even for same soil condition (GC-I, GC-II or GC-III), Bending Moment values of Base Slab increase significantly. With the changes of seismic level from lower to higher seismic, bending moment of Base Slab at wall junction is increased by 25–38%.

References

1. Hashash YMA, Hook JJ, Schmidt B, Yao JIC (2001) Seismic design and analysis of underground structures. Tunnel Underground Space Technol 16:247–293
2. Patil M, Choudhury D, Ranjith PG, Zhao J (2018) Behavior of shallow tunnel in soft soil under seismic conditions. Tunnel Underground Space Technol 82:30–38
3. Gillis KM (2015) Seismic response of shallow underground structures in dense urban environments
4. Delhi Metro Railway Corporation, Technical Specification: DMRC out line design specification for underground structure
5. Wang (Joe) JN (1993) Seismic design of tunnels. Parsons Brinckerhoff Quade & Douglas, Inc.
6. Pitilakis K, Tsinidis G (2014) Performance and seismic design of underground structures. https://doi.org/10.1007/978-3-319-03182-8_11

7. Sivarajan (2016) Seismic load considerations in the design of underground structures for hydropower projects in the Himalayan Region. In: Recent advances in rock engineering (RARE 2016)
8. STAAD.Pro V8i (SELECT Series 6) 20.07.11.33
9. IS: 2950 (Part I) (1981) Code of practice for design and construction of raft foundations, Part 1: design
10. IS: 1893 (Part I) (2016) Criteria for earthquake resistant design of structures

Analysis of Lateral Loads on Piles Supporting Liquid Storage Tanks

Akhila Manne, P. V. S. R. Prasad, and Madan Kumar Annam

Abstract Liquid storage tanks are usually located in nearshore or coastal regions with soil profiles containing thick layers of compressible soils. These storage tanks are usually of large diameter up to 90 m and carry high loads, and the tanks are often placed on heavy foundations such as piles. Piles supporting such tanks are to be designed for high lateral loads due to wind and earthquake, and any damage to storage tanks with highly inflammable liquids leads to disastrous conditions (Niigata and Alaska, 1964; 2011 Tohoku), etc. Performance of piles in liquefying ground under earthquake loading has been extensively studied; however, seismic behavior of piles in very soft clays has received relatively less attention, especially on their lateral capacity. The design of laterally loaded piles due to soil movement relies on several theoretical and numerical approaches. The subgrade reaction method (IS 2911 Part-1/Sect. 2: 2010) is most widely used for the design of laterally loaded piles in India and using this method, estimation of the magnitude of soil movement with reasonable confidence and accuracy is difficult. This paper discusses the analysis of lateral load on piles supporting storage tanks using the subgrade reaction method and load-deflection curves (p–y). The scope of this paper is limited to analysis using these methods. The results of the study indicate that the maximum bending moment in the piles that occurred during the earthquake using 3D FEM analysis is comparable to their moment capacities.

Keywords Piles · Seismic load · Storage tanks · LPILE · PLAXIS 3D

1 Introduction

Pile foundations are designed to transfer vertical, lateral and torsional loads from the superstructure to the bearing stratum. The design engineer considers factors involving both performance of the foundation to support loading and the costs and methods of construction for different types of foundations. The behavior of a pile

A. Manne (✉) · P. V. S. R. Prasad · M. K. Annam
Keller Ground Engineering (India) Pvt. Ltd., Kodambakkam, Chennai 600024, India
e-mail: akhila@kellerindia.com

T. G. Sitharam et al. (eds.), *Earthquakes and Structures*, Lecture Notes in Civil Engineering 188, https://doi.org/10.1007/978-981-16-5673-6_28

under lateral loading is dependent on the soil reaction (resistance) at any point along a pile and it is a function of pile deflection. Pile deflection, on the other hand, is dependent on the soil resistance; therefore, estimating the response of a pile under lateral loading is a soil-structure-interaction problem. Simplified analyses such as the pseudo-static analysis procedure can be examined to understand the behavior of piles under lateral loads. In pseudo-static analysis, a beam spring model is modeled and site investigation data such as the SPT blow count can be used to capture the basic mechanism of pile behavior.

Failure of a pile is either due to excessive bending moment that causes the development of a plastic hinge or due to excessive deflection and in minor cases by the shear failure of the pile. Piles are relatively vulnerable to lateral loads such as those imposed by ground shaking during strong earthquakes. Failures or damage of tanks with an insufficient freeboard or due to sloshing of stored fluids such as oil or chemicals may result in the contamination of the soil or serious disasters. In the case of soil liquefaction, this vulnerability is particularly pronounced since the loss of strength and stiffness in the liquefied soil results in a significant loss of lateral support for the embedded piles (1964 Niigata and 1995 Kobe earthquake).

In this paper, analysis of lateral load on pile foundation supporting storage tanks using IS 2911 (Part-1/Sect.-2): 2010 and load-deformation curves is considered. The scope of this paper is limited to simple calculations, 1D analysis and comparison of same with 3D FEM analysis results.

2 Lateral Load on Tank Foundation

To determine the static/seismic load on the piles, computations are to be made. The determination of seismic load on the foundation of liquid-containing tanks is calculated based on the hydrodynamic force exerted by the liquid on tank walls and based on the impulsive (V_i) and convective (V_c) components. The impulsive or convective component is expressed as $V = C_s \times W$, where C_s is the impulsive/convective base shear coefficient and W is the seismic weight of the impulsive/convective component. The estimation of total lateral load due to earthquake can be arrived at based on the site-specific spectra and API-650 (Annexure-E) [1] or IS 1893 (Part II) [2]. Since tanks have higher utility and damage consequences, codes specify a higher importance factor for liquid-containing tanks, which further increases design seismic forces for tanks.

In this paper, for the analysis and design of piles for lateral loads, a project site located near shore containing thick layers of compressible soils supporting liquid storage tanks (Fig. 1) is considered. The site consists of soft marine clay of 10 m thick followed by hard sandy clay of 7 m thick and highly weathered granitic formation (Fig. 1). The tank is of diameter 41 m $\times$ height 20 m with floating roof for storing inflammable fluids. The base of the tank rests on the pile cap (unanchored) and the pile cap connects all the piles supporting the tank. The total lateral loads due to wind and earthquake are to be estimated for the design of piles supporting the tank.

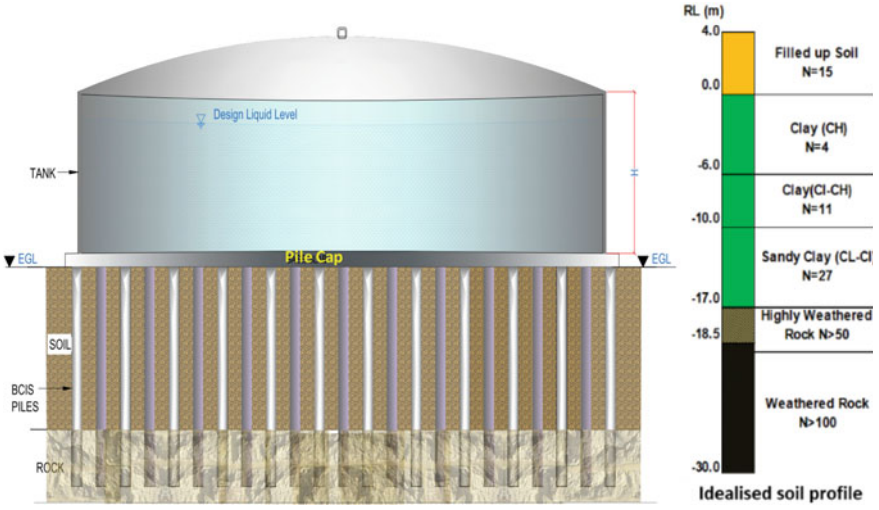

Fig. 1 Schematic of tank foundation and soil profile of the project site

Based on API-650 and site-specific seismic spectra, max. lateral load and maximum moment on the pile foundation are estimated. However, seismic moment shall not be transferred to the tank as it is unanchored support.

Based on the estimated total seismic load, the number of piles/required capacity for each pile is to be derived. However, liquefaction susceptibility of the soil or in this case, susceptibility to 'cyclic failure' of the soil is to be checked and further design is to be continued. IS 1893 (Part-1): 2016 suggests that if there is any presence of a liquefiable layer within the design depth of pile foundation, lateral load on the pile is to be estimated by neglecting the lateral resistance of that specific layer.

3 Preliminary Screening

For the design of the tank foundation, seismic zone III (IS 1893 Part-1: 2016 is considered. To check for any possibility of cyclic failure, Chinese Criteria [3] can be used for the screening of soil for cyclic failure. Seed et al. [4] based on post-earthquake data and laboratory tests revised the criteria. Boulanger and Idriss [5] identified that soils with plastic fines have been found to fail during earthquakes if the liquid limit (LL) is less than 47 and the plasticity index (PI) is less than 20. The soil was assessed as shown in Fig. 2 and does not fall under liquefiable criteria. Therefore, lateral resistance of all soil layers can be considered while estimating the lateral capacity of the pile.

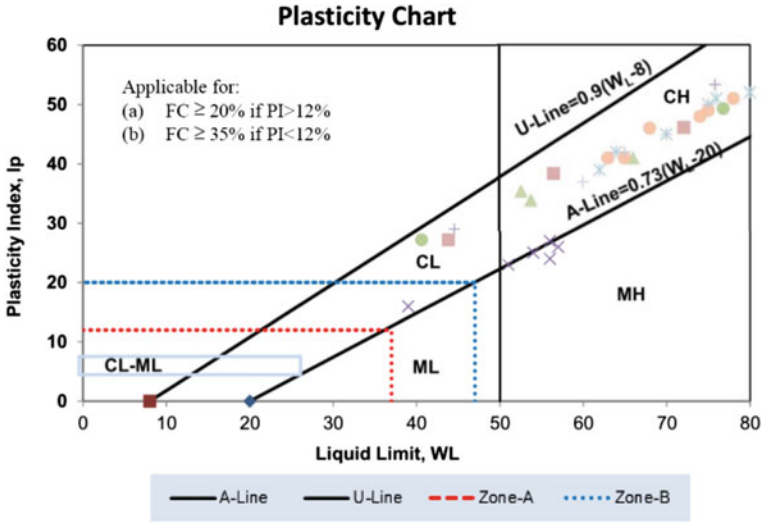

Fig. 2 Check for cyclic failure based on Idriss and Boulanger [5]

4 Static Analysis of Pile

The design of laterally loaded piles due to soil movement relies on several theoretical and numerical approaches. The analysis of a pile under only lateral loading is complex, as mobilized soil reaction varies in proportion to the pile movement, and the pile movement, on the other hand, is dependent on the soil response. This is the basic problem of soil-structure interaction. The subgrade reaction method suggested in IS 2911 (Part-1/Sect. 2) is based on the theory of a beam on an elastic foundation. The theory considers a continuous flexural member with stiffness El supported by infinitely closely spaced independent springs with a single stiffness value 'k'. However, the load-deformation characteristics of soils are not linear, and it is necessary to use the modulus (stiffness/unit deflection) compatible with the deflection of the flexural member. The load-deformation characteristics (p–y curves) were assessed by various researchers from field tests on fully instrumented piles. The static p–y curves can be thought of as backbone curves that can be correlated to some extent with soil properties.

For the project site considered, for the design of piles, single pile analysis using IS method and p–y curves [6] is considered for an 800 mm dia for both fixed and free head conditions. pile. In the IS method, a single spring constant/idealized modulus of subgrade reaction (k_s) of soil is considered for the estimation of lateral loads. Whereas, in LPILE, the load-deformation characteristics for each soil layer are considered based on the established soil models. Soil properties considered in LPILE analysis are listed in Table 1.

To estimate the load-carrying capacity based on the limiting deflection and pile reinforcement based on the bending moment of the pile, analysis is run for various

Table 1 Soil parameters used for the analysis

S. No.	RL (m)		Soil description	SPT N	Unit weight	Cu	φ
	From	To			(kN/m^3)	(kPa)	(deg)
1	4	0	Filled up soil	15	17	–	29
2	0	4	Clay (CH)	4	14.5	20	–
3	−7	−13	Clay (CI–CH)	11	16	20	–
4	−13	−17	Clayey silty sand	27	18.5	135	–
5	−17	−18.5	Highly weathered rock	>60	20	300	–
6	−18.5		Weathered rock	>100	20	600	–

loading conditions and head conditions. A pinned or free head condition assumption usually overestimates the pile head displacement, and based on the pile-pile cap connection in the proposed foundation, for practical purposes, the fixed head condition is accurate. Figures 3 and 4 show the variation in deflection and bending moment along the length of the pile for various head conditions. As predicted, max. pile head deflection and max bending moment in the pile are greater in free head condition compared to fixed head condition.

Apart from LPILE analysis, single pile analysis in free head condition was done to compare the max. deflection and bending moment in free head condition. It is understood that WALLAP [7] underestimates the deflection and bending moment in comparison. Comparison of BM from both the analysis is plotted in Fig. 5. LPILE results in comparison with IS method for both head conditions are shown in Fig. 6.

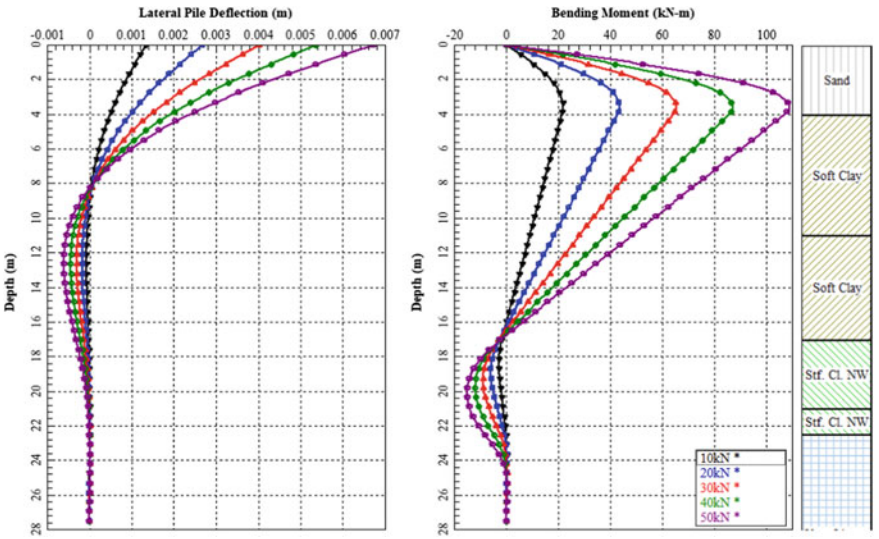

Fig. 3 Deflection and bending moment along the pile length for different lateral loads in free head condition

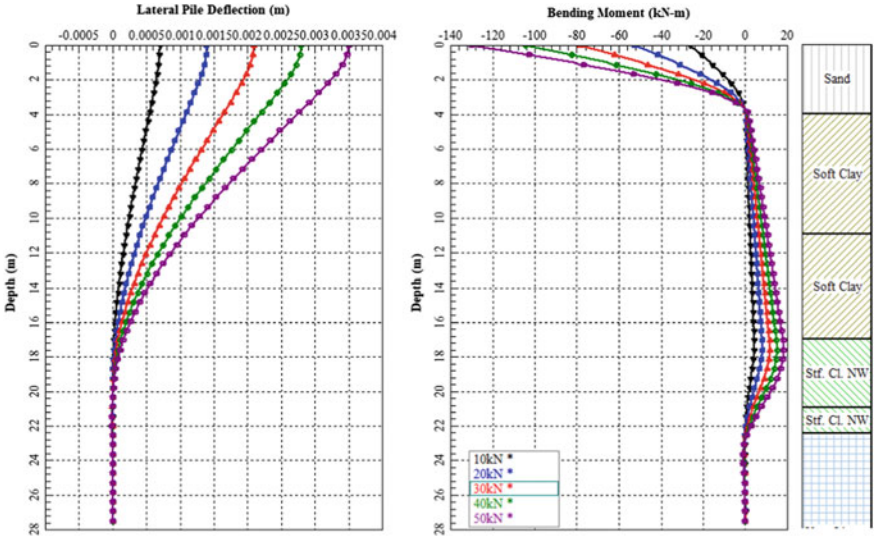

Fig. 4 Deflection and bending moment along the pile length for different lateral loads in fixed head condition

From the pile load tests conducted on piles up to 2.5 × load estimated from IS method revealed that the lateral capacity of piles (Fig. 7) in the free head condition is higher than that of predicted values.

From the estimated total lateral load encountered by tank foundation, lateral capacity and bending moment for a single pile in this section, the total number of piles required to support the tank and minimum reinforcement in the pile are calculated.

5 Dynamic Analysis of Piles Supporting Tank

When the performance of the piles as a group is considered, computation of the distribution of loading, moments and forces to each pile in the pile is to be understood. To estimate these parameters, a 3D seismic response analysis of the piles is to be conducted for which a computer program such as PLAXIS 3D is required. The magnitude of soil movement is difficult to estimate with reasonable confidence and accuracy in the subgrade reaction method.

In the 3D FEM model, in-situ soil condition, piles, pile cap and tank are modeled as shown in Fig. 8. Load due to tank fluid with a density of 8.45 kN/m^3 is considered as 154 kPa for a fluid height of 18.5 m. After rendering the model, site-specific accelerogram is then applied to the base of the underlying bedrock. Load combinations for the analysis are based on Cl.6.3.4 of IS 1893 (Part-1): 2016. In the analysis, unfactored seismic signal is used.

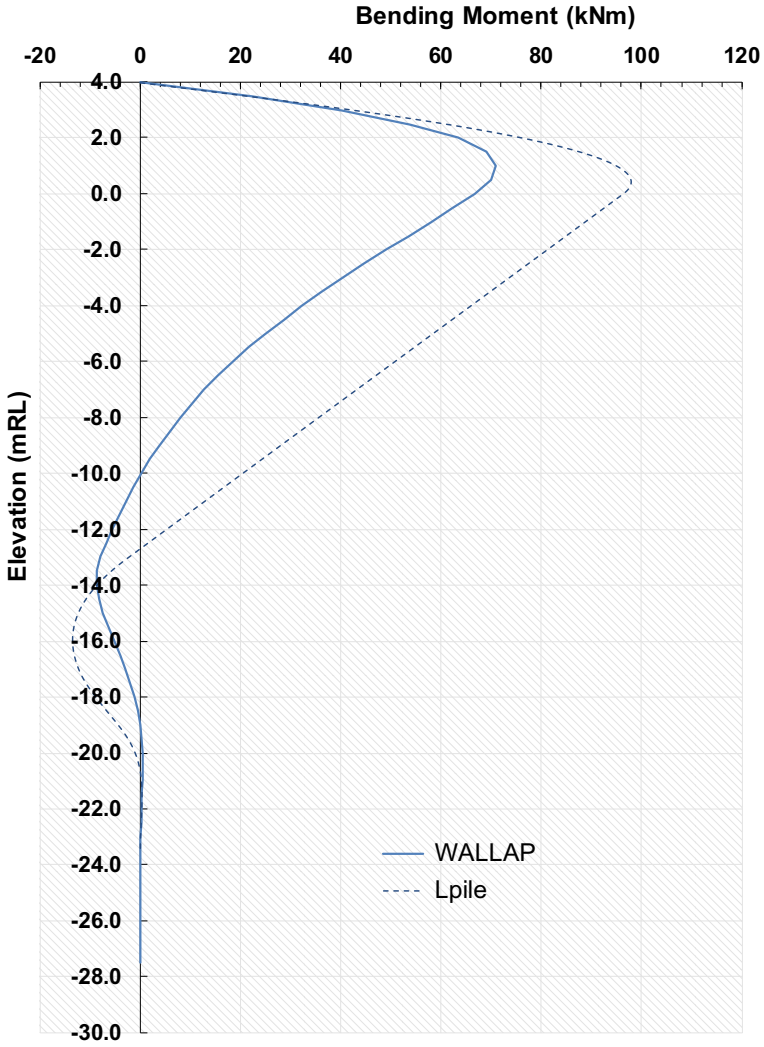

Fig. 5 Comparison of BM from WALLAP and LPILE for free head condition

From the analysis, a maximum transient pile movement of about 142 mm occur momentarily during the earthquake. However, the post-earthquake (at the end of the earthquake) residual pile deflection is only about 18.4 mm in tank full condition. The maximum bending moment during and post-earthquake in the piles is about 375 and 141 kNm. This occurred at the outermost three rows of piles leading and trailing of the earthquake shaking direction only. While the center piles show much less bending moment, the bending moments of the pile that occurred during the earthquakes are comparable to the moment capacity of the pile. The results confirm

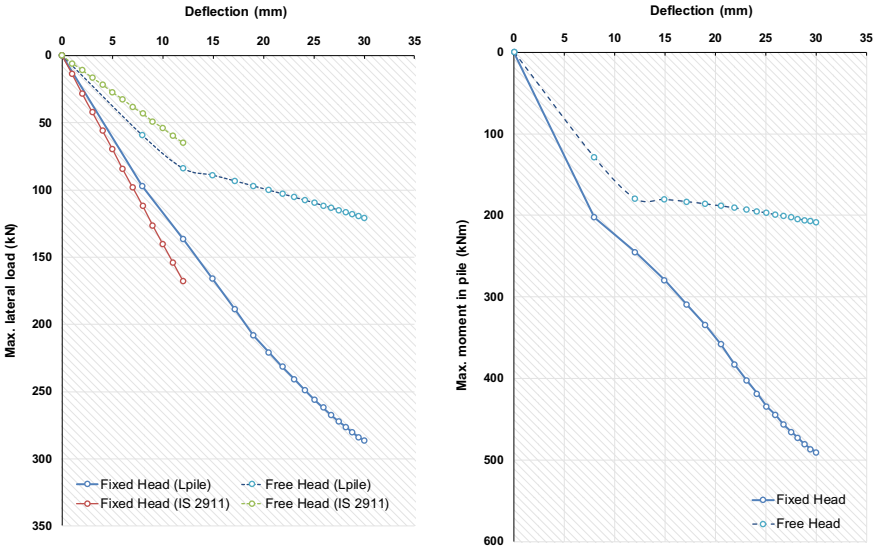

Fig. 6 Deflection and bending moment of the pile for different conditions

that the reinforcement considered based on the analysis using beam on subgrade reaction approach is adequate.

6 Conclusions

Damage to the foundation of the storage tank during an earthquake can be catastrophic. For the design of piles in soft soils supporting storage tanks, analysis is conducted using the subgrade modulus approach. This approach is the basis for IS code methods and for various software for lateral pile analysis. Using IS method and LPILE software, maximum lateral load-carrying capacity and bending moment in the pile are estimated for different pile head conditions. The estimated lateral capacity and bending moment are helpful to arrive at the total number of piles required to support the tank and minimum reinforcement in the pile. Since the sub-soils (clays) are not susceptible to cyclic failure during the earthquake, the total estimated lateral capacity is considered without any reduction.

To check the adequacy of the pile design during the earthquake, 3D PLAXIS analysis is carried out with a site-specific seismic accelerogram. The analysis shows that during the earthquake shaking process and after the earthquake in both the tank full and empty conditions the re-bars provided are sufficient.

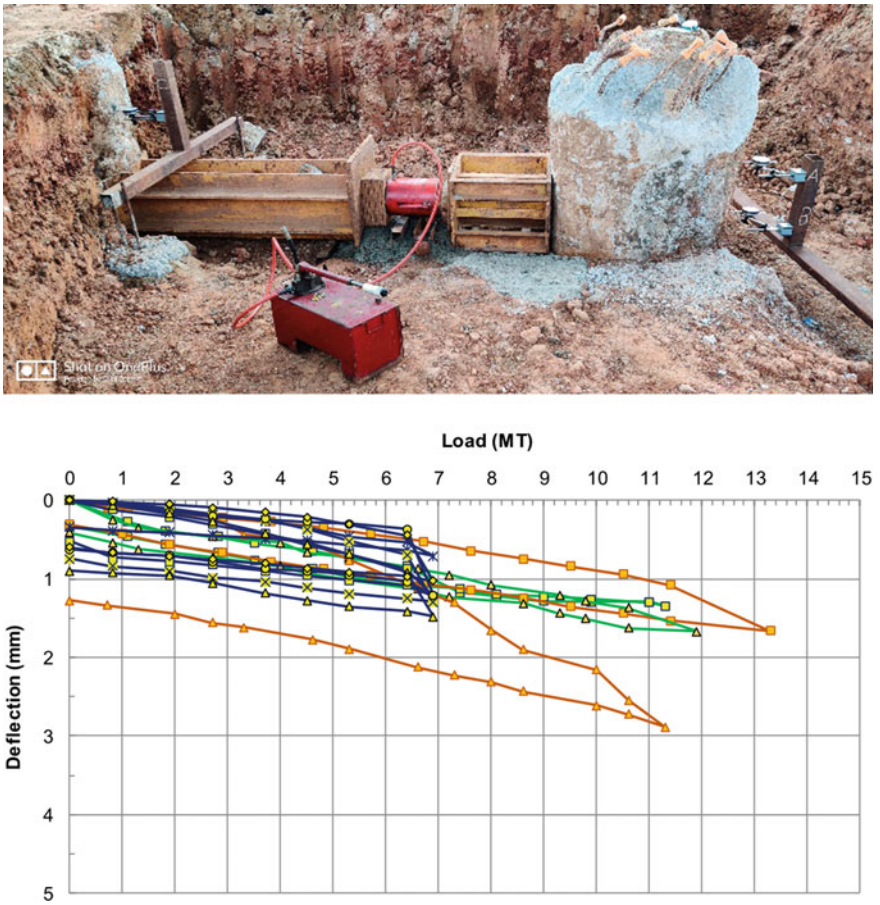

Fig. 7 Pile deflection recorded in in-situ lateral pile load test (free head condition)

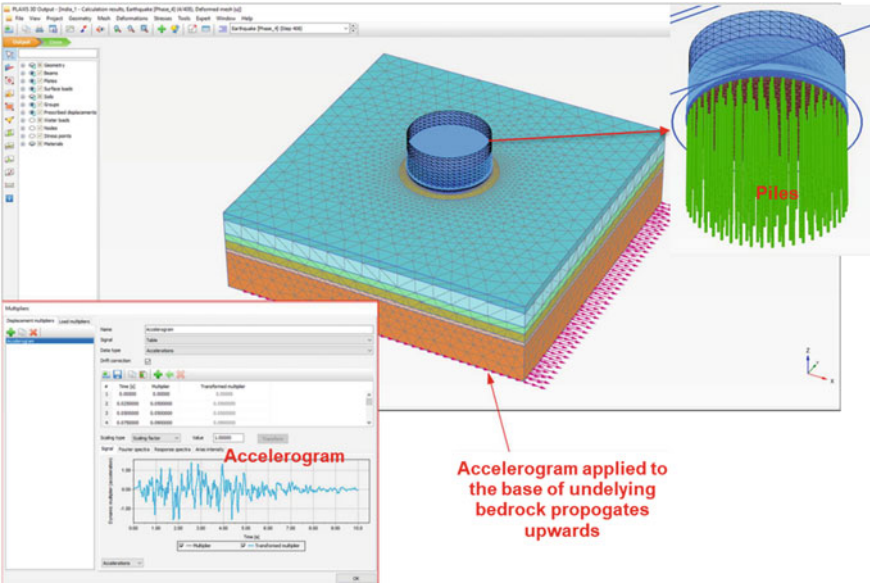

Fig. 8 PLAXIS model and accelerogram used for the analysis

Acknowledgements The authors would like to thank Keller management and other colleagues for their continuous support in the compilation of this paper. Thanks are also due to Keller India site management for providing execution data. The authors wish to thank Dr. Shen Rui Fu for his valuable guidance and suggestions during this study.

References

1. American Petroleum Institute (API) (2012) Welded storage tanks for oil storage, API 650. American Petroleum Institute Standard, Washington, DC
2. IS 1893 (Part-2) (2014) Criteria for earthquake resistant design structures, Part 2. Bureau of Indian Standards, New Delhi, India
3. Seed HB, Idriss IM (1982) Ground motions and soil liquefaction during earthquakes. Earthquake Engineering Research Institute Monograph, Oakland, California
4. Seed RB, Cetin KO, Moss RE, Kammerer AM, Wu J, Pestana JM, Riemer MF, Sancio RB, Bray JD, Kayen RE, Faris A (2003) Recent advances in soil liquefaction engineering: a unified and consistent framework. In: 26th annual ASCE Los Angeles geotechnical spring seminar, Long Beach, CA
5. Boulanger RW, Idriss IM (2004) Evaluating the potential for liquefaction or cyclic failure of silts and clays. Center for Geotechnical Modeling, Davis, CA
6. LPILE (2018) A program to analyze deep foundations under lateral loading. Ensoft, Inc., Austin, Texas
7. WALLAP (2012) Propped, anchored and cantilever retaining wall analysis program. Geosolve, London, UK

Dynamic Response Characteristics of Pile Group Under Axial Harmonic Loading

Shiva Shankar Choudhary, Sanjit Biswas, and Bappaditya Manna

Abstract This study is intended to check the performance of linear and nonlinear theories to determine the dynamic characteristics of the pile supported machine foundations. Forced vibration tests are performed in the field on a 3-pile group having pile length of 3 m and outer diameter of 0.114 m subjected to axial harmonic loading. The dynamic tests are performed for four different eccentric moments under a static load of 12 kN. The frequency-amplitude responses are measured for each eccentric moment. Theoretical study is also performed using both the linear and nonlinear solutions which are based on continuum approach method. The theoretically predicted frequency-amplitude responses are compared with the dynamic field test results for all the eccentric moments. It is found that the predicted responses of the linear solution indicate lower values of the resonant amplitude and much higher values of the resonant frequency as compared to the test results. In the case of nonlinear solution, the predicted dynamic response curves are reasonably well matched with the tests results. Such agreement with the nonlinear analysis results are achieved by considering precise values of boundary zone parameters and soil-pile separation lengths.

Keywords Pile group · Dynamic field test · Axial harmonic loading · Dynamic responses · Continuum approach analysis

S. S. Choudhary (✉)
National Institute of Technology Patna, Bihar 800005, India
e-mail: shiva@nitp.ac.in

S. Biswas
National Institute of Technology Warangal, Telangana 506004, India
e-mail: sbiswas@nitw.ac.in

B. Manna
Indian Institute of Technology Delhi, New Delhi 110016, India
e-mail: bmanna@civil.iitd.ac.in

T. G. Sitharam et al. (eds.), *Earthquakes and Structures*, Lecture Notes in Civil Engineering 188, https://doi.org/10.1007/978-981-16-5673-6_29

1 Introduction

Piles are used as foundations to resists controlled forces such as machinery and vibrating equipment or uncontrolled forces such as earthquake, ocean wave, and wind force. Geotechnical engineers usually face problems associated with the design of pile foundations under dynamic loads because of the complex pile-soil-pile behavior. Pile supported machine foundation behave in a nonlinear fashion with high displacements because of the soil nonlinearity, soil-pile separation, and slippage between pile and soil. Hence, in the case for machine induced harmonic loading, special considerations have to be taken in the analysis and design of pile foundations. To study the complex combined behavior of soil-pile, many researchers [1–3] performed various field tests on piles to determine the dynamic field and theoretical responses under machine induced harmonic loading. Many theoretical investigations have been done in order to predict the dynamic nonlinear response and impedance parameters (stiffness and damping) of the soil-pile system. Elkasabgy and Naggar [4] and Biswas and Manna [5] performed the dynamic field tests on piles and compared the results with the nonlinear theoretical curves obtained using a continuum approach analysis. From the studies, it was observed that the theoretical analysis provided a reasonable estimation of frequency-amplitude response curves as compared to the field test results under dynamic loading. Khalil et al. [6] reveal that the soil-pile analysis based on Novak's approach yields similar trends to those obtained from the finite element model under axial harmonic loading. From the results, it is also observed that the loading frequency has a great impact on the dynamic impedance parameters and the induced amplitudes. It is found from the previous research work that the prediction of boundary zone parameters and separation lengths between pile and soil under harmonic loading is a basic need to predict the nonlinear response of piles which has not been thoroughly investigated so far. It has been also observed that the experimental verification of different theories was rarely studied. Hence, in the current study, behavior of a 3-pile group is investigated and the performance of the linear (without boundary zone) and nonlinear (with boundary zone) continuum method is monitored under machine induced axial harmonic loading.

2 Site Characterization and Location

In the present study, dynamic field tests are performed in between block II and III at the Indian Institute of Technology Delhi campus; New Delhi, India. Different in-situ and laboratory tests are performed to investigate the subsurface soil conditions. Standard penetration test (SPT) tests are conducted and simultaneously disturbed and undisturbed soil samples are collected from the borehole. Different laboratory tests are carried out to characterize the soil properties. It is found based on in-situ and laboratory test results that the soil layers are mainly clayey silt. The measured soil properties of with layers are presented in Table 1.

Table 1 Soil properties at test site

Soil property	Layer 1 (0.0–2.5 m)	Layer 2 (2.5–3.5 m)
Moisture content (%)	9.20	7.52
Bulk density (kN/m^3)	16.74	15.88
LL (%)	33.59	38.30
PL (%)	20.14	23.23
Particle size distribution	Sand—39%, Silt—43%, Clay—18%	Gravel—3%, Sand—36%, Silt—42%, Clay—19%
Shear modulus (kN/m^2)	1.3×10^4	2.3×10^4

3 Axial Harmonic Loading Test

The hollow steel pipes of 3.0 m long (l), 0.114 m outer diameter (d), and 0.003 m thickness (t) is used as pile. These dimensions of the pile are selected for testing because it is intended to use a plie having a standard slenderness ratio ($l/d = 26$) for the study. The piles are embedded into undersize boreholes (made by 0.1 m diameter augur) with the help of tripod and SPT hammer to create good contact between pile and soil. To ensure the end bearing, the bottom end of the pile is closed with steel plate. A pile spacing of $3d$ is maintained during the pile driving.

The harmonic force on pile foundation is generated by a mechanical oscillator. The magnitude of the force is controlled by adjusting the eccentricity (θ) of the rotating masses. The value of generated eccentric moment ($m.e$) can be written as

$$m.e = (W/g).e = [0.9 \sin(\theta/2)]/g\text{N sec}^2 \quad (1)$$

where W and m are the weight and mass of eccentric rotating parts, respectively. e = eccentric distance of the rotating masses, g = acceleration due to gravity.

A steel pile cap is placed on the top of the pile followed by a bunch of steel plates and a mechanical oscillator. The axial harmonic loading field tests are performed on 3-pile group setup under a static load (W_s) of 12 kN (including the weight of the pile cap, steel plates, and oscillator) for four different eccentric moments ($W.e$ = 0.868, 1.269, 1.631, and 1.944 Nm). The frequency-amplitude responses of the system are measured at different frequencies (0–50 Hz) by a data acquisition system. One accelerometer is attached vertically on the top most plate at the center of the soil-pile loading system to measure the acceleration. One frequency measuring sensor is attached to the DC motor to obtain the operating frequency during dynamic testing. The time-acceleration and time–frequency response are measured during the axial harmonic test and from these response curves, frequency versus amplitude curves are determined. The experimental test setup is shown in Fig. 1.

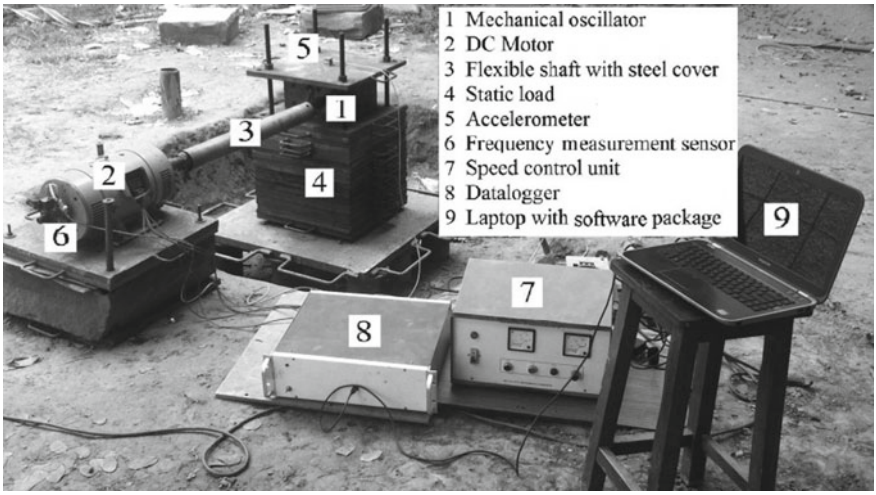

Fig. 1 Complete vertical vibration test setup of 3-pile group

4 Theoretical Analysis

In the present work, the continuum approach [7] is used to determine the linear and nonlinear dynamic response of 3-pile group. Two different soil models are analyzed in the present study, i.e., linear model (without boundary zone parameters) [8] and nonlinear model (with boundary zone parameters) [9]. The boundary zone is defined by an annular soil zone around the pile with reduced shear modulus and increased damping relative to the free field with no boundary zone soil mass to prevent wave reflections from the fictitious interface between the cylindrical zone and the outer region. This boundary zone can replicate the effect of soil nonlinearity, soil-pile separation, slippage on the dynamic pile response. This theoretical method is available as a software package named DYNA 5 which is used in this study.

4.1 Boundary Zone Parameters

The boundary soil zone is characterized by the boundary zone parameters, i.e., shear modulus reduction factor (G_m/G), weak zone soil damping (D_m), thickness ratio (t_m/R), and soil-pile separation (l_s) which are used to obtain the non-linear frequency-amplitude response of the pile group. These theoretical boundary zone parameters are arranged in such a way that the predicted response curves match with the field test results. The variation of shear modulus reduction factor and weak zone soil damping for different eccentric moment is shown in Fig. 2. In the analysis, the soil-pile separation lengths are also considered as $1.05d$ (= 0.12 m) for $W.e = 0.868$ Nm and $1.27d$ (= 0.145 m) for $W.e = 1.944$ Nm.

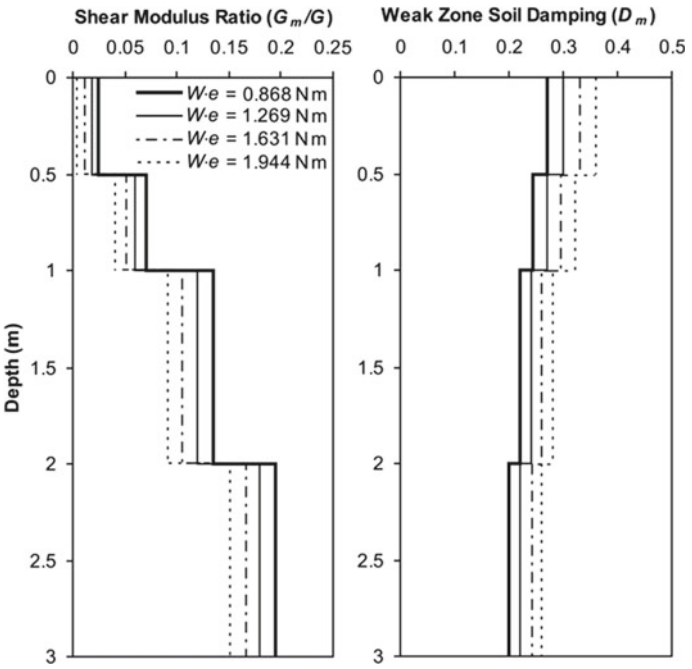

Fig. 2 Variations of boundary zone parameters with depth under axial loading condition

5 Theory Versus Experiment

5.1 Linear Analysis

Comparison between field test response and theoretical linear response curves is shown in Fig. 3 under varying eccentric moments. From the figure, it is observed that the predicted linear response shows lower values of the resonant axial amplitude and much higher values of resonant frequency as compared to the field test results. The theoretically predicted resonant frequency is found approximately 25% higher and resonant amplitude is found approximately 19% lower as compared to the field test results. These differences in the pile responses may occur due to the consideration of perfect bonding between the pile and soil and inconsideration of soil nonlinearity. However, in the actual field condition, the boundary soil zone and soil-pile separation may develop due to soil nonlinearity and soil-pile slippage which leads to the change in the stiffness of the soil-pile system due to the increase of dynamic loading.

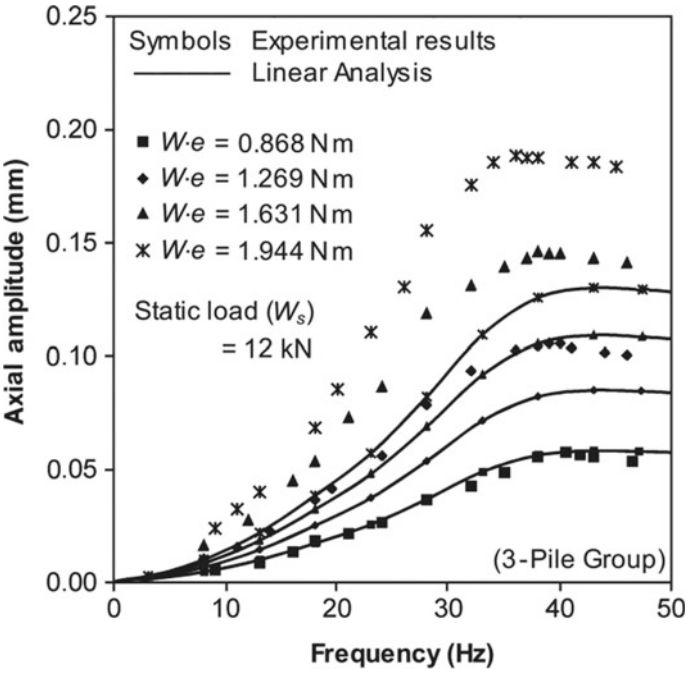

Fig. 3 Comparison of response curves of 3-pile group under axial loading obtained from experiments and linear analysis

5.2 Nonlinear Analysis

It is found that the linear analysis is not very suitable to predict the dynamic response of the pile foundation. Therefore, the nonlinear dynamic analysis is carried out with the help of DYNA 5 software to determine the frequency-amplitude response of the pile foundation by considering the boundary zone parameters. Comparisons of dy-namic response obtained from experimental testing and nonlinear solution are shown Fig. 4. It is noted that the differences between test and analytical results of resonant frequencies and amplitudes are reduced as compared to the linear analysis. From the comparison curves, it is also noted that the pattern of response curves indicate nonlinearity for both experimental and analytical solution as the resonant frequencies are decreased and resonant amplitudes are disproportionally increased with the increase of excitation forces.

A single resonant peak is observed from all the experimental and analytical dynamic responses of pile group for axial loading which indicate that the move-ment of the pile foundation is predominantly occurred in axial direction within that frequency range.

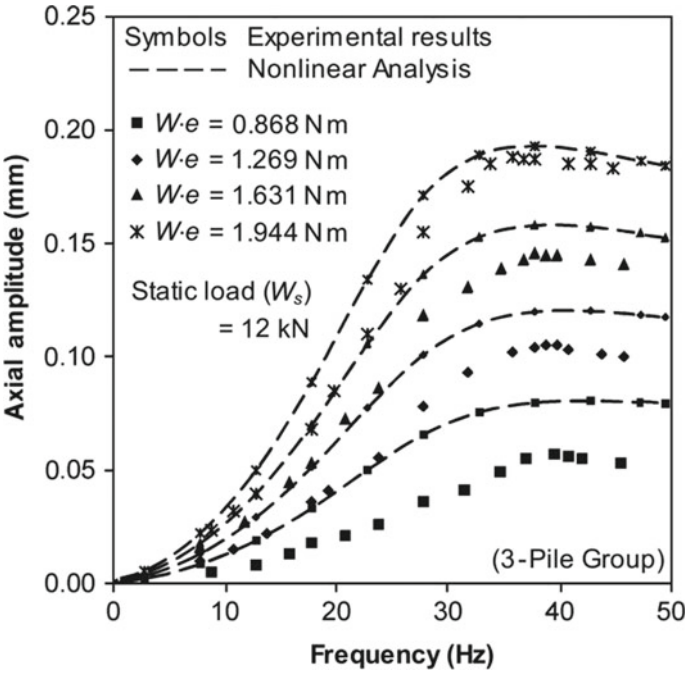

Fig. 4 Comparison of response curves of 3-pile group under axial loading obtained from experiments and nonlinear analysis

6 Conclusions

The frequency-amplitude response of the 3-pile group for different eccentric moments has been studied under axial harmonic loading. It is noted from the test results that the field response curves of piles indicate nonlinear behavior as the resonant frequencies decrease and resonant amplitudes disproportional increase with the variation of eccentric moments. From the theoretical analysis, it is observed that the resonant amplitudes of piles are underestimated and the resonant frequencies are overestimated by the linear approach under axial loading. In case of nonlinear analysis, the differences between predicted and test results of resonant frequencies and amplitudes values are reduced as compared to linear analysis. From the present investigation, it is also observed that the accuracy of predicting nonlinear responses mainly influence by the choice of boundary zone parameters. It can be concluded that nonlinear analysis with boundary zone and soil-pile separation is more capable to predict the resonant frequencies and amplitudes accurately for all eccentric moments as compared to linear analysis. Therefore, the nonlinear soil model can be used as realistic and versatile model for dynamic analysis of pile.

References

1. Novak M, Grigg RF (1976) Dynamic experiments with small pile foundations. Can Geotech J 13:372–385
2. El Sharnouby B, Novak M (1984) Dynamic experiments with group of piles. J Geotech Eng ASCE 110(6):719–737
3. El Marsafawi H, Han YC, Novak M (1992) Dynamic experiments on two pile groups. J Geotech Eng ASCE 118(4):576–592
4. Elkasabgy M, El Naggar MH (2013) Dynamic response of vertically loaded helical and driven steel piles. Can Geotech J 50:521–535
5. Biswas S, Manna B (2018) Experimental and theoretical studies on the nonlinear characteristics of soil-pile systems under coupled vibrations. J Geotech Geoenviron Eng ASCE 144(3). https://doi.org/10.1061/(ASCE)GT.19435606.0001850
6. Khalil MM, Hassan AM, Elmamlouk HH (2020) Dynamic behavior of pile foundations under vertical and lateral vibrations: review of existing codes and manuals. HBRC J 16(1):39–58
7. Novak M, Aboul-Ella F (1978a) Impedance functions for piles embedded in layered medium. J Eng Mech ASCE 104(3):643–661
8. Novak M, Aboul-Ella F (1978b) Stiffness and damping of piles in layered media. In: Proceedings of earthquake engineering and soil dynamics, ASCE specialty conference. Pasadena, California, pp 704–719
9. Novak M, Sheta M (1980) Approximate approach to contact problems of piles. In: Proceedings of the dynamic response of pile foundations: analytical aspects. New York, pp. 53–79

Comparison of Response of Pushover Analysis and Dynamic Analysis of Pile Foundation

Bidisha Borthakur and Arup Bhattacharjee

Abstract Pile foundations are the most vulnerable components of the entire structure and are prone to failure due to earthquake loading. Thus it is mandatory for proper seismic analyses to be conducted with the incorporation of all the necessary influencing factors to ensure no failure occurs to the pile foundation. Even though dynamic analysis has been the conventional seismic analysis method, a new nonlinear static analysis known as pushover analysis is seen to realistically predict earthquake response of the pile. This calls for proper research to be conducted to check if static pushover analysis can be used as an alternative to dynamic analysis for seismic analysis of structures to save time and ease on the complexity of dynamic analysis. In this research work, single piles of different diameter have been taken into consideration which has been embedded in stratified soil containing layers of different soil types. Dynamic analysis and static pushover analysis have been conducted for each case to compare the results of both the analyses. The Finite Element modeling as well as the analyses has been conducted in the user friendly interface of OpenSees known as OpenSees PL. From the results obtained, it is seen that pushover analysis can estimate the maximum bending moment witnessed by the pile while taking into account the effects of surrounding soil condition on it due to earthquake loading. Similar results of maximum bending moment have been obtained for both the analyses.s

Keywords Pushover analysis · Dynamic analysis · OpenSees PL

1 Introduction

1.1 General

Pile foundations have always been a solution to civil engineers when load has to be transferred from the superstructure through weaker soil strata onto less compressible soil or rock. However from various seismic investigations, it has been found that piles are the most vulnerable components of the entire structure and failure of pile has

B. Borthakur (✉) · A. Bhattacharjee
Department of Civil Engineering, Jorhat Engineering College, Jorhat, Assam, India

T. G. Sitharam et al. (eds.), *Earthquakes and Structures*, Lecture Notes in Civil Engineering 188, https://doi.org/10.1007/978-981-16-5673-6_30

been seen to result in the failure of the entire structure. The main reason behind this could be the unaccountability of surrounding soil condition while designing the pile foundation. In earthquake prone areas, the surrounding soil result in a combination of vertical and horizontal forces acting on the pile in addition to the load from the superstructure. Thus pile foundation should be designed by taking all the necessary factors into consideration such that no failure of foundation occurs due to seismic loading and proper seismic analyses should be conducted to do so. The dynamic analysis has been the conventional seismic analysis method for obtaining response of a structure due to earthquake loading. However, in recent times it has been seen that static nonlinear pushover analysis can be used in seismic design because of its ability to simulate equivalent peak load that occurs on the structure during earthquake. The ability of pushover analysis to simulate the peak dynamic response of structure decides the accuracy of this method [5]. The pushover analysis helps to improve understanding of post-yield structural behavior and results in more accurate prediction of global displacement along with realistic prediction of earthquake demand in individual structural elements [2]. It can also approximately take into account the redistribution of internal forces occurring in the structure due to inertia force which cannot be resisted within elastic range of the structure, thus helping to predict the seismic forces acting on the structure when seismic load is applied, which can further help in controlling the performance of the structure when subjected to earthquake [3].

Since pushover analysis can accurately simulate the dynamic response of a structure in spite of being a static analysis, its use as an alternative to dynamic analysis should be checked in order to make seismic analyses less complex and less time consuming. In this research work, single piles of different diameter embedded in different stratified soil conditions have been taken into consideration. Dynamic analysis as well as static pushover analysis has been conducted for each case to check the accuracy of response of pile due to pushover analysis with dynamic analysis.

1.2 3D Ground-Foundation Analyses Using OpenSees PL

A user-friendly interface of OpenSees, known as OpenSees PL was created using the using the pre- and post- processing efforts of OpenSees. OpenSees PL was created for 3D foundation-ground analyses such that the complicated soil-structure interaction mechanism could be incorporated while analyzing the foundation under seismic loading in order to represent the actual geometric configuration that is involved due to soil-structure interaction. It is a FE graphical user-interface for 3D ground-structure interaction response which allows conducting pushover analysis as well as seismic simulations [7]. This Finite Element Analysis software utilizes object-oriented design principles and programming approach and can incorporate element formulation, material relations, analysis algorithms and solution strategies.

1.3 Validation of Seismic Analysis Using OpenSees PL

The seismic analysis of pile foundation using OpenSees PL is validated with the results obtained by Lu et al. [4] and analytical results obtained by Abedzedah et al. [1]. A circular free-head pile of 10.15 m length and radius 203.20 mm, fully embedded in a 20.12 m soil domain of submerged unit weight 9.87 kN/m^3 is modeled in OpenSees PL [4]. The pile is modeled using linear beam-column elements so that bending moment, axial loads and shear force could be viewed easily with rigid beam-column elements representing the diameter and interface with the surrounding soil elements. The soil is modeled using 8-node brick elements with *MultiYield* material to capture seismic events accurately. Lateral incremental pushover loading is applied monotonically at the pile head up to a total load of 140.12 kN. Figure 1. shows the pile deflection and the bending moment experienced by the pile throughout its length due to pushover loading. From the results, it is seen that pile response in terms of deflection and bending moment obtained from pushover analysis in OpenSees PL is similar to the analytical results of pushover analysis obtained by [1]. Thus for the seismic analysis of pile foundation in OpenSees PL for this study, modeling is done as per [4].

2 Seismic Analyses of Pile Embedded in Stratified Soil

Single piles of diameters 0.4 m and 0.8 m are considered to be fully embedded in stratified soil containing different layers of cohesive soil and cohesionless soil.

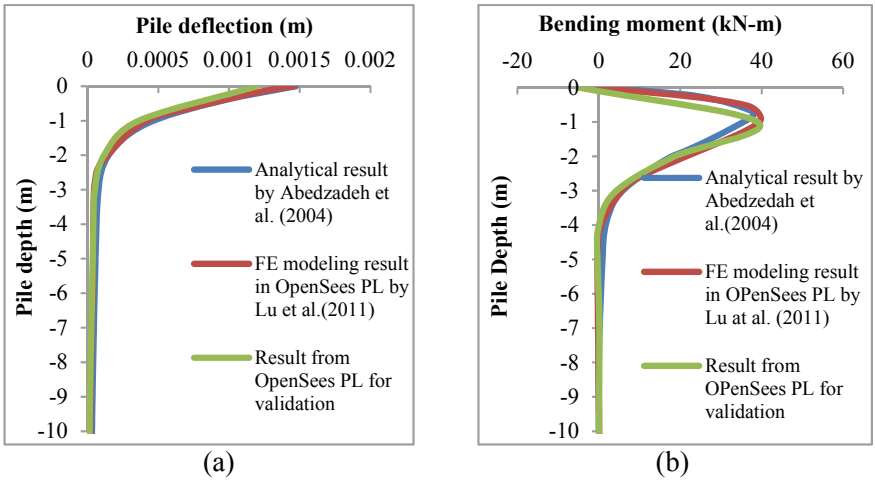

Fig. 1 Comparison of analytical results and FE modeling results in terms of (**a**) Pile deflection and (**b**) bending moment of pile for seismic analysis of pile-soil system for validation

Dynamic analysis as well as pushover analysis is conducted on each pile for each case of surrounding soil condition to compare to response of pile for both the analyses.

2.1 Numerical Modeling of Pile-Soil System in Opensees PL

The numerical modeling of pile is done in OpenSees PL according to [4]. To demonstrate the influence of non linear soil response, [7] considered a cohesion of 40.68 kPa in addition to the elastic properties specified by [4]. The fixed head circular piles of diameter are considered to be fully embedded in a 10 m soil domain consisting of various combinations of layers of soil. The pile is modeled using beam-column elements and rigid beam-column elements are used to represent the cross-sectional diameter and the interface with the soil elements surrounding the pile. The water table is considered to be up to the ground surface. The mass densities of the piles are taken as 2400 kg/m^3. The Young's modulus and the shear modulus are 3×10^7 kPa and 1.154×10^7 kPa respectively. For 0.4 m diameter pile, the moment inertia of the pile and torsion constant is 0.00125 m^4 and 0.00251 m^4 respectively. For 0.8 m diameter pile, the moment inertia of the pile and torsion constant is 0.02010 m^4 and 0.040212 m^4 respectively.

The modeling of the non linear soil domain is done using 8-node brick elements. Cohesionless soil is modeled using *PressureDependMultiYield* soil model and cohesive soil is modeled using *PressureIndependMultiYield* model. The water table is considered up to the pile head so as to consider liquefaction analysis while conducting dynamic or pushover analyses. The boundary condition is rigid box type and is considered to be fixed at the bottom in all directions. The plane of symmetry for half mesh configuration is fixed in Y direction while keeping it free in Z and X direction to model 3D full mesh scenario. The details about the soil elastic properties, soil nonlinear properties, fluid properties, dilatancy properties and liquefaction properties for the saturated cohesionless soil and cohesive soil are given in Table 1.

Wang [7] demonstrate the influence of non linear soil response in addition to the elastic response specified by [4]. On this pile-soil system, pushover analysis was conducted by Wang [7] by applying a total load of 420.36 kN incrementally at the pile head. Figure 2 shows the comparison of pushover curve for a typical case of single pile embedded in single layered soil as obtained by Wang [7] and in present analyses. It is seen from the results that the pushover analysis curve is comparable to that obtained by Wang [7] for both soil cases.

Table 1 Soil Properties of cohesionless and cohesive soil

	Cohesionless very loose sand	Cohesionless Dense sand	Cohesive medium soil	Cohesive stiff soil
Soil elastic properties				
Saturated mass density (Mg/m^3)	1.7	2.1	1.5	1.8
Reference pressure (kPa)	80	80	100	100
Reference Shear modulus (kPa)	55,000	130,000	60,000	150,000
Reference Bulk modulus (kPa)	150,000	390,000	300,000	750,000
Soil nonlinear properties				
Friction (deg)	29	40	0	0
Cohesion (kPa)	0.2	0.3	37	75
Fluid properties				
Fluid mass density (Mg/m^3)	1	1	1	1
Horizontal permeability (m/s)	6.6E-05	6.6E-05	1.00E-0.9	1.00E-0.9
Vertical permeability (m/s)	6.6E-05	6.6E-05	1.00E-0.9	1.00E-0.9
Dilatancy/liquefaction properties				
Phase transformation angle (deg)	29	27	–	–
Contraction parameter	0.21	0.03	–	–
Dilation parameter 1	0	0.8	–	–
Dilation parameter 2	0	5	–	–
Liquefaction parameter 1	10	0	–	–
Liquefaction parameter 2	0.02	0	–	–
Liquefaction parameter 3	1	0	–	–

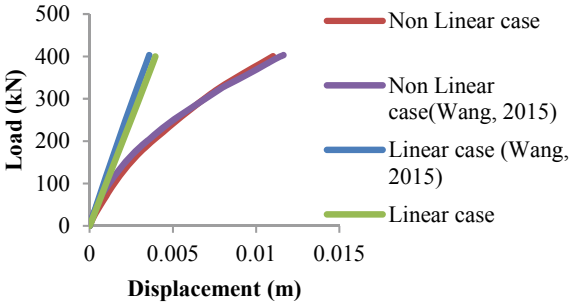

Fig. 2 Pushover analysis curves for typical case of single pile embedded in single layered soil

2.2 Numerical Modeling of Piles Embedded in Multi-Layered Soil

Using the validated model properties, the fixed head piles of different diameters embedded in various combinations of soil layers are considered for dynamic as well as pushover analysis. The soil domain of 10 m depth consist of two or three layers of different cohesive and cohesionless soil types considered in the present analysis is shown in Table 2 and Fig. 3.

2.3 Dynamic Analysis Results of Single Pile Embedded in Stratified Soil

In order to apply an earthquake of magnitude 7.0 in Richter scale [6], dynamic excitation in the form of sinusoidal wave of 0.3 g peak ground acceleration having frequency of 2 Hz is applied for 10 cycles at the base of the pile. Table 3 shows the maximum pile head displacement for each case of surrounding soil conditions obtained from dynamic analysis. The pile head displacement is seen to be high for soil containing layers of cohesionless very loose sand at any location.

Figure 4 shows the bending moment profiles of 0.4 m and 0.8 m diameter piles surrounded by double layered and triple layered soils. From the graphs, it is seen that presence of cohesionless very loose sand in any layer results in higher magnitude of bending moment witnessed by the piles for both 0.4 m and 0.8 m diameter piles. However, cohesionless dense soil in any layer is seen to result in lower magnitude of bending moment witnessed by the piles.

For 0.4 m diameter pile surrounded by cohesionless dense sand placed above cohesive medium soil, maximum magnitude of bending moment witnessed by pile is 176.42 kN-m. By interchanging the positions of layers i.e. cohesive medium soil placed above cohesionless dense sand, the maximum bending moment reduces to 87.01 kN-m. By replacing cohesionless dense sand layer with cohesionless very loose sand, the magnitude of maximum bending moment is 208.01 kN-m for sand

Table 2 Soil combinations of double and triple layered soil profile

Combination	Layer	Soil	Depth
Double layered soil			
1	Layer 1	Cohesionless dense sand	5 m
	Layer 2	Cohesive medium soil	5 m
2	Layer 1	Cohesive medium soil	5 m
	Layer 2	Cohesionless dense sand	5 m
3	Layer 1	Cohesionless very loose sand	5 m
	Layer 2	Cohesive medium soil	5 m
4	Layer 1	Cohesive medium soil	5 m
	Layer 2	Cohesionless very loose sand	5 m
Triple layered soil			
5	Layer 1	Cohesive medium soil	2 m
	Layer 2	Cohesionless dense sand	6 m
	Layer 3	Cohesive medium soil	2 m
6	Layer 1	Cohesive stiff soil	2 m
	Layer 2	Cohesionless dense sand	6 m
	Layer 3	Cohesive stiff soil	2 m
7	Layer 1	Cohesive medium soil	2 m
	Layer 2	Cohesionless very loose sand	6 m
	Layer 3	Cohesive medium soil	2 m
8	Layer 1	Cohesive stiff soil	2 m
	Layer 2	Cohesionless very loose sand	6 m
	Layer 3	Cohesive stiff soil	2 m

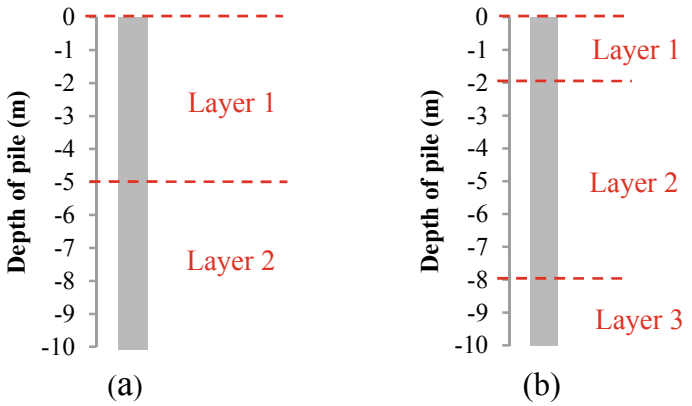

Fig. 3 Pile embedded in soil consisting of (**a**) double layered soil (**b**) triple layered soil

Table 3 Pile head displacements of piles surrounded by different soil combinations

Soil combination	0.4 m diameter	0.8 m diameter
Double layered soil		
Cohesionless dense sand + Cohesive medium soil	0.004999 m	0.005275 m
Cohesive medium soil + Cohesionless dense sand	0.001243 m	0.001197 m
Cohesionless very loose sand + Cohesive medium soil	0.01033 m	0.01437 m
Cohesive medium soil + Cohesionless very loose sand	0.0222 m	0.01827 m
Triple layered soil		
Cohesive medium soil + Cohesionless dense sand + Cohesive medium soil	0.003225 m	0.002436 m
Cohesive stiff soil + Cohesionless dense sand + Cohesive stiff soil	0.0006194 m	0.0006046 m
Cohesive medium soil + Cohesionless very loose sand + Cohesive medium	0.01915 m	0.01807 m
Cohesive stiff soil + Cohesionless very loose sand + Cohesive stiff	0.005404 m	0.009867 m

layer placed above cohesive medium soil layer. On interchanging the positions of soil layers, the magnitude of maximum bending moment increase to 742.39 kN-m. For triple layered soil containing cohesionless dense sand sandwiched between cohesive medium soil layers, the maximum magnitude of bending moment is 218.36 kN-m. By replacing cohesive medium soil layers with cohesive stiff soil, the magnitude of maximum bending moment reduces to 61.05 kN-m. For cohesionless very loose sand sandwiched between cohesive medium soil layers, the magnitude of maximum bending moment is the highest with magnitude 481.53 kN-m. However, on replacing cohesive medium soil layers with cohesive stiff soil, the maximum bending moment reduces to 394.92 kN-m.

For 0.8 m diameter piles, pile surrounded by cohesionless dense sand placed above cohesive medium soil layer, the maximum bending moment of magnitude is 992.65 kN-m. By interchanging the position of soil layers, the bending moment reduces to 809.65 kN-m. For cohesionless very loose sand placed above cohesive medium soil, the magnitude of maximum bending moment is 1897.81 kN-m. By interchanging position of soil layers, the bending moment is 3891.9 kN-m. Further, for triple layered soil, the maximum magnitude of bending moment of pile surrounded by cohesionless dense sand sandwiched between cohesive medium soil layers is 1127.7 kN-m. By replacing cohesive medium soil layers with cohesive stiff soil results in lower magnitude of maximum bending moment of 408.08 kN-m. For 0.8 m diameter pile surrounded by cohesionless very loose sand sandwiched between cohesive medium soil layer, the maximum magnitude of bending moment is 2934.02 kN-m. By replacing cohesive medium soil layer with cohesive stiff soil, the magnitude of maximum bending moment on pile is 2998.6 kN-m.

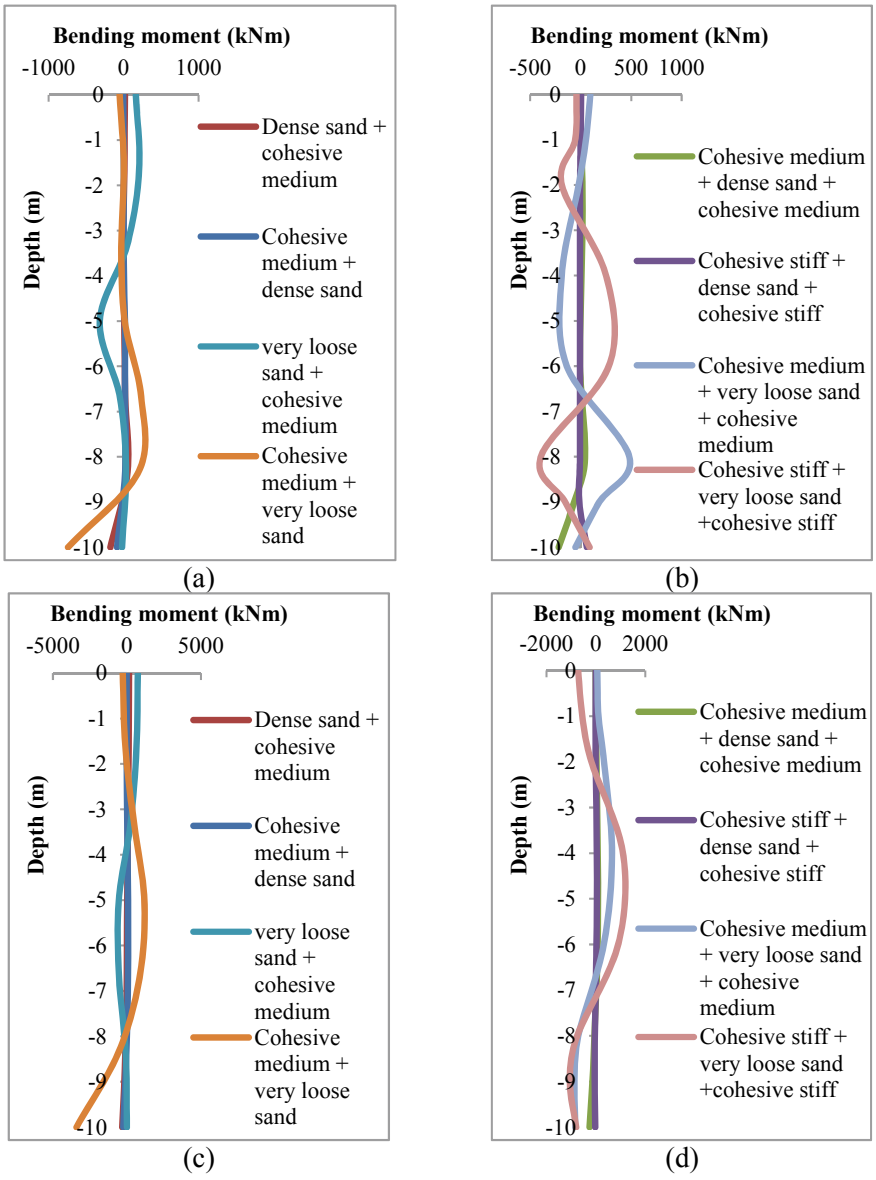

Fig. 4 Bending moment results of (**a**) 0.4 m diameter pile in double layered soil (**b**) 0.4 m diameter pile in triple layered soil (**c**) 0.8 m diameter pile in double layered soil and (**d**) 0.8 m diameter pile in tripe layered soil subjected to dynamic analysis with PGA 0.3 g

From the results of dynamic analysis, it is thus seen that bending moment witnessed by pile due to different surrounding soil conditions is influenced by the pile diameter, number of soil layers as well as with the positioning of soil types.

2.4 Pushover Analysis Results of Single Pile Embedded in Stratified Soil

The pushover analysis of pile surrounded by different soil combinations is conducted by pushing the pile until pile head displacement as obtained from dynamic analysis is achieved. Monotonically increasing horizontal load of 10 kN is applied at the pile head for static pushover analysis. Figure 5 shows the bending moment witnessed by each pile surrounded by different double layered and triple layered soil combinations due to pushover analysis.

For 0.4 m diameter pile surrounded by cohesionless dense sand placed above cohesive medium soil, the magnitude of maximum bending moment is 209.4 kN-m. The maximum bending moment reduces to 68.72 kN-m by interchanging position of the soil layers. By replacing cohesionless dense sand with cohesionless very loose sand, the maximum bending moment is 302.4 kN-m for very loose sand layer placed above cohesive medium soil layer. By interchaning of the positions of soil layers, the maximum bending moment increases to 861.5 kN-m. For triple layered cohesionless dense sand sandwiched between layers of cohesive medium soil surrounding 0.4 m diameter pile, maximum bending moment is 235.6 kN-m. By replacing cohesive medium soil with cohesive stiff soil, the maximum bending moment reduces to 83.63 kN-m. For pile surrounded by cohesionless very loose sand sandwiched between cohesive medium soil layers, the maximum bending moment is 561.5 kN-m. By replacing cohesive medium soil layer with cohesive stiff soil, the maximum bending moment is 459.6 kN-m.

For 0.8 m diameter pile surrounded by cohesionless dense sand placed above cohesive medium soil, maximum magnitude of bending moment is 1209 kN-m. By interchanging the position of soil layers, the maximum bending moment reduces to 904.7 kN-m. By replacing the cohesionless dense sand layer with cohesionless very loose sand, the magnitude of maximum bending moment is 1964 kN-m for sand layer placed above cohesive medium soil layer. By changing the position of soil layers, the magnitude of maximum bending moment increase to 4798 kN-m. For triple layered soil containing cohesionless dense sand sandwiched between cohesive medium soil layers, the maximum magnitude of bending moment is 844.9 kN-m. By replacing cohesive medium soil layers with cohesive stiff soil, the magnitude of maximum bending moment reduces to 341.7 kN-m. For cohesionless very loose sand sandwiched between cohesive medium soil layers, the magnitude of maximum bending moment is 3564 kN-m. However, by replacing cohesive medium soil layers with cohesive stiff soil, the maximum bending moment reduces to 3058 kN-m.

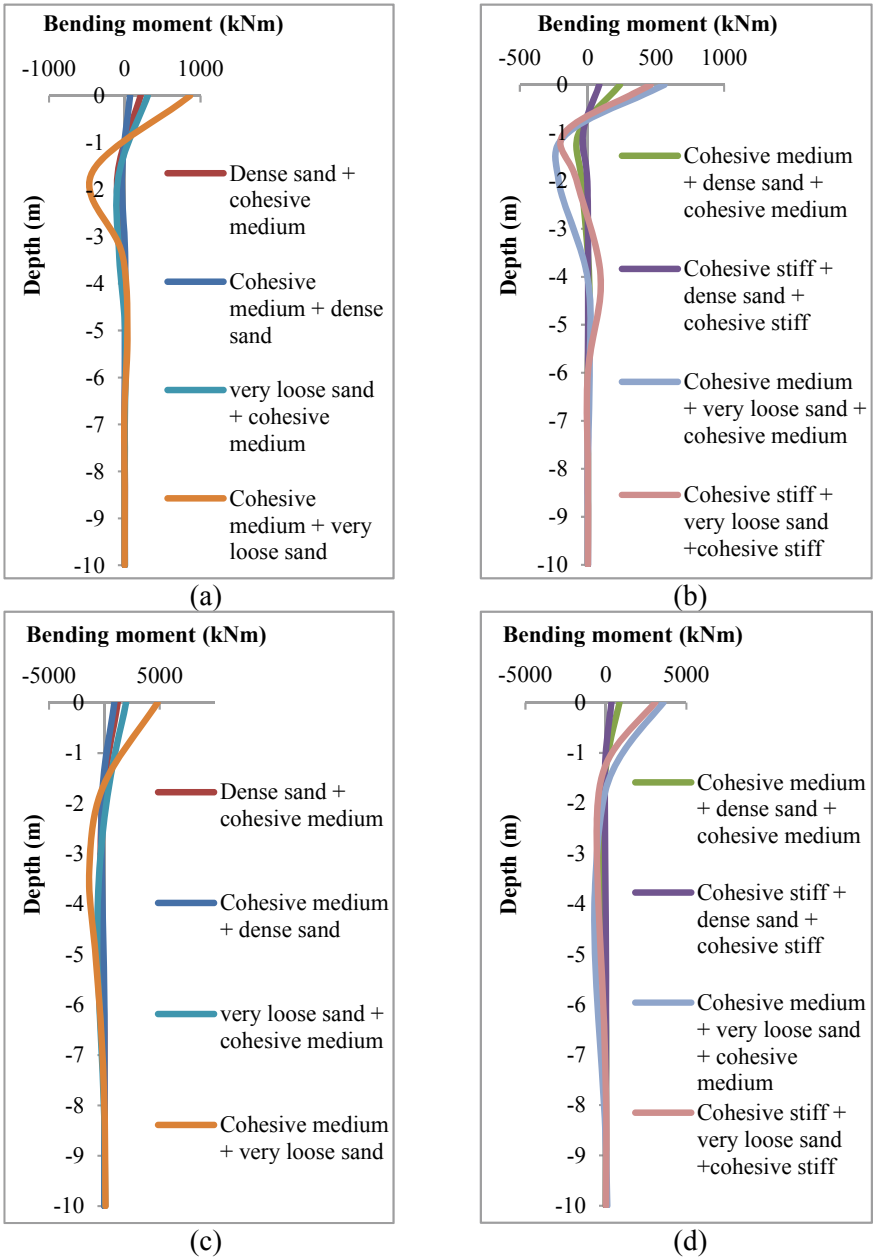

Fig. 5 Bending moment results of (**a**) 0.4 m diameter pile in double layered soil (**b**) 0.4 m diameter pile in triple layered soil (**c**) 0.8 m diameter pile in double layered soil and (**d**) 0.8 m diameter pile in tripe layered soil due to static pushover analysis

From the results of pushover analysis, it is thus seen that type of surrounding soil as well as the positioning of soil layers influence the maximum bending moment witnessed by 0.4 m as well as 0.8 m diameter pile.

2.5 Comparison of Pushover and Dynamic Analyses of Pile–Soil System

From the results of dynamic analysis and pushover analysis of 0.4 m and 0.8 m diameter piles surrounded by double layered and triple layered soil containing combinations of cohesionless soil and cohesive soil, it is observed that the surrounding soil influences the seismic response of pile. It is also observed that the bending moment profiles obtained for 0.4 m and 0.8 m diameter pile are different for both the analyses due to difference in location of load application for both the analyses. However, the magnitude of maximum bending moment witnessed by each pile is seen to be comparable for both the analyses for each surrounding soil condition. Figure 6 shows the comparison of maximum bending moment witnessed by each pile for each soil combination due to dynamic and static pushover analysis. It is seen that 0.4 m diameter pile experiences similar magnitudes of maximum bending moment for double layered as well as triple layered soils. For 0.8 m diameter pile surrounded by cohesionless dense sand sandwiched between layers of cohesive soil, dynamic analysis is seen to result in slightly higher magnitude of maximum bending moment than static pushover analysis.

Thus, from the comparison results it can be inferred that pushover analysis can estimate the maximum bending moment witnessed by pile due to dynamic analysis. Therefore it can be stated that static pushover analysis can be used to predict the maximum bending moment witnessed by pile due to seismic loading with the incorporation of soil-structure interaction.

3 Conclusion

From the analysis results and comparison of dynamic analysis and static pushover analysis of piles surrounded by startified soil, it can be concluded that:

- Pushover analysis as well as dynamic analysis results shows that the seismic response of pile embedded in stratified soil is influenced by the surrounding soil conditions.
- The type of soil and the position of soil layer influence the bending moment acting on the pile.
- Static pushover analysis can predict the magnitude of maximum bending moment witnessed by pile surrounded by stratified soil due to seismic loading.

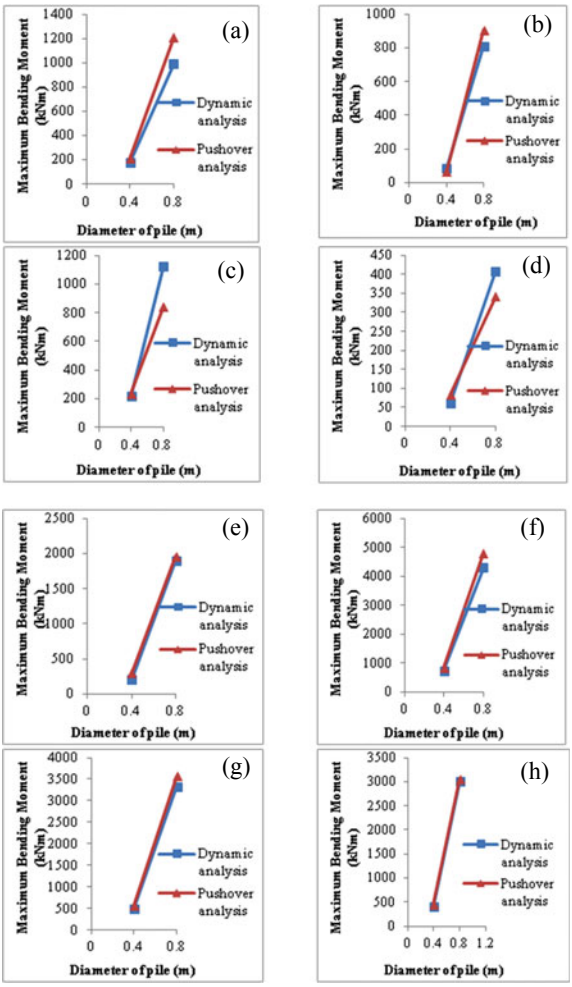

Fig. 6 Comparison of magnitude of maximum bending moment for 0.4 m and 0.8 m diameter pile surrounded by (**a**) Cohesionless dense sand + Cohesive medium soil (**b**) Cohesive medium soil + Cohesionless dense sand (**c**) Cohesive medium soil + Cohesionless dense sand + Cohesive medium soil (**d**) Cohesive stiff soil + Cohesionless dense sand + Cohesive stiff soil (**e**) Cohesionless very loose sand + Cohesive medium soil (**f**) Cohesive medium soil + Cohesionless very loose sand (**g**) Cohesive medium soil + Cohesionless very loose sand + Cohesive medium soil (**h**) Cohesive stiff soil + Cohesionless very loose sand + Cohesive stiff soil

- Static pushover analysis can be used to estimate the maximum bending moment witnessed by pile due to seismic loading with the incorporation of soil-structure interaction in place of dynamic analysis.

References

1. Abedzadeh F, Pak RYS (2004) Continuum mechanics of lateral soil-pile interaction. J Eng Mech 130(11):1309–1318
2. Kircher AC (1997) Overview of earthquake analysis methods with emphasis on nonlinear static methods, EERI Technical Seminar Series, Earthquake Engg Research Inst., Mountain View,

California
3. Krawinkler H, Seneviratna GK (1998) Pros and cons of a pushover analysis for seismic performance evaluation. Eng Struct 20(4–6):452–464
4. Lu J, Elgamal A, Yang Z (2011) OpenSees PL: 3D lateral pile-ground interaction. User manual. University of California, San Diego
5. Mukhopadhyay M, Choudhury D, Phanikanth VS, Reddy GR (2008) Pushover analysis of piles in stratified soil. In: The 14th world conference on earthquake engineering, Beijing, China
6. Seed HB, Idriss IM (1971) Simplified procedure for evaluating soil liquefaction potential. J Soil Mech Found 97:1249–1273. NoSM9,PROC PAPER 8371
7. Wang N (2015) Three-dimensional modeling of ground-pile systems and bridge foundations. PhD thesis, University of California, San Diego

Application of Wave Propagation with Low Strain Pile Integrity Test—A Case Study

J. Prakashvel, S. Harishkumaran, P. Vasudevan, and K. Sathishkumar

Abstract Piles should possess the structural integrity to carry the design load and transfer to the soil/rock below. As per Indian standard IS 14893:2001, in general following defects are observed in the pile, which may lead to catastrophic failure. (a) Pile shaft necking, (b) Discontinuity of concrete, (c) Intrusion of foreign matter, (d) Improper toe formation due to contamination of concrete at the base with soil particles, (e) Washing of concrete due to high water current, and (f) Poor quality control with improper construction methods. NDT-based low strain pile integrity testing can be effectively used for evaluation of quality and acceptance of pile foundations. Low strain pile integrity test is based on pulse echo method. Pile integrity tester gives the velocity plot versus time. The plot is observed for the reflections, which indicate the change in the property of wave passing medium. The reflections may be due to soil resistance (stiffness) effects, cross-sectional changes, and soil property changes. In this study, bored cast-in-situ piles are evaluated for its integrity.

Keywords Pile integrity · Wave propagation · Pile shaft

1 Introduction

NDT-based low strain pile integrity testing can be effectively used for evaluation of quality and acceptance of pile foundations. Piles should possess the structural integrity to carry the design load and transfer to the soil/rock below. As per Indian standard IS 14893:2001 [4], in general following defects are observed in the pile, which may lead to catastrophic failure. (a) Pile shaft necking, (b) Discontinuity of concrete, (c) Intrusion of foreign matter, (d) Improper toe formation due to contamination of concrete at the base with soil particles, (e) Washing of concrete due to high water current, and f)Poor quality control with improper construction methods. This is economical method to test all the piles in the site compared to the cost of doing load tests for 0.5 to 2% of total no of piles at site. Low strain pile integrity test is based on

J. Prakashvel (✉) · S. Harishkumaran · P. Vasudevan · K. Sathishkumar
CSIR-Structural Engineering Research Centre, Ch-113, Chennai, India
e-mail: jprakash@serc.res.in

T. G. Sitharam et al. (eds.), *Earthquakes and Structures*, Lecture Notes in Civil Engineering 188, https://doi.org/10.1007/978-981-16-5673-6_31

pulse echo method. The test is termed as low strain method because a small hammer is used to generate a short wave of appreciable acceleration with low strain levels. Many numbers of piles can be tested at the site with this method. Pile integrity tester gives the velocity plot versus time. The plot is observed for the reflections, which indicate the change in the property of wave passing medium. The reflections may be due to soil resistance (stiffness) effects, cross-sectional changes, and soil property changes. In this study, the details of investigations and the inferences drawn on bored cast-in-situ piles for its integrity carried out at site by way of performing low strain pile integrity tests on 160 piles of TG foundation at Thermal power plant are presented. Thilakasiri [1] have modeled the wave propagation through the pile using the Wave Equation Method. He has divided the pile into 200 elements with varying soil stiffness along the pile shaft. With an artificial velocity pulse, velocity of the same element for varying ground conditions and the defects commonly encountered in Sri Lanka is determined and the location of the defects and its appearance in the velocity plot is investigated. Surya J Varma et al have evaluated the structural integrity of pile foundations by Pile Integrity Testing at bridge construction site in Tamil Nadu [5].

2 Motivation and Objective(s)

To study the wave propagation in the piles to evaluate the integrity and depth of piles.

3 Methodology

We performed low strain pile integrity tests on all 160 piles of the Turbo Generator (TG) foundation of Unit-1 at 2 × 660 MW Super thermal Power Plant. The diameter of the pile is 760 mm. The piles are laid below the raft concrete block. The columns will be constructed from the raft concrete. The soil in the site is of clay and the site is ash dyke of a thermal power plant. They have consolidated the soil with the sand piles near all the concrete piles. This has increased the soil stiffness to significant level and hence in some cases we could not get the toe reflections. The subsoil is characterized by a filled up soil with fly-ash disposed from the nearby thermal power plant. The initial layer consists of very soft silty clay. Below this medium silty clay to stiff clay layer is observed. Near 40 meters level below the ground, dense silty sand and hard silty clay layer is found.

The pile topping may be prepared with Cement mortar 1:3 or Conbextra GP grout material with 50 mm thickness. The topping has to be prepared 7 days prior to integrity test. Sufficient time should be allowed for topping material to attain sufficient strength for integrity test. Ultrasonic pulse velocity in the piles to be tested for integrity is evaluated using PUNDIT Ultrasonic equipment. This is the required input to be given to the Pile Integrity Tester for the reliable integrity assessment. The average wave

velocity in concrete evaluated from Ultrasonic pulse velocity test measurements is 4173 m/s. Impact with less energy is imparted to the pile top. Accelerometer is fixed on the top of the pile surface after necessary preparations to get the response in time domain.

Pile Integrity Tests (PIT) are performed as per Indian Standard for Non-Destructive Integrity Testing of Piles (NDT)—Guidelines (IS 14893:2001 reaffirmed 2006) [4]; on all the 160 piles of the TG foundation using Pile Integrity Tester equipment (Make: Pile Dynamics Inc., USA; Model No.: PIT-FV). During the test, ASTM D5882—07 Standard Test Method for Low Strain Impact Integrity Testing of Deep Foundations [2] is also referred for guidelines of the test. The piles are constructed with M35 grade concrete. Prior to these PIT tests Ultrasonic Pulse Velocity (UPV) tests are performed as per Indian Standard for Non-Destructive Testing of Concrete—Methods of Test: Part 1 Ultrasonic Pulse velocity (IS 13311—Part 1: 1992; reaffirmed 2004) [3] on randomly selected 20 piles of the TG foundation from top concrete of 0.75 m depth from the cut-off level. In each of the selected pile, two sets of direct measurements along the diameter of the pile are taken at two different pile depths, namely 0.25 m and 0.75 m. For performing the UPV tests, a Portable Ultrasonic Non-destructive Digital Indicating Testing (PUNDIT) equipment (Make: Proceq, Switzerland; Model: PUNDIT Lab) is used. These UPV tests are performed to arrive at the representative stress wave velocity (C) of the pile concrete medium required for estimating the pile depth using PIT analysis software. In the present study, a mean stress wave velocity of 4173 m/s evaluated from UPV tests performed on the randomly selected 20 piles of the TG foundation is used in the PIT analysis to estimate the pile depth. The following aspects can be evaluated using pile integrity tester. Impedance change, Effects of surrounding soil and pile material in wave propagation, Maximum impact force given by the hammer. The wave reflections occur by change in the pile's impedance due to changes in either the cross-section or the material. Decreasing impedance shows tensile reflection, leading to wave velocity in the same direction as the impact. Increasing impedance leads to compressive reflection and velocity wave occurs in the direction opposite to the impact. For a stiff concrete pile in relatively weak soil (strength compared to the concrete), the toe reflection will have the same sign (positive) as the velocity input. For a pile with a fixed end (such as a rock socket), the toe reflection may be of the opposite sign (negative) as the velocity input. Other reflections, observed only in the velocity record, are caused by changes in the pile's impedance, ($E \times A \div c$,) where E is the elastic modulus, A is the cross-sectional area, and c is the stress wave speed. A local decrease (neck) would have a positive reflection followed by a negative reflection (positive negative cycle). A local increase (bulb) would have a negative reflection followed by a positive reflection (negative positive cycle). The reflections must be interpreted to determine whether the associated changes are normal or of major concern to the integrity of the shaft. ASTM D5882—07 [2] Standard Test Method for Low Strain Impact Integrity Testing of Deep Foundations have been referred in addition to the BIS code for conducting the test and analysis.

4 Results and Discussion

PIT tests involve low strain, stress wave propagation in the pile shaft. Non-uniformities observed in the cross-section of the pile shaft along the depth estimated from PIT analysis are discussed in this paper. UPV testing and pile integrity testing on a typical pile are shown in Fig. 1. Results of PIT in the form of wave velocity vs pile depth plots are analyzed using PIT software for all the 160 piles. These plots give the estimate of pile depth and pile depth locations where non-uniformity in the pile cross-section is likely to be present for each pile. The depth of the pile is estimated and uniformity of the cross-section is observed. Velocity time history of a pile with non-uniform cross-section and uniform cross-section are plotted. Higher soil stiffness is observed in some of the piles, which do not have well-defined toe reflection. Figure 2 shows the typical velocity profile of pile with uniform cross-section.

Most of the piles tested at site exhibits non-uniformity in the cross-section between 5 and 10 m. Due to the soil stiffness, many of the piles tested have shown early reflections rather than reflections at the toe and defects of the pile. From Fig. 3, it is inferred that due to the higher soil stiffness, there is no definite toe reflection. Due to the non-uniformity in the pile, between 7.5 m and 12.5 m there is additional reflections in the plot as shown in Fig. 3. In Fig. 4, it is noted that there is a non-uniformity in the cross-section near 7.5 m depth and toe reflection at 25.02 m.

It is observed from the PIT analysis performed, the estimated pile depths of 101 piles (out of 160 piles) are found to be higher than the 23.4 m (90% of the design depth of 26 m). 10 piles are found to be with estimated depth lower than 90% of

Fig. 1 UPV testing and pile integrity testing on a typical pile

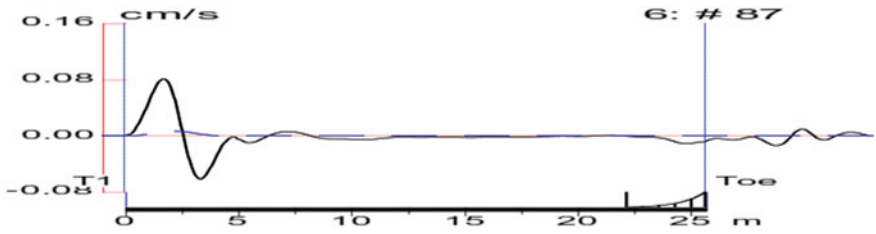

Fig. 2 Typical velocity profile of pile with uniform cross-section (Estimated depth is 25.69 m)

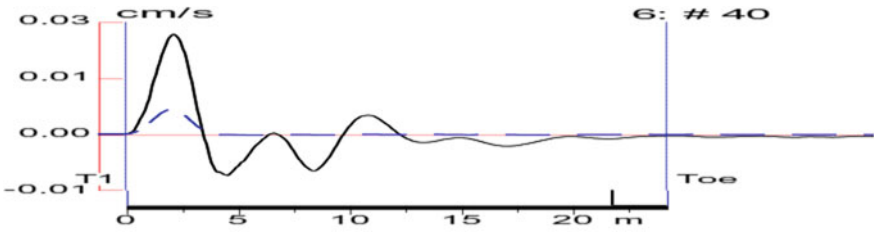

Fig. 3 Typical velocity profile of pile with non-uniformity in the cross-section between 7.5 m and 12.5 m depth

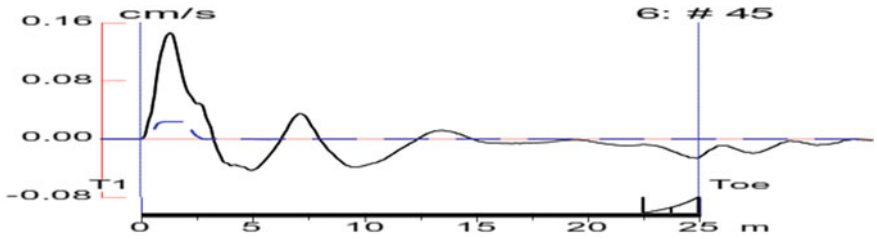

Fig. 4 Typical velocity profile of pile with non-uniformity in the cross-section near 7.5 m depth and the toe reflection at 25.02 m

design depth (i.e., 23.4 m). This could be due any one of the reasons stated above. 49 piles found to be with inconclusive depth due to the absence of well-defined wave reflection.

5 Conclusions

Pile integrity tester is a compact equipment, which also reflects the soil stiffness, in addition to abnormalities in the pile, which are tested. During the study, it is observed that few piles have the depth less than the design depth. The pile depth is estimated using PIT software based on the first reflection observed in the wave velocity profile beyond 20 m depth adopting a pile depth estimate of 26 m, 0.76 m pile diameter, and an average stress wave velocity of 4173 m/sec evaluated from UPV tests. This first wave reflection observed is mainly attributed to sudden variation of impedance (Z) ($Z = EA/C$, where E is the elastic modulus of the medium, A is the area of cross-section, and C is the stress wave velocity of the pile shaft) in the pile shaft through which the stress wave travels and could be due to any one of the following reasons. (a) Toe of the pile. In this case, the first reflection shows the end of the pile shaft. (b) Major reduction in the cross-section of the pile shaft in the form of necking or defect (crack). In this case, possibility of pile shaft material beyond this depth also exists. (c) Major non-homogeneity. In this case, possibility of mixing of concrete and soil

at this depth exists. The absence of well-defined wave reflection beyond 20 m depth shows that the low strain, stress wave generated at the top of the pile due to hammer impact gets attenuated fast and do not travel beyond this depth and could be due to any one of the following reasons. High soil stiffness is due to closely spaced piles within the group. Heterogeneity in the pile shaft material is due to poor concrete quality (like honeycombing and low grade concrete).

Acknowledgements Thanks are due to the Director, CSIR-SERC, Chennai, for the encouragement given to the project team during the pursuit of the project. The assistance and support provided by the technical staff of Advanced Seismic Testing and Research (ASTaR) Laboratory, CSIR-SERC deserves acknowledgement.

References

1. Thilakasiri HS (2006) Interpretation of Pile Integrity Test (PIT) results. Ann Trans IESL, 78–84
2. ASTM D5882–07 Standard test method for low strain impact integrity testing of deep foundations
3. IS 13311–Part 1: 1992 (1992) Indian standard for non-destructive testing of concrete—methods of test: Part 1 ultrasonic pulse velocity, Reaffirmed 2004
4. IS 14893:2001 Indian Standard for Non-Destructive Integrity Testing of Piles (NDT)—Guidelines (IS 14893:2001 reaffirmed 2006)
5. Varma SJ, Gopalakrishnan N, Sathish Kumar K, Eapen Sakaria P (2013) Structural integrity evaluation of pile foundations by pile integrity testing. Int J Struct Civil Eng Res 2(3):133140

Caisson Foundation Response During Liquefaction Induced Lateral Spreading

Shibayan Biswas and Deepankar Choudhury

Abstract Caisson foundations are widely used as the foundation system of bridges, transmission towers, and scour vulnerable structures for transmitting high structural load to the soil beneath. In seismically active regions having potentially liquefiable soils, one important consideration is the effect of liquefaction induced lateral spreading on deep foundations. During this phenomenon, caissons are subjected to seismic forces and simultaneously it loses the lateral support of surrounding soil due to liquefaction and an extra kinematic loading acts because of the flow of the liquefied soil. In this present study, a caisson embedded in liquefiable soil in gentle sloppy ground has been modeled in finite element-based software package PLAXIS 3D for capturing the response of the caisson in laterally spreading ground. The proposed numerical model has been found to compare well with the available centrifuge test results. Further parametric study has also been performed for lateral response of the caissons in liquefying soil for different ground slopes, embedment depth to caisson width ratio, frequency and amplitude of the dynamic motion. Behavior of the rigid caisson foundations subjected to liquefaction induced kinematic loading have been thoroughly discussed in the present study to assist the seismic design of caissons embedded in potentially liquefiable soil.

Keywords Caisson · Liquefaction · Lateral spreading · Kinematic

1 Introduction

Liquefaction-related phenomenon is associated with rapid loss of strength and stiffness of soil due to application dynamic loading. The excess pore pressure generated due to vibrations compensates the total stress in soil and the soil starts flowing like a viscous fluid. Whether the soil has been fully liquefied or not that can be estimated from the value of excess pore pressure ratio (r_u) of soil which is defined as

S. Biswas (✉) · D. Choudhury
Department of Civil Engineering, IIT Bombay, Powai, Mumbai 400076, India

D. Choudhury
e-mail: dchoudhury@iitb.ac.in

T. G. Sitharam et al. (eds.), *Earthquakes and Structures*, Lecture Notes in Civil Engineering 188, https://doi.org/10.1007/978-981-16-5673-6_32

the ratio of excess pore pressure to in-situ vertical effective stress. A r_u value of 1.0 (practically r_u value above 0.9–0.95) suggests full liquefaction. Liquefaction induced lateral spreading is mainly common in gentle sloping grounds and can be significant for partially liquefied soil also. When the reduced strength of slope soil falls below the static strength required to maintain the equilibrium in slopes, lateral spreading occurs. According to NCEER-92 workshop, lateral spreading generally occurs in 0.3–5% slopes [1], though, many researchers have suggested that it occurs in grounds having slope between 1° and 5°. Effect of kinematic loading on pile response due to lateral spreading has been investigated throughout the years using different methodologies such as force equilibrium method, p-y method, and finite element method. However, a very limited amount of work has been found on the lateral response of caisson foundation during lateral spreading condition. Due to the large cross-sectional area with high rigidity, caisson foundations were generally believed to have high capacity against the axial as well as the lateral loading and subsequently immune to seismic loading. However, this assumption was found to impart a fallacious hope only after several bridges founded on caisson foundations were reported to encounter damage in Kobe 1995 earthquake [2, 3]. Previous researchers [4, 5] have reported the girder failure of Nishinomiya-Ko Bridge and abutment failure of Kobe Bridge which occurred after Kobe 1995 earthquake. Although the caisson itself was found to be more or less unaffected, but bridge failure occurred due to displacement or rotation of caisson in the direction of laterally spreading soil. Therefore, the necessity for providing a systematic design guideline for caisson foundation design is instituted specifically for estimating the pressure coming from the flowing soil in lateral spreading phenomenon.

In the present study, numerical analysis using PLAXIS 3D [6] has been performed to investigate the different aspects of caisson-soil interaction under the liquefaction induced lateral spreading condition. The suitable constitutive model which can capture the liquefaction phenomenon as well as post liquefaction scenario has been discussed. The proposed model has been validated with the centrifuge test results and the results simulated by the proposed model has been found to be in good agreement with the available experimental results. After validation of the numerical model, detailed parametric study has been performed to observe the response of caissons embedded in liquefying soil for different frequency, amplitude of input dynamic motions, different ground slopes, and various caisson depth to width ratio.

2 Numerical Approach

2.1 Details of Numerical Methodology

A numerical method using finite element-based software package PLAXIS 3D [v.2018.01 (PLAXIS3D, 2018)] [6] has been adopted in this present study for simulating the effect of lateral spreading on a rigid caisson embedded in liquefying soil. A

3D model has been formed to capture the complete soil-structure interaction around the caisson. The optimized model dimensions were used for this analysis to ensure the non-significant effect of wave reflections. Free-field boundary condition has been used at the vertical sides of the boundary by employing free-field elements. Using this boundary condition, the free-field motion is transformed to the main domain by applying equivalent forces at the boundary. At the bottom of the 3D model, compliant base boundary condition has been employed to account for both absorption and application of dynamic input. The 3D soil and caisson elements have been modeled as 10-noded tetrahedral elements and the interface elements are modeled as 12-noded elements. In this analysis, caisson foundations have been modeled as rigid body where the relative displacement and angle between two points remain same before and after application of loads. That means the caisson will undergo rotation and/or translation depending upon the type of loading, but will not bend with respect to its longitudinal axis. This replicates the massive and heavy caisson of large dimensions with high stiffness contrast between caisson and soil. Ground water table has been considered at surface parallel to inclined ground and no slip condition at interface has been considered. An undrained analysis has been performed for the liquefaction problem. To facilitate free flow of soil during lateral spreading, the top ground surface has been kept in inclination with a certain percent of slope with the horizontal line throughout the domain. Therefore, the height of the soil block at two opposite ends has been kept at different elevations with the direction of slope staying along the direction of input motion (see Fig. 1).

In this dynamic analysis, damping has been incorporated inside the soil model through frequency dependent Rayleigh damping formulation, which can be defined as

$$2\omega\xi = \alpha + \beta\omega^2 \tag{1}$$

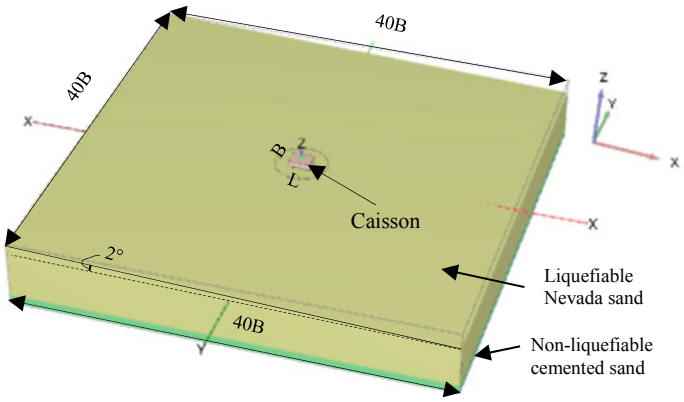

Fig. 1 3D model with slope used in the numerical analysis

$$\omega = 2\pi f \tag{2}$$

where ξ is the damping ratio, ω is the angular frequency and f is the frequency of input motion, α, β are Rayleigh damping coefficients. Two target frequencies (ω_1, ω_2) and their corresponding damping ratios (ξ_1, ξ_2) were set to compute the damping coefficients as below.

$$\alpha = 2\omega_1\omega_2 \frac{\omega_1\xi_2 - \omega_2\xi_1}{\omega_1^2 - \omega_2^2} \tag{3}$$

$$\beta = 2\frac{\omega_1\xi_1 - \omega_2\xi_2}{\omega_1^2 - \omega_2^2} \tag{4}$$

Generally, 1st and 2nd mode of natural frequencies are considered as the two target frequencies. In the analysis, 10% damping has been considered which is consistent with the practical range for soils. Sensitivity analyses of meshing have been performed to ensure optimized mesh density where both accuracy as well as numerical cost effectiveness were taken care off. The mesh size has been checked for the required element size from the time step calculation and seismic wave propagation criteria.

UBC3D PLM. To capture the rapid excess pore water pressure buildup and subsequent decrease in soil strength, a constitutive model named UBC3D-PLM has been used in this study. This model is generalized 3-D upgradation of UBCSAND model (University of British Columbia Sand) which was formulated by UBC researchers. Like UBCSAND, UBC3D-PLM is an effective-stress-based elasto-plastic model which follows the axioms of classical plasticity theory and consists of different rules for predicting soil behavior. A densification rule associated with secondary yield surface has been introduced in the UBC3D-PLM to simulate the generation of excess pore pressure with reasonable accuracy. To incorporate the degradation of stiffness after reaching liquefaction, i.e., post liquefaction phenomenon, a dilation factor has also been introduced in this model which can capture the gradual degradation of plastic shear modulus due to generation of plastic deviatoric strain at the time of dilation. Initially [7] performed several triaxial tests on soil response and proposed the equations for computation of parameters used for UBC3D-PLM. In their companion paper, [8] validated those expressions and proposed the modified expressions, mainly based on the in-situ corrected SPT value. In this present study, the constitutive model parameters are computed from the available relations provided by different researchers. Their proposed relations are based on the tests performed on the typical types of soils and for capturing a particular nature of soil. It is always advisable to perform tests for the model parameters evaluation for the response the researcher want to capture. In absence of test results, these relations can provide better estimate.

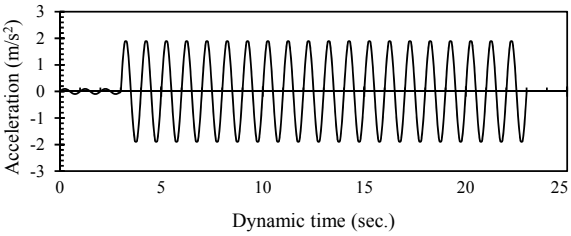

Fig. 2 Input motion used in the centrifuge experimental setup [9]

2.2 Validation of the Numerical Methodology

The proposed model is compared with the results found from the experiment performed by [9] in centrifuge at 50-g condition as a part of a NEES study at RPI. The stiff rigid caisson was made of aluminum which has external dimensions of 5 × 3.65 × 15.2 m in prototype. The soil layer consists of 10 m of potentially liquefiable Nevada sand with 2 m of bottom sand mixed with 5% Portland cement which provides soil-soil interaction with liquefiable soil and dense kind of behavior of bottom sand. The caisson was restrained at bottom to provide extra rotational stiffness. The whole container was kept at 2° with horizontal to facilitate lateral spreading. The similar condition has been replicated in PLAXIS 3D software. The depth of soil at one side was 10 m where in another side, it was 15.23 m to maintain the 2° slope throughout the soil domain (see Fig. 1). The input motion which was applied at bottom base consists of 3 low amplitude cycles of ±0.01 g and followed by 20 high amplitude cycles of ±0.2-g with a frequency of 1 Hz at prototype. Figure 2 shows the motion which was applied in the direction of lateral displacement.

The far-field displacement, excess pore water pressure variation, base acceleration with dynamic time, upslope passive earth pressure distribution along caisson depth, as shown in [9] and in their companion paper [10], have been generated in the numerical analysis and compared thoroughly. From Fig. 2, it can be seen that far-field displacement, excess pore pressure at different depths, and base acceleration at far-field location are in good agreement with the results obtained from [10]. Further, the variation of upslope passive pressure along the depth of caisson has been compared well with [9] result. Therefore, the suitable selection of UBC3D-PLM model in this numerical analysis to capture the liquefaction and post-liquefaction phenomenon has been found to work well (Figs. 3 and 4).

3 Parametric Study

After validation of the proposed model, a detailed parametric study has been performed. Various parameters such as depth of liquefiable soil, caisson height to width ratio, slope of ground to initiate lateral spreading post-liquefaction have been varied. In this study, four different types of sinusoidal motion covering the probable

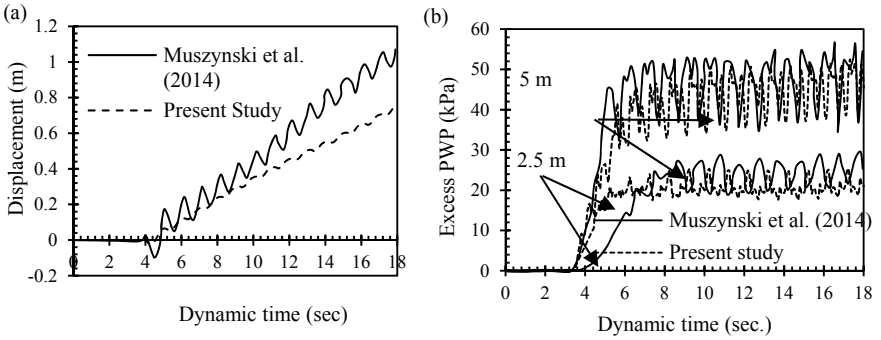

Fig. 3 Comparison of the numerical analysis results with the available centrifuge test results: **a** surface displacement at far-field location, **b** excess pore pressure at far-field location for 2.5 and 5 m depth from the ground surface

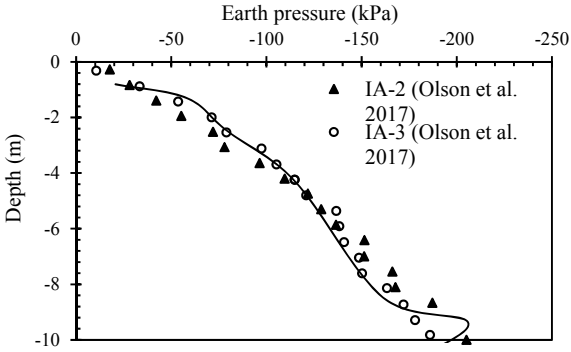

Fig. 4 Comparison of upslope passive pressure distribution obtained from the numerical analysis with the centrifuge test results

range of frequencies and amplitudes were used to observe the response of the caissons for different scenarios. Table 1 shows the details of the motions used in this analysis. Two different ground slope, i.e., 1% and 4% have been used in the present study and have been denoted as S1 and S4, respectively, for the rest of the paper. Soil properties have been kept same as used in the numerical analysis performed for validation.

Figure 5 shows that liquefaction has occurred for all the loading conditions. It

Table 1 Different types of input motion used in the parametric study

No	Frequency (Hz)	Amplitude (g)	Notation
1	2	0.4	M1
2	2	0.1	M2
3	1	0.4	M3
4	1	0.1	M4

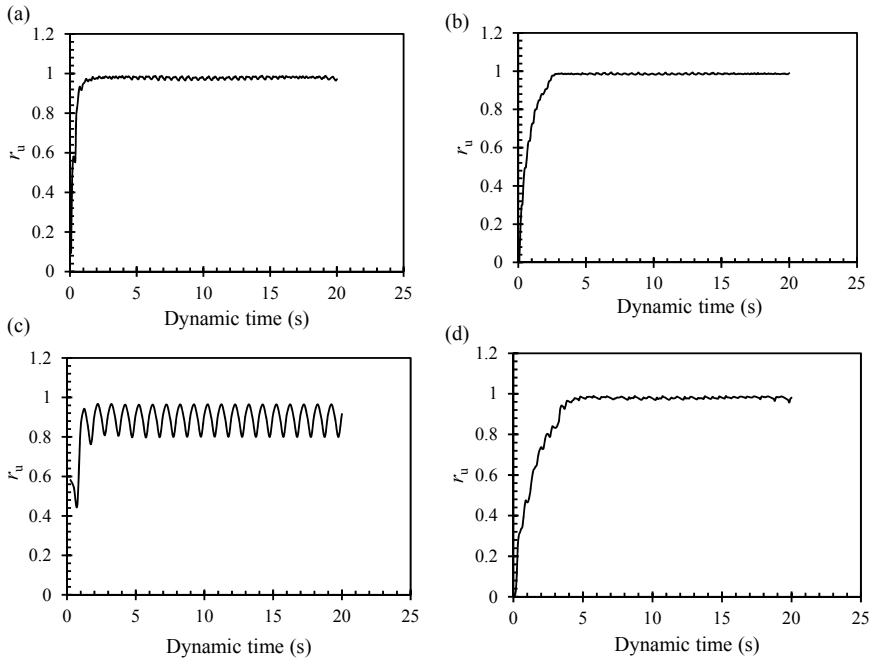

Fig. 5 Typical r_u versus dynamic time plot for **a** M1, **b** M2, **c** M3, **d** M4 motions for S1 ground slope inclination

also has been observed that for same motion frequency, if amplitude increases liquefaction occurs earlier as the cyclic shear stress applied is higher for higher amplitude motion. Also, liquefaction triggering depends on no. of stress reversals. Henceforth for same amplitude, no. of stress reversals increases with increment of frequency and subsequently liquefaction triggers earlier (see Fig. 5c, d).

Free-Field Displacement. Previous studies recommended that the response of deep foundations subjected to kinematic loading can be defined more profoundly by calculating the transfer function which is a ratio of the free-field ground displacement and foundation displacement. Present study indicated an increment in free-field displacement as the slope inclination increases. It can be due to the fact that with greater slope inclination, the driving stress for the flow of the soil increases which results in more displacement. Similar phenomenon can be observed for an increment of motion amplitude. However, the free-field displacement can be seen to decrease as the frequency of the input motion increases.

Caisson Response—Displacement and Rotation. Top head displacement and rotation of caisson are two major factors for the stability of caisson foundations subjected to lateral loading and have been investigated in the present study. Slender foundations like pile could follow more or less the wavy motion of the ground caused by the seismic waves. However, rigid foundations with high stiffness contrast compared to the surrounding soil generally don't follow free-field movement and

tend to modify the soil deformation. Henceforth the displacement of the caisson can be seen to be much different from the free-field ground motion. This phenomenon is known as the kinematic filtering effect of rigid foundations such as caissons. This filtering effect becomes more prominent for the foundations having high bending rigidity and low value of slenderness ratio. This can be compared in terms of wavelength of seismic shear waves in the soil and dimensions of a caisson, i.e., from the λ_{ff}/L value. Where λ_{ff} is the wavelength of the seismic wave which can be defined as V_s/f and L is caisson length. V_s is the shear wave velocity of the soil and f is the frequency of the input motion.

From Fig. 6, it can be observed that the caisson head displacement increases for increasing D/B ratio for S1 ground slope. Similar pattern has been found for the caisson embedded in S4 ground slope (see Fig. 7). According to the available literature, if λ_{ff}/L value decreases, the filtering effect of the caisson increases and the displacement of caisson decreases. For the same reason the rotation of the caisson reduces. That is why for D/B ratio of 3.75, the displacement and rotation is more. Though for D/B ratio of 2.5 and 1.67, the caisson height is same, but for D/B ratio

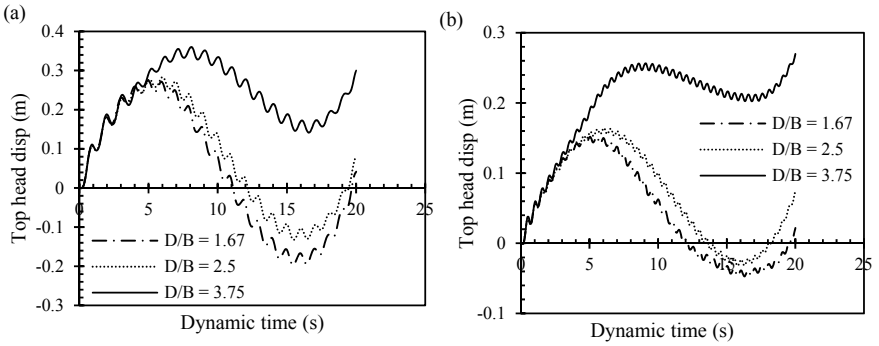

Fig. 6 Typical variation of top head displacement of caisson for 1% slope inclination (S1) for **a** M4 motion, **b** M2 motion

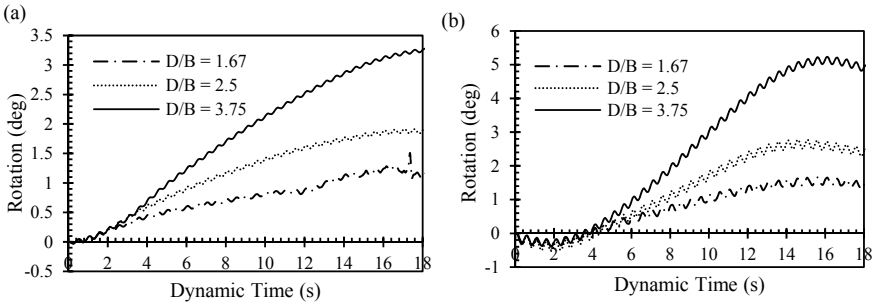

Fig. 7 Typical variation of caisson rotation for 4% slope inclination (S4) for **a** M2 motion, **b** M1 motion

of 1.67, the caisson width is more. This may be affecting the response and predicts less displacement and rotation for D/B ratio of 1.67. Figure 8 shows that the top head displacement and rotation of caisson increase as the slope inclination increases. This is due to the higher driving stress for the flow of the soil as discussed earlier. The effect of amplitude of input motion on caisson head displacement and rotation of caisson have been presented in Fig. 9. The top head displacement and rotation of the caisson increases with the increase in amplitude of the input motion. As the amplitude of the motion increases, the force imposed on the caisson increases which results in more displacement and rotation.

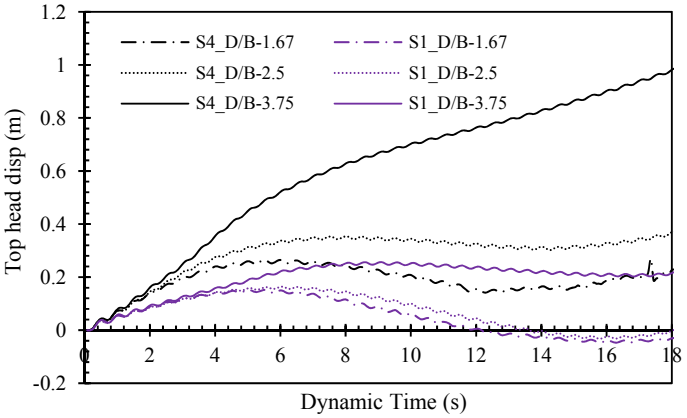

Fig. 8 Effect of ground slope inclination on top head displacement of caisson for M2 motion

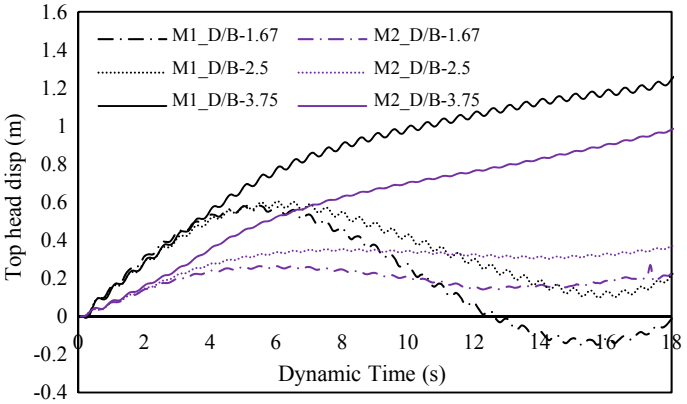

Fig. 9 Effect of amplitude of input motion on top head displacement of caisson for 4% ground slope inclination (S4)

4 Conclusions

This study presents the response of caisson foundations in liquefaction induced lateral spreading phenomenon in a qualitative way. Rigid foundations with high stiffness contrast compared to the surrounding soil generally don't follow free-field movement and tend to filter the soil deformation. Therefore, the caisson itself may be more or less unaffected due to the impact of lateral loading unlike piles but the slight movement and/or rotation of caisson due to the lateral flow pressure coming from the sub-soil ground movement initiates the failure of super-structures and subsequent damages. User defined PLAXIS 3D model UBC3D-PLM which can successfully capture the liquefaction phenomenon and flow of soil due to lateral spreading phenomenon has been used in the numerical analysis. This constitutive model is popular for its simplicity as well as for its effectiveness for successful prediction of soil behavior like triggering of liquefaction, post-liquefaction behavior, cyclic mobility, etc., using numerical and finite element formulation. The loss in capacity of surrounding soil due to seismically induced liquefaction when the caisson is has been found to affect the lateral stability of caissons embedded in potentially liquefiable soil through increase in top head displacement and rotation. The effect of different parameters on the extent of lateral spreading phenomenon which in turn affects the response of caisson has been observed through far-field ground displacement. The free-field displacement increases with slope, amplitude, and frequency of the input dynamic motion. It has also been observed that both the caisson head displacement and rotation increase for increase in amplitude of input motion, ground slope, caisson embedment to width ratio and decreases with the frequency of the input motion. The discussion on the behavior of the rigid caisson foundations subjected to liquefaction induced kinematic loading can be considered to provide the initial steps for the seismic design of caissons embedded in potentially liquefiable soil.

References

1. Youd TL (1978) Major cause of an earthquake damage is ground failure. Civil Eng ASCE 47–51
2. Biswas S, Choudhury D (2019) Seismic soil resistance for caisson design in sand. Proc Inst Civ Eng Geotech Eng 172(1):67–75
3. Biswas S, Choudhury D (2020) Caissons in cohesionless soils considering 3D wedge under earthquake loading. Int J Geomech 20(12):04020221
4. Finn WD, Thavaraj T (2001) Deep foundations in liquefiable soils: case histories, centrifuge tests and methods of analysis. In: Proceedings of international conferences on recent advances in geotechnical earthquake engineering and soil dynamics, USA
5. Matsui T, Oda K (1996) Foundation damage of structures. Soils Found 36(Special):189–200
6. Plaxis BV (2018) Netherlands user manuals. Plaxis 3D
7. Makra A (2013) Evaluation of the UBC3D-PLM constitutive model for prediction of earthquake induced liquefaction on embankment dams. MSc thesis, TU Delft
8. Petalas A, Galavi V (2013) Plaxis liquefaction model UBC3DPLM. Plaxis Rep

9. Olson SM, Hashash YM, Muszynski MR, Phillips C (2017) Passive wedge formation and limiting lateral pressures on large foundations during lateral spreading. J Geotech Geoenvironmental Eng 143(7):04017027
10. Muszynski MR, Olson SM, Hashash YM, Phillips C (2014) Repeatability of centrifuge tests containing a large, rigid foundation subjected to lateral spreading. Geotech Test J 37(6):1002–1015

Dynamic Analysis and Design of Foundations for Liquid Storage Tanks

Madan Kumar Annam and P. R. Sastry

Abstract Dealing with soft and loose soils is always a challenge to the practicing Civil Engineers. Foundations to support heavy loads on weak deposits in high seismic zones attracts more attention in design of foundations of structures. Seismic wave propagation and its impact on foundation elements induces additional bending moments and shear forces. This paper deals with analysis and design of foundations adopted for a 41 m diameter storage tank executed in the East Coast of India. The efficacy of lateral pile capacity has been assessed using PLAXIS 3D dynamic module. The performance of foundation system under earthquake loading was extensively studied and covered in this paper. A full geotechnical seismic site response analysis was conducted with a full mesh of soil layers and piles. Appropriate site-specific seismic acceleration history with time was imposed on the bedrock. Sloshing forces for both full and empty tank conditions were considered in the analysis. The 3D FEM seismic analysis of the pile movement and forces during and after earthquake were checked for structural adequacy of the piles against the M–N envelope.

Keywords Bored piles · Seismic loads · Storage tanks · Dynamic analysis · 3D FEM & PLAXIS 3D

1 Introduction

Storage tanks resting on pile foundations installed through soft soils and socketed into weathered rock and its performance under seismic conditions is great concern. The presence of soft soils plays important role in amplifying the ground motion, especially under seismic activity. Liquefaction of weak soils subjected to earthquake loading is key factor affecting the performance of pile foundation in seismically active zones where soil may experience liquefaction or cyclic mobility [1]. This paper presents

M. K. Annam (✉)
Head of Engg. Keller India, Chennai 600024, India
e-mail: madankumar@kellerindia.com

P. R. Sastry
Structural Consultant, Chennai 600032, India

T. G. Sitharam et al. (eds.), *Earthquakes and Structures*, Lecture Notes in Civil Engineering 188, https://doi.org/10.1007/978-981-16-5673-6_33

aspects of 3D FEM analysis applied to an oil storage tank founded on a group of piles installed through soft soils and all piles got socketed into rock. Numerical modelling was carried out using PLAXIS 3D dynamic module to assess adequacy of lateral pile capacity and efficacy of reinforcement in the event of earthquake [2]. The use of 3D Finite Element analysis for modelling of foundations in seismic conditions is often challenge to design engineers in understanding its behavior.

2 Project Background

An oil storage tank of 41 m diameter resting on 800 mm diameter bored cast in-situ (BCIS) piles along with reinforced concrete tank pad and associated civil works were executed in one of the oil tank farms. A full geotechnical seismic site response analysis was conducted with a full mesh of soil layers in order to evaluate seismic dynamic pile-soil interaction. Piles with an appropriate site-specific seismic acceleration history with time (accelerogram) was imposed on the underlying bedrock and propagates upward to the ground surface.

One of the requirements of design aspects in this project was to assess the concern of seismic impact on the pile foundation due to dynamic pile-soil interaction. This check was necessitated as the seismic wave propagates from the underlying bedrock upward to the ground surface [3]. A geotechnical 3D FEM seismic analysis was thus resorted as the present case is highly three dimensional in nature as seismic forces induce additional pile movements as well as additional bending moment & shear force along the pile shaft. The plan view and cross section of the proposed foundation system of storage tank is shown in Fig. 1 and 2 respectively.

3 Geological Conditions

The subsurface soil profile revealed by the relevant boreholes around the proposed tank is quite consistent with the SPT N with depth. Design soil parameters are presented in Table 1 and the ground conditions are uniform across the project site.

4 Load Combinations and Seismic Analysis

The site-specific seismic action characterized by the generated seismic response spectrum according to Clause 3.5 IS-1893 (Part 4): 2015 [4] was considered for a return period of 475 years. The site-specific seismic response spectrum is shown in Fig. 3. The seismic response spectrum matches reasonably with the target site specific seismic response spectrum.

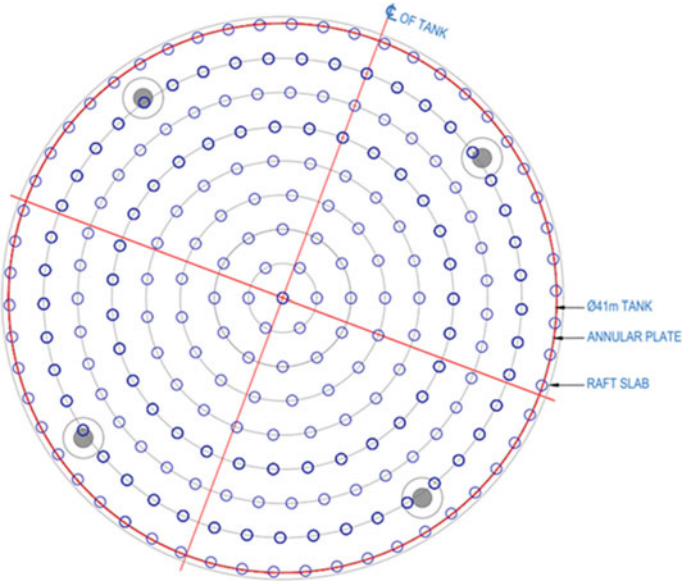

Fig. 1 Plan of the proposed tank foundation

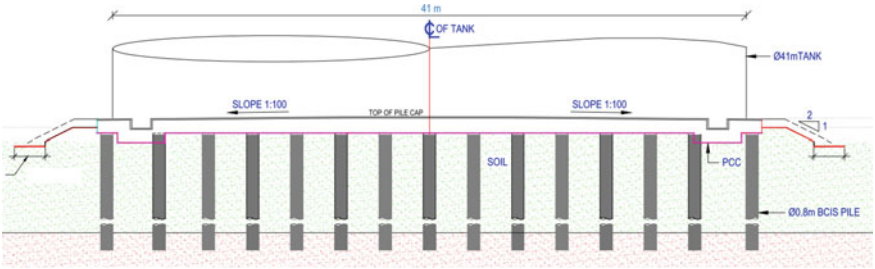

Fig. 2 Typical cross section of the foundation

Table 1 Soil parameters for the various soil types

S. No	RL (m)		Soil description	SPT N values	Unit weight	Cu	φ
	From	To			(kN/m^3)	(kPa)	(deg)
1	4	0	Filled up soil	8	17.0	–	29
2	0	−8	Clay (CH)	3	14.5	10	–
3	−8	−12	Clay (CI-CH)	6	16.0	20	–
4	−12	−17	Clayey silty sand	36	18.5	180	–
5	−17	−19	Highly weathered rock	>60	20.0	300	–
6	−19		Weathered rock	>100	20.0	600	–

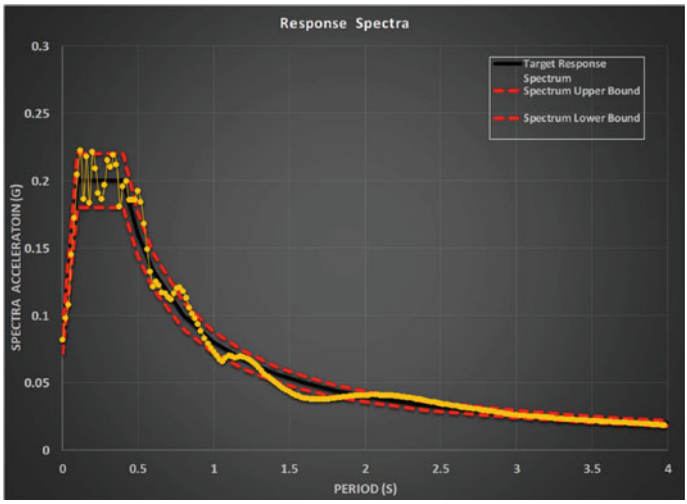

Fig. 3 The seismic response spectrum

The methodology adopted for Geotechnical 3D seismic analysis was based on the guidelines stipulated in IS-1893 Part 1 CL.6.3.4 [4] viz. (a) unfactored seismic signal as per DBE and (b) load combinations covering tank full and empty conditions with appropriate load factors, were checked along the full pile length.

5 Geotechnical 3D FEM Seismic Analysis

Latest version of Geotechnical 3D FEM (Plaxis 3D) dynamic module was used as it is highly three-dimensional in nature. The model was made initially with in-situ soil conditions followed by construction of piles and pile cap. The steel tank with base thickness of 10 mm and shell thickness of 25 mm at bottom to 8 mm at top was then erected as illustrated in Fig. 4. The load intensity of about 150 kPa was considered as content load acting on the foundation raft (reinforced concrete tank pad, resting on pile foundations).

Illustration of forces applied in Plaxis 3D model for seismic analysis is presented in Fig. 5.

The accelerogram was then applied to the base of underlying bedrock and propagate waves upwards. The accelerogram time history was sub-divided into 25 ms sub-steps for dynamic time-stepping analysis. Snapshots of intermediate moments of the tank movements during the earthquake is illustrated Fig. 6.

Based on the PLAXIS 3D study, it is assessed that for the full tank case, the calculated post-earthquake pile movement and forces are much smaller after the earthquake. Figure 7 presents the induced bending moment profiles of the piles during the earthquake with a maximum value of about 375 kNm.

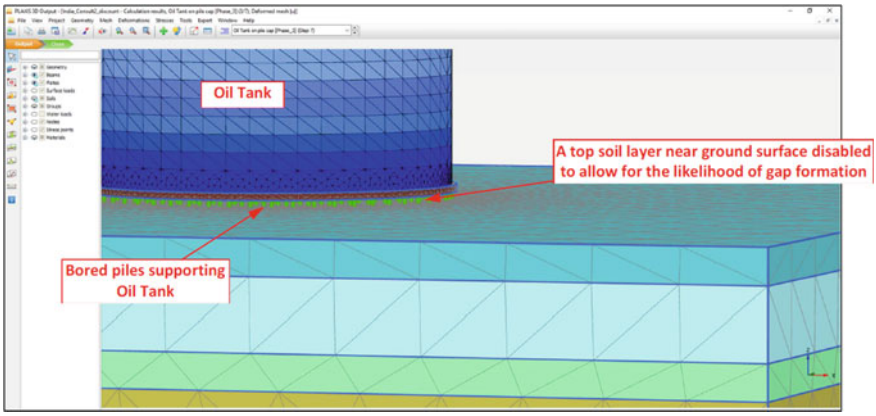

Fig. 4 Geotechnical 3D FEM model

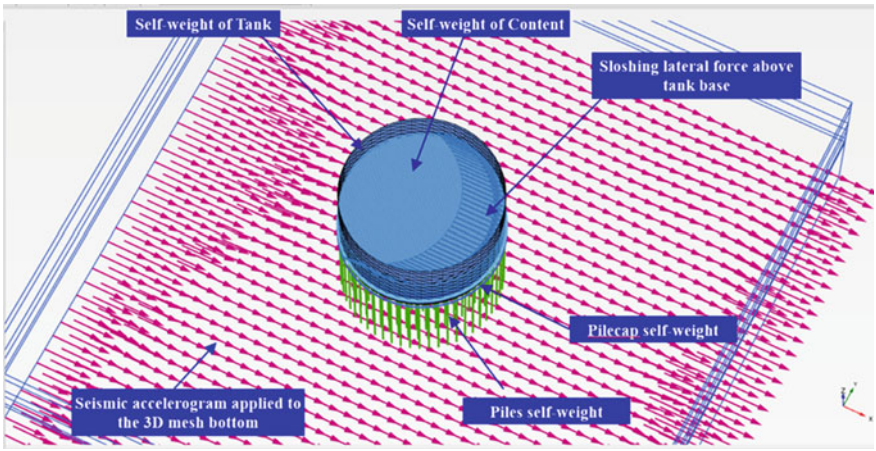

Fig. 5 Forces applied in Plaxis 3D model for seismic analysis

The induced pile forces are much smaller for the empty tank case due to much less inertial effect during earthquake. Load combinations for empty tank case and tank full conditions were complying with the IS1893 CL.6.3.4 [4] consistently.

6 Structural Analysis of the Foundation

Structural analysis of the foundation system was carried out using 'STAAD PRO'. Base raft was modeled as a circular reinforced concrete slab of 42.0 m diameter using plate elements resting on piles. Analysis and design of tank structure is not covered

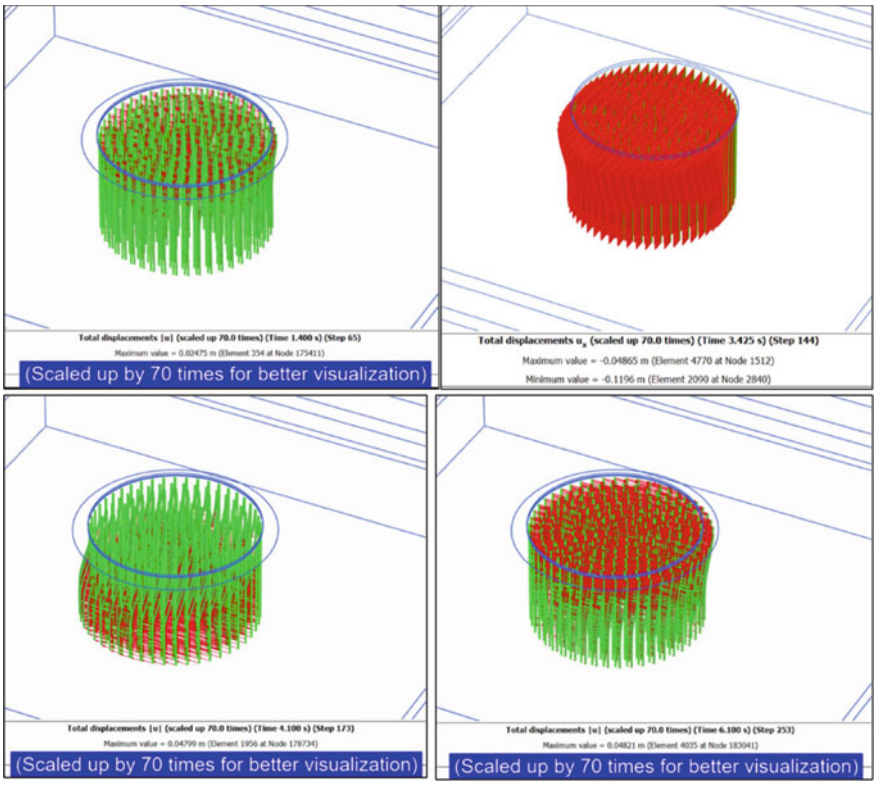

Fig. 6 Illustration of pile deflection during the earthquake (scaled up by 70 times)

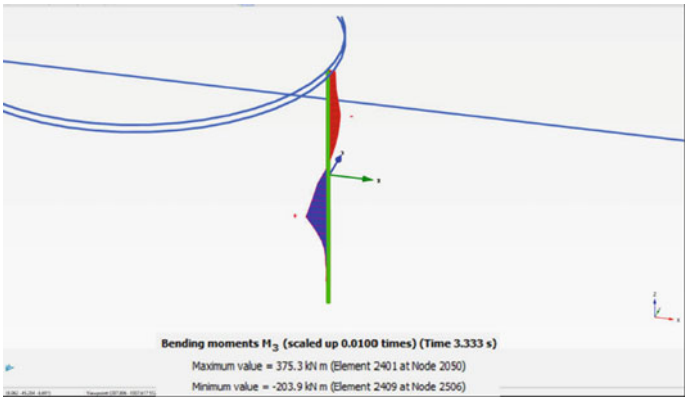

Fig. 7 The BM profile of the most critical pile during earthquake

in this paper. Foundation analysis was performed according to the forces supplied by client are applied in the structural model. Plate elements were modelled as annular grids and piles are considered as spring supports. Stiffness values of piles derived from its capacity and settlement. A concealed ring beam with nominal properties was placed at the edge of tank raft on which loads can be applied on the tank walls. The analysis was made for three scenarios namely empty condition, test load (with water) and service conditions. Loads due to empty tank and contents weight along with external loads viz. wind load and earthquake loads on the tank structure were applied on the model appropriately including the sloshing effects during operation stage.

The analyses revealed that for the tanks supported on piles, the number of piles solely based on geotechnical capacity for static loads and Design Basis Earthquake (DBE) conditions. The number of piles were selected to meet structural capacity requirements. The results of the structural analyses found that in most instances, the design of the tanks and the foundations are governed by the DBE. Bending moment and shear stress at critical locations for factored load combinations were obtained. Figure 8 illustrates the induced maximum M–N forces in the pile M–N envelope for both during & post-earthquake conditions.

It can be seen from the geotechnical 3D FEM seismic and structural analysis that the proposed number of bored piles are sufficient to resist the earthquake impact and hence foundation system is adequate.

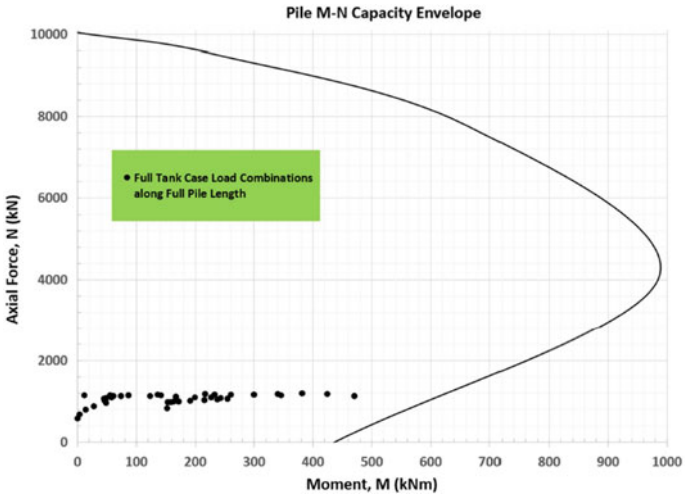

Fig. 8 Load combination along the full pile length on pile M–N capacity envelope

7 Results and Discussions

A full geotechnical 3D seismic analysis with a full mesh of soil layers was conducted for the storage tank foundation resting on piles. Dynamic pile-soil interaction with appropriate site-specific seismic accelerogram was imposed on the underlying bedrock. Seismic wave to propagate upward direction from the bed rock to ground surface was considered to evaluate the soil-structure interaction. The lateral loads arrived from geotechnical 3D FEM seismic analysis confirms structural integrity through M–N envelope that the re-bar provided is enough. On the other hand, the calculated post-earthquake pile movement and forces are much smaller after the earthquake, and a structural integrity check based on M–N envelope show the re-bar provided is more than sufficient for the post-earthquake forces.

Seismic analysis of the pile movement and forces during and after earthquake are checked for structural adequacy against the pile M–N structural capacity envelope and found satisfactory.

Acknowledgements The authors acknowledge with gratitude to Keller India management for their continuous support and encouragement in finalization of this paper. Appreciations are due to other colleagues who have helped the authors in compilation of this paper. Thanks also due to Keller India site management for providing execution and monitoring data. The authors wish to thank Dr Shen Rui Fu, Geotechnical Expert, Singapore for his valuable guidance and suggestions during this study.

References

1. Ashutosh K, Deepankar C, Jaykumar S, Shah DL (2015) Seismic design of pile foundation for oil tank. Disaster advances, pp 1–13
2. Design recommendation for storage tanks and their supports with emphasis on seismic design (2010 edition), pp 1–173
3. Poulos HG, Practical design procedures for piled raft foundations, Design applications of raft foundations, Practical design of piled rafts, pp 425–467
4. IS 1893 (Part 1) (2016) Criteria for earthquake resistant design of structures, Part 1 general provisions and buildings (sixth revision); BIS 2016

Performance of Mechanically Stabilized Earth Structures in Seismic Conditions

Atanu Adhikari and Deepak Manjunath

Abstract Mechanically Stabilized Earth (MSE) or Reinforced Soil structures are composite structures consisting of alternating layers of compacted backfill and soil reinforcement elements that are fixed to a facing. The stability of MSE structures is derived from the interaction between the backfill and soil reinforcements, involving friction and tension. The facing is relatively thin and is intended to perform the primary function of preventing erosion of the structural backfill. The significant relative cost saving that can be realized when this system is used compared to traditional RCC retaining structures, combined with ease of construction has resulted in widespread adoption of this technology in India and around the world. MSE structures have been found to perform satisfactorily when subjected to seismic loading conditions provided that recommended practices are adopted during their construction. This paper presents case studies of superior performance of MSE structures when subjected to seismic loading both during and after completion of construction including a case study on the behaviour of MSE structures founded on soft silt deposit in seismically active hilly terrain in the stretch from Quazigund to Baramulla where an earthquake measuring 5.4 on the Richter scale occurred during construction of the structure.

Keywords Reinforced earth · MSE wall · Mononabe-Okabe · Pseudo-static seismic loading

1 Introduction

One of the fundamental characteristics of earthquake resistant structures is the ability to dissipate energy induced due to earthquake loading by means of deformation within serviceability limits. Such structures are constructed with materials

A. Adhikari · D. Manjunath (✉)
Terre Armee India, New Delhi 110044, India
e-mail: deepak.manjunath@terrearmeeindia.com

A. Adhikari
e-mail: atanu.adhikari@terrearmeeindia.com

T. G. Sitharam et al. (eds.), *Earthquakes and Structures*, Lecture Notes in Civil Engineering 188, https://doi.org/10.1007/978-981-16-5673-6_34

that can resist shear and tension, with simple, regular shaped individual members joined to form a continuous system that is capable of redistributing the earthquake forces. Mechanically Stabilized Earth (MSE) structures possess all these properties. Mechanically Stabilized Earth (MSE) or Reinforced Soil structures are composite structures consisting of alternating layers of compacted backfill and soil reinforcement elements that are fixed to a facing. The stability of MSE structures is derived from the interaction between the backfill and soil reinforcements, involving friction and tension. The facing is relatively thin and is intended to perform the primary function of preventing erosion of the structural backfill. The significant relative cost saving that can be realized when this system is used compared to traditional RCC retaining structures, combined with ease of construction has resulted in widespread adoption of this technology in India and around the world.

2 Experimental Models and Structures

Over the years, the response of MSE structures to seismic loading has been extensively studied by means of three types of experimental models and structures [6], namely:

1. Scale Models
2. ½ Scale Models and
3. Full Scale structures.

2.1 Scale Models

Initial studies pertaining to seismic response of MSE structures were conducted on scale models of MSE structures on which seismic loading was induced by means of vibrating tables (Fig. 1).

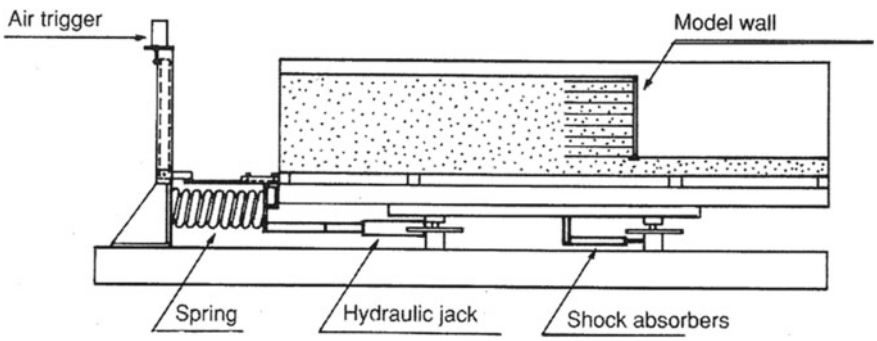

Fig. 1 Scale model on vibrating table [6]

However, drawing inferences and conclusions from such studies was a risky proposition due to inability of such models to represent behaviour of actual full size structures, specifically with respect to replicating adherence conditions, ductility of the reinforcements, the proportions of the structure, the period of vibration and so on. Moreover, it was difficult to observe the mode of reinforcement failure i.e. rupture or pull out [6].

2.2 ½ Scale Models

The short comings of scale models were addressed in the form of half scale models conceptualized by Professor Chida. These half scale models were placed on a vibrating table inside a box arrangement. This arrangement was instrumented with accelerometers and extensometers to record measurements during the experiments (Fig. 2). In this set up, earthquake loading was simulated through of a range of frequencies and accelerations that were induced by the vibrating table. Analysis of measurements recorded during experiments conducted using this set up, indicated a relatively even increase of tension in the reinforcements with increase in the induced acceleration. However, the rigidity of the frame was observed to influence the results at high frequencies [6].

2.3 Full Scale Structures

The propagation of significant vibrations through the reinforced soil mass, their effect on tension and adherence of reinforcements and the actual period of the vibration of the structures was studied by experiments conducted on full scale structures. Through these experiments, it was inferred that while seismic loading influences vertical stress, it did not have an effect on friction and thereby did not have an effect on adherence of the reinforcements [6].

3 Analysis of Experimental Data

At the request of Reinforced Earth Group, a critical analysis of all previous studies was conducted by the late Professor H.B. Seed [6]. Based on the experimental data, he drew the following conclusions:

1. The fundamental period of vibration of a structure is a function of its height and is only a fraction of a second. The maximum acceleration is nearly equivalent to the acceleration at ground level.

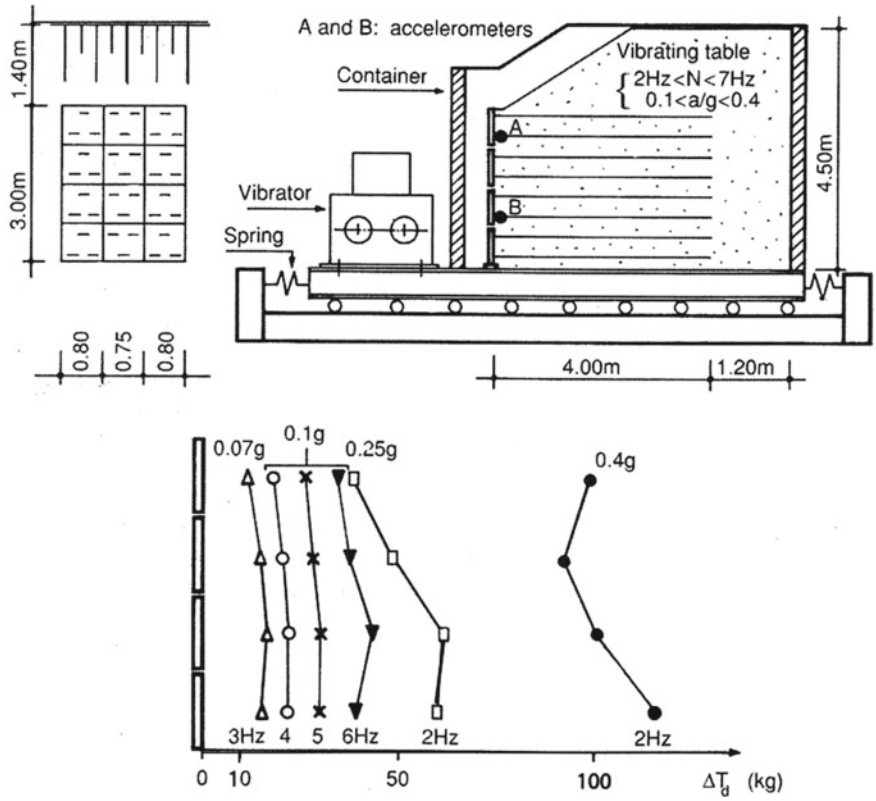

Fig. 2 ½ Scale model developed by Professor Chida and distribution of dynamic tension increments [6]

2. The excess dynamic tensile load that is developed in the reinforcements due to acceleration induced by seismic loading is practically constant throughout the height of a standard structure.
3. There is no residual deformation when MSE structures are subjected to accelerations up to 0.3 g

In addition, Professor Seed recommended that certain assumptions, like the width of the active zone, should be verified by other means, such as finite element method analysis.

4 Finite Element Analysis

When MSE structures using linear inextensible reinforcements were analyzed by finite elements method, the following inferences were drawn [6]:

1. The horizontal acceleration generally increases from the base to the top of the wall. While the average value is close to the input acceleration when the structure is founded on rock, the average acceleration transmitted to the structure is noticeably reduced when the structure is founded on less firm ground.
2. There is no residual deformation and a maximum elastic deformation of 13 mm results at the top of a 10 m tall MSE structure when it is subjected to seismic loading that induces an input acceleration of 0.4 g.
3. When compared with static loading, the location of the maximum tension line in the reinforcements doesn't change when MSE structures are subjected to seismic loading, even at high input accelerations.
4. When the reinforcements are evenly distributed in the structure, this internal dynamic force resulting due to seismic loading is equally distributed at all levels of reinforcements. The distribution is proportional to the shear resistance of the resistive zone, and hence is a function of the adherence length of the reinforcements.
5. When the reinforcements are unevenly distributed, the dynamic force is also distributed in proportion to the reinforcement density with the more heavily reinforced sections resisting more force.

5 Design Approach

Finite Element analyses have been adopted to analyse the behaviour of reinforced soil walls under static and seismic loading [1, 4, 9]. The design standards to be followed for design of reinforced soil walls and slopes in India find mention in Clause 3100 of Ministry of Road Transport & Highways (MoRTH) Specifications for Road & Bridge Works (5th Revision) as well as IRC:SP 102–2014. MoRTH Clause 3100 [10] allows for design to be done as per BS 8006:2010 [2] as well as FHWA-NHI-10–024 [3]. Since BS 8006:2010 does not cover the design checks to be carried out in seismic condition, the general design approach involves conducting the design checks for static case as per BS 8006 while the design checks for seismic case are carried out as per the Mononobe-Okabe pseudo-static approach presented in FHWA-NHI-10–024. MSE structures designed by adopting this design approach have been found to perform satisfactorily when subjected to seismic loading conditions provided that recommended practices are adopted during their construction.

6 Performance of MSE Structures Subjected to Seismic Loading

This section presents case studies to illustrate the performance of MSE structures subjected to seismic loading.

6.1 MSE Walls for Quazigund to Baramulla Rail Over Bridge Project

During the construction of eight Rail Over Bridge (ROB) approaches using MSE walls in the Quazigund to Baramulla project, the site experienced an earthquake of magnitude about 7.0 on Richter scale with epicenter about 150 km away from the site, in Pakistan. By means of extensive soil investigation, the foundation soil for most locations was found to be characterized by filled-up soil of 1–2 m followed by layers of fine grained clayey silt of low/ medium plasticity upto 15–20 m depth. In some locations sand was encountered at 16 m depth. Clayey silt upto 15 m depth was composed of 3–5% of sand, 80–95% of silt and 2–7% of clay. The SPT-N value was found to vary from 1–9 upto a depth range of 6–10 m.

MSE walls using discrete cruciform panels and high adherence steel strip reinforcement were adopted for the construction of the ROB approaches. The static design of the MSE structures was carried out as per BS 8006, 1995 and the seismic design was carried out as per AFNOR NF P 94–220, July 1992. The backfill used was well-graded riverbed material with engineering properties that conformed to the mechanical, physical and hydraulic and electrochemical criteria defined in the technical specifications. The foundation soil was reinforced with high tenacity polyester Geogrids as transition course to improve bearing capacity and to achieve global stability.

For reinforced soil walls upto a height of 4 m, no ground treatment was proposed. Walls exceeding 4 m height, the ground was proposed to be treated with one or two layers of high strength PET geogrid, which, were extended 3 m on both sides beyond the structure width depending on detailed analysis. Structures whose height exceeded 4 m were constructed in two or three stages with waiting period designed to dissipate excess pore pressures developed at the end of each stage of construction [5].

6.1.1 Seismic Event During Construction

The Kashmir earthquake (also known as the South Asia earthquake or the Great Pakistan earthquake) of 2005, was a major earhquake whose epicenter was located in the Pakistan administered Kashmir occurred at 08:50:38 h. Pakistan standard time (03:50:38 UTC) on 8th Oct. 2005. It registered 7.6 on the richer scale making it a major earthquake similar in intensity to the 1935 Quetta earthquake, the 2001 Gujarat earthquake, and the 1906 San Francisco earthquake. The equivalent magnitude of tremor on Richter scale at site was 5.4.

All the MSE walls on Baramula—Quazigund section experienced the impact of this earthquake. The constructed height of the wall was 6 m at the time of the seismic event. While many residential structures in the vicinity collapsed or were damaged due to earthquake, no damage was observed in the MSE walls (Fig. 3).

Fig. 3 (Top) Damage sustained by buildings in Uri 30 km from site and (Bottom) MSE approach wall for Bridge No. 127 after the earthquake [5]

The vertical alignment, individual panel joints, vertical and horizontal gap between the panels were found to be intact. No bulging, differential movement between the panels, or any damage in the panels was observed after the earthquake.

6.2 Performance of MSE Walls During the Northridge, Kobe and Izmit Earthquakes

6.2.1 Northridge Earthquake

23 MSE Wall structures measuring 5–10 m in height and located between 13–83 km from the epicentre were subjected to seismic loading during the 1994 Northridge earthquake. The earthquake subjected the structures to horizontal accelerations varying between 0.07–0.91 g and vertical accelerations varying between 0.04–0.62 g [7]. While the buildings and other structures in the vicinity of the MSE structures were severely damaged during the earthquake, the only damage observed in the MSE

walls was minor spalling of the concrete panels. It is of high importance to note that while over 75% of the MSE wall structures were designed using lesser horizontal ground accelerations than actually occurred, over 50% of the MSE wall structures were designed by not considering any horizontal ground accelerations at all [8].

6.2.2 Kobe Earthquake

Over 120 MSE wall structures ranging in height from 5 m to over 10 m were inspected after the 1995 Kobe earthquake. While the structures were designed using ground accelerations ranging from 0.15–0.2 g, the actual ground acceleration during the earthquake was 0.27 g. While ground deformation was observed next to 22 structures, 10 structures exhibited minor cracking of the concrete panels with 3 structures exhibiting significant lateral movement. While deformations recorded in walls at Awaji Island and Hosiga-oka Park varied between 4–113 mm, all the structures were recorded to remain functional after the earthquake [8].

6.2.3 Izmit Earthquake

One bridge and ramp structure located in Arifiye, in close proximity to the epicentre, was inspected after the 1999 Izmit earthquake. The differential settlements that were initiated by the seismic event caused panels to separate by as much as 75 mm at some locations. However, while the bridge collapsed, it was observed that the bridge approach MSE ramp walls remained stable and only sustained nominal damage. This is noteworthy, especially considering that the MSE walls were subjected to a ground accelearation of 0.4 g while they were actually designed considering a ground acceleration of 0.1 g only [8].

7 Conclusions

This paper presents inferences drawn from experiments that were conducted to study response of MSE structures to seismic loading. Selected case studies from around the world have been presented to support the conclusion that MSE structures remain structurally stable after experiencing significant seismic loading. MSE walls being flexible in nature, can be constructed over very soft soil where the expected settlement is very large and in areas prone to high seismic activity. Special arrangements like provision of slip joints are very important to ensure that MSE structures can accommodate large differential settlements.

References

1. Bathurst RJ, Hatami K (1998) Seismic response analysis of a geosynthetic reinforced soil retaining wall. Geosynth Int 5(1–2):127–166
2. BS 8006–1 (2010) Code of practice for strengthened/reinforced soils and other fills. BSI Standards Publication, London, UK
3. FHWA-NHI-10–024 (2009) Design and construction of mechanically stabilized earth walls and reinforced soil slopes. US Department of Transportation, Federal Highway Administration, Virginia, USA
4. Karpurapu R, Bathurst RJ (1995) Behavior of geosynthetic reinforced soil retaining walls using the finite element method. Comp Geotech 17(3):279–299
5. Mahajan P, Biwas S, Adhikari A (2008) Behaviour of reinforced earth structures founded on soft silt deposit in seismically active hilly terrains. In: Proceedings of the new horizons in earth reinforcement—otani, Miyata & Mukunoki, Taylor & Francis Group, London, pp 797–802
6. Reinforced Earth Management Services Sdn Bhd, Reinforced earth structures in seismic regions, Kuala Lumpur, Malaysia
7. Sandri D (1994) Retaining wall stand up to the northridge earthquake. Geotechnical Fabrics Report 12(4):30–31
8. Sankey JE, Segrestin P, Evaluation of seismic performance in Mechanically stabilized earth structures. https://www.tierra-armada.cl/descargas/Evaluation-of-Seismic-Performance-in-Mechanically-Stabilized-Earth.pdf
9. Segrestin P, Bastick MJ (1998) Seismic design of reinforced earth retaining walls—the contribution of finite element analysis. In: Yamanouchi T, Miura N, Ochiai H (eds) Proceedings of the international geotechnical symposium on theory and practice of earth reinforcement, Balkema, Rotterdam, pp 577–582
10. Specifications for road and bridge works (2013) Ministry of Road Transport & Highways, New Delhi, India